

The background of the cover features stylized silhouettes of three animals: a horse in the top right, a cow in the middle left, and a chicken in the bottom right. The horse is dark green, the cow is blue, and the chicken is light green. The title text is overlaid on the horse silhouette.

ADVANCES IN THE DIAGNOSIS AND CONTROL OF JOHNE'S DISEASE

EDITED BY: Marta Alonso-Hearn, Kumi de Silva and Miguel Salgado
PUBLISHED IN: Frontiers in Veterinary Science



frontiers

Frontiers eBook Copyright Statement

The copyright in the text of individual articles in this eBook is the property of their respective authors or their respective institutions or funders. The copyright in graphics and images within each article may be subject to copyright of other parties. In both cases this is subject to a license granted to Frontiers.

The compilation of articles constituting this eBook is the property of Frontiers.

Each article within this eBook, and the eBook itself, are published under the most recent version of the Creative Commons CC-BY licence.

The version current at the date of publication of this eBook is CC-BY 4.0. If the CC-BY licence is updated, the licence granted by Frontiers is automatically updated to the new version.

When exercising any right under the CC-BY licence, Frontiers must be attributed as the original publisher of the article or eBook, as applicable.

Authors have the responsibility of ensuring that any graphics or other materials which are the property of others may be included in the CC-BY licence, but this should be checked before relying on the CC-BY licence to reproduce those materials. Any copyright notices relating to those materials must be complied with.

Copyright and source acknowledgement notices may not be removed and must be displayed in any copy, derivative work or partial copy which includes the elements in question.

All copyright, and all rights therein, are protected by national and international copyright laws. The above represents a summary only. For further information please read Frontiers' Conditions for Website Use and Copyright Statement, and the applicable CC-BY licence.

ISSN 1664-8714

ISBN 978-2-88971-750-7

DOI 10.3389/978-2-88971-750-7

About Frontiers

Frontiers is more than just an open-access publisher of scholarly articles: it is a pioneering approach to the world of academia, radically improving the way scholarly research is managed. The grand vision of Frontiers is a world where all people have an equal opportunity to seek, share and generate knowledge. Frontiers provides immediate and permanent online open access to all its publications, but this alone is not enough to realize our grand goals.

Frontiers Journal Series

The Frontiers Journal Series is a multi-tier and interdisciplinary set of open-access, online journals, promising a paradigm shift from the current review, selection and dissemination processes in academic publishing. All Frontiers journals are driven by researchers for researchers; therefore, they constitute a service to the scholarly community. At the same time, the Frontiers Journal Series operates on a revolutionary invention, the tiered publishing system, initially addressing specific communities of scholars, and gradually climbing up to broader public understanding, thus serving the interests of the lay society, too.

Dedication to Quality

Each Frontiers article is a landmark of the highest quality, thanks to genuinely collaborative interactions between authors and review editors, who include some of the world's best academicians. Research must be certified by peers before entering a stream of knowledge that may eventually reach the public - and shape society; therefore, Frontiers only applies the most rigorous and unbiased reviews. Frontiers revolutionizes research publishing by freely delivering the most outstanding research, evaluated with no bias from both the academic and social point of view. By applying the most advanced information technologies, Frontiers is catapulting scholarly publishing into a new generation.

What are Frontiers Research Topics?

Frontiers Research Topics are very popular trademarks of the Frontiers Journals Series: they are collections of at least ten articles, all centered on a particular subject. With their unique mix of varied contributions from Original Research to Review Articles, Frontiers Research Topics unify the most influential researchers, the latest key findings and historical advances in a hot research area! Find out more on how to host your own Frontiers Research Topic or contribute to one as an author by contacting the Frontiers Editorial Office: frontiersin.org/about/contact

ADVANCES IN THE DIAGNOSIS AND CONTROL OF JOHNE'S DISEASE

Topic Editors:

Marta Alonso-Hearn, Animalien Osasuna, NEIKER-Instituto Vasco de Investigación y Desarrollo Agrario, Spain

Kumi de Silva, The University of Sydney, Australia

Miguel Salgado, Austral University of Chile, Chile

Citation: Alonso-Hearn, M., de Silva, K., Salgado, M., eds. (2021). Advances in the Diagnosis and Control of Johne's Disease. Lausanne: Frontiers Media SA.
doi: 10.3389/978-2-88971-750-7

Table of Contents

- 05 Editorial: Advances in the Diagnosis and Control of Johne's Disease**
Marta Alonso-Hearn, Miguel Salgado and Kumudika de Silva
- 07 Effectiveness and Economic Viability of Johne's Disease (Paratuberculosis) Control Practices in Dairy Herds**
Philip Rasmussen, Herman W. Barkema and David C. Hall
- 27 Corrigendum: Effectiveness and Economic Viability of Johne's Disease (Paratuberculosis) Control Practices in Dairy Herds**
Philip Rasmussen, Herman W. Barkema and David C. Hall
- 28 Serum Metabolomic Profiles of Paratuberculosis Infected and Infectious Dairy Cattle by Ambient Mass Spectrometry**
Alessandra Tata, Ivana Pallante, Andrea Massaro, Brunella Miano, Massimo Bottazzari, Paola Fiorini, Mauro Dal Prà, Laura Paganini, Annalisa Stefani, Jeroen De Buck, Roberto Piro and Nicola Pozzato
- 38 Diagnostic Sequences That Distinguish *M. avium* Subspecies Strains**
John P. Bannantine, Judith R. Stabel, Darrell O. Bayles, Cyril Conde and Franck Biet
- 55 Detection of *Mycobacterium avium* ssp. paratuberculosis in Cultures From Fecal and Tissue Samples Using VOC Analysis and Machine Learning Tools**
Philipp Vitense, Elisa Kasbohm, Anne Klassen, Peter Gierschner, Phillip Trefz, Michael Weber, Wolfram Miekisch, Jochen K. Schubert, Petra Möbius, Petra Reinhold, Volkmar Liebscher and Heike Köhler
- 70 Detection of *Mycobacterium avium* Subspecies paratuberculosis (MAP) Microorganisms Using Antigenic MAP Cell Envelope Proteins**
Shanmugasundaram Karuppusamy, Lucy Mutharia, David Kelton, Brandon Plattner, Sanjay Mallikarjunappa, Niel Karrow and Gordon Kirby
- 84 Survey of Candidate Single-Nucleotide Polymorphisms in *SLC11A1*, *TLR4*, *NOD2*, *PGLYRP1*, and *IFN γ* in Ankole Longhorn Cattle in Central Region of Uganda to Determine Their Role in *Mycobacterium avium* Subspecies paratuberculosis Infection Outcome**
Julius Boniface Okuni, Mathias Afayoa and Lonzy Ojok
- 94 Comparative Genomics of *Mycobacterium avium* Subspecies Paratuberculosis Sheep Strains**
Rachel Mizzi, Verlaine J. Timms, Marian L. Price-Carter, Milan Gautam, Richard Whittington, Cord Heuer, Patrick J. Biggs and Karren M. Plain
- 108 Alpha-2-Macroglobulin as a New Promising Biomarker Improving the Diagnostic Sensitivity of Bovine Paratuberculosis**
Hyun-Eui Park, Jin-Sik Park, Hong-Tae Park, Jeong-Gyu Choi, Jeong-Ih Shin, Myunghwan Jung, Hyung-Lyun Kang, Seung-Chul Baik, Woo-Kon Lee, Donghyuk Kim, Han Sang Yoo and Min-Kyoung Shin
- 118 Electrochemical Detection of Serum Antibodies Against *Mycobacterium avium* Subspecies paratuberculosis**
Kaoru Hatate, J. Hunter Rice, Karsten Parker, J. Jayne Wu, Amy Turner, Judith R. Stabel and Shigetoshi Eda

- 126 Bacteriophage-Based Methods for Detection of Viable *Mycobacterium avium* subsp. *paratuberculosis* and Their Potential for Diagnosis of Johne's Disease**
Irene R. Grant
- 134 Identification of Long Non-coding RNA Isolated From Naturally Infected Macrophages and Associated With Bovine Johne's Disease in Canadian Holstein Using a Combination of Neural Networks and Logistic Regression**
Andrew Marete, Olivier Ariel, Eveline Ibeagha-Awemu and Nathalie Bissonnette
- 148 Engineering Synthetic Lipopeptide Antigen for Specific Detection of *Mycobacterium avium* subsp. *paratuberculosis* Infection**
Sylvie Bay, Douglas Begg, Christelle Ganneau, Maxime Branger, Thierry Cochard, John P. Bannantine, Heike Köhler, Jean-Louis Moyaen, Richard J. Whittington and Franck Biet
- 158 Functional Variants Surrounding Endothelin 2 Are Associated With *Mycobacterium avium* Subspecies *paratuberculosis* Infection**
Jennifer N. Kiser, Zeping Wang, Ricardo Zanella, Erik Scraggs, Mahesh Neupane, Bonnie Cantrell, Curtis P. Van Tassell, Stephen N. White, Jeremy F. Taylor and Holly L. Neibergs
- 168 Early Detection of *Mycobacterium avium* subsp. *paratuberculosis* Infected Cattle: Use of Experimental Johnins and Innovative Interferon-Gamma Test Interpretative Criteria**
Sara Corneli, Antonella Di Paolo, Nicoletta Vitale, Martina Torricelli, Linda Petrucci, Carla Sebastiani, Marcella Ciullo, Ludovica Curcio, Massimo Biagetti, Paola Papa, Silva Costarelli, Monica Cagiola, Alessandro Dondo and Piera Mazzone
- 182 Development of a Method to Detect *Mycobacterium paratuberculosis* in the Blood of Farmed Deer Using Actiphage® Rapid**
Anton Kubala, Tania M. Perehinec, Catherine Evans, Andrea Pirovano, Benjamin M. C. Swift and Catherine E. D. Rees



Editorial: Advances in the Diagnosis and Control of Johne's Disease

Marta Alonso-Hearn^{1*}, Miguel Salgado² and Kumudika de Silva³

¹ NEIKER- Basque Institute for Agricultural Research and Development, Department of Animal Health, Basque Research and Technology Alliance (BRTA), Derio, Spain, ² Facultad de Ciencias Veterinarias, Instituto de Medicina Preventiva Veterinaria, Universidad Austral de Chile, Valdivia, Chile, ³ Faculty of Science, School of Veterinary Science, The University of Sydney, Sydney, NSW, Australia

Keywords: Johne's disease, diagnosis, control, vaccines, genetic resistance

Editorial on the Research Topic

Advances in the Diagnosis and Control of Johne's Disease

We are delighted to have contributed as Guest Editors to this special Research Topic entitled: "Advances in the Diagnosis and Control of Johne's Disease." This Research Topic is a collection of 15 manuscripts (14 original research papers and 1 minireview article) from 112 authors. *Mycobacterium avium* subsp. *paratuberculosis* (MAP) causes Johne's disease or paratuberculosis (PTB), an infectious chronic enteritis in domestic and wildlife ruminants with important welfare, economic, and potential public health consequences. This Research Topic explores novel technologies that have the potential both to advance our understanding of the immunopathology of MAP infection and to improve current diagnostic and control strategies.

The contribution of host genetic factors is one of the fundamental issues in understanding PTB pathogenesis and host resistance, tolerance, and resistance. Microarrays and high-throughput next-generation sequencing (NGS) are the cutting-edge technologies for genomics and transcriptomics studies. In this special issue, two studies by Kiser et al. and Okuni et al. analyzed loci associated with disease susceptibility that could be used by producers to select cattle that were less susceptible to PTB. Kiser et al. identified 18 single-nucleotide polymorphisms (SNPs) associated with MAP tissue infection through resequencing and fine-mapping of the region between the *EDN2* and *HIVEP3* genes in Holstein and Jersey breeds. Okuni et al. surveyed a population of Ankole cattle in Uganda, where there are no control measures against PTB, to determine associations between ELISA test results and allelic variants in the *SLC11A1*, *IFN γ* , *TLR4*, *NOD2*, and *PGLYRP1* genes. NGS-based RNA sequencing (RNA-Seq) can identify and quantify a variety of RNA species including long non-coding RNAs (lncRNAs). lncRNAs play an important role in regulating the immune response of macrophages to bacterial infections, including PTB. The novelty of the study by Marete et al. is that it identified genome-wide lncRNAs with potential roles in host immunity using RNA-Seq from macrophages of Canadian Holsteins naturally infected with MAP. In parallel to the revolutionary progress of NGS technology, direct analysis in real-time coupled to high-resolution mass-spectrometry (DART-HRMS) is another innovative approach to overcome the lack of efficient diagnostic methods in the subclinical stages of PTB. This technology allowed the identification of several metabolic markers associated with infected and infectious stages of PTB as was demonstrated in this special issue by Tata et al.

Diagnostic tests are central to limit the spread of PTB and are hampered by the lack of MAP-specific targets. In this special Research Topic, several studies describe MAP-specific genes and antigens that have the potential to improve the specificity of PTB diagnostic tests. Bannantine et al. aimed to define a more complete catalog of *M. avium* subspecies-specific genes. They confirm 86 genes as MAP-specific, seven as *M. avium* subspecies *avium*-specific, and three as *M. avium*

OPEN ACCESS

Edited and reviewed by:

Michael Kogut,
Agricultural Research Service,
United States Department of
Agriculture (USDA), United States

*Correspondence:

Marta Alonso-Hearn
malonso@neiker.eus

Specialty section:

This article was submitted to
Veterinary Infectious Diseases,
a section of the journal
Frontiers in Veterinary Science

Received: 07 September 2021

Accepted: 09 September 2021

Published: 04 October 2021

Citation:

Alonso-Hearn M, Salgado M and de
Silva K (2021) Editorial: Advances in
the Diagnosis and Control of Johne's
Disease. *Front. Vet. Sci.* 8:771891.
doi: 10.3389/fvets.2021.771891

subspecies *hominissuis*-specific. A single-tube PCR reaction was conducted as a proof-of-concept to quickly distinguish *M. avium* complex (MAC) strains. Karuppusamy et al. evaluated the potential of ELISAs based on six antigenically distinct recombinant MAP cell envelope proteins (SdhA, FadE25_2, FadE3_2, Mkl, DesA2, and hypothetical protein MAP1233) to detect antibodies against MAP in the sera of infected cattle. Their results suggested that antigenically distinct MAP cell envelope proteins and antibodies to these proteins may have the potential to detect MAP infection in dairy cattle. Unlike other MAC members, MAP does not produce glycopeptidolipids on the surface of the cell wall but a lipopentapeptide called L5P. Bay et al. produced by chemical synthesis a water-soluble variant of L5P and evaluated this compound for the serological diagnosis of MAP using well-defined serum banks. L5P and its water-soluble derivative used alone in ELISA had lower sensitivity (Se 82% for L5P and Se 62% for the water-soluble variant of L5P) compared to the Se of a commercial test (98%). The fact that L5P could not be validated in the context of ovine PTB highlighted the need to better characterize the antigens expressed from the different genetic lineages of MAP. In this context, Mizzi et al. investigated sheep MAP isolates from Australia and New Zealand using whole-genome sequencing. The genetic differences identified in this report may represent important epidemiological and virulence traits specific to sheep MAP strains. This knowledge could potentially contribute to improved vaccine development and control measures for these strains.

It is also widely acknowledged that the current tests for the diagnosis of PTB do not detect all MAP-infected animals. Consequently, PTB control efforts based on fecal culture and serum- or milk-ELISA results have not been as effective as national governments would have liked. In this special issue, several methods to improve MAP detection were described. Vitense et al. described a method to improve detection of MAP from fecal and tissue samples measuring volatile organic compounds. Biomarkers to improve differentiation between PTB disease outcomes have been studied in recent years. The use of the alpha 2 macroglobulin as a biomarker for PTB is presented by Park et al. where they assessed serum proteins in MAP exposed animals. Interferon-gamma (IFN γ) release from antigen-stimulated whole blood is a well-known marker of MAP exposure but is currently not used as a diagnostic test. Corneli et al. used antigens (Johnins) prepared from MAP isolates from a specific region and monitored herds over a few years. This allowed them to propose new criteria to better interpret IFN- γ test results. Hatate et al. described a new electrochemical detection method for MAP antibody testing that could distinguish samples of MAP-infected cattle from those of uninfected cattle with greater separation enabling on-site diagnostic testing for PTB.

Phage-based methods are a relatively recent addition to the PTB diagnostic toolbox. In this special issue, Grant reviewed the basis of the phage-based tests and described modifications made to the original plaque assay-based phage amplification assay (FASTPlaqueTBTM) over time to simplify the assay and make it more user-friendly. Finally, the performance of the phage assays for testing veterinary specimens (bovine milk, blood, and feces) relative to current PTB diagnostic methods (culture, fecal PCR, and blood-ELISA) was summarized. In addition, Kubala et al. developed a method of blood preparation for phage assays. Their results showed that this improved sample preparation method and Actiphage blood testing can be used to test blood samples from deer, and the full diagnostic potential of the method was evaluated.

Rasmussen et al. delve into modeling the effectiveness and benefits of long-term strategies for controlling PTB in dairy herds, focusing on the Canadian context. Current vaccines only induce protective immunity or suppress MAP shedding in some animals. Importantly, these factors were considered in this analysis. While the economic viability of PTB control strategies is the central theme, this work also holds clues for future PTB vaccine developers when testing novel vaccines for their ability to control the spread of disease.

We hope you enjoy reading and reflecting on these important topics while developing new integrated and multidisciplinary collaborations which will enable better detection of MAP infection and strategies for controlling John's disease.

AUTHOR CONTRIBUTIONS

All authors listed have made a substantial, direct and intellectual contribution to the work, and approved it for publication.

Conflict of Interest: The authors declare that the research was conducted in the absence of any commercial or financial relationships that could be construed as a potential conflict of interest.

Publisher's Note: All claims expressed in this article are solely those of the authors and do not necessarily represent those of their affiliated organizations, or those of the publisher, the editors and the reviewers. Any product that may be evaluated in this article, or claim that may be made by its manufacturer, is not guaranteed or endorsed by the publisher.

Copyright © 2021 Alonso-Hearn, Salgado and de Silva. This is an open-access article distributed under the terms of the Creative Commons Attribution License (CC BY). The use, distribution or reproduction in other forums is permitted, provided the original author(s) and the copyright owner(s) are credited and that the original publication in this journal is cited, in accordance with accepted academic practice. No use, distribution or reproduction is permitted which does not comply with these terms.



Effectiveness and Economic Viability of Johne's Disease (Paratuberculosis) Control Practices in Dairy Herds

Philip Rasmussen¹, Herman W. Barkema² and David C. Hall^{1*}

¹ Department of Ecosystem and Public Health, University of Calgary, Calgary, AB, Canada, ² Department of Production Animal Health, University of Calgary, Calgary, AB, Canada

OPEN ACCESS

Edited by:

Kumi de Silva,
The University of Sydney, Australia

Reviewed by:

Rebecca Lee Smith,
University of Illinois at
Urbana-Champaign, United States
Yosuke Sasaki,
University of Miyazaki, Japan

*Correspondence:

David C. Hall
dchall@ucalgary.ca

Specialty section:

This article was submitted to
Veterinary Epidemiology and
Economics,
a section of the journal
Frontiers in Veterinary Science

Received: 12 October 2020

Accepted: 10 December 2020

Published: 15 January 2021

Citation:

Rasmussen P, Barkema HW and
Hall DC (2021) Effectiveness and
Economic Viability of Johne's Disease
(Paratuberculosis) Control Practices in
Dairy Herds.
Front. Vet. Sci. 7:614727.
doi: 10.3389/fvets.2020.614727

Johne's disease (JD or paratuberculosis) control programs have been established in many dairy-producing regions. However, the effectiveness (reduction of within-herd prevalence) and the relative economic impact as measured by, for example, the ratio of benefits to costs (BCR) across a comprehensive selection of regions and potential control practices require further investigation. Within a Markovian framework using region-specific economic variables, it was estimated that vaccination was the most promising type of JD control practice modeled, with dual-effect vaccines (reducing shedding and providing protective immunity) having BCRs between 1.48 and 2.13 in Canada, with a break-even period of between 6.17 and 7.61 years. Dual-effect vaccines were also estimated to yield BCRs greater than one in almost all major dairy-producing regions, with greater ratios in regions characterized by above-average farm-gate prices and annual production per cow. Testing and culling was comparably effective to a dual-effect vaccine at test sensitivities >70% but would remain economically unviable in almost all regions modeled.

Keywords: MAP, Johne's disease, paratuberculosis, vaccination, testing and culling, control practice, Markov chain, economic analysis

INTRODUCTION

Johne's disease (JD), or paratuberculosis, is an infectious chronic inflammatory disorder of the intestines that can affect domestic and wild ruminants including dairy cattle (1). The disease is caused by an infection with *Mycobacterium avium* subspecies *paratuberculosis* (MAP), a relatively resistant bacterium (2–4). As the infection progresses in cattle, the clinical effects worsen in severity from diarrhea and reduced milk production to lethargy, hypoproteinemia, and severe emaciation (5). These clinical effects result in substantial economic losses for dairy producers (6), with decreased milk production (7, 8), decreased slaughter value (9–11), and premature culling (12, 13) among the primary sources of losses. Annual losses per cow among MAP-infected herds in the United States have been estimated at US\$21 (12), US\$35 (14), and up to US\$79 per cow (15), while annual losses among infected herds in Canada have been estimated at CA\$49 (16) and between US\$35 and US\$57 per cow (17). Globally, average annual losses in major dairy-producing regions have been estimated at US\$33 per cow, or ~1% of gross milk revenue (17). Although national control programs have already been established in several countries including Australia, Ireland, Japan, the Netherlands, and the United States (18), there are few estimates of the economic impact of potential control practices across major dairy-producing regions. It has been estimated that an average benefit of US\$8.03 per animal per year is associated with vaccination

in US dairy herds (19), and it has also been suggested through simulation that the most profitable strategy in average Danish herds is no control practice at all, with testing and culling being the most profitable in low-hygiene herds (20). Similarly, a recent stochastic simulation study found that no paratuberculosis control was the highly preferred strategy in small herds with 10% initial within-herd prevalence and frequently preferred in other herd scenarios (21). Intuitively, it may seem obvious that these economic losses warrant investment in control of the disease, but the precise mechanisms of control require further investigation; there is a need to estimate the effectiveness and economic impact of potential control practices with consideration for region-specific economic characteristics. Accordingly, this study estimates the effectiveness in terms of reducing within-herd prevalence, the economic impact in terms of the ratio of benefits to costs, and the break-even period in terms of years required for benefits to equal costs of various potential JD control practices across a comprehensive selection of dairy-producing regions within a Markovian framework.

MATERIALS AND METHODS

Within the Markovian framework established in Rasmussen et al. (17), a MAP-positive herd with no intervention was modeled over a 10-year horizon. Various control practices were then introduced to the simulated herds, ranging from a vaccine that reduced shedding among MAP-positive animals to more comprehensive control programs such as a “dual-effect” vaccine (a vaccine that both reduces shedding and also provides some protective immunity) combined with annual fecal PCR testing and culling of MAP-positive animals. The herds with JD control measures in place were then simulated over a 10-year horizon and compared to a positive herd with the same economic characteristics with no intervention to determine the changes in herd structure associated with each control practice. By incorporating economic variables into the Markovian framework, the region-specific benefits per cow, costs per cow, 10-year benefit-cost-ratios (BCRs), and break-even periods of each control practice were estimated. In all scenarios, regional adoption of the control practice was assumed, meaning that the replacement pool from which annual purchased replacements were acquired was assumed to be operating under the same conditions modeled for the herd.

Markovian Framework

The spread of MAP-infection within a dairy herd was modeled over a 10-year horizon using a MAP-positive herd model with a separately modeled replacement pool (17). In this MAP-positive model, the animal can remain negative and continue aging, become infected and continue aging, or be culled. Once an animal is infected, it can either be culled or its stage of infection can progress, regress, or remain the same. Each stage of infection is associated with a different risk of being culled, and each stage has some non-shedding, lightly-shedding, moderately-shedding, and heavily-shedding states within it. Infection pressure on animals in the herd is determined by the number and degree of shedding animals in the herd in each period, and all other

potential outcomes are functions of that infection pressure. For MAP-negative animals, the probability of being culled remains the steady-state MAP-negative value according to their age category. For MAP-positive animals, the probability of being culled depends on the stage of their infection, with the probability increasing with the severity of infection. After the initial age parameters were set, the herd and pool were modeled for 50 1-year periods stabilizing with an annual cow-culling rate of 27%, a young-stock percentage (including calves <1 year) of 48%, and for a 100-cow herd, 1.36 cows and 3.07 young-stock between 1 and 2 years of age brought in from the external replacement pool each year. These numbers are similar to those observed in Canadian dairy herds, which have an average cow-culling rate between 26 and 33% (22), an average young-stock percentage of 48% (23), and purchase an average of 1.37 cows and 3.09 young-stock between 1 and 2 years of age per 100 cows per year (24). Purchased replacements enter the herd at a MAP infection prevalence according to the region's animal-level prevalence, which is determined by the product of the region's average within-herd prevalence and average herd-level prevalence. For each economic region, a baseline MAP-positive herd is then compared to a MAP-positive herds with various JD control practices in place to estimate changes in herd structure, JD prevalence, and three sources of losses associated with JD in dairy cattle: premature culls; MAP-positive animals salvaged; and MAP-positive cows producing reduced amounts of milk. Lastly, because the current efficacies of available MAP vaccines in terms of reduced shedding and protective immunity are unknown, a range of vaccine efficacies are modeled.

Vaccine: Shedding

In this control scenario, a vaccine that reduces shedding among MAP-infected animals is administered to the entire herd at time zero and then administered to natural replacements at birth and purchased replacements at the time of purchase. Once animals are vaccinated, two main mechanisms operate: (i) the probability of an animal transitioning from a MAP-negative state to a shedding state of MAP-infection is decreased by the percentage reduction in shedding attributable to the vaccine; and (ii) the probability of an animal transitioning from a shedding state of MAP-infection to another shedding state of MAP-infection is decreased by the percentage reduction in shedding attributable to the vaccine. In other words, shedding states of MAP-infection become less likely outcomes and non-shedding states become more likely according to the MAP shedding-reducing properties of the vaccine.

Vaccine: Protective Immunity

In this control scenario, a vaccine that provides protective immunity from MAP infection is administered to the entire herd at time zero and then administered to natural replacements at birth and purchased replacements at the time of purchase. Once animals are vaccinated, a percentage of the MAP-negative animals are provided with protective immunity and separated into a new, immune cohort within the model according to the vaccine's efficacy (expressed as a percentage). The remainder

of the MAP-negative animals continue in the original non-immune cohort along with the MAP-positive animals in the herd, which although vaccinated, cannot be provided with protective immunity. Animals within the immune cohort either continue aging or are culled according the MAP-negative steady-state probability for their age but can never become infected in their lifetimes. Animals that remain in the non-immune cohort are subject to infection pressure according to the number of infected animals in the herd and the degree to which those infected animals are shedding MAP. These non-immune animals can continue to age, be culled, become infected, or have their existing infections progress, regress, or remain the same.

Vaccine: Dual-Effect

In this control scenario, a vaccine that both reduces shedding and provides protective immunity from MAP infection is administered to the entire herd at time zero and then administered to natural replacements at birth and purchased replacements at the time of purchase. The percentage of animals that are successfully provided with protective immunity enter the immune cohort, and because they are MAP-negative and remain so for their lifetimes, are not directly affected by the shedding-reducing effects of the vaccine. MAP-negative animals that remain in the non-immune cohort are still subject to infection pressure as previously described, while MAP-positive animals in this cohort transition from period to period according to the altered transition probabilities of the shedding-reduction vaccine model.

Testing and Culling

In this control scenario, animals aged 1–7 years are tested annually using a combination of pooled and individual fecal PCR tests. They are first tested at time zero, and then retested after each transition period (year) along with purchased replacements aged 1–3 years, which are tested only at the individual level. For all testing periods, the probability of a pooled test containing samples from an r number of MAP-positive animals given the pool size n , or $pr(TP) | C(n, r)$, is determined using the following equation:

$$pr(TP) | C(n, r) = \frac{n!}{r! * (n - r)!} \left(\frac{TP_s}{animals_{(1-7)}} \right)^r * \left(1 - \left(\frac{TP_s}{animals_{(1-7)}} \right) \right)^{n-r} \quad (1)$$

where: TP_s equals the number of true positive animals aged 1–7 years in a shedding state and $animals_{(1-7)}$ equals the number of animals aged 1–7 years in the herd. A testing pool size of five animals is assumed, or $n = 5$. Pooled tests and individual tests are assumed to share the same sensitivities and specificities, or that $se_p = se_i$ and $sp_p = sp_i$.

The number of true positive pools detected TP_p given pooled test sensitivity se_p is determined using the following equation:

$$TP_p = \sum_{r=1}^n (pr(TP) | C(n, r)) * \frac{animals_{(1-7)}}{n} * se_p \quad (2)$$

The number of false-positive pools detected FP_p given pooled test specificity sp_p is determined using the following equation:

$$FP_p = \left(\frac{animals_{(1-7)}}{n} - TP_p \right) * \frac{(1 - sp_p)}{sp_p} \quad (3)$$

The number of individual tests required T given the total number of positive pools detected, including true and false-positive pools, is determined using the following equation:

$$T = (TP_p + FP_p) * n \quad (4)$$

The number of true positive individuals detected TP_i given individual test sensitivity se_i is determined using the following equation:

$$TP_i = T * \frac{\sum_{r=1}^n (pr(TP) | C(n, r)) * r}{(\sum_{r=1}^n (pr(TP) | C(n, r)) + FP_p) * n} * se_i \quad (5)$$

Finally, the number of false-positive individuals detected FP_i given individual test specificity sp_i is determined using the following equation:

$$FP_i = (T - TP_i) * \frac{(1 - sp_i)}{sp_i} \quad (6)$$

where the total number of culls resulting from testing and culling equals the sum of true positive and false-positive individuals detected, or $TP_i + FP_i$. These culls are then distributed across the herd according to the herd structure in that period, with the false-positive culls coming from among the MAP-negative animals and the true positive culls coming from among the MAP-positive animals. The culled animals are then replaced with animals from the replacement pool, which is assumed to be operating under the same test-and-cull conditions.

Economic Analyses

Benefits per cow, costs per cow, benefit-cost ratios, and break-even periods of the various control practices were estimated using general input variables, region-specific dairy sector characteristics, and region-specific economic variables (17) (also available in **Supplementary Files**). The following values were assumed for control-specific economic variables: a fecal PCR direct testing cost of US\$40 per test, a pooled testing labor cost of 30 min per test, an individual testing labor cost of 5 min per test, a vaccination direct cost of \$US20 per dose for all vaccine types, and a vaccination labor cost of 1 min per dose. After each period, the herds with control practices in place were compared to a region-specific baseline MAP-positive herd with no intervention. The reduced economic losses in the herd with control practices relative to economic losses in the herd with no intervention were recorded as economic benefits for the various control practices. Premature culling benefits were estimated by tallying additional exits in the herd with no intervention and assigning those exits a value according to their age-at-exit and associated replacement price. The aggregated labor cost of seeking out, purchasing, and introducing a replacement to the

herd was also accounted for. Salvage benefits were estimated by tallying additional MAP-positive exits and assigning them a reduced salvage value according to their stage of infection. Production benefits were estimated in two different ways: (i) for the comprehensive selection of major dairy-producing regions, production benefits were measured as the value of the additional milk produced (the product of quantity and farm-gate price) by the herd due to the reduced number of MAP-positive cows; and (ii) for Canada, due to the unique market conditions that arise due to supply management, production benefits were re-estimated as the reduction in variable costs from requiring fewer cows to maintain a fixed production level. The three sources of benefits in the model (reduced premature culling losses, reduced salvage losses, and reduced production losses) were summed and divided by the number of cows in the herd to obtain an estimate of benefits per cow for each control scenario in each region.

The direct cost per dose of the vaccine was added to the labor cost per dose (i.e., time required to administer a single dose multiplied by the aggregate wage rate) to obtain an estimated total cost per dose. At time zero, the entire herd was vaccinated, with only purchased and natural replacements being vaccinated after each transition period. As overall herd health improved in the model, the culling rate decreased and animals remained in the herd for a longer period, leading to fewer doses being required over time. Each period, the total cost of vaccination was divided by the number of cows in the herd to obtain an estimate of annual vaccination costs per cow for each control practice that included vaccination in each region. Similarly, the direct cost per fecal PCR test was added to the labor cost per test, with pooled tests requiring more labor than individual tests. Syringe and alcohol swab material costs for vaccine delivery were trivial (pennies per cow) at the herd-level and were not accounted for in the simulations. However, in the case of a national or widespread JD control campaign, these costs would likely be significant when aggregated across thousands of herds. The direct cost of replacing culled animals that tested positive was added to the labor cost per replacement, with the direct cost being dependent on the age of the replacement animal. The total costs of testing and replacing animals were summed each period and divided by the number of cows in the herd to obtain an estimate of annual testing and culling costs per cow for each control scenario that included testing and culling in each region.

Annual benefits and costs per cow were discounted over time at an assumed rate of 5% per annum, averaged over the 10-year horizon to obtain the reported benefit and cost estimates. This discount rate is consistent with small private firm investment in a family enterprise, falling between a public investment return rate of ~3% (25) and a private investment return rate of ~10% (26). Similarly, the Treasury Board of Canada selected a discount rate of 7% in its 2007 Cost-Benefit Analysis Guide but noted that it would likely be reduced in future years (27). Once discounted, these benefits and costs were summed over the 10-year horizon, then divided by the sum of the costs to obtain an estimate of the benefit-cost ratio for each control scenario in each region. The annual cumulative costs were subtracted from the annual cumulative benefits, and for scenarios and regions where this value was greater than zero within the 10-year horizon, the

number of years required for the benefits to equal costs were recorded to obtain an estimate of the break-even period.

Monte Carlo Simulations

Monte Carlo simulations of 10,000 iterations were run using Palisade's @RISK software version 8.0 (28) and used to estimate the distribution of possible outcomes of the Markov chain models and their sensitivity to various input variables. For these simulations, assumptions of an initial mean within-herd prevalence of 10% and an initial mean herd-level prevalence of 50% were used in all scenarios, both with normal distributions and standard deviations of 20% of their mean values. Also assumed were mean values of 50% for the vaccine's reduction in shedding, 50% for the vaccine's protective immunity efficacy, 50% for both pooled and individual fecal PCR testing sensitivities, and 99% for testing specificities. These variables were also simulated with normal distributions but with standard deviations of 20% of their means, except for testing specificities; these were simulated with normal distributions truncated from 95 to 100% and standard deviations of 10% of their means. All general input variables, region-specific economic variables, and control-specific economic variables were assumed to have normal distributions and standard deviations of 10% of their mean values. Although the data required to determine the true standard deviations of these variables are unavailable, the selected standard deviations capture a wide range of input values without destabilizing the simulations and their results.

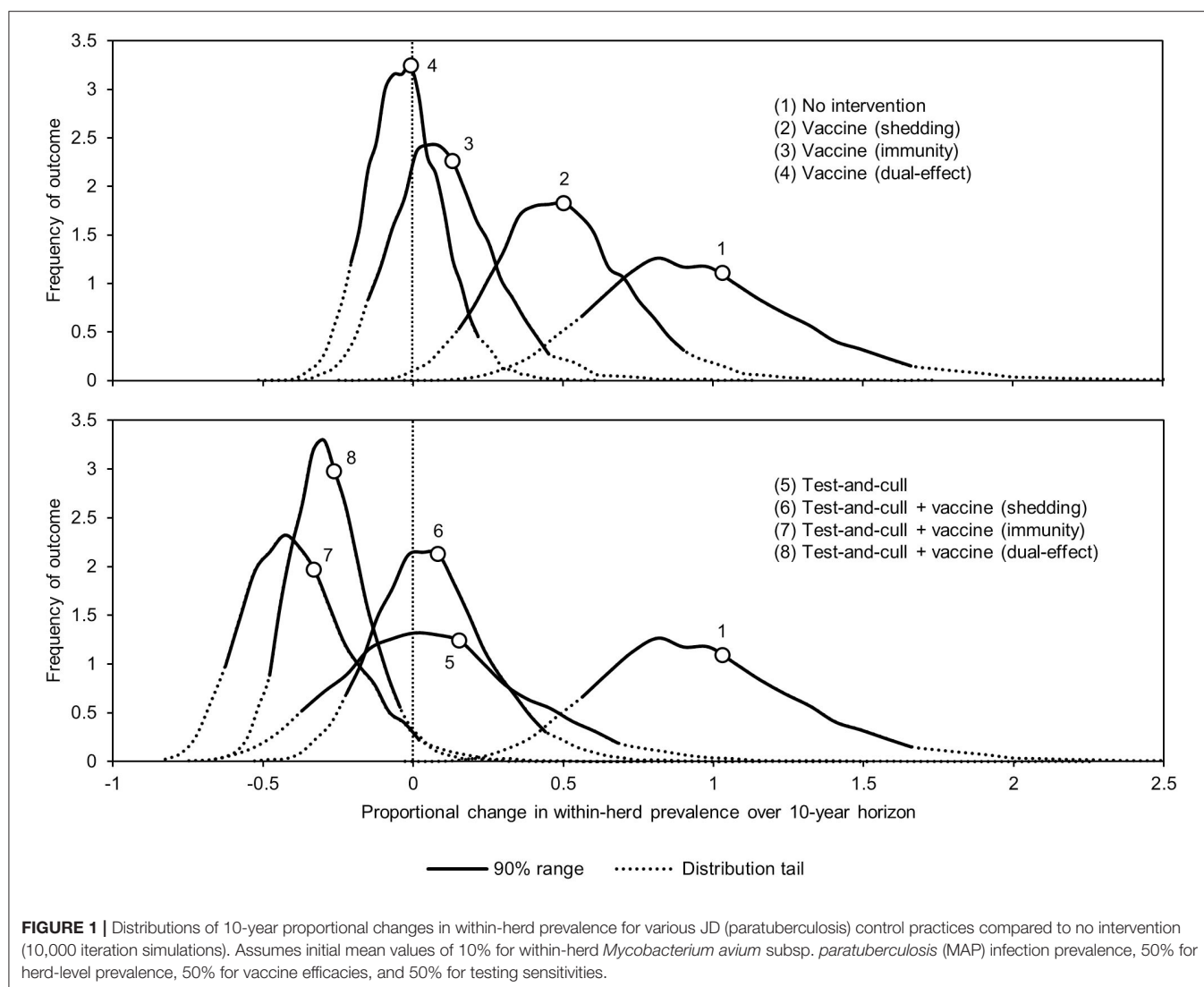
RESULTS

Distribution of Possible Outcomes

The proportional changes in within-herd prevalence (the differences between the final 10-year within-herd prevalence and the initial within-herd prevalence divided by the initial within-herd prevalence) from its initial mean value of 10% based on 10,000-iteration simulations of the various control practices are presented in **Figure 1** and **Table 1**. For the MAP-positive herd with no intervention, 90% of the iterations resulted in proportional increases of within-herd prevalence ranging from ~0.5 to 1.65, with a mean of 1.02, equivalent to a doubling of within-herd prevalence from 10 to 20% over 10 years. Only vaccines that provided protective immunity, dual-effect vaccines, and testing and culling combined with various vaccine types had 90% confidence ranges that did not overlap with the positive herd with no intervention. Additionally, only dual-effect vaccination and testing and culling combined with either a protective immunity vaccine or a dual-effect vaccine had 90% confidence ranges entirely below zero indicative of absolute decreases in within-herd prevalence over 10 years relative to its initial value.

Effects of JD Control on Herd Structure

The effects of the various control practices on within-herd prevalence, the percentage of shedding animals within the herd, and the cow-culling rate over time can be seen in **Figure 2**. In all control scenarios, prevalence decreased relative to the MAP-positive herd with no intervention. The greatest decreases



relative to no intervention were observed in the scenarios of dual-effect vaccination, testing and culling combined with protective immunity vaccination, and testing and culling combined with dual-effect vaccination. After year three, the within-herd prevalence in the testing and culling scenario began to increase relative to its minimum value within the 10-year horizon. When looking at the percentage of animals shedding in the herd, overall trends are similar to those observed when looking at within-herd prevalence, including the same upward trend after year three in the testing and culling scenario. The greatest decreases were observed in the dual-effect vaccination, testing and culling combined with vaccination to reduce shedding, and testing and culling combined with dual-effect vaccination scenarios. A sharp and immediate decrease in shedding animals as a percentage of animals in the herd was observed in scenarios involving vaccines with a shedding reduction effect. As within-herd MAP prevalence and the prevalence of MAP-shedding animals changed over time in the various scenarios, so did the

cow-culling rates. In the various vaccination scenarios, after 2 years the cow-culling rate began to decrease relative to the rate observed in the MAP-positive herd with no intervention, approaching the MAP-negative baseline rate of 0.275. This was indicative of both improving overall herd health and a decline in the severity of infections among MAP-positive animals as infection pressure in the herd began to fall due to the various control practices. In scenarios involving testing and culling, an initial increase in culling of cows was observed relative to the scenario with no intervention as MAP-positive animals were detected and removed from the herd. However, as the number of animals detected began to decrease with time, culling rates also fell, and by year 4, in the scenario combining testing and culling with a dual-effect vaccine, they were near or below the culling rate of cows in the positive herd with no intervention. Once again, only in the exclusive testing and culling scenario was there an eventual upward trend in the culling rate after an initial decline.

TABLE 1 | Summary statistics of the distributions of 10-year proportional changes in within-herd *Mycobacterium avium* subsp. *paratuberculosis* (MAP) infection prevalence for various JD (paratuberculosis) control practices (10,000 iteration simulations).

Statistic	No intervention	Vaccine (shedding)	Vaccine (immunity)	Vaccine (dual-effect)
Minimum	−0.03	−0.25	−0.47	−0.52
Maximum	3.35	1.75	1.14	0.61
Mean	1.02	0.53	0.13	−0.13
90% range	0.51 to 1.66	0.18 to 0.92	−0.13 to 0.44	−0.22 to −0.20
Standard deviation	0.36	0.23	0.18	0.13

Statistic	Test-and-cull	Test-and-cull with vaccine (shedding)	Test-and-cull with vaccine (immunity)	Test-and-cull with vaccine (dual-effect)
Minimum	−0.75	−0.53	−0.83	−0.66
Maximum	2.26	1.51	1.16	0.79
Mean	0.01	0.09	−0.35	−0.26
90% range	−0.36 to 0.66	−0.20 to 0.44	−0.62 to −0.02	−0.46 to −0.04
Standard deviation	0.32	0.20	0.19	0.13

Assumes initial mean values of 10% for within-herd MAP infection prevalence, 50% for herd-level prevalence, 50% for vaccine efficacies, and 50% for testing sensitivities.

Changes in the sources of economic losses in the models (forgone production, premature culling, and reduced salvage value due to MAP-positive culls) over time are presented in **Figure 3**. In all scenarios, forgone production, or the production lost due to MAP infection, as percentage of potential production decreased relative to the MAP-positive herd with no intervention. The greatest reductions were observed in scenarios with dual-effect vaccination and scenarios where testing and culling was combined with either a protective immunity vaccine or a dual-effect vaccine. The previously observed upward trend in the testing and culling scenario was once again observed for all sources of losses in the model. Premature culls (culls that would not have occurred in the MAP-negative baseline herd) as a percentage of total culls decreased relative to the MAP-positive herd with no intervention within 10 years in all scenarios except testing and culling, with dual-effect vaccination showing the greatest decrease. The greatest decreases in MAP-positive culls as a percentage of total culls were observed in scenarios combining testing and culling with protective immunity vaccination, testing and culling combined with dual-effect vaccination, and dual-effect vaccination only.

Economic Analysis: Major Dairy-Producing Regions

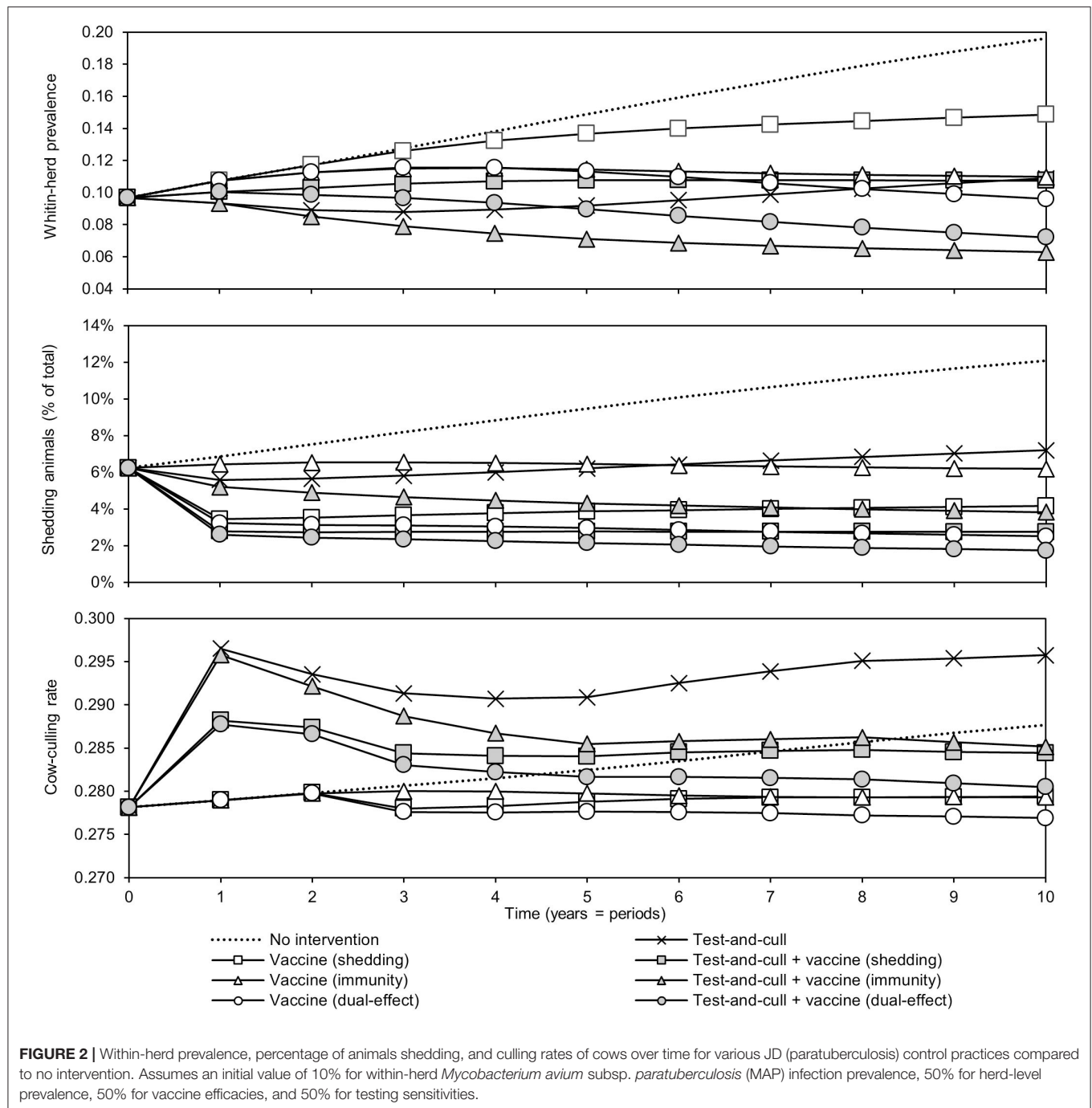
With a 50% reduction in shedding and a 50% efficacy of protective immunity, dual-effect vaccination resulted in BCRs greater than one for all regions except Poland, Brazil, China, Russia, and Turkey with revenue-weighted average values of 1.24 and 7.88 years for the scenario's BCR and break-even period, respectively (**Table 2**). Even at the 90% efficacy level in the dual-effect vaccination scenario, the BCRs remain <1 for these countries. For control practices involving testing and culling (**Table 3**), all revenue-weighted average BCR values are less than one, with the exception of testing and culling combined with a dual-effect vaccine at the 90% efficacy and test sensitivity levels,

which resulted in a BCR value of 1.22 and a break-even period of 9.17 years.

Economic Analysis: Canada

Benefits and costs for the various control practices were first estimated using the same method used for other major dairy-producing regions. They were then estimated again with consideration for the market conditions that arise due to supply management: fixed annual production and higher farm-gate prices. To account for these conditions, production losses were estimated as the increase in variable costs due to the presence of additional less productive MAP-positive cows in the herd required to maintain a fixed production level. Once again, the results are summarized using revenue-weighted average values at the bottom of each table.

With production losses measured as forgone production (**Table 4**), protective immunity vaccination and dual-effect vaccination scenarios resulted in mean BCRs >1 for all provinces within Canada, with the highest revenue-weighted average BCRs resulting from scenarios with dual-effect vaccination until control variables reach the 90%, when protective immunity vaccination has a slightly higher BCR. Testing and culling did not result in a BCR greater than one for any province at any test sensitivity modeled, and testing and culling combined with a shedding reduction vaccine only resulted in a BCR greater 1 in Alberta and Newfoundland and Labrador in the 90% vaccine efficacy and 90% test sensitivity scenario. Testing and culling combined with a protective immunity vaccine had a revenue weighted average BCR >1 (1.03) only at the 70% efficacy and sensitivity level, while testing and culling combined with dual-effect vaccination resulted in revenue-weighted average BCRs and provincial BCRs >1 at all vaccine efficacy and testing sensitivities modeled. Dual-effect vaccination also had the shortest break-even periods across vaccine efficacy scenarios. When production losses were



instead measured as increased variable costs from additional cows in the herd being required to maintain production levels (Table 5), similar trends were observed but with lower BCRs and longer break-even periods. Dual-effect vaccination was still the most promising control practice, resulting in BCRs greater than one for all provinces with a revenue-weighted average of 1.48 in the 50% control variable scenario, and the shortest break-even periods across all efficacy and test sensitivity scenarios.

Sensitivity Analyses

For simplicity, a generalized MAP-positive herd with no region-specific variables was selected to test the sensitivity of estimated within-herd prevalence to various input variables. For the shedding reduction vaccine, once the shedding reduction reached 70%, a slight overall downward trend in within-herd prevalence was observed (Figure 4). However, it was not until the shedding reduction exceeded 90% that an absolute decrease in within-herd prevalence relative to its initial value within the 10-year

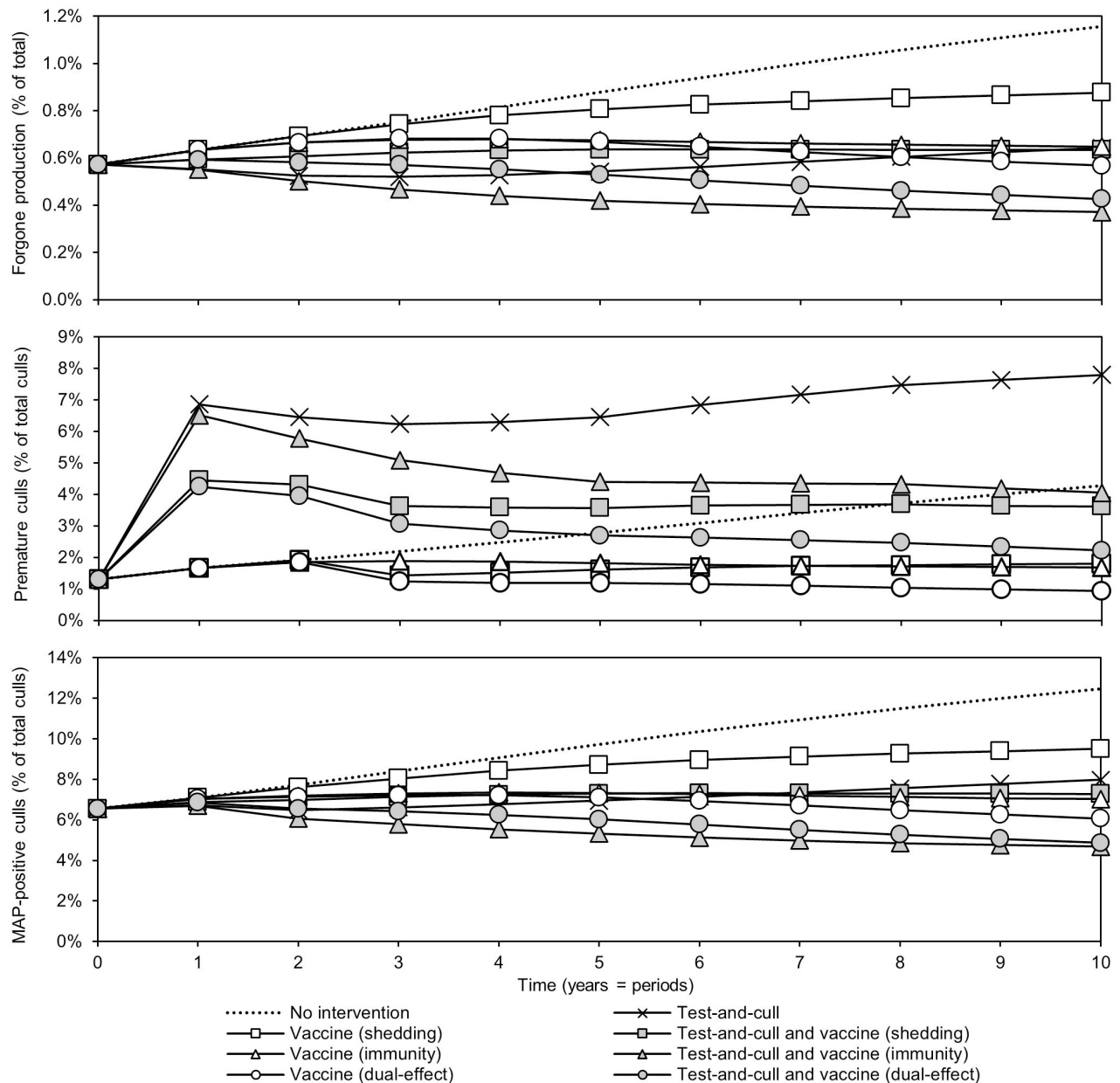


FIGURE 3 | Sources of economic losses due to JD (paratuberculosis) over time for various control practices compared to no intervention. Forgone production as a percentage of potential production over time, premature culls as a percentage of total culls, and *Mycobacterium avium* subsp. *paratuberculosis* (MAP) -positive culls as a percentage of total culls. Assumes an initial value of 10% for within-herd MAP infection prevalence, 50% for herd-level prevalence, 50% for vaccine efficacies, and 50% for testing sensitivities.

horizon was observed. For the protective immunity vaccine, at only 50% protective immunity a downward trend was observed, and an absolute decrease in within-herd prevalence within the 10-year horizon relative to its initial value was observed at <60% protective immunity. The relationship between protective immunity, shedding reduction, and the final 10-year within-herd prevalence in the dual-effect vaccination scenario is explored in **Figure 5**; the results suggest that the protective immunity

effect drove the overall effectiveness of dual-effect vaccines in the model, particularly at moderate control variable values. For example, a vaccine with 0% shedding reduction but 70% protective immunity resulted in a final 10-year within-herd prevalence of ~ 0.08 (assuming an initial within-herd prevalence of 0.10), whereas a vaccine with 70% shedding reduction and 0% protective immunity resulted in a final prevalence of 0.13. There was no significant 10-year decrease in within-herd prevalence

TABLE 2 | Estimated benefit-cost ratios (BCRs), and revenue-weighted average benefits and costs per cow (US\$), BCRs, and break-even periods (BEP) of various JD (paratuberculosis) vaccine types in major dairy-producing regions across a range of vaccine shedding reduction and protective immunity percentages.

Region	Vaccine (shedding)			Vaccine (immunity)			Vaccine (dual-effect)		
	50%	70%	90%	50%	70%	90%	50%	70%	90%
European Union (28)	0.69	0.94	1.18	0.99	1.32	1.60	1.23	1.47	1.60
Germany	0.80	1.10	1.37	1.14	1.52	1.84	1.43	1.70	1.85
France	0.69	0.95	1.18	0.99	1.31	1.59	1.23	1.46	1.59
Great Britain	0.73	1.00	1.26	1.07	1.42	1.72	1.32	1.57	1.71
Poland	0.36	0.51	0.65	0.62	0.82	1.01	0.73	0.87	0.95
Netherlands	0.94	1.28	1.61	1.34	1.78	2.16	1.67	1.99	2.16
Italy	0.69	0.95	1.19	1.02	1.36	1.65	1.26	1.50	1.63
Ireland	1.03	1.38	1.70	1.27	1.67	2.00	1.66	1.96	2.13
Spain	0.59	0.81	1.03	0.93	1.24	1.51	1.12	1.34	1.46
Denmark	1.06	1.45	1.80	1.49	1.98	2.40	1.87	2.22	2.42
Belgium	0.75	1.02	1.27	1.06	1.41	1.71	1.33	1.58	1.71
Austria	0.78	1.06	1.32	1.07	1.42	1.72	1.35	1.61	1.75
Czechia	0.54	0.76	0.97	0.90	1.21	1.48	1.07	1.29	1.40
Sweden	0.91	1.25	1.55	1.29	1.71	2.07	1.61	1.92	2.08
Finland	0.95	1.31	1.63	1.38	1.83	2.22	1.71	2.04	2.21
United States	0.93	1.27	1.59	1.33	1.76	2.14	1.66	1.97	2.14
California	0.91	1.24	1.56	1.31	1.73	2.10	1.63	1.93	2.10
Wisconsin	0.81	1.11	1.40	1.21	1.61	1.96	1.49	1.77	1.93
Idaho	0.70	0.97	1.23	1.12	1.50	1.83	1.35	1.61	1.75
New York	0.96	1.32	1.65	1.37	1.82	2.20	1.71	2.04	2.21
Texas	0.85	1.17	1.47	1.26	1.68	2.04	1.56	1.85	2.01
Michigan	0.79	1.10	1.39	1.24	1.65	2.02	1.50	1.80	1.95
Pennsylvania	0.79	1.08	1.35	1.14	1.51	1.84	1.42	1.69	1.83
Minnesota	0.84	1.14	1.43	1.21	1.60	1.94	1.50	1.78	1.94
New Mexico	0.75	1.04	1.32	1.18	1.57	1.92	1.43	1.71	1.86
Washington	0.91	1.25	1.57	1.33	1.76	2.14	1.65	1.96	2.13
Brazil	0.17	0.24	0.30	0.26	0.34	0.42	0.32	0.38	0.41
China	0.26	0.36	0.46	0.41	0.54	0.66	0.49	0.59	0.64
Russia	0.25	0.35	0.45	0.42	0.57	0.70	0.50	0.60	0.66
New Zealand	0.55	0.74	0.91	0.71	0.94	1.14	0.92	1.09	1.18
Turkey	0.21	0.29	0.37	0.34	0.46	0.56	0.41	0.49	0.54
Australia	0.71	0.96	1.18	0.92	1.22	1.47	1.19	1.41	1.53
Japan	1.66	2.28	2.87	2.48	3.30	4.01	3.05	3.63	3.95
Revenue-weighted average benefits and costs (US\$/cow/year), BCRs (ratio), and BEPs (years)									
Benefit	6.20	8.48	10.60	9.00	11.94	14.47	11.14	13.24	14.37
Cost	9.05	9.02	9.01	9.05	9.03	9.02	9.02	9.00	8.99
BCR	0.69	0.94	1.18	0.99	1.32	1.60	1.24	1.47	1.60
BEP	8.38	8.67	8.22	8.47	7.60	6.89	7.88	7.05	6.58

Assumes an initial within-herd *Mycobacterium avium* subsp. *paratuberculosis* (MAP) infection prevalence of 10% and a herd-level prevalence of 50%.

relative to its initial value resulting from testing and culling until test sensitivity exceeded 50% (**Figure 6**). However, even within the 50% to 70% sensitivity range, within-herd prevalence began to trend upwards in the later periods of the 10-year horizon. This upward trend did not clearly disappear until test sensitivity exceeded the 70% level.

The sensitivity of the proportional changes in within-herd prevalence over the 10-year horizons to a variety of input variables based on 10,000 iteration Monte Carlo simulations are

presented in **Figures 7, 8**. In the shedding reduction vaccine scenario, the proportional change was most sensitive to the initial within-herd prevalence, with above-mean within-herd prevalence values resulting in lesser proportional increases and therefore more effective JD control. Other impactful and negatively related variables were the shedding reduction efficacy of the vaccine and the additional culling risk associated with Stage 1 MAP infection. The degree of bacterial shedding among lightly shedding infected animals and herd-level prevalence

TABLE 3 | Estimated benefit-cost ratios (BCRs), and revenue-weighted average benefits and costs per cow (US\$), BCRs, and break-even periods (BEP) of various JD (paratuberculosis) control practices involving testing and culling in major dairy-producing regions across a range of testing sensitivities and vaccine shedding reduction and protective immunity percentages.

Region	Test-and-cull			Test-and-cull with vaccine (shedding)			Test-and-cull with vaccine (immunity)			Test-and-cull with vaccine (dual-effect)		
	50%	70%	90%	50%	70%	90%	50%	70%	90%	50%	70%	90%
European Union (28)	0.44	0.54	0.59	0.42	0.52	0.58	0.59	0.71	0.79	0.69	0.85	1.07
Germany	0.46	0.56	0.60	0.47	0.57	0.65	0.64	0.74	0.82	0.76	0.93	1.19
France	0.43	0.52	0.57	0.42	0.51	0.58	0.58	0.69	0.77	0.68	0.84	1.05
Great Britain	0.46	0.57	0.62	0.45	0.55	0.62	0.63	0.75	0.84	0.73	0.90	1.13
Poland	0.39	0.53	0.62	0.30	0.37	0.38	0.48	0.64	0.78	0.49	0.63	0.73
Netherlands	0.50	0.59	0.64	0.52	0.64	0.74	0.70	0.80	0.88	0.85	1.04	1.34
Italy	0.47	0.57	0.63	0.44	0.54	0.60	0.62	0.75	0.85	0.71	0.89	1.10
Ireland	0.39	0.44	0.45	0.47	0.57	0.68	0.56	0.61	0.64	0.74	0.89	1.19
Spain	0.48	0.61	0.70	0.42	0.51	0.56	0.63	0.78	0.92	0.68	0.86	1.04
Denmark	0.51	0.60	0.64	0.56	0.68	0.79	0.73	0.83	0.89	0.90	1.11	1.44
Belgium	0.45	0.54	0.58	0.44	0.54	0.61	0.60	0.71	0.79	0.71	0.88	1.12
Austria	0.43	0.51	0.54	0.44	0.54	0.62	0.59	0.68	0.74	0.71	0.87	1.11
Czechia	0.50	0.66	0.76	0.41	0.51	0.54	0.64	0.83	0.99	0.68	0.86	1.03
Sweden	0.48	0.57	0.62	0.51	0.62	0.71	0.67	0.77	0.85	0.82	1.00	1.29
Finland	0.52	0.61	0.66	0.54	0.65	0.75	0.72	0.83	0.91	0.87	1.07	1.37
United States	0.50	0.59	0.63	0.52	0.63	0.73	0.69	0.80	0.87	0.84	1.03	1.33
California	0.50	0.59	0.64	0.51	0.63	0.72	0.69	0.80	0.88	0.83	1.03	1.32
Wisconsin	0.52	0.63	0.69	0.50	0.61	0.69	0.70	0.84	0.94	0.82	1.01	1.27
Idaho	0.55	0.69	0.78	0.48	0.60	0.65	0.72	0.89	1.03	0.80	1.00	1.23
New York	0.50	0.59	0.64	0.53	0.64	0.75	0.70	0.80	0.88	0.85	1.05	1.36
Texas	0.51	0.62	0.67	0.51	0.62	0.71	0.70	0.83	0.92	0.83	1.02	1.30
Michigan	0.55	0.68	0.76	0.52	0.64	0.71	0.75	0.90	1.03	0.85	1.06	1.32
Pennsylvania	0.47	0.57	0.62	0.47	0.57	0.65	0.64	0.76	0.84	0.76	0.94	1.19
Minnesota	0.48	0.58	0.63	0.49	0.60	0.68	0.66	0.78	0.86	0.79	0.98	1.24
New Mexico	0.54	0.67	0.75	0.50	0.61	0.68	0.72	0.88	1.01	0.82	1.02	1.26
Washington	0.51	0.61	0.66	0.52	0.64	0.73	0.71	0.82	0.91	0.85	1.05	1.34
Brazil	0.18	0.25	0.29	0.14	0.17	0.17	0.21	0.28	0.35	0.22	0.28	0.32
China	0.27	0.36	0.41	0.20	0.25	0.27	0.32	0.42	0.52	0.33	0.42	0.50
Russia	0.29	0.40	0.48	0.21	0.26	0.27	0.35	0.47	0.59	0.35	0.45	0.52
New Zealand	0.33	0.39	0.42	0.32	0.39	0.44	0.43	0.51	0.57	0.51	0.63	0.79
Turkey	0.24	0.33	0.39	0.17	0.22	0.22	0.29	0.39	0.48	0.29	0.37	0.43
Australia	0.37	0.44	0.47	0.39	0.47	0.55	0.51	0.58	0.63	0.62	0.76	0.97
Japan	0.69	0.80	0.85	0.79	0.96	1.16	1.02	1.13	1.21	1.30	1.59	2.13
Revenue-weighted average benefits and costs (US\$/cow/year), BCRs (ratio), and BEPs (years)												
Benefit	15.36	23.82	29.45	14.29	17.25	16.34	20.84	27.16	31.10	18.26	20.60	19.46
Cost	31.65	40.59	45.98	29.85	29.41	24.65	31.52	34.79	35.68	23.49	21.41	16.01
BCR	0.49	0.59	0.64	0.48	0.59	0.66	0.66	0.78	0.87	0.78	0.96	1.22
BEP	—	—	—	—	—	10.00	10.00	10.00	10.00	10.00	10.00	9.17

Assumes an initial within-herd *Mycobacterium avium* subsp. *paratuberculosis* (MAP) infection prevalence of 10% and a herd-level prevalence of 50%.

were also determined to be impactful, but positively related to the proportional increase in within-herd prevalence, with above-mean values resulting in greater proportional increases in within-herd prevalence. The protective immunity vaccine estimate was sensitive to similar variables, with the percentage of protective immunity being the most impactful, as was the dual-effect vaccine scenario estimate, with protective

immunity having a significantly larger impact than shedding reduction. In all scenarios involving testing and culling, both alone and in combination with some type of vaccination, proportional changes to within-herd prevalence were most sensitive to test sensitivity, with initial within-herd prevalence, vaccine efficacy, and the degree of bacterial shedding among lightly shedding animals being consistently impactful to lesser

TABLE 4 | Estimated benefit-cost ratios (BCRs), and revenue-weighted average benefits and costs per cow (US\$), BCRs, and break-even periods (BEP) of various JD (paratuberculosis) control practices in Canadian regions across a range of vaccine shedding reduction, protective immunity percentages, and testing sensitivities.

Region	Vaccine (shedding)			Vaccine (immunity)			Vaccine (dual-effect)		
	50%	70%	90%	50%	70%	90%	50%	70%	90%
Canada	1.15	1.59	2.00	1.74	2.32	2.82	2.14	2.55	2.77
Québec	1.05	1.45	1.83	1.62	2.16	2.63	1.97	2.35	2.56
Ontario	1.12	1.55	1.95	1.69	2.26	2.74	2.08	2.48	2.69
British Columbia	1.26	1.74	2.19	1.92	2.55	3.11	2.34	2.80	3.04
Alberta	1.45	1.98	2.48	2.08	2.76	3.35	2.59	3.08	3.35
Manitoba	1.11	1.53	1.93	1.71	2.29	2.79	2.08	2.49	2.71
Saskatchewan	1.29	1.77	2.22	1.91	2.54	3.09	2.36	2.81	3.05
Nova Scotia	0.99	1.37	1.74	1.57	2.10	2.56	1.90	2.27	2.47
New Brunswick	0.99	1.37	1.73	1.54	2.06	2.51	1.88	2.24	2.44
Prince Edward Isl.	0.99	1.38	1.75	1.58	2.11	2.58	1.91	2.28	2.48
Nfld. and Labrador	1.56	2.15	2.70	2.34	3.12	3.80	2.88	3.43	3.73
Revenue-weighted average benefits and costs (US\$/cow/year), BCRs (ratio), and BEPs (years)									
Benefit	10.44	14.34	18.03	15.80	21.00	25.51	19.29	22.97	24.94
Cost	9.10	9.08	9.06	9.11	9.09	9.07	9.07	9.06	9.05
BCR	1.15	1.58	1.99	1.73	2.31	2.81	2.13	2.54	2.76
BEP	9.14	7.56	6.64	7.05	5.97	5.32	6.17	5.45	5.08

Region	Test-and-cull			Test-and-cull with vaccine (shedding)			Test-and-cull with vaccine (immunity)			Test-and-cull with vaccine (dual-effect)		
	50%	70%	90%	50%	70%	90%	50%	70%	90%	50%	70%	90%
Canada	0.61	0.73	0.79	0.64	0.79	0.91	0.87	1.00	1.10	1.05	1.30	1.68
Québec	0.62	0.75	0.82	0.62	0.76	0.87	0.86	1.02	1.13	1.02	1.27	1.61
Ontario	0.61	0.72	0.78	0.63	0.77	0.89	0.85	0.99	1.09	1.03	1.27	1.64
British Columbia	0.65	0.77	0.83	0.69	0.84	0.98	0.93	1.06	1.16	1.13	1.39	1.81
Alberta	0.60	0.69	0.74	0.69	0.84	1.01	0.88	0.98	1.04	1.13	1.37	1.84
Manitoba	0.64	0.77	0.85	0.65	0.80	0.91	0.90	1.05	1.17	1.07	1.32	1.69
Saskatchewan	0.62	0.73	0.78	0.68	0.82	0.97	0.89	1.01	1.10	1.10	1.35	1.78
Nova Scotia	0.64	0.79	0.87	0.62	0.76	0.86	0.89	1.06	1.19	1.03	1.27	1.61
New Brunswick	0.62	0.75	0.83	0.61	0.74	0.84	0.85	1.01	1.14	1.00	1.24	1.57
Prince Edward Isl.	0.65	0.79	0.88	0.62	0.77	0.86	0.89	1.06	1.20	1.03	1.28	1.61
Nfld. and Labrador	0.68	0.79	0.85	0.77	0.94	1.12	1.00	1.12	1.20	1.26	1.54	2.06
Revenue-weighted average benefits and costs (US\$/cow/year), BCRs (ratio), and BEPs (years)												
Benefit	23.79	37.15	46.34	21.79	26.36	24.86	32.38	42.51	48.98	28.12	31.78	29.95
Cost	37.67	49.45	56.71	33.01	32.66	26.65	36.17	41.11	43.08	25.92	23.79	17.33
BCR	0.63	0.75	0.82	0.66	0.81	0.93	0.90	1.03	1.14	1.08	1.34	1.73
BEP	—	—	—	—	—	—	—	10.00	10.00	10.00	9.72	8.17

Assumes an initial within-herd *Mycobacterium avium* subsp. *paratuberculosis* (MAP) infection prevalence of 10% and a herd-level prevalence of 50.

degrees. Similar variables were identified as impactful in the 10,000 iteration Monte Carlo simulation sensitivity analyses of estimated 10-year BCRs using an average Canadian dairy herd (Figures 9, 10).

The stochasticity introduced through the Monte Carlo simulations resulted in values ranging from ~5 to 15% for the initial within-herd prevalence over the 10,000 iterations, with the 10-year proportional change in within-herd prevalence varying accordingly, as presented in Figure 7 through Figure 10. However, additional economic and production variables such as the vaccine price per dose, farm-gate price of milk, annual

production per cow, and the effect of MAP infection on milk production were also identified. The degree of bacterial shedding among lightly shedding animals was once again consistently found to be impactful and positively related to BCR estimates in all scenarios. All significantly impactful variables in these BCR sensitivity analyses were positively related to estimated BCRs, aside from the vaccine price per dose, which was negatively related. In all control scenarios, within-herd prevalence was inversely related to the 10-year proportional change in within-herd prevalence and directly related to the benefit-cost ratio of the control practice.

TABLE 5 | Estimated benefit-cost ratios (BCRs), and revenue-weighted average benefits and costs per cow (US\$), BCRs, and break-even periods (BEP) of various JD (paratuberculosis) control practices in Canadian regions across a range of vaccine shedding reduction, protective immunity percentages, and testing sensitivities, and with consideration for supply management (fixed output over time and production losses allocated as increased variable costs necessary to maintain production).

Region	Variable cost ^a (US\$/cow/year)	Vaccine (shedding)			Vaccine (immunity)			Vaccine (dual-effect)		
		50%	70%	90%	50%	70%	90%	50%	70%	90%
Canada	2,476	0.89	1.20	1.48	1.15	1.52	1.83	1.48	1.76	1.91
Québec	2,430	0.79	1.07	1.33	1.05	1.39	1.67	1.34	1.59	1.72
Ontario	2,256	0.85	1.15	1.42	1.09	1.44	1.74	1.42	1.68	1.82
British Columbia	3,204	1.00	1.35	1.68	1.34	1.77	2.13	1.70	2.02	2.19
Alberta	3,106	1.20	1.62	1.99	1.53	2.01	2.42	1.98	2.34	2.54
Manitoba	3,014	0.87	1.18	1.46	1.18	1.57	1.89	1.50	1.78	1.93
Saskatchewan	2,785	1.02	1.37	1.69	1.31	1.73	2.08	1.69	2.00	2.17
Nova Scotia	2,515	0.73	0.99	1.23	1.00	1.32	1.59	1.26	1.50	1.63
New Brunswick	2,464	0.75	1.02	1.26	1.01	1.34	1.61	1.28	1.52	1.65
Prince Edward Isl.	2,144	0.70	0.95	1.18	0.93	1.23	1.48	1.19	1.41	1.53
Nfld. and Labrador	4,112	1.27	1.73	2.14	1.70	2.25	2.72	2.17	2.58	2.80
Revenue-weighted average benefits and costs (US\$/cow/year), BCRs (ratio), and BEPs (years)										
	Benefit	8.04	10.85	13.38	10.48	13.80	16.59	13.44	15.88	17.21
	Cost	9.10	9.08	9.06	9.11	9.09	9.07	9.07	9.06	9.05
	BCR	0.88	1.20	1.48	1.15	1.52	1.83	1.48	1.75	1.90
	BEP	9.05	9.05	7.61	9.11	7.60	6.75	7.61	6.71	6.23

Region	Test-and-cull			Test-and-cull with vaccine (shedding)			Test-and-cull with vaccine (immunity)			Test-and-cull with vaccine (dual-effect)		
	50%	70%	90%	50%	70%	90%	50%	70%	90%	50%	70%	90%
Canada	0.41	0.47	0.49	0.45	0.55	0.64	0.57	0.64	0.68	0.71	0.87	1.14
Québec	0.40	0.47	0.50	0.43	0.52	0.60	0.55	0.63	0.69	0.68	0.83	1.07
Ontario	0.39	0.45	0.47	0.44	0.53	0.62	0.55	0.61	0.65	0.69	0.84	1.09
British Columbia	0.45	0.52	0.55	0.50	0.61	0.72	0.64	0.71	0.77	0.80	0.98	1.29
Alberta	0.44	0.50	0.51	0.53	0.64	0.78	0.64	0.69	0.72	0.84	1.02	1.38
Manitoba	0.44	0.52	0.55	0.47	0.57	0.66	0.61	0.70	0.76	0.75	0.92	1.19
Saskatchewan	0.43	0.49	0.51	0.49	0.59	0.71	0.60	0.67	0.71	0.77	0.94	1.25
Nova Scotia	0.41	0.49	0.52	0.42	0.51	0.58	0.55	0.64	0.71	0.67	0.82	1.04
New Brunswick	0.40	0.48	0.51	0.42	0.51	0.59	0.55	0.64	0.70	0.67	0.82	1.05
Prince Edward Isl.	0.38	0.45	0.48	0.39	0.48	0.55	0.52	0.59	0.65	0.62	0.77	0.98
Nfld. and Labrador	0.49	0.56	0.59	0.59	0.71	0.86	0.72	0.79	0.83	0.94	1.14	1.53
Revenue-weighted average benefits and costs (US\$/cow/year), BCRs (ratio), and BEPs (years)												
	Benefit	16.23	24.68	29.79	15.73	18.86	18.08	21.83	27.86	31.36	19.59	22.00
	Cost	37.92	49.83	57.17	33.15	32.79	26.74	36.37	41.38	43.39	26.02	23.89
	BCR	0.43	0.50	0.52	0.47	0.58	0.68	0.60	0.67	0.72	0.75	0.92
	BEP	—	—	—	—	—	—	—	—	—	9.26	8.48

Assumes an initial within-herd *Mycobacterium avium* subsp. *paratuberculosis* (MAP) infection prevalence of 10% and a herd-level prevalence of 50%.

^aSTATCAN—Table 32-10-0136-01 Farm operating revenues and expenses, annual (29). Sum of "Feed, supplements, straw, and bedding," "Veterinary fees, medicine, and breeding fees," and "Salaries and wages, including benefits related to employee salaries" for average dairy farms across all revenue levels in 2018. Total per farm divided by number of cows per farm. Number of cows per farm obtained by number of cattle divided by number of farms: CDIC—Number of farms with shipments of Milk (30). Number of cattle: STATCAN—Table 32-10-0130-01—Number of cattle, by class and farm type (23).

DISCUSSION

With the assumptions of mean within-herd MAP infection prevalence of 10%, a mean herd-level MAP infection prevalence of 50%, vaccine efficacies (reduction in shedding and protective

immunity) of 50%, mean test sensitivity of 50%, and mean test specificity of 99%, no scenarios resulted in the elimination of JD within a 10-year horizon. However, all control practices reduced within-herd MAP prevalence relative to no intervention within a 10-year horizon. However, at the 50% vaccine efficacy

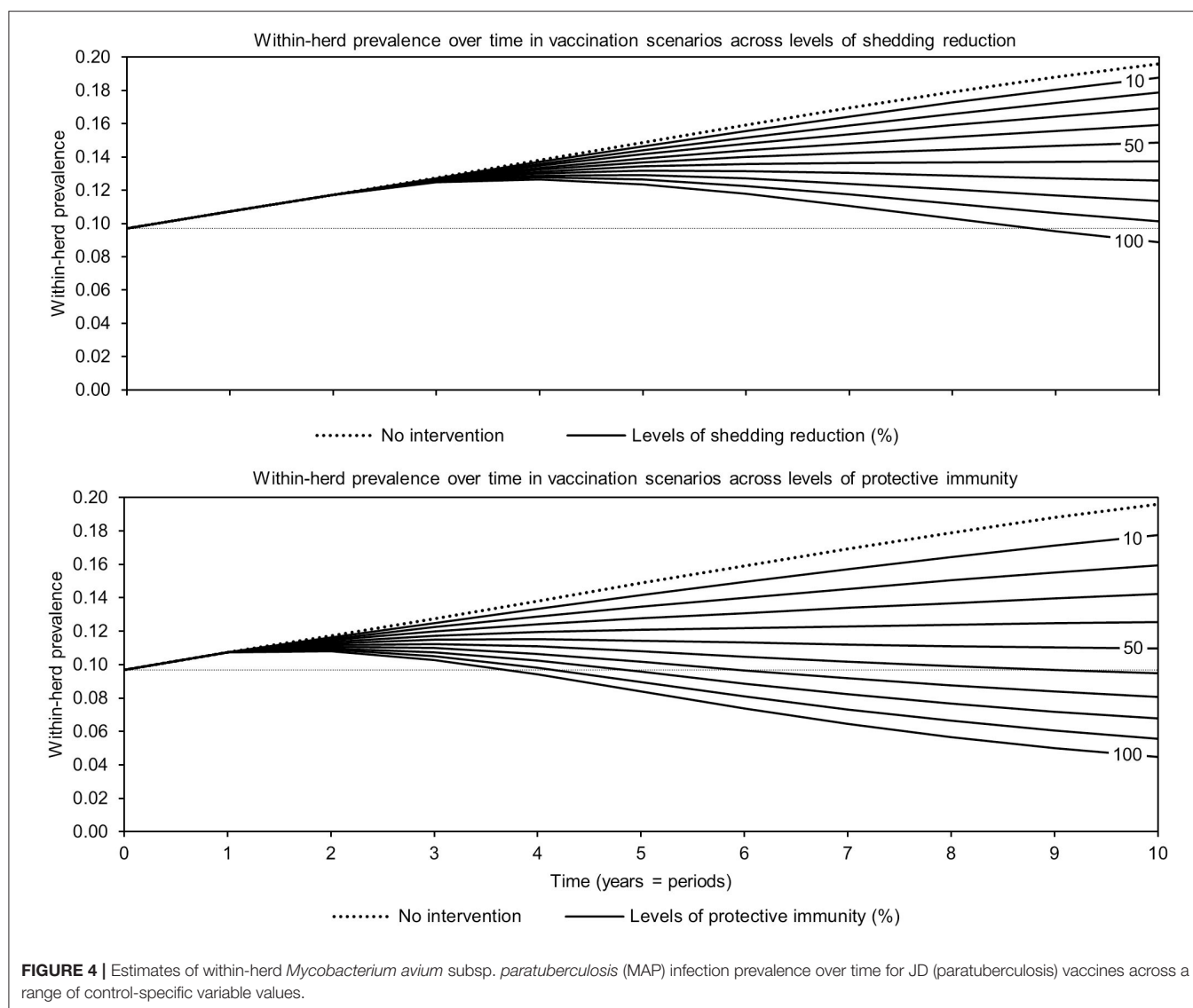


FIGURE 4 | Estimates of within-herd *Mycobacterium avium* subsp. *paratuberculosis* (MAP) infection prevalence over time for JD (paratuberculosis) vaccines across a range of control-specific variable values.

and 50% test sensitivity level, the only control practices that resulted in absolute reductions relative to initial within-herd MAP prevalence within the horizon were dual-effect vaccines, and protective immunity and dual-effect vaccines combined with testing and culling. Testing and culling alone did not; after three to four periods, an upward trend in within-herd prevalence was observed as new MAP infections occurred. Kudahl et al. (31) found that testing and culling alone only delayed an increase in within-herd prevalence, whereas Kirkeby et al. (20) found that that even with currently available testing tools, eradication of JD was attainable within seven to 10 years through testing and culling in Danish dairy herds. However, in the latter model, MAP infection was treated as an endemic situation, and therefore modeled using a density-dependent transition model as opposed to modeling the probability of infection as a function of the number and degree of infected animals in the herd. Also, their model explicitly considered a range of hygiene

levels across herds, whereas in this model, variations in herd hygiene are instead implicitly captured using a range of possible disease progression rates and MAP-specific input variables. The upward trend observed in the testing and culling scenarios was also accentuated by the 10-year horizon of the simulations; at test sensitivity levels in the 50–70% range, testing, and culling did not lower infection pressure within the herd quickly enough to overcome the disease progression of false-negative, subclinically infected, and non-shedding animals to stages of infection characterized by moderate and heavy shedding. As infections in those strata progressed, infection pressure within the herd, and therefore within-herd prevalence, began to rise again. If testing and culling were continued, with each passing 5- or 10-year horizon these oscillations would lessen in amplitude and an overall downward trend would be observed. However, from an economic and epidemiologic modeling perspective, it is unrealistic to assume that herd compositions, management

techniques, testing procedures, and even market structures would remain unchanged for more than 10 years. Therefore, the time horizon of the model was not extended.

Control variable values such as vaccine efficacy and testing sensitivity were clearly impactful on the effectiveness (ability to reduce within-herd prevalence within a 10-year period), economic impact (the ratio of benefits to costs per cow accrued

as a result of implementation), and break-even period (years for cumulative benefits to equal cumulative costs). The results suggest that the effectiveness of the dual-effect vaccine was primarily driven by the protective immunity effect of the vaccine as opposed to the shedding reduction effect. At higher ranges of protective immunity, the reduced-shedding effect of the dual-effect vaccine ceased to have impact on the final MAP prevalence; at levels >80% protective immunity, reduced shedding among MAP-positive animals actually had the reverse effect, resulting in a final prevalence greater than the final prevalence that would have been achieved using a single-effect protective immunity vaccine. In the model, disease progression is related to the degree and number of shedding animals in the herd. Therefore, a reduction in shedding among MAP-infected animals resulted in less severe but more prolonged subclinical infections; these non-shedding, subclinically infected animals remained in the herd rather than developing clinical signs of JD and being culled. Once again, if the horizon of the model were extended by five or 10 periods, this result would likely not be observed as the remaining subclinically infected animals would eventually exit the herd. However, for reasons already described, the model was not extended past its 10-year horizon.

Through the Monte Carlo sensitivity analyses, the degree of bacterial shedding among lightly shedding animals was identified as an impactful variable, highlighting the need for further research into this area. Also impactful were the farm-gate price of milk and annual production per cow due to their positive relationships with production, and therefore forgone production losses due to MAP infection. For the selection of major dairy-producing regions that were modeled, production benefits were measured as potential increases in milk sales. Dual-effect vaccines were among the most successful control practices in terms of their reduction in within-herd prevalence and were economically viable with BCRs greater than one in all

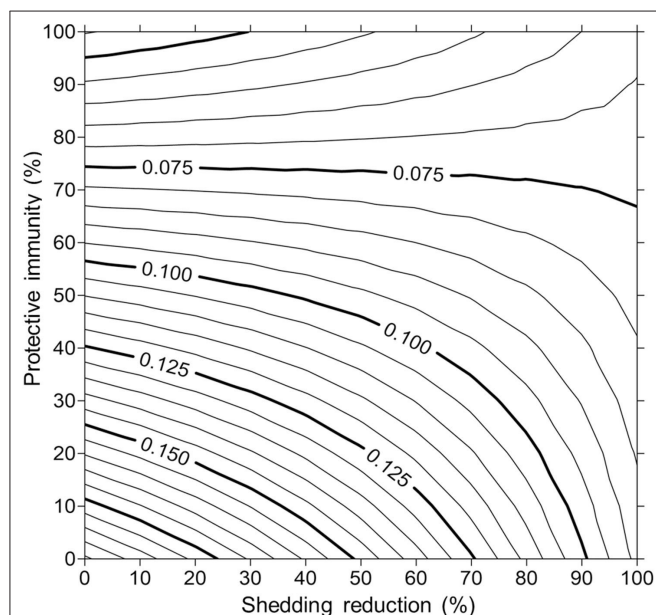


FIGURE 5 | Estimates of final 10-year within-herd prevalence across a range of protective immunities and shedding reductions given an initial within-herd *Mycobacterium avium* subsp. *paratuberculosis* (MAP) infection prevalence of 0.10.

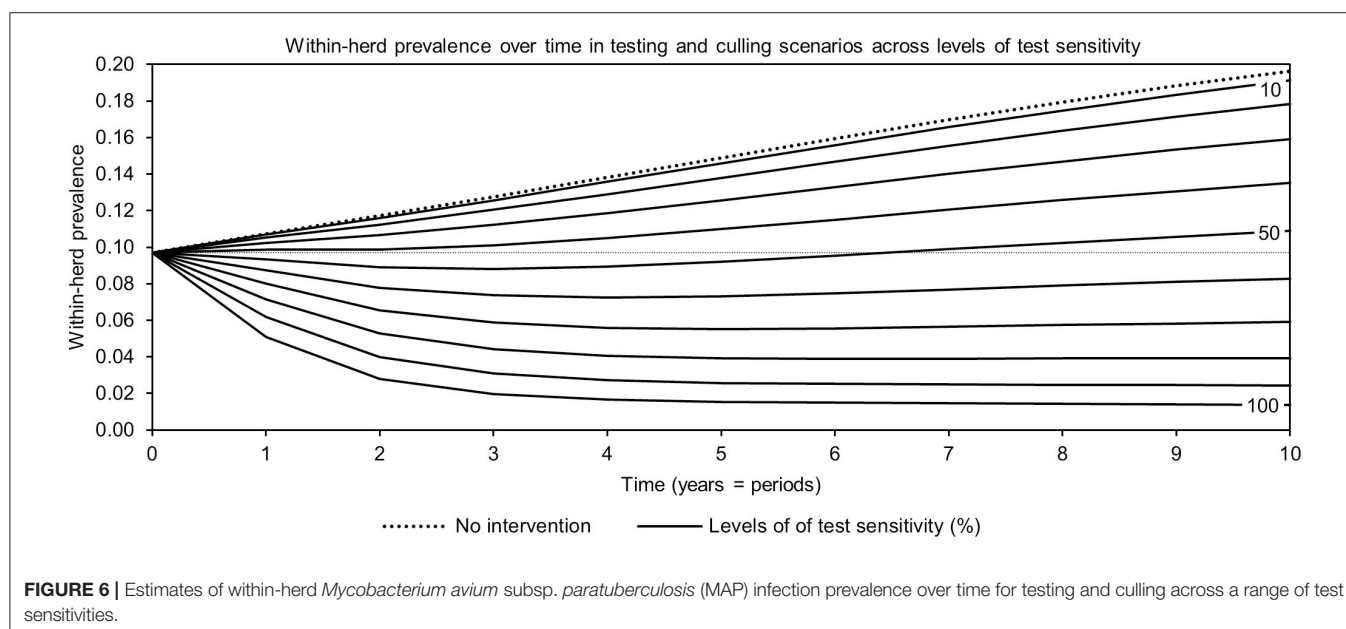
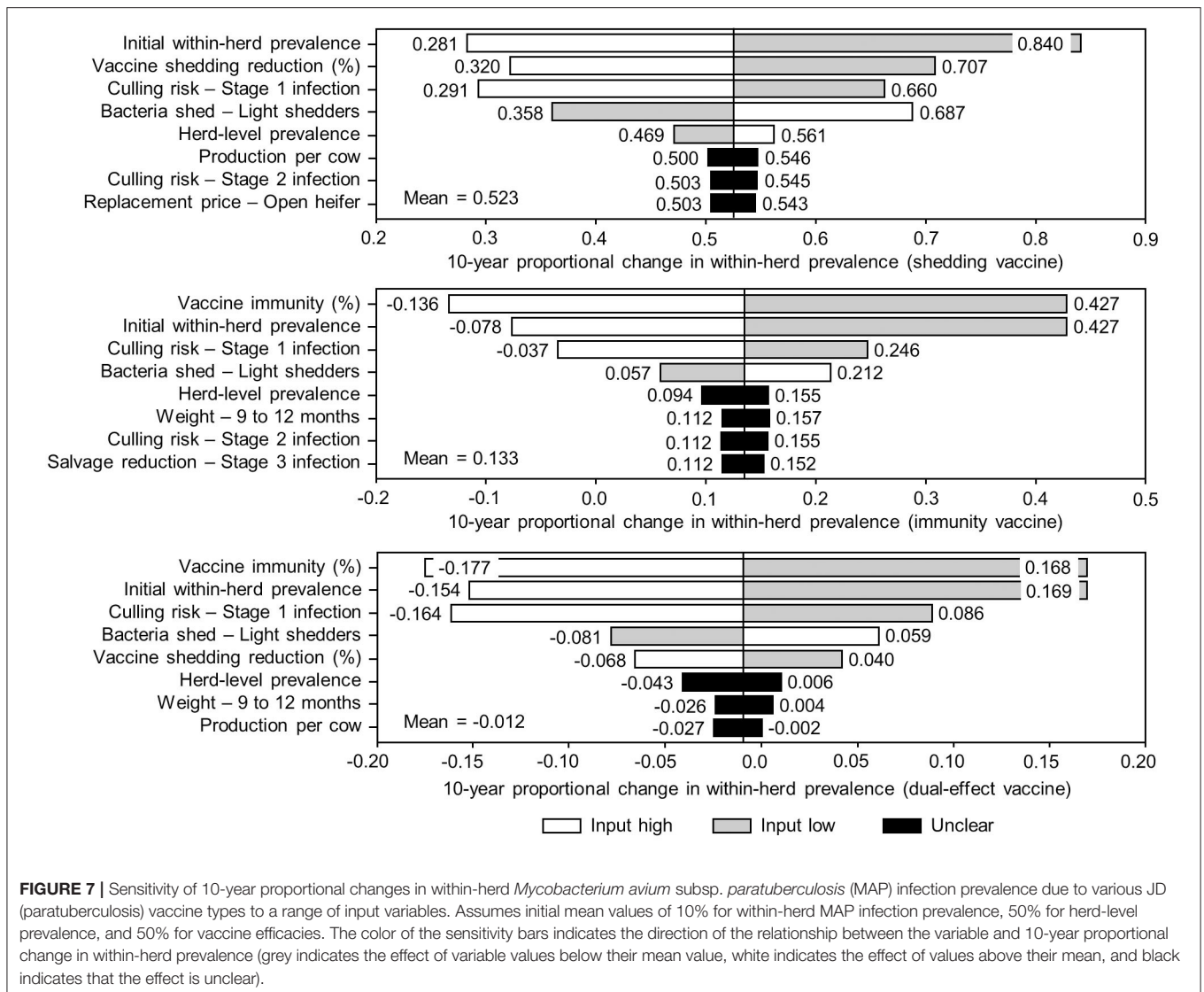


FIGURE 6 | Estimates of within-herd *Mycobacterium avium* subsp. *paratuberculosis* (MAP) infection prevalence over time for testing and culling across a range of test sensitivities.



countries except Poland, Brazil, China, Russia, and Turkey. These countries are five of the seven countries with the lowest annual milk production per cow that were modeled, along with Ireland and New Zealand. However, Ireland and New Zealand have significantly greater aggregated salvage prices and replacement costs than the other five countries. The combination of relatively low costs and low annual production resulted in lower economic losses due to JD, and therefore less economic benefits from controlling JD in those five countries.

Two interesting patterns emerged across a range of control variable values (test sensitivity, shedding reduction, and protective immunity), both related to testing and culling. Firstly, testing and culling and testing and culling combined with a protective immunity vaccine were the only control scenarios where estimated annual costs per cow increased as the control variable values increased. In the vaccine scenarios without testing and culling, as within-herd MAP prevalence decreased with more effective controls, the culling rate also decreased as

overall herd health improved. Because the vaccine was only administered to natural and purchased replacements after the initial time 0 whole-herd vaccination, costs per cow decreased over time as there were relatively fewer replacements requiring vaccination in each period. However, with testing and culling, this effect was outweighed by the fact that a more sensitive test detected more positive animals, which then needed to be culled and replaced at a relatively high cost. While testing and culling was effective at reducing within-herd prevalence relative to its initial value at test sensitivities >70%, this effectiveness depended entirely on aggressive culling of test-positive animals which may be impractical in a real-world setting, particularly in moderate and high prevalence herds. Similarly, in their simulations, Groenendaal et al. (32) found that while a test with 80% sensitivity in all infected animals was effective at reducing within-herd prevalence, the strategy was economically unviable because of the high culling rate of test-positive animals, particularly young ones, required to achieve that reduction

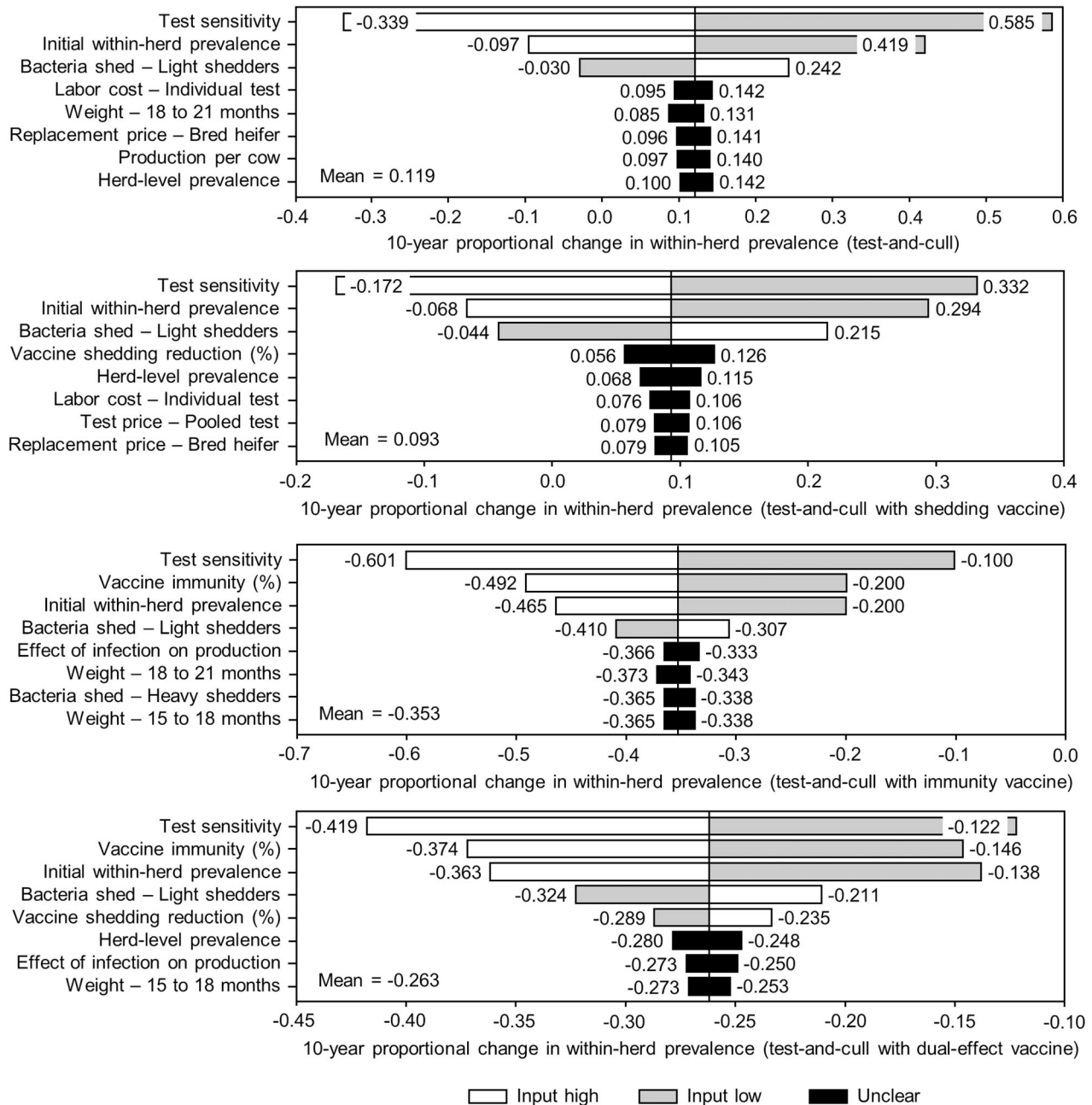


FIGURE 8 | Sensitivity of 10-year proportional changes in within-herd *Mycobacterium avium* subsp. *paratuberculosis* (MAP) infection prevalence due to various JD (paratuberculosis) practices involving testing and culling to a range of input variables. Assumes initial mean values of 10% for within-herd MAP infection prevalence, 50% for herd-level prevalence, 50% for vaccine efficacies, and 50% for testing sensitivities. The color of the sensitivity bars indicates the direction of the relationship between the variable and 10-year proportional change in within-herd prevalence (grey indicates the effect of variable values below their mean value, white indicates the effect of values above their mean, and black indicates that the effect is unclear).

in prevalence. Unless the costs of replacing test-positive and subsequently culled animals can be reduced for producers, this model also suggests that the benefits of testing and culling may not equal or exceed the costs, even if new, more sensitive and specific tests are developed. However, it is important to note

that the simulated testing protocol remained static throughout the 10-year horizon; a desirable real-world testing and culling program would not only need to reduce replacement costs, but also reduce testing costs by using a dynamic testing strategy (e.g., environmental testing instead of pooled and individual

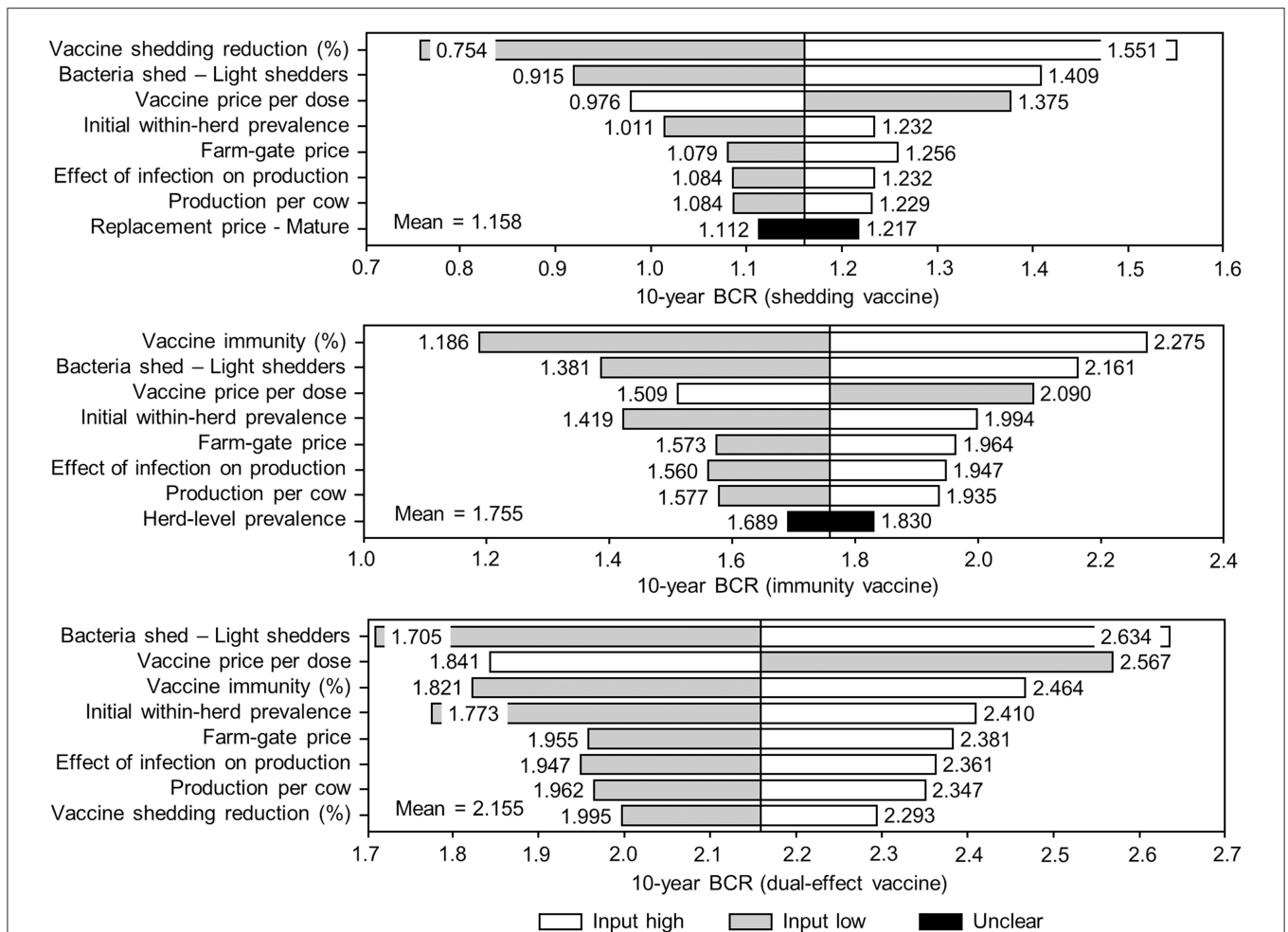


FIGURE 9 | Sensitivity of 10-year benefit-cost ratios (BCRs) associated with various JD (paratuberculosis) vaccine types in average Canadian dairy herds to a range of input variables. Assumes initial mean values of 10% for within-herd *Mycobacterium avium* subsp. *paratuberculosis* (MAP) infection prevalence, 50% for herd-level prevalence, and 50% for vaccine efficacies. The color of the sensitivity bars indicates the direction of the relationship between the variable and 10-year BCR (grey indicates the effect of variable values below their mean value, white indicates the effect of values above their mean, and black indicates that the effect is unclear).

testing once within-herd prevalence is reduced to a certain level). For herds with low initial within-herd prevalence, a dynamic testing strategy alone could reduce costs to the point where testing and culling becomes economically viable, particularly in closed herd scenarios where all replacements come from within the herd. If more sensitive tests were also developed, these low prevalence closed herds could become reliable and certifiable sources of MAP-negative replacements for higher prevalence open herds seeking to reduce within-herd MAP prevalence or low prevalence herds seeking to rapidly expand, with these replacements potentially being sold at an economic premium. The second interesting pattern that emerged related to testing and culling was that when combined with a vaccine that reduced shedding and when combined with a dual-effect vaccine, benefits per cow decreased as the control variable values (vaccine efficacy and test sensitivity) increased from 70 to 90%. Because a fecal PCR test was

modeled, the test could only detect animals in shedding states of infection. Therefore, as the shedding-reducing effects of the vaccine were increased, the number of animals detectable by fecal PCR testing was reduced, and the prevalence-reducing effects of improved testing sensitivity were partially offset. Because of this reduced ability to detect positive animals, the replacement costs associated with testing and culling also decreased. When these decreased costs were combined with the overall improvement in herd health due to vaccination and less aggressive testing and culling, the total costs per cow decreased at a greater rate than did benefits; the BCRs still increased with the control variable values despite the combination of vaccine-induced shedding reduction and fecal PCR testing being relatively inefficient.

While the general method described is appropriate for most dairy industries, the Canadian industry requires special attention. Canada's dairy sector operates with planned and

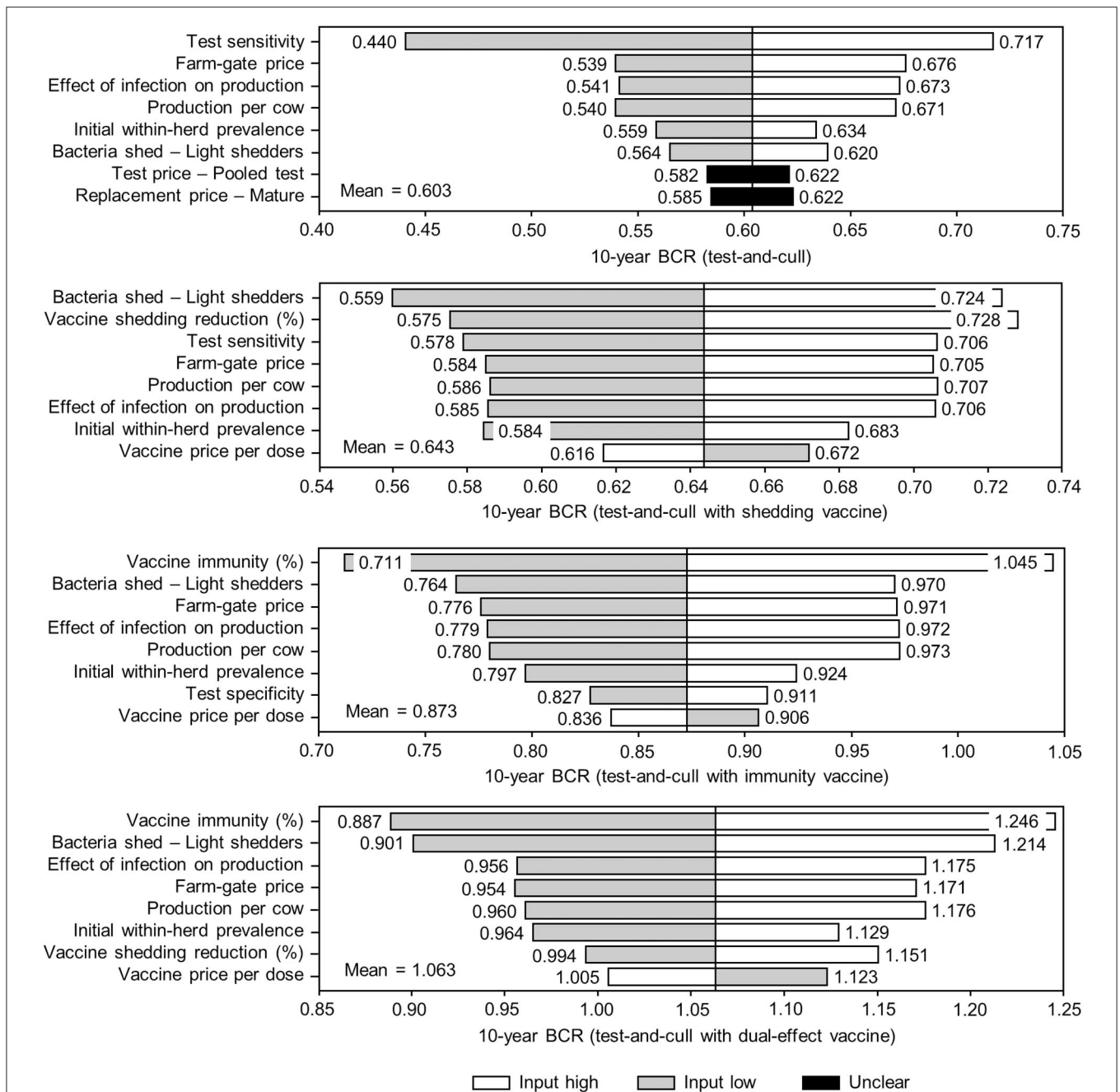


FIGURE 10 | Sensitivity of 10-year benefit-cost ratios (BCRs) associated with various JD (paratuberculosis) control practices involving testing and culling in average Canadian dairy herds to a range of input variables. Assumes initial mean values of 10% for within-herd *Mycobacterium avium* subsp. *paratuberculosis* (MAP) infection prevalence, 50% for herd-level prevalence, 50% for vaccine efficacies, and 50% for testing sensitivities. The color of the sensitivity bars indicates the direction of the relationship between the variable and 10-year BCR (grey indicates the effect of variable values below their mean value, white indicates the effect of values above their mean, and black indicates that the effect is unclear).

controlled production levels, administered cost-of-production-based pricing, and import controls. There are two consequences relevant to this model: (i) production losses, a significant contributor to the benefits of JD control, can no longer be measured as forgone milk sales due to the production quota

system; and (ii) Canada's above-average farm-gate price, which is the highest among countries modeled (aside from Japan) and much higher than the farm-gate price in the United States, Canada's most comparable counterpart. Apart from a higher level of annual output in the United States, both countries

have similar dairy sector characteristics in terms of genetics, marketing, consumer preferences, and annual production per cow, and assuming the same within-herd and herd-level MAP prevalence across the two countries, there should be similar per-cow benefits and costs associated with controlling JD. However, the above average farm-gate price in Canada results in a greater valuation of production losses and therefore benefits from JD control in Canada. While these differences are attributable in part to differing technical and allocative efficiencies across US and Canadian dairy sectors, which are not addressed by this study, the effects of the differing market structures are addressed; to reflect the constraint of fixed production, production losses were also estimated as the cost of having additional, less productive MAP-positive cows to maintain a fixed level of production. Once adjusted, the estimated BCRs of all control practices in Canada dropped and their break-even periods increased. For example, the Canadian revenue-weighted average BCR for dual-effect vaccination at 50% efficacy decreased from 2.13 to 1.48 when production levels were treated as fixed. While this is more in line with the BCR of 1.66 in average US herds for the same type of vaccination, this may be an overcorrection. Although overall production and farm-gate prices in Canada are predetermined and producers are not paid for production that exceeds their quota-based targets, the overall level of production generally increases year-over-year (33) and producers trade quota through an exchange market; essentially, more technically efficient producers purchase quota from less technically efficient ones to increase the size of their operations. Evidence of this competition is clear: the number of dairy farms in Canada has steadily decreased over the last several decades while the size of herds has increased (34). In other words, Canadian producers operate in an environment between fixed production and pure competition. Therefore, the true BCRs of the various potential JD control practices for Canadian dairy herds likely lie between the fixed production and variable production estimates.

Finally, it is also important to recognize the limitations of this study. The net costs associated with a higher culling rate may be overestimated in this model. Because only the economic impacts of culling due to MAP-infection were considered, this model ignores the potential benefits associated with having a greater proportion of younger animals in the herd. For example, age-related conditions such as reduced fertility, mastitis, and lameness are all potential sources of economic losses that could be partially offset as a direct result of an increased cow-culling rate. Also, the production benefits due to an increased conception rate resulting from JD control were not explicitly estimated. Instead, these benefits were only implicitly considered through the variations around the mean milk yield reduction estimated by McAloon et al. (8). Lastly, it is also important to note that production systems, grazing periods, cattle breeds, etc. were assumed to be uniform across herds within regions at the mean level. However, variations in these production factors were implicitly captured

through variations around the mean values used in the 10,000 iteration simulations.

CONCLUSIONS

Vaccination was the most economically viable type of JD control practice modeled, with dual-effect vaccines (reducing shedding and providing protective immunity) being the most promising. Even with modest 50% reductions in shedding and 50% protective immunity conferred by vaccination, BCRs for this type of vaccine were between 2.13 and 1.48 in Canada, with a break-even period of between 6.17 and 7.61 years. At this same level of efficacy, dual-effect vaccines were also estimated to be desirable with BCRs greater than one in almost all major-dairy producing regions, with a revenue-weighted average BCR of 1.24 and a revenue-weighted average break-even period of 7.88 years. Testing and culling was comparably effective to a dual-effect vaccine at test sensitivities >70% but would remain economically unviable in almost all regions modeled, even at levels of testing sensitivity above 70%. The results suggest that the main barrier to testing and culling programs for JD is the impractical nature of the aggressive culling that would have to accompany highly sensitive tests. Without a reduction in the replacement cost of culled animals, vaccination, particularly dual-effect vaccination, is the most promising potential JD control practice for dairy producers. This research is an important contribution to the policy discussion surrounding paratuberculosis control in Canada and internationally.

DATA AVAILABILITY STATEMENT

The raw data supporting the conclusions of this article will be made available by the authors, without undue reservation.

AUTHOR CONTRIBUTIONS

PR and DH conceived of the research and developed the models. PR performed the simulations and computations. HB and DH verified the methodology and validity of the results. HB provided expertise and knowledge regarding MAP transmission and existing control practices. DH supervised this research. All authors discussed the results and reviewed the final manuscript.

FUNDING

This research was supported by Genome Canada, Genome Prairie, and Genome British Columbia [225RVA].

SUPPLEMENTARY MATERIAL

The Supplementary Material for this article can be found online at: <https://www.frontiersin.org/articles/10.3389/fvets.2020.614727/full#supplementary-material>

REFERENCES

1. Fecteau ME, Whitlock RH. Paratuberculosis in cattle. In Behr MA, Collins DM, editors. *Paratuberculosis: Organism, Disease, Control*, Wallingford: CABI, (2010) 144–56.
2. Manning EJ, Collins MT. *Mycobacterium avium* subsp. paratuberculosis: pathogen, pathogenesis and diagnosis. *Rev Off Int Epizoot.* (2001) 20:133–50. doi: 10.20506/rst.20.1.1275
3. Whittington RJ, Marshall DJ, Nicholls PJ, Marsh IB, Reddacliff LA. Survival and dormancy of *Mycobacterium avium* subsp. paratuberculosis in the environment. *Appl Environ Microbiol.* (2004) 70:2989–3004. doi: 10.1128/AEM.70.5.2989-3004.2004
4. Donaghy J, Keyser M, Johnston J, Cilliers FP, Gouws PA, Rowe MT. Inactivation of *Mycobacterium avium* ssp. paratuberculosis in milk by UV treatment. *Lett Appl Microbiol.* (2009) 49:217–21. doi: 10.1111/j.1472-765X.2009.02644.x
5. Tiwari A, VanLeeuwen JA, McKenna SLB, Keefe GP, Barkema HW. John's disease in Canada Part I: clinical symptoms, pathophysiology, diagnosis, and prevalence in dairy herds. *Can Vet J.* (2006) 47:874–82.
6. Garcia AB, Shalloo L. Invited review: the economic impact and control of paratuberculosis in cattle. *J Dairy Sci.* (2015) 98:5019–39. doi: 10.3168/jds.2014-9241
7. Lombard JE, Garry FB, McCluskey BJ, Wagner BA. Risk of removal and effects on milk production associated with paratuberculosis status in dairy cows. *J Am Vet Med Assoc.* (2005) 227:1975–81. doi: 10.2460/javma.2005.227.1975
8. McAloon CG, Whyte P, More SJ, Green MJ, O'Grady L, Garcia A, et al. The effect of paratuberculosis on milk yield—a systematic review and meta-analysis. *J Dairy Sci.* (2016) 99:1449–60. doi: 10.3168/jds.2015-10156
9. Benedictus G, Dijkhuizen AA, Stelwagen J. Economic losses to farms due to paratuberculosis in cattle. *Tijdschr Diergeneesk.* (1985) 110:310–9.
10. Raizman EA, Fetrow JP, Wells SJ. Loss of income from cows shedding *Mycobacterium avium* subspecies paratuberculosis prior to calving compared with cows not shedding the organism on two Minnesota dairy farms. *J Dairy Sci.* (2009) 92:4929–36. doi: 10.3168/jds.2009-2133
11. Kudahl AB, Nielsen SS. Effect of paratuberculosis on slaughter weight and slaughter value of dairy cows. *J Dairy Sci.* (2009) 92:4340–6. doi: 10.3168/jds.2009-2039
12. Ott SL, Wells SJ, Wagner BA. Herd-level economic losses associated with John's disease on US dairy operations. *Prev Vet Med.* (1999) 40:179–92. doi: 10.1016/S0167-5877(99)00037-9
13. Shephard RW, Williams SH, Beckett SD. Farm economic impacts of bovine John's disease in endemically infected Australian dairy herds. *Aust Vet J.* (2016) 94:232–9. doi: 10.1111/avj.12455
14. Groenendaal H, Nielen M, Jalvingh AW, Horst SH, Galligan DT, Hesselink JW. A simulation of John's disease control. *Prev Vet Med.* (2002) 54:225–45. doi: 10.1016/S0167-5877(02)00027-2
15. Pillars RB, Grooms DL, Wolf CA, Kaneene JB. Economic evaluation of John's disease control programs implemented on six Michigan dairy farms. *Prev Vet Med.* (2009) 90:223–32. doi: 10.1016/j.prevetmed.2009.04.009
16. Tiwari A, VanLeeuwen JA, Dohoo IR, Keefe GP, Weersink A. Estimate of the direct production losses in Canadian dairy herds with subclinical *Mycobacterium avium* subspecies paratuberculosis infection. *Can Vet J.* (2008) 49:569–76.
17. Rasmussen P, Barkema HW, Mason S, Beaulieu E, Hall DC. Economic losses due to John's disease (paratuberculosis) in dairy cattle. *J Dairy Sci.* (2020).
18. Whittington R, Donat K, Weber MF, Kelton D, Nielsen SS, Eisenberg S, et al. Control of paratuberculosis: who, why and how. A review of 48 countries. *BMC Vet Res.* (2019) 15:198. doi: 10.1186/s12917-019-1943-4
19. Groenendaal H, Zagmutt FJ, Patton EA, Wells SJ. Cost-benefit analysis of vaccination against *Mycobacterium avium* ssp. paratuberculosis in dairy cattle, given its cross-reactivity with tuberculosis tests. *J Dairy Sci.* (2015) 98:6070–84. doi: 10.3168/jds.2014-8914
20. Kirkeby C, Græsbøll K, Nielsen SS, Christiansen LE, Toft N, Rattenborg E, et al. Simulating the epidemiological and economic impact of paratuberculosis control actions in dairy cattle. *Front Vet Sci.* (2016) 3:90. doi: 10.3389/fvets.2016.00090
21. Smith RL, Al-Mamun MA, Gröhn YT. Economic consequences of paratuberculosis control in dairy cattle: a stochastic modeling study. *Prev Vet Med.* (2017) 138:17–27. doi: 10.1016/j.prevetmed.2017.01.007
22. OMAFRA. *Culling Decisions: Dairy Cows*. Ontario Ministry of Agriculture, Food, and Rural Affairs. (2020). Available online at: [http://www.omafra.gov.on.ca/english/livestock/dairy/facts/cullcowwelfare.htm#:~:sim\\$=text=Trends%20in%20culling%20and%20markets,low%20milk%20production%20\(16%25\)](http://www.omafra.gov.on.ca/english/livestock/dairy/facts/cullcowwelfare.htm#:~:sim$=text=Trends%20in%20culling%20and%20markets,low%20milk%20production%20(16%25)) (accessed September 13, 2020).
23. STATCAN. *Table 32-10-0130-01 Number of cattle, by class and farm type (x 1,000)*. Statistics Canada. (2020) Available online at: <https://www150.statcan.gc.ca/t1/tbl1/en/tv.action?pid=3210013001> (accessed September 13, 2020).
24. Van Biert P. *Economics of milk production in Alberta, 2018: the dairy cost study*. Alberta Agriculture and Forestry. (2019). Available online at: <https://open.alberta.ca/dataset/abca66b6-d117-4ee2-8615-248fcb53262c/resource/b43613f3-6128-407e-aa85-b7504e0f0907/download/economics-of-milk-production-2018.pdf> (accessed September 14, 2020).
25. USDA NRCS. *Rate for Federal Water Projects - NRCS Economics*. United States Department of Agriculture - National Resource Conservation Service. (2020) Available online at: https://www.nrcs.usda.gov/wps/portal/nrcs/detail/national/cntsc/?&cid=nrcs143_009685 (accessed May 21, 2020).
26. Macrotrends. *S&P 500 Historical Annual Returns* Macrotrends L. L. C. (2020). Available online at: <https://www.macrotrends.net/2526/sp-500-historical-annual-returns> (accessed May 21, 2020).
27. TBC. *Canadian Cost-Benefit Analysis Guide: Regulatory Proposals*. Treasury Board of Canada Secretariat (2007). Available online at: <https://www.tbs-sct.gc.ca/rtrap-parfa/analys/analys-eng.pdf> (accessed May 21, 2020).
28. Palisade. *@RISK v. 8.0 - Risk Analysis Software Using Monte Carlo Simulation for Microsoft Excel and Microsoft Project*. Palisade (2019). Available online at: <https://www.palisade.com/msoffice/risk.asp> (accessed November 24, 2020).
29. STATCAN. *Table 32-10-0136-01 Farm Operating Revenues and Expenses, Annual*. Statistics Canada. (2019) Available online at: <https://www150.statcan.gc.ca/t1/tbl1/en/tv.action?pid=3210013601> (Accessed September 16, 2020).
30. CDIC. *D056 - Number of Farms with Shipments of Milk by Province*. Canadian Dairy Information Centre. (2019) Available online at: <https://aimis-simia-cdic-ccil.agr.gc.ca/rp/index-eng.cfm?action=pR&r=220&pdctc=> (accessed October 10, 2019).
31. Kudahl AB, Østergaard S, Sørensen JT, Nielsen SS. A stochastic model simulating paratuberculosis in a dairy herd. *Prev Vet Med.* (2007) 78:97–117. doi: 10.1016/j.prevetmed.2006.05.015
32. Groenendaal H, Nielen M, Hesselink JW. Development of the Dutch John's disease control program supported by a simulation model. *Prev Vet Med.* (2003) 60:69–90. doi: 10.1016/S0167-5877(03)00083-7
33. CDIC. *D037-3 Average Production by Province*. Canadian Dairy Information Centre (2019). Available online at: <https://aimis-simia-cdic-ccil.agr.gc.ca/rp/index-eng.cfm?action=pR&r=215&pdctc=> (accessed October 10, 2019).
34. CDIC. *D056 Number of Farms with Shipments of Milk by Province*. Canadian Dairy Information Centre (2019). Available online at: <https://aimis-simia-cdic-ccil.agr.gc.ca/rp/index-eng.cfm?action=pR&r=220&pdctc=> (accessed October 10, 2019).

Conflict of Interest: The authors declare that the research was conducted in the absence of any commercial or financial relationships that could be construed as a potential conflict of interest.

Copyright © 2021 Rasmussen, Barkema and Hall. This is an open-access article distributed under the terms of the Creative Commons Attribution License (CC BY). The use, distribution or reproduction in other forums is permitted, provided the original author(s) and the copyright owner(s) are credited and that the original publication in this journal is cited, in accordance with accepted academic practice. No use, distribution or reproduction is permitted which does not comply with these terms.



Corrigendum: Effectiveness and Economic Viability of Johne's Disease (Paratuberculosis) Control Practices in Dairy Herds

Philip Rasmussen¹, Herman W. Barkema² and David C. Hall^{1*}

¹ Department of Ecosystem and Public Health, University of Calgary, Calgary, AB, Canada, ² Department of Production Animal Health, University of Calgary, Calgary, AB, Canada

Keywords: MAP, Johne's disease, paratuberculosis, vaccination, testing and culling, control practice, Markov chain, economic analysis

A Corrigendum on

Effectiveness and Economic Viability of Johne's Disease (Paratuberculosis) Control Practices in Dairy Herds

by Rasmussen, P., Barkema, H. W., and Hall, D. C. (2021). *Front. Vet. Sci.* 7:614727. doi: 10.3389/fvets.2020.614727

OPEN ACCESS

Edited and reviewed by:

Marta Alonso-Hernández,
Animalien Osasuna, NEIKER-Instituto
Vasco de Investigación y Desarrollo
Agrario, Spain

*Correspondence:

David C. Hall
dchall@ucalgary.ca

Specialty section:

This article was submitted to
Veterinary Epidemiology and
Economics,
a section of the journal
Frontiers in Veterinary Science

Received: 22 January 2021

Accepted: 04 February 2021

Published: 22 February 2021

Citation:

Rasmussen P, Barkema HW and
Hall DC (2021) Corrigendum:
Effectiveness and Economic Viability
of Johne's Disease (Paratuberculosis)
Control Practices in Dairy Herds.
Front. Vet. Sci. 8:657453.
doi: 10.3389/fvets.2021.657453

In the original article, there was a typographical error. A correction has been made to the exponent on the final bracket of Materials and Methods, Testing and Culling, Paragraph 1, **Equation (1)**. The corrected paragraph appears below.

"In this control scenario, animals aged 1–7 years are tested annually using a combination of pooled and individual fecal PCR tests. They are first tested at time zero, and then retested after each transition period (year) along with purchased replacements aged 1–3 years, which are tested only at the individual level. For all testing periods, the probability of a pooled test containing samples from an r number of MAP-positive animals given the pool size n , or $pr(TP) | C(n, r)$, is determined using the following equation:

$$pr(TP) | C(n, r) = \frac{n!}{r! * (n - r)!} * \left(\frac{TP_s}{animals_{(1-7)}} \right)^r * \left(1 - \left(\frac{TP_s}{animals_{(1-7)}} \right) \right)^{n-r} \quad (1)$$

where: TP_s equals the number of true positive animals aged 1–7 years in a shedding state and $animals_{(1-7)}$ equals the number of animals aged 1–7 years in the herd. A testing pool size of five animals is assumed, or $n = 5$. Pooled tests and individual tests are assumed to share the same sensitivities and specificities, or that $se_p = se_i$ and $sp_p = sp_i$."

The authors apologize for this error and state that this does not change the scientific results or conclusions of the article in any way. The original article has been updated.

Copyright © 2021 Rasmussen, Barkema and Hall. This is an open-access article distributed under the terms of the Creative Commons Attribution License (CC BY). The use, distribution or reproduction in other forums is permitted, provided the original author(s) and the copyright owner(s) are credited and that the original publication in this journal is cited, in accordance with accepted academic practice. No use, distribution or reproduction is permitted which does not comply with these terms.



Serum Metabolomic Profiles of Paratuberculosis Infected and Infectious Dairy Cattle by Ambient Mass Spectrometry

Alessandra Tata¹, Ivana Pallante¹, Andrea Massaro¹, Brunella Miano¹, Massimo Bottazzari¹, Paola Fiorini¹, Mauro Dal Prà¹, Laura Paganini¹, Annalisa Stefani¹, Jeroen De Buck², Roberto Piro¹ and Nicola Pozzato^{1*}

¹ Istituto Zooprofilattico delle Venezie (IZSVe), Legnaro, Italy, ² Department of Production Animal Health, University of Calgary, Calgary, AB, Canada

OPEN ACCESS

Edited by:

Marta Alonso-Hearn,
Animalien Osasuna, NEIKER-Instituto
Vasco de Investigación y Desarrollo
Agrario, Spain

Reviewed by:

Kenneth James Genovese,
United States Department of
Agriculture, United States
Ad Koets,
Wageningen Bioveterinary Research
(WBVR), Netherlands

*Correspondence:

Nicola Pozzato
npozzato@izsvenezie.it

Specialty section:

This article was submitted to
Veterinary Infectious Diseases,
a section of the journal
Frontiers in Veterinary Science

Received: 02 November 2020

Accepted: 21 December 2020

Published: 20 January 2021

Citation:

Tata A, Pallante I, Massaro A, Miano B, Bottazzari M, Fiorini P, Dal Prà M, Paganini L, Stefani A, De Buck J, Piro R and Pozzato N (2021) Serum Metabolomic Profiles of Paratuberculosis Infected and Infectious Dairy Cattle by Ambient Mass Spectrometry. *Front. Vet. Sci.* 7:625067. doi: 10.3389/fvets.2020.625067

Mycobacterium avium subsp. paratuberculosis (MAP) is the causative agent of paratuberculosis [Johne's disease (JD)], a chronic disease that causes substantial economic losses in the dairy cattle industry. The long incubation period means clinical signs are visible in animals only after years, and some cases remain undetected because of the subclinical manifestation of the disease. Considering the complexity of JD pathogenesis, animals can be classified as infected, infectious, or affected. The major limitation of currently available diagnostic tests is their failure in detecting infected non-infectious animals. The present study aimed to identify metabolic markers associated with infected and infectious stages of JD. Direct analysis in real time coupled with high resolution mass spectrometry (DART-HRMS) was, hence, applied in a prospective study where cohorts of heifers and cows were followed up annually for 2–4 years. The animals' infectious status was assigned based on a positive result of both serum ELISA and fecal PCR, or culture. The same animals were retrospectively assigned to the status of infected at the previous sampling for which all JD tests were negative. Stored sera from 10 infected animals and 17 infectious animals were compared with sera from 20 negative animals from the same herds. Two extraction protocols and two (-/+) ionization modes were tested. The three most informative datasets out of the four were merged by a mid-level data fusion approach and submitted to partial least squares discriminant analysis (PLS-DA). Compared to the MAP negative subjects, metabolomic analysis revealed the m/z signals of isobutyrate, dimethylethanolamine, palmitic acid, and rhamnitol were more intense in infected animals. Both infected and infectious animals showed higher relative intensities of tryptamine and creatine/creatinine as well as lower relative abundances of urea, glutamic acid and/or pyroglutamic acid. These metabolic differences could indicate altered fat metabolism and reduced energy intake in both infected and infectious cattle. In conclusion, DART-HRMS coupled to a mid-level data fusion approach allowed the molecular features that identified preclinical stages of JD to be teased out.

Keywords: metabolomic, paratuberculosis, biomarker, cattle, DART-MS, Jonhe's disease, *mycobacterium avium* subsp *paratuberculosis*

INTRODUCTION

Bovine paratuberculosis, known as John's disease (JD), is a chronic infectious disease of ruminants resulting in diarrhea, wasting, weight loss, emaciation, and eventual death (1–3). The etiologic agent of JD is *Mycobacterium avium* subsp. *paratuberculosis* (MAP), a slow growing, obligate intracellular pathogen (4).

JD is widespread worldwide, causes great economic losses, and is mainly transmitted through the fecal-oral route (2, 5, 6). The susceptibility is age-dependent, with young calves highly sensitive to infection. The susceptibility decreases in heifers, with adult cows being infected only in the case of high infectious doses or long exposure time (2, 5, 7). In JD, animals can be classified into three groups: infected when MAP is present intracellularly in the animal, infectious when the animal is shedding MAP via feces and affected when clinical signs are visible (8). Common diagnostic tests, such as fecal Polymerase Chain Reaction (PCR) and enzyme-linked immunosorbent assay (ELISA) lack of sensitivity in earlier stages of infection, characterized by intermittent MAP shedding and absence of specific Th-2 response (9). The biology of MAP infection, the long incubation period, the pathogenesis, and the difficulties in detecting infected animals in the absence of accurate diagnostic tests entail delayed diagnosis of JD, so disease control in infected herds is a challenge (10).

Over recent years, genomics, transcriptomics and proteomics were introduced to overcome the lack of efficient diagnostic methods in the preclinical stages of the disease (11–16); the aim was to identify specific pathways related to disease progression through the study of the expression of genes and proteins. In this way, biomarkers related to MAP infection can be determined (11, 14–16). In addition, metabolomics has emerged as a means to identify altered metabolic pathways in infected animals, by characterizing the metabolic profiles of cattle experimentally infected with MAP (13). Serum lipidomics of control and MAP infected cattle were also explored, utilizing high-resolution mass spectrometry, with the data showing that altered availability of choline-containing lipids occurs late in the disease process, and it is most likely a result of malnutrition and altered biosynthetic capacities of the liver and the gastrointestinal tract (17). Volatile organic signatures of breath were defined by gas-chromatography to differentiate healthy cattle from MAP infected cattle (18). In human medicine, the metabolomic approach was used to differentiate latent infection caused by *Mycobacterium tuberculosis* from active tuberculosis. The identification of mycobacterial biomarkers of infection could contribute to faster and more accurate diagnosis than the tuberculin skin or interferon gamma tests (19).

In the field of metabolomics, direct analysis in real time coupled to high resolution mass spectrometry (DART-HRMS) is considered an innovative, ambient mass spectrometric approach, successfully applied in clinical screening, microbiology, food safety, and toxicology (20–30). DART-HRMS requires minimal sample preparation and it has already demonstrated its accuracy, intra-sample repeatability and rapidity, with the aim of reducing the burden of chemical laboratories. In addition, DART-HRMS

allows screening the metabolic profile without any prior knowledge of the identity of the metabolic features or their physicochemical characteristics (31). In parallel with genomic and transcriptomic analysis (11, 14–16, 32), this non-targeted approach produces a large amount of information within a very short time by the application of different extraction procedures and instrumental modalities. Statistical strategies called data fusion can then be applied to adequately integrate the data into a unique global dataset that can be submitted to multivariate analysis (33, 34).

In the present study, sera collected from MAP infected, infectious and negative animals were submitted to polar and non-polar extraction, then analyzed by DART-HRMS in positive and negative ion modes. Latent variables extracted from partial least squares discriminant analysis (PLS-DA) of single datasets were merged and submitted to a fused-PLS-DA with the aim of teasing out the characteristic molecular markers of the MAP infected, infectious and negative status.

MATERIALS AND METHODS

Animal Selection and Time Course of the Study

Holstein cattle were selected from four dairy farms with known paratuberculosis initial seroprevalences of >10% and were divided into age-cohorts by reproduction cycle: heifers, primiparous, and pluriparous cows. A total of 356 animals were monitored up to 4 lactations, with blood and fecal sample collections at 30 ± 15 days before the expected calving date to minimize individual metabolic variations except for young heifers that were recruited at 13–15 months of age. During the pre-calving period, cows do not produce milk and the metabolic-hormonal changes that prepare the animal for calving are not established yet. MAP affected animals and cattle in bad health condition were excluded from the study. Blood sample collection was performed under authorization n. 506/2015 of the Italian Ministry of Health for the use of animals for experimental purposes.

Sample Collection and Testing for JD

Blood samples were collected from the jugular vein in an anticoagulant free vacutainer tube, left to coagulate at room temperature for 2–4 h and centrifuged at 2,500 rpm for 5 min. Aliquots from the sera obtained were used for detecting serum antibodies against MAP using a commercial enzyme-linked immunosorbent assay (ELISA) (IDEXX Paratuberculosis Screening Ab, IDEXX Laboratories, Inc.) and applying the manufacturer's instructions for analysis. Two other aliquots of each serum were stored at -80°C for metabolomic analyses and for possible future analyses. Suspect and positive sera were submitted to an ELISA biphasic confirmation test (IDEXX Paratuberculosis Verification Ab, IDEXX Laboratories, Inc.).

Individual fecal samples were collected from the rectal ampulla and analyzed applying microbiological and molecular diagnostic methods for MAP identification. One fecal aliquot from each animal was stored at -80°C for possible future analyses.

All samples were processed for testing by direct real-time PCR (qPCR) and culture on modified Middlebrook 7H9 liquid media (7H9+). In brief, 2 g of feces were resuspended in 10 ml of water; mixtures were rocked on a horizontal shaker for 30 min and left to sediment for an additional 30 min. At the end of this step, an aliquot of 300 μ l of supernatant was collected for PCR testing and 5 ml were processed for culture following a modified double-decontamination and centrifugation method (35). In brief, the supernatant was resuspended in 10 ml of 0.75% hexadecylpyridinium, incubated overnight at 37°C, centrifuged, resuspended in PANTA antimicrobial mixture and reincubated overnight at 37°C. The next day, 200 μ l were inoculated into two 7H9+ tubes and incubated at 37°C for 6 weeks. At the end of the period, the 7H9+ cultures were examined by Ziehl-Nielsen staining and the broth cultures were confirmed by real-time PCR.

The same PCR protocol was used for both confirmatory test and direct analysis. In brief, 300 μ l of supernatant or culture medium was subjected to a bead-beating step in order to enhance MAP DNA recovery as previously described (36). DNA extraction was performed manually with the High Pure PCR preparation kit (Roche Diagnostic, Mannheim, Germany) or by the automated MagMAX™ 96 Viral Isolation Kit (Ambion, Austin, USA) using the Microlab Starlet automated extraction platform (Hamilton Robotics, Bonaduz, Switzerland) or the KingFisher Flex instrument (ThermoFisher Scientific Inc., Worcester, MA, USA). In all cases, DNA extraction was performed according to the manufacturer's instructions. Real-time amplification was performed in a 7300 Real-Time PCR System (Applied Biosystems, Nieuwerkerk a/d IJssel, The Netherlands) or a CFX96 Touch Deep Well real-time PCR system (Bio-Rad Laboratories, Segrate, Italy). The amplification mixture contained 900 nM of each primer, 200 nM of probe, and 1X 1 \times Taq GOLD PCR Master Mix (Applied Biosystems) in a volume of 25 μ l. The primers (Map668F-5'-GGCTGAT CGGACCCG-3', Map791R-5'-TGGTAGCCAGTAAGCAG GATCA-3') and probe (Map718 5'-FAM-ATACTTTCGG CGCTGGAACGCGC-TAMRA) were designed on a MAP-specific portion of IS900. The real-time PCR program was 2 min at 50°C followed by 10 min at 95°C, 40 cycles at 95°C for 15 s and 60°C for 1 min. A cut-off value of 38 cycles was set according to the laboratory's validation procedure (35).

JD Health Status Assignment and Sample Selection for DART-HRMS Analysis

Out of 356 animals, a total of 854 samples were collected during the study period resulting in a mean value of 2.40 samplings per cattle (range 1–5). Regarding JD testing, the frequency of positive animals along the study period resulted to be 6.23% by serology and 11.05% by fecal PCR/culture. At the end of the prospective study, the infectious status was assigned to a serum sample based on a seroconversion for MAP by ELISA accompanied by a positive result to fecal PCR or culture. The infected status was retrospectively assigned to the previous sampling of the animals classified as infectious, in which all JD tests (ELISA, PCR and culture) produced negative results.

The negative status was eventually assigned to exposed cohort animals selected from the same infected herds with the presence of at least one subsequent JD negative result after the selected sampling. These control animals were matched to cases according to sampling date and age category (heifers, primiparous cows, and pluriparous cows) in order to minimize the variability due to dietary and management conditions. The average number of samplings for these animals was 2.84 (range 2–4).

From the collection of sera stored at –80°C, 17 sera of infectious animals, 10 sera of infected animals and 20 sera of negative animals were selected and then analyzed by “DART-HRMS.” The age of the selected animals averaged 51.4 months (range 13–119 months).

DART-HRMS Analysis

Sample Extraction

Frozen aliquots of sera were thawed and submitted to two different extraction procedures. In the first protocol, 200 μ L of serum were diluted in 800 μ L of water and methanol (H₂O:MeOH; 20:80 v/v) solution (MilliQ water and methanol HPLC-grade with 99.9% purity, from VWR International, Radnor, USA), vortexed for 30 s, sonicated for 15 min, and centrifuged for 5 min at 12,000 rpm. In the second extraction procedure, 200 μ L of serum were diluted in 800 μ L of pure ethyl acetate (EtAc) (99.9% purity, Carlo Erba Reagents, Cornaredo, Italy), vortexed for 30 s, sonicated for 15 min, and centrifuged for 5 min at 12,000 rpm.

DART-HRMS

The instrumental analyses were carried out using a DART SVP 100 ion source (IonSense, Saugus, USA) coupled with an Exactive Orbitrap (Thermo Fisher Scientific, Waltham, USA). The DART source was coupled with a Dip-it^(R) sampler (IonSense, Saugus, MA, USA). A Vapor interface (IonSense, Saugus, USA) facilitated the passage of the ions from the DART source to the mass spectrometer. The distance between the DART gun and the ceramic transfer tube of the Vapor interface was 12 mm. The optimized DART settings were as follows: grid voltage 250 V, temperature 300°C, sample speed 0.3 mm/s, and a single time analysis of 0.66 min. The system parameter settings for the mass spectrometer were as follows: 55 S-lens RF level, capillary temperature 300°C, and maximum injection time 10 ms. The resolution was set to 70,000 FWHM and the mass range was 50–1,000 Da in both positive and negative ion modes. In positive ion mode, a vial with an aqueous solution of 25% ammonia was positioned below the DART gun exit, working as a dopant to facilitate and stabilize the formation of [M+NH₄]⁺ ions.

All DART-MS analyses were run with an automated gain control target setting of 3×10^6 . Homemade Dip-it tips (IonSense, Saugus, USA) were inserted into a holder of the autosampler, and then 5 μ L of each extract were spotted onto each Dip-it tip. Subsequently, the Dip-it tips automatically moved at a constant speed of 0.3 mm/s throughout the DART gun exit and ceramic tube of the Vapor interface. The duration of desorption from the surface of each tip was about 20 s.

The samples were analyzed in triplicate and XCalibur QualBrowser software (Thermo Fisher Scientific, Waltham,

USA) was used to visualize the entire spectra in raw format. These were converted to mzML files using Proteowizard and then opened with mMass software (<http://www.mmass.org/>), which allowed interpretation of the mass spectrometry data and assignment of ions using the online METLIN (<https://metlin.scripps.edu>) and HUMAN METABOLOME DATABASE (www.hmdb.ca) libraries. Prior to statistical analysis, the spectra of the four datasets (two extraction solvents *per* two ion modes) were converted into .csv files with Rstudio 3.6.1 software (RStudio Team, 2016; RStudio Integrated Development for R; RStudio, Inc., Boston, USA).

Data Processing and Statistical Analysis

The DART-HRMS spectral data, acquired in triplicate and not averaged, were statistically analyzed using MetaboAnalyst 4.0 web platform (www.metaboanalyst.ca) and Rstudio 3.6.1 software (37). The three replicates were used independently as done previously in several chemometric studies (38, 39). The signals of the four datasets were loaded onto MetaboAnalyst 4.0 web platform and aligned with a tolerance of 0.008 Da. We removed the ion signals with more than 75% of missing values (no detected ion intensity) over all the samples. The ions with <75% of missing values had them replaced with 1/5 of the recorded lowest intensity (40). Isotopes were removed. Normalization by sum was applied to the signals, whereby each feature was normalized by Pareto scaling. First, supervised partial least squared discriminant analysis (PLS-DA) was performed on the four separate datasets (2 extraction solvents \times 2 instrumental ion modes) to evaluate the possible improved discrimination achieved by mid-level data fusion (**Supplementary Figures 1–4**).

A low level data fusion was also tested and described in the **Supplementary Material (Supplementary Figure 5)**.

Mid-Level Data Fusion

Using Rstudio 3.6.1 software, the first five PLS-DA score components of each dataset were fused (concatenated) and submitted to a new PLS-DA with the aim at discriminating the three groups of samples (30). Evaluating the R^2 , Q^2 , and accuracy of each separate PLS-DA, (–)DART-HRMS spectra of polar extraction were excluded because they provided poor information. Mid-level data fusion of the three most informative datasets was performed and the merged data submitted to fused-PLS-DA clustering (41). Ten-fold cross-validation was performed on the entire dataset to evaluate the performance of the fused-PLS-DA and to select the best number of components within the loading tables of each separate PLS-DA. As recommended by Borràs et al. (41), to extract the PLS-DA features, the best number of components (5) was chosen when the classification error obtained by cross-validation was minimized.

Finally, only the ions whose loadings had an absolute value higher than 0.3 were retained from the first five components of the three separate PLS-DA (**Figure 1**, blue boxes). A table with the samples in the rows and the selected significant ions in the columns was built (**Figure 1**, pink box). The obtained table was used to calculate Pearson's distance and Ward linkage to

determine the correlation of the selected ions among the three JD health status groups.

RESULTS

In this study, a dual mode DART-HRMS analysis was performed on sera extracted using polar and non-polar solvents with the aim of finding the changes in metabolites' level in MAP-infected and infectious cattle as compared to those negative. Four DART-HRMS spectral datasets were thus acquired. Once pre-processed, each dataset was submitted to PLS-DA.

To overcome the difficulty of handling high dimensional datasets, a data reduction was conducted to fade out the most significant variables capable of discriminating the three MAP status groups. To this aim, a mid-level data fusion strategy was attempted by operating at the level of features and thus capturing only the relevant differences in the four datasets (33, 41, 42). In this case, good separation was obtained within the PC1 vs. PC2 score space (**Supplementary Figure 6**), explaining 32.9 and 10.6% of the total variance of the model. Although we obtained a good separation, we removed the less informative dataset.

To further improve the discrimination, we evaluated the R^2 , Q^2 , and accuracy of each separate PLS-DA (data not shown) and realized that (–)DART-HRMS of polar extractions provided no informative data for the discrimination of the groups. Hence, we merged the scores of the three most informative datasets and performed a PLS-DA. The score plot showed an improvement in clustering (**Figure 2**), with most samples from the MAP negative group correctly assigned to their 0.95-ellipses confidence interval, and some samples that overlapped between the infected and infectious groups. In this case, PC1 vs. PC2 explained 37.3 and 11.9% of the total variance of the model.

The 12 most informative m/z values were extrapolated by selecting the loadings with absolute value higher than 0.3. They were then fused in a single dataset and submitted to Pearson's distance and Ward linkage calculation. In this way, correlation between ions and MAP status groups was obtained. **Table 1** reports the m/z values that codified each MAP status group in terms of the most abundant molecular features. Representative DART-HRMS spectra showing the most informative m/z values are reported in the **Supplementary Material (Supplementary Figures 8–10)**.

Figure 3 shows box plots with the relative intensities of the observed biomarkers. Sera of infected cattle presented higher relative abundances (compared to the other MAP groups studied) of dimethylethanolamine (m/z 72.0815 in positive ion mode), isobutyric acid (m/z 106.0867 in positive ion mode), creatine a/o creatinine (m/z 114.0665 in positive ion mode), rhamnitol (m/z 167.0917 in positive ion mode), tryptamine (m/z 178.1339 in positive ion mode), palmitic acid (m/z 255.2333 in positive ion mode), and the unassigned ion, m/z 90.0919. The serum profiles of infected cattle were also characterized by lower relative intensity of urea (the dimer of m/z 121.0722 in positive ion mode). In addition, the molecular signature of sera from infectious cattle showed higher relative abundance of dimethylethanolamine (m/z 72.0815 in positive ion mode),



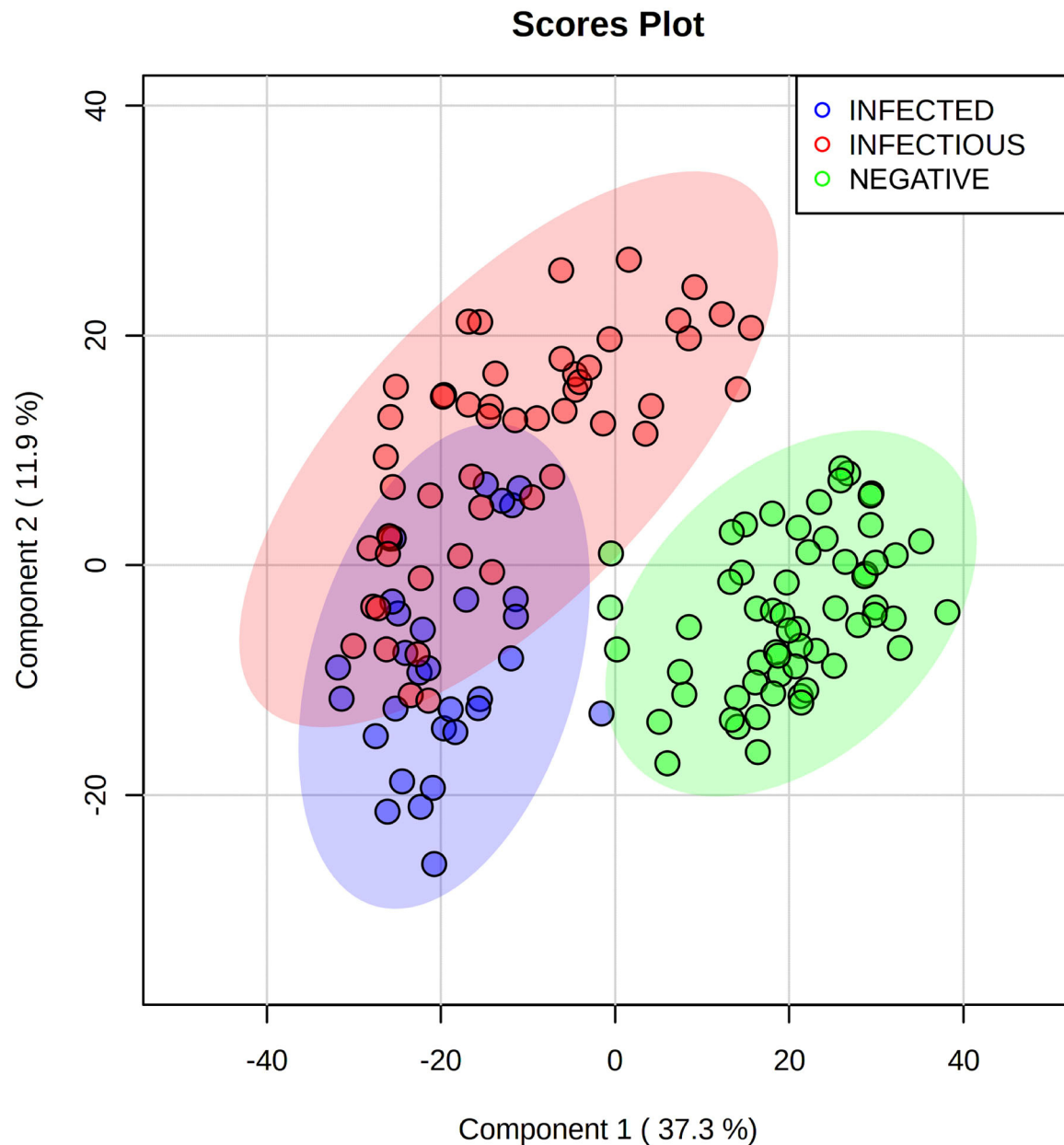


FIGURE 2 | Partial least squares discriminant analysis score plot of the three most informative Direct analysis in real-time high-resolution mass spectrometry datasets merged by mid-level data fusion. MAP infected (blue) and infectious (red) cattle are successfully discriminated from negative (green) cattle. A slight overlap can be seen between infected and infectious groups. Three repetitions for each sample were used.

We applied multimodality DART-HRMS that allows more comprehensive information to be obtained, although with the counterpart of its over-dispersion in the case of big dimensional data. To overcome this issue, we exploited a mid-level data fusion strategy, which demonstrated good discriminatory power. We confirmed that this technique can catch the existent variability among groups and that compression of the high dimensional data was imperative to fade out the existent correlations between markers (33, 34). DART-HRMS coupled

to statistical analysis demonstrated its capability to discriminate the negative group from infected and infectious cattle. On the other hand, this approach provided a tendency to discrimination between MAP infected and infectious animals due to a partial superposition of their metabolic profiles (**Figure 2** and **Supplementary Figures 8–10**).

MAP infected and infectious cattle had higher serum levels of creatine/creatinine, palmitic acid, dimethylethanolamine and tryptamine than did negative cattle.

TABLE 1 | List of discriminant (+/−) direct analysis in real time high resolution mass spectrometry metabolites observed in sera from groups of MAP infected, infectious and negative cattle.

Samples	<i>m/z</i> DART-HRMS	<i>m/z</i> theor	error (ppm)	Elemental formula	Type of ion	Instrument ion mode and extraction solvent	Tentative assignment
INFECTED SERA	72.0815	72.0814	−1.39	C ₄ H ₁₁ N ₃ O	[M+H−H ₂ O] ⁺	(+) Pure EtAc	Dimethylethanolamine
	90.0919					(+) MeOH:H ₂ O (80:20 v/v)	N/A
	106.0867	106.0863	−3.77	C ₄ H ₈ O ₂	[M+NH ₄] ⁺	(+) Pure EtAc	Isobutyric acid ⁺
						(+) MeOH:H ₂ O (80:20 v/v)	
	114.0665	114.0668	−2.6	C ₄ H ₉ N ₃ O ₂	[M+H−H ₂ O] ⁺	(+) MeOH:H ₂ O (80:20 v/v)	Creatine ⁺
		114.0663	1.75	C ₄ H ₇ N ₃ O	[M+H] ⁺		Creatinine ⁺
	167.0917	167.0914	1.80	C ₆ H ₁₄ O ₅	[M−H] ⁺	(+) Pure EtAc	Rhamnitrol
INFECTIOUS SERA	178.1339	178.1339	0	C ₁₀ H ₁₂ N ₂	[M+NH ₄] ⁺	(+) MeOH:H ₂ O (80:20 v/v)	Tryptamine
	255.2333	255.2330	1.18	C ₁₆ H ₃₂ O ₂	[M−H] [−]	(−) Pure EtAc	Palmitic acid (16:0)
	72.0815	72.0814	1.39	C ₄ H ₁₁ NO	[M+H−H ₂ O] ⁺	(+) MeOH:H ₂ O (80:20 v/v)	Dimethylethanolamine
	76.0764					(+) MeOH:H ₂ O (80:20 v/v)	N/A
	114.0665	114.0668	−2.6	C ₄ H ₉ N ₃ O ₂	[M+H−H ₂ O] ⁺	(+) Pure EtAc	Creatine ⁺
		114.0663	1.75	C ₄ H ₇ N ₃ O	[M+H] ⁺		Creatinine ⁺
	121.0722	121.0720	1.65	CH ₄ N ₂ O	[2M+H] ⁺	(+) MeOH:H ₂ O (80:20 v/v)	Urea dimer ⁺
NEGATIVE SERA	178.1339	178.1339	0	C ₁₀ H ₁₂ N ₂	[M+NH ₄] ⁺	(+) Pure EtAc	Tryptamine
	255.2333	255.2330	1.18	C ₁₆ H ₃₂ O ₂	[M−H] [−]	(−) Pure EtAc	Palmitic acid (16:0)
	59.9855					(−) Pure EtAc	N/A
	61.0404					(+) MeOH:H ₂ O (80:20 v/v)	N/A
	121.0722	121.0720	1.65	CH ₄ N ₂ O	[2M+H] ⁺	(+) MeOH:H ₂ O (80:20 v/v)	Urea dimer ⁺
	128.0353	128.0353	0	C ₅ H ₇ NO ₃	[M−H] [−]	(−) Pure EtAc	Pyroglutamic acid ⁺
		128.0348	−3.9	C ₅ H ₉ NO ₄	[M−H−H ₂ O] [−]		Glutamic acid ⁺

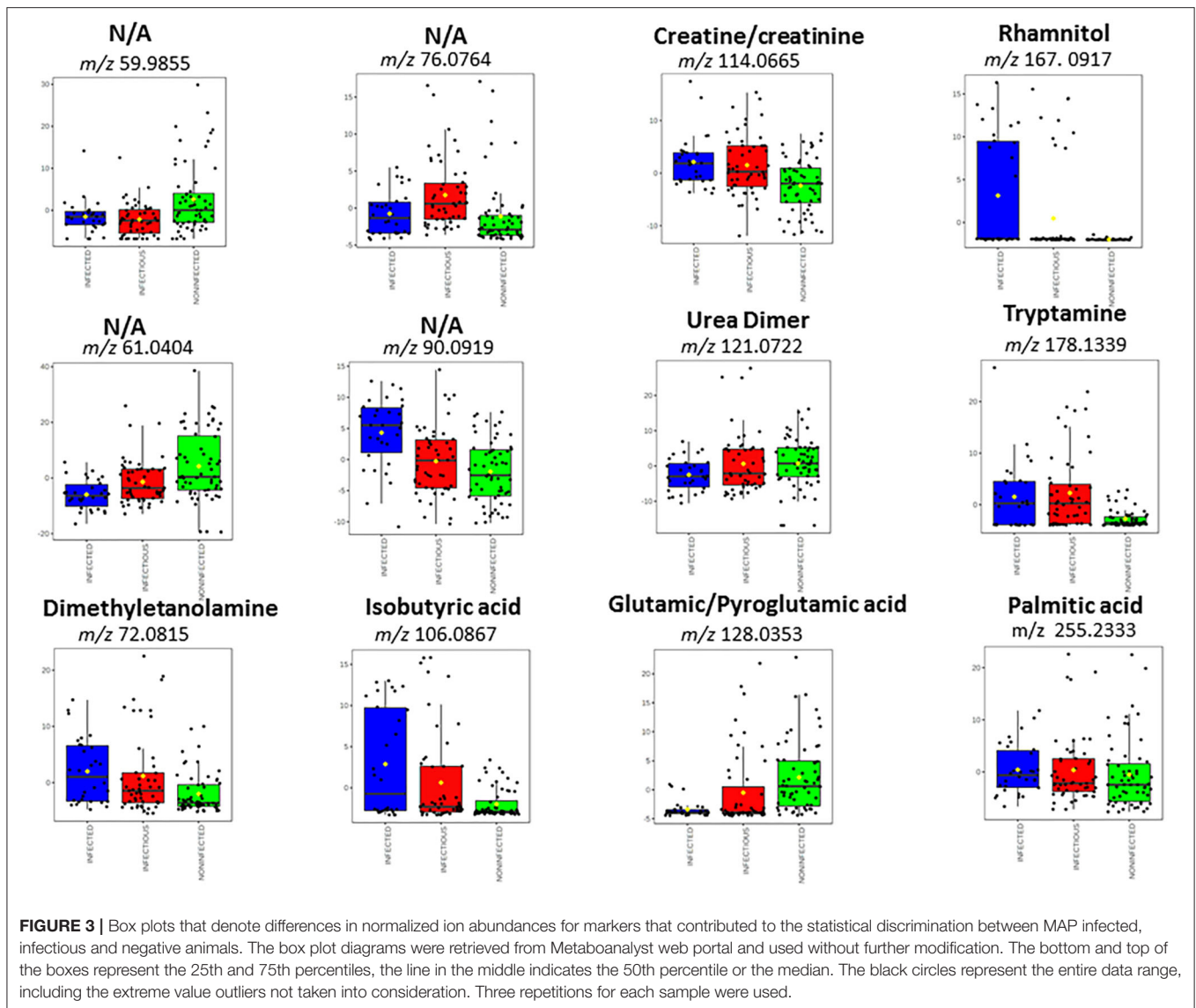
The *m/z* values, theoretical mass, error (ppm), elemental formula, type of ion, ion mode and extraction procedure, tentative assignment, and literature references are reported.

⁺(13).

The high creatine/creatinine abundances, already reported in experimental MAP infection (13), could be associated with muscle wasting due to the protein catabolism determined by the disease progression the led to a reduced energetic intake (47). In addition, we observed a higher abundance of palmitic acid in both MAP infected and infectious cattle than in negative animals. Alterations in the synthesis and absorption of phospholipids and sphingolipids presumably contribute to the circulation of high levels of the free fatty acid. In this context, Wood et al. found significant decrease in circulating levels of phospholipids and sphingolipids probably due to the dysfunction of the gastrointestinal (GI) epithelium and the liver (17). Furthermore, Thirunavukkarasu *et al* demonstrated the altered expression of genes associated with cholesterol and lipid metabolism (48). In parallel, in patients with active *Mycobacterium tuberculosis* infection, phosphatidylglycerol (PG 16:0_18:1), the structural components of which are oleic acid and palmitic acid, was one

of the molecules significantly elevated in the plasma (49). In the present study, the hydrolysis of phospholipids could have occurred during the extraction procedure or DART ionization.

In the same vein, high relative abundances of dimethylethanolamine were found in sera of both infected and infectious cattle. Dimethylethanolamine is a structural analogue of choline that is involved in the metabolism of phospholipids, absorption of which can be altered by gastrointestinal microbiome alteration (50). High levels of tryptamine (involved in tryptophan metabolism), observed in both infected and infectious animals, can be explained by important changes in protein turnover or deficiencies in MAP infected cattle (13). Interestingly, higher levels of isobutyric acid were measured in infected animals than in negative animals (Table 1 and Figure 3). Higher relative intensities of isobutyric acid in infected than in negative sera could be related to inflammation of the gut due to MAP infection.



The lower urea level in MAP-infected cattle has already been reported by De Buck et al. (13), who interpreted this phenomenon as being due to increased muscle turnover, likely altering amino acid metabolism and reducing energy intake.

Interestingly, while De Buck et al. (13) observed increased glutamic acid in both MAP infected and control groups, due to the influence of developmental and diet changes of the life of the calves, we observed higher glutamic/pyroglutamic acid levels only in sera of negative animals. Glutamic acid is involved in energy metabolism, immunity and GI function. Its scarcity in infected and infectious animals could be explained by a low immune response when cattle are in the advanced JD stages and by the damage of GI system. Since glutamic acid is also produced by muscles, low serum levels could also be associated with muscle wasting.

Finally, pyroglutamic acid and glutamic acid are involved in glutathione (GSH) metabolism. Pyroglutamic acid is a downstream metabolite of GSH metabolism, and glutamic acid is involved in the synthesis of GSH. GSH is an important antioxidant that protects cells from oxidative stress. Both were lower in the sera of infected and infectious cattle than in that of negative cattle, suggesting that MAP alters GSH metabolism.

In conclusion potential caveats of this prospective field study on natural MAP infection in dairy cattle must be taken into account. Considering the long MAP incubation period, we do not exclude that negative animals could have changed their status after the latest sampling carried out at least 1 year after the selected time-point.

Note that we made any possible effort to reduce metabolic variability due to season, feeding and management, by: (i) testing

all animals (except young heifers) during the pre-calving period and (ii) matching negative animals to cases by sampling date and age category. Finally, individual differences could have affected the results because of the small sized groups.

CONCLUSION

The main goal of mid-level data fusion is to optimize high dimensional information, exploit the synergies of information provided by different analytical strategies, and fade out the existent correlations between markers and groups. The construction of this model using DART-HRMS data revealed the characteristic serum metabolites of MAP infected, infectious, and negative cattle. The model, built by fusing the three most informative DART-HRMS datasets, produced a reasonably high degree of accuracy, suggesting the markers are capable of discriminating the health status of cattle with regard to MAP infection. In the future, the model will be populated with results from more animals in order to improve its robustness and performance. Proper validation of the model will be performed to evaluate its discriminative capacity and verify its potential for diagnostic purposes. Prospectively producing an earlier diagnosis, it will then be easier to manage infected cattle, prevent the diffusion of the pathogen and, thus, control JD on dairy farms.

DATA AVAILABILITY STATEMENT

The raw data supporting the conclusions of this article will be made available by the authors, without undue reservation.

REFERENCES

- Chacon O, Bermudez LE, Barletta RG. John's disease, inflammatory bowel disease, and *Mycobacterium paratuberculosis*. *Annu Rev Microbiol.* (2004) 58:329–63. doi: 10.1146/annurev.micro.58.030603.123726
- Clarke CJ. The pathology and pathogenesis of paratuberculosis in ruminants and other species. *J Comp Pathol.* (1997) 116:217–61. doi: 10.1016/S0021-9975(97)80001-1
- Whitlock RH, Buerget C. Preclinical and clinical manifestations of paratuberculosis (including pathology). *Vet Clin North Am Food Anim Pract.* (1996) 12:345–56. doi: 10.1016/S0749-0720(15)30410-2
- Lambrecht RS, Collins MT. *Mycobacterium paratuberculosis*. Factors that influence mycobactin dependence. *Diagn Microbiol Infect Dis.* (1992) 15:239–46. doi: 10.1016/0732-8893(92)90119-E
- Sweeney RW. Transmission of paratuberculosis. *Vet Clin North Am Food Anim Pract.* (1996) 12:305–12. doi: 10.1016/S0749-0720(15)30408-4
- Whittington R, Donat K, Weber MF, Kelton D, Nielsen SS, Eisenberg S, et al. Control of paratuberculosis: who, why and how. A review of 48 countries. *BMC Vet Res.* (2019) 15:198. doi: 10.1186/s12917-019-1943-4
- Rankin JD. The experimental infection of cattle with mycobacterium johnei: IV. Adult cattle maintained in an infectious environment. *J Comp Pathol.* (1962) 72:113–7. doi: 10.1016/S0368-1742(62)80013-7
- Nielsen SS, Toft N. Ante mortem diagnosis of paratuberculosis: a review of accuracies of ELISA, interferon- γ assay and faecal culture techniques. *Vet Microbiol.* (2008) 129:217–35. doi: 10.1016/j.vetmic.2007.12.011
- Whitlock RH, Wells SJ, Sweeney RW, Van Tiem J. ELISA and fecal culture for paratuberculosis (John's disease): sensitivity and specificity of each method. *Vet Microbiol.* (2000) 77:387–98. doi: 10.1016/S0378-1135(00)00324-2
- Arsenault RJ, Maattanen P, Daigle J, Potter A, Griebel P, Napper S. From mouth to macrophage: mechanisms of innate immune subversion

ETHICS STATEMENT

The animal study was reviewed and approved by authorization n. 506/2015 of the Italian Ministry of Health. Written informed consent was obtained from the owners for the participation of their animals in this study.

AUTHOR CONTRIBUTIONS

NP, RP, LP, and JD designed the research. BM, MB, PF, MD, and AS performed the experiments. LP contributed to sampling. AM performed the statistical analyses. AT, IP, and AM interpreted the data and wrote the manuscript. NP, RP, and JD interpreted the results and edited the manuscript. All contributed to the editing the manuscript.

FUNDING

This work was supported by the Italian Ministry of Health [grant number IZS VE 08/15 RC] research project: Applicazione di metodi spettroscopici e spettrometrici ad elevata capacità per l'identificazione di biomarcatori sierici associati all'infezione paratuberculare nei bovini da latte.

SUPPLEMENTARY MATERIAL

The Supplementary Material for this article can be found online at: <https://www.frontiersin.org/articles/10.3389/fvets.2020.625067/full#supplementary-material>

- by *Mycobacterium avium* subsp. paratuberculosis *Vet Res.* (2014) 45:54. doi: 10.1186/1297-9716-45-54
- Casey JL, Sanalla AM, Tamvakis D, Thalmann C, Carroll EL, Parisi K, et al. Peptides specific for *Mycobacterium avium* subspecies paratuberculosis infection: diagnostic potential. *Protein Eng Des Sel.* (2011) 24:589–96. doi: 10.1093/protein/gzr026
- David J, Barkema HW, Mortier R, Ghosh S, De Buck J. Gene expression profiling and putative biomarkers of calves 3 months after infection with *Mycobacterium avium* subspecies paratuberculosis. *Vet Immunol Immunopathol.* (2014) 160:107–17. doi: 10.1016/j.vetimm.2014.04.006
- De Buck J, Shaykhtudinov R, Barkema HW, Vogel HJ. Metabolomic profiling in cattle experimentally infected with *Mycobacterium avium* subsp. Paratuberculosis. *PLoS One.* (2014) 9:e111872. doi: 10.1371/journal.pone.0111872
- Seth M, Lamont EA, Janagama HK, Widdel A, Vulchanova L, Stabel JR, et al. Biomarker discovery in subclinical mycobacterial infections of cattle. *PLoS One.* (2009) 4:e5478. doi: 10.1371/journal.pone.0005478
- Skovgaard K, Grell SN, Heegaard PM, Jungersen G, Pudrith CB, Coussens PM. Differential expression of genes encoding CD30L and P-selectin in cattle with John's disease: progress toward a diagnostic gene expression signature. *Vet Immunol Immunopathol.* (2006) 112:210–24. doi: 10.1016/j.vetimm.2006.02.006
- Zhong L, Taylor D, Begg DJ, Whittington RJ. Biomarker discovery for ovine paratuberculosis (John's disease) by proteomic serum profiling. *Comp Immunol Microbiol Infect Dis.* (2011) 34:315–26. doi: 10.1016/j.cimid.2011.03.001
- Wood PL, Erol E, Hoffis GF, Steinman M, DeBuck J. Serum lipidomics of bovine paratuberculosis: disruption of choline-containing glycerophospholipids and sphingolipids. *SAGE Open Med.* (2018) 6:2050312118775302. doi: 10.1177/2050312118775302

18. Bergmann A, Trefz P, Fischer S, Klepik K, Walter G, Steffens M, et al. *In vivo* volatile organic compound signatures of *Mycobacterium avium* subsp. *Paratuberculosis*. *PLoS One*. (2015) 10:e0123980. doi: 10.1371/journal.pone.0123980
19. Mehaffy C, Kruh-Garcia NA, Graham B, Jarlsberg LG, Willyerd CE, Borisov A, et al. Identification of *Mycobacterium tuberculosis* peptides in serum extracellular vesicles from persons with latent tuberculosis infection. *J Clin Microbiol*. (2020) 58:e00393-20. doi: 10.1128/JCM.00393-20
20. Cody RB, McAlpin CR, Cox CR, Jensen KR, Voorhees KJ. Identification of bacteria by fatty acid profiling with direct analysis in real time mass spectrometry. *Rapid Commun Mass Spectrom*. (2015) 29:2007–12. doi: 10.1002/rcm.7309
21. Gu H, Pan Z, Xi B, Asiago V, Musselman B, Raftery D. Principal component directed partial least squares analysis for combining nuclear magnetic resonance and mass spectrometry data in metabolomics: application to the detection of breast cancer. *Anal Chim Acta*. (2011) 686:57–63. doi: 10.1016/j.aca.2010.11.040
22. Guo T, Yong W, Jin Y, Zhang L, Liu J, Wang S, et al. Applications of DART-MS for food quality and safety assurance in food supply chain. *Mass Spectrom Rev*. (2017) 36:161–87. doi: 10.1002/mas.21466
23. Halouzka R, Zeljković SC, Klejdus B, Tarkowski P. Analytical methods in strigolactone research. *Plant Methods*. (2020) 16:1–13. doi: 10.1186/s13007-020-00616-2
24. Li Y. Application of DART-MS in clinical and pharmacological analysis. *Direct Anal Real Time Mass Spectrom*. (2018) 223–40. doi: 10.1002/9783527803705.ch9
25. Miano, B., Righetti, L., Piro, R., Dall'Asta, C., Folloni, S., Galaverna, G., et al. (2018). Direct analysis real-time-high-resolution mass spectrometry for *Triticum* species authentication. *Food Addit Contam A* 35:2291–7. doi: 10.1080/19440049.2018.1520398
26. Pavlovich MJ, Musselman B, Hall AB. Direct analysis in real time-Mass spectrometry (DART-MS) in forensic and security applications. *Mass Spectrom Rev*. (2018) 37:171–87. doi: 10.1002/mas.21509
27. Pozzato N, Piva E, Pallante I, Bombana D, Stella R, Zanardello C, et al. Rapid detection of asperphenamate in a hay batch associated with constipation and deaths in dairy cattle. The application of DART-HRMS to veterinary forensic toxicology. *Toxicon*. (2020) 187:122–8. doi: 10.1016/j.toxicon.2020.08.022
28. Song, Y.-q., Liao, J., Zha, C., Wang, B., and Liu, C. C. (2015). A novel approach to determine the tyrosine concentration in human plasma by DART-MS/MS. *Anal Methods*. 7:1600–5. doi: 10.1039/C4AY02566K
29. Wang C, Zhu H, Cai Z, Song F, Liu Z, Liu S. Newborn screening of phenylketonuria using direct analysis in real time (DART) mass spectrometry. *Anal Bioanal Chem*. (2013) 405:3159–64. doi: 10.1007/s00216-013-6713-8
30. Riuzzi G, Tata A, Massaro A, Bisutti V, Lanza I, Contiero B, et al. Authentication of forage-based milk by mid-level data fusion of (+/-) DART-HRMS signatures. *Int Dairy J*. (2021) 112:104859. doi: 10.1016/j.idairyj.2020.104859
31. Aszyk J, Kubica P, Wozniak MK, Namieśnik J, Wasik A, Kot-Wasik A. Evaluation of flavour profiles in e-cigarette refill solutions using gas chromatography-tandem mass spectrometry. *J Chromatogr A*. (2018) 1547:86–98. doi: 10.1016/j.chroma.2018.03.009
32. You Q, Verschoor CP, Pant SD, Macri J, Kirby GM, Karrow NA. Proteomic analysis of plasma from Holstein cows testing positive for *Mycobacterium avium* subsp. *paratuberculosis* (MAP). *Vet Immunol Immunopathol*. (2012) 148:243–51. doi: 10.1016/j.vetimm.2012.05.002
33. Biancolillo A, Bucci R, Magri AL, Magri AD, Marini F. Data-fusion for multiplatform characterization of an Italian craft beer aimed at its authentication. *Anal Chim Acta*. (2014) 820:23–31. doi: 10.1016/j.aca.2014.02.024
34. Pirro V, Oliveri P, Ferreira CR, González-Serrano AF, Machaty Z, Cooks RG. Lipid characterization of individual porcine oocytes by dual mode DESI-MS and data fusion. *Anal Chim Acta*. (2014) 848:51–60. doi: 10.1016/j.aca.2014.08.001
35. Pozzato N, Gwozd J, Gastaldelli M, Capello K, Dal Ben C, Stefani E. Evaluation of a rapid and inexpensive liquid culture system for the detection of *Mycobacterium avium* subsp. *paratuberculosis* in bovine faeces. *J. Microbiol. Methods*. (2011) 84:413–7. doi: 10.1016/j.mimet.2011.01.019
36. Pozzato N, Stefani E, Capello K, Muliari R, Vicenzoni G. *Mycobacterium avium* subsp. *paratuberculosis* as a template in the evaluation of automated kits for DNA extraction from bovine organs. *World J Microbiol Biotechnol*. (2011) 27:31–7. doi: 10.1007/s11274-010-0423-6
37. Chong, J., Soufan, O., Li, C., Caraus, I., Li, S., Bourque, G., et al. (2018). MetaboAnalyst 4.0: towards more transparent and integrative metabolomics analysis. *Nucleic Acids Res*. 46:W486–W94. doi: 10.1093/nar/gky310
38. Alves JO, Botelho BG, Sena MM, Augusti R. Electrospray ionization mass spectrometry and partial least squares discriminant analysis applied to the quality control of olive oil. *J Mass Spectrom*. (2013) 48:1109–15. doi: 10.1002/jms.3256
39. Woolman M, Ferry I, Kuzan-Fischer CM, Wu M, Zou J, Kiyota T, et al. Rapid determination of medulloblastoma subgroup affiliation with mass spectrometry using a handheld picosecond infrared laser desorption probe. *Chem Sci*. (2017) 8:6508–19. doi: 10.1039/C7SC01974B
40. Chong J, Wishart DS, Xia J. Using MetaboAnalyst 4.0 for comprehensive and integrative metabolomics data analysis. *Curr Protoc Bioinform*. (2019) 68:e86. doi: 10.1002/cpbi.86
41. Borràs, E., Ferré, J., Boqué, R., Mestres, M., Aceña, L., Calvo, A., et al. Olive oil sensory defects classification with data fusion of instrumental techniques and multivariate analysis (PLS-DA). *Food Chem*. (2016) 203:314–22. doi: 10.1016/j.foodchem.2016.02.038
42. Borràs E, Ferré J, Boqué R, Mestres M, Aceña L, Busto O. Data fusion methodologies for food and beverage authentication and quality assessment - a review. *Anal Chim Acta*. (2015) 891:1–14. doi: 10.1016/j.aca.2015.04.042
43. Blasco H, Błaszczyński J, Billaut J-C, Nadal-Desbarats L, Pradat P-F, Devos D, et al. Comparative analysis of targeted metabolomics: dominance-based rough set approach versus orthogonal partial least square-discriminant analysis. *J Biomed Inform*. (2015) 53:291–9. doi: 10.1016/j.jbi.2014.12.001
44. Worley B, Powers R. Multivariate analysis in metabolomics. *Curr Metab*. (2013) 1:92–107. doi: 10.2174/2213235X130108
45. Triba MN, Le Moyec L, Amathieu R, Goossens C, Bouchemal N, Nahon P, et al. PLS/OPLS models in metabolomics: the impact of permutation of dataset rows on the K-fold cross-validation quality parameters. *Mol BioSyst*. (2015) 11:13–9. doi: 10.1039/C4MB00414K
46. Kiralj R, Ferreira M. Basic validation procedures for regression models in QSAR and QSPR studies: theory and application. *J Braz Chem Soc*. (2009) 20:770–87. doi: 10.1590/S0103-50532009000400021
47. Roy GL, De Buck J, Wolf R, Mortier RAR, Orsel K, Barkema HW. Experimental infection with *Mycobacterium avium* subspecies *paratuberculosis* resulting in decreased body weight in Holstein-Friesian calves. *Can Vet J*. (2017) 58:296–8.
48. Thirunavukkarasu S, Plain KM, de Silva K, Begg D, Whittington RJ, Purdie AC. Expression of genes associated with cholesterol and lipid metabolism identified as a novel pathway in the early pathogenesis of *Mycobacterium avium* subspecies *paratuberculosis*-infection in cattle. *Vet Immunol Immunopathol*. (2014) 160:147–57. doi: 10.1016/j.vetimm.2014.04.002
49. Collins JM, Walker DI, Jones DP, Tukvadze N, Liu KH, Tran VT, et al. High-resolution plasma metabolomics analysis to detect *Mycobacterium tuberculosis*-associated metabolites that distinguish active pulmonary tuberculosis in humans. *PLoS One*. (2018) 13:e0205398. doi: 10.1371/journal.pone.0205398
50. Shipkowski KA, Sanders JM, McDonald JD, Garner CE, Doyle-Eisele M, Wegerski CJ, et al. Comparative disposition of dimethylaminoethanol and choline in rats and mice following oral or intravenous administration. *Toxicol Appl Pharmacol*. (2019) 378:114592. doi: 10.1016/j.taap.2019.05.011

Conflict of Interest: The authors declare that the research was conducted in the absence of any commercial or financial relationships that could be construed as a potential conflict of interest.

Copyright © 2021 Tata, Pallante, Massaro, Miano, Bottazzari, Fiorini, Dal Prà, Paganini, Stefani, De Buck, Piro and Pozzato. This is an open-access article distributed under the terms of the Creative Commons Attribution License (CC BY). The use, distribution or reproduction in other forums is permitted, provided the original author(s) and the copyright owner(s) are credited and that the original publication in this journal is cited, in accordance with accepted academic practice. No use, distribution or reproduction is permitted which does not comply with these terms.



Diagnostic Sequences That Distinguish *M. avium* Subspecies Strains

John P. Bannantine^{1*}, Judith R. Stabel¹, Darrell O. Bayles¹, Cyril Conde² and Franck Biet²

¹ USDA-Agricultural Research Service, National Animal Disease Center, Ames, IA, United States, ² INRAE, Université de Tours, ISP, Nouzilly, France

OPEN ACCESS

Edited by:

Miguel Salgado,
Austral University of Chile, Chile

Reviewed by:

Marta Alonso-Hearn,
NEIKER-Instituto Vasco de
Investigación y Desarrollo
Agrario, Spain
Min Yue,
Zhejiang University, China

*Correspondence:

John P. Bannantine
john.bannantine@usda.gov

Specialty section:

This article was submitted to
Veterinary Infectious Diseases,
a section of the journal
Frontiers in Veterinary Science

Received: 21 October 2020

Accepted: 31 December 2020

Published: 28 January 2021

Citation:

Bannantine JP, Stabel JR, Bayles DO,
Conde C and Biet F (2021) Diagnostic
Sequences That Distinguish *M. avium*
Subspecies Strains.
Front. Vet. Sci. 7:620094.
doi: 10.3389/fvets.2020.620094

Over a decade ago *Mycobacterium avium* subspecies *paratuberculosis* (*Map*) specific genes were initially identified in a whole genome context by comparing draft genome sequences of *Map* strain K-10 with *Mycobacterium avium* subspecies *hominissuis* (*Mah*) strain 104. This resulted in identification of 32 *Map* specific genes, not including repetitive elements, based on the two-genome comparison. The goal of this study was to define a more complete catalog of *M. avium* subspecies-specific genes. This is important for obtaining additional diagnostic targets for Johne's disease detection and for understanding the unique biology, evolution and niche adaptation of these organisms. There are now over 28 complete genome sequences representing three *M. avium* subspecies, including *avium* (*Maa*), *Mah*, and *Map*. We have conducted a comprehensive comparison of these genomes using two independent pan genomic comparison tools, PanOCT and Roary. This has led to the identification of more than 250 subspecies defining genes common to both analyses. The majority of these genes are arranged in clusters called genomic islands. We further reduced the number of diagnostic targets by excluding sequences having high BLAST similarity to other mycobacterial species recently added to the National Center for Biotechnology Information database. Genes identified as diagnostic following these bioinformatic approaches were further tested by DNA amplification PCR on an additional 20 *M. avium* subspecies strains. This combined approach confirmed 86 genes as *Map*-specific, seven as *Maa*-specific and three as *Mah*-specific. A single-tube PCR reaction was conducted as a proof of concept method to quickly distinguish *M. avium* subspecies strains. With these novel data, researchers can classify isolates in their freezers, quickly characterize clinical samples, and functionally analyze these unique genes.

Keywords: *M. avium*, *Mycobacterium*, *paratuberculosis* (*Map*), whole genome comparison, diagnostics, PCR

INTRODUCTION

Accurate diagnosis of mycobacterial infections is important for effective disease management within the livestock production industry. National and state veterinary laboratories are routinely confronted with unresolved cases of non-tuberculous mycobacterial (NTM) infections that are not further delineated due to complicated cross-reactive results as well as a lack of time and funds. However, correct identification of *M. avium* subspecies is very important because of the divergent, yet prominent, clinical relevance that exists among these strains (1). The *Mycobacterium avium*

subspecies comprise three predominant, closely-related subspecies, *M. avium* subspecies *avium* (*Maa*), *M. avium* subspecies *hominissuis* (*Mah*), and *M. avium* subspecies *paratuberculosis* (*Map*) and their genetic similarity has limited the identification of diagnostic targets that distinguish each subspecies. A forth subspecies has been reported (*silvaticum*), but the lack of circulating strains and sequences in public databases suggests this subspecies designation may be artifactual (2). *Map* is the causative agent of Johne's disease, which is a chronic intestinal ailment of ruminants that results in significant economic loss to dairy, meat and wool industries (3, 4). *Mah* is an opportunistic pathogen of swine and humans that manifests most commonly as a pulmonary infection in humans (5), while *Maa* is primarily a pathogen of birds (6).

In this report, the terms *Map* and non-*Map* are used to divide the *M. avium* subspecies. This is due to the focus on diagnostic *Map* sequences, which are major tools for research and surveillance of Johne's disease. Conversely, very few studies have reported sequences that are diagnostic for non-*Map* subspecies. The only known sequences that are specific for the *Maa* and *Mah* subspecies include IS1245 (7) and genes contained within insertions or other genetic rearrangements termed large sequence polymorphisms (LSPs) (8). Whole genome comparative methods are a comprehensive approach for identifying specific genes useful in molecular diagnostic tests. In this approach, genomes from closely related organisms are compared to identify genes uniquely correlated with particular groups. A complicating factor is that *M. avium* subspecies strains studied thus far all share >98% average nucleotide identity across the entire genome (2). In addition, the core genome appears stable for *Map* with 80% of the genome sequence comprising genes present in all strains, whereas the core genomes of non-*Map* subspecies comprise only 40% of genes (2). Despite strong genetic similarity and availability of commonly used diagnostic targets (i.e., IS900), there are still undiscovered and unexplored genetic targets that may be used in diagnostic tests to distinguish the *M. avium* subspecies. These sequences are also important to understanding the unique biology, evolution and niche adaptation of these strains. A primary goal of this study is to identify genetic targets that can distinguish *M. avium* subspecies from each other.

Despite high sequence identity among these subspecies, some specific sequences have long been identified and used for diagnostics of Johne's disease. The most commonly used target is the repetitive sequence, IS900, which is present in 16–22 copies in *Map*. This insertion element was identified as *Map*-specific long before whole-genome sequences became available (9, 10). Other sequences reported as specific to *Map* include the single-copy genes *hspX* (MAP_RS11095; MAP2182c) (11, 12), F57 (MAP_RS22535; MAP_0865) (13), and locus 251 (MAP_RS14130; MAP2765c) (14, 15). Locus 251 was originally identified from shotgun sequence data shortly before the first complete genome of an *M. avium* subspecies was assembled (15) and later used as a target in commercial PCR assays. F57 was originally identified from a genomic DNA library screen (16) and was later discovered as part of the MAP_0865 coding sequence present on a large sequence polymorphism termed LSP4 (17). This gene has also been a common target in real

time PCR assays (13, 18, 19). Thirty-two *Map*-specific genes were identified by genomic hybridizations to DNA microarrays (20–22), but this approach lacked the resolution and completeness of whole-genome sequences.

To identify all remaining sequences specific for *Map* and new diagnostic sequences for *Maa* and *Mah*, complete genomes from several strains were compared and candidate genes identified. Two independent bioinformatic analyses were first conducted to obtain subspecies specific genes in *M. avium*. These analyses included Roary (23) and PanOCT (24) pan genome tools, which identify core and accessory genes for a group of closely related organisms. PanOCT works by joining homologous and conserved gene neighborhoods to cluster orthologous proteins while Roary preclusters highly similar protein sequences before BLASTP similarity searching. PanOCT analysis yields a variety of comparative data about the input genomes (24), but one of the more useful outputs are the match tables. These tables list orthologous clusters of genes along with information on the cutoff metrics that would result in genes being declared absent in the match table. Match tables were constructed from PanOCT analysis showing all genomes, including their corresponding genes and percent identity of their gene products. These tools were used previously to determine the core genome of *Map* and non-*Map* strains (2). Finally, once specific genes are identified, DNA amplification primers can then be designed for further testing on a panel of organisms representing additional *M. avium* strains.

MATERIALS AND METHODS

In silico Identification of Subspecies Specific Genes

PanOCT output includes a match table of all genes in every input genome (Genbank flatfile format) with orthologs arranged in rows and genomes arranged in columns. The input genomes included the 29 *M. avium* genomes reported in **Tables 1, 2** of (2). When orthologs are not present in a genome(s), this is interpreted as one of several possibilities: the amino acid percent identity is <35%, the BLAST E-value was $>1 \times 10^{-5}$, the minimum percent match length of subject and query (default is 1%) was not met, the frame-shift overlap parameter (default is 1.33) triggered a non-match, there were more than 20 amino acids at the beginning or end of a match that were missing, and finally, there was not at least one match that confirmed a protein fragment/frame-shift. Roary (v3.11.2) was used to define the accessory genome of each subspecies and was launched with *-e* and *-n* options to compute rapid core gene alignment. Coding sequences from both analyses were assembled and compared. Only subspecies-specific genes identified by both approaches were analyzed by DNA amplification.

Primer Design

Primers were designed using the National Center for Biotechnology Information (NCBI) primer search software (<https://www.ncbi.nlm.nih.gov/tools/primer-blast/>). Parameters that differed from the defaults included minimum product size of 300 bp, maximum product size of 800 bp, optimal primer

TABLE 1 | Genomic DNA templates used in DNA amplification experiments.

Species	Subspecies	Strain	Culture no.	Host	Notes
<i>Avium</i>	<i>Paratuberculosis</i>	K10	6121	Cow	
<i>Avium</i>	<i>Paratuberculosis</i>	Linda	6100	Human	
<i>Avium</i>	<i>Paratuberculosis</i>	ATCC 19698-1974	6002	Cow	
<i>Avium</i>	<i>Paratuberculosis</i>	Isolate 4025		Cow	Isolated from the jejunum of a Guernsey cow
<i>Avium</i>	<i>Paratuberculosis</i>	Sheep 407	6096	Sheep	Distal ileum isolate from a Suffolk in the US
<i>Avium</i>	<i>Paratuberculosis</i>	Bovine isolate	6013	Cow	From a high shedding cow by Dr. Whitlock, U Penn
<i>Avium</i>	<i>Paratuberculosis</i>	Bovine isolate	5077	Cow	From the IC valve of a Holstein cow in 1993
<i>Avium</i>	<i>Paratuberculosis</i>	117p	6116	Goat	Isolate from the Veterinary institute of Norway
<i>Avium</i>	<i>Paratuberculosis</i>	S397	6101	Sheep	A sheep isolate in the US
<i>Avium</i>	<i>Hominissuis</i>	H.S. 09-5894	6138	Cow	
<i>Avium</i>	<i>Hominissuis</i>	H.S. 10-1725	6140	Cow	
<i>Avium</i>	<i>Hominissuis</i>	MA 1115	6106		
<i>Avium</i>	<i>Hominissuis</i>	H.S. 10-05561	6124	Pig	Swine isolate in 2008
<i>Avium</i>	<i>Hominissuis</i>	H.S. 10-1519	6139	Cow	
<i>Avium</i>	<i>Avium</i>	ATCC 35719	6004	Chicken	MAIS complex 2
<i>Avium</i>	<i>Avium</i>	wood pigeon A	6007	Bird	
<i>Avium</i>	<i>Avium</i>	Strain 18	6005		Former vaccine strain
<i>Avium</i>	<i>Avium</i>		6084	Rabbit	Pygmy rabbit isolate
<i>Intracellulare</i>		ATCC 35773	6010	Swine	MAIS complex 6

TABLE 2 | Number of *M. avium* subspecies specific genes identified by each analysis.

Subspecies (n)	PanOCT	Roary	Both
<i>Maa</i> (2)	158	213	157
<i>Mah</i> (13)	9	13	8
<i>Map</i> (13)	115	155	114

melting temperature of 68°C with a max melting temperature of 70°C, and database selection was RefSeq genomes. At least 10 candidate primer pairs obtained from NCBI primer searches were tested on each gene *in silico* using MacVector version 17.5. Primer pairs were discarded if any bound within the product or if they formed hairpin and self-duplex structures. Only one set of primers was kept for each gene to use in DNA amplification studies. Accepted primer pairs are shown in **Supplementary Table 1** for all genes analyzed. If the open reading frames were small and adjacent to each other, a forward primer was designed in one coding sequence and the reverse primer was designed in the neighboring coding sequence. This approach provided more sequence to design optimal primer pairs and lessened the number of PCRs to be conducted. In one case, a primer pair was designed that spanned three small coding sequences, MAP_RS10970, MAP_RS10975, and MAP_RS10980.

Functional Analysis of Genes

All Roary *Map*-specific protein sequences of each gene (155 total) were extracted using an in-house python script (**Supplementary Materials**) based on Biopython (<https://biopython.org>). KEGG orthologs for each protein sequence

were assigned using kofamscan tool (https://github.com/takaram/kofam_scan) based on HMM profile search with default parameters. Kofamscan results were parsed using another in-house python script (searchKEGG.py). Briefly, for each gene, we selected the best result based either on the ratio value compute as score / threshold_score where available or on the lower e-value. K numbers were then used to retrieve the complete KEGG hierarchies and functional classes were assigned based on the KEGG hierarchies. For functional analysis using eggNOG, all Roary *Map*-specific protein sequences were again extracted. Proteins were aligned against the eggNOG database v5.0 using Diamond (<https://github.com/bbuchfink/diamond>) and functional annotation was assigned to each protein sequence when available using emapper.py python script from eggNOG-Mapper tool. Results were parsed using an in-house python script (**Supplementary Materials**) in order to extract relevant information.

DNA Amplification

Genomic DNA was purified from mycobacterial strains shown in **Table 1** using the method described previously (15). Advantage GC-2 (Takara Bio) was used for all amplifications on 100 ng of DNA and 100 μM of each primer. All reactions were repeated twice and if an unexpected result occurred, the reaction was again tested using EconoTaq PLUS GREEN master mix (Lucigen). All amplification reactions were conducted on an Applied Biosystems GeneAmp PCR System 9700 as follows: a single denaturation step at 94°C for 8 min; then 25 cycles of 94°C for 30 s, 70°C for 1 min, 72°C for 1 min; then a final extension at 72°C for 5 min. The single reaction multiplex PCRs were performed using the same conditions above, except three sets of primers (highlighted red in **Supplementary Table 1**)

were included in each reaction. *In silico* PCR was performed with MacVector 17.5 using the primer test feature and the same primers listed in **Supplementary Table 1**. DNA templates for *in silico* PCR consisted of complete genome sequences of *Mycobacterium* available in public sequence databases.

Data Availability

Raw sequence data supporting the results of this article were deposited in the European Nucleotide Archive (ENA) and NCBI under accession PRJEB2204.

RESULTS

Bioinformatic Analysis of *M. avium* Subspecies-Specific Genes

Map

The initial number of subspecies-specific gene candidates were obtained by two comparative genomic methods, Roary and PanOCT analysis. The same set of 28 complete genomes that were used in our previous study (2) was included herein. PanOCT analysis revealed a total of 115 genes that are present in all *Map* genomes, but absent in all non-*Map* genomes while Roary analysis identified 155 *Map*-specific genes (**Table 2; Supplementary Table 2**). The total number of *Map*-specific genes identified by either Roary or PanOCT analysis was 156 (**Supplementary Table 2**).

Of the 156 total genes, Roary analysis uncovered 41 genes not found by PanOCT analysis whereas one gene was identified by PanOCT analysis that was not listed by Roary. The reason for this single-gene discrepancy is due to different translational start sites in one of the 13 *Map* orthologs (EGA31_RS21685 in the Telford strain) encoding an alpha/beta hydrolase, which made this gene appear as though it was not present in all *Map* strains analyzed (**Supplementary Figure 1; Table 3**). Thus, it was excluded by Roary analysis. The 41 genes present by Roary analysis but absent by PanOCT is due to the different clustering methods used by these bioinformatic tools. However, it is of interest to further explore this subset of 41 genes to understand which bioinformatic approach might be better for defining these gene targets. BLAST analysis of these 41 genes against the NCBI database showed reasonably strong homologies to other, more distantly related, *Mycobacterium* species (**Supplementary Table 3**). These results suggest that PanOCT may be better suited to consider more evolutionarily distant strains than Roary. Nonetheless, 114 *Map*-specific gene candidates are present in both analyses (**Supplementary Table 2**). This result excludes *Map*-specific repetitive sequences, such as IS900, which are not annotated in the E1 and E93 genome sequences (2).

Non-map

The *Mah*-specific and *Maa*-specific genes were also obtained using similar analyses. There are only nine *Mah*-specific genes identified by PanOCT and 13 by Roary analysis (**Table 2; Supplementary Table 4**). Eight of these genes are present in both analyses. One gene, encoding hydroxycinnamic acid hydroxylase (**Table 3**), that is uniquely present in the PanOCT analysis was due to differences in the clustering of orthologous genes. In

this case, the BLAST score ratio, when used alone, would not classify these orthologs as a cluster. Therefore, Roary excluded it. However, when the conserved gene neighborhood is factored in the PanOCT analysis, these genes are found rooted in the same source. This might be what one would expect if there was a single event that introduced an entire cluster followed by divergence of a gene within that cluster. Conversely, there are five *Mah* genes identified as specific only by Roary analysis. As before, these differences were due to the clustering methods used by these bioinformatic tools (see Discussion). The largest set of subspecies-specific genes were obtained for *Maa* strains, which included 157 genes identified by both analyses (**Table 2; Supplementary Table 5**).

Location of *M. avium* Subspecies-Specific Genes

Subspecies specific genes are not randomly distributed over the entire genome but tend to be organized in clusters, termed large sequence polymorphisms (LSPs) (8, 17). This fact is supported by the results of this study, where several specific genes are contained within LSPs regardless of the subspecies (**Figure 1**). *Maa* shows the most clusters (26 total), followed by *Map* and then *Mah*, which only has four clusters of eight total genes. For example, the largest genomic island is just over 100 kb in *Maa* and it contains 97 *Maa*-specific genes. This island was previously described as LSP1 by Semret et al. (8). The location of LSP1 is at 7 o'clock on the *Maa* genome map in **Figure 1**. Likewise, the largest genomic island in *Map* includes 30 genes spanning 55 kb and was previously named LSP^P 14 (17). Not all genes within any defined LSP were found specific to a given subspecies in this study.

BLAST Similarity and *in silico* PCR Analysis

The 114 *Map*-specific genes were next analyzed by similarity searches against other complete mycobacterial genomes including members of the *M. tuberculosis* complex and non-tuberculosis mycobacteria closely related to the MAC complex (25, 26). Several *Map*-specific genes showed surprisingly strong similarity to mycobacterial genomes that were recently added to public sequence databases (**Supplementary Table 6**). These include *M. marseillense*, *M. lepraemurium*, *M. branderi*, and *Mycolicibacterium doricum*. *In silico* PCR using primers designed for this study (**Supplementary Table 1**) were tested on the strongest matching genome sequences obtained from BLAST analysis and amplification products of the correct size were obtained for nine *Map* genes (**Supplementary Table 6**). Removing these nine targets reduced the list of *Map* genes to 104 that are defined as *Map*-specific following PanOCT, Roary and *in silico* PCR analysis. Within that group of 104 genes, 54 were highly specific to *Map* as they had no matches in the NCBI sequence database (indicated by “no result” in **Supplementary Table 6**). Two additional *M. avium* genomes, *Map* DSM 44135 (27) and *Maa* ATCC 25291 (28), were published after this study began and *in silico* PCR on those genome sequences shows agreement with subspecies specificity for all genes except FCV17_RS22495, a *Mah* gene that yielded a correct size product in *Maa* ATCC 25291 (**Supplementary Table 4**).

TABLE 3 | *M. avium* subspecies-specific gene discrepancy in Roary analysis.

Subspecies	Strain	Locus tag	Description	Amino acids	Roary
<i>paratuberculosis</i>	K-10	MAP_RS19250	Alpha/beta hydrolase	MAVSATAGI...	Yes
<i>paratuberculosis</i>	MAP4	MAP4_RS00065	Alpha/beta hydrolase	MAVSATAGI...	Yes
<i>paratuberculosis</i>	E1	RC58_RS00065	Alpha/beta hydrolase	MAVSATAGI...	Yes
<i>paratuberculosis</i>	E93	RE97_RS00065	Alpha/beta hydrolase	MAVSATAGI...	Yes
<i>paratuberculosis</i>	India 2008	A0V42_RS19260	Alpha/beta hydrolase	MAVSATAGI...	Yes
<i>paratuberculosis</i>	FDAARGOS	CEP84_RS06855	Alpha/beta hydrolase	MAVSATAGI...	Yes
<i>paratuberculosis</i>	JII-1961	CEG92_RS19670	Alpha/beta hydrolase	MAVSATAGI...	Yes
<i>paratuberculosis</i>	MAPK_CN7/15	EC391_RS14825	Alpha/beta hydrolase	MAVSATAGI...	Yes
<i>paratuberculosis</i>	MAPK_CN9/15	EC390_RS07915	Alpha/beta hydrolase	MAVSATAGI...	Yes
<i>paratuberculosis</i>	MAPK_CN4/13	EGM63_RS09965	Alpha/beta hydrolase	MAVSATAGI...	Yes
<i>paratuberculosis</i>	MAPK_JB16/15	EGM64_RS22685	Alpha/beta hydrolase	MAVSATAGI...	Yes
<i>paratuberculosis</i>	MAPK_JJ1/13	EGM60_RS19585	Alpha/beta hydrolase	MAVSATAGI...	Yes
<i>paratuberculosis</i>	Telford	EGA31_RS21685	Alpha/beta hydrolase	MLLRASRYF...	No
<i>hominissuis</i>	104	MAV_RS08635	Hydroxycinnamic acid hydroxylase	MTDSPAYK...	Yes
<i>hominissuis</i>	TH135	MAH_RS07880	Propionate hydroxylase	MPVWVGAG...	No
<i>hominissuis</i>	OCU464	KV38_RS08390	Hydroxycinnamic acid hydroxylase	MTDSPAYK...	Yes
<i>hominissuis</i>	H87	BS641_RS14715	Propionate hydroxylase	MTDSPAYK...	Yes
<i>hominissuis</i>	HP17	BEP52_RS08480	Hydroxycinnamic acid hydroxylase	MPVWVGAG...	No
<i>hominissuis</i>	OCU901_S2_2s	BJP78_RS08465	Hydroxycinnamic acid hydroxylase	MPVWVGAG...	No
<i>hominissuis</i>	OCU873s_P7_4s	BJP74_RS08005	Hydroxycinnamic acid hydroxylase	MPVWVGAG...	No
<i>hominissuis</i>	MAC109	DFS55_RS16395	Hydroxycinnamic acid hydroxylase	MTDSPAYK...	Yes
<i>hominissuis</i>	mc2 2500	EX350_RS14220	Hydroxycinnamic acid hydroxylase	MTDSPAYK...	Yes
<i>hominissuis</i>	101174	FCV17_RS18625	Hydroxycinnamic acid hydroxylase	MTDSPAYK...	Yes
<i>hominissuis</i>	101034	FCV16_RS11165	Hydroxycinnamic acid hydroxylase	MTDSPAYK...	Yes
<i>hominissuis</i>	101115	FCV18_RS02655	Hydroxycinnamic acid hydroxylase	MTDSPAYK...	Yes
<i>hominissuis</i>	JP-H-1	JPH1_RS10225	Hydroxycinnamic acid hydroxylase	MTDSPAYK...	Yes

Genes listed in the above table are all orthologs in PanOCT, but those in red font have different translational starts. All the sequences in red font also indicate they are not listed in the Roary analysis.

This translational start for Telford was downstream of that for the rest of the *Map* genomes.

Gene Ontology of Map-Specific Genes

Functional analysis was performed on *Map*-specific genes using Kyoto Encyclopedia of Genes and Genomes (KEGG) (29) and evolutionary genealogy of genes: Non-supervised Orthologous Groups (eggNOG) (30). These genes were separated into 16 functional classifications by KEGG and 18 by eggNOG (Figure 2). Other than the most predominant unknown function class, KEGG analysis revealed 14 lipid transport system proteins, which likely remodel the cell wall in some way. EggNOG analysis showed the presence of Mce family proteins (n=6), and ABC transporters (n=5), but were predominantly genes of unknown function (n=45). The high number of genes with no assigned function suggests there are a lot of unknowns about what makes *Map* unique to other bacteria.

DNA Amplification of Subspecies Specific Genes

Taq polymerase-based DNA amplification of selected genes was performed on purified genomic DNA from 16 additional *M. avium* subspecies strains and *Map* K-10 as a control. All 104 *Map*-specific genes (Supplementary Table 2) and all eight

Mah-specific genes (Supplementary Table 4) were tested. In addition, a subset of eight genes from the 157 *Maa*-specific genes (Supplementary Table 5) were also tested by DNA amplification. IS900 and IS1245 repetitive element targets were included as controls. The results show that 106 of 120 genes tested were confirmed as subspecies-specific (Table 4). A gene was dropped from the subspecies-specific gene list if it failed to amplify in any target strains or if it did amplify in any non-target strains. Such unexpected reactions are highlighted in yellow (if negative) and green (if positive) in Table 4.

Map

Eighty-six genes were confirmed as *Map*-specific by DNA amplification (Table 4). Conversely, four genes amplified non-*Map* DNA and thus are no longer considered *Map*-specific (Table 4). The primers designed from the MAP_RS01130-MAP_RS01135 combination amplified the correct size product in the *M. intracellulare* strain, but only faintly, perhaps indicating nucleotide mismatches in the primers. Primers to MAP_RS22390-MAP_RS00525 along with MAP_RS00515-MAP_RS00520 are all clustered together in the genome and amplified a correct sized product in two *Mah* strains

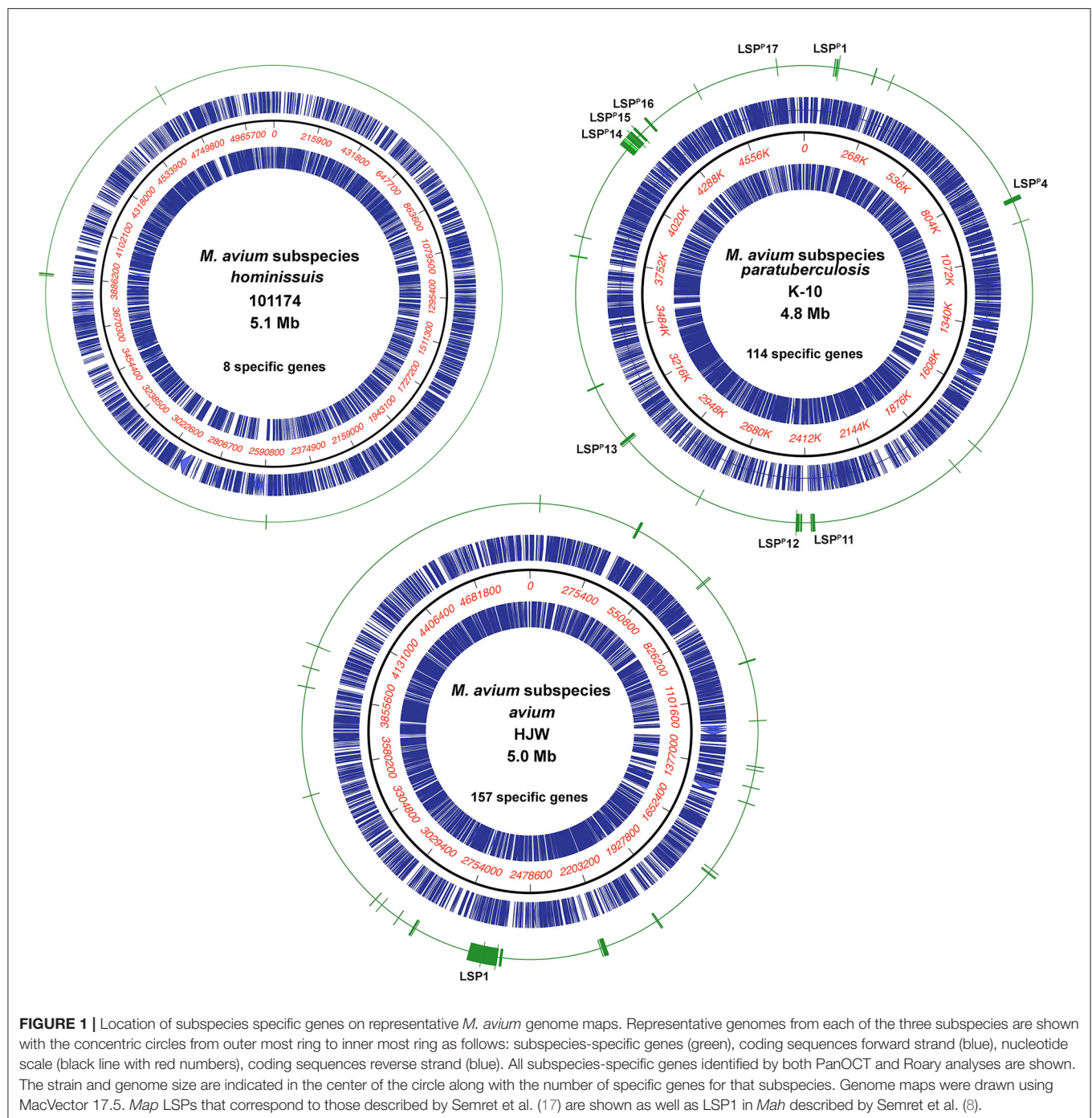
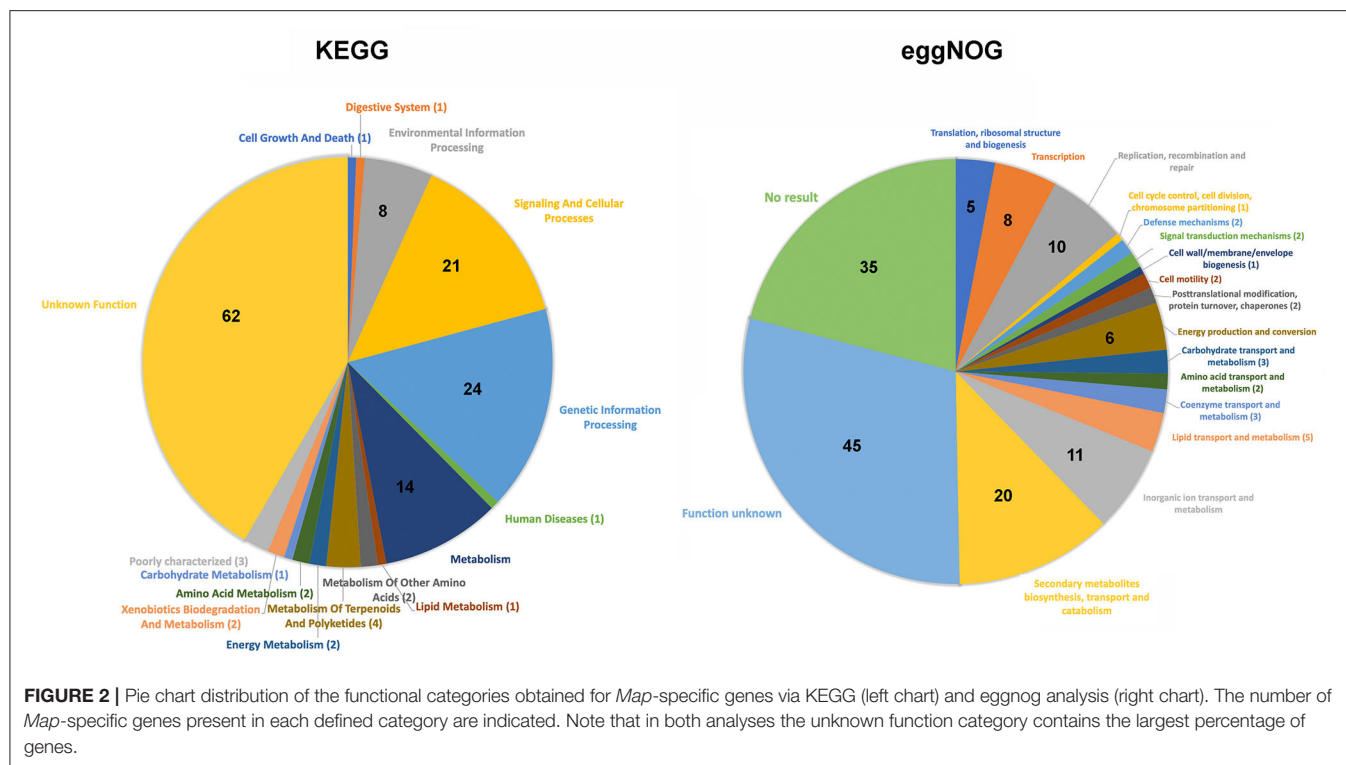


(Table 4). MAP_RS08655 was the most conserved gene, amplifying a product in six of the nine non-*Map* strains tested (Table 4). Conversely, *Map* strain Linda failed to amplify seven genes, despite testing different *Taq* enzyme mixtures. A search of sequence read archive data from accession PRJEB2204 suggests all seven genes are present in the Linda strain, similar to all other *Map* strains. One primer pair designed from MAP_RS14095 failed to amplify DNA from any strain tested.

Non-map

Gene candidates that are diagnostic for *Mah* are very limited. Among the eight genes identified as specific to *Mah* by bioinformatic approaches, only three (FCV17_RS18630, FCV17_RS18640, and FCV17_RS18645) remained specific following PCR analysis as the other five genes were amplified a correct sized product from *M. intracellulare* DNA (Table 4). Of the eight *Maa*-specific genes selected for PCR analysis, seven were confirmed specific while only one (DBO90_RS13535)



showed amplification in three *Map* strains. However, there are 149 other *Maa* gene candidates that were not tested, but could be *Maa*-specific (Supplementary Table 4).

The collective results identified 86 genes that are *Map*-specific, seven *Maa*-specific, and three *Mah*-specific. Thus, a final list of the subspecies-specific genes is included in Table 5. Collectively, these results further extended the number diagnostic targets tested for Johne's disease against 10 additional *Map* strains and 10 non-*Map* strains.

A Single Reaction PCR Distinguishes All *M. avium* Subspecies

As a proof of concept, primer combinations were tested that can distinguish any *M. avium* subspecies using a single-tube amplification reaction. Although other PCR reactions have been developed to distinguish *M. avium* subspecies (31), this approach eliminates the need for three reactions to accomplish the same result. This primer combination was used on selected genomic DNAs from *M. avium* subspecies. The single DNA amplification was able to distinguish each subspecies on the basis of size by gel electrophoresis (Figure 3), but can also be adapted to real time PCR using different Taqman probes and concentrations (32).

DISCUSSION

A total of 32 *Map*-specific genes were initially identified by comparing *Map* K-10 with *Mah* strain 104 (17, 20, 22). These genes have aided the specific detection of *Map*, but are single-copy genes compared to IS900, a repetitive element that was known to be diagnostic for *Map* long before whole-genome

comparisons were performed (9, 10). Using a comparative genomic approach combined with PCR analysis, this study confirmed 18 of the original 32 genes and identified 68 additional *Map*-specific genes as diagnostic targets (Table 5) yielding a total of 86 genes. Some genes were initially identified as potentially subspecies specific after PanOCT and Roary analysis, but were subsequently found to be conserved in other mycobacteria after additional strains were tested by *in silico* PCR or *Taq*-based PCR analysis. For example, eight *Mah*-specific genes were identified by bioinformatic analysis, but only three were still deemed *Mah*-specific following DNA amplification experiments. The number of subspecies-specific genes will likely be further reduced as additional *Map* and non-*Map* strains are analyzed. Significantly more genes specific to *Map* vs. *Mah* are likely attributed to the closed, stable genome of *Map*, which increases the chance that specific genes are present in all strains. The opposite is true for *Mah*, which has a more dynamic, open genome containing a smaller number of core sequences (2) and therefore, the number of specific genes is very small. *Maa* had the highest number of subspecies specific genes, possibly because only two complete genome sequences were bioinformatically analyzed for members of this subspecies. Only eight of the 157 *Maa* genes were selected for DNA amplification studies and seven genes remained specific to *Maa*. Nonetheless, with these novel data, researchers can classify isolates in their freezers, quickly characterize clinical samples, and functionally analyze these unique genes.

A total of 40% of the *Map*-specific genes and 24% of *Maa*-specific genes are annotated as hypothetical. This large percentage of *Map* hypothetical proteins is interesting considering the updated RefSeq annotation has resulted in a

TABLE 4 | DNA amplification of purified genomic DNA from additional *M. avium* subspecies strains.

Locus tag	PCR product Length (bp)	<i>M. avium</i> subspecies <i>paratuberculosis</i>								<i>M. avium</i> subspecies <i>hominissuis</i>				<i>M. avium</i> subspecies <i>avium</i>			<i>M. intracellulare</i>
		K-10	Linda	ATCC19698	4025	Bovine str.	Goat-bov	Sheep 407	S397	2 strains	10-1519	10-1725	6084	6106/6007	ATCC35719	Strain 18	ATCC35773
MAP_RS00485- MAP_RS00490	520	+	—	+	+	+	+	+	+	—	—	—	—	—	—	—	—
MAP_RS00515- MAP_RS00520	307	+	+	+	+	+	+	+	+	—	+	—	+	—	—	—	—
MAP_RS22390- MAP_RS00525	560	+	+	+	+	+	+	+	+	—	+	—	+	—	—	—	—
MAP_RS00540	300	+	+	+	+	+	+	+	+	—	—	—	—	—	—	—	—
MAP_RS00545	458	+	+	+	+	+	+	+	+	—	—	—	—	—	—	—	—
MAP_RS01130- MAP_RS01135	365	+	+	+	+	+	+	+	+	—	—	—	—	—	—	—	+
MAP_RS04345- MAP_RS04350	301	+	+	+	+	+	+	+	+	—	—	—	—	—	—	—	—
MAP_RS04355	302	+	+	+	+	+	+	+	+	—	—	—	—	—	—	—	—
MAP_RS04705	300	+	+	+	+	+	+	+	+	—	—	—	—	—	—	—	—
MAP_RS08655	334	+	+	+	+	+	+	+	+	—	+	—	+	+	—	+	+
MAP_RS10920	319	+	+	+	+	+	+	+	+	—	—	—	—	—	—	—	—
MAP_RS10925- MAP_RS10930	353	+	—	+	+	+	+	+	+	—	—	—	—	—	—	—	—
MAP_RS10940	312	+	+	+	+	+	+	+	+	—	—	—	—	—	—	—	—
MAP_RS10945	355	+	+	+	+	+	+	+	+	—	—	—	—	—	—	—	—
MAP_RS10965	364	+	+	+	+	+	+	+	+	—	—	—	—	—	—	—	—
MAP_RS10970- MAP_RS10980	353	+	—	+	+	+	+	+	+	—	—	—	—	—	—	—	—
MAP_RS11080	300	+	+	+	+	+	+	+	+	—	—	—	—	—	—	—	—
MAP_RS11085	301	+	+	+	+	+	+	+	+	—	—	—	—	—	—	—	—
MAP_RS11090	384	+	+	+	+	+	+	+	+	—	—	—	—	—	—	—	—
MAP_RS11095	336	+	+	+	+	+	+	+	+	—	—	—	—	—	—	—	—
MAP_RS11100	372	+	+	+	+	+	+	+	+	—	—	—	—	—	—	—	—
MAP_RS11105	328	+	+	+	+	+	+	+	+	—	—	—	—	—	—	—	—
MAP_RS11130	527	+	+	+	+	+	+	+	+	—	—	—	—	—	—	—	—
MAP_RS11135	402	+	+	+	+	+	+	+	+	—	—	—	—	—	—	—	—
MAP_RS11140	403	+	+	+	+	+	+	+	+	—	—	—	—	—	—	—	—
MAP_RS11155	628	+	—	+	+	+	+	+	+	—	—	—	—	—	—	—	—
MAP_RS11160	309	+	+	+	+	+	+	+	+	—	—	—	—	—	—	—	—
MAP_RS11165- MAP_RS11170	428	+	+	+	+	+	+	+	+	—	—	—	—	—	—	—	—

(Continued)

TABLE 4 | Continued

Locus tag	PCR product Length (bp)	<i>M. avium</i> subspecies <i>paratuberculosis</i>								<i>M. avium</i> subspecies <i>hominissuis</i>				<i>M. avium</i> subspecies <i>avium</i>			<i>M. intracellulare</i>
		K-10	Linda	ATCC19698	4025	Bovine str.	Goat-bov	Sheep 407	S397	2 strains	10-1519	10-1725	6084	6106/6007	ATCC35719	Strain 18	ATCC35773
MAP_RS12615	300	+	+	+	+	+	+	+	+	-	-	-	-	-	-	-	-
MAP_RS14055	180	+	+	+	+	+	+	+	+	-	-	-	-	-	-	-	-
MAP_RS14060	301	+	+	+	+	+	+	+	+	-	-	-	-	-	-	-	-
MAP_RS14070	191	+	+	+	+	+	+	+	+	-	-	-	-	-	-	-	-
MAP_RS14095	231	-	-	-	-	-	-	-	-	-	-	-	-	-	-	-	-
MAP_RS14110	272	+	+	+	+	+	+	+	+	-	-	-	-	-	-	-	-
MAP_RS14120	225	+	+	+	+	+	+	+	+	-	-	-	-	-	-	-	-
MAP_RS14130	381	+	+	+	+	+	+	+	+	-	-	-	-	-	-	-	-
MAP_RS14135	211	+	+	+	+	+	+	+	+	-	-	-	-	-	-	-	-
MAP_RS14140	489	+	+	+	+	+	+	+	+	-	-	-	-	-	-	-	-
MAP_RS15170	419	+	-	+	+	+	+	+	+	-	-	-	-	-	-	-	-
MAP_RS17665	380	+	+	+	+	+	+	+	+	-	-	-	-	-	-	-	-
MAP_RS17670	264	+	+	+	+	+	+	+	+	-	-	-	-	-	-	-	-
MAP_RS19105	333	+	+	+	+	+	+	+	+	-	-	-	-	-	-	-	-
MAP_RS19110	333	+	+	+	+	+	+	+	+	-	-	-	-	-	-	-	-
MAP_RS19115	353	+	+	+	+	+	+	+	+	-	-	-	-	-	-	-	-
MAP_RS19120	300	+	+	+	+	+	+	+	+	-	-	-	-	-	-	-	-
MAP_RS19130	333	+	+	+	+	+	+	+	+	-	-	-	-	-	-	-	-
MAP_RS19135	316	+	+	+	+	+	+	+	+	-	-	-	-	-	-	-	-
MAP_RS19140	310	+	+	+	+	+	+	+	+	-	-	-	-	-	-	-	-
MAP_RS19145	368	+	+	+	+	+	+	+	+	-	-	-	-	-	-	-	-
MAP_RS19150	760	+	+	+	+	+	+	+	+	-	-	-	-	-	-	-	-
MAP_RS19155	340	+	+	+	+	+	+	+	+	-	-	-	-	-	-	-	-
MAP_RS19160	426	+	+	+	+	+	+	+	+	-	-	-	-	-	-	-	-
MAP_RS19165	406	+	-	+	+	+	+	+	+	-	-	-	-	-	-	-	-
MAP_RS19170	620	+	+	+	+	+	+	+	+	-	-	-	-	-	-	-	-
MAP_RS19185	597	+	+	+	+	+	+	+	+	-	-	-	-	-	-	-	-
MAP_RS19190	616	+	+	+	+	+	+	+	+	-	-	-	-	-	-	-	-
MAP_RS19195	470	+	+	+	+	+	+	+	+	-	-	-	-	-	-	-	-
MAP_RS19200	308	+	+	+	+	+	+	+	+	-	-	-	-	-	-	-	-
MAP_RS19205	492	+	+	+	+	+	+	+	+	-	-	-	-	-	-	-	-
MAP_RS19215	340	+	+	+	+	+	+	+	+	-	-	-	-	-	-	-	-
MAP_RS19220	342	+	+	+	+	+	+	+	+	-	-	-	-	-	-	-	-
MAP_RS19225	316	+	+	+	+	+	+	+	+	-	-	-	-	-	-	-	-

(Continued)

TABLE 4 | Continued

Locus tag	PCR product Length (bp)	<i>M. avium</i> subspecies <i>paratuberculosis</i>								<i>M. avium</i> subspecies <i>hominissuis</i>				<i>M. avium</i> subspecies <i>avium</i>			<i>M. intracellulare</i>
		K-10	Linda	ATCC19698	4025	Bovine str.	Goat-bov	Sheep 407	S397	2 strains	10-1519	10-1725	6084	6106/6007	ATCC35719	Strain 18	ATCC35773
MAP_RS19230	602	+	+	+	+	+	+	+	+	-	-	-	-	-	-	-	-
MAP_RS19240- MAP_RS19245	326	+	+	+	+	+	+	+	+	-	-	-	-	-	-	-	-
MAP_RS19255	331	+	+	+	+	+	+	+	+	-	-	-	-	-	-	-	-
MAP_RS19265	328	+	+	+	+	+	+	+	+	-	-	-	-	-	-	-	-
MAP_RS19270	445	+	+	+	+	+	+	+	+	-	-	-	-	-	-	-	-
MAP_RS19275	364	+	+	+	+	+	+	+	+	-	-	-	-	-	-	-	-
MAP_RS19280	462	+	+	+	+	+	+	+	+	-	-	-	-	-	-	-	-
MAP_RS19305- MAP_RS19310	323	+	+	+	+	+	+	+	+	-	-	-	-	-	-	-	-
MAP_RS19325- MAP_RS19330	356	+	+	+	+	+	+	+	+	-	-	-	-	-	-	-	-
MAP_RS19335	380	+	+	+	+	+	+	+	+	-	-	-	-	-	-	-	-
MAP_RS19345	352	+	+	+	+	+	+	+	+	-	-	-	-	-	-	-	-
MAP_RS19350	335	+	+	+	+	+	+	+	+	-	-	-	-	-	-	-	-
MAP_RS19355	351	+	+	+	+	+	+	+	+	-	-	-	-	-	-	-	-
MAP_RS19565	343	+	+	+	+	+	+	+	+	-	-	-	-	-	-	-	-
MAP_RS19570	150	+	+	+	+	+	+	+	+	-	-	-	-	-	-	-	-
MAP_RS19575	458	+	+	+	+	+	+	+	+	-	-	-	-	-	-	-	-
MAP_RS19580	310	+	+	+	+	+	+	+	+	-	-	-	-	-	-	-	-
MAP_RS22425	322	+	+	+	+	+	+	+	+	-	-	-	-	-	-	-	-
MAP_RS22505	342	+	+	+	+	+	+	+	+	-	-	-	-	-	-	-	-
MAP_RS22515	420	+	+	+	+	+	+	+	+	-	-	-	-	-	-	-	-
MAP_RS22520	492	+	+	+	+	+	+	+	+	-	-	-	-	-	-	-	-
MAP_RS22525	371	+	+	+	+	+	+	+	+	-	-	-	-	-	-	-	-
MAP_RS22535	305	+	+	+	+	+	+	+	+	-	-	-	-	-	-	-	-
MAP_RS22540	221	+	+	+	+	+	+	+	+	-	-	-	-	-	-	-	-
MAP_RS22625	333	+	+	+	+	+	+	+	+	-	-	-	-	-	-	-	-
MAP_RS22710	338	+	+	+	+	+	+	+	+	-	-	-	-	-	-	-	-
MAP_RS22805	307	+	+	+	+	+	+	+	+	-	-	-	-	-	-	-	-
MAP_RS22810	314	+	+	+	+	+	+	+	+	-	-	-	-	-	-	-	-
MAP_RS22985	343	+	+	+	+	+	+	+	+	-	-	-	-	-	-	-	-
MAP_RS23005	327	+	+	+	+	+	+	+	+	-	-	-	-	-	-	-	-
IS900	229	+	+	+	+	+	+	+	+	-	-	-	-	-	-	-	-
FCV17_RS12965	377	-	-	-	-	-	-	-	-	+	+	+	+	-	-	-	+

(Continued)

TABLE 4 | Continued

Locus tag	PCR product Length (bp)	<i>M. avium</i> subspecies <i>paratuberculosis</i>								<i>M. avium</i> subspecies <i>hominissuis</i>				<i>M. avium</i> subspecies <i>avium</i>			<i>M. intracellulare</i>
		K-10	Linda	ATCC19698	4025	Bovine str.	Goat-bov	Sheep 407	S397	2 strains	10-1519	10-1725	6084	6106/6007	ATCC35719	Strain 18	ATCC35773
FCV17_RS12970	411	-	-	-	-	-	-	-	-	+	+	+	+	-	-	-	+
FCV17_RS18600	315	-	-	-	-	-	-	+	-	+	+	+	+	-	-	-	+
FCV17_RS18630	463	-	-	-	-	-	-	-	-	+	+	+	+	-	-	-	-
FCV17_RS18635	481	-	-	-	-	-	-	-	-	+	+	+	+	-	-	-	+
FCV17_RS18640	309	-	-	-	-	-	-	-	-	+	+	+	+	-	-	-	-
FCV17_RS18645	316	-	-	-	-	-	-	-	-	+	+	+	+	-	-	-	-
FCV17_RS22495	184	-	-	-	-	-	-	-	-	+	+	-	+	+	+	+	+
DBO90_RS12280	366	-	-	-	-	-	-	-	-	-	-	-	-	+	+	+	-
DBO90_RS12340	402	-	-	-	-	-	-	-	-	-	-	-	-	+	+	+	-
DBO90_RS12410	330	-	-	-	-	-	-	-	-	-	-	-	-	+	+	+	-
DBO90_RS12500	308	-	-	-	-	-	-	-	-	-	-	-	-	+	+	+	-
DBO90_RS12630	368	-	-	-	-	-	-	-	-	-	-	-	-	+	+	+	-
DBO90_RS13535	469	+	-	-	+	-	+	-	-	-	-	-	-	+	+	+	-
DBO90_RS18520	358	-	-	-	-	-	-	-	-	-	-	-	-	+	+	+	-
DBO90_RS12105	310	-	-	-	-	-	-	-	-	-	-	-	-	+	+	+	-
IS1245	427	-	-	-	-	-	-	-	-	+	+	+	+	+	+	+	-

Amplification results with a green highlight indicate an unexpected positive reaction while results with a yellow highlight indicate an unexpected negative reaction.

Bovine str. = 3 bovine strains that gave identical results. These include 6013, ATCC19698 and 5077.

goat-bov = This column represents 1 goat strain and 1 bovine strain that gave identical results (4025 and 117p).

2 strains = *M. avium* subs *hominissuis* strains 10-5894 and 10-05561, which had identical results.

6106/6007 = Two *M. avium* subspecies *avium* strains that gave identical results.

TABLE 5 | *M. avium* subspecies-specific genes confirmed in this study.

Original Locus tag	RefSeq Locus tag	Protein ID	Description	Amino acids
NA	MAP_RS00540	WP_003876878.1	XRE family transcriptional regulator	114
MAP0106c	MAP_RS00545	WP_003876023.1	Integrase	343
NA	MAP_RS04345	WP_016705558.1	Hypothetical protein	88
NA	MAP_RS04350	WP_003877462.1	Hypothetical protein	86
NA	MAP_RS04355	WP_003877465.1	Hypothetical protein	173
NA	MAP_RS04705	WP_003877504.1	Hypothetical protein	99
MAP2148	MAP_RS10920	WP_003878324.1	Recombinase XerD	227
MAP2151	MAP_RS10940	WP_003878325.1	Hypothetical protein	145
NA	MAP_RS10945	WP_019305592.1	Hypothetical protein	174
MAP2158	MAP_RS10965	WP_010949499.1	Hypothetical protein	193
MAP2179	MAP_RS11080	WP_003878349.1	Hypothetical protein	121
MAP2180c	MAP_RS11085	WP_016706156.1	Hypothetical protein	110
MAP2181c	MAP_RS11090	WP_003878351.1	TetR/AcrR family transcriptional regulator	206
MAP2182c	MAP_RS11095	WP_019305660.1	Nitroreductase family deazaflavin-dependent oxidoreductase	133
MAP2183c	MAP_RS11100	WP_003878354.1	Cytochrome P450	416
MAP2184c	MAP_RS11105	WP_003875947.1	NAD(P)-dependent oxidoreductase	261
MAP2189	MAP_RS11130	WP_003875942.1	MCE family protein	418
MAP2190	MAP_RS11135	WP_003875941.1	MCE family protein	341
MAP2191	MAP_RS11140	WP_003875940.1	MCE family protein	354
MAP2195	MAP_RS11160	WP_010949512.1	Hypothetical protein	448
NA	MAP_RS11165	WP_019305659.1	Hypothetical protein	72
NA	MAP_RS11170	WP_019305658.1	Hypothetical protein	159
MAP2473	MAP_RS12615	WP_003877285.1	Hypothetical protein	145
MAP2754	MAP_RS14055	WP_003875312.1	Hypothetical protein	85
MAP2755	MAP_RS14060	WP_003875311.1	Hypothetical protein	100
MAP2757	MAP_RS14070	WP_003875309.1	Hypothetical protein	79
NA	MAP_RS14110	WP_003878582.1	Hypothetical protein	92
MAP2763c	MAP_RS14120	WP_003878583.1	Hypothetical protein	74
MAP2765c	MAP_RS14130	WP_016706030.1	Hypothetical protein	296
NA	MAP_RS14135	WP_016706028.1	Helix-turn-helix domain-containing protein	70
MAP2767c	MAP_RS14140	WP_003875297.1	Hypothetical protein	183
MAP3436c	MAP_RS17665	WP_003878992.1	Hypothetical protein	231
NA	MAP_RS17670	WP_016705884.1	XRE family transcriptional regulator	87
MAP3726	MAP_RS19105	WP_019305717.1	Iron ABC transporter permease	324
MAP3727	MAP_RS19110	WP_003876873.1	ABC transporter ATP-binding protein	271
MAP3728	MAP_RS19115	WP_003873998.1	Fe ³⁺ -citrate ABC transporter substrate-binding protein	345
MAP3729	MAP_RS19120	WP_003873995.1	TauD/TfdA family dioxygenase	258
MAP3731c	MAP_RS19130	WP_010950082.1	Cobalt ABC transporter	500
MAP3732c	MAP_RS19135	WP_003873992.1	Energy-coupling factor transporter transmembrane protein EcT	230
MAP3733c	MAP_RS19140	WP_003873991.1	Membrane protein	208
MAP3734c	MAP_RS19145	WP_003876870.1	ABC transporter ATP-binding protein	531
MAP3735c	MAP_RS19150	WP_019305718.1	ABC transporter ATP-binding protein	468
MAP3737	MAP_RS19155	WP_010950084.1	PPE family protein	504
MAP3738c	MAP_RS19160	WP_003876866.1	Class I SAM-dependent methyltransferase	244
MAP3740	MAP_RS19170	WP_010950086.1	Non-ribosomal peptide synthetase	3,068
MAP3743	MAP_RS19185	WP_019305720.1	Hypothetical protein	343
MAP3744	MAP_RS19190	WP_003873982.1	Thiazolinyli imide reductase	344
MAP3745	MAP_RS19195	WP_010950089.1	Thioesterase	250

(Continued)

TABLE 5 | Continued

Original	RefSeq			
Locus tag	Locus tag	Protein ID	Description	Amino acids
MAP3746	MAP_RS19200	WP_003873980.1	Metal-sensitive transcriptional regulator	104
MAP3747c	MAP_RS19205	WP_010950090.1	Hypothetical protein	406
MAP3749	MAP_RS19215	WP_003873977.1	NAD(P)-dependent oxidoreductase	286
MAP3750	MAP_RS19220	WP_019305722.1	Transport accessory protein MmpS	140
MAP3751	MAP_RS19225	WP_010950093.1	MMPL family transporter	979
MAP3752	MAP_RS19230	WP_010950094.1	Acyl-CoA synthetase	578
NA	MAP_RS19240	WP_003876850.1	Hypothetical protein	131
MAP3756c	MAP_RS19245	WP_003876849.1	LLM class F420-dependent oxidoreductase	286
MAP3758c	MAP_RS19255	WP_019684230.1	AraC family transcriptional regulator	240
MAP3760c	MAP_RS19265	WP_003879162.1	Class I SAM-dependent methyltransferase	128
MAP3761c	MAP_RS19270	WP_003879163.1	GAP family protein	242
MAP3762c	MAP_RS19275	WP_003873965.1	Glycosyltransferase	408
MAP3763c	MAP_RS19280	WP_016705775.1	Acyltransferase	498
MAP3767c	MAP_RS19305	WP_003873957.1	30S ribosomal protein S18	88
MAP3768c	MAP_RS19310	WP_003873956.1	30S ribosomal protein S14	101
MAP3771	MAP_RS19325	WP_003873953.1	50S ribosomal protein L31 type B	97
NA	MAP_RS19330	WP_003879173.1	ANTAR domain-containing protein	87
MAP3772c	MAP_RS19335	WP_003873951.1	GTP-binding protein	380
MAP3774c	MAP_RS19345	WP_003879175.1	Metal ABC transporter permease	285
MAP3775c	MAP_RS19350	WP_003873948.1	ABC transporter	262
MAP3776c	MAP_RS19355	WP_019305700.1	ABC transporter substrate-binding protein	263
MAP3815	MAP_RS19565	WP_019305842.1	Hypothetical protein	254
NA	MAP_RS19570	WP_003873898.1	Hypothetical protein	49
MAP3817c	MAP_RS19575	WP_019305841.1	Carotenoid biosynthesis protein	278
MAP3818	MAP_RS19580	WP_016705755.1	Cytochrome P450	397
NA	MAP_RS22425	WP_023877748.1	Hypothetical protein	158
MAP0853	MAP_RS22505	WP_010948992.1	Hypothetical protein	219
MAP0856c	MAP_RS22515	WP_003872872.1	Hypothetical protein	575
MAP0860c	MAP_RS22520	WP_003872868.1	Hypothetical protein	296
MAP0862	MAP_RS22525	WP_003877468.1	Hypothetical protein	360
MAP0865	MAP_RS22535	WP_010949001.1	Cell division protein FtsK	423
NA	MAP_RS22540	WP_064469008.1	DNA-binding protein	75
MAP1610	MAP_RS22625	WP_010949277.1	Hypothetical protein	194
MAP2152c	MAP_RS22710	WP_010949495.1	Hypothetical protein	124
NA	MAP_RS22805	WP_073578986.1	Hypothetical protein	104
MAP2766c	MAP_RS22810	WP_003878585.1	DUF2742 domain-containing protein	158
MAP3730	MAP_RS22985	WP_003876872.1	Class I SAM-dependent methyltransferase	210
MAP3773c	MAP_RS23005	WP_003873950.1	Transcriptional repressor	139
	FCV17_RS18600	WP_084055242.1	Oxidoreductase	283
	FCV17_RS18640	WP_137987598.1	TetR/AcrR family transcriptional regulator	222
	FCV17_RS18645	WP_062890787.1	EVE domain-containing protein	138
	DBO90_RS12280	WP_009976179.1	Dihydrodipicolinate reductase	361
	DBO90_RS12340	WP_023879882.1	Hypothetical protein	134
	DBO90_RS12410	WP_009976156.1	Amidohydrolase	394
	DBO90_RS12500	WP_009976134.1	Zn-ribbon domain-containing OB-fold protein	137
	DBO90_RS12630	WP_009976097.1	SDR family oxidoreductase	267
	DBO90_RS18520	WP_009974923.1	IS110 family transposase	401
	DBO90_RS12105	WP_009976221.1	Cupin domain-containing protein	136

"NA" indicates that gene is either not present or changed from the initial annotation, hence there is no original locus tag.

RefSeq locus tag prefix DBO90 is based on Maa HJW.

RefSeq locus tag prefix FCV17 is based on Mah 101174.

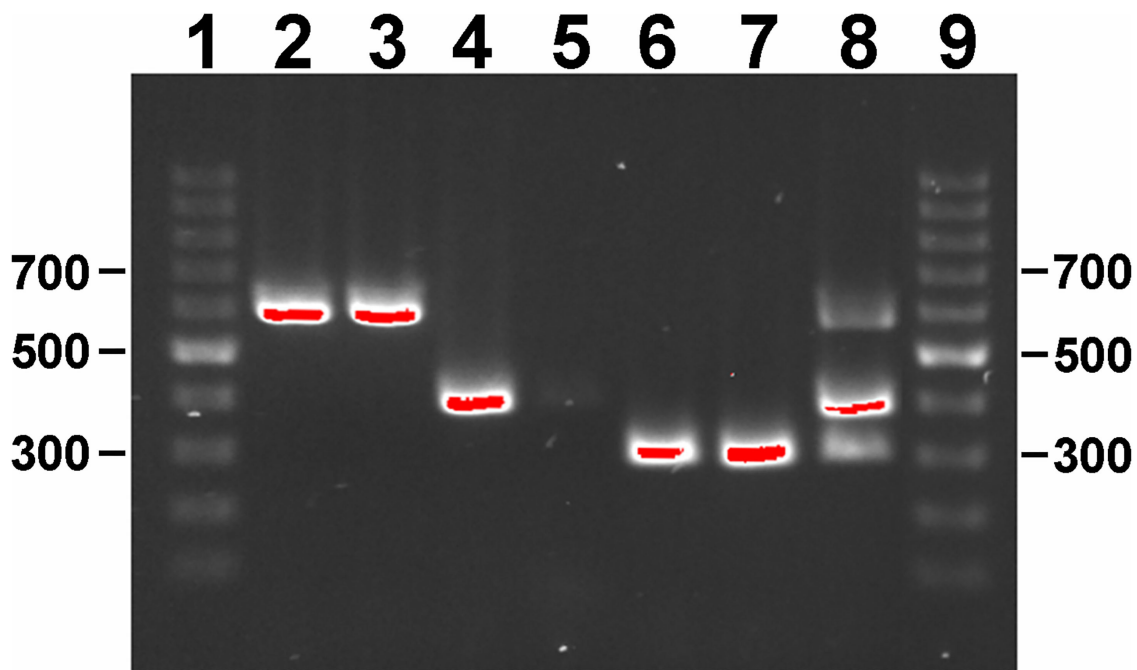


FIGURE 3 | Gel electrophoresis of single-reaction PCR products on a 1% agarose gel stained with ethidium bromide. Lane assignments: 1 and 9 = 100 bp ladder; 2 = *Map* K-10; 3 = *Map* ATCC 19698; 4 = *Maa* Strain 18; 5 = *Maa* ATCC 35719; 6 = *Mah* HS 09-5894; 7 = *Mah* HS 10-1725; 8 = 117p-6084-MA 1115 mixture. Size standards are indicated in the left and right margins. Red indicates DNA band saturation.

significant drop in the overall number of hypothetical proteins, but it suggests how little is known about these novel subspecies-specific genes. Also notable among this group is an operon of genes encoding Mce family proteins (Table 5), some of which are surface exposed and play a role in virulence and lipid transport (33). These proteins are typically conserved among the mycobacteria, and at least one gene this group is no different as *in silico* PCR analysis showed that the correct sized amplification product is obtained using MAP_RS11145 primers on *M. marseillense* strains (Supplementary Table 6). This species of *Mycobacterium* is considered a member of the *Mycobacterium avium* complex based on 16S rRNA, *rpoB*, and *hsp65* sequence similarity (25).

There are significant differences between PanOCT and Roary analysis in terms of genes assigned to subspecies-specific orthologous clusters. There are 41 genes identified as *Map*-specific by Roary that are not considered specific by PanOCT analysis. These discrepancies are attributed to differences in the algorithms of these two bioinformatic tools. PanOCT uses a single clustering tool compared to Roary, which uses two clustering mechanisms and then merges the results. In addition, Roary appears more stringent in the gene cluster formation through the use of BLASTP identity thresholds of 95%, which yields more gene clusters. This may explain why the Roary output listed more gene clusters specific to *Map* than PanOCT. Roary stringency results in more gene clusters overall since Roary will not cluster genes less identical than the threshold. Thus,

Roary will generate more groups of subspecies-specific genes than PanOCT causing Roary to estimate a higher number of subspecies-specific genes. On the other hand, PanOCT will group some of the genes because of its lower stringency and the number of specific groups will be lower.

Other discrepancies not related to mechanistic processes used by each tool can be traced to unexpected annotation differences in very similar orthologs. It is important to note that PanOCT is designed to give context to its findings in relation to genome organization and works off annotation data. This may be the reason why there is only one *Map*-specific gene identified by PanOCT analysis that is not listed by Roary. That one gene, encoding alpha/beta hydrolase (MAP_RS19250 in K-10), has the same translational start for all of the *Map* strains except Telford, which starts 95 codons downstream of the other strains (Supplementary Figure 1). This prevented its inclusion by Roary, and thus it was not considered a *Map*-specific gene, but it is indeed *Map*-specific. The same situation can be applied to the *Mah*-specific gene (MAV_RS08635 in strain 104), which encodes hydroxycinnamic acid hydroxylase (Table 3). These results pose the question of which bioinformatic approach works better for defining these diagnostic gene targets. Since agreement of both pipelines was required, the more conservative method would drive the final list of targets. Is the conservative assessment by PanOCT too strict or is Roary too liberal? Or is it somewhere in between? The only way to answer the question of whether the conservative nature of PanOCT was warranted would be

to test those genes identified only by Roary to determine their diagnostic specificity. When the 41-gene subset from Roary analysis was further analyzed by BLAST against the NCBI database, most of these genes (31 of 41) showed reasonably strong homologies to other, more distantly related, *Mycobacterium* species (**Supplementary Table 3**). Therefore, PanOCT might be the better bioinformatic tool to use in this approach.

There are several possible reasons for the non-specific amplification of selected genes that were reported as specific by PanOCT and Roary analysis. First, the region amplified in non-*Map* strains may not have been called as a protein coding region (pseudogene, intergenic region, or frameshifted protein). Second, the region amplified in non-*Map* strains may be in a protein coding region that is annotated in a different reading frame compared to *Map* strains. Third, underlying errors in genomic sequence could produce both these types of annotation deviations or the regions may be near a site where one of the strain clusters is reorganized compared to the other cluster. One example is MAP_RS22905, a gene specific to *Map* based on PanOCT and Roary, but amplifies a product in non-*Map* strains by *in silico* PCR and Taq-based PCR. This gene encodes a hypothetical protein and is immediately upstream of MAP_RS17350 in *Map* K-10, but with a significant 27-amino acid overlap in these coding sequences. MAP_RS17350 is annotated as a frameshifted non-functional protein that contains several internal stop codons. The primers to this gene were designed such that the forward primer binds within the MAP_RS22905 coding sequence while the reverse primer binds within the coding sequence that overlaps with MAP_RS17350. In the non-*Map* strains (as well as other *Map* strains) there is a single protein that is functional and encompasses the sequence that corresponds to MAP_RS22905 and MAP_RS17350. Therefore, it is important to examine the location of predicted amplicons in the genome context to clear up some ambiguities.

While some Taq-based amplification reactions were unexpectedly positive, and thus non-specific, other reactions were unexpectedly negative. One *Map*-specific gene (MAP_RS14095) did not amplify any of the genomic DNAs using the primer pairs (**Table 4**). These primers were carefully selected using strict parameters which resulted in a PCR product of the correct size by *in silico* PCR, but still did not amplify a product using purified genomic DNAs. Therefore, this primer pair was considered bad and MAP_RS14095 has yet to be confirmed as subspecies-specific. An additional six *Map*-specific genes failed to amplify using only the *Map* strain Linda template, although all of the other genes were successfully amplified with this genomic DNA sample. It is unclear why these genes did not amplify with this one template, since a search of unfinished contigs for the Linda strain suggests these six genes are indeed present. Nonetheless, these genes were not included among the *Map*-specific genes because they didn't amplify using two independent commercial recipes.

The insertion sequence IS900 and many other repeat elements were not identified by PanOCT or Roary analysis. This is due to the lack of such elements included in the two *Map* Egyptian isolates E1 (CP010113.1) and E93 (CP010114.1) (34). Applying the criteria used in this study that the gene must be present in all

Map and absent in all non-*Map*, these sequences do not appear in the E1 and E93 strains for reasons speculated previously (2), and hence they did not make the list. Nonetheless, there is no doubt that these two commonly used repetitive sequences are indeed *Map* specific and present in all *Map* strains. Surprisingly, the ISMap02 sequence did show positive PCR reactions with some *Mah* strains, but not with *Maa* (data not shown), casting doubt on its diagnostic specificity. Repetitive sequences specific to *Mah* and *Maa* were also identified in this study. One example is DBO90_RS18520 (from *Maa* HJW), an IS110 family transposase that has 14–16 copies in *Maa* strains.

F57, *hspX*, and locus 251 have been widely used as diagnostic sequences for *Map* (11, 13, 18, 35). These genes were checked against the subspecies-specific gene lists obtained from the current analyses. The F57 sequence occurs within MAP_RS22535 (MAP_0865) and was also identified as *Map*-specific in this study. Likewise, *hspX* was originally discovered as a *Map*-specific gene before the whole genome sequence was available (11) and was subsequently shown to be expressed within *Map*-infected macrophages (12). The locus tag for this sequence is MAP_RS11095 (MAP_2182c) and has been used in studies to determine antigenic reactivity (36). Locus 251 has been tested in a real-time PCR platform and was considered *Map*-specific in that context (14). All three of these sequences were also identified in this study as *Map*-specific by Roary, PanOCT, and PCR analysis.

One area where annotations have improved dramatically has been in G+C rich organisms like the mycobacteria. RefSeq annotation has identified new coding sequences that were previously hidden in the same genome because original annotation software either missed them or called distinctly different start sites or reading frames for the same gene. Because of the consistency in the RefSeq annotation pipeline, genomes can now be directly compared at the gene feature level. Several subspecies specific genes identified in this study do not list an outdated locus tag, but only the updated RefSeq locus tag. Among the *Map*-specific genes, 17 do not have an original locus tag designation (**Table 5**), representing 20% of the *Map*-specific genes identified in this study that might have been “missed” or changed significantly from the initial sequence annotation (37). For example, closer inspection of MAP_RS04350, which does not list an original locus tag in **Table 5** and is annotated as a hypothetical protein, actually encodes the C-terminal 86 amino acids of MAP_0852 which was previously shown to be *Map*-specific (22). Other similar examples of shifted coding sequences that result in dropped locus tags from the original annotation exist as well. In our previous studies, we expressed *Map*-specific coding sequences identified by the original annotation and tested them for antibody reactivity (38). Although specific antigens were identified, additional testing revealed low antibody reactivity to all *Map*-specific coding sequences known at that time. Now with these updated RefSeq coding sequences identified by the prokaryotic genome annotation pipeline (PGAP), there still remains a possibility to obtain a truly specific and strong antigen for *Map*. Therefore, these updated RefSeq coding sequences should be recombinantly expressed and examined

for antigenicity as has been done with previous *Map*-specific genes (38).

DATA AVAILABILITY STATEMENT

The original contributions presented in the study are included in the article/**Supplementary Materials**, further inquiries can be directed to the corresponding author/s.

AUTHOR CONTRIBUTIONS

JB conceived and designed the study. All authors made substantial contributions to the experimentation, analysis, and writing of the manuscript.

REFERENCES

- Biet F, Boschioli ML. Non-tuberculous mycobacterial infections of veterinary relevance. *Res Vet Sci.* (2014) 97(Suppl):S69–77. doi: 10.1016/j.rvsc.2014.08.007
- Bannantine JP, Conde C, Bayles DO, Branger M, Biet F. Genetic diversity among *Mycobacterium avium* subspecies revealed by analysis of complete genome sequences. *Front Microbiol.* (2020) 11:1701. doi: 10.3389/fmicb.2020.01701
- Gautam M, Anderson P, Ridler A, Wilson P, Heuer C. Economic cost of ovine John's disease in clinically affected New Zealand flocks and benefit-cost of vaccination. *Vet Sci.* (2018) 5:16. doi: 10.3390/vetsci5010016
- Losinger WC. Economic impact of reduced milk production associated with John's disease on dairy operations in the USA. *J Dairy Res.* (2005) 72:425–32. doi: 10.1017/S0022029905001007
- Tran QT, Han XY. Subspecies identification and significance of 257 clinical strains of *Mycobacterium avium*. *J Clin Microbiol.* (2014) 52:1201–6. doi: 10.1128/JCM.03399-13
- Dhama K, Mahendran M, Tiwari R, Dayal Singh S, Kumar D, Singh S, et al. Tuberculosis in birds: insights into the *Mycobacterium avium* infections. *Vet Med Int.* (2011) 2011:712369. doi: 10.4061/2011/712369
- Johansen TB, Djonje B, Jensen MR, Olsen I. Distribution of IS1311 and IS1245 in *Mycobacterium avium* subspecies revisited. *J Clin Microbiol.* (2005) 43:2500–2. doi: 10.1128/JCM.43.5.2500-2502.2005
- Semret M, Zhai G, Mostowy S, Cleto C, Alexander D, Cangelosi G, et al. Extensive genomic polymorphism within *Mycobacterium avium*. *J Bacteriol.* (2004) 186:6332–4. doi: 10.1128/JB.186.18.6332-6334.2004
- Green EP, Tizard ML, Moss MT, Thompson J, Winterbourne DJ, McFadden JJ, et al. Sequence and characteristics of IS900, an insertion element identified in a human Crohn's disease isolate of *Mycobacterium paratuberculosis*. *Nucleic Acids Res.* (1989) 17:9063–73. doi: 10.1093/nar/17.22.9063
- Collins DM, Gabric DM, De Lisle GW. Identification of a repetitive DNA sequence specific to *Mycobacterium paratuberculosis*. *FEMS Microbiol Lett.* (1989) 51:175–8. doi: 10.1111/j.1574-6968.1989.tb03440.x
- Ellingson JL, Bolin CA, Stabel JR. Identification of a gene unique to *Mycobacterium avium* subspecies *paratuberculosis* and application to diagnosis of *paratuberculosis*. *Mol Cell Probes.* (1998) 12:133–42. doi: 10.1006/mcpr.1998.0167
- Bannantine JP, Stabel JR. HspX is present within *Mycobacterium paratuberculosis*-infected macrophages and is recognized by sera from some infected cattle. *Vet Microbiol.* (2000) 76:343–58. doi: 10.1016/S0378-1135(00)00247-9
- Tasara T, Stephan R. Development of an F57 sequence-based real-time PCR assay for detection of *Mycobacterium avium* subsp. *paratuberculosis* in milk. *Appl Environ Microbiol.* (2005) 71:5957–68. doi: 10.1128/AEM.71.10.5957-5968.2005
- Rajeev S, Zhang Y, Sreevatsan S, Motiwala AS, Byrum B. Evaluation of multiple genomic targets for identification and confirmation of *Mycobacterium avium* subsp. *paratuberculosis* isolates using real-time PCR. *Vet Microbiol.* (2005) 105:215–21. doi: 10.1016/j.vetmic.2004.10.018
- Bannantine JP, Baechler E, Zhang Q, Li L, Kapur V. Genome scale comparison of *Mycobacterium avium* subsp. *paratuberculosis* with *Mycobacterium avium* subsp. *avium* reveals potential diagnostic sequences. *J Clin Microbiol.* (2002) 40:1303–10. doi: 10.1128/JCM.40.4.1303-1310.2002
- Poupart P, Coene M, Van Heuverswyn H, Cocito C. Preparation of a specific RNA probe for detection of *Mycobacterium paratuberculosis* and diagnosis of John's disease. *J Clin Microbiol.* (1993) 31:1601–5. doi: 10.1128/JCM.31.6.1601-1605.1993
- Semret M, Alexander DC, Turenne CY, de Haas P, Overduin P, van Soolingen D, et al. Genomic polymorphisms for *Mycobacterium avium* subsp. *paratuberculosis* diagnostics. *J Clin Microbiol.* (2005) 43:3704–12. doi: 10.1128/JCM.43.8.3704-3712.2005
- Sidoti F, Banche G, Astegiano S, Allizond V, Cuffini AM, Bergallo M. Validation and standardization of IS900 and F57 real-time quantitative PCR assays for the specific detection and quantification of *Mycobacterium avium* subsp. *paratuberculosis*. *Can J Microbiol.* (2011) 57:347–54. doi: 10.1139/w11-022
- Slana I, Liapi M, Moravkova M, Kralova A, Pavlik I. *Mycobacterium avium* subsp. *paratuberculosis* in cow bulk tank milk in Cyprus detected by culture and quantitative IS900 and F57 real-time PCR. *Prev Vet Med.* (2009) 89:223–6. doi: 10.1016/j.prevetmed.2009.02.020
- Paustian ML, Kapur V, Bannantine JP. Comparative genomic hybridizations reveal genetic regions within the *Mycobacterium avium* complex that are divergent from *Mycobacterium avium* subsp. *paratuberculosis* isolates. *J Bacteriol.* (2005) 187:2406–15. doi: 10.1128/JB.187.7.2406-2415.2005
- Paustian ML, Zhu X, Sreevatsan S, Robbe-Austerman S, Kapur V, Bannantine JP. Comparative genomic analysis of *Mycobacterium avium* subspecies obtained from multiple host species. *BMC Genomics.* (2008) 9:135. doi: 10.1186/1471-2164-9-135
- Paustian ML, Bannantine JP, Kapur V. *Mycobacterium avium* subspecies *paratuberculosis* Genome. In: Behr MA, Collins DM, editors. *Paratuberculosis: Organism, Disease, Control*. Oxfordshire: CAB International (2010). p. 73–82.
- Page AJ, Cummins CA, Hunt M, Wong VK, Reuter S, Holden MT, et al. Roary: rapid large-scale prokaryote pan genome analysis. *Bioinformatics.* (2015) 31:3691–3. doi: 10.1093/bioinformatics/btv421
- Fouts DE, Brinkac L, Beck E, Inman J, Sutton G. PanOCT: automated clustering of orthologs using conserved gene neighborhood for pan-genomic analysis of bacterial strains and closely related species. *Nucleic Acids Res.* (2012) 40:e172. doi: 10.1093/nar/gks757
- Ben Salah I, Cayrou C, Raoult D, Drancourt M. *Mycobacterium marseillense* sp. nov., *Mycobacterium timonense* sp. nov. and *Mycobacterium bouchadurhonnense* sp. nov., members of the *Mycobacterium avium* complex. *Int J Syst Evol Microbiol.* (2009) 59(Pt 11):2803–8. doi: 10.1099/ijs.0.010637-0
- Matsumoto Y, Kinjo T, Motooka D, Nabeya D, Jung N, Uechi K, et al. Comprehensive subspecies identification of 175 nontuberculous mycobacteria

FUNDING

This work was funded by the USDA Agricultural Research Service.

ACKNOWLEDGMENTS

We thank Kayla E. Straight for excellent technical support.

SUPPLEMENTARY MATERIAL

The Supplementary Material for this article can be found online at: <https://www.frontiersin.org/articles/10.3389/fvets.2020.620094/full#supplementary-material>

- species based on 7547 genomic profiles. *Emerg Microbes Infect.* (2019) 8:1043–53. doi: 10.1080/22221751.2019.1637702
27. Goethe R, Basler T, Meissner T, Goethe E, Sproer C, Swiderski J, et al. Complete genome sequence and manual reannotation of *Mycobacterium avium* subsp. *paratuberculosis* strain DSM 44135. *Microbiol Resour Announc.* (2020) 9:e00711–20. doi: 10.1128/MRA.00711-20
 28. Goethe R, Laarmann K, Sproer C, Bunk B. Complete genome sequence of *Mycobacterium avium* subsp. *avium* Chester (DSM 44156). *Microbiol Resour Announc.* (2020) 9:e01549–19. doi: 10.1128/MRA.01549-19
 29. Kanehisa M, Furumichi M, Tanabe M, Sato Y, Morishima K. KEGG: new perspectives on genomes, pathways, diseases and drugs. *Nucleic Acids Res.* (2017) 45:D353–61. doi: 10.1093/nar/gkw1092
 30. Huerta-Cepas J, Szklarczyk D, Heller D, Hernandez-Plaza A, Forslund SK, Cook H, et al. eggNOG 5.0: a hierarchical, functionally and phylogenetically annotated orthology resource based on 5090 organisms and 2502 viruses. *Nucleic Acids Res.* (2019) 47:D309–14. doi: 10.1093/nar/gky1085
 31. Semret M, Turenne CY, de Haas P, Collins DM, Behr MA. Differentiating host-associated variants of *Mycobacterium avium* by PCR for detection of large sequence polymorphisms. *J Clin Microbiol.* (2006) 44:881–7. doi: 10.1128/JCM.44.3.881-887.2006
 32. Rajagopal A, Yurk D, Shin C, Menge K, Jacky L, Fraser S, et al. Significant expansion of real-time PCR multiplexing with traditional chemistries using amplitude modulation. *Sci Rep.* (2019) 9:1053. doi: 10.1038/s41598-018-37732-y
 33. Casali N, Riley LW. A phylogenomic analysis of the actinomycetales mce operons. *BMC Genomics.* (2007) 8:60. doi: 10.1186/1471-2164-8-60
 34. Amin AS, Hsu CY, Darwish SE, Ghosh P, AbdEl-Fatah EM, Behour TS, et al. Ecology and genomic features of infection with *Mycobacterium avium* subspecies *paratuberculosis* in Egypt. *Microbiology.* (2015) 161(Pt 4):807–18. doi: 10.1099/mic.0.000051
 35. Motiwala AS, Amonsin A, Strother M, Manning EJ, Kapur V, Sreevatsan S. Molecular epidemiology of *Mycobacterium avium* subsp. *paratuberculosis* isolates recovered from wild animal species. *J Clin Microbiol.* (2004) 42:1703–12. doi: 10.1128/JCM.42.4.1703-1712.2004
 36. Bannantine JP, Paustian ML, Waters WR, Stabel JR, Palmer MV, Li L, et al. Profiling bovine antibody responses to *Mycobacterium avium* subsp. *paratuberculosis* infection by using protein arrays. *Infect Immun.* (2008) 76:739–49. doi: 10.1128/IAI.00915-07
 37. Li L, Bannantine JP, Zhang Q, Amonsin A, May BJ, Alt D, et al. The complete genome sequence of *Mycobacterium avium* subspecies *paratuberculosis*. *Proc Natl Acad Sci USA.* (2005) 102:12344–9. doi: 10.1073/pnas.0505662102
 38. Paustian ML, Amonsin A, Kapur V, Bannantine JP. Characterization of novel coding sequences specific to *Mycobacterium avium* subsp. *paratuberculosis*: implications for diagnosis of John's Disease. *J Clin Microbiol.* (2004) 42:2675–81. doi: 10.1128/JCM.42.6.2675-2681.2004

Conflict of Interest: The authors declare that the research was conducted in the absence of any commercial or financial relationships that could be construed as a potential conflict of interest.

Copyright © 2021 Bannantine, Stabel, Bayles, Conde and Biet. This is an open-access article distributed under the terms of the Creative Commons Attribution License (CC BY). The use, distribution or reproduction in other forums is permitted, provided the original author(s) and the copyright owner(s) are credited and that the original publication in this journal is cited, in accordance with accepted academic practice. No use, distribution or reproduction is permitted which does not comply with these terms.



Detection of *Mycobacterium avium* ssp. *paratuberculosis* in Cultures From Fecal and Tissue Samples Using VOC Analysis and Machine Learning Tools

OPEN ACCESS

Edited by:

Kumi de Silva,
The University of Sydney, Australia

Reviewed by:

Kenneth James Genovese,
United States Department of
Agriculture, United States
Eric Altermann,
AgResearch Ltd., New Zealand

*Correspondence:

Heike Köhler
heike.koehler@flii.de

† Present address:

Anne Klassen,
Thüringer Tierseuchenkasse,
Rindergesundheitsdienst, Jena,
Germany;
Peter Gierschner,
Albutec GmbH, Rostock, Germany

Specialty section:

This article was submitted to
Veterinary Infectious Diseases,
a section of the journal
Frontiers in Veterinary Science

Received: 22 October 2020

Accepted: 13 January 2021

Published: 03 February 2021

Citation:

Vitense P, Kasbohm E, Klassen A,
Gierschner P, Trefz P, Weber M,
Miekisch W, Schubert JK, Möbius P,
Reinhold P, Liebscher V and Köhler H
(2021) Detection of *Mycobacterium*
avium ssp. *paratuberculosis* in
Cultures From Fecal and Tissue
Samples Using VOC Analysis and
Machine Learning Tools.
Front. Vet. Sci. 8:620327.
doi: 10.3389/fvets.2021.620327

Philipp Vitense¹, Elisa Kasbohm¹, Anne Klassen^{2†}, Peter Gierschner^{3†}, Phillip Trefz³,
Michael Weber², Wolfram Miekisch³, Jochen K. Schubert³, Petra Möbius⁴,
Petra Reinhold², Volkmar Liebscher¹ and Heike Köhler^{4*}

¹ Institute of Mathematics and Computer Science, University of Greifswald, Greifswald, Germany, ² Institute of Molecular Pathogenesis, Friedrich-Loeffler-Institut, Jena, Germany, ³ Department of Anaesthesia and Intensive Care, University Medicine Rostock, Rostock, Germany, ⁴ National Reference Laboratory for Paratuberculosis, Institute of Molecular Pathogenesis, Friedrich-Loeffler-Institut, Jena, Germany

Analysis of volatile organic compounds (VOCs) is a novel approach to accelerate bacterial culture diagnostics of *Mycobacterium avium* subsp. *paratuberculosis* (MAP). In the present study, cultures of fecal and tissue samples from MAP-infected and non-suspect dairy cattle and goats were explored to elucidate the effects of sample matrix and of animal species on VOC emissions during bacterial cultivation and to identify early markers for bacterial growth. The samples were processed following standard laboratory procedures, culture tubes were incubated for different time periods. Headspace volume of the tubes was sampled by needle trap-micro-extraction, and analyzed by gas chromatography-mass spectrometry. Analysis of MAP-specific VOC emissions considered potential characteristic VOC patterns. To address variation of the patterns, a flexible and robust machine learning workflow was set up, based on random forest classifiers, and comprising three steps: variable selection, parameter optimization, and classification. Only a few substances originated either from a certain matrix or could be assigned to one animal species. These additional emissions were not considered informative by the variable selection procedure. Classification accuracy of MAP-positive and negative cultures of bovine feces was 0.98 and of caprine feces 0.88, respectively. Six compounds indicating MAP presence were selected in all four settings (cattle vs. goat, feces vs. tissue): 2-Methyl-1-propanol, 2-methyl-1-butanol, 3-methyl-1-butanol, heptanal, isoprene, and 2-heptanone. Classification accuracies for MAP growth-scores ranged from 0.82 for goat tissue to 0.89 for cattle feces. Misclassification occurred predominantly between related scores. Seventeen compounds indicating MAP growth were selected in all four settings, including the 6 compounds indicating MAP presence. The concentration levels of 2,3,5-trimethylfuran, 2-pentylfuran, 1-propanol, and 1-hexanol were indicative for MAP cultures before visible growth was apparent. Thus,

very accurate classification of the VOC samples was achieved and the potential of VOC analysis to detect bacterial growth before colonies become visible was confirmed. These results indicate that diagnosis of paratuberculosis can be optimized by monitoring VOC emissions of bacterial cultures. Further validation studies are needed to increase the robustness of indicative VOC patterns for early MAP growth as a pre-requisite for the development of VOC-based diagnostic analysis systems.

Keywords: bacterial culture, diagnostics, machine learning, *Mycobacterium avium* ssp. *paratuberculosis*, paratuberculosis, random forests, variable selection, volatile organic compound

INTRODUCTION

Detection of volatile organic compounds (VOCs) derived from bacterial metabolism has been proposed as a novel approach in diagnostic microbiology. VOCs originate from metabolic processes of the bacteria. Due to their physicochemical properties, they transform into gaseous state already at low temperatures. Appearing in very low concentrations (nmol/L—pmol/L or ppbV—pptV) they belong to all classes of organic substances (1). Technologies in use for the analysis of volatiles include (high-resolution) mass spectrometry (MS) approaches, including soft chemical ionization mass spectrometry (SCIMS) or gas chromatography-mass spectrometry (GC-MS), spectroscopic techniques, and sensors. Analyzers can be allocated to two categories, namely *offline* systems, which require sample workup such as pre-concentration prior to analysis, and *online* instrumentation, which can analyze samples directly without manipulation (2). Online monitoring of bacteria-specific VOC-profiles during cultivation would enable direct species identification without further processing of samples, and would thus reduce labor and costs. In addition, highly sensitive detection of VOCs released by growing bacteria could allow detection of bacterial growth earlier than currently possible. This is of special interest for slow-growing bacteria, such as *Mycobacterium avium* ssp. *paratuberculosis* (MAP).

Bacterial culture on solid or liquid media with subsequent species confirmation via polymerase chain reaction (PCR) is still considered the most sensitive and robust diagnostic method for the detection of MAP in different types of samples (3). This labor-intensive and time-consuming procedure takes weeks to months until reliable results are available (4). Automated liquid culture systems, which were adopted recently for MAP, resulted in reduced cultivation times, but still demand further processing of the samples for species identification (5, 6). In an attempt to reduce time to result, (real-time) PCR based techniques have been established and introduced in routine diagnostics (7–9). The performance of PCR based methods depends largely on the efficacy of the protocol used for nucleic acid extraction from clinical samples (10, 11). The detection rate is reduced when samples with low bacterial load are tested (12, 13). On the other hand, due to their high analytic sensitivity, these methods are prone to sample misclassification by false positive results because of cross contaminations (own unpublished results). The main advantage of PCR techniques compared to bacterial culture is the short time necessary until results are

available. A diagnostic approach combining the advantages of both techniques without increased risk of misclassification is highly desirable.

Recent studies have shown that it is possible to detect growth of MAP by measuring volatile organic compounds in the headspace of bacterial cultures (14, 15), even before colonies become visually apparent (16). Instead of individual indicative substances, these studies recorded a selection of several VOCs (i.e., a “VOC profile”) in order to differentiate growing MAP cultures from control vials and from cultures of other mycobacterial species. The composition of the VOC profiles varied to some extent depending on MAP strain (14, 15), culture medium (15), bacterial density (14, 15), and duration of incubation (15). However, it was possible to define a core profile of 28 VOCs related to growth of MAP cultures by a meta-analysis (17).

As a common feature of these studies, pure bacterial cultures were grown using laboratory strains of different field isolates. In practical diagnostics, however, MAP is being isolated from different matrices, such as feces and tissue samples of variable animal species, solid or liquid manure and even dust from the housing environment of the animals. These matrices may emit additional VOCs during cultivation, which might possibly interfere with the MAP-specific VOC profile. This problem has not been addressed so far (17).

Matrix-related VOC emissions were investigated in this study as a necessary step toward practical application. Cultures of native diagnostic samples from MAP infected and non-suspect cattle and goats were examined to elucidate the effects of the sample matrix (feces or tissue) and of the animal species on VOC emissions during cultivation. On this basis, the applicability of the MAP-specific core-profile to diagnose MAP cultures was reviewed.

Previous studies showed that VOC concentrations above MAP cultures varied in relation to bacterial density (14, 15). The majority of substances increased with increasing bacterial counts, others decreased, or they decreased after an initial increase (15). Therefore, a data analysis workflow based on random forests was developed to capture those varying VOC patterns in a multivariate fashion. The workflow comprises also a random forest-based variable selection procedure to pick all relevant VOCs from the full panel of volatile compounds that were detected in the headspace volume of the bacterial cultures. Repeated cross-validation was deployed to robustify the results of the workflow.

We analyzed the data, on the one hand, focusing on MAP presence and, on the other hand, focusing on different stages of MAP growth in native samples, taking into account varying patterns of VOC emission in relation to bacterial growth. Thus, by using a tailored machine learning workflow, we aimed at identifying MAP-specific VOC profiles that allow sample classification already after short periods of cultural incubation.

MATERIALS AND METHODS

Samples

Fecal and tissue samples ($n = 80$) with culturally pre-defined MAP status were derived from the sample collection of the German National Reference Laboratory for paratuberculosis at the Friedrich-Loeffler-Institut. Fecal samples from cattle and goats originated from different animals and herds enrolled in a field study performed in 2016 and 2017. The study protocol was approved by the responsible authority, the Animal Health and Welfare Unit of the “Thüringer Landesamt für Verbraucherschutz” (permit number 04-102/16, date of permission: 20.04.2016). Goat tissue samples (mesenteric lymph nodes, tissue from ileum or jejunum) were obtained from different goats necropsied in the course of an experimental infection trial in 2011 and 2012. The animal experiment was approved by the responsible authority (see above, permit number 04-001/11, date of permission: 03.03.2011). Cattle tissue samples were collected after slaughter from different cattle during a slaughterhouse survey in 2007 (18). Presence or absence of MAP was originally examined after admission to the laboratory by cultural isolation following standard laboratory procedures. After first processing, the samples were stored at -20°C (cattle and goat feces, goat tissue) and -80°C (cattle tissue) until preparation for the present study. An overview of the samples is given in **Table 1**. The MAP isolates obtained from cattle and goat feces and from cattle tissue represent eight different MAP genotypes (see **Supplementary Table 1**). The MAP isolates from goat tissue were all derived from MAP strain JII-1961 (19), which was used for inoculation of the animals in the experimental infection trial.

Sample Preparation

The procedures followed in this study conform to protocols established in previous studies (15, 17) in order to enable comparability.

To prepare the test tubes for a fecal sample, 3 g of feces were decontaminated in 30 mL of 0.75% hexadecylpyridinium chloride (HPC, Merck, Darmstadt, Germany) for 48 h in order to eliminate non-MAP flora (20). The supernatant was discarded and the sediment (1–2 mL) was further processed as described below. The tissue samples originated from different parts of ileum, jejunum, or mesenteric lymph nodes. After separating tissue and fat, approximately 1 g of tissue from different parts of the sample were gathered. Decontamination was performed with 0.9% HPC for 24 h at room temperature. The tissue samples were centrifuged and the sediment resuspended with 1 mL of sterile phosphate buffered saline (PBS) to maintain a physiological pH (20).

For both fecal samples as well as tissue samples, nine tubes of slanted Herrold's Egg Yolk Medium with Mycobactin J and Amphotericin, Nalidixic Acid and Vancomycin (HEYM, Becton Dickinson, Heidelberg, Germany) were inoculated with 200 μL of the resulting sediments. After spreading the inoculum evenly over the surface of the solid medium, the tubes were incubated at about 37°C under aerobic conditions. For each set of samples (goat or cattle, negative or MAP-positive), inoculation was performed at a separate day to eliminate carry-over effects. Parallel to these samples, 30 control tubes were prepared for each set either with 200 μL of 0.75% HPC (for feces) or with 200 μL of a 1:1 mixture of PBS and 0.9% HPC (for tissue) without fecal or tissue matter. The control tubes were treated and incubated under the same conditions as the test tubes.

Colony growth was assessed regularly by visual inspection, colony counts up to 50 colonies were counted, higher colony counts were estimated following a standard laboratory procedure. Growth was scored at the end of the pre-determined incubation period in the following way: score 0—no growth visible, score 0.5—one to 20 colonies, score 1—21 to 50 colonies, score 2—51 to 100 colonies, score 3—loose layer, score 4—dense layer. The duration of culture incubation was defined depending on the expected growth characteristics of the MAP isolates in order to cover different growth stages of the individual samples. Of the nine test tubes per original sample, three were randomly selected at the pre-determined end of the incubation period after 4, 6, and 8 weeks for cattle feces and tissue and goat tissue, and after 16, 18, or 20 weeks for goat feces. An exception had to be made for MAP cultures from goat feces: The cultures of two samples grew unexpectedly fast. Incubation of three randomly selected culture tubes was therefore interrupted after 4, 6, and 8 weeks and the tubes were moved to a refrigerator to limit further growth. Before GC-MS measurement, these tubes were again incubated for 7 days at 37°C . Finally, they were measured 16–20 weeks after inoculation. The test tubes of the other MAP-positive and negative samples and the control tubes were incubated for the pre-determined period of 16, 18, or 20 weeks. The final sample sizes can be seen in **Table 2**.

VOC Analysis

The headspace volume of the tubes was sampled by means of needle trap microextraction (NTME) and analyzed by GC-MS as described elsewhere (14, 15). The GC-MS system consisted of an Agilent 7890A gas chromatograph and an Agilent 5975C inert XL MSD mass spectrometer. In order to identify unknown VOCs from the mass spectra, first, a mass spectral library search (NIST 2005 Gatesburg, PA, USA) was carried out and, subsequently, compounds were verified and quantified by measurements of pure reference substances. Altogether, more than 100 volatile substances were detected in the headspace volumes. VOCs which could not be identified unequivocally, which could not be quantified or which were assigned to contamination from room air were excluded from the VOC panel in a pre-processing screening of the GC-MS spectra.

TABLE 1 | Overview of the samples included in the study.

Matrix	Species	MAP-negative Number of Herds/ Animals/Samples	MAP-positive Number of Herds/ Animals/Samples/ MAP genotypes
Feces	Cattle	5/10/10	4/10/10/3
	Goat	3/10/10	3/7/10/2
Tissue	Cattle	1/2/10	5/5/10/6
	Goat	1/5/10	1/5/10/1

Numbers represent the number of herds, number of animals, number of samples and number of MAP genotypes, respectively, for each set of samples (for details on the genotypes see **Supplementary Table 1**).

TABLE 2 | Sample sizes for VOC analysis per species and matrix with regard to incubation periods in accordance with the study design (4/6/8 weeks in general and 16/18/20 weeks for goat feces, respectively).

Matrix	Species	Control vials	MAP-negative	MAP-positive
Feces	Cattle	20/20/20	20/20/20	18/20/20
	Goat	20/18/20	20/20/20	20/20/20
Tissue	Cattle	20/20/20	20/20/20	20/20/20
	Goat	20/20/20	20/20/20	20/20/20

Data Analysis

Exploratory data analysis included heat maps to visualize normalized concentrations of each VOC in the individual samples, and principal component analysis (PCA) to assess if differentiation of MAP-positive and negative samples is possible in general. Basic graphical representations of the data (e.g., box-whisker plots, scatterplots) were explored interactively by means of a specially tailored R Shiny app. A correlation analysis using Spearman's rank correlation coefficient was performed for VOC measurements of bacterial cultures with visible growth to detect clusters of compounds with similar or opposite trends which might be related to MAP growth.

VOC emissions of control vials were considered baselines and used for quality assessment. Effects of the extended incubation period of 16–20 weeks in comparison to 2–8 weeks on VOC concentration in the headspace volume above pure media was assessed using two-sided Mann–Whitney–U-tests with Bonferroni *p*-value correction. A tentative screening for potential influences from exogenous sources was performed by assessing variations of control vials between different days of inoculation (using Kruskal–Wallis tests with Bonferroni *p*-value correction) and comparing concentration levels of control vials with those of actual samples (using two-sided Mann–Whitney–U-tests with Bonferroni correction; details in **Supplementary Table 4**).

In order to assess which VOCs might originate from traces of original sample material, feces or tissue, VOC concentration of MAP-negative test tubes was compared to control vials prepared at the same day using one-sided Mann–Whitney–U-tests with Benjamini–Hochberg *p*-value correction. We deployed a one-sided test to capture only VOCs with higher concentration values above MAP-negative test tubes compared to control vials.

Identification of MAP-specific VOC emissions was tackled using machine learning tools: Since the absence or presence of MAP was known for each sample and MAP growth had been scored for each VOC measurement, both could be used as targets for a supervised learning task. The objective of our workflow was to classify samples based on their VOC measurements with high accuracy and to identify VOCs supporting the classification. We decided to base our approach on random forests to be able to consider arbitrary patterns of multiple VOCs in combination. Random forests are completely data-driven and do not assume a specific underlying distribution of the data. In brief, a random forest classifier consists of a large number (typically several hundreds) of decision trees (21–23). Hence, their results are always aggregated across their decision trees, as an inspection of individual trees is not insightful. One result that can be drawn from random forests is a ranking of variable importance. The importance of a variable is determined for each decision tree using the observations that had not been used to construct the respective tree and scored by the loss of classification accuracy after resampling the measurements of the variable. This approach is based on the idea that an informative variable contributes considerably to the classification accuracy of a decision tree and thus resampling of an informative variable will lead to a high loss in accuracy, whereas resampling of a non-informative variable will hardly affect the classification accuracy. The loss of accuracy for each variable is reported as average across all decision trees of the random forest.

The variable selection algorithm Boruta (24) was used to reduce the set of VOCs to those that show variations related to MAP presence or growth. The Boruta algorithm uses random forest variable importance measures to compare variables with randomly permuted copies of themselves. Only if an original variable outperforms the best among all copies it is considered important and used further.

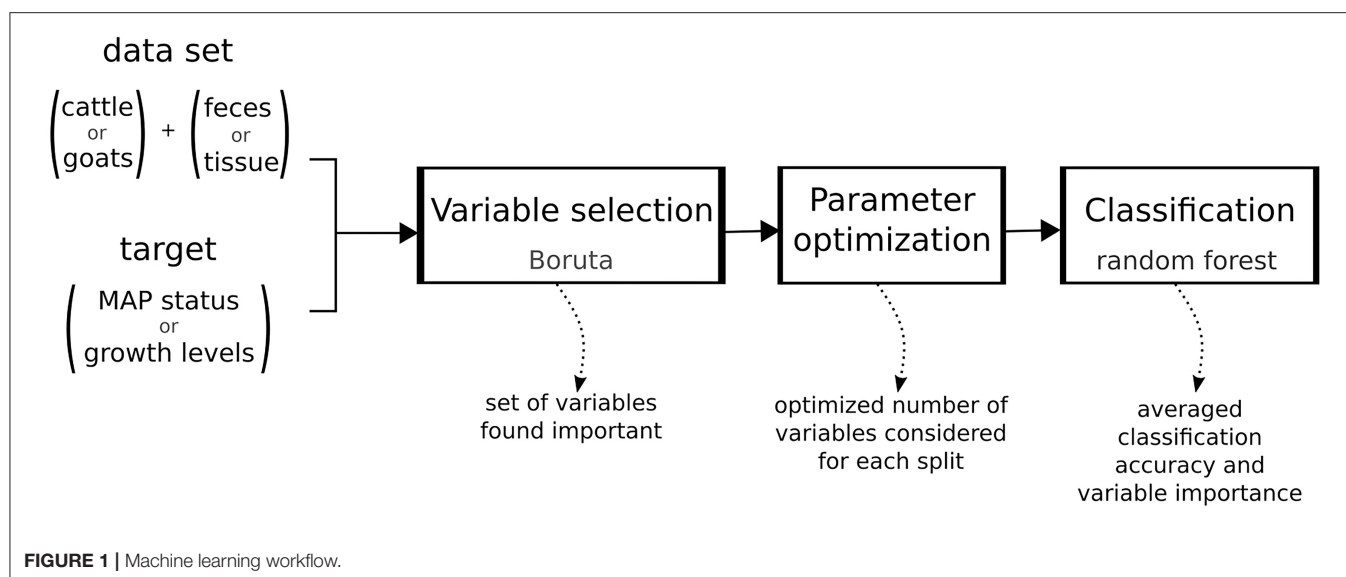
Using the methods described above a robust machine learning workflow was set up as follows (**Figure 1**):

Step 1: *Variable selection with Boruta*. To decrease variance of the decision, the algorithm was applied 30 times and only variables found important in more than 27 of the iterations were used further.

Step 2: *Parameter optimization for random forest*. We optimized the number of variables considered for a split in a decision tree (parameter *mtry*) to maximize classification accuracy.

Step 3: *Classification using random forest*. A random forest classifier consisting of 500 decision trees using the variables selected in step 1 and the optimized parameter from step 2 was trained and the results averaged over 10 repeats of 10-fold cross-validation. For each VOC used in classification the importance measure is the mean decrease in accuracy when randomizing the values of that VOC.

The caret package (25) was used to streamline steps 2 and 3 such that the parameter optimization used the same cross-validation sets as the final classification. As the Boruta algorithm is not yet implemented in the caret package, the variable selection process is based on the complete data set outside of cross-validation.



This workflow was applied to address the two central objectives of the study, first, classification of MAP-positive vs. negative samples to find VOCs specific to MAP presence, and second, differentiation between the different stages of growth (scores from 0 to 4 as described above) and negative samples to find VOCs indicative of the stages of bacterial growth and thus possible candidates enabling accelerated cultural detection.

These analyses were performed for both species and both sample matrices separately. For the growth classifiers, the data was distributed unevenly over different growth stages and upsampling was applied for balancing, except for growth scores that were not observed for a set of samples. To summarize the results, we report the number of selected variables (step 1), the optimized number of variables considered for each new split (step 2) and the averaged classification accuracy of the final model (step 3).

The workflow was implemented in R v3.6.2. (26) with packages Boruta v6.0.0 (24) and caret v6.0-86 (25), which depends on the package randomForest (27). Packages used for data manipulation were dplyr (28) and tidyr (29), and packages used for data visualization were ggplot2 (30), pheatmap (31), factoextra (32), corrplot (33), ggridges (34), ggstance (35), plotly (36), and shiny (37).

RESULTS

VOC Panel

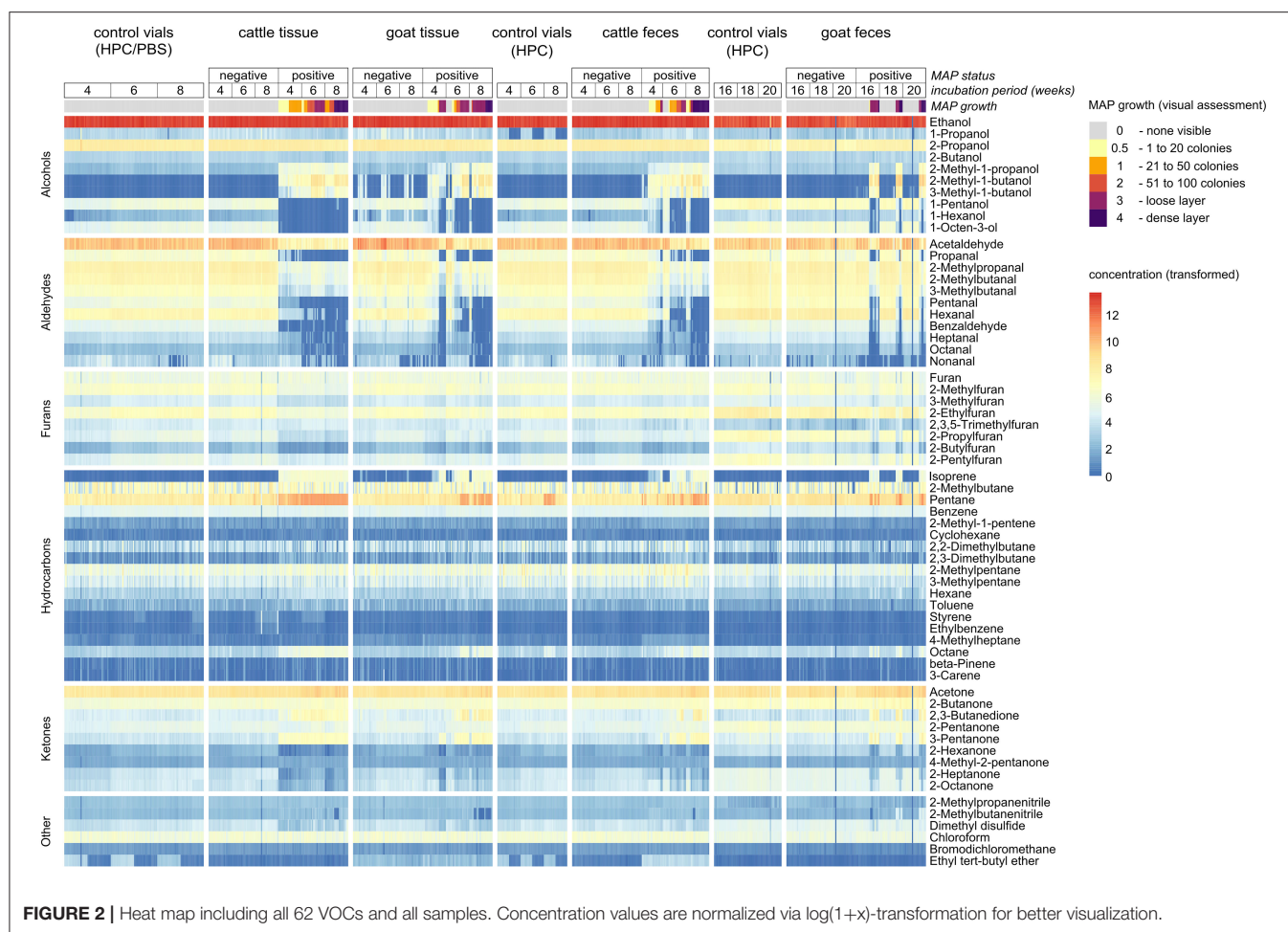
VOC analyses resulted in a panel of 62 volatile substances (Supplementary Tables 2, 3). They belong to the classes of hydrocarbons including acyclic hydrocarbons, alcohols, ketones, aldehydes, furans, nitriles, organosulfur compounds, halogenated hydrocarbons, and ethers. Visual data exploration revealed that some of these compounds showed distinctive differences in concentration for MAP-positive samples in comparison to negative samples and control vials. This became evident in the heat map including all VOCs and all samples (Figure 2)

and also in the visualization based on principal component analysis (PCA, Supplementary Figure 1). Not only increased, but also decreased concentrations above MAP-positive cultures were observed (Figure 2). Some of the MAP-positive goat feces samples did not show any bacterial growth, even after 20 weeks of incubation, which is very likely the reason why their VOC composition resembles negative samples in these visualizations. Correlation analysis revealed clusters of highly correlated compounds in the headspace of bacterial cultures with visible growth (Supplementary Figure 2).

The extended incubation period of 16–20 weeks affected most of the compounds (both increase and decrease in concentration, Supplementary Table 4). Tentative screening for VOCs from exogenous sources captured a single compound: Ethyl tert-butyl ether (ETBE) showed increased levels on 3 consecutive days for both control vials and test tubes irrespective of the content of the test tube (Supplementary Figure 3 and Supplementary Table 4). This compound is a fuel additive and therefore most likely contamination from laboratory room air. Thus, ETBE was excluded from the VOC panel as it introduced a systematic bias.

VOCs Originating From Feces or Tissue

VOC emissions from sample material were analyzed by comparing measurements of negative samples with control vials (see Supplementary Table 5). Fecal samples showed significantly higher concentrations of cyclohexane than control vials, whereas tissue samples showed significantly higher concentrations of acetaldehyde and 1-propanol. Cattle samples were characterized by higher levels of ethanol, propanal, 2-methylpropanal and acetone. In addition, cattle feces samples showed increased concentration levels of 2-propanol, and cattle tissue samples exhibited higher levels of furan, chloroform and 2-methylpropanenitrile. The latter was also elevated in goat feces samples, whereas goat tissue samples were characterized by 4-methylheptane, 2,3-butanedione, 2-methyl-1-butanol and



3-methyl-1-butanol. The last two compounds were detected above LOQ only in goat tissue samples, apart from MAP-positive samples.

VOCs Indicating MAP Presence

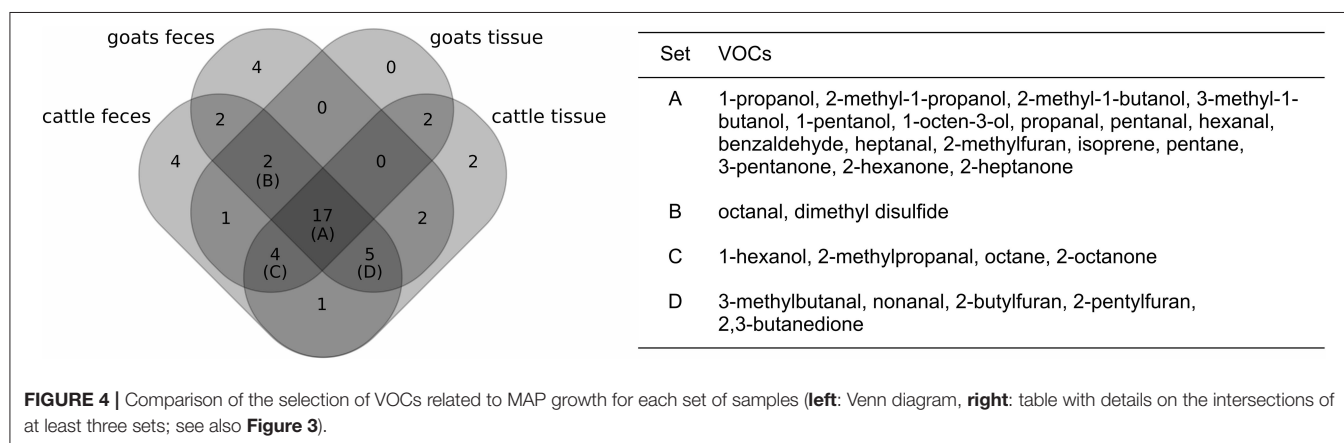
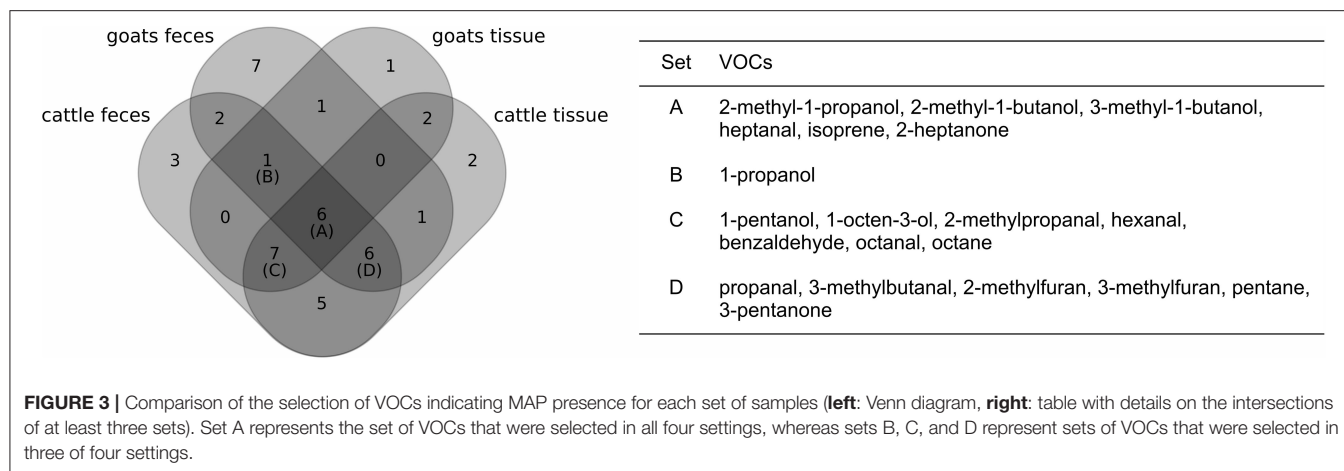
By comparing headspace VOC compositions of MAP-positive and negative samples by our random forest-based workflow, 44 of 61 VOCs were found to show indicative variations between these two groups in at least one of the four settings. The number of selected VOCs ranges from 18 VOCs for goat tissue to 30 VOCs for cattle feces (see **Supplementary Table 6**). Six compounds were selected in all four settings (**Figure 3**): 2-Methyl-1-propanol, 2-methyl-1-butanol, 3-methyl-1-butanol, heptanal, isoprene, and 2-heptanone. Further, 14 compounds were selected in three settings, comprising six aldehydes (propanal, 2-methylpropanal, 3-methylbutanal, hexanal, benzaldehyde, octanal), three alcohols (1-propanol, 1-pentanol, 1-octen-3-ol), two hydrocarbons (pentane, octane), two furans (2-methylfuran, 3-methylfuran), and one ketone (3-pentanone).

We observed that 3-methyl-1-butanol exhibited the maximum variable importance in two of four settings (for fecal samples). However, the relative variable importance

values of the compounds varied considerably between the four settings (**Supplementary Figure 4**). While, three settings yielded a rather steep decline in variable importance from the top compound to the least informative compound of the selection, the results for cattle tissue samples showed that a large proportion of compounds reached comparatively high variable importance values. Ranking compounds by their respective importance value reflects the high variance in variable importance between different settings: Only 2-methylbutanal, pentanal and heptanal were consistently ranked among the top ten variables and selected in at least two settings. However, for all four settings, the random forest classifiers reached high accuracies in discriminating between negative and MAP-positive samples (cross-validated accuracy between 0.89 for goat feces and 1.00 for cattle tissue, **Supplementary Table 6**).

VOCs Related to MAP Growth

The refined analysis targeting the varying bacterial growth densities resulted in a similar selection of VOCs as before: 42 of the 44 VOCs that had been considered before were also selected to differentiate between levels of MAP growth in at least one of the four settings (**Figure 4**). Four VOCs were found



to be related to MAP growth additionally. One of them, 2-pentylfuran, was selected in three of the four settings, whereas the other three compounds (2-pentanone, bromodichloromethane, 2-methylbutanenitrile) had been selected only once.

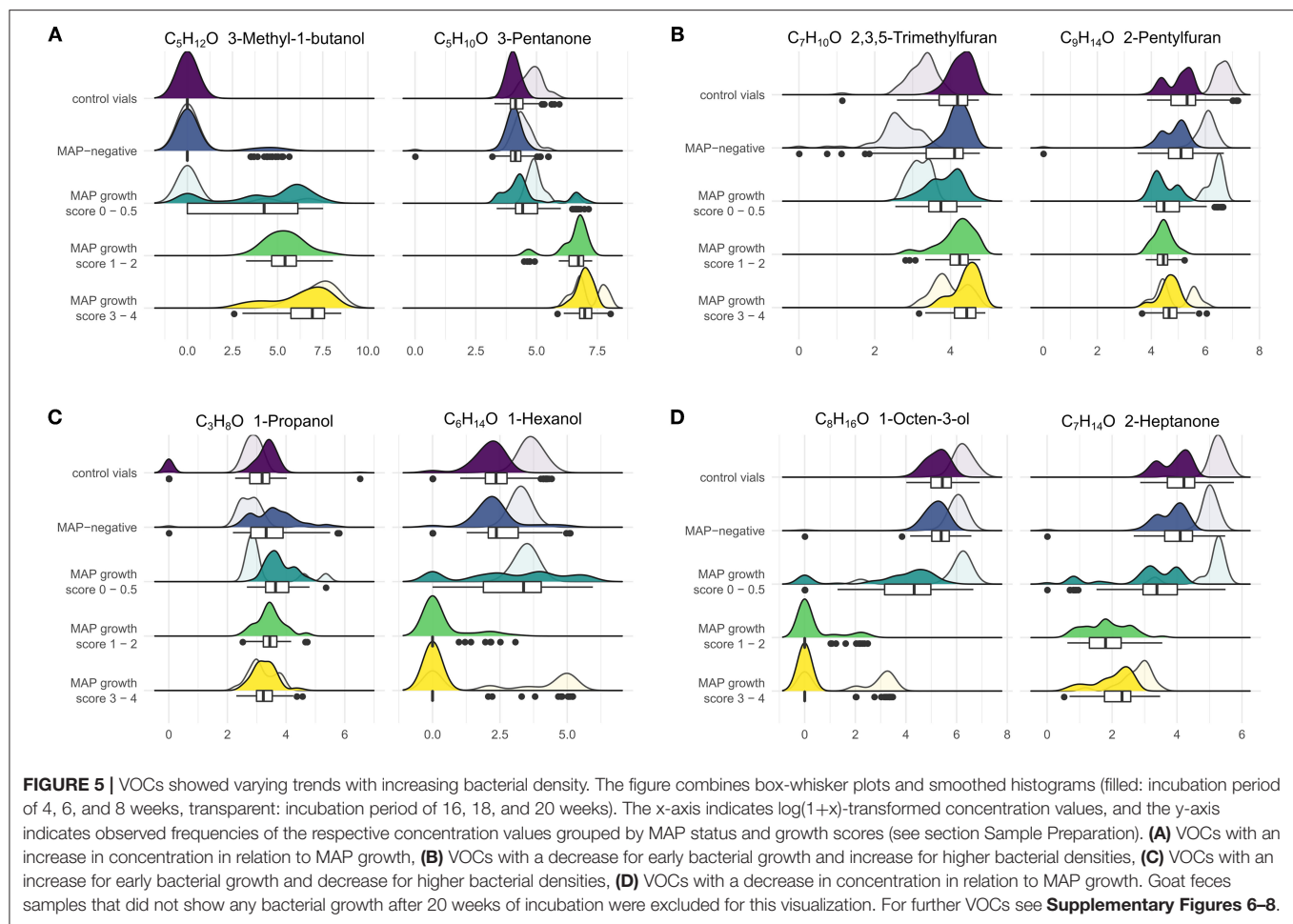
For each of the four settings, the number of selected compounds increased by four to eight compounds in the refined analysis (**Supplementary Table 6**). Thus, some VOCs were in total selected more often than in the previous analysis. 2-Hexanone and pentanal, which had previously passed the selection criteria only in one and two settings, respectively, were now included in all four settings. Acetaldehyde and octanal were excluded for the refined analysis regarding cattle tissue samples, while they had been selected for this setting in the previous analysis. However, both were selected in another setting (cattle feces and goat feces, respectively), for which they had not been considered in the previous analysis. Apart from these four compounds, the remaining 40 compounds of the previous analysis differed only in regard to a single setting.

An overview of the relative importance of selected VOCs per setting is given in **Supplementary Figure 4**. Due to different selections of VOCs and the redefined target of classification,

relative importance values for the refined analysis deviate from those of the previous analysis. It should be noted that an increase in importance does not necessarily correspond to an increase in concentration and vice versa, as pictured in **Supplementary Figure 5**. Instead, the importance of a single compound for a specific level of bacterial growth should be considered in relation to the importance of other compounds in the same setting.

Cross-validated classification accuracies ranged from 0.82 for goat tissue samples to 0.89 for cattle feces samples (**Supplementary Table 6**). Misclassifications mainly occurred between related classes (e.g., between “MAP-negative” and “score 0,” but not between “MAP-negative” and “score 4,” **Supplementary Tables 7–10**).

Regarding VOCs which were included in at least two settings for classifying growth scores, compounds of some substance classes showed variable tendencies: Alcohols and ketones with up to five carbon molecules (except for 1-propanol and 1-pentanol) increased above growing MAP cultures, while substances of the same classes with higher carbon numbers (up to C8) decreased in concentration (**Figure 5**). The concentrations of hydrocarbons, including isoprene, but except for styrene, increased in the



headspace of MAP cultures in comparison to control vials. All aldehydes showed a decrease in concentration with growing MAP cultures.

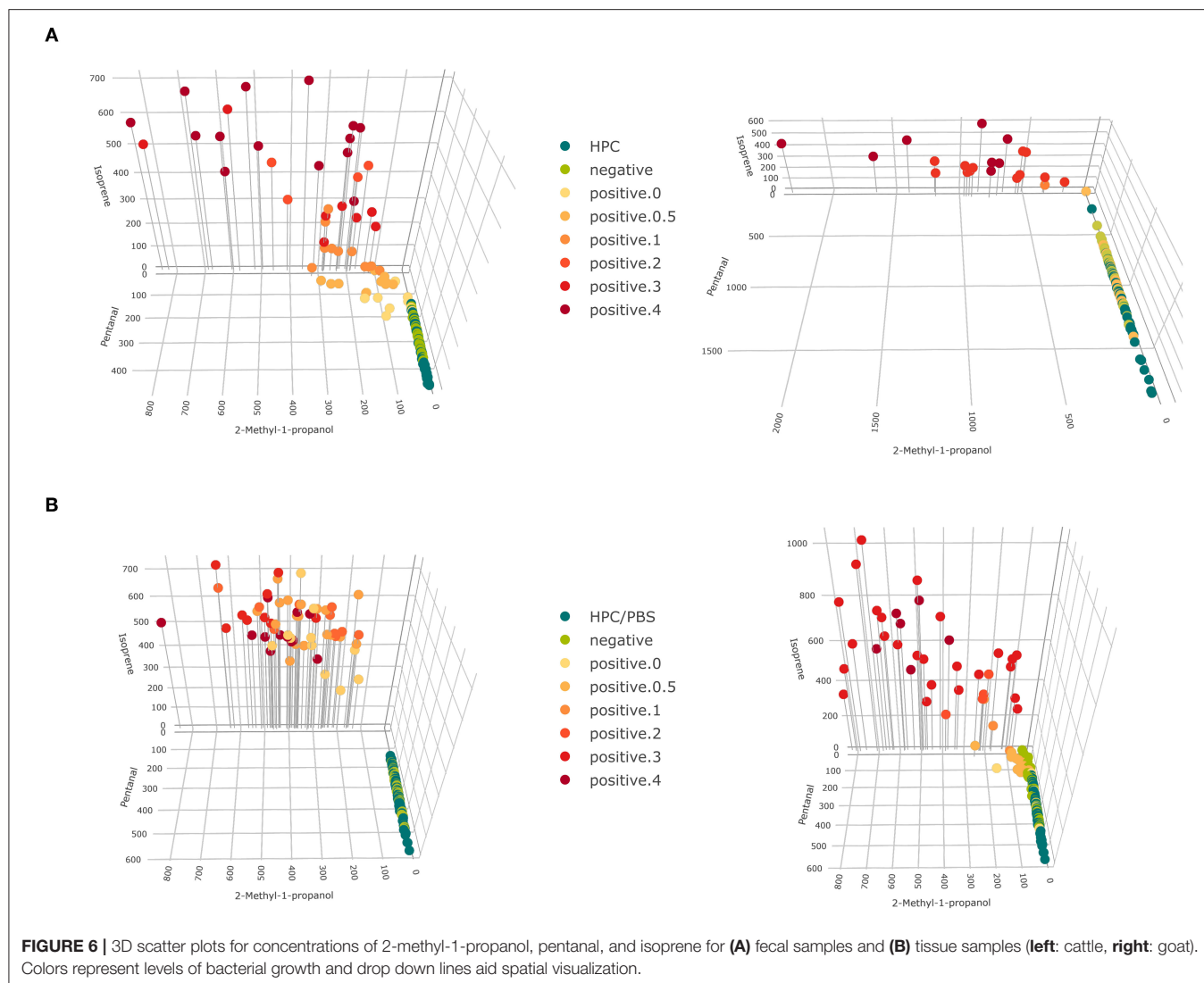
Furan concentrations did not differ markedly between negative and MAP-positive cultures and tended to be lower in the headspace of positive cultures. As an exception, concentrations of 2,3,5-trimethylfuran and 2-pentylfuran decreased above MAP cultures without visible growth or with few colonies (score 0–0.5) and slightly increased again for higher bacterial densities (score 1–4). Conversely, 1-propanol and 1-hexanol tended to increase above MAP cultures with score 0–0.5 and decreased with score 1–4. While, these changes were less pronounced for 1-propanol, 1-hexanol showed a steep decline below the limit of quantification from early phases of bacterial growth to higher bacterial densities (Figure 5).

VOCs that have been selected in at least two settings for classifying growth scores have also been selected in at least two settings for classifying MAP presence, due to the higher selection frequency in the refined analysis. Thus, we consider the selection of VOCs presented in **Supplementary Figures 6–8** as a final set of VOCs indicating growth of MAP cultures in the present study. This selection represents all relevant compounds for the present study, not a minimum selection. Indeed, stages of

bacterial growth could be discriminated with few compounds, as pictured in **Figure 6**.

DISCUSSION

VOC measurements of biological samples are typically characterized by a high naturally occurring variance. In our analysis, we considered effects from the sample material and from pre-processing steps on VOC emissions of bacterial cultures, and also confounding effects by different inoculation days, incubation periods and varying bacterial densities for each set of samples. Nevertheless, a common set of VOCs related to the growth of MAP cultures was detected. They were assembled based on random forest classifiers, which reached high classification accuracies for their respective set of samples. Thus, we conclude that these VOCs allow to discriminate MAP-positive and negative samples despite of additional emissions from sample material. More precisely, identification of marker substances relied on three different categories of samples, (i) culture tubes containing only plain medium which were treated with either HPC or HPC/PBS, respectively, at the beginning of the cultivation period (controls), (ii) culture tubes inoculated with MAP-negative tissue or feces, and (iii) culture tubes



inoculated with MAP-positive tissue or feces. The control tubes were measured concurrently to the test tubes at all time points to unveil VOCs originating from laboratory air and to elucidate the effects of sample preparation and of aging of the medium during the cultivation time of up to 20 weeks. Inclusion of control tubes enabled identification of ETBE as contaminant of laboratory air, because it was elevated in all three categories of samples only at specific dates of sample preparation. Thus, measurements of control tubes were a crucial point of our study design to identify true marker substances. If parallel measurement of control tubes will be necessary also during practical application of VOC diagnostics remains to be elucidated in further analyses.

The study design included two animal species and two matrices to exemplify the variety of settings in practical diagnostics. The MAP isolates considered in this study represent eight different genotypes of MAP type II, the most frequently observed MAP type in samples of cattle and goat (details in **Supplementary Table 1**). Thus, differences in VOC profiles related to different MAP strains, as reported earlier for pure

bacterial cultures (14), were taken into account. Although the effects of the different MAP strains included in this study were not analyzed separately, they are expected to be negligible for the aims of the present study. For example, while cattle tissue samples exhibited the highest variance of MAP types (six different strains), they could still be classified with high accuracy, in both analyses, with a moderate number of selected VOCs.

A few VOCs related to animal species and matrix were identified. Since these effects are expected to be similar for MAP-positive and negative samples, they would not be considered informative by the variable selection procedure. Thus, the inclusion of MAP-negative diagnostic samples was crucial to identify truly MAP-related VOC emissions.

As discussed in previous studies (17, 38), random forests' ability to consider multiple compounds simultaneously makes it suitable for analysis of patterns in VOC data. Random forests have been applied before to analyze VOC patterns for other settings [see e.g., (39–43)], and the random forest-based variable selection algorithm Boruta has been deployed in other VOC

studies too to select relevant compounds (44–48). In the present study, the Boruta algorithm was favored over other variable selection methods to reduce the number of VOCs to a set of potential MAP marker compounds because of its proven performance in the context of random forest classifiers (49). The number of repeated Boruta applications we chose for this analysis does not need to be as high as 30, as the algorithm is computationally expensive and a lower number would not have changed the outcome in a major way, as long as the cutoff point is similar. The averaged accuracy of the random forest classifiers is potentially biased, since Boruta was applied out of the cross-validation scheme (50). This resulted as a drawback from our decision to base our workflow on the R package *caret*, which enables to create reproducible workflows by using the available built-in functions, but does not yet include the Boruta algorithm.

While, random forests are straightforward to apply, as they do not require pre-processing and use only a small number of parameters, there are also some disadvantages. As random forest classifiers consist of hundreds of decision trees summarizing myriads of decision rules, it is hardly feasible to pin down the complex interplay of variables in the classifier to simple statements. Instead, we investigated variable importance values to gain insight into the results of the random forest analyses. These values are measurements of predictive power of VOCs for the particular classification task on a specific class of samples and should only be compared within the same class. Their relative rankings can be unstable (51, 52), e.g., correlated variables can produce similar importance values and also lead to underestimated importance values (53). Thus, for a cluster of variables with similar importance values, small changes in absolute importance may be associated with a large (but not meaningful) skip in ranks.

Moreover, the top compounds according to random forests' variable importance measure are not necessarily the best choice for diagnostic use. Random forests do not discriminate between VOCs with low and high concentration ranges, but screen for variables which allow to single out samples of the same class by simple decision rules. Therefore, also top VOCs with high variable importance values may not be applicable for diagnostic use, if their concentration values are too close to LOQ.

With our workflow, we analyzed the data sets two-fold: We targeted the classification procedure on (i) MAP presence and (ii) MAP growth scores, as we think of the two analyses as complementary to each other. While, the analyses targeting MAP presence are directly motivated from the study design and might profit from balanced classes, the second group of analyses targeting MAP growth scores gives additional insight into the relation of VOCs to bacterial density.

Furthermore, the different sets of samples had to be analyzed separately (goat or cattle and tissue or feces) in order to detect variations specific for the respective sample material. Comparative analyses finally showed similarities between the VOC selections for the different set of samples, especially considering MAP growth. However, since the different classes of samples were analyzed separately, quantitative differences in concentration values between these sets were not considered and consistency across the different sets of samples could not

be inferred directly from our workflow, but explorative analysis showed comparable trends.

As a novelty, the present study described VOC profiles for MAP cultures derived from original sample material. Nevertheless, some VOCs of our final selection had also been included in the VOC profile for pure MAP cultures (17) and showed a consistent tendency with the previously described trend above growing MAP cultures (pentane, octane, 2-methyl-1-butanol, 3-methyl-1-butanol, acetone, 2-butanone, 2,3-butanedione, 3-pentanone, hexanal, heptanal, and benzaldehyde). In addition, further VOCs conformed to results of previous studies on VOC emissions of pure MAP cultures (15, 16), but had not been included in the VOC profile because they were described only in a single study (2-methyl-1-propanol, 1-pentanol, 1-octen-3-ol, acetaldehyde, propanal, and pentanal). However, while furans included in the published MAP core profile had consistently shown an increase in concentration above MAP, for our samples furans tended to decrease with increasing bacterial density or exhibited a varying pattern. For example, 2-pentylfuran was reported to be an important marker compound among the VOCs of the MAP core profile (17) and had been detected in high concentration ranges above MAP cultures (14), but for the present samples 2-pentylfuran showed only slight variations with respect to bacterial growth densities and did not indicate MAP presence in general. Other VOCs have been investigated before as potential MAP markers but showed differing tendencies above MAP cultures (17) (2-methylpropanal, 2-methylbutanal, 3-methylbutanal, 2-heptanone). Furthermore, some VOCs have not been described in any of the previous studies on MAP cultures (2-hexanone, 2-octanone, octanal, and nonanal).

Remarkably, the majority of MAP-positive samples without visible bacterial growth could be distinguished from negative samples by our workflow (as indicated by the confusion matrices, **Supplementary Tables 6–9**), apart from goat tissue samples. This underlines the potential of an early *in vitro* MAP diagnosis using VOC analysis. Compounds with a considerable difference in concentration above MAP cultures with none or scant visible bacterial growth (score 0 and 0.5) in comparison to negative samples and control vials are alcohols such as 2-methyl-1-propanol, 2-methyl-1-butanol, 3-methyl-1-butanol, and 1-octen-3-ol, aldehydes such as 2-methylbutanal, 3-methylbutanal, pentanal, hexanal, benzaldehyde, heptanal, and octanal, and furans such as 2-methylfuran, 2-ethylfuran, and 2-butylfuran (see **Figure 5**). Aldehydes have been described before as potential marker substances of early MAP growth (15, 16). However, these studies identified an increase in concentration of some aldehydes before MAP growth was visually apparent and a decrease with increasing bacterial density. In the present study, an increase of aldehydes could not be confirmed, which may be due to the fact that the previous study also analyzed samples after only 2 weeks of incubation.

Microorganisms can produce a wide variety of volatiles. The reasons why they produce volatiles is unclear, but several functions such as communication (54) and defense have been suggested (55). The VOCs of bacteria (pathogenic and non-pathogenic) have been studied extensively (1, 55).

A variety of VOCs has been identified over mycobacterial cultures, especially *M. tuberculosis* (Mtb) and *M. bovis* strains. Most of the substances described in our study were already reported previously (56). However, the knowledge about the origin and fate of VOCs within the metabolism of MAP is still limited. Therefore, conclusions have to be drawn from other (myco)bacteria.

The majority of the substances considered important for the classification of MAP-positive samples most likely originate from carbon and fatty acid metabolism of MAP. Carbon catabolism provides the bacterial cell with energy and essential biosynthetic precursors (57). In contrast to other bacterial genera, which use catabolite repression as a regulatory mechanism to maximize growth by consuming individual carbon substrates in a preferred sequence, Mtb is able to catabolize multiple carbon sources simultaneously to augment growth (58). Consequentially, a whole range of intermediates is to be expected. The same can be assumed for MAP, although it was not demonstrated so far.

Herrold's Egg Yolk Medium, which was used for cultivation in this study, provides several carbon sources, e.g., polysaccharides of the agar, egg yolk derived cholesterol, the fatty acids oleic acid and linoleic acid, sodium pyruvate, and glycerol.

Emerging evidence, predominantly originating from studies with Mtb, suggests that fatty acids, rather than carbohydrates, might be the dominant carbon substrate utilized during infection. Fatty acids, cholesterol, glycerol as well as pyruvate are degraded to acetyl-CoA. Acetyl-CoA is further oxidized to CO₂ by the citric acid cycle, which provides reducing equivalents for respiration-mediated ATP synthesis and essential precursors for multiple biosynthetic pathways, such as glucose-6-phosphate, acetyl-CoA and others (57). However, the actual metabolic origin of most VOCs found in the present study remains unknown.

Isoprene was produced by MAP-positive cultures and increased in concentration with increasing growth rate. It was considered highly important as indicator for the presence of MAP and for MAP growth by random forest analysis. In general, it is an important atmospheric hydrocarbon that is emitted to the atmosphere from terrestrial plants, phytoplankton sources and soil bacteria (59). Various bacterial species, both Gram-positive and Gram-negative, were found to produce it (60). One major source of isoprene is the bacterial methylerythritol phosphate pathway (61, 62), which is also utilized by Mtb for the biosynthesis of five-carbon building blocks of isoprenoids. Isoprenoids are crucial for survival of Mtb and other microorganisms. They are the parent compounds of many secondary metabolites involved in membrane function, respiratory electron transport and bacterial cell wall synthesis (63).

As far as alcohols and ketones are concerned, it is noticeable that, in the present study, substances with up to 5 carbons are rising in concentrations in the headspace of MAP-positive tubes in relation to growth, while at the same time, substances with more than 5 carbons are decreasing in concentration. It seems that the former compounds result from catabolic processes while the latter may be consumed within biosynthetic pathways. This is feasible because hydrocarbons, aliphatic alcohols and ketones presumably are formed by modification of products of

the fatty acid biosynthetic pathway (55). Reverse reactions with similar intermediates take place during degradation of fatty acids through the β -oxidation pathway. Every single intermediate can potentially be the precursor of volatile compounds emitted by the bacteria (64).

For the classification of MAP and for MAP growth, 3-methyl-1-butanol, 2-methyl-1-propanol, 2-methyl-butanol and 2-heptanone were considered most important in all eight and 3-pentanone in 4 and 3 classifiers, respectively. The best discrimination was achieved by 2-methyl-propanol and 3-pentanone. McNerney et al. (65) identified seven potential markers of *M. bovis* BCG above cultures on Loewenstein-Jensen medium, a whole egg medium, among them 2-methyl-1-propanol, 2-methyl-1-butanol, 3-methyl-1-butanol, and 2-butanone, which were indicative for MAP-positive cultures in the present study. These compounds are not unique to mycobacteria. Identical methyl alcohols were identified in the headspace above fungal and other bacteria species (66, 67). This underlines that the compounds are of limited value as individual markers for detecting specific bacteria, but that their value may increase if used in combination as components of a VOC profile or "fingerprint" (65).

Methyl ketones derive from two principle metabolic pathways. First, they are formed from alkanes by α -oxidation with no change in the carbon skeleton. In some hydrocarbon-oxidizing bacteria of the genus *Mycobacterium*, for example, the pathway of propane metabolism involves an initial hydroxylation reaction producing isopropanol, which is oxidized subsequently to acetone (68). This may be the way of acetone formation during cultural growth of MAP. Second, methyl ketones with an odd number of carbon atoms (acetone to pentadecan-2-one) are derived from even-numbered β -keto acids by decarboxylation, and occur in many bacteria (55). 2-Butanone, 2-pentanone, 2-heptanone, and others were detected in the VOCs released by *Lactobacillus casei* (69). 2-Heptanone is produced by endophytic bacteria in plants such as *Bacillus* (*B.*) *pumilus* and *B. safensis*, and is one of several compounds with antifungal activities (70).

Mycobacteria are not only able to produce, but have also an affinity for growing on a variety of methyl ketones (71). Different rapid growing mycobacteria were shown to utilize acetone, 2-butanone, 2-pentanone, 2-tridecanone or octadecanone. The short-chain ketones supported more rapid and abundant growth than the long-chain ketones (68).

Interestingly, the concentrations of aldehydes with two to eight carbon molecules tend to decrease or are significantly lower above the MAP-positive cultures compared to negative cultures or control tubes. Different sources of these compounds have to be considered. Obviously, the culture medium is itself a source of volatiles, particularly as the autoclaving process forms several VOCs (55). Emission of aldehydes by control tubes containing HEYM was demonstrated in a previous study (15). Otherwise, aldehydes were produced by MAP cultures with a characteristic dynamic pattern, as the headspace of MAP cultures with low bacterial density contained higher concentrations of these compounds than control tubes and then cultures with higher bacterial density (15). In Mtb, aldehydes proved to be toxic metabolites of the cholesterol degradation pathway (72).

In contrast to our results, the headspace of BCG cultures contained significantly more acetaldehyde than was present in the headspace of the controls (65). On the other hand, aldehydes seem to be intermediates in the biosynthesis of the lipids composing the mycobacterial cell envelope (73). Benzaldehyde and octanal, among others, are substrates of the *M. bovis* BCG alcohol dehydrogenase, which seems to play a role in this pathway (74). Furthermore, aldehydes as well as ketones could result from enzymatic or thermic degradation of mycolic acids of the mycobacterial cell wall (75, 76).

As mentioned above, furans tended to decrease above MAP-positive cultures or showed variable tendencies. Their impact on classification of cultures from diagnostic samples was not as pronounced as shown previously on pure MAP cultures (14). Similar to aldehydes, furan derivatives seem to be involved in mycobacterial cell wall formation and degradation, since mycobacterial surface glycolipids contain D-galactofuran and arabinofuranosyl-residues (77, 78). The balance between these processes may determine the kind of substances and their concentrations in the cultures. 2-Pentylfuran was suggested as marker of *Aspergillus* infection in humans (79, 80).

Dimethyl disulfide, an organosulfur compound and intermediate of methionine and cysteine degradation, was identified in varying concentrations above pure HEYM, MAP-negative and MAP-positive culture tubes. Interestingly, the lowest concentrations occurred above MAP-positive tubes with growth score 2–4. This is most likely due to consumption of the substance by replicating MAP. Recent findings that members of the *Actinobacteria* in bio-filters assimilate dimethyl disulfide contained in air emissions from livestock facilities support this assumption (81).

The results of previous (14–17) and the present study provide proof of principle that detection of MAP presence and replication is possible by analysis of VOCs in the headspace of culture tubes already at very low bacterial density and before colony growth becomes visible. Sampling was done at discrete time points during the cultivation process by pre-concentration of VOCs using different micro-extraction techniques. Volatiles were identified later *offline* by GC-MS. This enabled the detection of VOCs in very low concentrations in the ppbV–pptV range (see also **Supplementary Tables 2, 3**). Utilization of VOC analysis in practical diagnosis would demand a different approach. VOC emission has to be measured continuously to enable monitoring of the concentration dynamics of individual marker substances. Analytical platforms that allow online analysis of VOC emissions, such as ion mobility spectrometry (IMS), ion flow tube-mass spectrometry (SIFT-MS) or proton transfer reaction-mass spectrometry (PTR-MS), respectively, are available and could be adapted for this purpose. The incubation time of cultures minimally necessary for correct classification of samples has to be defined. A broader knowledge about the sources of the potential marker compounds and an assessment of their robustness in respect to further matrices and increased sample sizes is needed. Finally, the discriminatory performance of the adapted analysis systems compared to established diagnostic methods, in particular to direct PCR against the same samples, has to be evaluated.

CONCLUSION

The present paper described VOC profiles of MAP cultures from native samples for the first time. MAP-related changes in headspace VOC composition were clearly detectable and not masked by emissions from original sample material. Most VOCs highlighted in this paper have been described for pure MAP cultures before, and some of them were included in the MAP core profile (17) showing a consistent tendency above MAP cultures in comparison to control vials. In contradiction to the published core profile, furans exhibited a decrease in concentration above MAP cultures in the present study. The reasons for this reversal remain unclear. However, the potential of VOC analysis to detect bacterial growth before colonies become visible could still be confirmed. Thus, cultural diagnosis of paratuberculosis could eventually be accelerated by monitoring VOC emissions of growing MAP bacteria. In order to develop a VOC-based diagnostic test, further validation studies are needed to increase the robustness of indicative VOC patterns for early MAP growth.

The techniques presented in this paper are not restricted to MAP, but could be applied to other bacterial cultures as well. However, influencing parameters must be taken into consideration, such as medium composition and measuring technique (pre-concentration, detection, and quantification of VOCs), which will affect the resulting VOC panel. Defined framework conditions are a prerequisite to assess a reliable VOC profile. For a first screening for putative VOC markers, the selected technique should cover a wide range of substance classes. Indicative compounds can be extracted from the full panel by random forest-based approaches, as presented here, which facilitate the consideration of multivariate VOC patterns and return a ranking of the compounds with few preconditions on the VOC data.

DATA AVAILABILITY STATEMENT

The original contributions presented in the study are included in the article/**Supplementary Material**, further inquiries can be directed to the corresponding author/s.

ETHICS STATEMENT

The samples of the present study were part of the sample collection of the German National Reference Laboratory for paratuberculosis at the Friedrich-Loeffler-Institut and originated from different previous studies. One study was a slaughterhouse survey, the others were approved by the Animal Health and Welfare Unit of the Thüringer Landesamt für Verbraucherschutz (permit numbers 04-102/16 and 04-001/11).

AUTHOR CONTRIBUTIONS

PR, HK, JS, and WM conceived the study. AK planned the experiment and carried out sample preparations. PG carried out GC-MS measurements. PG and PT analyzed the GC-MS spectra. PM carried out genotype analyses of the MAP-isolates. Data analysis was carried out by PV and EK, while the

data analysis strategy was conceived by PV, EK, and HK. PV created the workflow and the R Shiny app. PV, EK, and HK drafted the manuscript. All authors discussed the results and commented on the manuscript. All authors read and approved the final manuscript.

FUNDING

This study received funding by the Deutsche Forschungsgemeinschaft (<https://www.dfg.de/>), grant no.

REFERENCES

- Bos LDJ, Sterk PJ, Schultz MJ. Volatile metabolites of pathogens: a systematic review. *PLoS Pathog.* (2013) 9:e1003311. doi: 10.1371/journal.ppat.1003311
- Beauchamp J, Miekisch W. Breath sampling standardization. In: Beauchamp J, Davis C, Pleil J, editors. *Breathborne Biomarkers the Human Volatilome*. Boston, MA: Elsevier (2006). p. 23–41. doi: 10.1016/B978-0-12-819967-1.00002-5
- Stabel JR. An improved method for cultivation of *Mycobacterium paratuberculosis* from bovine fecal samples and comparison to three other methods. *J Vet Diagnostic Investig.* (1997) 9:375–80. doi: 10.1177/104063879700900406
- Whittington RJ, Marsh I, Turner MJ, McAllister S, Choy E, Eamens GJ, et al. Rapid detection of *Mycobacterium paratuberculosis* in clinical samples from ruminants and in spiked environmental samples by modified BACTEC 12B radiometric culture and direct confirmation by IS900 PCR. *J Clin Microbiol.* (1998) 36:701–7. doi: 10.1128/jcm.36.3.701-707.1998
- Williams-Bouyer N, Yorke R, Lee HI, Woods GL. Comparison of the BACTEC MGIT 960 and ESP culture system II for growth and detection of *Mycobacteria*. *J Clin Microbiol.* (2000) 38:4167–70. doi: 10.1128/jcm.38.11.4167-4170.2000
- Gumber S, Whittington RJ. Comparison of BACTEC 460 and MGIT 960 systems for the culture of *Mycobacterium avium* subsp. *paratuberculosis* S strain and observations on the effect of inclusion of ampicillin in culture media to reduce contamination. *Vet Microbiol.* (2007) 119:42–52. doi: 10.1016/j.vetmic.2006.08.009
- Vansnick E, de Rijk P, Vercammen F, Geysen D, Rigouts L, Portaels F. Newly developed primers for the detection of *Mycobacterium avium* subspecies *paratuberculosis*. *Vet Microbiol.* (2004) 100:197–204. doi: 10.1016/j.vetmic.2004.02.006
- Stabel JR, Bannantine JP. Development of a nested PCR method targeting a unique multicopy element, ISMap02, for detection of *Mycobacterium avium* subsp. *paratuberculosis* in fecal samples. *J Clin Microbiol.* (2005) 43:4744–50. doi: 10.1128/JCM.43.9.4744-4750.2005
- Herthnek D, Bölske G. New PCR systems to confirm real-time PCR detection of *Mycobacterium avium* subsp. *paratuberculosis*. *BMC Microbiol.* (2006) 6:87. doi: 10.1186/1471-2180-6-87
- Sting R, Hrubenja M, Mandl J, Seemann G, Salditt A, Waibel S. Detection of *Mycobacterium avium* subsp. *paratuberculosis* in faeces using different procedures of pre-treatment for real-time PCR in comparison to culture. *Vet J.* (2014) 199:138–42. doi: 10.1016/j.tvjl.2013.08.033
- Husakova M, Kralik P, Babak V, Slana I. Efficiency of DNA isolation methods based on silica columns and magnetic separation tested for the detection of *Mycobacterium avium* subsp. *Paratuberculosis* in milk and faeces. *Materials.* (2020). 13:5112. doi: 10.3390/ma13225112
- Bögli-Stuber K, Kohler C, Seibert G, Glanemann B, Antognoli MC, Salman MD, et al. Detection of *Mycobacterium avium* subspecies *paratuberculosis* in Swiss dairy cattle by real-time PCR and culture: a comparison of the two assays. *J Appl Microbiol.* (2005) 99:587–97. doi: 10.1111/j.1365-2672.2005.02645.x
- Prendergast DM, Pearce RA, Yearsley D, Ramovic E, Egan J. Evaluation of three commercial PCR kits for the direct detection of *Mycobacterium avium* subsp. *paratuberculosis* (MAP) in bovine faeces. *Vet J.* (2018) 241:52–7. doi: 10.1016/j.tvjl.2018.09.013
- Trefz P, Koehler H, Klepik K, Moebius P, Reinhold P, Schubert JK, et al. Volatile emissions from *Mycobacterium avium* subsp. *paratuberculosis* mirror bacterial growth and enable distinction of different strains. *PLoS ONE.* (2013) 8:e76868. doi: 10.1371/journal.pone.0076868
- Küntzel A, Fischer S, Bergmann A, Oertel P, Steffens M, Trefz P, et al. Effects of biological and methodological factors on volatile organic compound patterns during cultural growth of *Mycobacterium avium* ssp. *paratuberculosis*. *J Breath Res.* (2016) 10:037103. doi: 10.1088/1752-7155/10/3/037103
- Küntzel A, Oertel P, Fischer S, Bergmann A, Trefz P, Schubert J, et al. Comparative analysis of volatile organic compounds for the classification and identification of mycobacterial species. *PLoS ONE.* (2018) 13:e0194348. doi: 10.1371/journal.pone.0194348
- Küntzel A, Weber M, Gierschner P, Trefz P, Miekisch W, Schubert JK, et al. Core profile of volatile organic compounds related to growth of *Mycobacterium avium* subspecies *paratuberculosis* - A comparative extract of three independent studies. *PLoS ONE.* (2019) 14:e0221031. doi: 10.1371/journal.pone.0221031
- Elze J, Liebler-Tenorio E, Ziller M, Köhler H. Comparison of prevalence estimation of *Mycobacterium avium* subsp. *paratuberculosis* infection by sampling slaughtered cattle with macroscopic lesions vs. systematic sampling. *Epidemiol Infect.* (2013) 141:1536–44. doi: 10.1017/S0950268812002452
- Möbius P, Nordsiek G, Hölzer M, Jarek M, Marz M, Köhler H. Complete genome sequence of JII-1961, a bovine *Mycobacterium avium* subsp. *paratuberculosis* field isolate from Germany. *Genome Announc.* (2017) 5:e00870-17. doi: 10.1128/genomeA.00870-17
- Köhler H, Soschinka A, Meyer M, Kather A, Reinhold P, Liebler-Tenorio E. Characterization of a caprine model for the subclinical initial phase of *Mycobacterium avium* subsp. *paratuberculosis* infection. *BMC Vet Res.* (2015) 11:74. doi: 10.1186/s12917-015-0381-1
- Breiman L, Friedman JH, Stone CJ, Olshen RA. *Classification and Regression Trees*. Boca Raton, FL: Chapman & Hall/CRC (1984).
- Breiman L. Random forests. *Mach Learn.* (2001) 45:5–32. doi: 10.1023/A:1010933404324
- Smolinska A, Hauschild A-C, Fijten RRR, Dallinga JW, Baumbach J, van Schooten FJ. Current breathomics—a review on data pre-processing techniques and machine learning in metabolomics breath analysis. *J Breath Res.* (2014) 8:027105. doi: 10.1088/1752-7155/8/2/027105
- Kursa MB, Rudnicki WR. Feature selection with the Boruta Package. *J Stat Softw.* (2010) 36:1–13. doi: 10.18637/jss.v036.i11
- Kuhn M. Building predictive models in R using the caret package. *J Stat Softw.* (2008) 28:1–26. doi: 10.18637/jss.v028.i05
- R Core Team. *R: A Language and Environment for Statistical Computing.* (2019). Available online at: <https://www.r-project.org/>
- Liaw A, Wiener M. Classification and regression by randomForest. *R News.* (2002) 2:18–22. Available online at: https://cran.r-project.org/doc/Rnews/Rnews_2002-3.pdf
- Wickham H, François R, Henry L, Müller K. *dplyr: A Grammar of Data Manipulation* (2020). Available online at: <https://cran.r-project.org/package=dplyr>
- Wickham H, Henry L. *tidyr: Tidy Messy Data.* (2020). Available online at: <https://cran.r-project.org/package=tidyr>

SUPPLEMENTARY MATERIAL

The Supplementary Material for this article can be found online at: <https://www.frontiersin.org/articles/10.3389/fvets.2021.620327/full#supplementary-material>

30. Wickham H. *ggplot2: Elegant Graphics for Data Analysis*. New York, NY: Springer-Verlag (2016). Available online at: <https://ggplot2.tidyverse.org>
31. Kolde R. *pheatmap: Pretty Heatmaps*. (2019). Available online at: <https://cran.r-project.org/package=pheatmap>
32. Kassambara A, Mundt F. *factoextra: Extract and Visualize the Results of Multivariate Data Analyses*. (2017). Available online at: <https://cran.r-project.org/package=factoextra>
33. Wei T, Simko V. *R package "corrplot": Visualization of a Correlation Matrix*. (2017). Available online at: <https://github.com/taiyun/corrplot>
34. Wilke CO. *ggridges: Ridgeline Plots in "ggplot2"*. (2020). Available online at: <https://cran.r-project.org/package=ggridges>
35. Henry L, Wickham H, Chang W. *ggstance: Horizontal "ggplot2" Components*. (2020). Available online at: <https://cran.r-project.org/package=ggstance>
36. Sievert C. *Interactive Web-Based Data Visualization with R, Plotly, and Shiny*. Boca Raton, FL: Chapman and Hall/CRC (2020). Available online at: <https://plotly-r.com>
37. Chang W, Cheng J, Allaire JJ, Xie Y, McPherson J. *Shiny: Web Application Framework for R*. (2019). Available online at: <https://cran.r-project.org/package=shiny>
38. Kasbohm E, Fischer S, Kuntzel A, Oertel P, Bergmann A, Trefz P, et al. Strategies for the identification of disease-related patterns of volatile organic compounds: prediction of paratuberculosis in an animal model using random forests. *J Breath Res*. (2017) 11:047105. doi: 10.1088/1752-7163/aa83bb
39. Cappellin L, Soukoulis C, Aprea E, Granitto P, Dallabetta N, Costa F, et al. PTR-ToF-MS and data mining methods: a new tool for fruit metabolomics. *Metabolomics*. (2012) 8:761–70. doi: 10.1007/s11306-012-0405-9
40. Phillips CO, Syed Y, Parthalain N, Mac, Zwigglelaar R, Claypole TC, Lewis KE. Machine learning methods on exhaled volatile organic compounds for distinguishing COPD patients from healthy controls. *J Breath Res*. (2012) 6:036003. doi: 10.1088/1752-7155/6/3/036003
41. Kistler M, Muntean A, Szymczak W, Rink N, Fuchs H, Gailus-Durner V, et al. Diet-induced and mono-genetic obesity alter volatile organic compound signature in mice. *J Breath Res*. (2016) 10:016009. doi: 10.1088/1752-7155/10/1/016009
42. Di Gilio A, Catino A, Lombardi A, Palmisani J, Facchini L, Mongelli T, et al. Breath analysis for early detection of malignant pleural mesothelioma: volatile organic compounds (VOCs) determination and possible biochemical pathways. *Cancers*. (2020) 12:1262. doi: 10.3390/cancers12051262
43. Runyon JB, Gray CA, Jenkins MJ. Volatiles of high-elevation five-needle pines: chemical signatures through ratios and insight into insect and pathogen resistance. *J Chem Ecol*. (2020) 46:264–74. doi: 10.1007/s10886-020-01150-0
44. Martinez-Lozano Sinues P, Landoni E, Miceli R, Dibari VF, Dugo M, Agresti R, et al. Secondary electrospray ionization-mass spectrometry and a novel statistical bioinformatic approach identifies a cancer-related profile in exhaled breath of breast cancer patients: a pilot study. *J Breath Res*. (2015) 9:031001. doi: 10.1088/1752-7155/9/3/031001
45. Aggio RBM, de Lacy Costello B, White P, Khalid T, Ratcliffe NM, Persad R, et al. The use of a gas chromatography-sensor system combined with advanced statistical methods, towards the diagnosis of urological malignancies. *J Breath Res*. (2016) 10:017106. doi: 10.1088/1752-7155/10/1/017106
46. Kalske A, Shiojiri K, Uesugi A, Sakata Y, Morrell K, Kessler A. Insect herbivory selects for volatile-mediated plant-plant communication. *Curr Biol*. (2019) 29:3128–33.e3. doi: 10.1016/j.cub.2019.08.011
47. Geraldino CGP, Arbilla G, da Silva CM, Corrêa SM, Martins EM. Understanding high tropospheric ozone episodes in Bangu, Rio de Janeiro, Brazil. *Environ Monit Assess*. (2020) 192:156. doi: 10.1007/s10661-020-8119-3
48. Muchlinski A, Ibdah M, Ellison S, Yahyaa M, Nawade B, Laliberte S, et al. Diversity and function of terpene synthases in the production of carrot aroma and flavor compounds. *Sci Rep*. (2020) 10:9989. doi: 10.1038/s41598-020-66866-1
49. Degenhardt F, Seifert S, Szymczak S. Evaluation of variable selection methods for random forests and omics data sets. *Brief Bioinform*. (2019) 20:492–503. doi: 10.1093/bib/bbx124
50. Varma S, Simon R. Bias in error estimation when using cross-validation for model selection. *BMC Bioinformatics*. (2006) 7:91. doi: 10.1186/1471-2105-7-91
51. Calle ML, Urrea V. Letter to the editor: stability of random forest importance measures. *Brief Bioinform*. (2011) 12:86–9. doi: 10.1093/bib/bbq011
52. Nicodemus KK. Letter to the editor: on the stability and ranking of predictors from random forest variable importance measures. *Brief Bioinform*. (2011) 12:369–73. doi: 10.1093/bib/bbr016
53. Gregorutti B, Michel B, Saint-Pierre P. Correlation and variable importance in random forests. *Stat Comput*. (2017) 27:659–78. doi: 10.1007/s11222-016-9646-1
54. Chernin L, Toklikishvili N, Ovadis M, Kim S, Ben-Ari J, Khmel I, et al. Quorum-sensing quenching by rhizobacterial volatiles. *Environ Microbiol Rep*. (2011) 3:698–704. doi: 10.1111/j.1758-2229.2011.00284.x
55. Schulz S, Dickschat JS. Bacterial volatiles: the smell of small organisms. *Nat Prod Rep*. (2007) 24:814. doi: 10.1039/b507392h
56. Maurer DL, Ellis CK, Thacker TC, Rice S, Koziel JA, Nol P, et al. Screening of microbial volatile organic compounds for detection of disease in cattle: development of lab-scale method. *Sci Rep*. (2019) 9:12103. doi: 10.1038/s41598-019-47907-w
57. Muñoz-Elias EJ, McKinney JD. Carbon metabolism of intracellular bacteria. *Cell Microbiol*. (2006) 8:10–22. doi: 10.1111/j.1462-5822.2005.00648.x
58. de Carvalho LPS, Fischer SM, Marrero J, Nathan C, Ehrt S, Rhee KY. Metabolomics of *Mycobacterium tuberculosis* reveals compartmentalized co-catabolism of carbon substrates. *Chem Biol*. (2010) 17:1122–31. doi: 10.1016/j.chembiol.2010.08.009
59. Fall R, Copley SD. Bacterial sources and sinks of isoprene, a reactive atmospheric hydrocarbon. *Environ Microbiol*. (2000) 2:123–30. doi: 10.1046/j.1462-2920.2000.00095.x
60. Kuzma J, Nemecek-Marshall M, Pollock WH, Fall R. Bacteria produce the volatile hydrocarbon isoprene. *Curr Microbiol*. (1995) 30:97–103. doi: 10.1007/BF00294190
61. Eisenreich W, Schwarz M, Cartayrade A, Arigoni D, Zenk MH, Bacher A. The deoxyxylulose phosphate pathway of terpenoid biosynthesis in plants and microorganisms. *Chem Biol*. (1998) 5:R221–33. doi: 10.1016/S1074-5521(98)90002-3
62. Eisenreich W, Bacher A, Arigoni D, Rohdich F. Biosynthesis of isoprenoids via the non-mevalonate pathway. *Cell Mol Life Sci*. (2004) 61:1401–26. doi: 10.1007/s00018-004-3381-z
63. Wang X, Dowd CS. The methylerythritol phosphate pathway: promising drug targets in the fight against tuberculosis. *ACS Infect Dis*. (2018) 4:278–90. doi: 10.1021/acscinfecdis.7b00176
64. Bhaumik P, Koski MK, Glumoff T, Hiltunen JK, Wierenga RK. Structural biology of the thioester-dependent degradation and synthesis of fatty acids. *Curr Opin Struct Biol*. (2005) 15:621–8. doi: 10.1016/j.sbi.2005.10.010
65. McNerney R, Mallard K, Okolo PI, Turner C. Production of volatile organic compounds by mycobacteria. *FEMS Microbiol Lett*. (2012) 328:150–6. doi: 10.1111/j.1574-6968.2011.02493.x
66. Kiviranta H, Tuomainen A, Reiman M, Laitinen S, Liesivuori J, Nevalainen A. Qualitative identification of volatile metabolites from two fungi and three bacteria species cultivated on two media. *Cent Eur J Public Health*. (1998) 6:296–9.
67. Thorn RMS, Reynolds DM, Greenman J. Multivariate analysis of bacterial volatile compound profiles for discrimination between selected species and strains *in vitro*. *J Microbiol Methods*. (2011) 84:258–64. doi: 10.1016/j.mimet.2010.12.001
68. Lukins HB, Foster JW. Methyl ketone metabolism in hydrocarbon-utilizing mycobacteria. *J Bacteriol*. (1963) 85:1074–87. doi: 10.1128/JB.85.5.1074-1087.1963
69. Gallegos J, Arce C, Jordano R, Arce L, Medina LM. Target identification of volatile metabolites to allow the differentiation of lactic acid bacteria by gas chromatography-ion mobility spectrometry. *Food Chem*. (2017) 220:362–70. doi: 10.1016/j.foodchem.2016.10.022
70. Erjaee Z, Shekarforoush SS, Hosseinzadeh S. Identification of endophytic bacteria in medicinal plants and their antifungal activities against food spoilage fungi. *J Food Sci Technol*. (2019) 56:5262–70. doi: 10.1007/s13197-019-03995-0
71. Forney FW, Markovetz AJ. The biology of methyl ketones. *J Lipid Res*. (1971) 12:383–95.
72. Carere J, McKenna SE, Kimber MS, Seah SYK. Characterization of an aldolase-dehydrogenase complex from the cholesterol degradation

- pathway of *Mycobacterium tuberculosis*. *Biochemistry*. (2013) 52:3502–11. doi: 10.1021/bi400351h
73. Chhabra A, Haque AS, Pal RK, Goyal A, Rai R, Joshi S, et al. Nonprocessive [2 + 2]e⁻ off-loading reductase domains from mycobacterial nonribosomal peptide synthetases. *Proc Natl Acad Sci USA*. (2012) 109:5681–6. doi: 10.1073/pnas.1118680109
 74. Wilkin J-M, Soetaert K, Stelandre M, Buysens P, Castillo G, Demoulin V, et al. Overexpression, purification and characterization of *Mycobacterium bovis* BCG alcohol dehydrogenase. *Eur J Biochem*. (1999) 262:299–307. doi: 10.1046/j.1432-1327.1999.00369.x
 75. Barry CE, Lee RE, Mdluli K, Sampson AE, Schroeder BG, Slayden RA, et al. Mycolic acids: structure, biosynthesis and physiological functions. *Prog Lipid Res*. (1998) 37:143–79. doi: 10.1016/S0163-7827(98)00008-3
 76. Yuan Y, Mead D, Schroeder BG, Zhu Y, Barry CE. The biosynthesis of mycolic acids in *Mycobacterium tuberculosis*. *J Biol Chem*. (1998) 273:21282–90. doi: 10.1074/jbc.273.33.21282
 77. Dhiman RK, Dinadayala P, Ryan GJ, Lenaerts AJ, Schenkel AR, Crick DC. Lipoarabinomannan localization and abundance during growth of *Mycobacterium smegmatis*. *J Bacteriol*. (2011) 193:5802–9. doi: 10.1128/JB.05299-11
 78. Appelmek BJ, den Dunnen J, Driessen NN, Ummels R, Pak M, Nigou J, et al. The mannose cap of mycobacterial lipoarabinomannan does not dominate the *Mycobacterium*–host interaction. *Cell Microbiol*. (2008) 10:930–44. doi: 10.1111/j.1462-5822.2007.01097.x
 79. Syhre M, Scotter JM, Chambers ST. Investigation into the production of 2-Pentylfuran by *Aspergillus fumigatus* and other respiratory pathogens *in vitro* and human breath samples. *Med Mycol*. (2008) 46:209–15. doi: 10.1080/13693780701753800
 80. Chambers ST, Bhandari S, Scott-Thomas A, Syhre M. Novel diagnostics: progress toward a breath test for invasive *Aspergillus fumigatus*. *Med Mycol*. (2011) 49:S54–61. doi: 10.3109/13693786.2010.508187
 81. Kristiansen A, Lindholm S, Feilberg A, Nielsen PH, Neufeld JD, Nielsen JL. Butyric acid- and dimethyl disulfide-assimilating microorganisms in a biofilter treating air emissions from a livestock facility. *Appl Environ Microbiol*. (2011) 77:8595–604. doi: 10.1128/AEM.06175-11

Conflict of Interest: The authors declare that the research was conducted in the absence of any commercial or financial relationships that could be construed as a potential conflict of interest.

Copyright © 2021 Vitense, Kasbohm, Klassen, Gierschner, Trefz, Weber, Miekisch, Schubert, Möbius, Reinhold, Liebscher and Köhler. This is an open-access article distributed under the terms of the Creative Commons Attribution License (CC BY). The use, distribution or reproduction in other forums is permitted, provided the original author(s) and the copyright owner(s) are credited and that the original publication in this journal is cited, in accordance with accepted academic practice. No use, distribution or reproduction is permitted which does not comply with these terms.



Detection of *Mycobacterium avium* Subspecies *paratuberculosis* (MAP) Microorganisms Using Antigenic MAP Cell Envelope Proteins

Shanmugasundaram Karuppusamy¹, Lucy Mutharia², David Kelton³, Brandon Plattner⁴, Sanjay Mallikarjunappa⁵, Niel Karrow⁵ and Gordon Kirby^{1*}

¹ Department of Biomedical Sciences, Ontario Veterinary College, University of Guelph, Guelph, ON, Canada, ² Department of Molecular and Cellular Biology, College of Biological Science, University of Guelph, Guelph, ON, Canada, ³ Department of Population Medicine, Ontario Veterinary College, University of Guelph, Guelph, ON, Canada, ⁴ Department of Pathobiology, Ontario Veterinary College, University of Guelph, Guelph, ON, Canada, ⁵ Department of Animal Biosciences, Ontario Agricultural College, University of Guelph, Guelph, ON, Canada

OPEN ACCESS

Edited by:

Kumi de Silva,
The University of Sydney, Australia

Reviewed by:

Marta Alonso-Hearn,
NEIKER-Instituto Vasco de
Investigación y Desarrollo
Agrario, Spain
Rahul K. Nelli,
Iowa State University, United States

*Correspondence:

Gordon Kirby
gkirby@uoguelph.ca

Specialty section:

This article was submitted to
Veterinary Infectious Diseases,
a section of the journal
Frontiers in Veterinary Science

Received: 07 October 2020

Accepted: 13 January 2021

Published: 03 February 2021

Citation:

Karuppusamy S, Mutharia L, Kelton D,
Plattner B, Mallikarjunappa S,
Karrow N and Kirby G (2021)
Detection of *Mycobacterium avium*
Subspecies *paratuberculosis* (MAP)
Microorganisms Using Antigenic MAP
Cell Envelope Proteins.
Front. Vet. Sci. 8:615029.
doi: 10.3389/fvets.2021.615029

Cell envelope proteins from *Mycobacterium avium* subspecies *paratuberculosis* (MAP) that are antigenically distinct from closely related mycobacterial species are potentially useful for Johne's Disease (JD) diagnosis. We evaluated the potential of ELISAs, based on six antigenically distinct recombinant MAP cell envelope proteins (SdhA, FadE25_2, FadE3_2, Mkl, DesA2, and hypothetical protein MAP1233) as well as an extract of MAP total cell envelope proteins, to detect antibodies against MAP in the sera of infected cattle. The sensitivity (Se) and specificity (Sp) of an ELISA based on MAP total cell envelope proteins, when analyzing 153 bovine serum samples, was 75 and 96%, respectively. Analysis of the same samples, using a commercial serum ELISA resulted in a Se of 56% and Sp of 99%. Results of ELISA analysis using plates coated with recombinant cell envelope proteins ranged from a highest Se of 94% and a lowest Sp of 79% for Sdh A to a lowest Se of 67% and a highest Sp of 95% for hypothetical protein MAP1233. Using polyclonal antibodies to MAP total cell envelope proteins, immunohistochemical analysis of intestinal and lymph node tissues from JD-positive cattle detected MAP organisms whereas antibodies to recombinant proteins did not. Finally, polyclonal antibodies to MAP total cell envelope protein and to recombinant SdhA, FadE25_2, and DesA2 proteins immunomagnetically separated MAP microorganisms spiked in PBS. These results suggest that antigenically distinct MAP cell envelope proteins and antibodies to these proteins may have potential to detect MAP infection in dairy cattle.

Keywords: mycobacterium, cell envelope, ELISA, immunohistochemistry, immunomagnetic separation

INTRODUCTION

Johne's disease (JD) is a non-treatable chronic granulomatous enteritis of cattle and small ruminants caused by *Mycobacterium avium* subspecies *paratuberculosis* (MAP) (1). JD is associated with profuse diarrhea, emaciation, submandibular edema, and eventually death of infected animals due to poor nutrient absorption. JD is endemic in North America, prevalent worldwide and imposes considerable economic burden to the cattle industry due to production losses and herd

replacement costs (2, 3). There are four stages in JD. In the silent stage I, infected animals are healthy without shedding of MAP in the feces (4). In stage II, the disease is subclinical and infected animals appear healthy and can intermittently shed MAP in the feces, thereby contaminating the environment and acting as a source of infection to herd-mates (4). Current laboratory tests have very limited sensitivity in the diagnosis of animals at stage I and II of infection and cattle may remain undiagnosed for several years (5). In stages III (clinical disease) and IV (advanced clinical disease), infected animals exhibit typical clinical signs of JD such as intermittent to continuous diarrhea, weight loss, and emaciation and shed large numbers of MAP in the feces (4).

Currently, JD is diagnosed by clinicians and pathologists using fecal culture, PCR, ELISA, and the identification of gross and histopathological lesions in infected tissues including the presence of acid-fast bacilli (6). Culturing MAP from infected tissues is considered to be the most accurate direct detection test for JD diagnosis (7). However, due to the low numbers of MAP in infected tissues and the disparate distribution, multiple tissue samples are necessary to isolate and culture MAP microorganisms, a process that typically takes 5–16 weeks (7). While direct visualization of MAP by acid-fast staining of intestinal smears and sections is also employed, acid-fast staining has limited sensitivity and specificity as it requires a minimum of 10^6 MAP organisms per gram of tissue and non-specific staining of other acid-fast bacterial species occurs (8, 9). Alternatively, direct detection of MAP in infected tissue by immunohistochemistry using MAP-specific antibodies is a more accurate technique that can detect both intact and lysed MAP organisms (9).

The design of studies to assess tests for JD is problematic due to the difficulty in identifying a suitable reference standard for comparison purposes. While fecal culture is considered to be the gold standard test for identification of MAP microorganisms (7), there are several inadequacies in that the test has limited sensitivity, is time-consuming, labor-intensive, and expensive (7). Moreover, the use of chemical decontaminants reduces the viability of MAP microorganisms and affects the sensitivity of the assay (10). In addition, MAP microorganisms are often shed intermittently in the feces and the number of microorganisms shed by low and medium shedders is minimal (5, 11) and the lack of efficient methods to concentrate MAP from the samples reduces the sensitivity and specificity of MAP detection by culture. Detection of MAP DNA in the feces is also used in JD diagnosis. Isolation of high quality MAP DNA from feces is also challenging due to low numbers of MAP microorganisms in the feces and difficulty in lysing cells to extract DNA (7). In addition, the presence of PCR inhibitors in fecal matter affects the sensitivity of PCR-based identification of

MAP (12). Immunomagnetic capture of MAP allows a selective concentration of the organism from other non-specific bacteria and inhibitory substances (13). Captured bacteria can then be identified by other methods such as culture, or amplification via phage display methods or PCR (10, 13).

ELISA is a commonly used test by clinicians and pathologists to diagnose JD, due to its simplicity and cost-effectiveness. In general, the sensitivity and specificity of commercial ELISA kits varies from 45 to 57% and 85 to 99%, respectively, for fecal culture-positive cases (1, 14). Part of the variations in ELISA sensitivity are due to fluctuations in the antibody titer depending on the stage of infection (15). While comparisons of different tests are questionable when data are not paired, there is variability between commercial ELISA kits with samples showing seropositivity by one and seronegativity by another (16, 17). Moreover, a recent analysis of cow serum samples from MAP-infected and uninfected animals with a commercial ELISA revealed a sensitivity of 4.5% in comparison to an ELISA using recombinant MAP1985 antigen (18). Indeed, none of the commercial ELISA kits can be used as a single test to identify early stage MAP infection in dairy cattle (19). Selection and incorporation of MAP antigens that are both specific and sensitive in an ELISA is a challenging task due to genetic similarity of MAP with other subspecies within the *M. avium* complex and sharing of antigenic epitopes with other mycobacterial and non-mycobacterial species (6). Exposure of animals to related bacterial species may generate antibodies that cross-react with MAP antigens affecting the specificity of MAP ELISA tests (20). Identification of MAP-specific antigens that could be incorporated into ELISAs might be valuable in JD diagnosis. Indeed, flow cytometry analysis has shown that antibody binding to MAP cell surface antigens is particularly sensitive and subspecies-specific (21).

While commercial ELISAs are most commonly used in the serodiagnosis of JD, test specificity is limited by the use of crude antigen preparations such as purified protein derivative, protoplasmic antigens, and lipoarabinomannan that contain epitopes expressed in other mycobacterial and non-mycobacterial species (22, 23). This can lead to false positive diagnoses of JD due to cross-reacting antibodies that are not related to MAP exposure (21). For instance, estimated specificities and sensitivities of five commercial ELISA tests for the diagnosis of JD varied from 87.4 to 99.8% and 27.8 to 44.5%, respectively, in comparison to fecal culture (14). A previous study revealed that ELISA plates with formalin-treated whole MAP organisms or cell surface proteins extracted from formalin-treated, sonicated MAP organisms produced a sensitivity and specificity of more than 95% in the serodiagnosis of JD (1). Another study used flow cytometry to detect MAP subspecies-specific IgG antibodies against MAP cell surface antigens from cattle subclinically infected with MAP and showed that these antigens could be used in the serodiagnosis of JD (24).

We have recently identified several MAP cell envelope proteins that are antigenically distinct from genetically close species including *M. avium* subsp. *hominisuis* (MAH) and *M. smegmatis*, an environmental mycobacterium (25). In this study we investigate whether the use of extracts of

Abbreviations: AUC_{ROC}, area under the receiver operating characteristic curve; CFU, colony forming units; FC, fecal culture; FITC, fluorescein isothiocyanate; H&E, Hematoxylin and eosin; IF, immunofluorescence; IHC, immunohistochemistry; IM, immunomagnetic; JD, John's Disease; MAH, *M. avium* subsp. *hominisuis*; MAP, *Mycobacterium avium* subsp. *paratuberculosis*; MS, *M. smegmatis*; Ni-NTA, Nickel-Nitrilotriacetate; OADC, oleic acid-albumin-dextrose-catalase; PBST, phosphate-buffered saline with Tween; Se, sensitivity; Sp, specificity.

MAP total cell envelope proteins or individual antigenically distinct recombinant MAP-specific cell envelope proteins in an ELISA format would improve the sensitivity and specificity of *M. phlei*-preabsorbed sera as has been demonstrated in similar studies (20, 21, 26). Thus, the objectives of this study are to assess the potential of ELISAs that incorporate six antigenically distinct MAP recombinant cell envelope proteins SdhA, FadE25_2, FadE3_2, Mkl, DesA2, and hypothetical protein MAP1233 to detect serum antibodies to MAP. In general, the functional roles of these specific cell envelope proteins are to support MAP survival and persistence during infection as we have previously discussed (25). Briefly, succinate dehydrogenase (SdhA) allows mycobacteria to adapt to hypoxic environments by maintaining ATP synthesis, Acyl coA dehydrogenase (FadE25_2 and FadE3_2) participates in β -oxidation of cholesterol producing carbon as an energy source; little is known about the Mkl gene product in MAP, however, it is involved in the acquisition of carbohydrates by *Mycobacterium tuberculosis* in host macrophages; disruption of the DesA2 gene, encoding Acyl-ACP desaturase reduces viability of pathogenic mycobacteria, and hypothetical protein MAP1233 has sequence similarity with the methyltransferase FkbM family which is associated with cell wall biogenesis and remodeling. An ELISA using an extract of MAP total cell envelope proteins was also assessed. In addition, we tested the utility of polyclonal antibodies to MAP total cell envelope proteins in the identification of MAP organisms by immunohistochemistry and by immunomagnetic separation. As such, the goal of this proof-of-concept study was to assess the accuracy of a variety of approaches using MAP cell envelope proteins, and polyclonal antibodies to these proteins, in identifying the presence of MAP microorganisms in a small population of cattle ($n = 153$).

MATERIALS AND METHODS

Bacterial Strains, Media, and Growth Conditions

Three MAP strains (Madonna, gc86, and gd30 strains), isolated from bovine clinical cases from southern Ontario, Canada were graciously grown in Middlebrook 7H9 broth medium at 37°C for 6–8 week as described in our previous study (25). Cultures were harvested by centrifugation at 1,000 g for 30 min at 4°C and washed three times with ice-cold phosphate buffered saline (PBS) (pH 7.4). Bacterial pellets were then washed with a 0.16 M NaCl solution. Subcellular fractionation of MAP was done to obtain the cell wall core and cytoplasmic membranes using lysozyme digestion, bead beating and ultracentrifugation as previously described (25).

Recombinant Protein Antigen Purification

Six antigenic proteins were purified from the MAP cell envelope expressed in *Escherichia coli* BL21 (DE3) based on our previous study (25). Five recombinant proteins (SdhA, FadE25_2, FadE3_2, Mkl, and DesA2) were purified under native conditions with immobilized metal affinity chromatography techniques

using HiTrapTMTALON[®] crude resins (GE Healthcare, Bio-Sciences AB, Uppsala, Sweden) as per manufacturer's instructions. A hypothetical protein MAP1233 was purified under denaturing conditions using HisPurTM Ni-NTA (Nickel-Nitrilotriacetate) resin (Thermo Scientific, Rockford, IL, USA), as per the manufacturer's instructions. Protein purity was assessed by sodium dodecyl sulfate–polyacrylamide gel electrophoresis (SDS-PAGE) and Coomassie blue staining (27). Proteins purified under native conditions were dialyzed in PBS (10 mM, pH 7.4) and 10–20% glycerol was added. Protein concentrations were quantified by bicinchoninic acid assay using a Pierce BCA Protein Assay kit (Thermo Scientific, Rockford, IL, USA), and samples were aliquoted and stored at –80°C until further use. It was not possible to solubilize the denatured hypothetical protein so the denatured form was subsequently used for ELISA experiments.

Sample Collection

Fecal and serum samples were obtained from 153 adult milking dairy cows (ranging from 2 to 6 years of age) from three dairy herds in southwestern Ontario. Cattle had been tested for JD based on both fecal culture (FC) and commercial ELISA kits for antibodies to MAP in serum (MAP Ab Test, IDEXX Laboratories Inc., Westbrook, ME; USA) and milk (Prionics ParaChek test kit analysis of milk, Prionics, Zurich, Switzerland). Herd R1 had an average of 90 milking cows (70% Jersey and 30% Holstein) with an average herd prevalence of 20% based on 6 whole herd milk ELISA tests over 6 years. Herd R2 had an average of 38 milking cows (all Jerseys) with an average herd prevalence of 11% based on 11 whole herd milk ELISA tests over 6 years. Herd R3 had an average of 120 milking cows (all Holsteins) with an average herd prevalence of 8% based on 8 whole herd milk ELISA tests over 3 years. In **Supplementary Table 1**, fecal culture results revealed that 39 cows were positive and 114 were MAP-negative for MAP microorganisms. Commercial serum ELISA results revealed that 24 were positive for MAP serum antibodies and 129 were negative.

Serum Absorption

One isolate of each of three mycobacterial species i.e., *M. avium* subsp. *hominisuis* (MAH), *M. smegmatis*, and *M. phlei* were used for serum absorption. In brief, frozen glycerol stock cultures were streaked on Middlebrook 7H11 agar plates and incubated at 37°C. From these plates, single colonies for each isolate were picked and sub-cultured in 15 mL of Middlebrook 7H9 broth at 37°C after incubation, 4 mL of culture from each isolate was aseptically aliquoted and sub-cultured into Middlebrook 7H9 culture media (250 mL \times 2 flasks/bacteria) and cultures were harvested separately by centrifugation at 3,000 g for 20 min at 4°C and washed twice with PBST. One suspension was heat-killed at 100°C for 15 min, cooled at room temperature and washed three times with PBS. The other pellets had neutral buffered formalin added (0.5% final concentrations) and was incubated at room temperature for 2 h on a rotating platform followed by repeated washing (3 times) with PBS. Heat and formalin-killed bacterial pellets were suspended in PBS, pooled

and stored at 4°C until further processing. Serum samples were diluted (1:100) in 2% bovine serum albumin (BSA) in PBS with 0.5% Tween 20 containing killed MAH, *M. smegmatis*, and *M. phlei* (10% v/v) and were then incubated at 4°C overnight on a rotating platform. Absorbed serum samples were centrifuged at 13,000 g for 20 min at 4°C. Supernatants were then transferred into new microcentrifuge tubes and stored at -20°C until further processing.

Validation of ELISA With MAP Cell Envelope Proteins and Recombinant Proteins

The checkerboard titration method was used to optimize the indirect ELISA components such as coating buffer, blocking buffer, antigen concentrations, primary antibody dilutions, and conjugate dilutions as previously described (28). To optimize the primary antibody dilutions, a total of 10 bovine serum samples that were JD test-positive by fecal culture and IDEXX serum ELISA were pooled and served as a positive control. Similarly, bovine serum samples ($n = 10$) that were JD test-negative by fecal culture and IDEXX serum ELISA were pooled and served as negative controls. After this optimization of ELISA components, subsequent ELISAs were performed with single dilutions of antigens and antibodies. A total of 153 serum samples from cows with known status for MAP based on fecal culture results were used so that relative sensitivities and specificities could be calculated in order to validate the new assay. In brief, MAP cell envelope proteins were diluted in bicarbonate coating buffer to a final concentration of 250 ng/mL and 100 μ L of diluted antigen was added to each well of the 96-well microtiter plates. Plates were incubated at 4°C on a shaker (45 rpm) overnight and washed three times with PBS using an automated plate washer. Wells were blocked with 2% BSA (IgG-free) (Santa Cruz Biotechnology, Dallas, USA) in PBS, incubated for 2 h at room temperature on a shaker (85 rpm) and washed three times with PBS. Absorbed serum samples were diluted to 1:1,000 for MAP total cell envelope proteins and 1:500 for recombinant proteins in 2% BSA in PBS with 0.5% Tween 20 and each sample was added into duplicate wells. For non-absorbed serum, samples were diluted 1:1,000 in 2% BSA in PBS with 0.5% Tween 20 and each sample was added into duplicate wells. The remaining procedures were common for both the absorbed and non-absorbed samples. Plates were incubated at room temperature for 2 h on a shaker (85 rpm) and washed 6 times with PBST. Wells were then incubated with horse radish peroxidase (HRP)-linked conjugate antibody (affinity-purified rabbit anti-bovine IgG) (Jackson ImmunoResearch Laboratories Inc., West Gove, PA), diluted (1:7,500) in 2% BSA in PBS with 0.5% Tween 20 for 2 h at room temperature on a shaker and washed six times with PBST. Each well-received 100 μ L of highly sensitive 3,3',5,5'-tetramethylbenzidine (TMB) substrate (Bio legend, USA), incubated for 20 min at room temperature and reactions were stopped with 100 μ L of 2 N H₂SO₄. Readings were measured at OD₄₅₀ using a microtiter plate reader. Experiments were repeated twice to test repeatability and reproducibility.

Statistical Analysis

Fecal culture results were chosen as the gold standard of JD diagnosis in order to compare serum samples and to calculate the sensitivity and specificity of the ELISAs. Sensitivity and specificity of the MAP cell envelope protein ELISA and five recombinant proteins ELISAs including confidence intervals of 95% (CI-95%) were calculated from MAP-positive and -negative serum samples. The ability of the tested antigens to discriminate between MAP test-positive and test-negative animals was assessed by plotting the area under the receiver operating characteristic curve (AUC_{ROC}) using MedCalc 10.3.0.0 statistical software (MedCalc®, Mariakerke, Belgium). Sensitivities and specificities were estimated based on maximum Youden index *J*. The influence of serum absorption on specificity of the MAP cell envelope protein ELISA was assessed using the McNemar test which accounts for paired data.

Generation of Polyclonal Antibodies to MAP Total and Recombinant Cell Envelope Proteins

Total MAP cell envelope proteins from the three MAP isolates (Madonna, gc86, and gd30) were extracted as described above. Protein extracts were dialyzed against descending concentrations of urea, thiourea and 3-[(3-cholamidopropyl) dimethylammonio]-1-propanesulfonate (CHAPS) buffers with a final dialysis with 10 mM PBS (pH 7.2). Following collection of pre-immune serum samples, three female adult Sprague-Dawley rats were immunized intramuscularly with emulsions of MAP total cell envelope proteins (150 μ g/rat) mixed with equal volumes of TiterMax gold adjuvant (Sigma-Aldrich). Polyclonal antibodies were previously generated against only three recombinant proteins (SdhA, FadE25_2, and DesA2) due to issues with folding of the other proteins and the specificity of these antibodies to the respective proteins has been described (25).

Immunoblot Analysis of Polyclonal Antibodies Generated to MAP Total Cell Envelope Proteins

For immunoblot analysis of the specificity of rat anti-MAP polyclonal antibodies, 25 μ g of cell envelope proteins from MAP, MAH, and MS were electrophoretically transferred to nitrocellulose membranes. Non-specific sites were blocked with 5% skim milk in TBST and membranes were incubated with serum (1:6,000 in 2% BSA in TBST) from rats immunized with MAP total cell envelope proteins, as described above. Membranes were washed with TBST and incubated with anti-rat HRP-linked conjugate (1:2,000 dilution in 5% skim milk in TBST) for 1 h at room temperature and then probed with ClarityTM Western ECL substrate (Bio-Rad Laboratories, Inc., USA).

Immunohistochemistry (IHC) and Immunofluorescence (IF)

IHC was performed as previously described (29) using intestinal tissues and lymph nodes from adult cattle naturally infected with MAP. For negative controls, intestinal tissues and lymph

nodes were obtained from calves not previously exposed to MAP (kindly provided by Dr. Brandon Plattner, Department of Pathobiology, University of Guelph). Tissue sections (5 μ m) were prepared and antigens were retrieved in sodium citrate buffer at 95°C for 20 min in a water bath and allowed to cool at room temperature for 30 min. Sections were repeatedly washed with distilled water and endogenous peroxidase activity was blocked with 3% hydrogen peroxide in distilled water for 30 min at RT. Non-specific sites were blocked with goat serum for 1 h in a humidified chamber at RT, washed with Tris-buffered saline Tween-20 and incubated with rat polyclonal antibodies (1:25) against each of the three recombinant proteins (SdhA, FadE25_2, and DesA2) or polyclonal antibodies to the MAP total cell envelope proteins diluted to 1:50 in 1% BSA in TBST overnight at 4°C in a humidified chamber. Sections were then incubated with anti-rat-HRP-linked conjugate (Cell Signaling Technology, Inc., Danvers, MA, USA) diluted 1:50 in 5% skim milk in TBST and incubated for 1 h at room temperature in a humidified chamber. Tissue sections were then washed and incubated with 200 μ L of ImmPACTNovaRed peroxidase substrate (Vector Lab, Burlingame, CA, USA) in the dark for 5–20 min. Slides were washed with distilled water and counter-stained with Harris' haematoxylin solution and mounted with cover slips. Slides were examined under a light microscope for the presence of antigen antibody reactions. For immunofluorescence experiments, tissue sections were processed in a manner similar to that of IHC, except endogenous inactivation of peroxidases and secondary antibodies were labeled with fluorescein isothiocyanate and diluted 1:500 in 5% skim milk in TBST. Slides were then mounted with ProLong Gold Antifade Mountant (Invitrogen, Eugene, OR, USA) as per the manufacturer's instructions.

Immunomagnetic Separation of MAP

Magnetic protein G Dynabeads (Thermo Fisher Scientific, Mississauga, ON, Canada) were aliquoted (10 μ L/tube) into 1.5 mL microcentrifuge tubes and washed with PBST (0.1%, pH 7.5), suspended in 200 μ L of PBST and loaded with either 3 μ g of purified rat anti-SdhA, anti-FadE25_2, and anti-DesA2 polyclonal antibodies per tube or 5 μ L of rat anti-MAP (total cell envelope protein) polyclonal antibodies per tube. Tubes were incubated overnight at 4°C with gentle mixing and then placed on a magnetic stand where unbound antibodies were removed and beads were washed twice with PBST (0.1% Tween 20, pH 7.4). MAP cultures were harvested by centrifugation at 6,500 g for 10 min at room temperature followed by three washing steps with PBST and bacterial pellets were re-suspended in PBST. MAP organisms were then passed through 25-gauge needles to break the bacterial clumps as previously described (30). MAP organisms were quantified by measuring optical density at 600 nm with an optical density of 0.6–0.9 at 600 nm considered to be equivalent to approximately 10^8 CFU of MAP organisms per mL as previously described (31). For exact numbers, optical density-adjusted MAP organisms (OD₆₀₀ 0.6) were serially diluted from 10^8 to 10^1 in 1 mL of PBST and 100 μ L from each dilution was plated on Middlebrook 7H11 agar plates supplemented with mycobactin J and on Middlebrook

Oleic Albumin Dextrose Catalase enrichment agar medium and plates were incubated at 37°C.

For the immunomagnetic (IM) separation, a volume of 100 μ L from each dilution or from a suspension of MAP organisms was mixed with 10 μ L of antibody-bound protein G beads and incubated at room temperature for 1 h with gentle mixing. For negative controls, beads were coated with polyclonal antibodies to unrelated proteins (i.e., anti- α -1 acid glycoprotein or anti-cytochrome P450 2A5) and incubated with MAP (10^7 CFU) bacteria. Beads were then washed 3 times with PBST buffer in a magnetic separator to remove unbound bacteria. Immunomagnetically separated MAP was then suspended in 50 μ L of sterile PBS stored at 4°C until further use.

PCR Assay With Immunomagnetically Separated MAP

To test whether IM separation of MAP was successful, a PCR assay was performed using DNA templates prepared from IM-separated MAP using MAP species-specific (*IS900*) primers previously described (32). In brief, 10 μ L of IM-separated MAP bound to beads in PBS from previous steps were transferred into new 1.5 mL microcentrifuge tubes, placed on a magnetic stand and the liquid removed carefully leaving the beads remaining in the tubes. IM-separated MAP bacteria were re-suspended in 20 μ L of 10 mM Tris EDTA (pH 7.6), heated at 95°C in a thermal cycler for 30 min and cooled on ice for 5 min. For positive controls, 25 μ L of MAP culture was boiled in 10 mM Tris EDTA (pH 7.6) for 10 min, then cooled on ice, followed by quick high-speed centrifugation. A 4 μ L aliquot of these suspensions was used as the DNA template for PCR and amplification was carried out as per the cycling conditions previously described (32). PCR-amplified products were then visualized on 2% agarose gels.

Confirmation of MAP Attachment to IM Beads by Culture

The efficiency of MAP recovery from IM-separated beads was assessed by bacterial culture by mixing a 10 μ L volume of beads from each dilution of MAP organisms with 90 μ L of sterile DNA grade water, plated on Middlebrook 7H11 agar plates supplemented with mycobactin J and OADC medium and plates were incubated at 37°C for 6–8 weeks. Colonies were counted and CFU were calculated as per standard procedures.

RESULTS

Sensitivity and Specificity of MAP Total Cell Envelope Protein ELISA

Results of preliminary absorbance experiments to determine optimal conditions for the ELISA coated with extracts of MAP total cell envelope proteins revealed that blocking with 2% BSA (IgG-free) in PBS produced the least amount of background and therefore was used for antibody dilutions. Based on data from checkerboard titrations the following conditions were

TABLE 1 | Calculated sensitivities, specificities, and ROC_(AUC) for the *Mycobacterium avium* subsp. *paratuberculosis* total cell envelope protein and IDEXX serum ELISAs.

ELISA type	Serum absorption	Se%	95% CI	Sp%	95% CI	ROC _(AUC)	95% CI	Youden index J	Cut-off
MAP ENV ELISA	No	72.22	54.8–85.8	90.35	83.4–95.1	0.808	0.735–0.867	0.626	>0.611
MAP ENV ELISA	Yes	75.00	57.8–87.9	95.61	90.1–98.6	0.896	0.836–0.940	0.706	>0.384
IDEXX Serum ELISA	Yes	55.56	38.1–72.1	99.12	95.2–100	0.833	0.766–0.888	0.669	0.600

established: 25 ng of protein/well, dilutions of 1:1,000 for serum and 1:7,500 for the HRP-conjugated secondary antibodies.

Validation of the ELISA was undertaken with serum samples from cattle with associated fecal culture (FC) results, 39 of which were FC test-positive and 114 that were test-negative. Our ELISA results were compared to FC as a gold standard in order to calculate the sensitivities and specificities determined at different cut-off points. At a cut-off value of 0.611 (OD₄₅₀), the sensitivity and specificity of the MAP total cell envelope protein ELISA without serum absorption was 72% (95% CI, 54.8–85.8) and 90% (95% CI, 83.4–95.1), respectively (Table 1). The calculated area under the ROC curve was 0.808 (95% CI, 0.735–0.867, $p < 0.0001$; Supplementary Figure 1).

We included a serum absorption step with MAH and *M. smegmatis* in addition to the routine serum absorption that was performed with *M. phlei* in order to improve the specificity of the ELISAs. Using a cut-off value of 0.384 (OD₄₅₀), the sensitivity and specificity of the MAP total cell envelope protein ELISA was 75 and 95.61%, respectively after absorption (Table 1). The calculated area under the ROC curve was 0.90 (Table 1 and Supplementary Figure 1). Statistical analysis revealed that serum absorption significantly improved the specificity of the ELISAs compared to non-absorption (one-tailed $p < 0.035$, exact test) with an Odds Ratio estimate of 7 and one-sided 95% CI >1.125, however, sensitivity was not improved. Thus, it is estimated that non-absorbed ELISA has 7 times the odds of giving false positives than does absorption.

In order to compare the efficiency of the MAP total cell envelope protein ELISA to the IDEXX ELISA, results were compared with FC as a gold standard. In relation to FC, IDEXX ELISA results, as per the cut-off value given by the manufacturer's recommendations, are also shown in Table 1. Of the 153 serum samples, 24 were test-positive with the IDEXX ELISA. Of these 24 animals, 23 were positive for MAP by fecal culture and one was negative. The calculated area under the ROC curve for the IDEXX ELISA was 0.833 compared to 0.896 for the MAP total cell envelope protein ELISA with serum absorption (Table 1). Comparison of ROC_(AUC) for the three ELISAs also revealed that the MAP total cell envelope protein ELISA using absorbed serum samples had the highest ROC_(AUC) value (Table 1 and Supplementary Figure 1).

Sensitivity and Specificity of ELISAs With Recombinant Proteins

Based on preliminary absorbance values and checkerboard titrations, similar conditions were used for ELISAs with recombinant proteins except that a serum dilution of 1:500 was chosen. For all six recombinant protein antigens, OD₄₅₀

values for MAP FC test-negative animals ($n = 114$) were less than for MAP FC test-positive animals ($n = 39$; Table 2). ROC_(AUC) analyses were performed to measure the discriminatory power of the MAP recombinant protein ELISA assay to differentiate positive and negative animals. ROC_(AUC) was above 0.7 for all recombinant protein antigens used in this study (Supplementary Figures 2A–F). SdhA had the highest ROC_(AUC) of 0.921 (95% CI 0.851–0.965) and FadE3_2 had the lowest ROC_(AUC) of 0.787 (95% CI 0.713–0.849) (Table 2). Youden index J analysis was performed to measure the trade-off between sensitivity and specificity at different cut-off values in order to assess the performance of the ELISAs with recombinant MAP proteins. ELISA results for SdhA protein revealed the highest Youden index J of 0.735 and FadE3_2 showed the lowest value of 0.522. Sensitivities and specificities at the selected cut-off points for individual recombinant proteins are also shown in Table 2. SdhA protein resulted in the highest sensitivity of 94% (95% CI, 80.3–99.3) and the lowest specificity of 79 (95% CI, 67.9–88.3) at a selected cut-off criterion of >0.483. Hypothetical protein MAP1233 produced the lowest sensitivity of 67% (95% CI, 49.0–81.4) and highest specificity of 95% (95% CI, 87.6–98.2) at a selected cut-off criterion of >0.543. Overall, ELISA results for the six recombinant proteins showed higher sensitivity and lower specificity than the IDEXX ELISA results.

Immunoblot Analysis of Rat Polyclonal Antibodies Against MAP Total Cell Envelope Proteins

The specificity of rat polyclonal antibodies to an extract of MAP total cell envelope proteins was assessed by immunoblot analysis of cell envelope protein extracts from MAP, MAH and *M. smegmatis* (Figure 1). The results revealed that these antibodies were strongly immunoreactive with MAP cell envelope protein extracts. However, some cross-reactivity with MAH and *M. smegmatis* cell envelope proteins was evident. Densitometric analysis of all the bands in the three lanes in Figure 1 revealed that bands in MAP, MAH and MS lanes represented 79.0, 5.9, and 15.1%, respectively, of total band density on the immunoblot.

Immunohistochemistry and Immunofluorescence

Hematoxylin and eosin (H&E) staining of formalin-fixed intestinal tissues from cattle infected with MAP demonstrated mononuclear inflammatory cell infiltrates (Figure 2A) and acid-fast staining indicated the presence of bacilli (Figure 2B). Immunohistochemistry with antibodies generated to extracts of MAP total cell envelope proteins showed strong immunoreactivity to MAP bacteria (Figure 2C). H&E staining

TABLE 2 | Calculated sensitivities and specificities at the selected cut-off points, ROC_{AUC}, and Youden index J for the ELISAs coated with recombinant protein antigens.

Accession ID	Protein name	Gene name	Mean OD ₄₅₀ values		Se%	95% CI	Sp%	95% CI	ROC _(AUC)	95% CI	Youden index J	Cut-off
			FC -ve	FC +ve								
R4MT83_MYCPC	Succinate dehydrogenase iron sulfur subunit	<i>SdhA</i>	0.400	0.711	94.1	80.3–99.3	79.41	67.9–88.3	0.921	0.851–0.965	0.735	>0.483
R4NF35_MYCPC	Acyl-CoA dehydrogenase	<i>FadE25_2</i>	0.383	0.630	70.6	52.5–84.9	89.66	82.6–94.5	0.845	0.777–0.899	0.602	>0.533
R4N5P6_MYCPC	Acyl-CoA dehydrogenase	<i>FadE3_2</i>	0.330	0.573	69.4	51.9–83.7	82.76	74.6–89.1	0.787	0.713–0.849	0.522	>0.456
R4N4C8_MYCPC	Ribonucleotide-transport ATP binding protein ABC transporter	<i>Mkl</i>	0.447	0.858	83.3	67.2–93.6	89.25	81.1–94.7	0.895	0.829–0.942	0.725	>0.579
R4MZZ5_MYCPC	Hypothetical protein		0.350	0.688	66.7	49.0–81.4	94.51	87.6–98.2	0.859	0.786–0.915	0.611	>0.543
R4N4U1_MYCPC	Acyl-ACP desaturase	<i>DesA2</i>	0.368	0.672	69.4	51.9–83.7	92.17	85.7–96.4	0.861	0.796–0.912	0.616	>0.546

of formalin-fixed control intestinal tissue sections from a calf not exposed to MAP showed normal histology (**Figure 2D**) and lacked any visible antigen-antibody reactivity (**Figure 2E**). Immunofluorescence using FITC-labeled antibodies identified MAP antigens in sections of intestine (**Figure 3A**) and lymph node (**Figure 3B**). There was no antigen-antibody reactivity in the control tissue sections of intestine (**Figure 3C**) and lymph node (**Figure 3D**). Finally, rat anti-SdhA, anti-FadE25_2, and anti-DesA2 polyclonal antibodies failed to identify any MAP antigens in these tissues.

Immunomagnetic Separation (IMS) of MAP

The capturing efficiency of polyclonal antibodies to MAP total cell envelope proteins as well as to recombinant proteins SdhA, FadE25_2, and DesA2 was assessed by analysis of captured microorganisms by PCR analysis as well as by culture. PCR amplification results revealed that IMS with rat polyclonal antibodies to MAP total cell envelope proteins was most efficient, yielding the expected product size of 0.215 kbp for as low as 10² CFU of MAP (**Supplementary Figure 3A**). These findings were confirmed by culture results. PCR analysis of IMS mRNA with rat anti-SdhA polyclonal antibodies yielded the expected product size for as low as 10³ CFU of MAP (**Supplementary Figure 3B**), whereas IMS with rat anti-FadE25_2 and DesA2 polyclonal antibodies yielded the expected product size for up to 10⁵ CFU of MAP (**Supplementary Figures 3C,D**). Negative control samples that included beads without antibodies or antibodies to unrelated proteins (i.e., Alpha-1 acid glycoprotein or CYP2A5) failed to produce a PCR product thereby confirming a lack of non-specific binding of antibodies. This indicates that the magnetic beads coated with polyclonal antibodies to MAP whole cell envelope protein extracts or antibodies to recombinant SdhA, FadE25_2, and DesA2 were able to bind and capture intact MAP bacteria.

DISCUSSION

In the first part of this study, we investigated the use of MAP total cell envelope antigens and six recombinant MAP cell envelope proteins in ELISAs developed to identify serum antibodies to MAP bacteria in naturally infected cattle. We showed that ELISAs with MAP total cell envelope proteins using absorbed serum samples significantly increased specificity. In general, ELISAs using unabsorbed serum samples are more sensitive but less specific thereby affecting test accuracy (33). In our study, serum absorption with MAH and *M. smegmatis* in addition to the traditional absorption with *M. phlei* significantly improved specificity of the assay possibly due to a reduction of cross-reacting antibodies which were generated due to environmental exposure of cattle to other mycobacterial species (34). This is in contrast to an earlier study in which two commercial ELISAs with absorbed serum samples revealed low sensitivities (13.9 and 16.6%) and specificities (95.9 and 97.1%) in comparison to fecal culture (33). In contrast, an ELISA with unabsorbed serum showed a sensitivity of 27.8% and specificity of 90% when compared to fecal culture (33). The possible reasons for the improved sensitivity in our study may be due to the use of MAP total cell envelope proteins with large numbers of MAP-specific epitopes, indigenous MAP strains, and serum absorption with MAH and *M. smegmatis*. For example, protein extracted from MAP cell surface antigens from American strains had a sensitivity of 97.1% when tested on serum samples from American origin and 21.8% when tested on serum samples from Indian origin (35, 36). Interestingly, **Supplementary Table 1** shows that 6 cows (KR3-470, KR2-154, KR2-26, KR2-142, KR3-1516, and KR3-365) were negative when analyzed by the IDExx serum ELISA and FC, but had OD₄₅₀ values above the cut-off value of 0.384 with MAP cell envelope protein ELISAs. While this may represent a false positive result, the presence of MAP-specific

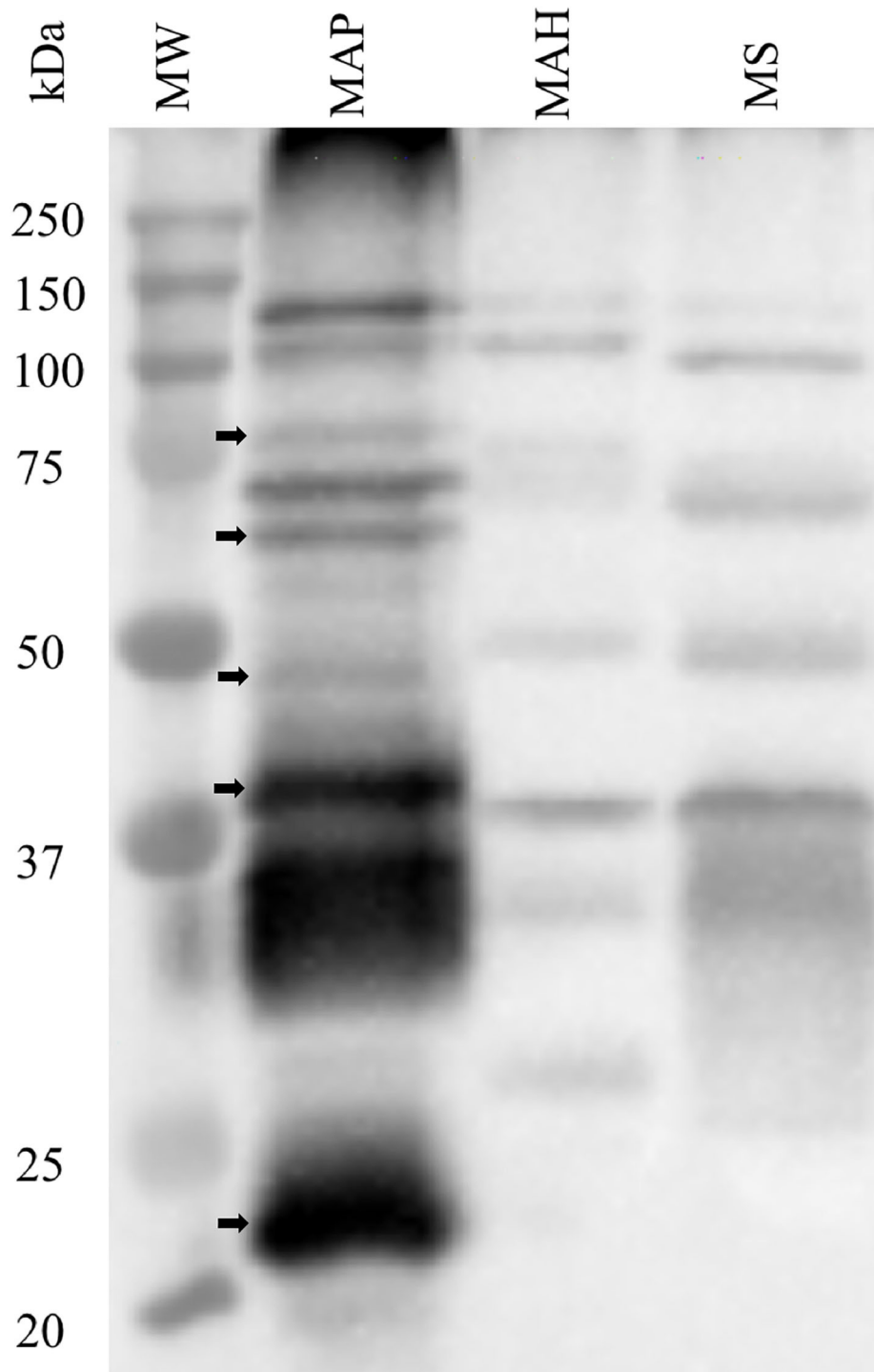


FIGURE 1 | Assessment of specificity of rat polyclonal antibodies generated against cell envelope proteins from *M. avium* subsp. *paratuberculosis* (MAP). Immunoblot analysis of cell envelope protein extracts from MAP, *M. avium* subsp. *hominisuis* (MAH), and *M. smegmatis* (MS). Arrows indicate bands that are apparently specific to MAP envelope proteins.

antibodies suggests that these animals may be in the early stages of MAP infection and were not detected by fecal culture and the commercial ELISA. This may also suggest that reliance on FC as a gold standard test reduces the specificity of the MAP

total cell envelope protein ELISA if indeed these cows were MAP-positive. Because intermittent shedding of MAP in the feces can limit the sensitivity of FC, tissue culture may be a more accurate gold standard method. However, confirming this contention

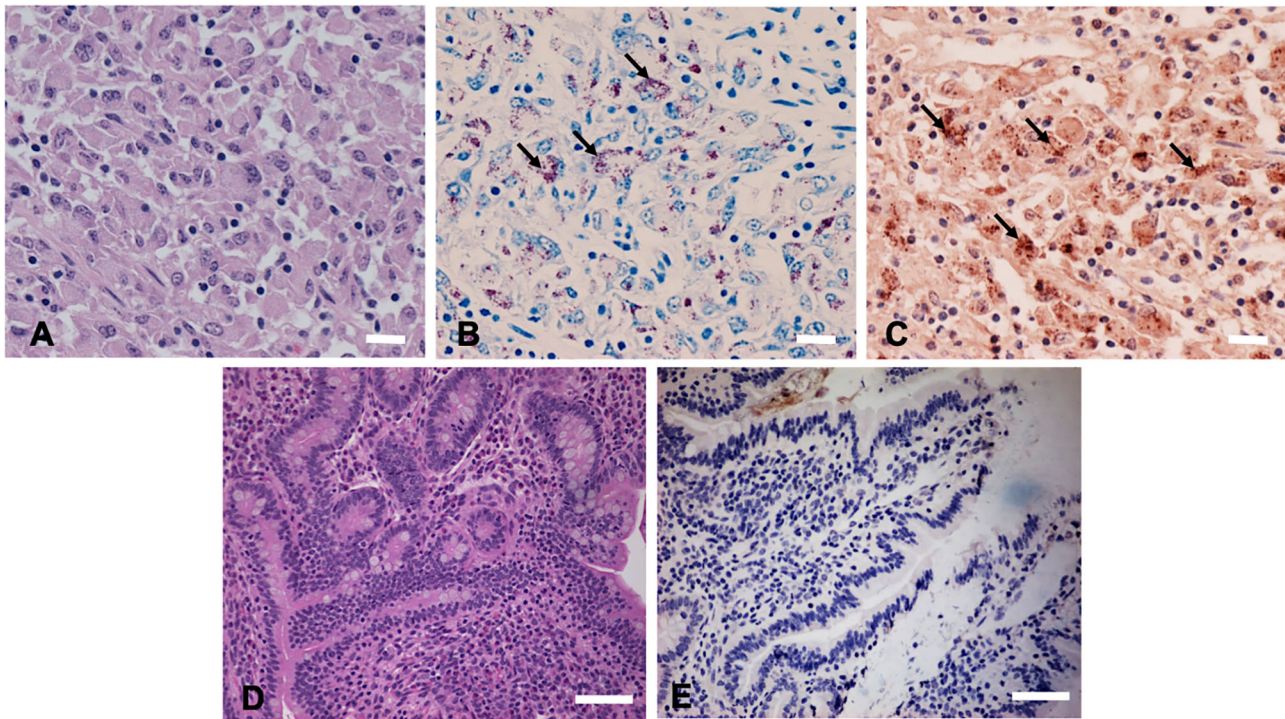


FIGURE 2 | Immunohistochemical (IHC) staining of tissues sections using anti-*M. avium* subsp. *paratuberculosis* (MAP) cell envelope antibodies. **(A)** Hematoxylin and eosin stain (H&E)-stained intestinal tissue section from a MAP-infected cow showing mononuclear inflammatory cell infiltrates. Bar = 25 μ m; **(B)** acid-fast staining of intestinal tissue showing the presence of MAP organisms (arrows indicating red bacilli), Bar = 25 μ m; **(C)** IHC of intestinal tissue section with antibodies to MAP whole cell envelope protein extracts showing strong immunoreactivity (arrows indicating brown immunoreactivity), Bar = 25 μ m; **(D)** H&E-stained intestinal tissue section from a calf not exposed to MAP, Bar = 50 μ m; and **(E)** IHC of intestinal tissue section from a calf not exposed to MAP, Bar = 50 μ m.

would require postmortem sampling of MAP-infected tissues and testing fecal or serum samples from “known negative” herds, options which are not currently available for this study.

A follow-up study might be useful to determine whether these animals will subsequently test positive by the IDEXX ELISA so that the accuracy of our new MAP ELISA assays can be assessed. Similarly, some of the animals were positive by fecal culture but negative by MAP total cell envelope protein ELISA. It is possible that these animals are infected with MAP but their MAP-specific antibody levels are below the detection limit. Another possible reason may be due to passive shedding of MAP rather than actual infection (37). Discrepancy between ELISA seropositivity and fecal shedding has been reported in a longitudinal study examining correlations between serology and fecal shedding patterns (38). Nonetheless, a definitive explanation awaits re-testing of these animals to gain further epidemiological information regarding their JD status.

The specificity and sensitivity of our assay is less than that of other studies that use MAP cell surface antigens. For example, flow cytometry analysis and ethanol vortex ELISA with MAP surface antigens revealed a specificity of 96.7 and 100% and sensitivity of 95.2 and 97.4%, respectively (21, 24). However, serum samples used in these two studies were from herds with a known JD status (JD-free or -positive) and animals with a known shedding pattern (mild, moderate, and heavy fecal shedding from high prevalence herds) possibly leading to bias in the calculation of sensitivity and specificity (39). Indeed, when the ethanol vortex

ELISA was tested with other serum samples ($n = 38$), results revealed that 70% of the animals were false positive for JD (35). This suggests that comparison of test accuracies between various tests for JD is not possible (39).

We also assessed an ELISA with six recombinant MAP cell envelope proteins (SdhA, FadE25_2, FadE3_2, Mkl, DesA2, and hypothetical protein MAP1233) that were identified as MAP species-specific based on our earlier two-dimensional difference gel electrophoresis comparative proteomic analysis and 2-dimensional electrophoresis immunoblot analysis (25). ELISAs with recombinant protein antigens were able to differentiate MAP-positive and -negative serum samples. This finding was in agreement with earlier studies that used similar approaches to evaluate the potential of recombinant MAP protein antigens to be used in the diagnosis of JD (40, 41). The ELISAs with SdhA and hypothetical protein MAP1233 showed the highest and lowest sensitivity of 94 and 67%, respectively. The low sensitivity of the recombinant protein ELISAs is not surprising in view of the complex nature of MAP infection. It has been shown that test using one antigen may not be sufficiently sensitive and specific during the entire course of infection and therefore future experiments with cocktails of MAP-specific recombinant protein antigens might improve the test sensitivity and allow for detection of animals at different stages of JD (42, 43).

Among the six recombinant proteins, hypothetical protein MAP1233 and DesA2 showed a high specificity of 95 and

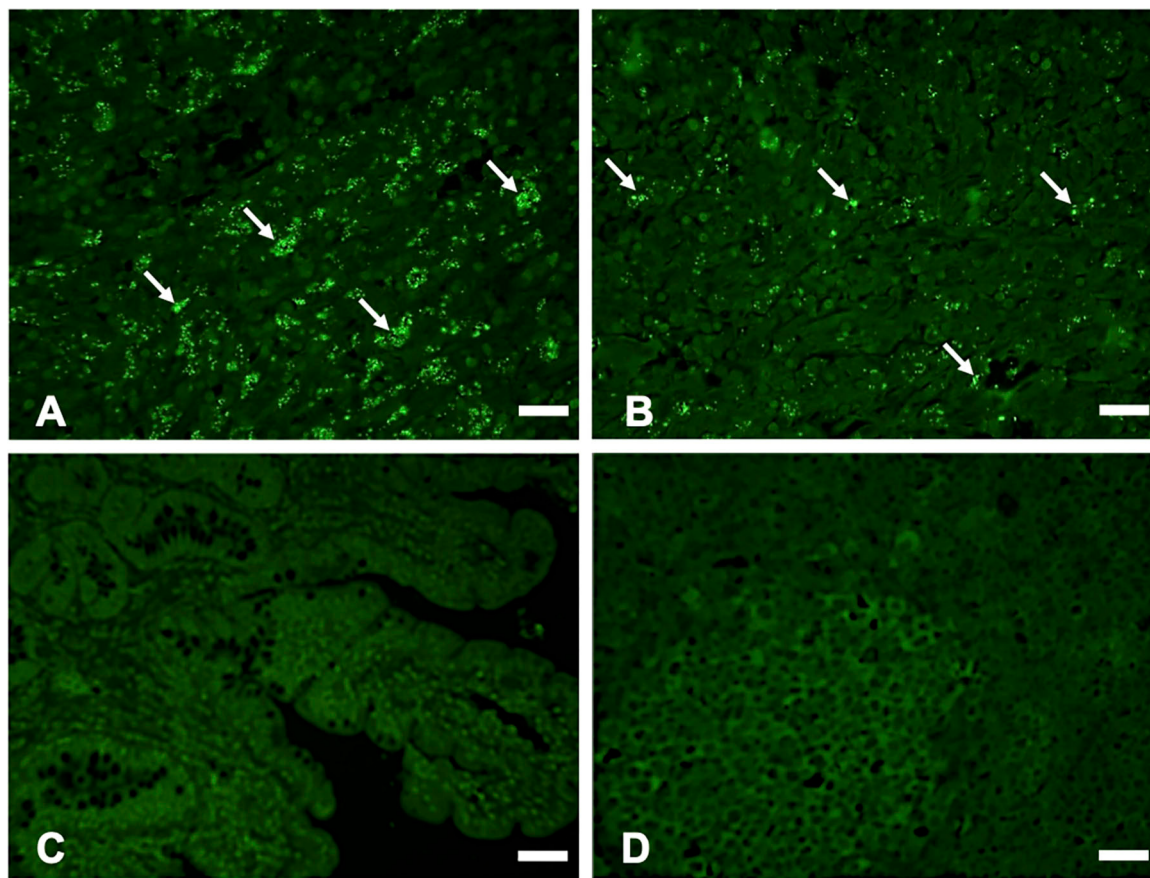


FIGURE 3 | Immunofluorescence (IF) staining of tissue sections using anti-*M. avium* subsp. *paratuberculosis* (MAP) cell envelope antibodies. IF staining of intestinal tissue **(A)** and lymph node sections **(B)** with antibodies to total MAP cell envelope protein extract showing strong immunoreactivity with MAP bacteria (arrows indicating bright green immunofluorescent spots), Bars = 25 μ m; IF staining of intestinal tissue **(C)** and lymph node sections **(D)** from a calf not exposed to MAP showing lack of immunoreactivity with antibodies to total MAP cell envelope protein extract, Bars = 25 μ m.

92%, respectively. The ELISA with DesA2 recombinant protein had a $ROC_{(AUC)}$ value of 0.84. Earlier studies with DesA2 recombinant protein ELISAs showed $ROC_{(AUC)}$ values of 0.69 and 0.70 (44, 45). However, these studies used refolded recombinant proteins that could have altered the protein properties such as structure, orientation and antigenicity resulting in low $ROC_{(AUC)}$ values. ELISAs with the other four recombinant proteins, SdhA, FadE25_2, FadE3_2, and Mkl, showed less specificity. In general, the specificities of ELISAs with recombinant proteins reported in this study were less than that of the commercial ELISA tests. Indeed, false positive reactions with recombinant protein-based ELISAs has been reported previously (44, 46) and considerable numbers of animals in the false positive and false negative categories are typically expected in JD diagnosis (47). In addition to the MAP-specific epitopes, it is possible that the antigens used in this study may contain other epitopes that may be present in other mycobacterial or non-mycobacterial species and environmental exposure of cattle to these microorganisms might have led to false positives. Future experiments with partial proteins or peptides as well as ELISAs coated with mixtures of different recombinant MAP cell envelope proteins could improve test specificity.

There were certain limitations to our experimental approach. In this study, we used serum samples collected from cattle from MAP-positive herds some of which were likely exposed to different levels of MAP bacteria. Moreover, a lack of true negative samples could result in a degree of bias in the calculation of sensitivity and specificity. Additional testing of true negative and true positive samples might yield a more definitive assessment of sensitivity and specificity. We acknowledge that establishing JD infection status is an important aspect of studies comparing tests for this disease. However, the dilemma is identifying a suitable reference standard test as there is no formal JD status program in Canada. The best available tests currently used for evaluation of JD in Canadian dairy herds are fecal culture (direct test) and ELISA analysis of serum antibodies to MAP (indirect test). Additional ELISA tests are available to assess antibodies in milk. However, limitations to the use of these tests associated with deficiencies in their accuracy require cautious interpretation of test results from individual cattle. For example, cattle in the early stages of infection may not have produced sufficient antibodies necessary for detection by ELISA. Moreover, MAP microorganisms may only be shed intermittently in the feces. Because only 45% of subclinically infected cattle are detected by fecal culture and <20% by serological methods, it is often

necessary to repeat testing periodically to determine whether a herd has a minimal risk for MAP infection¹.

In 2010, the USDA introduced national standards for a Voluntary Bovine Johne's Disease Control Program the purpose of which is to identify herds with low prevalence of JD (48). The program consists of a classification system with 6 levels based on annual testing with official JD tests with the highest classification levels identifying herds with 2 or more years of test negative results. However, there is no similar policy in Canada and Canadian dairy herds are typically referred to as "low prevalence" and "low risk" rather than "negative" due to limitations in existing reference tests (i.e., fecal culture and ELISA) to establish JD herd status. While the degree of infectivity can be calculated from fecal culture results as either low (<10 CFU), medium (between 10 and 50 CFU), or heavy (>50 CFU), Ontario animal diagnostic laboratories do not routinely report the number of CFUs that might reflect the level of MAP microorganisms being shed. In addition, serum samples from *M. bovis*-positive cattle could be used to further assess the level of cross-reactivity. Finally, an increase in sample size would increase the statistical power of the study.

In the second part of our study, we tested polyclonal antibodies generated to either MAP total cell envelope protein extracts, or recombinant proteins (SdhA, FadE25_2, and anti-DesA2) in order to identify MAP in tissues by IHC or immunomagnetic separation techniques. Polyclonal antibodies are routinely used in pathogen identification by immunoblot, IHC, biosensors and flow cytometry (49). Others have shown that polyclonal antibodies generated against MAP cell wall components are useful tools in the identification of MAP organisms (50). While antibodies specific to MAP are useful in the diagnosis of JD, generation of these antibodies is difficult due to the genetic similarity of MAP with other closely related mycobacterial species (51). Recently our 2-dimensional difference gel electrophoresis analysis of MAP, MAH, and *M. smegmatis* analysis showed that the MAP cell envelope proteome profile is different from genetically close relative species in the *M. avium* complex and many of the MAP-specific proteins were antigenically distinct based on 2-dimensional electrophoresis immunoblot analysis with JD-test positive cattle serum samples (25). This finding suggested that antibodies to MAP cell envelope proteins may be useful in JD diagnosis by specifically identifying MAP organisms.

IHC and IF analysis of MAP-infected intestinal and lymph node sections infected with MAP using rat polyclonal antibodies to total MAP cell envelope proteins revealed strong antigen-antibody reactions to MAP organisms. At present, there are no MAP species-specific antibodies available commercially and previous studies using commercial anti-*M. bovis* antibodies and in-house anti-MAP antibodies for IHC and IFC showed variable sensitivity when compared to various gold standard diagnostic approaches (52–54). For example, a very low sensitivity for IHC as compared to fecal culture has been reported (52). In contrast, others found that IHC was more sensitive in identifying MAP organisms in tissues sections compared to acid-fast staining

(29, 55, 56). Rat polyclonal antibodies to SdhA, FadE25_2, and DesA2 were not able to identify MAP organisms in tissue sections possibly because these antigens were either inaccessible to the antibodies or were damaged by formalin fixation. Interestingly, antigens of membrane origin are more susceptible to decay in formalin fixative than cytoplasmic antigens (57). Other possible reasons include masking of epitopes, protein-protein interactions and changes in protein conformation by formalin-mediated protein cross-linking (57). Therefore, further studies with frozen tissue sections or tissues fixed in formalin for shorter periods are necessary to test the use of anti-SdhA, FadE-25_2, and DesA2 antibodies in IHC and IF.

Additionally, polyclonal antibodies from chickens (IgY) are more specific and sensitive in MAP capturing by magnetic separation (53). In experiments involving immunomagnetic separation of MAP, we found that Dyna protein G beads coated with polyclonal antibodies generated against MAP total cell envelope proteins are capable of capturing MAP organisms at concentrations as low as 10² CFU. Others have used IMS-PCR based assays to identify 10³–10⁵ CFU of MAP (58, 59). While polyclonal antibodies to SdhA, FadE25_2, and DesA2 were able to bind and retrieve MAP organisms, the sensitivity of MAP recovery was variable. This may be because antibodies to recombinant MAP proteins target single antigens that may have reduced levels of abundance. Another possible reason is that recombinant proteins may lack the appropriate tertiary structure required for antibody recognition of native antigens on the MAP cell surface. More recently, studies found that magnetic nanoparticles coated with anti-MAP polyclonal or monoclonal antibodies were effective in the identification of MAP from clinical samples (30, 60). The advantages of immunomagnetic separation methods are that they concentrate the target bacterium from the non-specific bacterial pool and inhibitory substances. This then facilitates rapid and sensitive identification of MAP by the downstream detection tests such as PCR, culture, and acid-fast staining of MAP (13, 53, 61). Having determined the capacity of immunomagnetic separation to bind and extract MAP in PBS, future experiments will be conducted using relevant biological samples (e.g., milk or feces) that have been spiked with varying concentrations of MAP either alone or mixed with other bacterial species.

DATA AVAILABILITY STATEMENT

The original contributions presented in the study are included in the article/**Supplementary Material**, further inquiries can be directed to the corresponding author/s.

ETHICS STATEMENT

This animal study was reviewed and approved by Animal Care Committee of the University of Guelph.

AUTHOR CONTRIBUTIONS

GK, LM, DK, BP, and NK designed the overall study. SK and SM performed the experiments. LM, DK, and BP provided

¹<https://www.vet.cornell.edu/animal-health-diagnostic-center/testing/protocols/johnes-disease-program>

samples essential to the study. SK and GK wrote the manuscript. All authors contributed to the article and approved the submitted version.

FUNDING

This work was supported by the Indian Council of Agricultural Research (ICAR) for supporting SK with an ICAR International Fellowship.

ACKNOWLEDGMENTS

We would like to thank technicians in the Central Animal Facility at the University of Guelph for their help with immunization of rats and blood collection.

SUPPLEMENTARY MATERIAL

The Supplementary Material for this article can be found online at: <https://www.frontiersin.org/articles/10.3389/fvets.2021.615029/full#supplementary-material>

Supplementary Table 1 | Individual fecal culture (FC) and ELISA analysis results for *Mycobacterium avium* subsp. *paratuberculosis*.

REFERENCES

1. Speer C, Scott MC, Bannantine JP, Waters WR, Mori Y, Whitlock RH, et al. A novel enzyme-linked immunosorbent assay for diagnosis of *Mycobacterium avium* subsp. *paratuberculosis* infections (John's Disease) in cattle. *Clin Vaccine Immunol.* (2006) 13:535–40. doi: 10.1128/CDLI.13.5.535-540.2006
2. McKenna SL, Keefe GP, Tiwari A, VanLeeuwen J, Barkema HW. John's disease in Canada part II: disease impacts, risk factors, and control programs for dairy producers. *Can Vet J.* (2006) 47:1089–99.
3. Garcia A, Shalloo L. Invited review: The economic impact and control of paratuberculosis in cattle. *J Dairy Sci.* (2015) 98:5019–39. doi: 10.3168/jds.2014-9241
4. Whitlock RH, Buergelt C. Preclinical and clinical manifestations of paratuberculosis (including pathology). *Vet Clin North Am Food Anim Pract.* (1996) 12:345–56. doi: 10.1016/S0749-0720(15)30410-2
5. Logar K, Kopinc R, Bandelj P, Staric J, Lapanje A, Ocepik M. Evaluation of combined high-efficiency DNA extraction and real-time PCR for detection of *Mycobacterium avium* subsp. *paratuberculosis* in subclinically infected dairy cattle: comparison with faecal culture, milk real-time PCR and milk ELISA. *BMC Vet Res.* (2012) 8:49. doi: 10.1186/1746-6148-8-49
6. Collins MT. Diagnosis of paratuberculosis. *Vet Clin North Am Food Anim Pract.* (2011) 27:581–91, vi. doi: 10.1016/j.cvfa.2011.07.013
7. Gilardoni LR, Paolich FA, Mundo SL. Bovine paratuberculosis: a review of the advantages and disadvantages of different diagnostic tests. *Rev Argent Microbiol.* (2012) 44:201–5.
8. Thoresen OF, Falk K, Evensen Ø. Comparison of immunohistochemistry, acid-fast staining, and cultivation for detection of *Mycobacterium paratuberculosis* in goats. *J Vet Diagn Invest.* (1994) 6:195–9. doi: 10.1177/104063879400600210
9. Coetsier C, Havaux X, Mattelard F, Sadatte S, Cormont F, Buergelt K, et al. Detection of *Mycobacterium avium* subsp. *paratuberculosis* in infected tissues by new species-specific immunohistological procedures. *Clin Diagn Lab Immunol.* (1998) 5:446–51. doi: 10.1128/CDLI.5.4.446-451.1998
10. O'Brien LM, Stewart LD, Strain SA, Grant IR. Novel monoclonal antibody and peptide binders for *Mycobacterium avium* subsp. *paratuberculosis* and their application for magnetic separation. *PLoS ONE.* (2016) 11:e0147870. doi: 10.1371/journal.pone.0147870
11. Mortier RA, Barkema HW, Orsel K, Wolf R, De Buck J. Shedding patterns of dairy calves experimentally infected with *Mycobacterium avium* subspecies *paratuberculosis*. *Vet Res.* (2014) 45:71. doi: 10.1186/s13567-014-0071-1
12. Timms VJ, Gehring MM, Mitchell HM, Daskalopoulos G, Neilan BA. How accurately can we detect *Mycobacterium avium* subsp. *paratuberculosis* infection? *J Microbiol Methods.* (2011) 85:1–8. doi: 10.1016/j.mimet.2011.01.026
13. Foddai A, Elliott CT, Grant IR. Maximizing capture efficiency and specificity of magnetic separation for *Mycobacterium avium* subsp. *paratuberculosis* cells. *Appl Environ Microbiol.* (2010) 76:7550–8. doi: 10.1128/AEM.01432-10
14. Collins MT, Wells SJ, Petrini KR, Collins JE, Schultz RD, Whitlock RH. Evaluation of five antibody detection tests for diagnosis of bovine paratuberculosis. *Clin Diagn Lab Immunol.* (2005) 12:685–92. doi: 10.1128/CDLI.12.6.685-692.2005
15. Toft N, Nielsen SS, Jørgensen E. Continuous-data diagnostic tests for paratuberculosis as a multistage disease. *J Dairy Sci.* (2005) 88:3923–31. doi: 10.3168/jds.S0022-0302(05)73078-2
16. McKenna S, Barkema H, Keefe GP, Sockett D. Agreement between three ELISAs for *Mycobacterium avium* subsp. *paratuberculosis* in dairy cattle. *Vet Microbiol.* (2006) 114:285–91. doi: 10.1016/j.vetmic.2005.12.002
17. Buczinski S, Arsenault J, Kostoulas P, Corbière F, Fecteau G, Dendukuri N. Accuracy of paratuberculosis diagnostic tests in small ruminants: protocol for a systematic review and meta-analysis. *Anim Health Res Rev.* (2019) 20:98–102. doi: 10.1017/S1466252319000082
18. Bach E, Raizman EA, Vanderwal R, Soto P, Chaffer M, Keefe G, et al. Immunogenicity of PtpA secreted during *Mycobacterium avium* ssp. *paratuberculosis* infection in cattle. *Vet Immunol Immunopathol.* (2018) 198:1–5. doi: 10.1016/j.vetimm.2018.02.006
19. Khol J, Geisbauer E, Wassertheurer M, Revilla-Fernández S, Damoser J, Österreicher E, et al. Outcome of three commercial serum ELISAs and faecal detection of *Mycobacterium avium* subsp. *paratuberculosis* in consecutive samples from a cattle herd with low prevalence of paratuberculosis (John's Disease). *Transbound Emerg Dis.* (2012) 59:197–207. doi: 10.1111/j.1865-1682.2011.01256.x

20. Facciuolo A, Kelton DE, Mutharia LM. Novel secreted antigens of *Mycobacterium paratuberculosis* as serodiagnostic biomarkers for Johne's disease in cattle. *Clin Vaccine Immunol.* (2013) 20:1783–91. doi: 10.1128/CVI.00380-13
21. Eda S, Bannantine JP, Waters W, Mori Y, Whitlock RH, Scott MC, et al. A highly sensitive and subspecies-specific surface antigen enzyme-linked immunosorbent assay for diagnosis of Johne's disease. *Clin Vaccine Immunol.* (2006) 13:837–44. doi: 10.1128/CVI.00148-06
22. McKenna S, Sockett D, Keefe GP, McClure J, VanLeeuwen JA, Barkema H. Comparison of two enzyme-linked immunosorbent assays for diagnosis of *Mycobacterium avium* subsp. *paratuberculosis*. *J Vet Diagn Invest.* (2005) 17:463–6. doi: 10.1177/104063870501700510
23. Fukuda T, Matsumura T, Ato M, Hamasaki M, Nishiuchi Y, Murakami Y, et al. Critical roles for lipomannan and lipoarabinomannan in cell wall integrity of mycobacteria and pathogenesis of tuberculosis. *mBio.* (2013) 4:e00472-12. doi: 10.1128/mBio.00472-12
24. Eda S, Elliott B, Scott M, Waters W, Bannantine J, Whitlock R, et al. New method of serological testing for *Mycobacterium avium* subsp. *paratuberculosis* (Johne's disease) by flow cytometry. *Foodborne Pathog Dis.* (2005) 2:250–62. doi: 10.1089/fpd.2005.2.250
25. Karuppusamy S, Mutharia L, Kelton D, Karrow N, Kirby G. Identification of antigenic proteins from *Mycobacterium avium* subspecies *paratuberculosis* cell envelope by comparative proteomic analysis. *Microbiology.* (2018) 164:322–37. doi: 10.1099/mic.0.000606
26. Prieto JM, Balseiro A, Casais R, Abendaño N, Fitzgerald LE, Garrido JM, et al. Sensitive and specific enzyme-linked immunosorbent assay for detecting serum antibodies against *Mycobacterium avium* subsp. *paratuberculosis* in fallow deer. *Clin Vaccine Immunol.* (2014) 21:1077–85. doi: 10.1128/CVI.00159-14
27. Simpson RJ. Rapid coomassie blue staining of protein gels. *Cold Spring Harbor Protocols.* (2010) 2010.pdb.prot5413. doi: 10.1101/pdb.prot5413
28. Crowther JR. The ELISA guidebook. *Methods Mol Biol.* (2000) 149:iii-iv, 1–413. doi: 10.1385/1592590497
29. Hemida H, Kihal M. Detection of paratuberculosis using histopathology, immunohistochemistry, and ELISA in West Algeria. *Comp Clin Path.* (2015) 24:1621–9. doi: 10.1007/s00580-015-2126-8
30. Gilardoni LR, Fernández B, Morsella C, Mendez L, Jar AM, Paolicchi FA, et al. *Mycobacterium paratuberculosis* detection in cow's milk in Argentina by immunomagnetic separation-PCR. *Braz J Microbiol.* (2016) 47:506–12. doi: 10.1016/j.bjm.2016.01.013
31. Mead PJ. Infection of monocyte-derived macrophages with a reporter Map strain: validation of the susceptibility SNP (-298A/G) in the bovine MIF gene (Ph.D. dissertation). University of Guelph, Guelph, ON, Canada (2013).
32. Moravkova M, Hložek P, Beran V, Pavlik I, Preziuso S, Cuteri V, et al. Strategy for the detection and differentiation of *Mycobacterium avium* species in isolates and heavily infected tissues. *Res Vet Sci.* (2008) 85:257–64. doi: 10.1016/j.rvsc.2007.10.006
33. McKenna S, Keefe GP, Barkema H, Sockett D. Evaluation of three ELISAs for *Mycobacterium avium* subsp. *paratuberculosis* using tissue and fecal culture as comparison standards. *Vet Microbiol.* (2005) 110:105–11. doi: 10.1016/j.vetmic.2005.07.010
34. Osterstock JB, Fosgate GT, Norby B, Manning EJ, Collins MT, Roussel AJ. Contribution of environmental mycobacteria to false-positive serum ELISA results for paratuberculosis. *J Am Vet Med Assoc.* (2007) 230:896–901. doi: 10.2460/javma.230.6.896
35. Scott MC, Bannantine JP, Kaneko Y, Branscum AJ, Whitlock RH, Mori Y, et al. Absorbed EVELISA: a diagnostic test with improved specificity for Johne's disease in cattle. *Foodborne Pathog Dis.* (2010) 7:1291–6. doi: 10.1089/fpd.2010.0541
36. Chaubey K, Singh S, Bhatia A. Indigenous and 'Ethanol Vortex' ELISA kits for diagnosis of *Mycobacterium avium* subsp. *paratuberculosis* infection in cattle: is there a 'globally relevant kit' in the 'Reverse ice-burg' environment? *Indian J Exp Biol.* (2018) 56:279–86. doi: 10.5402/2011/636038
37. Sweeney RW, Whitlock RH, Hamir AN, Rosenberger AE, Herr SA. Isolation of *Mycobacterium paratuberculosis* after oral inoculation in uninfected cattle. *Am J Vet Res.* (1992) 53:1312–4.
38. Navarro-Gonzalez N, Fourichon C, Blanquefort P, Delafosse A, Joly A, Ngwa-Mbot D, et al. Longitudinal study of *Mycobacterium avium* ssp. *paratuberculosis* fecal shedding patterns and concurrent serological patterns in naturally infected dairy cattle. *J Dairy Sci.* (2019) 102:9117–37. doi: 10.3168/jds.2018-15897
39. Nielsen SS, Toft N. Ante mortem diagnosis of paratuberculosis: a review of accuracies of ELISA, interferon- γ assay and faecal culture techniques. *Vet Microbiol.* (2008) 129:217–35. doi: 10.1016/j.vetmic.2007.12.011
40. Bannantine JP, Rosu V, Zanetti S, Rocca S, Ahmed N, Sechi LA. Antigenic profiles of recombinant proteins from *Mycobacterium avium* subsp. *paratuberculosis* in sheep with Johne's disease. *Vet Immunol Immunopathol.* (2008) 122:116–25. doi: 10.1016/j.vetimm.2007.10.020
41. Leroy B, Viart S, Trinchero N, Roupie V, Govaerts M, Letesson J, et al. Use of *Mycobacterium avium* subsp. *paratuberculosis* specific coding sequences for serodiagnosis of bovine paratuberculosis. *Vet Microbiol.* (2009) 135:313–9. doi: 10.1016/j.vetmic.2008.09.065
42. Bannantine JP, Hansen JK, Paustian ML, Amonsin A, Li L-L, Stabel JR, et al. Expression and immunogenicity of proteins encoded by sequences specific to *Mycobacterium avium* subsp. *paratuberculosis*. *J Clin Microbiol.* (2004) 42:106–14. doi: 10.1128/JCM.42.1.106-114.2004
43. Hughes V, Bannantine JP, Denham S, Smith S, Garcia-Sanchez A, Sales J, et al. Immunogenicity of proteome-determined *Mycobacterium avium* subsp. *paratuberculosis*-specific proteins in sheep with paratuberculosis. *Clin Vaccine Immunol.* (2008) 15:1824–33. doi: 10.1128/CVI.00099-08
44. Gurung RB, Purdie AC, Begg DJ, Whittington RJ. *In silico* screened *Mycobacterium avium* subsp. *paratuberculosis* (MAP) recombinant proteins upregulated under stress conditions are immunogenic in sheep. *Vet Immunol Immunopathol.* (2012) 149:186–96. doi: 10.1016/j.vetimm.2012.06.026
45. Gurung RB, Begg DJ, Purdie AC, Bannantine JP, Whittington RJ. Antigenicity of recombinant maltose binding protein-*Mycobacterium avium* subsp. *paratuberculosis* fusion proteins with and without factor Xa cleaving. *Clin Vaccine Immunol.* (2013) 20:1817–26. doi: 10.1128/CVI.00596-13
46. Angkasekwinai N, Atkins EH, Romero S, Grieco J, Chao CC, Ching WM. An evaluation study of enzyme-linked immunosorbent assay (ELISA) using recombinant protein Pap31 for detection of antibody against *Bartonella bacilliformis* infection among the Peruvian population. *Am J Trop Med Hyg.* (2014) 90:690–6. doi: 10.4269/ajtmh.13-0131
47. Köhler H, Burkert B, Pavlik I, Diller R, Geue L, Conraths FJ, et al. Evaluation of five ELISA test kits for the measurement of antibodies against *Mycobacterium avium* subspecies *paratuberculosis* in bovine serum. *Berl Munch Tierarztl Wochenschr.* (2007) 121:203–10.
48. USDA. *Uniform Program Standards for the Voluntary Bovine Johne's Disease Control Program.* U.S.D.o. Agriculture (2010).
49. Frenzel A, Hust M, Schirrmann T. Expression of recombinant antibodies. *Front Immunol.* (2013) 4:217. doi: 10.3389/fimmu.2013.00217
50. Stabel JR, Ackermann MR, Goff JP. Comparison of polyclonal antibodies to three different preparations of *Mycobacterium paratuberculosis* in immunohistochemical diagnosis of Johne's disease in cattle. *J Vet Diagn Invest.* (1996) 8:469–73. doi: 10.1177/104063879600800412
51. Bannantine JP, Stabel JR, Lamont EA, Briggs RE, Sreevatsan S. Monoclonal antibodies bind a SNP-sensitive epitope that is present uniquely in *Mycobacterium avium* subspecies *paratuberculosis*. *Front Microbiol.* (2011) 2:163. doi: 10.3389/fmicb.2011.00163
52. Martinson SA, Hanna PE, Ikede BO, Lewis JP, Miller LM, Keefe GP, et al. Comparison of bacterial culture, histopathology, and immunohistochemistry for the diagnosis of Johne's disease in culled dairy cows. *J Vet Diagn Invest.* (2008) 20:51–7. doi: 10.1177/104063870802000109
53. Shin SJ, Lee SS, Manning EJ, Collins MT. Production of and applications for a polyclonal IgY diagnostic reagent specific for *Mycobacterium avium* subsp. *Paratuberculosis*. *J Microbiol.* (2009) 47:600–9. doi: 10.1007/s12275-009-0052-7
54. Pedersen JS, Clarke I, Mills J. Improved detection of mycobacteria species in formalin-fixed tissue sections. *Histopathology.* (2011) 59:993–1005. doi: 10.1111/j.1365-2559.2011.04015.x
55. Brees DJ, Reimer SB, Chevillat NF, Florance A, Thoen CO. Immunohistochemical detection of *Mycobacterium paratuberculosis* in formalin-fixed, paraffin-embedded bovine tissue sections. *J Vet Diagn Invest.* (2000) 12:60–3. doi: 10.1177/104063870001200111
56. Sonawane G, Tripathi BN. Comparative diagnosis of *Mycobacterium avium* subspecies *paratuberculosis* in the tissues of clinical and subclinical sheep

- of paratuberculosis endemic farm. *Comp Clin Path.* (2018) 28:549–55. doi: 10.1007/s00580-018-2837-8
57. Grillo F, Pigozzi S, Ceriolo P, Calamaro P, Fiocca R, Mastracci L. Factors affecting immunoreactivity in long-term storage of formalin-fixed paraffin-embedded tissue sections. *Histochem Cell Biol.* (2015) 144:93–9. doi: 10.1007/s00418-015-1316-4
 58. Grant I, Pope C, O'Riordan L, Ball H, Rowe M. Improved detection of *Mycobacterium avium* subsp. *paratuberculosis* in milk by immunomagnetic. *PCR Vet Microbiol.* (2000) 77:369–78. doi: 10.1016/S0378-1135(00)00322-9
 59. Chui LW, King R, Sim J. Development of an immunocapture-polymerase chain reaction assay using IgY to detect *Mycobacterium avium* subsp. *paratuberculosis*. *Can J Vet Res.* (2010) 74:102–7.
 60. Singh M, Singh SV, Gupta S, Chaubey KK, Stephan BJ, Sohal JS, et al. 'Nano-immuno test' for the detection of live *Mycobacterium avium* subspecies *paratuberculosis* bacilli in the milk samples using magnetic nano-particles and chromogen. *Vet Res Commun.* (2018) 42:183–94. doi: 10.1007/s11259-018-9721-5
 61. Khare S, Ficht TA, Santos RL, Romano J, Ficht AR, Zhang S, et al. Rapid and sensitive detection of *Mycobacterium avium* subsp. *paratuberculosis* in bovine milk and feces by a combination of immunomagnetic bead separation-conventional PCR and real-time PCR. *J Clin Microbiol.* (2004) 42:1075–81. doi: 10.1128/JCM.42.3.1075-1081.2004

Conflict of Interest: The authors declare that the research was conducted in the absence of any commercial or financial relationships that could be construed as a potential conflict of interest.

Copyright © 2021 Karuppusamy, Mutharia, Kelton, Plattner, Mallikarjunappa, Karrow and Kirby. This is an open-access article distributed under the terms of the Creative Commons Attribution License (CC BY). The use, distribution or reproduction in other forums is permitted, provided the original author(s) and the copyright owner(s) are credited and that the original publication in this journal is cited, in accordance with accepted academic practice. No use, distribution or reproduction is permitted which does not comply with these terms.



Survey of Candidate Single-Nucleotide Polymorphisms in SLC11A1, TLR4, NOD2, PGLYRP1, and IFN γ in Ankole Longhorn Cattle in Central Region of Uganda to Determine Their Role in *Mycobacterium avium* Subspecies *paratuberculosis* Infection Outcome

OPEN ACCESS

Edited by:

Miguel Salgado,
Austral University of Chile, Chile

Reviewed by:

Marta Alonso-Hernández,
NEIKER-Instituto Vasco de
Investigación y Desarrollo
Agrario, Spain

Amanda Jane Gibson,
Aberystwyth University,
United Kingdom

*Correspondence:

Julius Boniface Okuni
jbonkuni@gmail.com

Specialty section:

This article was submitted to
Veterinary Infectious Diseases,
a section of the journal
Frontiers in Veterinary Science

Received: 06 October 2020

Accepted: 06 January 2021

Published: 12 February 2021

Citation:

Okuni JB, Afayoa M and Ojok L (2021)
Survey of Candidate Single-Nucleotide
Polymorphisms in SLC11A1, TLR4,
NOD2, PGLYRP1, and IFN γ in Ankole
Longhorn Cattle in Central Region of
Uganda to Determine Their Role in
Mycobacterium avium Subspecies
paratuberculosis Infection Outcome.
Front. Vet. Sci. 8:614518.
doi: 10.3389/fvets.2021.614518

Julius Boniface Okuni^{1*}, Mathias Afayoa¹ and Lonzy Ojok^{1,2}

¹ Department of Pharmacy, Veterinary Clinical and Companion Animal Medicine, College of Veterinary Medicine, Animal Resources and Biosecurity (COVAB), Makerere University, Kampala, Uganda, ² Department of Pathology, Faculty of Medicine, Gulu University, Gulu, Uganda

Mycobacterium avium ssp. *paratuberculosis* (MAP) is the cause of Johne's disease (JD) in a wide range of domestic and wild ruminants. Single-nucleotide polymorphisms (SNPs) in several genes including solute-like carrier 11A1 (SLC11A1), interferon gamma (IFN γ), Toll-like receptor 4 (TLR4), nucleotide-binding oligomerization domain 2 gene (NOD2), and bovine peptidoglycan recognition protein 1 (PGLYRP1) have been implicated in influencing the infection outcome of MAP in cattle. We have carried out a survey in a population of Ankole cattle from three districts in the central region of Uganda including Isingiro, Lyantonde, and Rakai to determine the role played by several SNPs on the above genes in the infection outcome of local cattle in Uganda. Nine hundred fifty-five heads of cattle obtained from 93 herds were tested using ELISA. Thirty-five ELISA-positive cattle and 35 negative herd mates from a total of 955 cattle tested for MAP were genotyped using iPLEX MassARRAY genotyping systems to detect the presence of a total of 13 SNPs in five different genes (SLC11A1, IFN γ , TLR4, NOD2, and PGLYRP1). The cow-level prevalence of MAP infection in Ankole Longhorn cattle in the three districts was 3.98% (35/955), while the herd-level prevalence was 27.9% and within-herd prevalence was $12 \pm 1.5\%$ (95% CI = 9.1–14.8%). The genotypes and allele frequencies of the MAP-positive cattle were compared with those of their ELISA-negative herd mates to determine the significance of the polymorphisms. The results showed that SNPs rs109915208, rs110514940, and rs110905610 on SLC11A1, c.480G>A and c.625C>A on PGLYRP1, and c.2021C>T on TLR4 were monomorphic in both seropositive and seronegative cattle and therefore had no influence on the infection outcome. The remaining SNPs studied in the five genes [SLC11A1: rs109614179; TLR4: rs29017188 (c.226G>C), c.2021C>T; NOD2: rs110536091, rs111009394; PGLYRP1:

c.102G>C, c.480G>A, c.625C>A; *IFN γ* : rs110853455] were polymorphic, but their allele and genotype frequencies did not show any significant difference between the seropositive and seronegative cattle. No significant difference was observed for any haplotype at the gene level.

Keywords: *Mycobacterium avium* subspecies *paratuberculosis*, Ankole cattle, SNPs, SLC11A1, TLR4, Nod2, IFN γ , PGLYRP1

INTRODUCTION

Mycobacterium avium ssp. *paratuberculosis* (MAP) is the cause of paratuberculosis (PTB) or Johne's disease (JD), a chronic granulomatous enteritis characterized by projectile watery diarrhea in cattle (or loose feces in other species), marked weight loss, submandibular edema, and eventual death (1). PTB causes serious economic losses to the dairy industry in developed countries (2), and it is becoming increasingly relevant in Africa as well (3). Economic impacts of this disease stem from poor growth rate, progressive weight loss, reduced milk production, increased culling, death in affected animals, and loss of market for replacement heifers from affected farms (4).

The biggest risk factor for any herd or population of susceptible cattle is the presence of a clinically affected animal that is shedding the causative agent. In such herds, infected cattle shed MAP through colostrum, milk, and feces and are ingested through feeding of milk or contaminated pasture and water (5). For decades, control of PTB has relied on testing and culling of infected livestock, purchase of stock from JD-free herds, and addition of lime on pasture to render the environment unfavorable for survival of MAP (6). Unfortunately, there has been limited success in these measures due to various difficulties such as lack of a highly sensitive test for the disease during the early stages of infection (7). Diagnosis of the disease relies on antibody detection and demonstration of MAP in feces, which is only possible during the late stages. The other challenge is that culling is extremely expensive and could practically shut down some farms with no guarantee that the MAP-free stock to be introduced will not get infected, since it takes a long time to get rid of MAP from the farm environment (8).

Recently, efforts toward control of MAP infection have turned to the fact that some breeds of cattle (9) and deer (10) appear to be more resistant, while others are more susceptible. MAP infection does not necessarily lead to PTB, since it has been observed that certain breeds and lineages within specific breeds appear to be more resistant, while others are more susceptible. There are noted variations in the severity and spectrum of lesions even among infected cattle (9). This could be attributed to differences in strains of MAP or the genotypes of the host species (11). Indeed, a number of genetic association studies have linked single-nucleotide polymorphisms (SNPs) in some genes to increased susceptibility or resistance to MAP infection.

So far, studies on the effect of SNPs on the most significant genes that play key roles in innate immunity, including Toll-like receptors (TLRs) 1, 2, 4, and 9; nucleotide-binding oligomerization domain 2 (NOD2), solute-like carrier 11A1 (SLC11A1), interferon gamma (IFN γ), and peptidoglycan

recognition protein 1 (PGLYRP1), have been done on different breeds of cattle across the world mostly on *Bos taurus* breeds of cattle (12–18), but there is scarcely any report on the frequency of those polymorphisms and their influence on African cattle. The only study of *Bos indicus* but outside Africa is that of Sadana et al. (19), who investigated the association of MAP infection status with SNPs on SLC11A1, TLR2, NOD2, and IFN γ in Indian cattle.

African breeds of cattle have been recognized for their innate resistance to some of the most important diseases of cattle such as tickborne infections and nagana (20). In Uganda, two indigenous breeds, Ankole and zebu cattle, are the backbone of both milk and meat production in the country. These breeds are known for their natural resistance to many diseases (20, 21), but no investigation has been done to understand how they would respond to MAP infection. Ankole Longhorn cattle is a breed of *B. indicus* cattle that has a characteristic long horn phenotype and is one of the two indigenous breeds in Uganda (21). Two published surveys have indicated that MAP infections in Ankole cattle and their crossbreeds have similar rates of infection as exotic breeds of cattle (22, 23). This finding is of great concern because, at the moment, there is no control measure against PTB in Uganda as is the case in most African countries. However, the studies were carried out in mixed breed herds, and therefore, there was a likelihood that the disease incidences in Ankole cattle that tested positive could have been influenced by the herd characteristics such as high stocking density, presence of large number of very susceptible cattle, and husbandry practices. A report (24) noted earlier that there is a wide lesion spectrum in cattle that are slaughtered at an abattoir in Kampala, which suggests differences in either susceptibility, resistance of the cattle, or virulence of strains of infecting MAP organism or the stage of infection. This study has been carried out to determine allele frequency and the effect of previously studied SNPs in SLC11A1, NOD2, TLR-4, IFN γ , and PGLYRP1 on serostatus of Ankole cattle to MAP infection.

MATERIALS AND METHODS

Study Area

This study was carried out in three districts of south-central Uganda, namely, Isingiro, Lyantonde, and Rakai, which lie on the southern end of a semiarid belt known as the cattle corridor, which runs across Uganda from the south-south-west to the north-east and was historically well-known for pastoralism. The area lies between the southwestern shore of Lake Victoria known as Sango Bay to the East and the Uganda–Tanzania Border to the south in Rakai, to Nakivale in Isingiro, extending northward toward Lake Mburo and Kyotera. The area has one long dry spell

and two short rainy seasons. The vegetation cover consists of wooded semitropical grassland with undulating hills and valleys (Figure 1).

Study Population and Sample Collection

The study population consisted of Ankole Longhorn cattle populations in the three districts. Care was taken to include only cattle from farms and areas with only pure Ankole cattle in herds without mixed breeds. Consent was requested and obtained from the livestock owners to enroll and sample their cattle. Baseline information such as herd size, husbandry practices, history of clinical signs of PTB, and knowledge about the disease was obtained from each of the farmers who agreed to participate. A total of 93 herds that are kept under the traditional system of husbandry were sampled in the study, from which 955 samples were collected. Age of the cattle was obtained from the farmer and verified by checking the tooth eruption and wear. Age was recorded, and only cattle that was 2 years above were included in the study. Blood was obtained aseptically from the animals through the caudal or jugular vein following proper restraint. Two blood samples were obtained from each cow into a vacutainer: ~2 ml of blood into a heparinized tube and another 4 ml of blood into a plain vacutainer for serum extraction. The samples were both placed in a cool box and transported to the laboratory. Serum was extracted from the clotted blood collected in the plain vacutainers and was later tested for MAP.

Serological Testing for *M. avium* ssp. *paratuberculosis* Antibodies

ELISA was performed on sera to test for MAP antibodies using a commercial ELISA kit from IDVET (Montpellier, France) according to the manufacturer's instruction. Optical density readings of the plates were taken at 450 nm using SpectroStar Nano ELISA reader (BMG LABTECH GmbH). To determine the serostatus, a sample to positive ratio was calculated using the formula: $S/P = (\text{Sample OD} - \text{NC-OD}) / (\text{PC-OD} - \text{NC-OD}) \times 100$. Where S/P is the sample to positive ratio, Sample OD is the optical density reading for each sample, NC-OD is the mean optical density reading for the negative controls, and PC-OD is the mean optical density reading of the positive controls. A sample was considered positive if its S/P ratio is equal to or >70%.

Sources of Single-Nucleotide Polymorphisms Studied

The SNPs reported in this paper were discovered by other authors and have been referenced in GenBank and ENSEMBL databases. For SLC11A1 gene, the SNPs included rs109614179, rs109915208, rs110905610, and rs110514940 (19). For NOD2 gene, the investigated SNPs are rs110536091 and rs111009394 (19), while for IFN γ , SNP rs110853455 (19) was investigated. The others were c.102G>C (ss104807451), c.480G>A (ss104807452), and c.625C>A (ss104807453) on the PGLYRP1 gene (17) and rs29017188, rs8193060, and c.2021C>T on the TLR4 gene (25, 26).

Genotyping

A total of 35 ($n = 955$) ELISA-positive Ankole cattle from 26 farms across the three districts and 35 matched controls (Supplementary Table 1) were genotyped at different gene loci to determine the presence or absence of SNPs previously associated with MAP infection. DNA was extracted using Quick-DNATM Microprep Kit (Zymo Research Corp., Freiburg, Germany) according to the manufacturer's instructions. DNA was diluted to a final concentration of 25 ng/ μ l and stored at -20°C . The flanking sequences of the above SNPs were retrieved, and locus-specific and extension primers targeting each of the 13 SNPs across the five genes were designed using Agena Assay Design software and synthesized unmodified under standard purification (Table 1). Primers were synthesized by Inqaba Biotec Laboratories (Pretoria, SA). Genotyping was done using iPLEX MassARRAY platform, which is based on matrix-assisted laser desorption ionization-time of flight (MALDI-TOF) mass spectrometry (Agena Biosciences). The reagents (iPLEX Pro Genotyping reagents) used were custom made for use in Agena MassARRAY system. Briefly, equimolar concentrations of the amplification primers were pooled into a working primer solution containing 0.5 mM of each primer. A PCR mix consisting of 1.8 μ l of high-performance liquid chromatography (HPLC)-grade water, 0.5 μ l of 10 \times PCR buffer (20 mM MgCl_2), 0.4 μ l of MgCl_2 (25 mM), 0.1 μ l of dNTPs (25 mM each), 1 μ l of primers (0.5 mM each), and 0.2 μ l of polymerase (5 U/ μ l) was prepared in a total volume of 5 μ l. The reaction conditions consisted of initial denaturation at 94°C for 2 min and 45 cycles at 94°C for 30 s, 56°C for 30 s, 72°C for 60 s in each cycle, and a final extension of 72°C for 5 min and cooled to 4°C . After the PCR reaction, 2 μ l of shrimp alkaline phosphatase was added to each well and the mix was incubated at 37°C for 40 min and then at 80°C for 5 min. Single base extension of the reaction was carried out by addition of 2 μ l of iPLEX-SBE master mix followed by PCR cycle of 94°C for 30 s, 95°C for 5 s, 52°C for 3 s, and 80°C for 3 s repeated five times. The whole amplification was repeated 60 times then a final extension of 72°C for 3 min and held at 15°C . All PCR amplifications were done using Mastercycler[®] Nexus machines (Eppendorf). The products were purified using resin and then spotted into a 384-well microchip plate using a nanodispenser (MassARRAY System with CPM 384). The chip was then read by the MALDI-TOF Mass Spectrometer (MassARRAY[®] Analyzer 4, Agena Biosciences), and data were obtained using Typer 4.1. software. The spectrographs of each call were visually checked to confirm the identity of the base calls. Only samples with coverage >87.5% were included in the final analysis.

Data Analysis

Data were analyzed using SHEsisPlus software (<http://analysis.bio-x.cn/SHEsisMain.htm>) (28) to estimate the allele and genotype frequencies, pairwise linkage disequilibria, and odds ratio (OR) to compare the associations of alleles, genotypes, and haplotypes with MAP infection. Haplotypes were constructed using a threshold of 0.05 for lowest frequency. The p -values were corrected for multiple comparisons with Sidak correction, and a false discovery rate (FDR) was derived for each SNP.

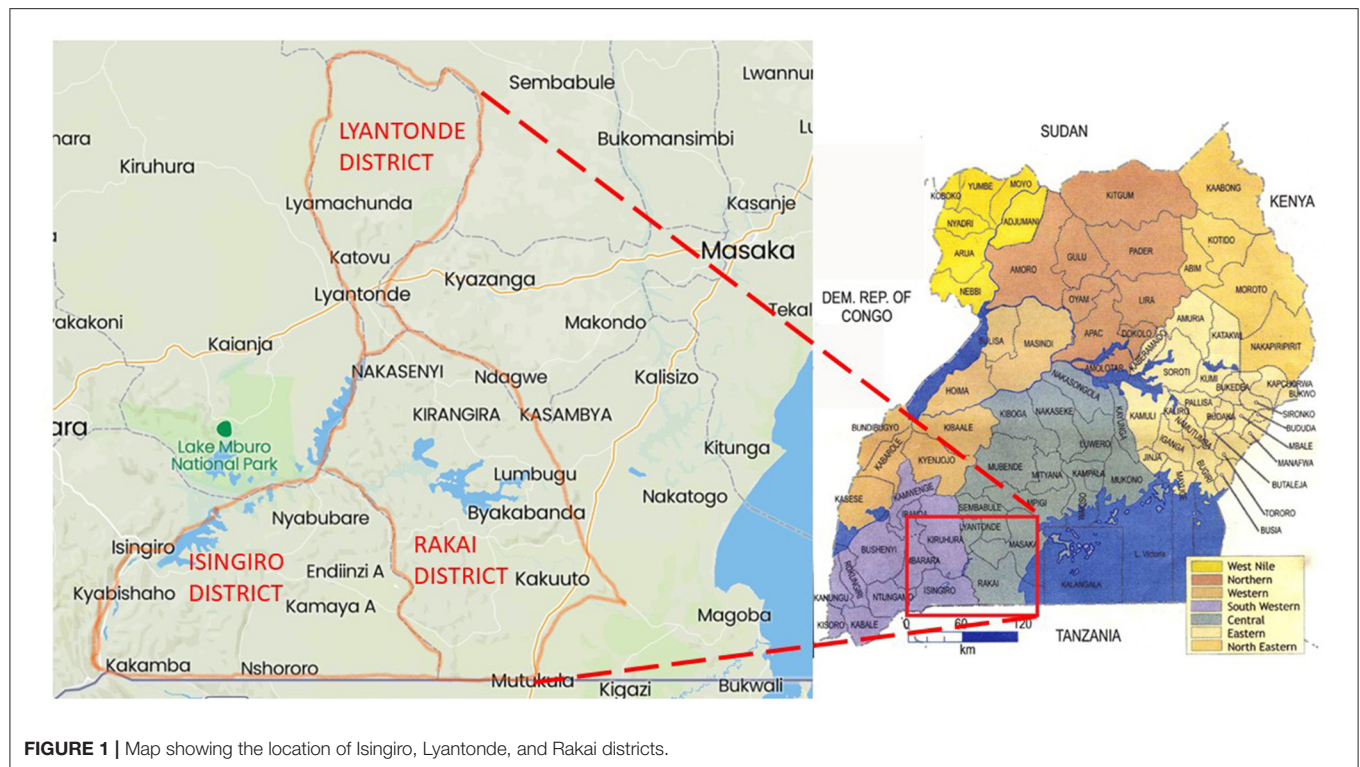


FIGURE 1 | Map showing the location of Isingiro, Lyantonde, and Rakai districts.

Ethical Approval

Ethical clearance for this study was granted by the Uganda National Council for Science and Technology (UNCST) under reference number A32ES. Sample collection was done according to the guidelines on the use of animals in research.

RESULTS

This study was done with the aim of determining the effect of selected SNPs on the seropositivity of Ankole Longhorn cattle to *M. avium* ssp. *paratuberculosis* in central Uganda. Ninety-three herds with only local Ankole cattle, ranging from 8 to 300 cattle and an average of 48 cattle were sampled. The mean age of the cows sampled was 5.95 ± 3.14 years. The herd-level prevalence was 27.9% (26/93), which is at least one cow infected within the herd. The cow-level prevalence was 3.98% and the within-herd prevalence rate ranged from 3 to 29% with a mean of $12 \pm 1.5\%$ (95% CI = 9.1–14.8%). The prevalence rates for the three districts were 4.9% for Rakai, 4.8% for Lyantonde, and 2.5% for Isingiro.

The husbandry practices among the farms consisted of communal grazing and shared water sources in communal valley dams, rivers, and streams. Few of the farmers owned private valley dams and had paddocked grazing land. Seventy-three percent ($n = 93$) of the farmers reported that they had experienced prolonged diarrheal episodes in their farms, and 30.4% of them reported that the diarrhea was non-responsive to treatment. There was considerable mobility for most of the herds during dry season and close sharing of both pasture and water

sources. Approximately 73% ($n = 93$) of the farmers reported regular introduction of new stock into their herds, either as gifts from other cattle keepers, purchases, or bulls for breeding but lacked knowledge (89.2%) about PTB. Water logging on the farms was reported by 17.3%.

The results of the MassARRAY genotyping indicated that SNP c.2021G>T on the TLR4 gene, c.480G>A and c.625C>A on the PGLYRP1 gene, and rs109915208, rs110905610, and rs110514940 on the SLC11A1 gene were monomorphic in both cases and controls and thus had no effect on the infection outcome in the population. The remaining SNPs, namely, rs29017188 (c.226G>C) and rs8193060 (c.1656C>T) on the TLR4 gene, c.480G>A and c.625C>A on the PGLYRP1 gene, rs109614179 on the SLC11A1 gene, and rs110536091 and rs111009394 on the NOD2 gene and finally rs110853455 on the IFN γ gene, did not have any significant differences between seropositive and seronegative animals. The alternative alleles for each of these SNPs are shown in **Table 2**. The frequencies of alleles and genotypes of the different SNPs across five genes SLC11A1, CARD15, IFN γ , TLR4, and PGLYRP1 and their individual effects are shown in **Tables 2, 3**. All polymorphic SNPs were in Hardy-Weinberg equilibrium, except rs109614179. There was a strong linkage disequilibrium for SNPs on NOD2 ($D' = 1$) and TLR4 ($D' = 0.98$). Haplotype analysis of SNPs within the different genes (**Table 4**) showed that haplotype CGCCT was significantly more represented in cases compared to controls ($p = 0.053$, OR = 2.236). Another haplotype CACGT has a stronger p -value 0.048 but with an OR < 1. However, in both cases, the FDR is 0.116.

TABLE 1 | List of SNPS studied and the primers used.

Gene	SNPs	Name of the oligo	Sequence of oligo	References
Toll-like receptor 4 (TLR4)	rs29017188	TLR4aF	ACGTTGGATGGGTCTGCAGACGTTTCTTC	(12)
		TLR4aR	ACGTTGGATGCTTAGCTTTCTGGACTTTG	
		TLR4aE	CCTCTAACTTCCCTC	
	rs8193060	TLR4bF	ACGTTGGATGTTATGAACCACTCCACTCGC	(27)
		TLR4bR	ACGTTGGATGTCCTTAGAGGCCATGATACG	
		TLR4bE	CCATGATACGGTTGAA	
	c.2021C>T	TLR4cF	ACGTTGGATGTTCCACCTGATGCTTCTTGC	(27)
		TLR4cR	ACGTTGGATGGGCTCGAGTAGATGACAAAG	
		TLR4cE	AGGGGCGAGAGCA	
Peptidoglycan recognition protein 1 (PGLYRP1)	c.102G>C	PGLYRP1aF	ACGTTGGATGTAGCGCACAGGCTGTCTTAG	(17)
		PGLYRP1aR	ACGTTGGATGTCAAGACTGCGGCAGCATC	
		PGLYRP1aE	GCACTTGGATGCCAGGGC	
	c.480G>A	PGLYRP1bF	ACGTTGGATGTTTATAGAGCTCGTCCCTG	(17)
		PGLYRP1bR	ACGTTGGATGCGGGGATACCTGACTCCTAA	
		PGLYRP1bE	CGGTGTCCTTTGAC	
	c.625C>A	PGLYRP1cF	ACGTTGGATGATGGCAGGACACAGGAATAC	(17)
		PGLYRP1cR	ACGTTGGATGACCCATCCCATCAGAAACCC	
		PGLYRP1cE	AGAAACCCACCGC	
Solute-like carrier 11A1 (SLC11A1)	rs109614179	SLC11A1bF	ACGTTGGATGCCAGATATGGCTCCATCTCC	(19)
		SLC11A1bR	ACGTTGGATGTTCTCACTTAGGTAGTCCC	
		SLC11A1bE	GAGCCACAGCAAGC	
	rs109915208	SLC11A1cF	ACGTTGGATGTTCACTACCCACAGTACG	(19)
		SLC11A1cR	ACGTTGGATGGAACAGGCCCTGAAGCAATG	
		SLC11A1cE	GAAGCAATGCTCCCTGA	
	rs110905610	SLC11A1dF	ACGTTGGATGCAAGACCCCTCATTCCACTC	(19)
		SLC11A1dR	ACGTTGGATGTGCGATGCTCATGAGGAATC	
		SLC11A1dE	CCACTCCCCCACCAGGGT	
Nucleotide-binding oligomerization domain 2 (NOD2)	rs110514940	SLC11A1eE	AAGGCCACAGCTTCC	(19)
	rs110536091	CARD15aF	ACGTTGGATGTCTCAATTTCTCCGGAGAG	
		CARD15aR	TCTCTTTGCTTTATCCC	
	rs111009394	CARD15aE	ACGTTGGATGACAACTCTGTGGGCGACATC	(19)
		CARD15bF	ACGTTGGATGAGCATCACTCACTAAAGAGC	
		CARD15bR	AAGAGCTTTGCAGAC	
	rs110853455	CARD15bE	ACGTTGGATGCCAGCGCAAAGCCATAATG	(19)
		IFN γ F	ACGTTGGATGGATTCTGACTTCTCTTCCGC	
		IFN γ R	CTGAGGTTAGATTTTGG	
Interferon gamma (IFN γ)	rs110853455	IFN γ E		

DISCUSSION

PTB is an emerging disease in Uganda and, owing to the lack of awareness and control, may be considered a neglected disease. The findings indicate that the prevalence of MAP infection in Ankole cattle is within the same range as it has been reported in mixed breed study in other districts within the central region of Uganda. This has disproved the long-held view that MAP infection of Ankole Longhorn cattle is due to transmission from highly susceptible exotic cattle. In the current study, the prevalence of 3.98% is comparable to 3.7% earlier on reported in Wakiso, Mpigi, and Luwero in mixed breed study (22); 4.7% in slaughtered cattle (24) but significantly lower than

reported in indigenous breeds in Wakiso (23). Overall, the cow-level prevalence of MAP infection in these districts is still low compared to some countries in the world like Canada (30) and Denmark (31), but the herd-level prevalence of 29.3 is considerably high and is a cause for worry if no control measures are instituted. The finding of MAP-infected cattle in an area with one of the most traditional systems of husbandry indicates that PTB is well-established in the local cattle population in Uganda. This is especially so because no single prevalence survey in Uganda has returned a zero-prevalence rate in any district. Practices such as communal grazing and watering, livestock movements in search of water, and pasture during the dry season, all of which were responded to in the affirmative by all the

TABLE 2 | Allele frequencies of the different SNPs in Ankole cattle with positive and negative serostatus for *Mycobacterium avium* ssp. *paratuberculosis*.

Gene	SNPs	Frequency of minor and major alleles			<i>p</i> -value	Corrected <i>p</i> -value (SSD)	FDR
		Alleles	MAP positive	MAP negative			
Toll-like receptor 4 (TLR4)	rs29017188	C	63 (0.900)	66 (0.943)	0.346025	–	–
		G	7 (0.100)	4 (0.057)			
	rs8193060	C	28 (0.400)	24 (0.343)	0.484160	0.929	0.968
		T	42 (0.600)	46 (0.657)			
	c.2021C>T	C	70 (1.000)	69 (0.986)	0.315563	–	–
Peptidoglycan recognition protein 1 (PGLYRP1)	c.102G>C	T	0 (0.000)	1 (0.014)			
		C	55 (0.786)	15 (0.214)	0.017254	0.099	0.103
		G	42 (0.600)	28 (0.400)			
		C	70 (1.000)	70 (1.000)	–	–	–
	c.480G>A	G	70 (1.000)	70 (1.000)	–	–	–
		A	0	0			
	c.625C>A	C	70 (1.000)	70 (1.000)	–	–	–
		A	0	0			
Solute-like carrier 11A1	rs109614179	A	42 (0.600)	30 (0.455)	0.089418	0.373	–
		G	28 (0.400)	36 (0.545)			
	rs109915208	C	70 (1.000)	66 (1.000)	–	–	–
	rs110905610	C	70 (1.000)	66 (1.000)	–	–	–
	rs110514940	C	70 (1.000)	66 (1.000)	–	–	–
Nucleotide-binding oligomerization domain 2 (NOD2)	rs110536091	C	47 (0.671)	42 (0.677)	0.941550	0.984	0.969
		T	23 (0.329)	20 (0.323)			
	rs111009394	C	47 (0.671)	45 (0.682)	0.959511	0.989	–
		T	23 (0.329)	21 (0.318)			
	rs110853455	A	21 (0.300)	20 (0.303)	0.969285	0.989	0.969
		G	49 (0.700)	46 (0.697)			

p, Pearson's *p*-value; SSD, Sidak step-down adjusted *p*-values for strong control of the familywise Type I error rate (FWER); FDR, adjusted *p*-values for the (29) step-up false discovery rate controlling procedure.

farmers mean that it will be very difficult to control the disease in this region.

The results of genotyping show that about half of the SNPs in this study are monomorphic in the Ugandan Ankole Longhorn cattle and therefore may not play any role in the resistance or susceptibility to MAP among Ankole cattle. The other SNPs that were polymorphic also did not show a significant difference between cases and control.

Pairwise and single-site analysis of the data from this study using SHESis Plus software (<http://analysis.bio-x.cn/SHEsisMain.htm>) with *p*-value correction and FDR has led us to conclude that there is no significant difference in the allele and genotype frequency between the cases and control. However, several other studies that had reported an association between some of the SNPs and serostatus (12, 14, 32) in different breeds did not report any *p*-value correction using Bonferroni, Holms, or Sidak methods, and none also reported FDR values, and yet in some instances, the *p*-values were also marginal. Based on this observation, we believe that some of our findings may be comparable to those in some of the published reports.

Although SNP c.102G>C on PGLYRP1 gene had an uncorrected *p*-value of 0.0172 (Table 2), when corrected for multiple comparisons, its *p*-value became 0.099 and the FDR

was 0.103 and thus was not significant. Pant et al. (17) have investigated the linkage between SNP c.102G>C, c.480G>A, and c.625C>A on the PGLYRP1 gene and MAP infection status in Holstein Friesian cattle and reported that c.480G>A is associated with MAP infection. In our study, however, c.480G>A was monomorphic and allele A has zero frequency. At present, there is scarcely any other study on the role of SNPs of this gene with respect to MAP or PTB.

SLC11A1 gene (SLC11A1) codes for the natural resistance-associated macrophage protein (NRAMP1) (33) and some alleles of SLC11A1 have been shown to confer the resistance against MAP to BALB/C mice (34), to cattle against diseases such as tuberculosis (35, 36), brucellosis (37), salmonellosis (38), and conferment of udder immunity (39). In this study, four SNPs on this gene identified as rs109614179, rs109915208, rs110905610, and rs110514940 were investigated for their association. Three of these SNPs (rs109915208, rs110905610, and rs110514940) were monomorphic, indicating that either they are monomorphic in the whole Ankole cattle population or the minor allele has very low allele frequency while rs109614179 was not significantly different in cases and controls. Regarding the significance of the SNPs on SLC11A1, our findings are similar to that of Sadana et al. (19), who did not find any significant association between these

TABLE 3 | Frequency of different genotypes among cattle with positive and negative serostatus for MAP.

Gene	SNPs	Genotype frequency			<i>p</i> -value	Corrected <i>p</i> -value SSD	FDR
		Genotype	MAP positive	MAP negative			
Toll-like receptor 4 (TLR4)	rs29017188	C/C	28 (0.800)	31 (0.886)	0.324487	-	-
		C/G	7 (0.200)	4 (0.114)			
		G/G	0 (0)	0 (0)			
	rs8193060	C/C	6 (0.171)	4 (0.114)	0.762290	0.986	0.959
		C/T	16 (0.457)	16 (0.457)			
		T/T	13 (0.371)	15 (0.429)			
	c.2021C>T	C/C	35 (1.000)	34 (0.971)	-	-	-
		C/T	0 (0)	1 (0.029)			
		T/T	0 (0)	0 (0)			
Peptidoglycan recognition protein 1 (PGLYRP1)	c.102G>C	C/C	22 (0.629)	12 (0.343)	0.051908	0.233	0.155
		C/G	11 (0.314)	18 (0.514)			
		G/G	2 (0.057)	5 (0.143)			
	c.480G>A	G/G	35 (1.000)	35 (1.000)	-		-
	c.625C>A	C/C	35 (1.000)	35 (1.000)	-		-
Solute-like carrier 11A1	rs109614179	A/A	9 (0.257)	7 (0.212)	0.028287	0.158	0.155
		A/G	24 (0.686)	16 (0.485)			
		G/G	2 (0.057)	10 (0.303)			
	rs109915208	C/C	35 (1.000)	33 (1.000)	-		-
	rs110905610	G/G	35 (1.000)	33 (1.000)	-		-
	rs110514940	C/C	35 (1.000)	33 (1.000)	-		-
	rs110536091	C/C	17 (0.486)	15 (0.484)	0.983237	0.997	0.959
		C/T	13 (0.371)	12 (0.387)			
Nucleotide-binding oligomerization domain 2 (NOD2)	rs111009394	T/T	5 (0.143)	4 (0.129)			
		C/C	17 (0.486)	16 (0.485)	0.959511	0.997	0.959
		C/T	13 (0.371)	13 (0.394)			
		T/T	5 (0.143)	4 (0.121)			
		A/A	4 (0.114)	2 (0.061)	0.551026	0.959	0.959
		A/G	13 (0.371)	16 (0.485)			
		G/G	18 (0.514)	15 (0.455)			

p, Pearson's *p*-value; SSD, Sidak step-down adjusted *p*-values for strong control of the familywise Type I error rate (FWER); FDR, adjusted *p*-values for the (29) step-up false discovery rate controlling procedure.

SNPs and MAP infection in Indian cattle. Likewise, there was no association between MAP serostatus and SNPs in IFN γ and TLR4, which we studied. Although other studies have reported an association, for example (19), found between MAP infection status with only IFN γ SNP rs110853455 and not with SNPs on SLC11A1, NOD2/CARD15, which were the focus of our investigation, and Sharma et al. (18) noted that the haplotype C/T of the SNPs c.226C>T and c.2021C>T on TLR4 was associated with susceptibility to MAP infection in Holsteins, yet in our case, both of these SNPs were not related to MAP infection status. Similarly, although Pinedo et al. (13) found an association between SNP c.2197T>C on the NOD2 gene and MAP infection in Holsteins and Brahman-Angus of Florida and Küpper et al. (15) reported an association between SNP g.521G>A on the same gene in German Holstein cattle, those SNPs were different from the ones in our study and therefore lacked a close comparison. Just like other innate immunity genes, NOD2 is known for

its role in natural host resistance to bacterial infection (40) and therefore warrants investigation of its polymorphisms in association with MAP.

We aimed at determining the effect of the SNPs in the five genes enumerated here because they have been studied in Indian cattle (19), since Ankole Longhorn cattle are also *B. indicus* and are therefore closer to the Indian breeds than the Holstein Friesian and other *B. taurus* breeds in other studies. While Sadana et al. (19) used PCR-RLFP for genotyping, we used iPLEX MassARRAY for genotyping except for SNP rs11053609, where we used both methods and obtained the same result, thus validating the use of MassARRAY genotyping. We note that although each of the SNPs had little or no significant effect, when considered together, some haplotypes, e.g., CGCCT (Table 4), may have significant association with the infection. This also may suggest that if the number of individuals in the study was bigger, in hundreds or thousands, it could have been possible to observe

TABLE 4 | Haplotypes inferred using SNPs rs109614179, rs110536091, rs110853455, rs111009394, c.102G>C (PGLYRP1), and rs8193060.

Haplotype	Case (freq)	Control (freq)	Chi2	Pearson's p	OR [95% CI]	SSD	FDR
CGCGT	3 (0.042)	8 (0.129)	2.466	0.116	0.347	0.579	0.215
TATCT	4 (0.057)	3 (0.048)	0.15	0.698	1.353	0.966	0.756
CGCCT*	18 (0.257)	9 (0.145)	3.716	0.053	2.346	0.363	0.116
CGCCC	9 (0.128)	11 (0.177)	0.233	0.629	0.791	0.966	0.743
CACGT*	2 (0.028)	8 (0.129)	3.876	0.048	0.227	0.363	0.116
TATCC	8 (0.114)	6 (0.096)	0.317	0.573	1.376	0.966	0.743
CACCT	6 (0.085)	2 (0.032)	2.121	0.145	3.187	0.61	0.236
CGCGC	8 (0.114)	4 (0.064)	1.458	0.227	2.129	0.724	0.328
TGTCT	9 (0.128)	8 (0.129)	0.066	0.795	1.143	0.966	0.795

FDR, false discovery rate; OR, odds ratio; Sidak SD (Sidak's correction of p-value).

*Haplotype CGCCT is significantly more represented in cases compared to controls with an OR of 2.346. CACGT also has a significant p-value but a small OR <1.

a clear association for some of the SNPs. Our sample size was small because the cases and controls were derived from a study aimed at determining the seroprevalence of MAP among pure Ankole cattle herds in the central region of the country. Overall, 955 heads of cattle were sampled, and 35 of them (3.6%) were seropositive. Due to the lack of well-characterized MAP-positive and MAP-negative herds or a database of JD-positive cattle in the country, it was difficult to come up with a large number of samples for this kind of study. It would have required a very large survey, which was beyond our resources, and furthermore, characterizing herds as MAP resistant would still be a challenge. There are also studies that have used small sample sizes due to the same reason and yet have reported interesting results (27). Given these limitations, we have used a method similar to that in other studies in which seronegative herd mates were considered controls (17, 25, 41), although we did not have the opportunity to confirm seronegative status by retesting. Based on our knowledge of this disease, these controls might be animals at preclinical stage or animals that may test positive on a second testing. We therefore believe that repeated studies especially with a larger number of animals will be necessary to concretely determine the significance of each of these SNPs in Ankole cattle with regard to MAP. Those SNPs that are monomorphic appear to be truly so or may represent SNPs whose minor alleles may be <5%, which would have been otherwise removed from the analysis, as this was the set limit for the minimum allele frequency during the analysis. It is not possible to draw comparisons between our findings and most of the previous studies, since most of the studies cited have used different SNPs, moreover, even with different nomenclature, and only one or a few SNPs being studied in each case. The studies cited point to the general indication that SLC11A1, TLR (1, 2, and 4), NOD2, PGLYRP1, and IFN γ have functional mutations that influence the outcome of cattle infection with MAP. More studies on the effect of the different SNPs on susceptibility or resistance within a breed are still necessary for future application for marker-assisted selection of individuals that are resistant and therefore achieve the control of PTB. To our knowledge, this is the first study done to assess the relevance of these SNPs in association with any infectious disease in Ankole cattle in Uganda and therefore provides key information regarding some of the SNPs, especially those that are now known to have limited allele diversity and those that may have significance for investigating

the association with MAP. More studies are necessary to unravel their significance, more so using a larger sample size and well-characterized herds. Future studies may also aim at discovering more SNPs and other polymorphic loci, especially using genome-wide association studies.

In conclusion, the prevalence of MAP infection in Ankole Longhorn cattle in the districts of Isingiro, Lyantonde, and Rakai in central Uganda is still low like it is in the neighboring districts but indicates that the infection is equally established in the native cattle population under its traditional farming system. Furthermore, genotyping of SNPs previously reported to be associated with seropositivity to MAP is monomorphic in our study population, whereas the remaining are not significantly associated with cases compared with controls, and therefore, there is a need to carry out more studies using larger sample sizes to determine their population significance and genome-wide association studies that can lead to the discovery of other genetic markers that might be more relevant to any future prospect of marker-assisted selection in Ankole cattle.

DATA AVAILABILITY STATEMENT

The datasets presented in this study can be found online in the **Supplementary Material**. The details of the SNPs used and their accession numbers can be found in GenBank database.

ETHICS STATEMENT

The animal study was reviewed and approved by Uganda National Council for Science and Technology (UNCST), Ministry of Science, Technology and ICT, Republic of Uganda (Ethical approval reference number: A32ES). Written informed consent was obtained from the owners for the participation of their animals in this study.

AUTHOR CONTRIBUTIONS

JO conceived the study and drafted the manuscript. JO, LO, and MA designed the study. JO and MA did the laboratory and fieldwork. LO and JO analyzed the data. All authors contributed to writing and approved the manuscript for publication.

FUNDING

This research was funded by the Carnegie Corporation New York through Makerere University Directorate of Research and Graduate Training under the theme Nurturing Emerging Research Leaders through Postdoctoral training (NERLP).

ACKNOWLEDGMENTS

We wish to acknowledge Carnegie Corporation New York for providing the funding for postdoctoral training at Makerere University. We also acknowledge support of the

Directorate of Research and Graduate Training in Makerere University and Inqaba Biotech Laboratory for providing the platform for MassARRAY genotyping and our field assistants, especially Mr. Magid Kisekka and Mr. Abubaker Musoba, the farmers and veterinary personnel for supporting our fieldwork.

SUPPLEMENTARY MATERIAL

The Supplementary Material for this article can be found online at: <https://www.frontiersin.org/articles/10.3389/fvets.2021.614518/full#supplementary-material>

REFERENCES

- Chaubey KK, Singh SV, Gupta S, Singh M, Sohal JS, Kumar N, et al. *Mycobacterium avium* subspecies *paratuberculosis* - an important food borne pathogen of high public health significance with special reference to India: an update. *Vet Q*. (2017) 37:282–99. doi: 10.1080/01652176.2017.1397301
- Smith RL, Al-Mamun MA, Grohn YT. Economic consequences of paratuberculosis control in dairy cattle: a stochastic modeling study. *Prev Vet Med*. (2017) 138:17–27. doi: 10.1016/j.prevetmed.2017.01.007
- Okuni JB, Hansen S, Eltom KH, Eltayeb E, Amanzada A, Omega JA, et al. Paratuberculosis: a potential zoonosis and a neglected disease in Africa. *Microorganisms*. (2020) 8:1–13. doi: 10.3390/microorganisms8071007
- Lombard JE. Epidemiology and economics of paratuberculosis. *Vet Clin North Am - Food Anim Pract*. (2011) 27:525–35. doi: 10.1016/j.cvfa.2011.07.012
- Doré E, Paré J, Côté G, Buczinski S, Labrecque O, Roy JP, et al. Risk factors associated with transmission of *Mycobacterium avium* subsp. *paratuberculosis* to calves within dairy herd: a systematic review. *J Vet Intern Med*. (2012) 26:32–45. doi: 10.1111/j.1939-1676.2011.00854.x
- Garcia AB, Shalloo L. Invited review: the economic impact and control of paratuberculosis in cattle. *J Dairy Sci*. (2015) 98:5019–39. doi: 10.3168/jds.2014-9241
- Barkema HW, Orsel K, Nielsen SS, Rutten VPMG, Bannantine JP, Keefe GP, et al. Knowledge gaps that hamper prevention and control of *Mycobacterium avium* subspecies *paratuberculosis* infection. *Transbound Emerg Dis*. (2018) 65:125–48. doi: 10.1111/tbed.12723
- Kirkeby C, Græsbøll K, Nielsen SS, Christiansen LE, Toft N, Rattenborg E, et al. Simulating the epidemiological and economic impact of paratuberculosis control actions in dairy cattle. *Front Vet Sci*. (2016) 3:90. doi: 10.3389/fvets.2016.00090
- Singh SV, Dhama K, Chaubey KK, Kumar N, Singh PK, Sohal JS, et al. Impact of host genetics on susceptibility and resistance to *Mycobacterium avium* subspecies *paratuberculosis* infection in domestic ruminants. *Pakistan J Biol Sci*. (2013) 16:251–66. doi: 10.3923/pjbs.2013.251.266
- Dobson B, Liggett S, O'Brien R, Griffin JFT. Innate immune markers that distinguish red deer (*Cervus elaphus*) selected for resistant or susceptible genotypes for Johne's disease. *Vet Res*. (2013) 44:5. doi: 10.1186/1297-9716-44-5
- Vazquez P, Ruiz-Larranaga O, Garrido JM, Iriondo M, Manzano C, Agirre M, et al. Genetic association analysis of paratuberculosis forms in Holstein-Friesian cattle. *Vet Med Int*. (2014) 2014:321327. doi: 10.1155/2014/321327
- Mucha R, Bhide MR, Chakurkar EB, Novak M, Mikula I. Toll-like receptors TLR1, TLR2 and TLR4 gene mutations and natural resistance to *Mycobacterium avium* subsp. *paratuberculosis* infection in cattle. *Vet Immunol Immunopathol*. (2009) 128:381–8. doi: 10.1016/j.vetimm.2008.12.007
- Pinedo PJ, Buerge CD, Donovan GA, Melendez P, Morel L, Wu R, et al. Association between CARD15/NOD2 gene polymorphisms and paratuberculosis infection in cattle. *Vet Microbiol*. (2009) 134:346–52. doi: 10.1016/j.vetmic.2008.09.052
- Pinedo PJ, Buerge CD, Donovan GA, Melendez P, Morel L, Wu R, et al. Candidate gene polymorphisms (BoIFNG, TLR4, SLC11A1) as risk factors for paratuberculosis infection in cattle. *Prev Vet Med*. (2009) 91:189–96. doi: 10.1016/j.prevetmed.2009.05.020
- Küpper JD, Brandt HR, Erhardt G. Genetic association between NOD2 polymorphism and infection status by *Mycobacterium avium* ssp. *paratuberculosis* in German Holstein cattle. *Anim Genet*. (2014) 45:114–6. doi: 10.1111/age.12097
- Canive M, Casais R, Jimenez JA, Blanco-Vazquez C, Amado J, Garrido JM, et al. Correlations between single nucleotide polymorphisms in bovine CD209, SLC11A1, SP110 and TLR2 genes and estimated breeding values for several traits in Spanish Holstein cattle. *Heliyon*. (2020) 6:e04254. doi: 10.1016/j.heliyon.2020.e04254
- Pant SD, Verschoor CP, Schenkel FS, You Q, Kelton DF, Karrow NA. Bovine PGLYRP1 polymorphisms and their association with resistance to *Mycobacterium avium* ssp. *paratuberculosis*. *Anim Genet*. (2011) 42:354–60. doi: 10.1111/j.1365-2052.2010.02153.x
- Sharma BS, Abo-Ismael MK, Schenkel FS, You Q, Verschoor CP, Pant SD, Karrow NA. Association of TLR4 polymorphisms with *Mycobacterium avium* subspecies *paratuberculosis* infection status in Canadian Holsteins. *Anim Genet*. (2015) 46:560–5. doi: 10.1111/age.12333
- Sadana T, Singh RV, Singh SV, Saxena VK, Sharma D, Singh PK, et al. Single nucleotide polymorphism of SLC11A1, CARD15, IFNG and TLR2 genes and their association with *Mycobacterium avium* subspecies *paratuberculosis* infection in native Indian cattle population. *Indian J Biotechnol*. (2015) 14:469–75.
- Kim J, Hanotte O, Mwai OA, Dessie T, Salim B, Diallo B, et al. The genome landscape of indigenous African cattle. *Genome Biol*. (2017) 18:1–14. doi: 10.1186/s13059-017-1153-y
- Magona JW, Walubengo J, Kabi F. Response of Nkedi Zebu and Ankole cattle to tick infestation and natural tick-borne, helminth and trypanosome infections in Uganda. *Trop Anim Health Prod*. (2011) 43:1019–33. doi: 10.1007/s11250-011-9801-9
- Okuni JB, Loukopoulos P, Reinacher M, Ojok L. Seroprevalence of *Mycobacterium avium* subspecies *paratuberculosis* antibodies in cattle from Wakiso, Mpigi and Luwero districts in Uganda. *Int J Anim Vet Adv*. (2011) 3:156–60.
- Erume J, Mutebi F. The prevalence and risk factors of para tuberculosis in indigenous and exotic cattle in Wakiso and Masaka districts, Uganda. *Int J Anim Vet Adv*. (2012) 4:244–51.
- Okuni JB, Reinacher M, Loukopoulos P, Ojok L. Prevalence and spectrum of Johne's disease lesions in cattle slaughtered at two abattoirs in Kampala, Uganda. *Trop Anim Health Prod*. (2013) 45:1197–202. doi: 10.1007/s11250-012-0346-3
- Ruiz-Larrañaga O, Manzano C, Iriondo M, Garrido JM, Molina E, Vazquez P, et al. Genetic variation of toll-like receptor genes and infection by *Mycobacterium avium* ssp. *paratuberculosis* in Holstein-Friesian cattle. *J Dairy Sci*. (2011) 94:3635–41. doi: 10.3168/jds.2010-3788

26. Sharma BS, Leyva I, Schenkel F, Karrow NA. Association of toll-like receptor 4 polymorphisms with somatic cell score and lactation persistency in holstein bulls. *J Dairy Sci.* (2006) 89:3626–35. doi: 10.3168/jds.S0022-0302(06)72402-X
27. Bhaladhare A, Sharma D, Kumar A, Sonwane A, Chauhan A, Singh R, et al. single nucleotide polymorphisms in toll-like receptor genes and casecontrol association studies with bovine tuberculosis. *Vet World.* (2016) 9:458–64. doi: 10.14202/vetworld.2016.458-464
28. Li Z, Zhang Z, He Z, Tang W, Li T, Zeng Z, et al. A partition-ligation-combination-subdivision em algorithm for haplotype inference with multiallelic markers: update of the SHEsis (<http://analysis.bio-x.cn>). *Cell Res.* (2009) 19:519–23. doi: 10.1038/cr.2009.33
29. Benjamini Y, Hochberg Y. Controlling the false discovery rate: a practical and powerful approach to multiple testing. *J R Statist B.* (1995) 57:289–300.
30. Wolf R, Barkema HW, De Buck J, Slomp M, Flaig J, Hauptstein D, et al. High herd-level prevalence of *Mycobacterium avium* subspecies *paratuberculosis* in Western Canadian dairy farms, based on environmental sampling. *J Dairy Sci.* (2014) 97:6250–9. doi: 10.3168/jds.2014-8101
31. Jakobsen MB, Alban L, Nielsen SS. A cross-sectional study of paratuberculosis in 1155 danish dairy cows. *Prev Vet Med.* (2000) 46:15–27. doi: 10.1016/S0167-5877(00)00138-0
32. Juste RA, Vazquez P, Ruiz-Larrañaga O, Iriondo M, Manzano C, Agirre M, et al. Association between combinations of genetic polymorphisms and epidemiopathogenic forms of bovine paratuberculosis. *Heliyon.* (2018) 4:e00535. doi: 10.1016/j.heliyon.2018.e00535
33. Stewart LC. *SLC11A1* polymorphisms in inflammatory bowel disease and *Mycobacterium avium* subspecies *paratuberculosis* status. *World J Gastroenterol.* (2010) 16:5727. doi: 10.3748/wjg.v16.i45.5727
34. Roupie V, Rosseels V, Piersoel V, Zinniel DK, Barletta RG, Huygen K. Genetic resistance of mice to *Mycobacterium paratuberculosis* is influenced by *Slc11a1* at the early but not at the late stage of infection. *Infect Immun.* (2008) 76:2099–105. doi: 10.1128/IAI.01137-07
35. Baqir M, Bhushan S, Kumar A, Sonawane A, Singh R, Chauhan A, et al. Association of polymorphisms in *SLC11A1* gene with bovine tuberculosis trait among Indian cattle. *J Appl Anim Res.* (2016) 44:380–3. doi: 10.1080/09712119.2015.1091333
36. Kadarmideen HN, Ali AA, Thomson PC, Müller B, Zinsstag J. Polymorphisms of the *SLC11A1* gene and resistance to bovine tuberculosis in African Zebu cattle. *Anim Genet.* (2011) 42:656–8. doi: 10.1111/j.1365-2052.2011.02203.x
37. Prakash O, Kumar A, Sonwane A, Rathore R, Singh RV, Chauhan A, et al. Polymorphism of cytokine and innate immunity genes associated with bovine brucellosis in cattle. *Mol Biol Rep.* (2014) 41:2815–25. doi: 10.1007/s11033-014-3136-3
38. Doorduyn Y, Van Pelt W, Siezen CLE, Van Der Horst F, Van Duynhoven YTHP, Hoebee B, et al. Novel insight in the association between salmonellosis or campylobacteriosis and chronic illness, and the role of host genetics in susceptibility to these diseases. *Epidemiol Infect.* (2008) 136:1225–34. doi: 10.1017/S095026880700996X
39. Zhang CL, Wang YH, Chen H, Gu CW, Fang XT. *SLC11A1* gene polymorphisms are not associated to somatic cell score and milk yield in Chinese Holstein. *Vet Immunol Immunopathol.* (2009) 127:389–92. doi: 10.1016/j.vetimm.2008.10.333
40. Salem M, Seidelin JB, Eickhardt S, Alhede M, Rogler G, Nielsen OH. Species-specific engagement of human nucleotide oligomerization domain 2 (NOD)2 and toll-like receptor (TLR) signalling upon intracellular bacterial infection: role of Crohn's associated NOD2 gene variants. *Clin Exp Immunol.* (2015) 179:426–34. doi: 10.1111/cei.12471
41. Kirkpatrick BW, Shi X, Shook GE, Collins MT. Whole-Genome association analysis of susceptibility to paratuberculosis in Holstein cattle. *Anim Genet.* (2011) 42:149–60. doi: 10.1111/j.1365-2052.2010.02097.x

Conflict of Interest: The authors declare that the research was conducted in the absence of any commercial or financial relationships that could be construed as a potential conflict of interest.

Copyright © 2021 Okuni, Afayoa and Ojok. This is an open-access article distributed under the terms of the Creative Commons Attribution License (CC BY). The use, distribution or reproduction in other forums is permitted, provided the original author(s) and the copyright owner(s) are credited and that the original publication in this journal is cited, in accordance with accepted academic practice. No use, distribution or reproduction is permitted which does not comply with these terms.



Comparative Genomics of *Mycobacterium avium* Subspecies *Paratuberculosis* Sheep Strains

Rachel Mizzi^{1*}, Verlaine J. Timms², Marian L. Price-Carter³, Milan Gautam⁴, Richard Whittington¹, Cord Heuer⁴, Patrick J. Biggs^{4,5} and Karren M. Plain¹

¹ Farm Animal Health Group, Sydney School of Veterinary Science, Faculty of Science, The University of Sydney, Camden, NSW, Australia, ² Centre for Infectious Diseases and Microbiology, Public Health, Westmead Hospital, Westmead, NSW, Australia, ³ AgResearch, Hopkirk Research Institute, Palmerston North, New Zealand, ⁴ School of Veterinary Science, Massey University, Palmerston North, New Zealand, ⁵ School of Fundamental Sciences, Massey University, Palmerston North, New Zealand

OPEN ACCESS

Edited by:

Miguel Salgado,
Austral University of Chile, Chile

Reviewed by:

Kumaragurubaran Karthik,
Tamil Nadu Veterinary and Animal
Sciences University, India
Hazem Ramadan,
US National Poultry Research Centre
(USDA-ARS), United States

*Correspondence:

Rachel Mizzi
rachel.mizzi@sydney.edu.au

Specialty section:

This article was submitted to
Veterinary Infectious Diseases,
a section of the journal
Frontiers in Veterinary Science

Received: 04 December 2020

Accepted: 25 January 2021

Published: 15 February 2021

Citation:

Mizzi R, Timms VJ, Price-Carter ML,
Gautam M, Whittington R, Heuer C,
Biggs PJ and Plain KM (2021)
Comparative Genomics of
Mycobacterium avium Subspecies
Paratuberculosis Sheep Strains.
Front. Vet. Sci. 8:637637.
doi: 10.3389/fvets.2021.637637

Mycobacterium avium subspecies *paratuberculosis* (MAP) is the aetiological agent of Johne's disease (JD), a chronic enteritis that causes major losses to the global livestock industry. Further, it has been associated with human Crohn's disease. Several strains of MAP have been identified, the two major groups being sheep strain MAP, which includes the Type I and Type III sub-lineages, and the cattle strain or Type II MAP lineage, of which bison strains are a sub-grouping. Major genotypic, phenotypic and pathogenic variations have been identified in prior comparisons, but the research has predominately focused on cattle strains of MAP. In countries where the sheep industries are more prevalent, however, such as Australia and New Zealand, ovine JD is a substantial burden. An information gap exists regarding the genomic differences between sheep strain sub-lineages and the relevance of Type I and Type III MAP in terms of epidemiology and/or pathogenicity. We therefore investigated sheep MAP isolates from Australia and New Zealand using whole genome sequencing. For additional context, sheep MAP genome datasets were downloaded from the Sequence Read Archive and GenBank. The final dataset contained 18 Type III and 16 Type I isolates and the K10 cattle strain MAP reference genome. Using a pan-genome approach, an updated global phylogeny for sheep MAP from *de novo* assemblies was produced. When rooted with the K10 cattle reference strain, two distinct clades representing the lineages were apparent. The Australian and New Zealand isolates formed a distinct sub-clade within the type I lineage, while the European type I isolates formed another less closely related group. Within the type III lineage, isolates appeared more genetically diverse and were from a greater number of continents. Querying of the pan-genome and verification using BLAST analysis revealed lineage-specific variations ($n = 13$) including genes responsible for metabolism and stress responses. The genetic differences identified may represent important epidemiological and virulence traits specific to sheep MAP. This knowledge will potentially contribute to improved vaccine development and control measures for these strains.

Keywords: Johne's disease, *Mycobacterium avium* subspecies *paratuberculosis*, pan-genome, sheep strain, whole genome sequencing, type I, type III

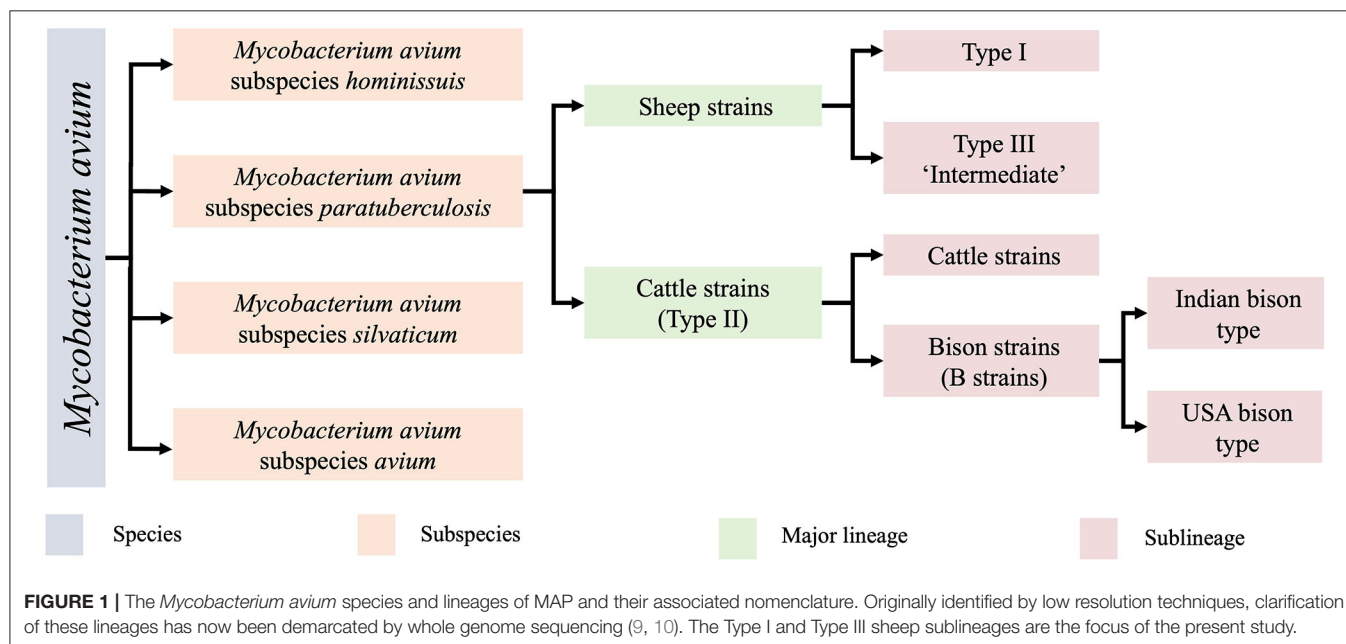
INTRODUCTION

Johne's Disease (JD) is a chronic gastroenteritis of ruminant species worldwide (1). Additionally, the causative agent, *Mycobacterium avium* subspecies *paratuberculosis* (MAP), has been implicated in the pathobiology of Crohn's disease in humans. Despite a strong association, causality has not been proven (2, 3). A major complication of JD is the extended subclinical phase. During this stage, low levels of intermittent bacterial shedding occurs in the faeces. Low levels of shedding may be difficult to detect with current diagnostic tests and may lead to false negative results. This insufficient sensitivity may allow for ongoing spread of the pathogen (4). Overall, losses due to clinical disease tend to be highest in dairy cattle since animals are retained in herds to older ages and hence have more time to develop disease. An Australian study estimated an average cost of \$2,491AUD per cow with clinical JD (5). A similar value of \$2,386AUD per clinical case was estimated by a French study (6). In sheep, the main losses are attributed to mortalities which have been estimated at 1–10% in Australian flocks (1, 7). Stud operations may become unviable if JD is prevalent due to restrictions imposed on sales and a reduced customer base (8). Thus, control of MAP and the ability to trace the spread of disease is critical. Further studies are required to inform producers of the economic losses and the cost-benefit for JD control measures in sheep enterprises.

MAP is one of four closely related subspecies within the species *Mycobacterium avium* (Figure 1). Within this subspecies, two major groups are recognised, the sheep strains (S strains) and cattle strains (C strains), which were named after the host from which they were originally isolated (11). S and C strains of MAP can be distinguished by a variety of molecular methods including variation in the IS1311 sequence (12), variable number

tandem repeats (VNTR) and short sequence repeat (SSR) loci (13, 14). Typing methods have helped to determine that MAP strains are cross transmissible between ruminant species (14–16), leading to some researchers preferring to designate S strains as Type I and C strain as Type II to avoid confusion. Within the two major groups, several sub-lineages of MAP strains exist. The C strain/Type II lineage contains a subcategory of bison strains, which were originally thought to be their own lineage (17, 18) but were recently demonstrated to be a sub-lineage of Type II by whole genome sequencing (WGS) (9) with regional lineages present in India and America (18). Within the S group there are two sub-lineages, Type I and Type III. The Type III strains were initially thought to be an intermediate of sheep and cattle strains (11, 19) but were later proven to be a sub-lineage of S strains by WGS (9) (Figure 1).

Accurate strain identification of MAP is vital for source attribution and mapping transmission pathways in epidemiological investigations. Furthermore, it improves the knowledge of bacterial population structure. This better our understanding of the genetic diversity that exists in a population and potentially links a genotype with a disease outcome, transmission risk factors or origin of infection in the case of a new outbreak if the transmission chain is unknown. Specific control strategies may be warranted in the case of a new outbreak if the transmission chain is known. This is particularly important for a pathogen such as MAP which has multiple host species, and therefore different potential agro-industrial or wildlife sources and may be zoonotic. Historically, strain typing required culture of MAP, a process that is very time-consuming and may result in false negative results (20) if an inappropriate culture medium is used. This is particularly important for sheep strains, which are notoriously difficult to culture; typing was originally undertaken after physically extracting bacterial cells from intestinal mucosa



(21). Phenotypic differences between S and C strains have been described that relate to culture requirements and virulence (22), with S strains appearing less virulent *in vivo* in terms of the ability to infect multiple species and also *in vitro* in models when human or bovine macrophages are used (23). Notably, when ovine derived cells were used in an *in vitro* model, virulence was restored in S strains (24). Thus far, these functional investigations of MAP have included a limited number of isolates, predominantly focused on differences between a few S and C strains (25–27). This is problematic, since S strains have been reported to be more heterogenic than C strains (13, 28).

Currently employed typing tools distinguish MAP isolates to varying degrees and numerous methods have been employed (29). IS1311 restriction fragment length polymorphism (RFLP) is widely used for distinguishing between C and S strains of MAP (30). However, this technique is insufficient for distinguishing between the sheep MAP Type I and III sub-lineages. Strain typing of sheep MAP sub-lineages has been reported using the *gyrA* and *gyrB* genes. While these genes have a very low mutation rate and have previously been reported for typing of closely related mycobacteria (31), this test is not widely used for typing MAP or other mycobacterial species. Furthermore, few studies distinguish between sheep MAP types, thus presenting an information gap. Later studies investigating the genetic diversity of MAP utilised genotyping methods such as Mycobacterial Interspersed Repetitive Unit-Variable Number Tandem Repeat (MIRU-VNTR) and short sequence repeat typing (SSR) and other PCR assays (13, 14, 32, 33), which use multiple loci and are more useful for determining population structures. In one study, MIRU-VNTR typing was unable to distinguish between Type I and Type III sheep strains (13). However, tests such as MIRU-VNTR, SSR and PCR-based assays are able to distinguish MAP strains with higher efficiency when combined with each other or other techniques such as IS900 RFLP (34–37). Despite these techniques being more advanced they still provide limited insight into the functional consequences of genetic diversity and have been shown at times to both underestimate and overestimate the diversity of MAP in some scenarios. In contrast, WGS enables high resolution genetic data to be obtained from bacterial isolates and enables more data to be obtained for each isolate than any other genotype test, leading to the resolution of relationships between lineages that has enabled a more complete overview of the population structure of MAP (9).

Studies on lineage-specific variants of MAP to date have focused on holistic differences between the S and C strains. Early literature utilised laborious subtractive hybridisation methods available at the time (38–41). This was followed by microarray hybridisation studies (42, 43). Today, WGS offers unique insights on comparative genomics. The first complete MAP whole genome sequence was on K10, a C strain isolate (44) and this is an invaluable resource for further comparative genomics work. In 2012, the draught sequence of S397, a Type III S strain, revealed differences between S and C strains at the whole genome level (45). Comparison of the K10 (type II) and S397 (type III) genome sequences revealed 10 large sequence polymorphisms in the type III isolate that contained >4 open reading frames, compared to the type II sequence (45). The presence of these polymorphisms

from genomic data agrees with pan-genome microarray data (42, 43). Moreover, analysis of microarray suggests that there is significant variability between the sub-lineages of MAP S strains (43).

Understanding genetic diversity within a population of bacterial pathogens may provide insights into virulence, antibiotic susceptibility and other phenotypic traits important for the treatment and control of infectious diseases. Better characterisation of existing MAP strains will likely provides insights into mechanisms of host preference in S strains (25) and inform diagnostic test and vaccine development. Detected differences between the type I and type III sheep subtypes may reveal important evolutionary, epidemiological and virulence traits specific to each sub-lineage. In the present study, we compare type I and type III sheep MAP genomes from several global locations and host species using a pan-genome approach.

MATERIALS AND METHODS

Isolate Collation

MAP genomes used in this study were from a variety of sources. Publicly available genomes were downloaded from the National Centre for Biotechnology Information (NCBI) GenBank and Sequence Read Archive (SRA) databases for *Mycobacterium avium* subspecies *paratuberculosis* on the 3rd of March 2020. Search philtres for genome, Illumina and DNA were used in the SRA. For isolates JQ5, JQ6, 88281, S397, JIII386 and Telford, raw reads were not available therefore assemblies were downloaded from GenBank. Additional New Zealand isolates AgS43 and AgS36 were originally sourced from sheep tissue or faecal samples from New Zealand Veterinary Pathology Limited (Palmerston North, New Zealand) and were regrown from the AgResearch Ltd. strain archive. Isolates 3410, 3443, 3413, 110b, 135b, 3324 and 3326 were sourced from the University of Sydney archive collection that were used in previous studies (22, 46). These isolates included four Australian isolates (3443, 135b, 110b, 3413 and 3410) and two Spanish isolates (3324 and 3326). Detailed information on isolates is available in **Supplementary Material 1**. Culture and extraction of isolates from the University of Sydney was done as described below.

MAP Culture and DNA Extraction

Isolates were cultured as previously described (47) and pellets were washed and placed in 300 μ L of Tris-EDTA (TE) (10 mM Tris, 1 mM EDTA, Ambion) buffer and stored at -80°C until further processing. MAP suspensions were thawed at room temperature prior to addition of 550 μ L of TE buffer. Declumping was achieved by drawing the suspension through a 25-gauge needle seven times followed by vigorous vortexing. Suspensions were heat inactivated at 85°C for 30 min, then mechanically lysed in a 2 ml conical base screw capped tube containing 0.3 g of Zirconia/Silica beads (BioSpec Products Inc, Daintree Scientific) using a Tissue lyser II (Qiagen) at a frequency of 30 for 1 min 40 s, twice followed by centrifugation at 16,000 \times g for 3 min and the supernatant was transferred to a new 1.5 ml tube. DNA extraction was performed based on the method of Choy et al. (21).

To disrupt the cell wall, 60 μ L of 200 mg/mL Lysozyme (Sigma-Aldrich) was added and the samples were incubated for 2 h at 37°C with gentle mixing. To remove contaminating RNA, 20 μ L 20 mg/mL RNase (Sigma-Aldrich) was added and incubated for a further 3 h. To complete cell wall breakdown, 200 units of Mutanolysin (Sigma-Aldrich) was added and lysates were incubated for 12–16 h at 37°C with gentle mixing. Following this, 35 μ L of Proteinase K solution (10 mg/mL) (Sigma-Aldrich) and 60 μ L of 10% sodium dodecyl sulphate were added and the suspensions were incubated for 24 h at 37°C with gentle mixing. The Proteinase K was inactivated by heating at 70°C for 10 min and then 97.5 μ L 5M NaCl and 82.5 μ L CTAB/ NaCl (Bioline) pre-warmed to 65°C were added and the lysates incubated at 65°C with gentle mixing for 10 min. On completion, 700 μ L of 25:24:1 phenol/ chloroform/ isoamyl alcohol (Sigma-Aldrich) was added and mixed vigorously for 30 s by pipetting. The upper aqueous phase was collected after centrifuging at 12,000 \times g for 10 min. To remove excess phenol, an approximately equal volume of chloroform:isoamyl alcohol (24:1) (Sigma-Aldrich) was added and centrifuged at 12,000 \times g for 10 min. The upper aqueous layer was collected and mixed well via inversion for 1 min with 1,000 μ L of 2-Propanol (Sigma-Aldrich). DNA was pelleted by centrifuging for 15 min at 12,000 \times g. The pellet was washed twice using 70% molecular-grade ethanol (Sigma-Aldrich) in nuclease-free water, cooled to –20°C, then centrifuged for 15 min at 12,000 \times g. The supernatant was removed and the pellet was resuspended in 30 μ L of 10 mM Tris buffer, pH 8.0 (Astral Scientific). Resolubilization of DNA occurred at room temperature overnight with gentle mixing. On completion, samples were stored at –80°C. DNA quality was assessed using a NanoDropTM 2000 spectrophotometer (Thermo Fisher Scientific). Samples with $A_{260/280}$ below 1.7 or $A_{230/280}$ < 1.2 were discarded and re-isolated. A Quant-iTTM PicoGreenTM dsDNA Assay Kit (Thermo Fisher Scientific) was used to measure DNA concentration.

New Zealand isolates AgS43 and AgS36 were re-cultured, extracted and sequenced as described by Gautam et al. (in preparation).

Library Preparation and Whole Genome Sequencing

WGS of isolates 3410, 3443, 3413, 110b, 135b 3324 and 3326 was carried out at the NSW Mycobacterium Tuberculosis Reference Laboratory at the Centre of Infectious Diseases and Microbiology, Westmead Hospital on the Illumina sequencing platform. A Nextera XT library preparation kit (Illumina, Scoresby, Victoria, Australia) was used to generate paired indexed libraries of 150 base pairs in length as per the manufacturer's instruction. Sequencing was done using the Illumina NextSeq platform.

Quality Control and Assembly

Fastq files were trimmed using Trimmomatic (version 0.36, RRID:SCR_011848) (48) with options set to -phred33, LEADING:3 TRAILING:3 SLIDINGWINDOW:4:20 MINLEN:36. Reads were assembled with SPAdes (version 3.12.0, RRID:SCR_000131) (49) using the default k-mer size

testing options. To improve the assemblies, the Bayes-Hammer read correction, and careful option for post-assembly Burrows Wheeler Aligner mismatch correction (50) were also used. Seven isolates retrieved from GenBank were only available as assemblies (fasta files). Quality assessment of the assemblies was done with Quast (version 5.0.2, RRID:SCR_001228) (51). Assemblies which had a GC% of <69%, number of contigs >500 or a total length outside of 4.5–5.3 Mb were removed from the final analysis.

Pan-genome Analysis

Genome annotation was undertaken with Prokka (version 1.13.3, RRID:SCR_014732) (52) with the minimum contig length set to 500 base pairs. GFF files from Prokka were used as an input for the Roary (version 3.12.0, RRID:SCR_018172) (53) pan-genome pipeline. Within this pipeline MAFFT (version 7.402) (54) was used to produce a nucleotide multifasta alignment of all core genes.

Phylogenetic Analyses and Pruning

IQ-Tree (version 1.6.7, RRID:SCR_017254) (55) was used to generate trees from the core gene alignment output from Roary. Within IQ-Tree, ModelFinder (56) was used to identify the best-fitting model, which turned out to be the general time reversible model (GTR+F+R4) (57). Trees were visualised and annotated in iTOL (RRID:SCR_018174) (58). Any isolates that clustered with the S397 (accession AFIF01000001) or Telford (accession CP033688.1) reference genomes were retained and used in the downstream comparative analysis. Those which were phylogenetically distant to known sheep MAP genomes Telford (accession CP033688.1) (59) and S397 (accession AFIF01000001) or clustered with the K10 reference were discarded.

The K10 reference and any sequences that did not meet quality criteria outlined in the Quality control and assembly section were removed and Treemmer (60) was used to reduce redundancies within the type I dataset and bias of downstream analyses. Some manual selection of isolates was undertaken to maximise the geographical diversity of isolates within the dataset. The final dataset of 34 isolates contained 16 type I and 18 type III isolates. This enabled 95% of the original diversity to be retained. The K10 reference was retained in the final dataset as a root for the phylogenetic tree.

Analysis of the *gyrA/B* Genes

The *gyrA* and *gyrB* genes from the Telford (accession CP033688.1) type I reference (59) and S397 (accession AFIF01000001) type III reference (45) genomes were used as a basis for *in silico* genotyping. BLAST analysis of the two versions of these two genes was used to confirm that the two major branches in the phylogeny were indeed Type I or Type III in the other analysed isolates. The online BLAST global align tool (available at <https://blast.ncbi.nlm.nih.gov/Blast.cgi>) from the National Centre for Biotechnology Information (NCBI) was used to compare the nucleotide and protein sequences of the genes between lineages.

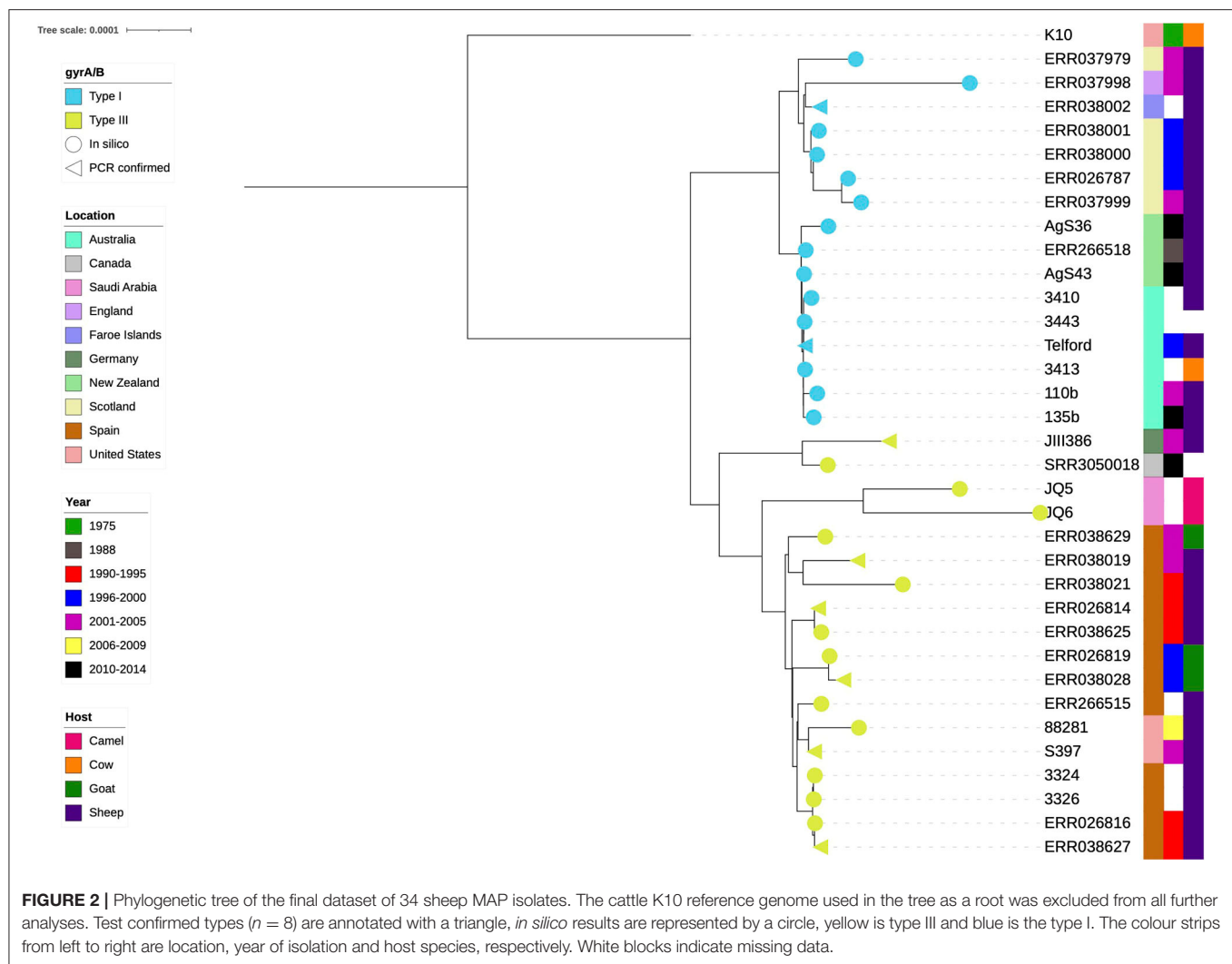


FIGURE 2 | Phylogenetic tree of the final dataset of 34 sheep MAP isolates. The cattle K10 reference genome used in the tree as a root was excluded from all further analyses. Test confirmed types ($n = 8$) are annotated with a triangle, *in silico* results are represented by a circle, yellow is type III and blue is the type I. The colour strips from left to right are location, year of isolation and host species, respectively. White blocks indicate missing data.

Querying the Pan-genome

The pan-genome analysis was repeated on the final dataset (Figure 2) to reduce the likelihood of noise due to misassemblies or mis-annotations and prevent bias towards large clusters of highly similar genomes. Genes of interest were those that were present in one lineage and absent from the other or had consistent lineage-specific variations. To minimise the likelihood of a lineage-specific gene being an assembly or annotation artefact, candidate genes of interest had to be identified by Prokka annotation in all isolates from one lineage and completely absent from the other. The gene presence/absence output from Roary was used as an input for Scoary (61). This tool was used to identify genes of interest and demonstrate a gene's association with a respective lineage. A fasta file containing all lineage specific coding sequences (CDS) was uploaded to the EggNOG web-tool (available <http://eggno-mapper.embl.de/>) (RRID:SCR_002456) to obtain functional categories for each gene. Contigs of draught genomes were reordered and aligned to the Telford reference genome (accession CP033688.1) with mauve (RRID:SCR_012852) (version 2.4.0) (62, 63) to view contig boundaries within isolates and confirm

there were no contig boundaries interfering with the genes of interest.

Blast

To obtain additional annotation data for hypothetical proteins potentially missed by automated annotation, a BLASTx of the nucleotide sequences of each gene of interest was undertaken using the NCBI online BLASTx tool (RRID:SCR_001653). The hit with the smallest e-value, a minimum of 99% identity and a minimum length of at least 99% of the query length was used. The nucleotide sequence of lineage-specific genes was obtained from the Roary pan-genome reference fasta output file. This file contains a representative nucleotide sequence for each protein annotated in the analysis. A nucleotide BLAST of each lineage-specific gene identified by Scoary to all sheep genomes in the study confirmed if the gene was present in the other lineage but had undergone mutations that led to an annotation failure by Prokka. The NCBI BLAST global align tool was used to compare lineage variants of protein sequences (available at <https://blast.ncbi.nlm.nih.gov/Blast.cgi>).

RESULTS

Whole Genome Sequencing and Assembly

Approximately 400 MAP genomes were available from the SRA and an additional 50 were available from GenBank. These genomes were screened and assemblies that did not reach quality thresholds described in the methods quality assessment section and those that clustered more closely with K10 than S Type references were removed. Treemmer culled an additional 40 S strain isolates that represented redundancies in the dataset. The final dataset included 16 Type I and 18 Type III isolates from 10 different geographical sources and five different hosts. The average GC% content across both lineages was 69.23% (Table 1). The average genome length was 4,819,192 bp and 4,794,996 bp for Type I and Type III isolates, respectively (Table 1). Overall, the average quality of the draught assemblies was similar with the number of contigs and N50 for Type I at 268.9 and 45,862 bp and 247.9 and 113,636.8 bp for Type III. Detailed information on isolate-specific assembly statistics from QUAST and strain metadata can be found in **Supplementary Material 1**. A phylogenetic tree including public sequences culled by Treemmer to optimise diversity and those that did not meet assembly quality thresholds is available in **Supplementary Material 2**.

Analysis of *gyrA/B* Genes

Eight isolates had previously undergone lineage typing using the *gyrA/B* genes using PCR and sequencing (9, 45, 59, 64, 65). The *gyrA/B* BLAST results of the present study were in agreement with these results. Only one *gyrA/B* type was present per lineage within the phylogeny (yellow and blue branch symbols, Figure 2).

A BLASTp global alignment between the *gyrA* translated proteins from the Type I (Telford, CP033688.1) and Type III (from S397, AFIF01000001) reference genomes revealed a single mismatch where the Type I reference contained a glutamic acid instead of a lysine at position 290. Alignment of the *gyrB* protein sequences revealed a glutamic acid instead of a lysine at position 594 in the Type I reference. This confirms one of the SNPs found in each nucleotide sequence is non-synonymous. No differences in gene or protein length were seen between the Type I and Type III.

Most of the type I isolates had a *gyrA* and *gyrB* nucleotide sequence that was identical to the type I reference genome. The one exception was the New Zealand isolate AgS36 which had a single, synonymous SNP in both the *gyrA* and *gyrB* gene. All Type I *gyrA* and *gyrB* protein sequences were identical.

Type III isolates contained two ($n = 16$ isolates) or three ($n = 2$ isolates) SNP differences compared to the type I *gyrA* gene. The type III nucleotide sequence of the *gyrA* gene was consistently different by two SNPs with all type I isolates. Within the Type III isolates, the S397 *gyrA* gene was 100% identical to 16 isolates and had a single SNP difference compared to two of the type III isolates. The two type III isolates which contained an additional SNP in the *gyrA* gene were JIII386 and SRR3050018.

Protein sequence BLASTs revealed a single mismatch between the Type I *gyrA* reference sequence and 16 Type III isolates. Type III isolates JIII386 and SRR3050018 had two mismatches compared to the type I *gyrA* which also had a mismatch to the type III *gyrA* protein sequence indicating a non-synonymous mutation. Protein sequences from these two isolates were identical. Alignment of the S397 *gyrA* protein to that of isolate JIII386 demonstrated a single mismatch of an arginine to a glycine at amino acid number 558. A schematic comparison of the Type I and III reference *gyrA* proteins to that of JIII386 is available in **Supplementary Material 3**.

The nucleotide sequence of the *gyrB* gene from the Type I reference genome differed by 2 or 3 SNPs compared to all Type III isolates. The nucleotide sequence of the type III *gyrB* gene from the Type III reference genome was two SNPs different to all type I isolates, 100% identical to 16 of the type III isolates and differed by one SNP in isolates JQ5 and JQ6. The protein sequence of all Type III isolates was identical, indicating that the SNP in isolate JQ5 and JQ6 was synonymous.

Isolates JIII386, SRR3050018, JQ5 and JQ6 were within the Type III cluster (Figure 2), their *gyr* genes more closely resembled the Type III lineage and previous typing of JIII386 (65), JQ5 and JQ6 (64) indicated they were Type III, thus in this investigation they were considered Type III.

Phylogeny

A clear distinction between the Type I and Type III isolates became obvious when the K10 reference was used as a tree root (Figure 2). The type I isolates were of Australian, New Zealand

TABLE 1 | Average basic assembly metrics and statistics for the isolates in this study and comparison of the sub-lineages.

	K10*	All sheep	Type I	Type III
No. genomes	1	34	16	18
GC%	69.3	69.23	69.24	69.22
Genome length (bp)	4,829,781	4,807,094	4,819,192.25	4,794,996
No. Contigs	1	258.38	268.87	247.89
N50**	4,829,781	79,749.39	45,862	113,636

Metrics were calculated on the final dataset after pruning with Treemmer and removal of assemblies which did not meet the quality standards of GC% > 69%, number of contigs <500 or a total length within 4.5–5.3 Mb. All figures are to two decimal places.

*Only one genome in this category, the K10 C strain reference, therefore these figures are not averages.

**N50 is the length (in base pairs) of the shortest contig at 50% of the total genome length.

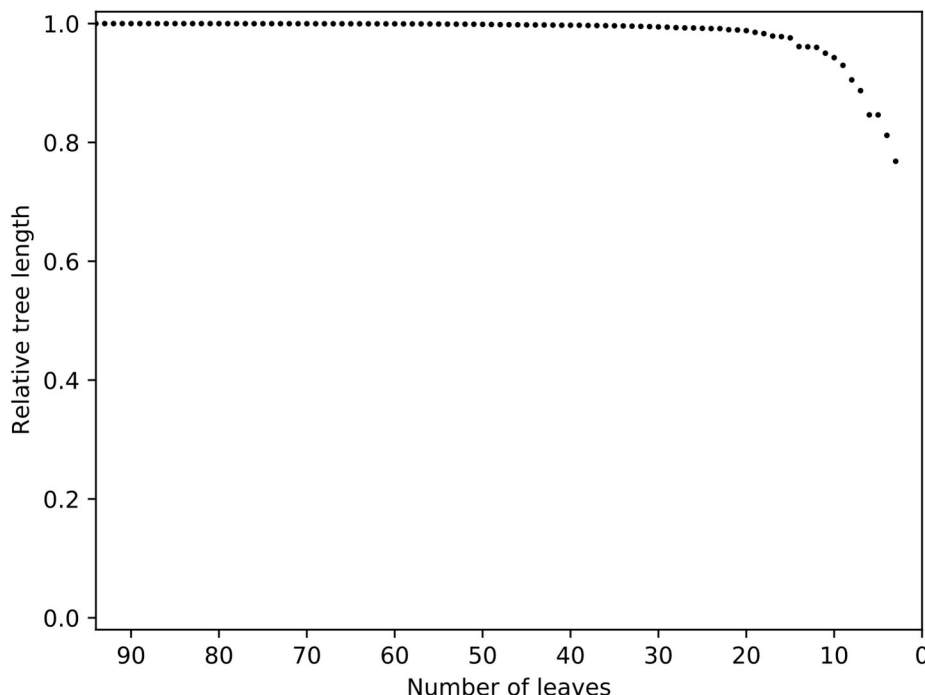


FIGURE 3 | Relative tree length plot of the dataset prior to trimming with Treemmer. Number of leaves is equal to the number of genomes present in a phylogenetic tree. Note the steep curve indicating that a small number of genomes represents a large amount of the diversity in this dataset. Additional genomes in this study would not have increased the genetic diversity within the dataset, thus redundant genomes were removed. K10 was not included in this process since it is an outlier in the tree.

and European origin, with a distinct and very closely related Australia and New Zealand clade present. The type III isolates appeared more diverse, both genetically as indicated by their branch lengths in the phylogenetic tree, and geographically.

Pan-genome Analysis

The increase in pan-genome size with the addition of new isolates or strains can be used to predict the discovery rate of new genes within a species (66). The initial tree demonstrated that several isolates were very distant (data not shown) and contrary to their labelling were unlikely to be MAP. Others clustered with the K10 reference genome, indicating they were likely to be C strains. After removal of C strains, distant isolates and those that did not meet the quality thresholds outlined earlier, the resulting phylogeny had one very large, flat clade of Australian isolates indicating low diversity and a potentially skewed dataset to the type I isolates (data not shown). A relative tree length plot from Treemmer (**Figure 3**) revealed low diversity of MAP isolates and many redundant sequences. Overall within the final dataset, the core genome (genes in 100% of isolates) contained 3,239 genes, soft core genome (95–99%) of 423 genes, accessory genome 1,408 and cloud genome (<15% of isolates) had 2,582 genes (**Table 2**).

Lineage-specific Genes and Variations

Scoary identified 13 candidate lineage-specific genes, with 9 in the Type I and four in the Type III isolates. All annotated genes of interest had a sensitivity and specificity of 100% and a Bonferroni corrected P -value of 4.54×10^{-10} . As described

TABLE 2 | Number of genes present in each category of genes in the pan-genome categorised by Roary.

Category	All*
Core (99–100%)	3,239
Soft core (95–99%)	423
Accessory (15–95%)	1,408
Cloud (<15%)	2,582
Total	7,652
No. genomes	34
No. genes of interest	13

Genes are categorised by Roary into core, soft core, accessory and cloud genes.

*These summary statistics exclude the K10 C strain reference genome.

in the methods, genes of interest were those that were present in one lineage and absent from the other or had consistent lineage-specific variations. BLAST analysis demonstrated that the lineage-specific genes called by Scoary were present in all isolates but contained consistent SNP variations and this had resulted in different annotations for these genes (**Table 3**).

The MAUVE alignment revealed no contig boundaries present in the genes of interest. The Type I genes of interest included *cinA1*, *mphA2* and seven hypothetical proteins. The Type III genes included four hypothetical proteins. BLASTx analysis of nucleotide sequences retrieved from the Roary pan-genome reference fasta file revealed additional

TABLE 3 | Lineage-specific genes and variation of type I and type III isolates.

Gene	Type	Annotation	Variations*
Group 4585	I	Putative nuclear transport factor 2 family protein	5 variable mismatches in the Type III protein
Group 4593	I	MMPL family transporter	No significant protein hit in Type III isolates
<i>cinA1</i>	I	1,8-cineole 2-endo-monooxygenase	Type III protein has 8–17 mismatches, length is identical between lineages
<i>mhpA2</i>	I	3-(3-hydroxy-phenyl)propionate/3-hydroxycinnamic acid hydroxylase	Type I isolate protein sequences are 62 amino acids longer and Type III isolates have a single mismatch
Group 4493	I	Hemolysin III family protein	Type III protein is 54 amino acids longer and contains 9 mismatches to the Type I version
Group 4363	III		
Group 4592	I	MMPL family protein	No significant protein hit in Type III isolates
Group 1815	I	Hypothetical protein	1-2 mismatches in Type III protein and Type III is 22 amino acids shorter
Group 4617	I	<i>TetR/AcrR</i> family transcriptional regulator	11 amino acid mismatches and the Type I protein is three amino acids shorter
Group 4778	III		
Group 4500	I	Nitroreductase family protein	Type I protein is 185 amino acids long and Type III is 171. Contains 11 mismatches
Group 4772	III		
Group 4781	III	Hypothetical protein	Type I isolates 37–164 amino acids long with 24–105 mismatches. Type III are all 299 amino acids long with a single mismatch present in four isolates

Where Prokka annotated the gene as a hypothetical protein but BLASTx was able to provide a putative annotation, the BLASTx annotation was used. Variations are from BLASTp results. *bp = base pairs.

annotations (Table 3). BLASTx results are available in **Supplementary Material 4**. Six genes were identified that are involved in metabolism, information processing and storage. Seven of the genes were uncharacterised and COG categories are unavailable (Figure 4).

Most genes called in the Type I lineage were present in type III, but due to inconsistent differences within the type III isolates, they were not recognised as lineage specific for type III (Table 3). This was found in the putative nuclear transport factor 2 family protein (group 4585), hypothetical protein 1815 and *cinA1*. Differences in the *mhpA2* protein were consistently different between Type I and III isolates. However, the very large difference in length between Type I and Type III BLAST result indicates this may be an inconsequential alignment in the Type III lineage. Type III specific hypothetical protein 4781 had no significant hits in 10 Type I isolates and hits with 82–105 mismatches in the remaining isolates. Some SNPs were present in group 4781 (hypothetical protein) within the Type III lineage, resulting in a single mismatch that did not affect the overall length of the protein (Table 3).

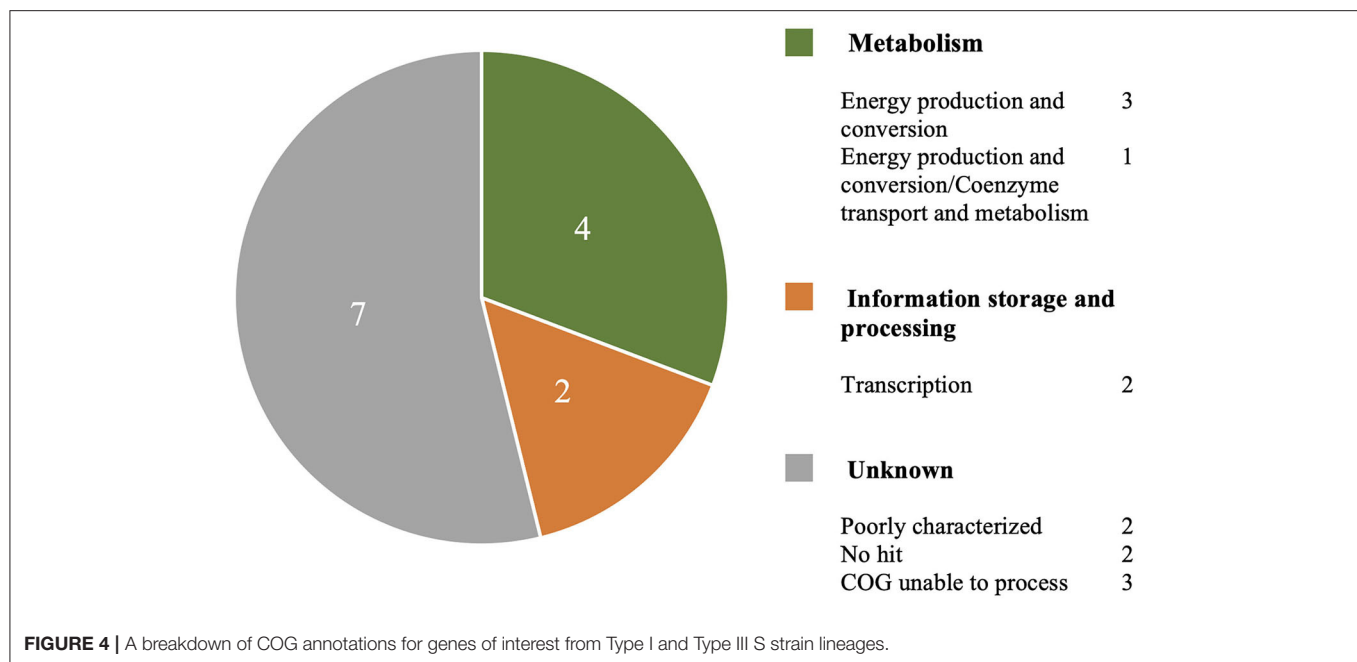
Some genes had similar BLASTx results and appeared to be variants of the same gene in each lineage. The Type I lineage-specific haemolysin family protein (group 4493) is 203 amino acids in length and 79% identical to the Type III haemolysin. The Type III haemolysin family protein (group 4363) is 257 amino acids in length and contains 9 mismatches compared to the Type I version. The TetR/AcrR family transcriptional regulator is 80% identical between lineages and differs by 11 mismatches and three amino acids in length. The nitroreductase family

proteins are 82% identical, differ by 11 amino acid mismatches and the Type III protein is 14 amino acids shorter. Two type I hypothetical proteins, group 4593 and group 4592 had no significant protein hit in type III isolates. The haemolysin III family protein found in both lineages was also discovered in a previous study (MAP2704) (43). BLASTx of MAP2704 produced similar results to that of the Type III variant (group4363). A summary of lineage-specific variants that match previously identified variable loci and a copy of Table 3 that summaries the differences between Type I and Type III genes of interest that also includes differences found in the K10 reference strain is available in **Supplementary Material 5**.

DISCUSSION

Most studies on Johne's disease and MAP epidemiology do not distinguish between S sub-types and thus the relative abundance and virulence of each is not widely known. In this investigation, we address the epidemiology of each of these sub-types with the view that conserved differences detected between lineages could be used for future studies into comparative virulence and larger epidemiological investigations. We also attempted to reveal genomic differences using a pan-genome approach.

The current test used to distinguish between Type I and Type III lineages of sheep MAP uses a PCR-based assay on the *gyrA/B* genes. Previously, these genes were demonstrated to have a low mutation rate and be ideal for the typing of slow growing mycobacteria (31). The presence of variable SNPs in these genes, which were identified in our study, indicate that



they are less conserved than suggested by Kasai and colleagues. This variability may cause problems if SNPs occur in the primer binding sites of the existing assay (67). Thus, additional markers identified by the present study may be useful.

Several attempts to understand the genetic diversity of MAP have been undertaken (9, 14, 33, 36, 68). Of those using WGS as a tool (9, 68), most isolates have been C strains (Type II lineages). These investigations have incorporated several human isolates, which have all clustered with the C strains of MAP (9, 69). One possible reason for this is that C strains have a broader host preference, while S strains of MAP are generally more host-specific, though still capable of cross-species transmission given the appropriate host-pathogen interactions and level of infection pressure (14, 20). Due to the relatively small number of S strains included in the published studies to date, minimal conclusions could be drawn for S strains of MAP. A major limitation of earlier studies is the use of culture media that did not support the growth of S strains of MAP (47). This may have led to a bias for inclusion of mainly C strains of MAP in the early studies and in contemporary studies which have used inappropriate culture media. Routine inclusion of S strain isolates in typing studies and improved ability to recognise the two sub-lineages may assist with tracing an S strain isolate in epidemiological investigations including human infections. Furthermore, historical (20) and contemporary reports of cross-species transmission of S strains in co-grazing properties (14) leading to economic losses and between wildlife reservoirs (16, 70) means that these strains have genuine relevance.

Overall, the Type III lineage isolates analysed here appeared to be more genetically heterogeneous than the Type I lineage but were derived from a broader array of geographical sources. Isolates of the Type III sub-lineage represent multiple continents including America, Europe and Asia in their locations. The Type

III lineage had a larger number of genes in the pan-genome, displayed longer branches on the tree, and only four lineage-specific genes were identified. In contrast, Type I isolates were less diverse and had a larger number of genes characterised as being in the core genome. These findings are supported by previous work, which found Type I isolates to be more homogenous (71). Similarly, the finding that Type III isolates are more heterogeneous than Type I isolates is also in agreement with earlier findings which utilised PFGE and IS900-RFLP typing techniques on a panel of isolates from a variety of countries (13, 28).

There appears to be association of lineage Type with different regions of Europe, with all Spanish and German isolates belonging to the type III lineage and all European type I isolates from Scotland, England and the Faroe Islands. One finding that was not supported by literature was that Type III is the predominant Type throughout the United States of America. Previous work using SSR and PFGE identified Type I isolates to be the predominant type throughout the United States (71). This discrepancy is potentially due to only two sheep MAP whole genome sequences being available from this location. Overall, these epidemiological findings must be interpreted with caution due to the small number of isolates used in the present study. Other biases include a lack of culturability of certain types of MAP, and both the sampling effort in particular countries and enthusiasm of people who have gathered and curated culture collections to facilitate such studies. These factors may introduce sampling bias to the apparent epidemiology of sheep MAP Types illustrated here.

Within Oceania, this study found low diversity in sheep MAP. This may reflect a small sample size of the present study or the slow rate that MAP accumulates genetic variation (9). A similar conclusion for sheep MAP isolates was found in an earlier study

that utilised IS900 RFLP and IS1311 polymorphism analyses of an Australia-wide panel of isolates. Only a single RFLP type (S1) was found in sheep strains (12). A recent epidemiological study of S strains of MAP in New Zealand using VNTR/SSR (14) and WGS (Gautam et al., in preparation) demonstrated low sequence diversity across the country. Akin to the present study, New Zealand isolates were solely of the Type I lineage and Australian and New Zealand isolates appeared to be closely related. Of relevance is that our methods differed from those of the New Zealand group, which mapped all isolates to the Telford reference genome, whereas the present study utilised *de novo* assembly. The similar grouping of sheep isolates from Australia and New Zealand in comparison to those from other countries helps validate both approaches when exploring MAP diversity. The tight clustering of Australian and New Zealand sheep isolates may indicate recent transmission between these countries and reflect geographical isolation from the rest of the world.

Thirteen genes were annotated as lineage-specific in this investigation, using the program Scoary. BLAST results demonstrated that each of these are not fully lineage-specific genes, but that each gene contained a lineage-specific mutation. Discrepancies between Roary and BLAST are potentially due to small variants within genes, such as insertions or deletions. These mutations may have moved the reading frame of the nucleotides, leading to alternate predicated protein sequences such that annotation software no longer recognised these proteins as being derived from the same gene. Eleven of the 13 genes of interest were annotated as hypothetical proteins, and in these cases, BLASTx was used to determine if they had functions previously identified in other, related species. BLASTx also served to find overlaps between lineage-specific genes from each group, where annotations from Prokka were ambiguous. Previous microarray data demonstrated several variable loci between Type I and Type III isolates (43). Many of these findings were supported by the present study including one locus (MAP2704) that encodes a haemolysin III family protein that was found in both studies (group4363 in Type III and group4493 in Type I). BLASTx of the MAP2704 nucleotide sequence retrieved an identical result as the Type III specific gene group4363 (**Supplementary Material 5**). MAP2325 was thought to be absent from Type I isolates (42) but was later found in Type I isolates from countries other than Australia (43). This gene was absent from all Australian Type I isolates tested but present in all other isolates with a single SNP present in some Type III isolates.

Type I isolates contained more conserved unique variants than Type III isolates, potentially due to their lower diversity. Proteins derived from most of these genes were found in the Type III isolates, but in the other lineage the sequences contained SNPs and polymorphisms which were inconsistent between isolates, whereas all the Type I sequences were identical. Genes in Type I isolates that were variable in Type III included a lineage-specific putative nuclear transport factor 2 family protein, mycobacterial membrane protein large (MMPL) family transporter, MMPL family protein, hydroxycinnamic acid hydroxylase (*mhpA2*) and a monooxygenase (*cinA1*). The MMPL genes are a subgroup of resistance-nodulation-division transporters involved in trans-envelop and trans-membrane export of immunomodulatory

lipid components in mycobacteria (72). Prior investigations discovered variation in these genes in S strains of MAP (38). Both MMPL proteins from the Type I isolates had no significant hits in the Type III isolates and no hits to any MAP genomes in the NCBI BLASTp database. The role of these proteins in lipid export would require further investigation in both lineages. The *mhpA* genes have not been extensively studied in mycobacteria but are involved in redox reactions (73). Similarly, the monooxygenase is a member of a superfamily of haemoprotein enzymes responsible for oxidative metabolism of fatty acids and acyl homoserine lactones (74). These enzymes are thought to give bacteria a competitive advantage since they can block signalling of other bacteria (75). Differences in these genes between lineages may offer a regional selective advantage against conditions encountered by each lineage. Alternatively, the higher similarity of Type I isolate may indicate clonal expansion of a more virulent isolate that diverged from the common ancestor of Type I and Type III isolates in the past.

Both lineages had consistent variations in genes involved in metabolism and transcription including a haemolysin III family protein, a nitroreductase family protein and a *TetR/AcrR* family transcriptional regulator. These genes have all been previously linked with virulence. Haemolysin III family proteins are surface associated and may be involved in the acquisition of nutrients and drug resistance in *M. tuberculosis* (76). Nitroreductase enzymes convert nitro-containing compounds to their corresponding amine and are associated with the stress response in mycobacteria (77). The *TetR/AcrR* family transcriptional regulator is a gene involved with a paired mechanism responsible for chemical signalling and bacterial homeostasis (78). Further *in vitro* work would be required to investigate if these differences have a functional impact on MAP lineages.

An unexpected finding in the present study was the variability of the *gyrA* and *gyrB* genes within sub-lineages. These genes have been described to have type-specific mutations between lineages (67). Non-synonymous SNPs were found within the type III isolates in the *gyrA* gene and synonymous SNPs found in the *gyrB* gene. These mutations may represent regional variants. Sequencing of PCR amplicons may have diagnostic value, but further work is needed to characterise the extent of these mutations in various regions. A lineage-specific *gyr* variant was not found by the pan-genome analysis, since the resulting proteins were of the same length between the lineages and thus annotation software successfully identified the proteins as the same. These genes have been the subject of multiple studies in *M. tuberculosis*, in which SNPs have been found to confer antimicrobial resistance (79, 80). Antimicrobial resistance is not typically a concern in MAP since the use of antibiotics to treat Johne's disease in ruminants is uncommon. However, keeping track of potential resistance markers may have human clinical relevance. The presence of within-lineage SNPs in these genes indicates that their use as lineage-specific markers may not be ideal and a new diagnostic test may be required for rapid lineage identification.

Initially, *de novo* assembly was chosen over mapping to a reference genome, since a wider variety of isolates were being used and a single reference genome was unlikely to

be appropriate for all isolates. At the time of this study, only a single reference genome was complete, the Australian Telford Type I (CP033688.1), all other available sheep strains were only available as draught assemblies. Using a reference genome on isolates that are diverse could have led to unmapped regions being missed by the analysis. To reduce the possibility that our genes of interest were assembly or annotation artefacts, genes annotated by Prokka had to be identified by Scoary as lineage-specific. These candidate genes of interest were further investigated by BLAST to confirm that within a lineage they were identical and that between lineages, there were consistent differences specific to their respective lineages.

Due to the possibility of assembly errors, poor and/or incomplete coverage, more lineage specific genes and variations may be present but were not identified by the present study. Repetitive regions such as the PPE/PE genes are difficult to assemble since the assembly software cannot be certain where raw sequencing reads belong if two regions are highly similar or repetitive. These genes have been the subject of numerous studies and can represent important virulence traits and genomic variation (81–86). Assembly errors in regions such as these can result in a loss of important information on isolate diversity. Efforts were made to include only high-quality genomic data in the study. Nevertheless, more lineage variations may have been missed due to their presence on a contig boundary or poor genome coverage in particular regions such as the PPE/PE genes of some isolates. This was partly seen in several genes that were identified using Scoary as lineage-specific in type I isolates but not type III, due to slight differences within the Type III group. Future investigations may require long read sequencing such as Nanopore long read sequencing so that reads span regions that are difficult to assemble, such that repetitive regions can be accurately assembled (87). This would enable the construction of complete sheep genomes so that more detailed comparisons can be made, a method which was recently employed to compare genomes across all of *M. avium* (88). Having a number of complete or closed sheep MAP genomes has the potential to reveal important differences in that we were unable to be identify.

CONCLUSION

Within sub-lineages of S strain MAP, there appear to be distinct regional clusters, such as the Australian-New Zealand group within the Type I lineage. The Type I lineage exhibits low genetic diversity compared to the Type III lineage. Within lineages, there is evidence for lineage-specific variants of genes associated with virulence in mycobacteria. By revealing lineage-specific markers for S strains of MAP, there is potential for improving diagnostics so that rapid identification of Type I and III strains can occur. These *in silico* findings require further testing *in vitro* prior to the development of a lineage-specific diagnostic test. This knowledge could reveal insights into the epidemiology and spread of these lineages without the need for full genome sequencing in future studies. Further *in vitro* work may assist in identifying the

functional differences of these genes and reveal how lineage differences relate to virulence and host adaptation.

DATA AVAILABILITY STATEMENT

The datasets generated for this study can be found in online repositories. The names of the repository/repositories and accession number(s) can be found below: NCBI Sequence Read Archive, SRR13214442 - SRR13214448.

AUTHOR CONTRIBUTIONS

RM was responsible for the data collection, bioinformatics analysis and writing of the manuscript. VT and KP assisted with the study design and editing of the manuscript. VT also assisted with the bioinformatics analyses. RW assisted in the collection, curation and description of some of the study isolates and editing of the manuscript. MP-C, MG, PB, and CH assisted with obtaining isolates and metadata from New Zealand and editing of the manuscript. All authors contributed to the article and approved the submitted version.

FUNDING

This study was a piece of the first author's P.hD. project funded by Meat and Livestock Australia (MLA) through project grant P.PSH.0813. The funding body (MLA) provided support in the form of some authors' salaries and research materials but did not have any role in the study design, data collection and analysis or preparation of the manuscript.

ACKNOWLEDGMENTS

The authors would like to acknowledge the Sydney Informatics Hub for enabling the use of the Artemis computer and for training received by the first author. Assistance from Keenan Pey and Winkie Fong with the bioinformatics in this study was greatly appreciated. Laboratory assistance from Anna Waldron and Ann-Michele Whittington is also acknowledged.

SUPPLEMENTARY MATERIAL

The Supplementary Material for this article can be found online at: <https://www.frontiersin.org/articles/10.3389/fvets.2021.637637/full#supplementary-material>

Supplementary Material 1 | Isolate metadata list and QUAST results Excel spreadsheet.

Supplementary Material 2 | Phylogenetic tree including public sequences culled by Treemmer and those that did not meet assembly quality thresholds.

Supplementary Material 3 | Type I and III reference and JIII386 *gyrA* protein alignment schematic.

Supplementary Material 4 | BLASTx results of lineage-specific genes.

Supplementary Material 5 | Previously identified variable loci from Castellanos et al. (43) in sheep MAP strains.

REFERENCES

- Whittington R, Donat K, Weber M, Kelton D, Nielsen S, Eisenberg S, et al. Control of *paratuberculosis*: who, why and how. A review of 48 countries. *BMC Vet Res*. (2019) 15:198. doi: 10.1186/s12917-019-1943-4
- Waddell LA, Rajić A, Stärk KDC, McEwen SA. The zoonotic potential of *Mycobacterium avium* ssp. *paratuberculosis*: a systematic review and meta-analyses of the evidence. *Epidemiol Infect*. (2015) 143:3135. doi: 10.1017/S095026881500076X
- Timms VJ, Daskalopoulos G, Mitchell HM, Neilan BA. The association of *Mycobacterium avium* subsp. *paratuberculosis* with inflammatory bowel disease. *PLoS ONE*. (2016) 11:e0148731. doi: 10.1371/journal.pone.0148731
- Britton LE, Cassidy JP, O'Donovan J, Gordon SV, Markey B. Potential application of emerging diagnostic techniques to the diagnosis of bovine Johne's disease (*paratuberculosis*). *Vet J*. (2016) 209:32–9. doi: 10.1016/j.tvjl.2015.10.033
- Shephard RW, Williams SH, Beckett SD. Farm economic impacts of bovine Johne's disease in endemically infected Australian dairy herds. *Aust Vet J*. (2016) 94:232–9. doi: 10.1111/avj.12455
- Garcia AB, Shalloo L. Invited review: the economic impact and control of *paratuberculosis* in cattle. *J Dairy Sci*. (2015) 98:5019–39. doi: 10.3168/jds.2014-9241
- Eppeleston J, Simpson G, O'Neill S, Thornberry K, Lugton I, Taylor P, et al. Reported levels of sheep mortalities in flocks infected with ovine Johne's disease in New South Wales. *Asian-Australas J Anim Sci*. (2000) 13:247–247.
- Webb Ware JK, Larsen JWA, Kluver P. Financial effect of bovine Johne's disease in beef cattle herds in Australia. *Aust Vet J*. (2012) 90:116–21. doi: 10.1111/j.1751-0813.2012.00896.x
- Bryant JM, Thibault VC, Smith DGE, McLuckie J, Heron I, Sevilla IA, et al. Phylogenomic exploration of the relationships between strains of *Mycobacterium avium* subspecies *paratuberculosis*. *BMC Genomics*. (2016) 17:79. doi: 10.1186/s12864-015-2234-5
- Stevenson K. Genetic diversity of *Mycobacterium avium* subspecies *paratuberculosis* and the influence of strain type on infection and pathogenesis: a review. *Vet Res*. (2015) 46:64. doi: 10.1186/s13567-015-0203-2
- Collins DM, Gabric DM, de Lisle GW. Identification of two groups of *Mycobacterium paratuberculosis* strains by restriction endonuclease analysis and DNA hybridization. *J Clin Microbiol*. (1990) 28:1591. doi: 10.1128/JCM.28.7.1591-1596.1990
- Whittington RJ, Hope AF, Marshall DJ, Taragel CA, Marsh I. Molecular epidemiology of *Mycobacterium avium* subsp. *paratuberculosis*: IS900 restriction fragment length polymorphism and IS1311 polymorphism analyses of isolates from animals and a human in Australia. *J Clin Microbiol*. (2000) 38:3240. doi: 10.1128/JCM.38.9.3240-3248.2000
- Biet F, Sevilla Iker A, Cochard T, Lefrançois Louise H, Garrido Joseba M, Heron I, et al. Inter- and Intra-subtype genotypic differences that differentiate *Mycobacterium avium* subspecies *paratuberculosis* strains. *BMC Microbiol*. (2012) 12:264. doi: 10.1186/1471-2180-12-264
- Verdugo C, Pleydell E, Price-Carter M, Prattley D, Collins D, de Lisle G, et al. Molecular epidemiology of *Mycobacterium avium* subsp. *paratuberculosis* isolated from sheep, cattle and deer on New Zealand pastoral farms. *Prev Vet Med*. (2014) 117:436–46. doi: 10.1016/j.prevetmed.2014.09.009
- Moloney B, Whittington R. Cross species transmission of ovine Johne's disease from sheep to cattle: an estimate of prevalence in exposed susceptible cattle. *Aust Vet J*. (2008) 86:117–23. doi: 10.1111/j.1751-0813.2008.00272.x
- Stevenson K, Alvarez J, Bakker D, Biet F, de Juan L, Denham S, et al. Occurrence of *Mycobacterium avium* subspecies *paratuberculosis* across host species and European countries with evidence for transmission between wildlife and domestic ruminants. *BMC Microbiol*. (2009) 9:212–212. doi: 10.1186/1471-2180-9-212
- Whittington RJ, Marsh IB, Whitlock RH. Typing of IS 1311 polymorphisms confirms that bison (*Bison bison*) with *paratuberculosis* in Montana are infected with a strain of *Mycobacterium avium* subsp. *paratuberculosis* distinct from that occurring in cattle and other domesticated livestock. *Mol Cell Probes*. (2001) 15:139–45. doi: 10.1006/mcpr.2001.0346
- Yadav D, Singh SV, Singh AV, Sevilla I, Juste RA, Singh PK, et al. Pathogenic "Bison-type" *Mycobacterium avium* subspecies *paratuberculosis* genotype characterized from riverine buffalo (*Bubalus bubalis*) in North India. *Comp Immunol Microbiol Infect Dis*. (2007) 31:373–87. doi: 10.1016/j.cimid.2007.06.007
- de Juan L, Mateos A, Domínguez L, Sharp JM, Stevenson K. Genetic diversity of *Mycobacterium avium* subspecies *paratuberculosis* isolates from goats detected by pulsed-field gel electrophoresis. *Vet Microbiol*. (2005) 106:249–57. doi: 10.1016/j.vetmic.2004.12.013
- Whittington RJ, Taragel CA, Ottaway S, Marsh I, Seaman J, Fridriksdottir V. Molecular epidemiological confirmation and circumstances of occurrence of sheep (S) strains of *Mycobacterium avium* subsp. *paratuberculosis* in cases of *paratuberculosis* in cattle in Australia and sheep and cattle in Iceland. *Vet Microbiol*. (2001) 79:311–22. doi: 10.1016/S0378-1135(00)00364-3
- Choy E, Whittington RJ, Marsh I, Marshall J, Campbell MT. A method for purification and characterisation of *Mycobacterium avium* subsp. *paratuberculosis* from the intestinal mucosa of sheep with Johne's disease. *Vet Microbiol*. (1998) 64:51–60. doi: 10.1016/S0378-1135(98)00252-1
- Whittington RJ, Marsh IB, Saunders V, Grant IR, Juste R, Sevilla IA, et al. Culture phenotypes of genomically and geographically diverse *Mycobacterium avium* subsp. *paratuberculosis* isolates from different hosts. *J Clin Microbiol*. (2011) 49:1822. doi: 10.1128/JCM.00210-11
- Kabara E, Kloss CC, Wilson M, Tempelman RJ, Sreevatsan S, Janagama H, et al. A large-scale study of differential gene expression in monocyte-derived macrophages infected with several strains of *M. avium* subspecies *paratuberculosis*. *Brief Funct Genomics*. (2010) 9:220–37. doi: 10.1093/bfpg/eq009
- Abendaño N, Tyukalova L, Barandika J, Balseiro A, Sevilla I, Garrido J, et al. *Mycobacterium avium* subsp. *paratuberculosis* isolates induce *in vitro* granuloma formation and show successful survival phenotype, common anti-inflammatory and antiapoptotic responses within ovine macrophages regardless of genotype or host of origin. *PLoS ONE*. (2014) 9:e104238. doi: 10.1371/journal.pone.0104238
- Motiwalla AS, Janagama HK, Paustian ML, Zhu X, Bannantine JP, Kapur V, et al. Comparative transcriptional analysis of human macrophages exposed to animal and human isolates of *Mycobacterium avium* subspecies *paratuberculosis* with diverse genotypes. *Infect Immun*. (2006) 74:6046. doi: 10.1128/IAI.00326-06
- Thibault VC, Grayon M, Boschirolu ML, Hubbans C, Overduin P, Stevenson K, et al. New variable-number tandem-repeat markers for typing *Mycobacterium avium* subsp. *paratuberculosis* and *M. avium* strains: comparison with IS900 and IS1245 restriction fragment length polymorphism typing. *J Clin Microbiol*. (2007) 45:2404. doi: 10.1128/JCM.00476-07
- Abendaño N, Sevilla IA, Prieto JM, Garrido JM, Juste RA, Alonso-Hearn M. *Mycobacterium avium* subspecies *paratuberculosis* isolates from sheep and goats show reduced persistence in bovine macrophages than cattle, bison, deer and wild boar strains regardless of genotype. *Vet Microbiol*. (2013) 163:325–34. doi: 10.1016/j.vetmic.2012.12.042
- Sevilla I, Garrido JM, Geijo M, Juste RA. Pulsed-field gel electrophoresis profile homogeneity of *Mycobacterium avium* subsp. *paratuberculosis* isolates from cattle and heterogeneity of those from sheep and goats. *BMC Microbiol*. (2007) 7:18. doi: 10.1186/1471-2180-7-18
- Fawzy A, Zschöck M, Ewers C, Eisenberg T. Genotyping methods and molecular epidemiology of *Mycobacterium avium* subsp. *paratuberculosis*. *Int J Vet Sci Med*. (2018) 6:258–64. doi: 10.1016/j.ijvsm.2018.08.001
- Whittington R, Marsh I, Choy E, Cousins D. Polymorphisms in IS1311, an insertion sequence common to *Mycobacterium avium* and *M. avium* subsp. *paratuberculosis*, can be used to distinguish between and within these species. *Mol Cell Probes*. (1998) 12:349–58. doi: 10.1006/mcpr.1998.0194
- Kasai H, Ezaki T, Harayama S. Differentiation of phylogenetically related slowly growing mycobacteria by their gyrB sequences. *J Clin Microbiol*. 38:301. doi: 10.1128/JCM.38.1.301-308.2000
- Collins DM, De Zoete M, Cavaignac SM. *Mycobacterium avium* subsp. *paratuberculosis* strains from cattle and sheep can be distinguished by a PCR test based on a novel DNA sequence difference. *J Clin Microbiol*. (2002) 40:4760. doi: 10.1128/JCM.40.12.4760-4762.2002
- Ahlstrom C, Barkema HW, Stevenson K, Zadoks RN, Biek R, Kao R, et al. Limitations of variable number of tandem repeat typing identified through whole genome sequencing of *Mycobacterium avium* subsp. *paratuberculosis* on a national and herd level. *BMC Genomics*. (2015) 16:161. doi: 10.1186/s12864-015-1387-6

34. Möbius P, Fritsch I, Luyven G, Hotzel H, Köhler H. Unique genotypes of *Mycobacterium avium* subsp. *paratuberculosis* strains of Type III. *Vet Microbiol.* (2009) 139:398–404. doi: 10.1016/j.vetmic.2009.06.011
35. Kasnitz N, Köhler H, Weigoldt M, Gerlach GF, Möbius P. Stability of genotyping target sequences of *Mycobacterium avium* subsp. *paratuberculosis* upon cultivation on different media, *in vitro*- and *in vivo* passage, and natural infection. *Vet Microbiol.* (2013) 167:573–83. doi: 10.1016/j.vetmic.2013.09.008
36. Sohal JS, Arsenault J, Labrecque O, Fairbrother J-H, Roy J-P, Fecteau G, et al. Genetic structure of *Mycobacterium avium* subsp. *paratuberculosis* population in cattle herds in Quebec as revealed by using a combination of multilocus genomic analyses. *J Clin Microbiol.* (2014) 52:2764. doi: 10.1128/JCM.00386-14
37. Park H-T, Park H-E, Park WB, Kim S, Hur TY, Jung Y-H, et al. Genetic diversity of bovine *Mycobacterium avium* subsp. *paratuberculosis* discriminated by IS1311 PCR-REA, MIRU-VNTR, and MLSSR genotyping. *J Vet Sci.* (2018) 19:627. doi: 10.4142/jvs.2018.19.5.627
38. Marsh IB, Whittington RJ. Deletion of an *mmpL* gene and multiple associated genes from the genome of the S strain of *Mycobacterium avium* subsp. *paratuberculosis* identified by representational difference analysis and *in silico* analysis. *Mol Cell Probes.* (2005) 19:371–84. doi: 10.1016/j.mcp.2005.06.005
39. Semret M, Turenne CY, Behr MA. Insertion sequence IS900 Revisited. *J Clin Microbiol.* (2006) 44:1081. doi: 10.1128/JCM.44.3.1081-1083.2006
40. Semret M, Turenne CY, de Haas P, Collins DM, Behr MA. Differentiating host-associated variants of *Mycobacterium avium* by PCR for detection of large sequence polymorphisms. *J Clin Microbiol.* (2006) 44:881. doi: 10.1128/JCM.44.3.881-887.2006
41. Marsh IB, Whittington RJ. Genomic diversity in *Mycobacterium avium*: single nucleotide polymorphisms between the S and C strains of *M. avium* subsp. *paratuberculosis* and with *M. a. avium*. *Mol Cell Probes.* (2007) 21:66–75. doi: 10.1016/j.mcp.2006.08.002
42. Marsh IB, Bannantine JP, Paustian ML, Tizard ML, Kapur V, Whittington RJ. Genomic comparison of *Mycobacterium avium* subsp. *paratuberculosis* sheep and cattle strains by microarray hybridization. *J Bacteriol.* (2006) 188:2290. doi: 10.1128/JB.188.6.2290-2293.2006
43. Castellanos E, Aranaz A, Gould KA, Linedale R, Stevenson K, Alvarez J, et al. Discovery of stable and variable differences in the *Mycobacterium avium* subsp. *paratuberculosis* type I, II, and III genomes by pan-genome microarray analysis. *Appl Environ Microbiol.* (2009) 75:676. doi: 10.1128/AEM.01683-08
44. Li L, Bannantine JP, Zhang Q, Amonsin A, May BJ, Alt D, et al. The complete genome sequence of *Mycobacterium avium* subspecies *paratuberculosis*. *Proc Natl Acad Sci USA.* (2005) 102:12344. doi: 10.1073/pnas.0505662102
45. Bannantine JP, Wu C-W, Hsu C, Zhou S, Schwartz DC, Bayles DO, et al. Genome sequencing of ovine isolates of *Mycobacterium avium* subspecies *paratuberculosis* offers insights into host association. *BMC Genomics.* (2012) 13:89. doi: 10.1186/1471-2164-13-89
46. Dhand NK, Eppeleston J, Whittington RJ, Windsor PA. Changes in prevalence of ovine *paratuberculosis* following vaccination with Gudair®: results of a longitudinal study conducted over a decade. *Vaccine.* (2016) 34:5107–13. doi: 10.1016/j.vaccine.2016.08.064
47. Whittington RJ, Whittington AM, Waldron A, Begg DJ, de Silva K, Purdie AC, et al. Development and validation of a liquid medium (M7H9C) for routine culture of *Mycobacterium avium* subsp. *paratuberculosis* to replace modified bactec 12B medium. *J Clin Microbiol.* (2013) 51:3993–4000. doi: 10.1128/JCM.01373-13
48. Bolger AM, Lohse M, Usadel B. Trimmomatic: a flexible trimmer for illumina sequence data. *Bioinformatics.* (2014) 30:2114–20. doi: 10.1093/bioinformatics/btu170
49. Bankevich A, Nurk S, Antipov D, Gurevich AA, Dvorkin M, Kulikov AS, et al. SPAdes: a new genome assembly algorithm and its applications to single-cell sequencing. *J Comput Biol.* (2012) 19:455–77. doi: 10.1089/cmb.2012.0021
50. Li H, Durbin R. Fast and accurate short read alignment with Burrows–Wheeler transform. *Bioinformatics.* (2009) 25:1754–60. doi: 10.1093/bioinformatics/btp324
51. Gurevich A, Saveliev V, Vyahhi N, Tesler G. QUAST: quality assessment tool for genome assemblies. *Bioinformatics.* (2013) 29:1072–5. doi: 10.1093/bioinformatics/btt086
52. Seemann T. Prokka: rapid prokaryotic genome annotation. *Bioinformatics.* (2014) 30:2068–9. doi: 10.1093/bioinformatics/btu153
53. Page AJ, Cummins CA, Hunt M, Wong VK, Reuter S, Holden MTG, et al. Roary: rapid large-scale prokaryote pan genome analysis. *Bioinformatics.* (2015) 31:3691–3. doi: 10.1093/bioinformatics/btv421
54. Katoh K, Misawa K, Kuma K-I, Miyata T. MAFFT: a novel method for rapid multiple sequence alignment based on fast Fourier transform. *Nucleic Acids Res.* (2002) 30:3059–66. doi: 10.1093/nar/gkf436
55. Nguyen L-T, Schmidt HA, Von Haeseler A, Minh BQ. IQ-TREE: a fast and effective stochastic algorithm for estimating maximum-likelihood phylogenies. *Mol Biol Evol.* (2015) 32:268. doi: 10.1093/molbev/msu300
56. Kalyaanamoorthy S, Minh BQ, Wong TKF, von Haeseler A, Jermin LS. ModelFinder: fast model selection for accurate phylogenetic estimates. *Nat Methods.* (2017) 14:587. doi: 10.1038/nmeth.4285
57. Rodríguez F, Oliver JL, Marín A, Medina JR. The general stochastic model of nucleotide substitution. *J Theor Biol.* (1990) 142:485–501. doi: 10.1016/S0022-5193(05)80104-3
58. Letunic I, Bork P. Interactive tree of life (iTOL) v4: recent updates and new developments. *Nucleic Acids Res.* (2019) 47:W256–W259. doi: 10.1093/nar/gkz239
59. Brauning R, Plain K, Gautam M, Russell T, Correa CC, Biggs P, et al. Complete genome sequence of the telford type S strain of *Mycobacterium avium* subsp. *paratuberculosis*. *Microbiol Res Announc.* (2019) 8:e00004–19. doi: 10.1128/MRA.00004-19
60. Menardo F, Loiseau C, Brites D, Coscolla M, Gygli SM, Rutaiwa LK, et al. Treemmer: a tool to reduce large phylogenetic datasets with minimal loss of diversity. *BMC Bioinformatics.* (2018) 19:164. doi: 10.1186/s12859-018-2164-8
61. Brynildsrud O, Bohlin J, Scheffer L, Eldholm V. Rapid scoring of genes in microbial pan-genome-wide association studies with Scoary. *Genome Biol.* (2016) 17:238. doi: 10.1186/s13059-016-1108-8
62. Darling ACE, Mau B, Blattner FR, Perna NT. Mauve: multiple alignment of conserved genomic sequence with rearrangements. *Genome Res.* (2004) 14:1394. doi: 10.1101/gr.2289704
63. Rissman AI, Mau B, Biehl BS, Darling AE, Glasner JD, Perna NT. Reordering contigs of draft genomes using the mauve aligner. *Bioinformatics.* (2009) 25:2071–3. doi: 10.1093/bioinformatics/btp356
64. Pallab G, Chungyi H, Essam JA, Maher MS, Musaad AA-D, Abdulmohsen A-N, et al. Genome-wide analysis of the emerging infection with *Mycobacterium avium* subspecies *paratuberculosis* in the Arabian camels (*Camelus dromedarius*). *PLoS ONE.* (2012) 7:e31947. doi: 10.1371/journal.pone.0031947
65. Möbius P, Hölzer M, Felder M, Nordsiek G, Groth M, Köhler H, et al. Comprehensive insights in the *Mycobacterium avium* subsp. *paratuberculosis* genome using new WGS data of sheep strain JIII-386 from Germany. *Genome Biol Evol.* (2015) 7:2585–601. doi: 10.1093/gbe/evv154
66. Vernikos G, Medini D, Riley DR, Tettelin H. Ten years of pan-genome analyses. *Curr Opin Microbiol.* (2015) 23:148. doi: 10.1016/j.mib.2014.11.016
67. Castellanos E, Aranaz A, Romero B, de Juan L, Alvarez J, Bezos J, et al. Polymorphisms in *gyrA* and *gyrB* Genes among *Mycobacterium avium* subsp. *paratuberculosis* type I, II, and III isolates. *J Clin Microbiol.* (2007) 45:3439. doi: 10.1128/JCM.01411-07
68. Ahlstrom C, Barkema HW, Stevenson K, Zadoks RN, Biek R, Kao R, et al. Genome-wide diversity and phylogeography of *Mycobacterium avium* subsp. *paratuberculosis* in Canadian dairy cattle. *PLoS ONE.* (2016) 11:e0149017. doi: 10.1371/journal.pone.0149017
69. Timms VJ, Hassan KA, Mitchell HM, Neilan BA. Comparative genomics between human and animal associated subspecies of the *Mycobacterium avium* complex: a basis for pathogenicity. *BMC Genomics.* (2015) 16:695. doi: 10.1186/s12864-015-1889-2
70. Elliott GN, Hough RL, Avery LM, Maltin CA, Campbell CD. Environmental risk factors in the incidence of Johne's disease. *Crit Rev Microbiol.* (2015) 41:488. doi: 10.3109/1040841X.2013.867830
71. Bannantine JP, Li LL, Sreevatsan S, Kapur V. How does a *Mycobacterium* change its spots? Applying molecular tools to track diverse strains of *Mycobacterium avium* subspecies *paratuberculosis*. *Lett Appl Microbiol.* (2013) 57:165–73. doi: 10.1111/lam.12109
72. Viljoen A, Dubois V, Girard-Misguich F, Blaise M, Herrmann JL, Kremer L. The diverse family of *MmpL* transporters in mycobacteria: from regulation to antimicrobial developments. *Mol Microbiol.* (2017) 104, 889–904. doi: 10.1111/mmi.13675

73. Ortega Ugalde S, de Koning CP, Wallraven K, Bruyneel B, Vermeulen NPE, Grossmann TN, et al. Linking cytochrome P450 enzymes from *Mycobacterium tuberculosis* to their cognate ferredoxin partners. *Appl Microbiol Biotechnol.* (2018) 102:9231. doi: 10.1007/s00253-018-9299-4
74. Hawkes DB, Adams GW, Burlingame AL, Ortiz de Montellano PR, De Voss JJ. Cytochrome P450(cin) (CYP176A), isolation, expression, and characterization. *J Biol Chem.* (2002) 277:27725–32. doi: 10.1074/jbc.M203382200
75. Chowdhary PK, Keshavan N, Nguyen HQ, Peterson JA, González JE, Haines DC. *Bacillus megaterium* CYP102A1 oxidation of acyl homoserine lactones and acyl homoserines. *Biochemistry.* (2007) 46:14429–37. doi: 10.1021/bi701945j
76. Ahmed N, Sneh A, Srivastava Saumya S, Rahman A, Krishnasastri Musti V. Molecular characterization of tlyA gene product, Rv1694 of *Mycobacterium tuberculosis*: a non-conventional hemolysin and a ribosomal RNA methyl transferase. *BMC Biochem.* (2010) 11:35. doi: 10.1186/1471-2091-11-35
77. Negri A, Javidnia P, Mu R, Zhang X, Vendome J, Gold B, et al. Identification of a mycothiol-dependent nitroreductase from *Mycobacterium tuberculosis*. *ACS Infect Dis.* (2018) 4:771–87. doi: 10.1021/acsinfecdis.7b00111
78. Deng W, Li C, Xie J. The underling mechanism of bacterial TetR/AcrR family. *Cell Signal.* (2013) 25:1608–13. doi: 10.1016/j.cellsig.2013.04.003
79. Monego F, Duarte RS, Biondo AW. gyrA and gyrB gene mutation in ciprofloxacin-resistant *Mycobacterium massiliense* clinical isolates from Southern Brazil. *Microbial Drug Resist.* (2012) 18:1–6. doi: 10.1089/mdr.2011.0047
80. Bernard C, Veziris N, Brossier F, Sougakoff W, Jarlier V, Robert J, et al. Molecular diagnosis of fluoroquinolone resistance in *Mycobacterium tuberculosis*. *Antimicrob Agents Chemother.* (2015) 59:1519–24. doi: 10.1128/AAC.04058-14
81. Karboul A, Mazza A, Gey van Pittius NC, Ho JL, Brousseau R, Mardassi H. Frequent homologous recombination events in *Mycobacterium tuberculosis* PE/PPE multigene families: potential role in antigenic variability. *J Bacteriol.* (2008) 190:7838. doi: 10.1128/JB.00827-08
82. Mackenzie N, Alexander DC, Turenne CY, Behr MA, De Buck JM. Genomic Comparison of PE and PPE genes in the *Mycobacterium avium* complex. *J Clin Microbiol.* (2009) 47:1002. doi: 10.1128/JCM.01313-08
83. Nagata R, Kawaji S, Minakawa Y, Wang X, Yanaka T, Mori Y. A specific induction of interleukin-10 by the Map41 recombinant PPE antigen of *Mycobacterium avium* subsp. *paratuberculosis*. *Vet Immunol Immunopathol.* (2010) 135:71–8. doi: 10.1016/j.vetimm.2009.11.002
84. Castellanos E, Aranaz A, de Juan L, Dominguez L, Linedale R, Bull TJ. A 16kb naturally occurring genomic deletion including mce and PPE genes in *Mycobacterium avium* subspecies *paratuberculosis* isolates from goats with John's disease. *Vet Microbiol.* (2012) 159:60–8. doi: 10.1016/j.vetmic.2012.03.010
85. Ahmad J, Khubaib M, Sheikh JA, Pansa R, Kumar S, Srinivasan A, et al. Disorder-to-order transition in PE–PPE proteins of *Mycobacterium tuberculosis* augments the pro-pathogen immune response. *FEBS Open Bio.* (2020) 10:70–85. doi: 10.1002/2211-5463.12749
86. Wu L, Wanyan D, Jianping X. Expression and regulatory networks of *Mycobacterium tuberculosis* PE/PPE family antigens. *J Cell Physiol.* (2018) 234:7742–51. doi: 10.1002/jcp.27608
87. Sohn J-I, Nam J-W. The present and future of de novo whole-genome assembly. *Brief Bioinform.* (2018) 19:23–40. doi: 10.1093/bib/bbw096
88. Bannantine JP, Conde C, Bayles DO, Branger M, Biet F. Genetic diversity among *Mycobacterium avium* subspecies revealed by analysis of complete genome sequences. *Front Microbiol.* (2020) 11:1701. doi: 10.3389/fmicb.2020.01701

Conflict of Interest: The authors declare that the research was conducted in the absence of any commercial or financial relationships that could be construed as a potential conflict of interest.

Copyright © 2021 Mizzi, Timms, Price-Carter, Gautam, Whittington, Heuer, Biggs and Plain. This is an open-access article distributed under the terms of the Creative Commons Attribution License (CC BY). The use, distribution or reproduction in other forums is permitted, provided the original author(s) and the copyright owner(s) are credited and that the original publication in this journal is cited, in accordance with accepted academic practice. No use, distribution or reproduction is permitted which does not comply with these terms.



Alpha-2-Macroglobulin as a New Promising Biomarker Improving the Diagnostic Sensitivity of Bovine Paratuberculosis

Hyun-Eui Park^{1,2}, Jin-Sik Park¹, Hong-Tae Park², Jeong-Gyu Choi^{1,3}, Jeong-Ih Shin^{1,3}, Myunghwan Jung^{1,3}, Hyung-Lyun Kang^{1,3}, Seung-Chul Baik^{1,3}, Woo-Kon Lee^{1,3}, Donghyuk Kim⁴, Han Sang Yoo^{2*} and Min-Kyoung Shin^{1,3*}

OPEN ACCESS

Edited by:

Kumi de Silva,
The University of Sydney, Australia

Reviewed by:

Mohanned Naif Alhussien,
National Dairy Research Institute
(ICAR), India
Eduard Otto Roos,
Pirbright Institute, United Kingdom

*Correspondence:

Han Sang Yoo
yoohs@snu.ac.kr
Min-Kyoung Shin
mkshin@gnu.ac.kr

Specialty section:

This article was submitted to
Veterinary Infectious Diseases,
a section of the journal
Frontiers in Veterinary Science

Received: 04 December 2020

Accepted: 08 February 2021

Published: 05 March 2021

Citation:

Park H-E, Park J-S, Park H-T,
Choi J-G, Shin J-I, Jung M, Kang H-L,
Baik S-C, Lee W-K, Kim D, Yoo HS
and Shin M-K (2021)
Alpha-2-Macroglobulin as a New
Promising Biomarker Improving the
Diagnostic Sensitivity of Bovine
Paratuberculosis.
Front. Vet. Sci. 8:637716.
doi: 10.3389/fvets.2021.637716

¹ Department of Microbiology, Institute of Health Sciences, Gyeongsang National University School of Medicine, Jinju, South Korea, ² Department of Infectious Diseases, College of Veterinary Medicine, BK21 Four and Bio-Max/N-Bio Institute, Seoul National University, Seoul, South Korea, ³ Department of Convergence Medical Sciences, Gyeongsang National University, Jinju, South Korea, ⁴ Schools of Energy & Chemical Engineering and Life Sciences, Ulsan National Institute of Science and Technology, Ulsan, South Korea

Johne's disease (JD) is a chronic granulomatous enteritis of ruminants caused by *Mycobacterium avium* subsp. *paratuberculosis* (MAP), which induces persistent diarrhea and cachexia. JD causes huge economic losses to the dairy industry due to reduced milk production and premature culling. Infected animals excrete MAP via feces during the prolonged subclinical stage without exhibiting any clinical signs. Therefore, accurate detection of subclinical stage animals is crucial for successful eradication of JD in the herd. In the current study, we analyzed serum samples of MAP-infected and non-infected cattle to identify potential biomarker candidates. First, we identified 12 differentially expressed serum proteins in subclinical and clinical shedder groups compared to the healthy control group. Second, we conducted ELISA for three selected biomarkers (alpha-2-macroglobulin (A2M), alpha-1-beta glycoprotein, and transthyretin) and compared their diagnostic performance with that of two commercial ELISA diagnostic kits. Serum A2M levels were significantly higher in the MAP-exposed, subclinical shedder, subclinical non-shedder, and clinical shedder groups than in the healthy control group, suggesting its possible use as a diagnostic biomarker for MAP infection. Furthermore, A2M demonstrated a sensitivity of 90.4%, and a specificity of 100% while the two commercial ELISA kits demonstrated a sensitivity of 67.83 and 73.04% and a specificity of 100%, respectively. In conclusion, our results suggest that measuring A2M by ELISA can be used as a diagnostic tool to detect MAP infection, considerably improving the detection rate of subclinical shedders and MAP-exposed animals that are undetectable using current diagnostic tools.

Keywords: Johne's disease, biomarkers, alpha-2-macroglobulin, cattle, serum

INTRODUCTION

Johne's disease (JD) is a chronic granulomatous enteritis of ruminants caused by *Mycobacterium avium* subsp. *paratuberculosis* (MAP) that causes significant economic damage to dairy industries worldwide (1). The primary hosts of MAP are farmed and free-range ruminants, including cattle, lamb, goat, and deer (1). In addition, several researchers have also isolated MAP from various non-ruminant wildlife and captive animals such as rabbit, mice, rat, fox, raccoon, opossum, skunk, coyote, Cuban hutia, parrot, wallaby, and baboon which suggests the possibility of inter-species transmission (2–4). Furthermore, with the possibility of an association between MAP and human autoimmune diseases such as Crohn's disease, multiple sclerosis, type 1 diabetes, and rheumatoid arthritis, JD has become an important public health disease (5–7).

The prominent clinical features of JD are persistent diarrhea, progressive weight loss, decreased milk production, and debilitation after a prolonged incubation period (1). During disease progression, infected cattle shed MAP with their feces, and bacterial shedding subsequently contaminates water, feed, milk, and the surrounding environment (1, 8). Due to the waxy mycolic acid layer, MAP endure harsh environmental conditions, including dryness, low pH, and high or low temperatures; MAP viability in pastures can be maintained for over 1 year and much longer periods in water (9, 10). Ingestion of MAP-contaminated materials is the primary route of infection. Therefore, rapid detection and culling of subclinical fecal shedder from herd are needed for the control of the JD (1, 8).

The diagnosis of JD is mainly divided into two categories. The presence of MAP in clinical specimens such as feces, milk, colostrum, and intestinal tissues can be detected by PCR and bacterial culture (11). Bacterial culture from a fecal sample is the gold standard for diagnosis of JD and the only available method to detect viable MAP. However, observation of visible colonies takes at least 4 weeks after inoculation due to a slow growth rate (11). Furthermore, different disease progression rates, especially in subclinical stages, induce intermittent bacterial shedding and subsequently result in false-negative results for infected animals (11). Detection of MAP by PCR is a fast and high-throughput method that detects MAP-specific genes such as *IS900*, *ISMap02*, and *f57* (12–14). Nevertheless, PCR-based detection has several limitations (15). First, PCR inhibitors in feces may interfere with the reaction and subsequently lead to false-negative results. Second, non-specific amplification from the host and other bacterial DNA can result in false-positive results (15). Third, most subclinically infected animals typically shed bacteria intermittently, which leads to false-negative results (15). Enzyme-linked immunosorbent assay (ELISA) is generally easy to conduct with a simple protocol and high-throughput method for herd-level diagnosis (16). However, diagnosis of MAP-infected cattle at subclinical stage is hampered by the low sensitivity of currently developed commercial ELISA. Furthermore, co-infection with other pathogens such as *Mycobacterium bovis*, *Fasciola hepatica*, and non-tuberculous mycobacteria may reduce diagnostic specificity by altering the immune response (17, 18). Taken together, alternative diagnostic methods that can detect

subclinically infected animals are urgently needed for the control and eradication of JD.

Biomarkers are measurable indicators that represent physiological alterations during disease progression. A number of studies have previously identified potential biomarkers in MAP-infected animals (16, 19, 20). Acute phase proteins such as haptoglobin and serum amyloid A were significantly increased in various stages of paratuberculosis infection with different types of lesions (20). Shaughnessy *et al.* identified three fecal biomarkers (hsa-miR-658, hsa-miR-92a-3p, and hsa-miR-501-5p) that were significantly upregulated in fecal samples of cattle with JD (19). Several proteins, including ABCA13, FAM84A, DES, ABCA13, MMP8, and SPARC, were abundant in serum of MAP-infected animals with different pathological lesions compared to non-infected animals, suggesting their potential for diagnosis of subclinical stages of JD (16). In previous studies, efforts have been made to identify biomarker candidates by analyzing host transcripts in MAP-infected cells, mice and bovine models (21–23), and also by discovering several genes that are upregulated in cattle infected with MAP (24–26). However, mRNA and protein expression of these genes demonstrated poor correlation (27) and previous studies have been conducted with relatively small sample sizes. To overcome these limitations, we analyzed the proteomic profiles of serum samples from MAP-infected cattle in different stages of disease progression for biomarker discovery and evaluated the diagnostic potential of the novel biomarker candidates in naturally MAP-infected cattle.

MATERIALS AND METHODS

Animal Subjects and Sample Collection

Cattle were selected from one farm in Chungcheongnam province and two farms in Gangwon province of South Korea. For proteomic analysis for the serum proteins, 28 cattle were selected and classified into three groups according to the results of fecal qPCR analysis and the level of serum MAP antibodies detected by ELISA as follows: (1) Healthy control group ($n = 10$): selected from a JD-free farm, negative for fecal PCR and serum ELISA. (2) Subclinical shedder group ($n = 8$): fecal PCR positive and ELISA negative. (3) Clinical shedder group ($n = 10$): exhibiting typical JD clinical signs, positive for fecal PCR and ELISA. For the evaluation of biomarker candidates, 126 cattle were selected according to ELISA results for serum samples detected using two commercial ELISA diagnostic kits (IDEXX Laboratories, Inc., Westbrook, ME, USA; ID Screen Paratuberculosis Indirect, ID Vet, Montpellier, France) and detection of MAP in fecal samples by qPCR targeting *IS900* and *ISMap02* (12, 28). In detail, 126 cattle were divided into four groups as follows: (1) Healthy control group ($n = 11$): selected from a JD-free farm, negative for fecal PCR and ELISA negative for both commercial kits. (2) MAP-exposed group ($n = 20$): selected from a JD-positive farm, negative for fecal PCR and ELISA negative for both commercial kits. (3) Subclinical shedder group ($n = 27$): fecal PCR positive and ELISA negative for both commercial kits. (4) Subclinical non-shedder group ($n = 50$): fecal PCR negative and ELISA positive for at least one commercial kit. (5) Clinical shedder group ($n = 18$): exhibiting

typical JD clinical signs, fecal PCR positive, and ELISA positive for at least one commercial kit. Blood samples were collected by caudal vein venipuncture with Vacutainer Plus Plastic Serum Tubes (BD Biosciences, San Jose, CA, USA). Serum was separated by centrifugation at 2,500 *g* for 10 min. Separated serum was transferred to a 1.5 mL tube and stored at -80°C until use. The animal study was reviewed and approved by the Animal Ethics Committee of Seoul National University (SNU-200525-4).

Two-Dimensional Gel Electrophoresis (2-DE) Analysis

For 2-DE analysis for the serum proteins, the pooled serum samples were prepared from three groups. Calbiochem ProteoExtract™ Removal Kits (Merck Millipore, Darmstadt, Germany) was used for the removal of albumin and IgG from pooled serum samples according to the manufacturer's instructions. 2-DE and image analysis with 2-DE samples were conducted as previously described (29). Serum protein samples were washed with 40 mmol/L Tris-hydrochloride (HCl) (pH 7.2) and 1 mmol/L ethylenediaminetetraacetic acid (EDTA) and lysed using a buffer containing 9.5 mol/L urea, 4% 3-((3-cholamidopropyl)dimethylammonium)-1-propanesulfonate (CHAPS), and 35 mmol/L Tris-HCl (pH 7.2). The rehydration solution containing 8 mol/L urea, 4% CHAPS, 10 mmol/L dithiothreitol (DTT), and 0.2% carrier ampholytes (pH 3.0–10.0) was mixed with the solubilized protein samples (30 μg) and applied to immobilized pH gradient (IPG) strips (7 cm; Bio-Rad Laboratories, Hercules, CA, USA) at pH 3.0–10.0 in a re-swelling tray (Bio-Rad). Isoelectric focusing (IEF) was performed using a Protein IEF Cell (Bio-Rad), and 3 preset programs consisting of the first conditioning step (15 min, 250 Vh), the linear voltage ramping step (3 h, 4,000 Vh), and the maximum voltage ramping step (up to 30,000 Vh). After IEF, the strips were equilibrated with 0.375 mol/L Tris buffer (pH 8.8) containing 6 mol/L urea, 2% sodium dodecyl sulfate (SDS), 20% glycerol, 2% DTT, and 0.01% bromophenol blue. The equilibrated strips were equilibrated again with the same buffer supplemented with 2.5% iodoacetamide. 2D SDS-PAGE was conducted overnight with 12.5% separating polyacrylamide gel (8–10 cm) without a stacking gel at 20 mA per gel.

Image Analysis and In-gel Protein Digestion

Visualization of resolved protein spots on the gels was carried out by silver staining and scanned using a Fluor-S MultiImager (Bio-Rad). PDQUEST 2D Gel Analysis Software version 6 (Bio-Rad) was used to analyze spot intensities of each sample. After silver staining, individual spots were excised from the 2-DE gels and transferred into 1.5 mL tubes. Then, 30 mmol/L potassium ferricyanide and 100 mmol/L sodium thiosulfate were mixed (1:1 ratio) and 100 μL of the mixture was added to the sample and vortexed until the brownish color disappeared. Distilled water was added to the samples 3x to cease the reaction. Then, 500 μL of 200 mmol/L ammonium bicarbonate was added to cover the gel for 20 min. The solution was discarded, and the gel piece was dehydrated with 100 μL acetonitrile, followed

by drying using vacuum centrifugation. In-gel digestion was conducted as previously described (30). Briefly, digestion buffer with 12.5 ng/mL trypsin was added to the gel pieces containing protein spots and incubated for 45 min on ice. Next, the enzyme solution was removed and 20 μL of buffer without enzyme was added to maintain hydration during the enzymatic reaction overnight at 37°C . The gel pieces were then subjected to vigorous vortexing for 30 min. The digested solution was transferred into a new 1.5 mL tube and dried using vacuum centrifugation. Finally, the samples were dissolved in 2 μL 0.1% trifluoroacetic acid (TFA).

Peptide Mass Fingerprinting

For peptide mass fingerprinting, a matrix solution containing α -cyano-4-hydroxycinnamic acid (40 mg/mL) in 50% acetonitrile and 0.1% TFA was prepared. An equal volume of matrix solution was added to the sample solution and 2 μL was transferred to the matrix-assisted laser desorption/ionization time of flight (MALDI-TOF)/TOF target plate, quickly dried, and washed with deionized water. After drying for 10 min at room temperature, the mixture solution was subjected to MALDI-TOF-mass spectrometry (MS) and MS/MS analysis using an ABI 4800 Plus TOF-TOF Mass Spectrometer (Applied Biosystems, Framingham, MA, USA). The apparatus was set at 200-Hz Nd:355-nm YAG laser operation for analysis. Peaks with signal/noise ratios >25 were selected, and the 10 most intense ions were used for MS/MS analysis in 1 kV mode and 1,000–1,250 consecutive laser exposures. *Bos taurus* proteins from the National Center for Biotechnology Information (NCBI) protein database (version 20140415; 2,845 sequences, 921,323 residues) were used for analysis of all MALDI-TOF-MS spectra with a molecular mass range of $\pm 15\%$ of that estimated from 2-DE, allowing a peptide mass accuracy of 50 ppm. Protein Pilot V.3.0 database software (with the MASCOT V.2. 3.02 database search engine) was used for analysis of MS/MS spectral data at a mass tolerance of 50 ppm. Individual peptide ion scores were detected using a statistically significant threshold value of $P = 0.05$. The MS proteomic data have been presented in **Supplementary Data 1**.

ELISA

For quantitative detection of the three selected biomarkers (alpha-2-macroglobulin [A2M], transthyretin [TTR], and alpha-1-beta glycoprotein [A1BG]) in the serum of each animal, commercially available ELISA kits were used according to the manufacturer's instructions (MyBioSource, San Diego, CA, USA). The detection ranges of A2M, TTR, and A1BG were 0.156–10 $\mu\text{g/mL}$, 312.5–5,000 ng/mL, and 2.5–50 ng/mL, respectively. The intra and inter assay CV of ELISA kits were $<8\%$ and $<10\%$, respectively. A standard curve was generated to determine the concentration of each biomarker in the serum samples.

Statistical Analysis

ANOVA with Tukey's *post-hoc* test between different infection groups was conducted using GraphPad Prism software version 7.00 (GraphPad Software, Inc., La Jolla, CA, USA). A P -value < 0.05 was considered statistically significant. Receiver operating

characteristic (ROC) curve analysis was carried out for the determination of the area under the curve (AUC) and optimal cut-off values for each biomarker candidate. ROC curve analysis was performed using MedCalc software version 19.4 (MedCalc Software, Ostend, Belgium). The optimal cut-off values were determined as the value showing the maximum Youden Index ($J = Se + Sp - 1$). The ability to differentiate between different infection groups and the healthy control group was determined with the following meaning. In detail, biomarkers with AUC values ≥ 0.9 were considered to possess excellent discriminatory power. AUC values ≥ 0.8 and < 0.9 were considered to possess good discriminatory power. AUC values ≥ 0.7 and < 0.8 were considered to possess fair discriminatory power. AUC values < 0.7 were considered to have poor discriminatory power (31).

RESULTS

Animal Subjects

The characteristics of the 28 animals selected for serum profiling are summarized in **Table 1A**. The mean ELISA sample/positive (S/P) ratios of the healthy control, subclinical shedder, and clinical shedder groups were 4.16, 7.31, and 235.93, respectively. The mean ages of the cattle between the groups were not significantly different. The characteristics of the 126 animals selected for evaluation of the biomarker candidates are also summarized in **Table 1B**. The mean IDEXX ELISA S/P ratios for the healthy control, MAP-exposed, subclinical shedder, subclinical non-shedder, and clinical shedder groups were 3.73, 8.58, 5.84, 114.14, and 207.67, respectively. Similarly, the mean IDVET ELISA S/P ratios for these groups were 2.49, 8.01, 2.69, 90.25, and 183.35, respectively. Collectively, the mean ages of the cattle between the groups were not significantly different.

Protein Identification

In total, 12 significant regions were identified through MALDI-TOF/MS analysis, and a meaningful protein list was prepared (**Table 2** and **Figure 1**). Two proteins (complement C3 and TTR) were abundant only in the subclinical shedder group compared to the healthy control group, while four proteins (complement component 3d, A1BG precursor, complement component C9 precursor, and uncharacterized protein) were abundant only in the clinical shedder group. Furthermore, four proteins (apolipoprotein A-IV, A2M, IgM heavy chain constant region, and Kallikrein G) were abundant in both the subclinical and clinical shedder groups. Identification of the hIgG1 heavy chain constant region or bovine serum albumin suggested the possibility of incomplete removal of immunoglobulin and albumin. A2M, A1BG, and TTR were selected for further evaluation of diagnostic performance.

Biomarker ELISA

The serum levels of each biomarker candidate within different infection groups based on the results of serum ELISA and fecal PCR are shown in **Figure 2**. Serum A2M levels were significantly higher in the MAP-exposed ($p < 0.01$), subclinical shedder ($p < 0.0001$), subclinical non-shedder ($p < 0.0001$), and clinical shedder ($p < 0.0001$) groups than in the healthy control group.

The serum A1BG level was significantly higher in the MAP-exposed group than in the healthy control group ($p < 0.05$) and significantly lower in the subclinical shedder group than in the MAP-exposed group ($p < 0.01$). Additionally, the subclinical non-shedder group demonstrated a higher serum A1BG level than the subclinical shedder group ($p < 0.01$). The serum TTR level was significantly higher in the subclinical non-shedder group than in the healthy control group ($p < 0.05$), but did not differ significantly among the other infection groups.

Diagnostic Utility of Selected Biomarkers

Compared with the commercial ELISA kits, the diagnostic performance of candidate biomarker proteins was presented according to groups (**Table 3**). All subjects in groups 1, 2 and 3 corresponding to the clinical shedder were positive in A2M-ELISA. In particular, 25 out of 26 subjects in groups 5 and 6, which were subclinical non-shedder and showed positive only in one of the commercial kits, were diagnosed as positive by A2M-ELISA. Above all, in group 7 belonging to the subclinical shedder and group 8 belonging to the exposed group, 23 out of 27 subjects and 18 out of 20 subjects were diagnosed as positive in the diagnosis using A2M-ELISA, respectively (**Table 3**). ROC curve analysis suggested the possibility of discrimination between the different infection groups using biomarker-based ELISA. AUCs and their optimal cut-off values were calculated (**Figure 3**). Comparing the healthy control group ($n = 11$) and the infected cattle group altogether ($n = 115$), A2M ELISA possessed excellent discriminatory power with an AUC = 0.973 (95% confidence interval [CI]: 0.946–1.000, $p < 0.0001$), a sensitivity of 90.4%, and a specificity of 100%. Conversely, A1BG ELISA possessed poor discriminatory power with an AUC = 0.641 (95% CI: 0.543–0.739, $p = 0.0048$), a sensitivity of 50.4%, and a specificity of 100%. Similarly, TTR ELISA demonstrated poor discriminatory ability with an AUC value of 0.512 (95% CI: 0.348–0.677, $p = 0.8840$), a sensitivity of 15.7%, and a specificity of 100%. The IDEXX commercial ELISA kit demonstrated fair discriminatory ability with an AUC value of 0.796 (95% CI: 0.720–0.872, $p < 0.0001$), a sensitivity of 67.83%, and a specificity of 100%. In addition, the IDVET commercial ELISA kit demonstrated good discriminatory ability with an AUC value of 0.828 (95% CI: 0.753–0.904, $p < 0.0001$), a sensitivity of 73.04%, and a specificity of 100%. Comparison of ROC curves obtained using the three biomarkers to those obtained using the two commercial kits revealed that A2M demonstrated superior diagnostic performance (**Figure 3**).

DISCUSSION

Detection of protein biomarkers in biological fluids can be a promising method to diagnose and predict disease progression in mycobacterial infections in both animal and human medicine (32). Eradication of JD in the herd can be achieved by detecting subclinical MAP infection, but the current diagnostic tools require improvement. The present study revealed differences in host protein expression within the serum of MAP-infected cattle during different stages of JD progression, suggesting the

TABLE 1 | Clinical characteristics of the animal subjects in this study.**(A) Animals for the serum profiling for biomarker discovery**

		Healthy control (n = 10)	Subclinical shedder (n = 8)	Clinical shedder (n = 10)
Age, years, mean \pm SD		2.80 \pm 1.31	3.50 \pm 1.51	5.42 \pm 1.61
Sex, female		10 (100)	8 (100)	10 (100)
MAP isolation		0 (0)	1 (12.5)	8 (80)
Fecal PCR positive		0 (0)	8 (100)	10 (100)
Serum ELISA S/P ratio, mean \pm SD	IDEXX	4.06 \pm 1.85	7.31 \pm 4.15	235.93 \pm 27.67

(B) Animals for the evaluation of the biomarker candidates

		Healthy control (n = 11)	Exposed (n = 20)	Subclinical shedder (n = 28)	Subclinical non-shedder (n = 50)	Clinical shedder (n = 18)
Age, years, mean \pm SD		5.69 \pm 1.6	4.33 \pm 1.6	3.83 \pm 2.33	4.73 \pm 1.43	5 \pm 1.71
Sex, female		11 (100)	20 (100)	28 (100)	50 (100)	18 (100)
MAP isolation		0 (0)	0 (0)	1 (3.6)	0 (0)	14 (77.8)
Fecal PCR positive		0 (0)	0 (0)	28 (100)	0 (0)	18 (100)
Serum ELISA S/P ratio, mean \pm SD	IDEXX	3.73 \pm 1.82	8.58 \pm 11.74	5.84 \pm 7.79	114.21 \pm 54.14	207.67 \pm 102.30
	IDVet	2.49 \pm 1.24	8.01 \pm 5.59	2.69 \pm 2.16	90.25 \pm 77.14	183.35 \pm 60.99

Data are presented as numbers (percentages) unless otherwise stated.

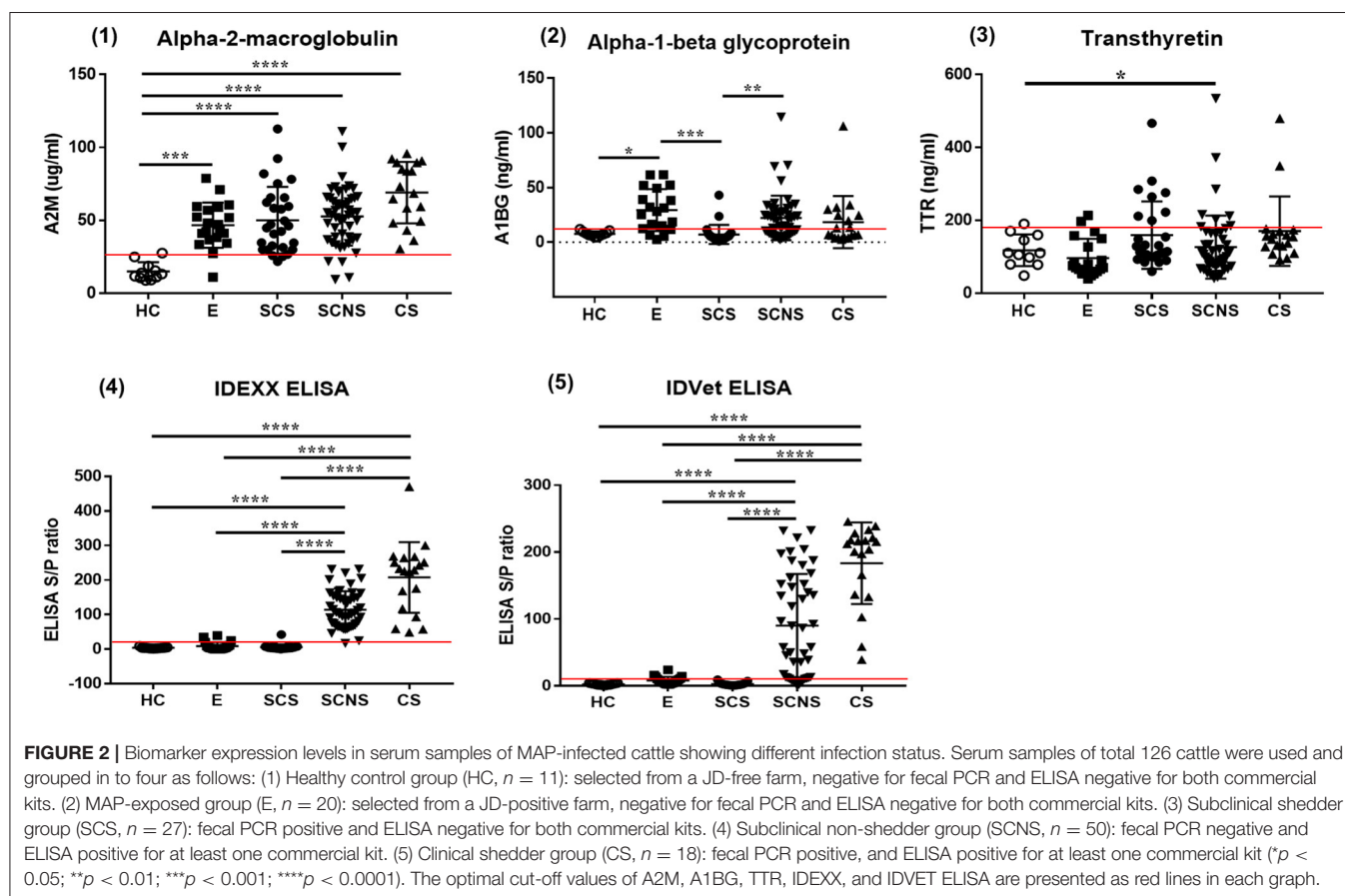
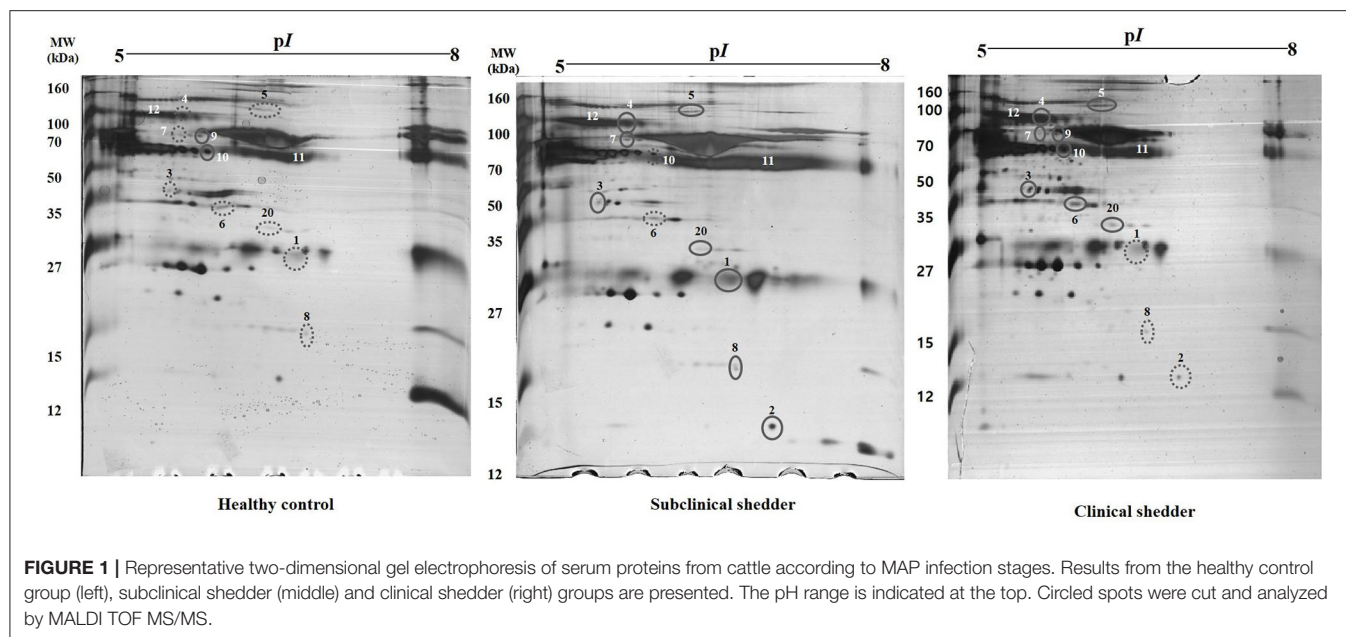
TABLE 2 | Identification of differentially expressed serum biomarkers in MAP-infected animals.

Spot No.	Protein Name	ID(NCBI)	MW (Da)	pI	Expectation value	Upregulation in group
1	Complement C3	A0A4W2D411	190190	8.36	3.20E-04	Subclinical shedder
2	Transthyretin	A0A4W2BU20	15831	5.91	2.40E-04	Subclinical shedder
3	Apolipoprotein A-IV	V6F7X3	42963	5.3	6.70E-24	Subclinical and clinical shedder
4	Alpha-2-macroglobulin	R9QSM8	134613	5.75	1.40E-04	Subclinical and clinical shedder
5	IgM heavy chain constant region	2232299	48512	5.68	3.10E+02	Subclinical and clinical shedder
6	Complement component 3d	Q693V9	34593	6.68	1.10E-20	Clinical shedder
7	alpha-1B-glycoprotein precursor	Q2KJF1	54091	5.29	2.40E-05	Clinical shedder
8	Kallikrein G	A0A1R3UGP4	28249	9.07	3.40E-02	Subclinical and clinical shedder
9	complement component C9 precursor	A0A3Q1MU98	58618	5.66	1.10E-08	Clinical shedder
10	Uncharacterized protein	A0A3Q1M3L6	41077	5.16	7.90E-04	Clinical shedder
11	hlgG1 heavy chain constant region	7547266	36510	6.09	2.70E-08	–
12	Inter-alpha-trypsin inhibitor heavy chain	F1MMD7	101620	6.22	5.00E-03	–

usefulness of a host biomarker-based diagnostic approach that provides improved sensitivity for subclinical infection.

We discovered 12 protein biomarkers for JD with the serum samples which have different stage of infection. Among the discovered biomarkers, three proteins (A2M, A1BG, and TTR) were selected according to their biological significance. One of the biologically significant protein was A2M. A2M is a large glycoprotein that involved in trapping a broad range of proteases for the host defense (33). A2M possesses available bait region for diverse proteases of pathogen and snares proteases using a cage-like structure through the structural rearrangement process with proteolytic activation (34). Mycobacterial proteases facilitate the invasion of host cells and promote growth during infection, and subsequently play an important role in intracellular survival and

disease progression (35). MAP0403 is a transmembrane protein that has 86% amino acid homology to Rv3671c, a serine protease of *M. tuberculosis* (36). The transposon mutant, which has an insertion in Rv3671c, exhibited increased susceptibility to an acidic environment and growth defects in a mouse model (37). Furthermore, a previous study revealed that the essentiality of serine protease MAP0403 for maintaining the intra-bacterial pH and response to acid stress *in vitro* and *in vivo* for intracellular survival (36). Another serine protease, MAP3292c, significantly enhanced intracellular survival and damage to the liver, spleen, and lung in mice (38). Further, MAP3292c facilitated the release of inflammatory cytokines such as IL-1 β , IL-6, and TNF- α in mice (38). Although the interaction between A2M and mycobacterial proteases has not yet been identified, the elevated serum A2M



level in MAP-infected animals might be in response to the release of MAP serine protease during infection. The interaction between A2M and mycobacterial proteases will be elucidated in further research.

In addition to inhibiting proteases, A2M modulates the biological activity of cytokines and growth factors such as TNF- α , IL-1 β , IL-2, IL-6, IL-10, bFGF, β -NGF, PDGF, and TGF- β (39). During the early stage of MAP infection, pro-inflammatory

TABLE 3 | Comparison of diagnostic performance using candidate biomarker proteins and commercial ELISA kits.

	Group*			A2M		A1BG		TTR		IDEXX ELISA		IDVET ELISA	
	PCR	IDEXX ELISA	IDVET ELISA	P	N	P	N	P	N	P	N	P	N
1	P	P	P	15	0	7	8	1	14	15	0	15	0
2	P	P	N	2	0	1	1	0	2	2	0	0	2
3	P	N	P	1	0	0	1	1	0	0	1	1	0
4	N	P	P	21	3	17	7	1	23	24	0	24	0
5	N	P	N	23	1	13	11	3	21	24	0	0	24
6	N	N	P	2	0	1	1	2	0	0	2	2	0
7	P	N	N	23	4	2	25	8	19	0	27	0	27
8	N	N	N	18	2	16	4	2	18	0	20	0	20
9	N	N	N	0	11	0	11	0	11	0	11	0	11

*Groups 1, 2, and 3 belong to the clinical shedder, groups 4, 5, and 6 to the subclinical non-shedder, and group 7 to the subclinical shedder. In addition, group 8 is occupied to the exposed group, and group 9 to the healthy control group. P, positive; N, negative.

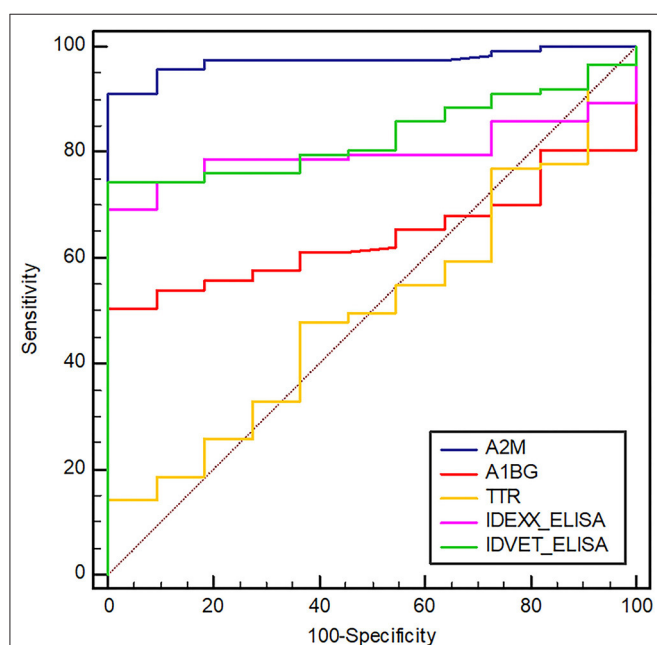


FIGURE 3 | Receiver operating characteristic (ROC) curves of selected biomarkers and two commercial ELISAs (IDEXX and IDVET). A2M, alpha-2-macroglobulin; A1BG, alpha-1-beta glycoprotein; TTR, transthyretin. The area under the ROC of A2M, A1BG, TTR, IDEXX, and IDVET ELISAs is 0.973, 0.641, 0.512, 0.796, and 0.828, respectively. The optimal cut-off values of A2M, A1BG, TTR, IDEXX, and IDVET ELISA are 27.56, 11.93, 190.13, 8.92, and 4.37, respectively.

cytokines such as IFN- γ , IL-12, TNF- α and IL-6 are significantly increased in MAP-infected animals compared to healthy control which indicating Th1 dominant immune response (40). On the contrary, immunologic shift arises from Th1 to Th2 with the progression of the disease suggesting the modulation of host immune response by pathogen. Therefore, upregulation of A2M in MAP-infected animals might be related to modulation of the immune response during disease progression. Elevated plasma A2M levels in tuberculous lymphadenitis, pulmonary

tuberculosis, and latent tuberculosis patients compared to healthy controls suggested a positive correlation between higher A2M levels and progression of mycobacterial infection (41). Similarly, A2M was also significantly increased in the serum of malnourished patients with active tuberculosis, suggesting a role for A2M in mycobacterial pathogenesis (42). A2M is mainly synthesized in liver and its production is affected by various cytokines such as TNF- α , IL-1 and IL-6 (42). In that regard, up-regulation of A2M can be induced by highly abundant pro-inflammatory cytokines in MAP-infected animal. In our study, A2M levels were significantly higher in MAP-infected animals which including exposed and subclinical cases. Taken together, we propose that A2M may serve as a promising biomarker for differentiation between MAP-infected and non-infected animals.

Other biologically significant proteins were A1BG and TTR. A1BG is a plasma glycoprotein which belongs to immunoglobulin supergene family that containing immunoglobulin like domains (43). TTR is a tetrameric plasma protein which involved in the transport of thyroid hormones and retinol (44). A1BG was significantly elevated only in exposed group compared to healthy control group. Also, elevated serum TTR level was detected in subclinical non-shedder group. However, there are no consistent changes between non-infected and infected cattle suggesting the low diagnostic value of A1BG and TTR in JD. These findings are contrary to previous research which have suggested that up-regulation of serum A1BG in experimentally MAP-infected cattle at 12 months post-infection (PI) compared to *M. bovis*-infected cattle (45). Furthermore, serum A1BG level was also up-regulated in MAP-infected cattle at 3 months PI while decreased in non-infected cattle at same time point (45). In addition, abundance of TTR in serum was increased in experimentally MAP-infected cattle at 3 months PI compared to non-infected cattle and elevated serum TTR level was consistent up to 10 months PI compared to non-infected cattle (45). Differences of A1BG and TTR expression in our study may be elucidated by the origin of sample. In detail, we used serum samples from naturally infected cattle which have over 1 year of age at least while Seth et al. (45) used experimentally

infected neonatal calves at 6 weeks of age which leading to different immune response compared to adult cattle.

Our results indicated that A2M ELISA yielded higher AUC value and sensitivity than the two commercial ELISA kits for detection of subclinical MAP-infected animals. Indeed, A2M ELISA demonstrated superior diagnostic performance for detection of MAP-infected animals, including subclinical cases. A2M ELISA detected 85.18% of subclinical shedder animals, while the IDEXX and IDVET ELISA kits detected 0%. Further, A2M ELISA detected 90% of subclinical non-shedder cases, while the IDEXX and IDVET ELISA kits detected 96 and 52%, respectively. Similarly, A2M ELISA detected 100% of clinical shedder animals, while the IDEXX and IDVET ELISA kits detected 94.44 and 88.88%, respectively. Taken together, A2M ELISA improved the detection rate of MAP-infected animals, especially for the subclinical shedder group.

The MAP-exposed animals were negative for fecal PCR and both commercial ELISA kits. However, all exposed animals were raised together with MAP-infected animals, and some exposed animals demonstrated fecal PCR positivity at different time points, suggesting the high possibility of MAP infection within the exposed group. Serum A2M levels in the MAP-exposed and subclinical shedder groups were significantly higher than those in the healthy control group, while this was not observed for serum levels of the other two biomarkers. Furthermore, elevated serum A2M levels were consistent in subclinical shedder, subclinical non-shedder, and clinical shedder groups. Therefore, increased serum A2M levels might be related to the host immune response against MAP infection at early stage.

The current study provides valuable information regarding host serum biomarkers for JD at different infection stages. However, despite rigorous effort, we were unable to collect a significant number of truly healthy control animal samples due to difficulty finding a JD-free farm. Furthermore, the detailed infection status of each animal, such as histological observations and results from cytokine assays and tissue bacterial cultures, would provide more reliable information for statistical analysis.

In conclusion, the urgent need for JD biomarkers to diagnose MAP-exposed and subclinical MAP-infected cattle arises due to the low sensitivity of current diagnostics methods such as commercial ELISA kits and fecal PCR. The identified serum protein A2M may improve the diagnosis of JD, especially in subclinical cases. Furthermore, the significant change in serum A2M levels in infected animals suggests its important role in JD pathogenesis. The current study reveals new possibilities to improve current JD diagnostic tools with further testing of serum biomarkers for accurate detection of subclinical cases, which may help eradicate JD in the herd.

REFERENCES

- Whitlock R H, Buergelt C. Preclinical and clinical manifestations of paratuberculosis (including pathology). *Vet Clin North Am Food Anim Pract.* (1996) 15:30410–2.

DATA AVAILABILITY STATEMENT

The original contributions presented in the study are included in the article/**Supplementary Material**, further inquiries can be directed to the corresponding author.

ETHICS STATEMENT

The animal study was reviewed and approved by In accordance with local legislation, all animal procedures used in this study were approved by the Animal Ethics Committee of Seoul National University (SNU-200525-4). Written informed consent was obtained from the owners for the participation of their animals in this study.

AUTHOR CONTRIBUTIONS

H-EP, HSY, and M-KS: conceptualization. H-EP, J-GC, and J-SP: investigation. H-TP and J-IS: resources. DK: software. MJ and H-LK: validation. S-CB and W-KL: data curation. M-KS and H-EP: writing—original draft preparation. HSY and M-KS: funding acquisition. All authors read and approved the final manuscript.

FUNDING

This research was supported by the Basic Science Research Program (2019R1A2C1006789) of the National Research Foundation (NRF) funded by the Ministry of Science, ICT (Information and Communication Technologies), and by a Grant (918020-4) from the Strategic Initiative for Microbiomes in Agriculture and Food, Ministry of Agriculture, Food and Rural Affairs, (as part of the (multi-ministerial) Genome Technology to Business Translation Program), Republic of Korea.

ACKNOWLEDGMENTS

The authors wish to thank Dr. Dong Won Bae of the section of Center for Research Facilities, Gyeongsang National University, for excellent technical supports.

SUPPLEMENTARY MATERIAL

The Supplementary Material for this article can be found online at: <https://www.frontiersin.org/articles/10.3389/fvets.2021.637716/full#supplementary-material>

Supplementary Data 1 | Mascot search results and raw data files for LC-MS/MS analysis for the identification of specific blood proteins in cattle with Johne's disease.

- Anderson JL, Meece JK, Koziczowski JJ, Clark DL Jr, Radcliff RP, Nolden CA, et al. *Mycobacterium avium* subsp. *paratuberculosis* in scavenging mammals in Wisconsin. *J Wildl Dis.* (2007) 43:302–8. doi: 10.7589/0090-3558-43.2.302
- Shaughnessy LJ, Smith LA, Evans J, Anderson D, Caldwell G, Marion G, et al. High prevalence of paratuberculosis in rabbits is associated with

- difficulties in controlling the disease in cattle. *Vet J.* (2013) 198:267–70. doi: 10.1016/j.tvjl.2013.08.030
4. Florou M, Leontides L, Kostoulas P, Billinis C, Sofia M, Kyriazakis I, et al. Isolation of *Mycobacterium avium* subspecies *paratuberculosis* from non-ruminant wildlife living in the sheds and on the pastures of Greek sheep and goats. *Epidemiol Infect.* (2008) 136:644–52. doi: 10.1017/S095026880700893X
 5. Bo M, Arru G, Niegowska M, Erre GL, Manchia PA, Sechi LA. Association between lipoprotein levels and humoral reactivity to *Mycobacterium avium* subsp. *paratuberculosis* in multiple sclerosis, type 1 diabetes mellitus and rheumatoid arthritis. *Microorganisms.* (2019) 7:423. doi: 10.3390/microorganisms7100423
 6. Bo M, Erre GL, Niegowska M, Piras M, Taras L, Longu MG, et al. Interferon regulatory factor 5 is a potential target of autoimmune response triggered by Epstein-Barr virus and *Mycobacterium avium* subsp. *paratuberculosis* in rheumatoid arthritis: investigating a mechanism of molecular mimicry. *Clin Exp Rheumatol.* (2018) 36:376–81.
 7. Dow CT, Sechi LA. Cows get crohn's disease and they're giving us diabetes. *Microorganisms.* (2019) 7:466. doi: 10.3390/microorganisms7100466
 8. Tiwari A, VanLeeuwen JA, McKenna SLB, Keefe GP, Barkema HW. John's disease in Canada Part I: Clinical symptoms, pathophysiology, diagnosis, and prevalence in dairy herds. *Can Vet J.* (2006) 47:874–82.
 9. Whittington RJ, Marsh IB, Reddacliff LA. Survival of *Mycobacterium avium* subsp. *paratuberculosis* in dam water and sediment. *Appl Environ Microbiol.* (2005) 71:5304–8. doi: 10.1128/AEM.71.9.5304-5308.2005
 10. Sung N, Collins MT. Variation in resistance of *Mycobacterium paratuberculosis* to acid environments as a function of culture medium. *Appl Environ Microbiol.* (2003) 69:6833–40. doi: 10.1128/AEM.69.11.6833-6840.2003
 11. Laurin E, McKenna S, Chaffer M, Keefe G. Sensitivity of solid culture, broth culture, and real-time PCR assays for milk and colostrum samples from *Mycobacterium avium* ssp. *paratuberculosis*-infectious dairy cows. *J Dairy Sci.* (2015) 98:8597–609. doi: 10.3168/jds.2014-8758
 12. Sevilla IA, Garrido JM, Molina E, Geijo MV, Elguezal N, Vázquez P, et al. Development and evaluation of a novel multicopy-element-targeting triplex PCR for detection of *Mycobacterium avium* subsp. *paratuberculosis* in feces. *Appl Environ Microbiol.* (2014) 80:3757–68. doi: 10.1128/AEM.01026-14
 13. Tasara T, Stephan R. Development of an F57 sequence-based real-time PCR assay for detection of *Mycobacterium avium* subsp. *paratuberculosis* in milk. *Appl Environ Microbiol.* (2005) 71:5957–68. doi: 10.1128/AEM.71.10.5957-5968.2005
 14. Stabel JR, Bannantine JP. Development of a nested PCR method targeting a unique multicopy element, ISMAP02, for detection of *Mycobacterium avium* subsp. *paratuberculosis* in fecal samples. *J Clin Microbiol.* (2005) 43:4744–50. doi: 10.1128/JCM.43.9.4744-4750.2005
 15. Acharya KR, Dhand NK, Whittington RJ, Plain KM. PCR inhibition of a quantitative PCR for detection of *Mycobacterium avium* subspecies *paratuberculosis* DNA in feces: diagnostic implications and potential solutions. *Front Microbiol.* (2017) 8:115. doi: 10.3389/fmicb.2017.00115
 16. Blanco Vázquez C, Alonso-Hearn M, Juste RA, Canive M, Iglesias T, Iglesias N, et al. Detection of latent forms of *Mycobacterium avium* subsp. *paratuberculosis* infection using host biomarker-based ELISAs greatly improves paratuberculosis diagnostic sensitivity. *PLoS ONE.* (2020) 15:e0236336. doi: 10.1371/journal.pone.0236336
 17. Tewari D, Hovingh E, Linscott R, Martel E, Lawrence J, Wolfgang D, et al. *Mycobacterium avium* subsp. *paratuberculosis* antibody response, fecal shedding, and antibody cross-reactivity to *Mycobacterium bovis* in *M. avium* subsp. *paratuberculosis*-infected cattle herds vaccinated against John's disease. *Clin Vaccine Immunol.* (2014) 21:698–703. doi: 10.1128/CVI.00032-14
 18. Naranjo-Lucena A, García-Campos A, Garza-Cuartero L, Britton L, Blanco A, Zintl A, et al. Fasciola hepatica products can alter the response of bovine immune cells to *Mycobacterium avium* subsp. *paratuberculosis*. *Parasite Immunol.* (2020) 42:e12779. doi: 10.1111/pim.12779
 19. Shaughnessy RG, Farrell D, Stojkovic B, Browne JA, Kenny K, Gordon SV. Identification of microRNAs in bovine faeces and their potential as biomarkers of John's Disease. *Sci Rep.* (2020) 10:5908. doi: 10.1038/s41598-020-62843-w
 20. Espinosa J, de la Morena R, Benavides J, García-Pariente C, Fernández M, Tesouro M, et al. Assessment of acute-phase protein response associated with the different pathological forms of bovine paratuberculosis. *Animals (Basel).* (2020) 10:1925. doi: 10.3390/ani10101925
 21. Cha SB, Yoo A, Park HT, Sung KY, Shin MK, Yoo HS. Analysis of transcriptional profiles to discover biomarker candidates in *Mycobacterium avium* subsp. *paratuberculosis*-infected macrophages. *RAW 264.7. J Microbiol Biotechnol.* (2013) 23:1167–75. doi: 10.4014/jmb.1302.02021
 22. Shin MK, Park H, Shin SW, Jung M, Lee S, K DY, et al. Host transcriptional profiles and immunopathologic response following *Mycobacterium avium* subsp. *paratuberculosis* infection in mice. *PLoS ONE.* (2015) 10:e0138770. doi: 10.1371/journal.pone.0138770
 23. Shin MK, Park H, Shin SW, Jung M, Im YB, Park H, et al. Whole-blood gene-expression profiles of cows infected with *Mycobacterium avium* subsp. *paratuberculosis* reveal changes in immune response and lipid metabolism. *J Microbiol Biotechnol.* (2015) 25:255–67. doi: 10.4014/jmb.1408.08059
 24. Park HE, Shin MK, Park HT, Jung M, Cho YI, Yoo HS. Gene expression profiles of putative biomarker candidates in *Mycobacterium avium* subsp. *paratuberculosis*-infected cattle. *Pathog Dis.* (2016) 74:ftw022. doi: 10.1093/femspd/ftw022
 25. Park HE, Park HT, Jung YH, Yoo HS. Establishment a real-time reverse transcription PCR based on host biomarkers for the detection of the subclinical cases of *Mycobacterium avium* subsp. *paratuberculosis*. *PLoS ONE.* (2017) 12:e0178336. doi: 10.1371/journal.pone.0178336
 26. Park HE, Park HT, Jung YH, Yoo HS. Gene expression profiles of immune-regulatory genes in whole blood of cattle with a subclinical infection of *Mycobacterium avium* subsp. *paratuberculosis*. *PLoS ONE.* (2018) 13:e0196502. doi: 10.1371/journal.pone.0196502
 27. De Sousa Abreu R, Penalva LO, Marcotte EM, Vogel C. Global signatures of protein and mRNA expression levels. *Mol Bio Syst.* (2009) 5:1512–26. doi: 10.1039/b908315d
 28. Zhang MZ, Zhang S. An efficient DNA extraction method for polymerase chain reaction-based detection of *Mycobacterium avium* subspecies *paratuberculosis* in bovine fecal samples. *J Vet Diagnostic Investig.* (2011) 23:41–8. doi: 10.1177/104063871102300106
 29. Seo JH, Youn JH, Kim EA, Jun JS, Park JS, Yeom JS, et al. *Helicobacter pylori* antigens inducing early immune response in infants. *J Korean Med Sci.* (2017) 32:1139–46. doi: 10.3346/jkms.2017.32.7.1139
 30. O'Connell KL, Stults JT. Identification of mouse liver proteins on two-dimensional electrophoresis gels by matrix-assisted laser desorption/ionization mass spectrometry of *in situ* enzymatic digests. *Electrophoresis.* (1997) 18:349–59. doi: 10.1002/elps.1150180309
 31. Muller MP, Tomlinson G, Marrie TJ, Tang P, McGeer A, Low DE, et al. Can routine laboratory tests discriminate between severe acute respiratory syndrome and other causes of community-acquired pneumonia? *Clin Infect Dis.* (2005) 40:1079–86. doi: 10.1086/428577
 32. Palmer MV, Thacker TC, Rabideau MM, Jones GJ, Kanipe C, Vordermeier HM, et al. Biomarkers of cell-mediated immunity to bovine tuberculosis. *Vet Immunol Immunopathol.* (2020) 220:109988. doi: 10.1016/j.vetimm.2019.109988
 33. Cater JH, Wilson MR, Wyatt AR. Alpha-2-macroglobulin, a hypochlorite-regulated chaperone and immune system modulator. *Oxid Med Cell Longev.* (2019) 2019:5410657. doi: 10.1155/2019/5410657
 34. Budd A, Blandin S, Levashina EA, Gibson TJ. Bacterial alpha2-macroglobulins: colonization factors acquired by horizontal gene transfer from the metazoan genome? *Genome Biol.* (2004) 5:R38. doi: 10.1186/gb-2004-5-6-r38
 35. Ribeiro-Guimarães ML, Pessolani MCV. Comparative genomics of mycobacterial proteases. *Microb Pathog.* (2007) 43:173–8. doi: 10.1016/j.micpath.2007.05.010
 36. Kugadas A, Lamont EA, Bannantine JP, Shoyama FM, Brenner E, Janagama HK, et al. A *Mycobacterium avium* subsp. *paratuberculosis* predicted serine protease is associated with acid stress and intraphagosomal survival. *Front Cell Infect Microbiol.* (2016) 6:85. doi: 10.3389/fcimb.2016.00085
 37. Vandal OH, Pierini LM, Schnappinger D, Nathan CF, Ehrh S. A membrane protein preserves intrabacterial pH in intraphagosomal *Mycobacterium tuberculosis*. *Nat Med.* (2008) 14:849–54. doi: 10.1038/nm.1795
 38. Liu H, Dang G, Zang X, Cai Z, Cui Z, Song N, Liu S. Characterization and pathogenicity of extracellular serine protease MAP3292c from

- Mycobacterium avium* subsp. *paratuberculosis*. *Microb Pathog.* (2020) 142:104055. doi: 10.1016/j.micpath.2020.104055
39. Armstrong PB, Quigley JP. Alpha2-macroglobulin: an evolutionarily conserved arm of the innate immune system. *Dev Comp Immunol.* (1999) 23:375–90. doi: 10.1016/S0145-305X(99)00018-X
 40. Stabel JR, Bannantine JP. Divergent antigen-specific cellular immune responses during asymptomatic subclinical and clinical states of disease in cows naturally infected with *Mycobacterium avium* subsp. *paratuberculosis*. *Infect Immun.* (2020) 88:e00650–19. doi: 10.1128/IAI.00650-19
 41. Kathamuthu GR, Moideen K, Kumar NP, Sridhar R, Baskaran D, Babu S. Altered systemic levels of acute phase proteins in tuberculous lymphadenitis and modulation after treatment. *PLoS ONE.* (2020) 15:e0233426. doi: 10.1371/journal.pone.0233426
 42. Bapat PR, Satav AR, Husain AA, Shekhawat SD, Kawle AP, Chu JJ, et al. Differential levels of alpha-2-macroglobulin, haptoglobin and sero-transferrin as adjunct markers for TB diagnosis and disease progression in the malnourished tribal population of Melghat, India. *PLoS ONE.* (2015) 10:e0133928. doi: 10.1371/journal.pone.0133928
 43. Ishioka N, Takahashi N, Putnam FW. Amino acid sequence of human plasma alpha 1B-glycoprotein: homology to the immunoglobulin supergene family. *Proc Natl Acad Sci U S A.* (1986) 83:2363–7. doi: 10.1073/pnas.83.8.2363
 44. Ingenbleek Y, Young V. Transthyretin (prealbumin) in health and disease: nutritional implications. *Annu Rev Nutr.* (1994) 14:495–533. doi: 10.1146/annurev.nu.14.070194.002431
 45. Seth M, Lamont EA, Janagama HK, Widdel A, Vulchanova L, Stabel JR, et al. Biomarker discovery in subclinical mycobacterial infections of cattle. *PLoS ONE.* (2009) 4:e5478. doi: 10.1371/journal.pone.0005478

Conflict of Interest: The authors declare that the research was conducted in the absence of any commercial or financial relationships that could be construed as a potential conflict of interest.

Copyright © 2021 Park, Park, Park, Choi, Shin, Jung, Kang, Baik, Lee, Kim, Yoo and Shin. This is an open-access article distributed under the terms of the Creative Commons Attribution License (CC BY). The use, distribution or reproduction in other forums is permitted, provided the original author(s) and the copyright owner(s) are credited and that the original publication in this journal is cited, in accordance with accepted academic practice. No use, distribution or reproduction is permitted which does not comply with these terms.



Electrochemical Detection of Serum Antibodies Against *Mycobacterium avium* Subspecies *paratuberculosis*

Kaoru Hatate¹, J. Hunter Rice², Karsten Parker², J. Jayne Wu³, Amy Turner⁴, Judith R. Stabel⁴ and Shigetoshi Eda^{1,2*}

¹ Department of Forestry, Wildlife and Fisheries, University of Tennessee Institute of Agriculture, Knoxville, Knoxville, TN, United States, ² Department of Microbiology, University of Tennessee, Knoxville, Knoxville, TN, United States, ³ Department of Electrical Engineering and Computer Science, University of Tennessee, Knoxville, Knoxville, TN, United States, ⁴ Agricultural Research Service, United States Department of Agriculture, National Animal Disease Center, Ames, IA, United States

OPEN ACCESS

Edited by:

Kumi de Silva,
The University of Sydney, Australia

Reviewed by:

Ratna B. Gurung,
National Centre for Animal Health,
Bhutan
Bharat Bhandari,
Anand Agricultural University, India

*Correspondence:

Shigetoshi Eda
seda@utk.edu

Specialty section:

This article was submitted to
Veterinary Infectious Diseases,
a section of the journal
Frontiers in Veterinary Science

Received: 16 December 2020

Accepted: 03 February 2021

Published: 09 March 2021

Citation:

Hatate K, Rice JH, Parker K, Wu JJ,
Turner A, Stabel JR and Eda S (2021)
Electrochemical Detection of Serum
Antibodies Against *Mycobacterium*
avium Subspecies *paratuberculosis*.
Front. Vet. Sci. 8:642833.
doi: 10.3389/fvets.2021.642833

Mycobacterium avium subsp. *paratuberculosis* (MAP) causes a chronic inflammatory intestinal disease, called Johne's disease (JD) in many ruminants. In the dairy industry, JD is responsible for significant economic losses due to decreased milk production and premature culling of infected animals. Test-and-cull strategy in conjunction with risk management is currently recommended for JD control in dairy herds. However, current diagnostic tests are labor-intensive, time-consuming, and/or too difficult to operate on site. In this study, we developed a new method for the detection of anti-*M. paratuberculosis* antibodies from sera of *M. paratuberculosis*-infected animals. *M. paratuberculosis* antigen-coated magnetic beads were sequentially reacted with bovine serum followed by a horseradish peroxidase (HRP)-labeled secondary antibody. The reaction of HRP with its substrate was then quantitatively measured electrochemically using a redox-active probe, ferrocyanide. After optimization of electrochemical conditions and concentration of the redox-active probe, we showed that the new electrochemical detection method could distinguish samples of *M. paratuberculosis*-infected cattle from those of uninfected cattle with greater separation between the two groups of samples when compared with a conventional colorimetric testing method. Since electrochemical detection can be conducted with an inexpensive, battery-operated portable device, this new method may form a basis for the development of an on-site diagnostic system for JD.

Keywords: Johne's disease, diagnosis, antibody, immunoassay, electrochemical sensing

INTRODUCTION

A bacterial pathogen, *Mycobacterium avium* subsp. *paratuberculosis* (MAP) infects the intestinal tissue of animals and causes a chronic wasting disease called Johne's disease (JD). JD affects domestic animals such as farm deer, sheep, and dairy cattle. The prevalence of JD in cattle in Australia, New Zealand, Europe, and the United States was estimated to range from 10 to 60% (1–4). United States Department of Agriculture (USDA) reported that 68.1% of dairy herds in the US are contaminated with MAP, and the most recent report estimated that the actual herd-level prevalence of MAP was higher than 90% (5). Clinical symptoms of JD include submandibular edema, emaciation, severe diarrhea, and reduction in milk production (6). Economic loss caused by JD in dairy herds is mostly due to the reduced milk production and premature

culling of JD-affected cattle (7). In the USA, JD causes an estimated annual loss of \$220 million to the agricultural economy (4, 8–10).

The current recommendation for JD control in dairy herds involves test-and-cull strategies in conjunction with risk management and intervention (11, 12). However, multiple mathematical modeling studies have suggested that this approach (test-and-cull) would require long-term effort, investment, and widespread compliance to effectively reduce JD prevalence in dairy herds (13–15). In a 6-years field study, the prevalence of JD in 9 dairy herds was reduced from 11.6 to 5.6% by applying ELISA-based control measures, but no statistically significant difference could be detected across the same population when MAP prevalence was estimated by the slower but more sensitive fecal culture test (16). Therefore, the test-and-cull approach itself is unlikely a cost-effective control measure and should be accompanied by the prevention of within-farm MAP transmission.

The fecal-oral mode of transmission has been identified as the most important route of infection for JD, while the contribution of alternative routes, such as infection through MAP-contaminated milk or colostrum, has more slowly gained attention (17, 18). Young animals (1-year-old or younger) are known to be especially susceptible to MAP infection (19–21), and a longitudinal study demonstrated JD in dairy farms could be reduced by preventing infection of young animals (calves and heifers) through feces and milk/colostrum (16). To achieve this, the results of ELISAs were used to inform animal segregation based on disease state and for the selection of MAP-free colostrum for feeding. A recent study showed a direct correlation between ELISA-positivity and rate of shedding of MAP into milk (up to 10^6 /ml of milk) (22), supporting the strategy of using ELISA results for the prevention of MAP transmission to young animals.

Currently, ELISA tests for JD are conducted in diagnostic laboratories, incurring long turnaround time (days to a week) and excess labor/shipment costs. Thus, the effectiveness of the aforementioned ELISA-based JD risk management measures could significantly be improved if all the steps of the assay were performed at the site of sample collection, on the farm. Also, since JD is often mischaracterized as an infection with another type of enteric pathogen, on-site diagnosis of JD could reduce unnecessary treatment of the animal with antibiotics. This study aims to develop a platform technology for rapid, on-site detection of antibodies against MAP for JD diagnosis. The principle of antibody detection in our method is based on the conventional ELISA, but for implementation into an inexpensive portable device, we utilized a magnetic-bead-based immunoassay (23) and a new electrochemical method for antibody detection.

The last step of the ELISA test is to quantify the reaction of enzyme tagged to the secondary antibody. A widely used enzyme is horseradish peroxidase (HRP), and the quantification of HRP can be done by measuring color, fluorescence, or chemiluminescence produced by HRP-substrate reaction. Since such detection requires bulky and/or expensive equipment, electrochemical detection approaches have been evaluated in previous studies. This study demonstrated that the analytical

sensitivity of the new electrochemical detection of HRP is comparable to a conventional optical method. Further, we tested the new electrochemical method for detecting anti-MAP antibodies in serum samples of JD-affected (MAP-infected) animals using magnetic beads for antibody binding future automation as described in our previous work (23).

MATERIALS AND METHODS

Reagents

A solution of 10 mM phosphate-buffered saline (pH 7.4, PBS) supplemented with 0.05% (v/v) surfactant Tween-20 (Thermo Fisher Scientific, Waltham, MA, USA) served as the wash solution (PBST). A buffer for serum dilution and blocking (Buffer B) was prepared by adding SuperBlock blocking solution (10 v/v%, Thermo Fisher Scientific/Pierce, Waltham, MA, USA) and Tween 20 (0.05 v/v, % Thermo Fisher Scientific, Waltham, MA, USA) to 10 mM (pH 7.4, PBS). Bovine serum albumin (BSA, Sigma-Aldrich, St. Louis, MO, USA) solution (1 w/v%) was prepared in PBST. HRP-labeled goat anti-bovine immunoglobulin G (H+L) obtained from Jackson ImmunoResearch (West Grove, PA, USA) was diluted in Buffer B immediately before use. Potassium ferrocyanide $\{K_4[Fe(CN)_6]\}$ and potassium ferricyanide $\{K_3[Fe(CN)_6]\}$ purchased from Thermo Fisher Scientific/ACROS Organics (Waltham, MA, USA) were stored dry and prepared fresh before each experiment. Purified HRP enzyme and 3,3', 5,5'-tetramethylbenzidine (TMB) substrate were purchased from Thermo Fisher Scientific (Waltham, MA, USA). Other chemicals such as acetone and 2-propanol were purchased from Thermo Fisher Scientific/Fisher Chemical (Waltham, MA, USA).

Serum Samples

A total of 15 bovine serum samples were obtained from USDA-National Animal Disease Center (NADC; Ames, IA, USA). The samples had been collected from Holstein dairy cows purchased from dairy farms in the USA (IA, MN, and ND) from 2014 to 2019. Among the 15 samples, five samples were collected from female Holstein cattle (3–12 years old, mean \pm SD = 5.2 ± 3.8) that had been diagnosed as negatives for JD by interferon-gamma, ELISA, and fecal culture test. All the negative samples were from animals maintained separately in the dairy barn at the USDA-NADC. The other 10 samples were collected from female Holstein cattle (4–8 years old, mean \pm SD = 5.8 ± 1.3) that had been diagnosed as JD positives by interferon-gamma, ELISA, and fecal culture test. Among the 10 infected animals tested in this study, five of them were shedding over 100 MAP/g of feces, four were shedding <100 (one of them was only <3 MAP/g feces), and the other one was unknown (culture contaminated). HyClone™ fetal bovine serum (FBS, GE Healthcare, Wauwatosa, WI, USA) was also used as a negative reference serum, and a pool of JD-ELISA (IDEXX)-positive bovine samples obtained from BioVet Inc. (called BV+, Beaudry Saint-Hyacinthe, Canada) was used as a positive reference serum. All serum samples were diluted 1:1 with glycerol and stored at -20°C until use.

Antibody Detection Assay

a. Ethanol-Vortex ELISA Test

Ethanol-Vortex ELISA test (EVELISA) was conducted as described in the previous report (24). Briefly, a 96-well plate was prepared by an overnight immobilization of 50 μ l ethanol-extracted MAP antigen and then blocked with Buffer B for 1 h, before 50 μ l of diluted serum samples (1:100 dilution in Buffer B) were inoculated for 30 min at room temperature. After washing the wells four times with PBS-T, 50 μ l of HRP-labeled goat anti-bovine secondary antibody (diluted 1:1,000 in Buffer B) was added and incubated at the room temperature another 30 min. After four more washes with PBST, 100 μ l of TMB substrate solution was added to each well, and optical density (OD) was measured at 655 nm after 16 min of reaction time had elapsed.

b. Bead-Based Antibody Detection Assay

The principle of the assay used in this study is depicted in **Figure 1**. In brief, MAP-antigen-coated magnetic beads were incubated with a bovine serum samples from a JD-infected or uninfected animal, and bound antibody was labeled with an HRP-tagged secondary antibody. After washing, the HRP-tagged secondary antibody remaining on the beads was detected either calorimetrically (OD measurement) or electrochemically [electrochemical impedance spectroscopy (EIS) measurement]. The detailed procedures are described below (**b-1** and **b-2**).

b-1. Bead-Based Antibody Binding Assay

The preparation of 80% ethanol extract (EE) of MAP Linda (human isolate) antigen was conducted as described previously (25, 26), and the protocol for antibody reactions on magnetic beads was similar to our previous work (23). Polystyrene coated magnetic beads (\varnothing 4.13 μ m, SpheroTech, Lake Forest, IL, USA) were suspended in diluted MAP EE (1:40 in absolute ethanol) with gently agitated on a shaker overnight at room temperature. The antigen-coated beads were blocked by 1% BSA for 30 min and the magnetic separation rack (Thermo Fisher Scientific, Waltham, MA) was used by acclimating the beads to replace supernatant with 100 μ l of diluted serum samples (1:50 in 1% BSA in PBST). After 30 min incubation at room temperature, the supernatant was removed and replaced with 100 μ l of diluted HRP-labeled goat anti-bovine secondary antibody (1:500 in 1% BSA in PBST) on the magnetic rack. Again for 30 min incubation on a shaker, the beads were washed with 500 μ l of PBST four times and a half portion of the last wash was left for the OD measurement, and the other half was left until electrochemical measurement.

b-2. Measurement of HRP Activity

b-2-1. Optical Density Measurement

To determine the limit of detection (LOD) for electrochemical measurement described below, the OD of the TMB solution reacted with different concentrations of HRP was compared with those measured by the electrochemical measurement. The A series of diluted HRP solutions was prepared by serially diluting HRP with PBST to make 1, 2, 4, 8, and 16 pM (the final concentrations). Fifty microliters of each HRP solution were reacted with 100 μ l of TMB substrate in a 96-well plate for 6 min, and OD value was read at 655 nm using a microplate reader (Bio-Rad, Hercules, CA). Simultaneously, the electrochemical reading of the same samples was performed as described below.

Each measurement was performed in triplicate. Similarly, the OD (655 nm) was measured after reacting a TMB solution with magnetic beads prepared as described in the Bead-based antibody binding assay section.

b-2-2. Electrochemical Measurement

A portable potentiostat (Autolab, PGSTAT204, Metrohm, Riverview, FL, USA) in coordination with NOVA software was used for the EIS measurement. Gold interdigitated microelectrodes (IDE, printed on a ceramic substrate with 100 mm gaps, Metrohm, Riverview, FL, USA) were immersed in an acetone bath and rinsed with 2-propanol and purified water ($>18 \text{ M}\Omega \times \text{cm}$) sequentially before use. Before measurement, the impedance of a solution of 5 mM ferrocyanide and ferricyanide mixture was recorded to ensure the quality (cleanness) of each IDE microelectrode. IDE electrodes that gave 500 Ω or less on the imaginary axis at the peak of the hemisphere on the Nyquist plot were used for the assay. After the sample was reacted with TMB substrate for 6 min in the dark, a ferrocyanide solution was added to the sample (2–20 μ l of the sample) to make the concentration indicated in each figure before loading onto the IDE microelectrode. The impedance was recorded at frequencies ranging from 100 to 10 kHz. The IDE microelectrode was rinsed thoroughly with purified water and air-dried between readings. Each measurement was performed in duplicate. For EIS analysis, the values of charge transfer impedance (R_{ct}) were calculated by using the NOVA software.

The R_{ct} of a control buffer was used to normalize R_{ct} of the tested samples. Reciprocal of the ratio (RR) was calculated by dividing the R_{ct} of a control buffer [a mixture of 20 μ l TMB buffer and 2 μ l ferrocyanide solution [50 mM]] by that of each tested sample. The reciprocal value was used since R_{ct} decreases as the HRP–TMB reaction proceeds.

$$RR = \left\{ \frac{R_{ct} \text{ of the control buffer}}{R_{ct} \text{ of the sample}} \right\} \quad (1)$$

Statistical Analysis

Sample-to-positive (S/P) ratios were calculated according to the following equation:

$$S/P = \left\{ \frac{\text{Value of sample} - \text{value of FBS control}}{\text{Value of BV}^+ \text{ control} - \text{value of FBS control}} \right\}, \quad (2)$$

where “value” refers to either RR or OD. Pearson’s correlation analysis and Mann–Whitney U test were performed in Excel and R, respectively. The LOD was estimated as described previously (27, 28). Briefly, the RR or OD values were plotted against the HRP concentrations (1–4 pM and 1–16 pM, respectively). A linear regression generated in Excel was used to find the values of slope and y-intercept of the line of best fit. The SD of the data was multiplied by 3 and added to the y-intercept, which was then used to find the LOD (i.e., the corresponding concentration of HRP on the linear regression line).

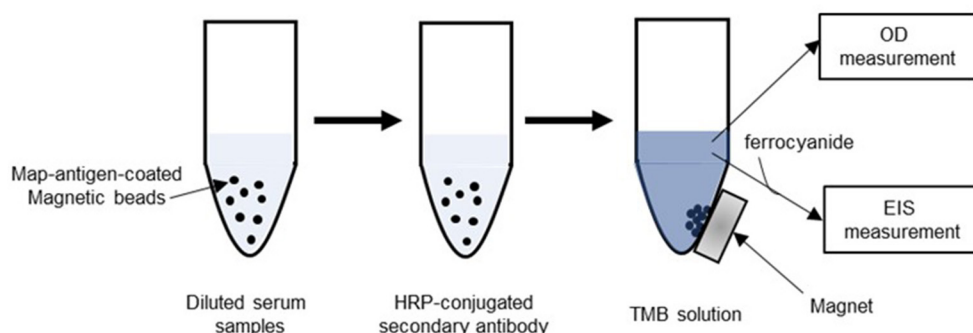


FIGURE 1 | Schematic of bead-based antibody binding assay. Magnetic beads coated with antigen of *Mycobacterium avium* subsp. *paratuberculosis* (MAP) were treated with diluted bovine serum samples from Johne's disease (JD)-positive and negative animals. After removal of the serum solution, the beads were then incubated with secondary antibody (anti-bovine immunoglobulin antibody) conjugated with horseradish peroxidase (HRP). After washing, the beads were reacted with 3,3',5,5'-tetramethylbenzidine (TMB) followed by a 6-min incubation. The TMB solution was subjected to the colorimetric or electrochemical measurement. For the electrochemical measurement, a ferrocyanide solution was added to the TMB solution prior to the measurement.

RESULTS

Optimization of Assay Conditions for Electrochemical Measurement of HRP Activity

A solution of HRP at 8 pM was used for the optimization of the electrochemical detection method. The solution was reacted with TMB solution, mixed with a ferrocyanide solution, and loaded onto an IDE microelectrode followed by an EIS measurement. In **Figure 2A**, different voltages were applied to the IDE microelectrode for the EIS measurement. The highest RR value was obtained at 1 mV but the variation among the triplicate measurements (SD of 109.3) was higher than that obtained at other voltages. Based on this result, 5 mV was used in the following experiments. As shown in **Figure 2B**, the highest RR value was obtained at 0.16 mM ferrocyanide (labeled 1/32X in the figure), and the concentration was used in the following experiments.

Comparison of Electrochemical and Colorimetric Measurements of HRP Activity

The electrochemical measurement of HRP activity was compared with a conventional colorimetric measurement by testing different HRP concentrations ranging from 1 to 16 pM. A strong linear correlation was observed when the electrochemical (RR) and colorimetric measurements (OD) were plotted on a semi-log scattered plot ($R^2 = 0.9376$, $RR = 0.0331e^{56.3OD}$) (**Figure 3**). The difference of ODs at the level of 0.01 (1 and 2 pM HRP) could be differentiated by the electrochemical method with a statistical significance (t -test, $p < 0.05$). Under the tested condition (6 min reaction of HRP and TMB), the LODs of the colorimetric and electrochemical method for the detection of HRP were estimated to be 0.94 pM (41 pg/ml) and 1.35 pM (58.9 pg/ml), respectively.

Comparison of Anti-MAP Antibody Detection Using the New Electrochemical Method and EVELISA

Fifteen bovine serum samples were collected from dairy cattle with known JD status and tested for anti-MAP antibody by using the new electrochemical method and the EVELISA test (24, 29) (**Figure 4**). For the electrochemical method, MAP antigen was immobilized on magnetic beads and reacted with bovine serum followed by an HRP-conjugated secondary antibody. In both methods, JD-negative (N) and JD-positive (P) samples were clearly separated, and the differences between the two groups (N and P) were statistically significant ($p < 0.01$, Mann-Whitney U test). As shown in the figure, the separation between the highest negative and lowest positive was greater when the samples were tested by the electrochemical method (0.02 vs. 0.586) than when they were tested by the EVELISA test (0.285 vs. 0.454).

DISCUSSION

Due to the lack of practical treatment for JD control, the detection and removal of JD-positive animals are recommended for the reduction of the burden of the disease on the dairy farms (30). Our group developed the ELISA test (named EVELISA) that showed a higher sensitivity for the detection of anti-MAP antibodies in serum and milk of cattle tested positive for MAP infection by the fecal culture test (29, 31, 32). However, mathematical modeling studies (15, 33, 34) indicated that ELISA-based JD control can be prohibitively costly, especially in the first few years after implementation of more stringent control measures, and the approach may not be economically feasible for many dairy farmers. Also, there is still a requirement for the ELISA procedure to be conducted in well-equipped diagnostic laboratories, causing a long turnaround time (from days to a week). Despite the drawbacks of the ELISA and the difficulties with implementing an effective MAP-management strategy, "on-site" detection of anti-MAP antibodies in serum or milk may still be useful in some scenarios, such as (1)

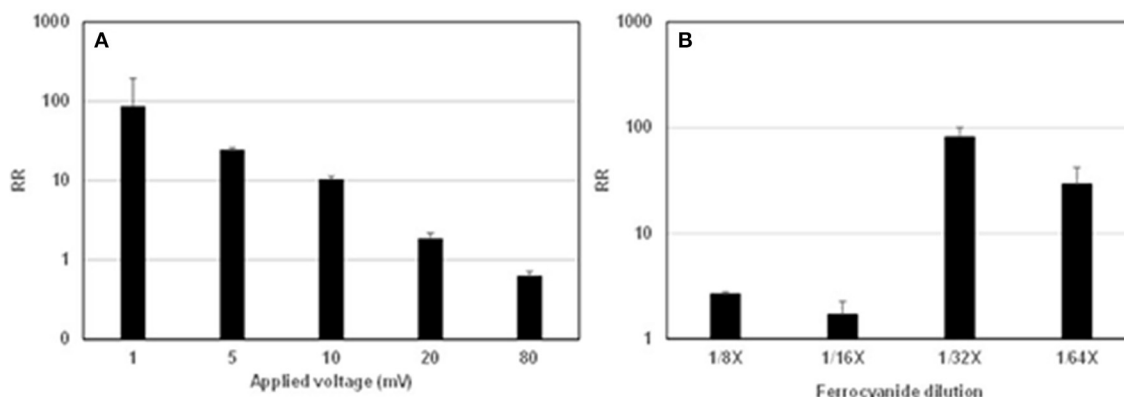


FIGURE 2 | Optimization of assay conditions for electrochemical measurement of HRP activity. The y-axis represents the reciprocal ratio (RR) values calculated as described in the method section. **(A)** Different voltages were applied to the interdigitated microelectrode (IDE) at the measurement of HRP activity. The experiment was conducted with three replicates. A similar result was obtained in a separate experiment. **(B)** Concentrations of ferrocyanide [1/8X (0.6 mM), 1/16 (0.3 mM), 1/32X (0.15 mM), and 1/64 (0.08 mM)] were added to the HRP–TMB reaction solution prior to the electrochemical measurement of HRP activity.

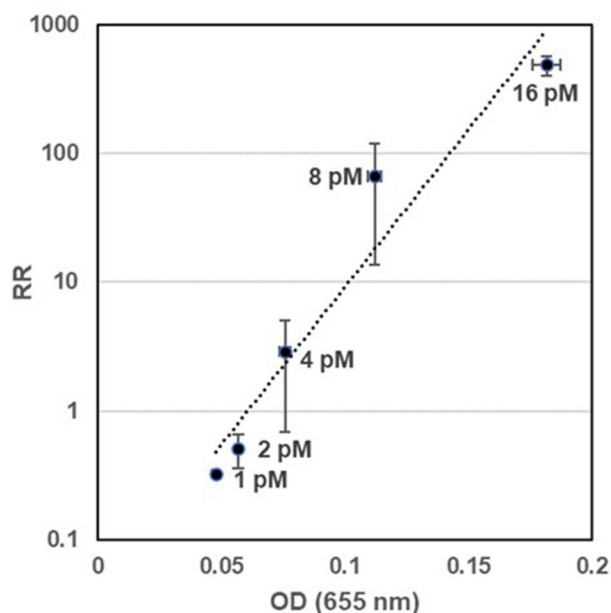


FIGURE 3 | Comparison of electrochemical and colorimetric measurements of HRP activity. HRP–TMB reaction was measured using the optimized electrochemical method and a conventional colorimetric method [measurement of the optical density (OD) at 655 nm] at different HRP concentrations. HRP concentrations (pM) used in the experiment were indicated next to each dot. The experiment was conducted with three replicates. A similar result was obtained in a separate experiment.

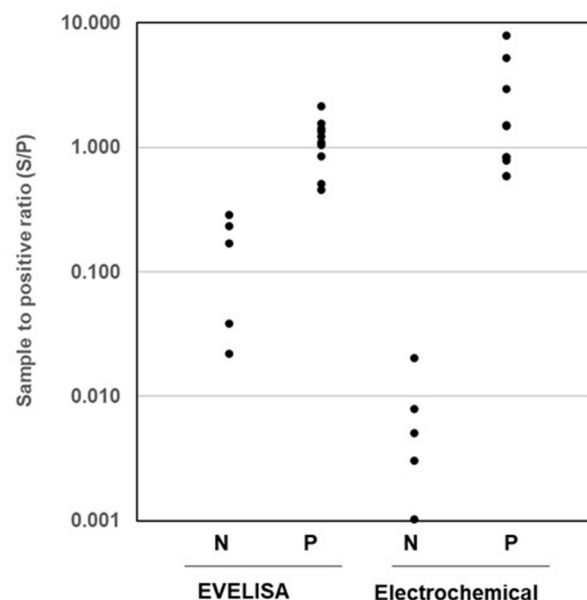


FIGURE 4 | Comparison of anti-MAP antibody detection using the Ethanol-Vortex ELISA test (EVELISA) and new electrochemical method. Serum samples from 5 JD-negative (N) and 10 JD-positive (P) samples were tested by the EVLISA and the electrochemical method. The experiment was conducted with two replicates. A similar result was obtained in a separate experiment.

rapid screening of animals for JD before importing them into a new dairy herd, (2) examining dams for JD status to avoid feeding calves with colostrum/milk contaminated with MAP, and (3) segregating anti-MAP antibody-positive and negative cattle within maternity pens (16). This study aimed to develop base technology for on-site detection of anti-MAP antibodies in dairy

cattle by combining magnetic-bead-based immunoassay and a new electrochemical method for HRP detection.

Several studies used electrochemical methods, such as chronoamperometry (CA) and cyclic voltammetry (CV), for the detection of HRP–TMB reaction (35–38). All the studies directly detected TMB oxidized by HRP and did not use ferrocyanide. For example, Singh et al. used CA for electrochemical direct detection of oxidized TMB for the detection of serum antibodies against

parasitic nematode, *Ostertagia ostertagi* (35). The antibody-antigen reaction was conducted in a regular ELISA plate and, after the reaction, the TMB-containing solution was transferred onto an electrode for the electrochemical measurement. The difference between positive and negative serum samples was found to be 1.6 times greater than an optical ELISA method. In the present study, the difference between positive and negative samples observed with the new electrochemical method (293-fold, 0.586/0.02) was much greater than that obtained with an optical ELISA method (1.6-fold, 0.454/0.285). There are several potential explanations for this improvement in our protocol including the difference in the antibody-antigen reaction format [i.e., plate-based in Singh's vs. magnetic bead-based in our study (23)]. Another difference is that our protocol included a redox reagent, ferrocyanide, to facilitate charge transfer at the surface of the electrode. Another recent study by Barhoumi et al. also utilized CA for direct detection of HRP-TMB reaction (36). In the study, a capture antibody against tumor necrosis factor (TNF)- α was immobilized onto an electrode through magnetic microparticles, reacted with a TNF-containing solution followed by reaction with a detection anti-TNF antibody labeled with HRP. After reacting with TMB, CA reading was conducted to quantify TMB oxidized by the HRP on the electrode. The LOD of the method for TNF quantification was estimated to be 0.2 pg/ml (0.01 pM). The LOD of our method for HRP detection was much higher 58.9 pg/ml (1.35 pM); however, such direct comparison may not be meaningful as (1) the secondary antibody used in the Barhoumi study may have been labeled with multiple HRP molecules, (2) TMB reaction was occurring at the electrode in their study while ours occur in a solution, and, more importantly, (3) the LOD of our method is likely improved if we extend the HRP-TMB reaction time. For direct comparison, we tested JD-negative and JD-positive samples with the new electrochemical method (impedance analysis of ferrocyanide-mediated oxidized TMB detection), which performed better than previously reported protocols (direct detection of oxidized TMB with CA or CV) and found that the new protocol differentiated the positive samples from negative samples with much greater separation than the previous protocols (**Supplementary Figure 1**).

By using the MAP antigen used in EVELISA, we demonstrated that a magnetic-bead-based immunoassay for anti-MAP antibody detection can be carried out in a microfluidic system (23). Magnetic-bead-based immunoassay has some advantages over ELISA, such as a high surface-to-volume ratio for antigen immobilization and compatibility with the microfluidic system. However, since our previous study utilized a fluorescent tag for the detection of secondary antibody (23), it required bulky and expensive equipment for the assay. Therefore, in this study, the new electrochemical detection method was combined with the magnetic-bead-based immunoassay we developed in the previous work. A similar concept has been used in several previous studies (36, 39, 40), but this study is unique in that

the new electrochemical method was used for the diagnosis the target disease, JD. Since we tested a limited number of samples in this study, the diagnostic sensitivity and specificity cannot be discussed; however, further studies are warranted based on the observation that the separation between negative and positive samples was greater when the samples were tested by the electrochemical method than that tested by the EVELISA test. In summary, this study provides a base technology for the development of an on-site detection of serum antibodies against MAP for JD control. Once developed, the costs for the on-site detection system (\$2 per sample and \$200 for equipment) are expected to be less expensive than the ELISA test (\$5 per sample and \$5,000 for equipment).

DATA AVAILABILITY STATEMENT

The raw data supporting the conclusions of this article will be made available by the authors, without undue reservation.

AUTHOR CONTRIBUTIONS

SE and JR: conceptualization. KH, JR, and KP: data curation. KH, SE, JR, KP, and JW: data analysis. SE, JW, and JS: funding acquisition and supervision. JR and KH: methodology. SE: project administration. SE, JW, JS, and AT: resources. KH, SE, and JR: visualization. KH and SE: writing (original draft). KH, JR, KP, JW, AT, JS, and SE: writing (review and editing). All authors contributed to the article and approved the submitted version.

FUNDING

This study has been supported by funding from the University of Tennessee (UT) Research Foundation Technology Maturation Grant, UT Student Faculty Award, and USDA—Foreign Agricultural Service Borlaug Fellowship Program.

ACKNOWLEDGMENTS

We would like to thank Haley Dylewski, Xin Xia, and Yu Jiang for their excellent technical support.

SUPPLEMENTARY MATERIAL

The Supplementary Material for this article can be found online at: <https://www.frontiersin.org/articles/10.3389/fvets.2021.642833/full#supplementary-material>

Supplementary Figure 1 | Comparison of (A) electricalchemical impedance spectroscopy (EIS), (B) cyclic voltammetry (CV), and (C) chronoamperometry (CA) for detection of oxidized TMB. JD-negative [fetal bovine serum (FBS), gray dots] and JD-positive control (BV+, black dots) samples were tested by using the new electrochemical method (A) with ferrocyanide and previously reported direct TMB detection with CV (B) and CA (C). It clearly shows that the new method performed better than the previous methods in separating the positive sample from negative sample.

REFERENCES

- Harris NB, Barletta RG. *Mycobacterium avium* subsp. paratuberculosis in veterinary medicine. *Clin Microbiol Rev.* (2001) 14:489–512. doi: 10.1128/CMR.14.3.489-512.2001
- Kennedy DJ, Benedictus G. Control of *Mycobacterium avium* subsp. paratuberculosis infection in agricultural species. *Rev Sci Tech.* (2001) 20:151–79. doi: 10.20506/rst.20.1.1274
- Linnabary RD, Meerdink GL, Collins MT, Stabel JR, Sweeney RW, Washington MK, et al. *Johne's Disease in Cattle, Council for Agricultural Science and Technology*. Ames, IA (2001). p. 1–10.
- Garvey M. *Mycobacterium avium* paratuberculosis: a disease burden on the dairy industry. *Animals.* (2020) 10:1773. doi: 10.3390/ani10101773
- Lombard JE, Gardner IA, Jafarzadeh SR, Fossler CP, Harris B, Capsel RT, et al. Herd-level prevalence of *Mycobacterium avium* subsp. paratuberculosis infection in United States dairy herds in 2007. *Prev Vet Med.* (2012) 108:234–8. doi: 10.1016/j.prevetmed.2012.08.006
- Fecteau ME, Whitlock RH. Paratuberculosis in cattle. In: Behr MA, Collins DM, editors. *Paratuberculosis Organism, Disease, Control*. Cambridge, MA: CAB International (2010). p. 144–56. doi: 10.1079/9781845936136.0144
- Wilson DJ, Rossiter C, Han HR, Sears PM. Association of *Mycobacterium paratuberculosis* infection with reduced mastitis, but with decreased milk production and increased cull rate in clinically normal dairy cows. *Am J Vet Res.* (1993) 54:1851–7.
- Sweeney RW. Transmission of paratuberculosis. *Vet Clin North Am Food Anim Pract.* (1996) 12:305–12. doi: 10.1016/S0749-0720(15)30408-4
- Stabel JR. Johne's disease: a hidden threat. *J Dairy Sci.* (1998) 81:283–8. doi: 10.3168/jds.S0022-0302(98)75577-8
- Ott SL, Wells SJ, Wagner BA. Herd-level economic losses associated with Johne's disease on US dairy operations. *Prev Vet Med.* (1999) 40:179–92. doi: 10.1016/S0167-5877(99)00037-9
- Collins MT, Gardner IA, Garry FB, Roussel AJ, Wells SJ. Consensus recommendations on diagnostic testing for the detection of paratuberculosis in cattle in the United States. *J Am Vet Med Assoc.* (2006) 229:1912–9. doi: 10.2460/javma.229.12.1912
- Sweeney RW, Collins MT, Koets AP, McGuirk SM, Roussel AJ. Paratuberculosis (Johne's Disease) in cattle and other susceptible species. *J Vet Intern Med.* (2012) 26:1239–50. doi: 10.1111/j.1939-1676.2012.01019.x
- Kudahl AB, Sorensen JT, Nielsen SS, Ostergaard S. Simulated economic effects of improving the sensitivity of a diagnostic test in paratuberculosis control. *Prev Vet Med.* (2007) 78:118–29. doi: 10.1016/j.prevetmed.2006.10.004
- Lu Z, Schukken YH, Smith RL, Grohn YT. Stochastic simulations of a multi-group compartmental model for Johne's disease on US dairy herds with test-based culling intervention. *J Theor Biol.* (2010) 264:1190–201. doi: 10.1016/j.jtbi.2010.03.034
- Massaro T, Lenhart S, Spence M, Drakes C, Yang G, Agosto F, et al. Modeling for cost analysis of Johne's disease control based on EVELISA testing. *J Biol Syst.* (2013) 21:13400101–17. doi: 10.1142/S021833901340010X
- Collins MT, Eggleston V, Manning EJ. Successful control of Johne's disease in nine dairy herds: results of a six-year field trial. *J Dairy Sci.* (2010) 93:1638–43. doi: 10.3168/jds.2009-2664
- Dore E, Pare J, Cote G, Buczinski S, Labrecque O, Roy JP, et al. Risk factors associated with transmission of *Mycobacterium avium* subsp. paratuberculosis to calves within dairy herd: a systematic review. *J Vet Intern Med.* (2012) 26:32–45. doi: 10.1111/j.1939-1676.2011.00854.x
- Whittington RJ, Windsor PA. *In utero* infection of cattle with *Mycobacterium avium* subsp. paratuberculosis: a critical review and meta-analysis. *Vet J.* (2009) 179:60–9. doi: 10.1016/j.tvjl.2007.08.023
- Mitchell RM, Medley GF, Collins MT, Schukken YH. A meta-analysis of the effect of dose and age at exposure on shedding of *Mycobacterium avium* subspecies paratuberculosis (MAP) in experimentally infected calves and cows. *Epidemiol Infect.* (2012) 140:231–46. doi: 10.1017/S0950268811000689
- Larsen AB, Merkall RS, Cutlip RC. Age of cattle as related to resistance to infection with *Mycobacterium paratuberculosis*. *Am J Vet Res.* (1975) 36:255–7.
- Windsor PA, Whittington RJ. Evidence for age susceptibility of cattle to Johne's disease. *Vet J.* (2010) 184:37–44. doi: 10.1016/j.tvjl.2009.01.007
- Steuer P, Collado B, Avilez C, Tejeda C, Soto JP, Salgado M. Is the transmission of *Mycobacterium avium* subspecies paratuberculosis (MAP) infection through milk intended to feed calves an overlooked item in paratuberculosis control programs? *Trop Anim Health Prod.* (2020) 52:89–94. doi: 10.1007/s11250-019-01988-x
- Wadhwa A, Foote RS, Shaw RW, Eda S. Bead-based microfluidic immunoassay for diagnosis of Johne's disease. *J Immunol Methods.* (2012) 382:196–202. doi: 10.1016/j.jim.2012.06.006
- Eda S, Bannantine JP, Waters WR, Mori Y, Whitlock RH, Scott MC, et al. A highly sensitive and subspecies-specific surface antigen enzyme-linked immunosorbent assay for diagnosis of Johne's disease. *Clin Vaccine Immunol.* (2006) 13:837–44. doi: 10.1128/0140-06
- Bannantine JP, Wadhwa A, Stabel JR, Eda S. Characterization of ethanol extracted cell wall components of *Mycobacterium avium* Subsp. paratuberculosis. *Vet Sci.* (2019) 6:88. doi: 10.3390/vetsci6040088
- Wadhwa A, Johnson RE, Eda K, Waters WR, Palmer MV, Bannantine JP, et al. Evaluation of ethanol vortex ELISA for detection of bovine tuberculosis in cattle and deer. *BMC Vet Res.* (2014) 10:147. doi: 10.1186/1746-6148-10-147
- Alankar Shrivastava VBH. Methods for the determination of limit of detection and limit of quantitation of the analytical methods. *Chron Young Sci.* (2011) 2:21–5. doi: 10.4103/2229-5186.79345
- Fanjul-Bolado P, Gonzalez-Garcia MB, Costa-Garcia A. Amperometric detection in TMB/HRP-based assays. *Anal Bioanal Chem.* (2005) 382:297–302. doi: 10.1007/s00216-005-3084-9
- Wadhwa A, Bannantine JP, Byrem TM, Stein TL, Saxton AM, Speer CA, et al. Optimization of serum EVELISA for milk testing of Johne's disease. *Foodborne Pathog Dis.* (2012) 9:749–54. doi: 10.1089/fpd.2011.1115
- Gardner IA, Nielsen SS, Whittington RJ, Collins MT, Bakker D, Harris B, et al. Consensus-based reporting standards for diagnostic test accuracy studies for paratuberculosis in ruminants. *Prev Vet Med.* (2011) 101:18–34. doi: 10.1016/j.prevetmed.2011.04.002
- Scott MC, Bannantine JP, Kaneko Y, Branscum AJ, Whitlock RH, Mori Y, et al. Absorbed EVELISA: a diagnostic test with improved specificity for Johne's disease in cattle. *Foodborne Pathog Dis.* (2010) 7:1291–6. doi: 10.1089/fpd.2010.0541
- Speer CA, Scott MC, Bannantine JP, Waters WR, Mori Y, Whitlock RH, et al. A novel enzyme-linked immunosorbent assay for diagnosis of *Mycobacterium avium* subsp. paratuberculosis infections (Johne's Disease) in cattle. *Clin Vaccine Immunol.* (2006) 13:535–40. doi: 10.1128/0140-06
- Robins J, Bogen S, Francis A, Westhoek A, Kanarek A, Lenhart S, et al. Agent-based model for Johne's disease dynamics in a dairy herd. *Vet Res.* (2015) 46:68. doi: 10.1186/s13567-015-0195-y
- De Silva KR, Eda S, Lenhart S. Modeling environmental transmission of MAP infection in dairy cows. *Math Biosci Eng.* (2017) 14:1001–17. doi: 10.3934/mbe.2017052
- Singh B, Flampouri E, Dempsey E. Electrochemical enzyme-linked immunosorbent assay (e-ELISA) for parasitic nematode *Ostertagia ostertagi* (brown stomach worm) infections in dairy cattle. *Analyst.* (2019) 144:5748–54. doi: 10.1039/C9AN00982E
- Barhoumi L, Bellagambi FG, Vivaldi FM, Baraket A, Clement Y, Zine N, et al. Ultrasensitive immunosensor array for TNF-alpha detection in artificial saliva using polymer-coated magnetic microparticles onto screen-printed gold electrode. *Sensors (Basel).* (2019) 19:692. doi: 10.3390/s19030692
- Shoae N, Forouzandeh M, Omidfar K. Voltammetric determination of the *Escherichia coli* DNA using a screen-printed carbon electrode modified with polyaniline and gold nanoparticles. *Mikrochim Acta.* (2018) 185:217. doi: 10.1007/s00604-018-2749-y
- Lin M, Song P, Zhou G, Zuo X, Aldalbahi A, Lou X, et al. Electrochemical detection of nucleic acids, proteins, small molecules and cells using a DNA-nanostructure-based universal biosensing platform. *Nat Protoc.* (2016) 11:1244–63. doi: 10.1038/nprot.2016.071
- Fabiani L, Saroglia M, Galata G, De Santis R, Fillo S, Luca V, et al. Magnetic beads combined with carbon black-based screen-printed electrodes for COVID-19: a reliable and miniaturized electrochemical immunosensor for SARS-CoV-2 detection in saliva. *Biosens Bioelectron.* (2020) 171:112686. doi: 10.1016/j.bios.2020.112686
- Zitka O, Krizkova S, Skalickova S, Dospivova D, Adam V, Kizek R. Microfluidic tool coupled with electrochemical assay for

detection of lactoferrin isolated by antibody-modified paramagnetic beads. *Electrophoresis*. (2013) 34:2120–8. doi: 10.1002/elps.201200631

Conflict of Interest: The authors declare that the research was conducted in the absence of any commercial or financial relationships that could be construed as a potential conflict of interest.

Copyright © 2021 Hatate, Rice, Parker, Wu, Turner, Stabel and Eda. This is an open-access article distributed under the terms of the Creative Commons Attribution License (CC BY). The use, distribution or reproduction in other forums is permitted, provided the original author(s) and the copyright owner(s) are credited and that the original publication in this journal is cited, in accordance with accepted academic practice. No use, distribution or reproduction is permitted which does not comply with these terms.



Bacteriophage-Based Methods for Detection of Viable *Mycobacterium avium* subsp. *paratuberculosis* and Their Potential for Diagnosis of Johne's Disease

Irene R. Grant*

School of Biological Sciences, Institute for Global Food Security, Queen's University Belfast, Belfast, United Kingdom

OPEN ACCESS

Edited by:

Kumi de Silva,
The University of Sydney, Australia

Reviewed by:

Michael Thomas Collins,
University of Wisconsin-Madison,
United States
Raul G. Barletta,
University of Nebraska-Lincoln,
United States

*Correspondence:

Irene R. Grant
i.grant@qub.ac.uk

Specialty section:

This article was submitted to
Veterinary Infectious Diseases,
a section of the journal
Frontiers in Veterinary Science

Received: 23 November 2020

Accepted: 12 February 2021

Published: 11 March 2021

Citation:

Grant IR (2021) Bacteriophage-Based
Methods for Detection of Viable
Mycobacterium avium subsp.
paratuberculosis and Their Potential
for Diagnosis of Johne's Disease.
Front. Vet. Sci. 8:632498.
doi: 10.3389/fvets.2021.632498

Bacteriophage-based methods for detecting *Mycobacterium avium* subsp. *paratuberculosis* (MAP) are a potential new approach for diagnosis of Johne's disease (JD). The basis of these tests is a mycobacteriophage (D29) with a lytic lifecycle that is able to infect a range of *Mycobacterium* spp., not just MAP. When added to a test sample, the phages will bind to and infect mycobacterial cells present. If the host mycobacterial cells are viable, the phages will take over the metabolic machinery of the cells to replicate and produce multiple copies of themselves (phage amplification), before weakening the host cell walls by enzyme action and causing cell lysis. Cell lysis releases the host cell contents, which will include ATP, various enzymes, mycobacterial host DNA and progeny D29 phages; all of which can become the target of subsequent endpoint detection methods. For MAP detection the released host DNA and progeny phages have principally been targeted. As only viable mycobacterial cells will support phage amplification, if progeny phages or host DNA are detected in the test sample (by plaque assay/phage ELISA or qPCR, respectively) then viable mycobacteria were present. This mini-review will seek to: clearly explain the basis of the phage-based tests in order to aid understanding; catalog modifications made to the original plaque assay-based phage amplification assay (FASTPlaqueTB™) over the years; and summarize the available evidence pertaining to the performance of the various phage assays for testing veterinary specimens (bovine milk, blood and feces), relative to current JD diagnostic methods (culture, fecal PCR, and blood-ELISA).

Keywords: Johne's disease diagnosis, *Mycobacterium avium* subsp. *paratuberculosis*, phage-based detection methods, phage amplification assay, phagomagnetic separation, viability test

INTRODUCTION

Paratuberculosis, or Johne's disease (JD), caused by *Mycobacterium avium* subsp. *paratuberculosis* (MAP), is a chronic enteritis of domesticated ruminant animals that is very much a hidden and often endemic problem for farmers worldwide (1, 2). It is widely acknowledged that the available tests for the diagnosis of JD are imperfect and do not detect all MAP infected animals (3). Consequently, JD control efforts based on fecal culture and serum- or milk-ELISA results have

not been as effective as national governments would have liked (2). Culture remains the definitive diagnostic test for JD, but takes too long to deliver results; it has been the only method available to confirm the presence of viable MAP, i.e., the infectious agent, in veterinary specimens for many years. Phage-based methods are a relatively recent potential addition to the JD diagnostic toolbox; their development being principally progressed by two research groups in the United Kingdom (Professor Catherine Rees' group at University of Nottingham and the author's group at Queen's University Belfast) since the mid 2000s. Currently, other than culture and some viability dye-based qPCR methods (4–6), phage-based tests represent the only other means of specifically detecting and distinguishing viable MAP. This mini-review will seek to, firstly, clearly explain the basis of the phage-based tests in order to aid understanding of how such tests work. Secondly, it will catalog modifications made to the original plaque assay-based phage amplification assay (FASTPlaqueTB™) over time in an effort to simplify the assays and make them more user-friendly. Finally, the available evidence pertaining to the performance of the phage assays for testing veterinary specimens (bovine milk, blood, and feces), relative to current JD diagnostic methods (culture, fecal PCR, and blood-ELISA), will be summarized.

HOW DO PHAGE-BASED TESTS FOR DETECTION OF VIABLE MAP WORK?

A mycobacteriophage with a lytic (virulent) lifecycle, known as D29 (7), has been employed for all MAP phage assays developed to date. D29 has a broad host range amongst the *Mycobacterium* spp., including *M. tuberculosis*, *M. bovis*, *M. avium*, *M. scrofulaceum*, and *M. ulcerans* (8–10). Hence, a test based on D29 phages alone will never be specific for MAP; although it will be specific for viable mycobacterial cells (i.e., host cells with functioning metabolism that facilitate replication of the infecting phage within them). To add specificity for MAP, PCR or qPCR have needed to be applied as a confirmatory final step in the vast majority of published phage-based methods. The different published phage-based tests all have at their core phage amplification (multiplication) within viable host mycobacterial cells, as illustrated in **Figure 1**. Differences between phage-based tests for detection of MAP principally relate to: (1) how the mycobacterial cells are prepared prior to addition of phages; (2) how the phages are added to the test sample; and (3) what is detected once mycobacterial cells present in a sample lyse (burst) due to phage action, i.e., progeny phages and/or MAP DNA. Each of the published phage-based methods developed for detection of viable MAP will be briefly described, categorized by what they detect.

METHODS TO DETECT PROGENY PHAGES AFTER PHAGE AMPLIFICATION AND MAP CELL LYSIS

Plaque Assays

The starting point for phage-based methods for detection of viable MAP was when the commercially available

FASTPlaqueTB™ assay (Biotec Laboratories Ltd., Ipswich, UK), originally developed for detection of *Mycobacterium tuberculosis* complex in sputum for human Tuberculosis diagnosis (12), was successfully applied with minimal adaptation to detect viable MAP in milk by Stanley et al. (13). This test is a plaque assay which involves fast-growing *Mycobacterium smegmatis* cells to provide the bacterial lawn in which zones of clearing (plaques) form, as a consequence of phage-infected MAP cells bursting within the agar and releasing D29 phages which then repeatedly infect and lyse nearby *M. smegmatis* cells to form plaques during an overnight incubation (**Figure 1**). However, because the D29 mycobacteriophage involved is not specific for MAP, Stanley et al. (13) added in plaque harvesting, DNA extraction (by heating agar plaques) and IS900 PCR (termed plaque PCR) steps to achieve specificity for MAP. Stanley et al. (13) termed their test the Phage-PCR assay. Subsequently, the use of Zymoclean DNA Clean and Concentrator columns (Zymo Research, Irvine, CA, USA, or similar) to extract DNA from plaques, rather than simple boiling of plaques, was recommended by the Nottingham research group in order to increase the detection sensitivity of the Phage-PCR assay (14, 15). This Phage-PCR assay is marketed as the Actiphage® Core 2-day assay (PBD Biotech Limited, Thurston, Suffolk, UK). It has been used by the Rees research group for many years to test for viable MAP in raw (16) and pasteurized milk (17), other dairy products including infant formula and cheeses (18, 19), and in cattle blood (14). The Phage-PCR assay has also been used for detection of *Mycobacterium bovis* in cattle blood (15, 20).

Altic et al. (21) and Donaghy et al. (22) applied the original FASTPlaqueTB™ assay to detect and enumerate viable MAP in milk after UV treatment, and both groups observed that plaque numbers did not correlate well with MAP colony counts. Foddai et al. (23) optimized the conditions of the original phage amplification assay to achieve accurate enumeration of viable MAP in milk. This was considered to be important because even though the test is more rapid than culture unless the phage-based test is able to accurately indicate the number of viable MAP the true story about prevalence of viable MAP in bovine milk or blood will not be uncovered. The main changes made to the test protocol were an extended incubation time from 1 to 3.5 h before plating with *M. smegmatis* mc² 155 and molten agar, and virucide treatment 2 h into this incubation period rather than just before plating (23).

Subsequently, Foddai et al. (24) inserted a peptide-mediated magnetic separation (PMS) step (25) to selectively separate MAP cells from complex sample matrices and concentrate them into a smaller volume in front of the optimized phage amplification assay (23). The PMS step gives the assay greater specificity for MAP than the earlier Phage-PCR or optimized phage assays. The Peptide-mediated magnetic separation (PMMS)-phage assay referred to by Swift et al. (14) is the same PMS step linked to the Phage-PCR method rather than to the optimized phage amplification assay. Subsequent tweaks to milk sample preparation protocols and application of the PMS-phage assay to test naturally contaminated milk samples were reported (26, 27), but no further changes were made to conditions of the optimized PMS-phage assay *per se*.

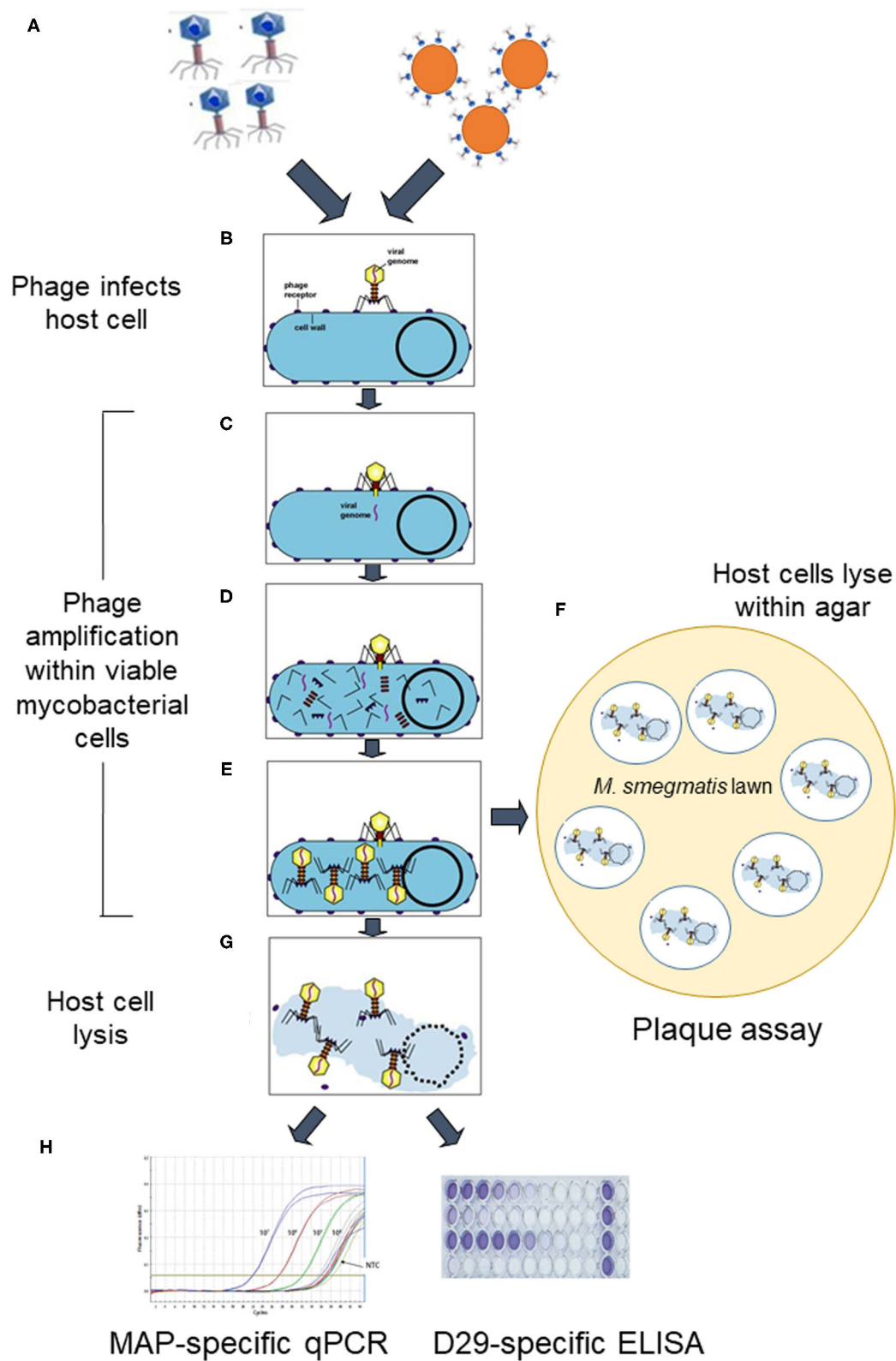


FIGURE 1 | Schematic overview of how lytic phage-based assays for detection of viable *Mycobacterium avium* subsp. *paratuberculosis* work. D29 phages are added to the sample as either free phages or as phage-coated paramagnetic beads (step **A**). They specifically bind irreversibly to host mycobacterial cells (step **B**) in the (Continued)

FIGURE 1 | sample and then infect the cells by injecting their genome (step **C**). The host cell's machinery is hi-jacked to reproduce phage component parts (step **D**), which assemble into mature phages within the host cell (step **E**). At this point the phage-treated sample is either plated in agar before mycobacterial cells burst to release progeny phages which infect a *Mycobacterium smegmatis* lawn and form zones of clearing (plaques) (step **F**), or incubation proceeds until after burst of mycobacterial cells occurs due to action of phage endolysins in suspension (step **G**). When cells burst, host cell DNA and progeny phages are released, which can be detected by a MAP-specific qPCR or D29-specific ELISA, respectively (step **H**) (Elements of this figure are not to scale and are for illustrative purposes only.). Certain elements of this figure are used under licence BY-NC-SA 3.0 from Kaiser (11) 10.7A: The Lytic Lifecycle of Bacteriophages. Biology LibreTexts™.

D29-Specific ELISA

In an effort to achieve a more rapid phage-based test for viable MAP, Stewart et al. (28) spent time producing a D29-specific polyclonal antibody to form the basis of a competitive ELISA assay to be used after phage amplification, rather than applying the plaque assay. The new immunoassay, which still included PMS to separate and concentrate MAP cells from a milk or feces sample first, was called the PMS-Phage-ELISA assay (28). Although the PMS step added considerable specificity for MAP detection to the overall assay, some non-MAP mycobacterial cells (e.g., *M. bovis* or environmental mycobacteria) could potentially be captured from naturally contaminated samples, and hence all of the D29 phages detected by the ELISA may not necessarily be due to viable MAP cells. A working assay was achieved that was quicker than the PMS-phage assay (24 h instead of 48 h) and that had good detection sensitivity, however no further work on the PMS-phage-ELISA assay was ever reported.

METHODS TO DETECT MAP DNA AFTER MAP CELLS HAVE LYSED DUE TO PHAGE ACTION

Two rapid, 1-day phage- and qPCR-based tests for viable MAP have been reported most recently - the Actiphage® Rapid assay (15) and the Phagomagnetic separation (PhMS)-qPCR assay (29). The Actiphage® technology is subject of a patent [(30), PCT/GB2014/052970], and the Actiphage® Rapid assay is commercially available (PBD Biotech Limited). The PhMS-qPCR assay is patent pending [(31), PCT/EP2020/076632], but not yet a commercial test. Whilst the two tests may seem similar, the latter has a different *modus operandi*. Phages are added to the test sample bound to paramagnetic beads rather than as a free phage suspension, as in the Actiphage Rapid® assay. The D29 phages are attached to tosylactivated paramagnetic beads by covalent bonding with capsid (head) proteins, so that tails are orientated outwards to permit binding between phage and MAP cell surface. The phage-coated paramagnetic beads facilitate physical separation of phage-captured MAP cells from potentially inhibitory sample constituents by means of a magnet. Once the bead-bound D29 phages attach to MAP cells, they inject their DNA to infect the host MAP cells and initiate phage amplification (the lytic cycle) within viable cells only. The magnetic beads remain attached to the MAP cells facilitating subsequent washing of the bead-cell complexes, and then resuspension of the beads in a small volume (50 µl) of broth. When the D29 phage-infected mycobacterial cells subsequently burst from the inside out due to phage enzyme action, DNA is released into this small volume and no further DNA extraction

or purification is necessary prior to its use as template DNA for MAP-specific Taqman qPCR (6). In contrast, purification of mycobacterial DNA using extraction columns is recommended for the Actiphage Rapid® assay to maximize detection sensitivity (15). **Supplementary Table 1** compares the steps involved for the two rapid phage- and qPCR-based assays when testing 50 ml milk. The MAP detection capabilities of these two rapid phage-based tests for viable MAP have yet to be directly compared.

WHAT DOES A PHAGE ASSAY POSITIVE RESULT MEAN?

There appears to be a degree of misunderstanding amongst MAP researchers about what a phage assay positive result means, and also considerable skepticism about positive phage assay results that are not supported by parallel culture positive results, or other positive JD diagnostic test result. In theory, the presence of a plaque is due to a single viable mycobacterial cell or a clump of viable mycobacterial cells bursting within the agar, and the progeny phages released infecting and repeatedly bursting *M. smegmatis* cells in the surrounding bacterial lawn. In practice, potential false positive results may arise with plaque-based phage assays due to ineffective viricide treatment, meaning that some plaques would be due to non-inactivated D29 phages, or some cells bursting before plating in agar happens, also releasing D29 phages that will interact with *M. smegmatis* lawn to form plaques. Early adopters of the phage-PCR assay or PMS-phage assay have run into such issues, and have found the multiple steps and transfers involved, the timed incubation steps, the need for molten agar and an *M. smegmatis* culture, and one or two overnight incubations tedious (32). In my experience of transferring our optimized Phage assay or PMS-phage assays to a number of other laboratories, this has rarely proved to be a straightforward process and a lot of follow-up troubleshooting activity has ensued. It seems that many years of practice with the plaque assays at University of Nottingham and Queen's University Belfast make perfect, and that some degree of proficiency in their use must be acquired before reliable results can be consistently obtained in other laboratories.

The two most recently published 1-day phage assays (Actiphage® Rapid and PhMS-qPCR assays) are no longer reliant on plaque assays and subsequent plaque PCR for confirmation of a positive result. These tests have clear advantages compared to plaque assay-based tests, not just in terms of speed of results but also in terms of greater sensitivity of detection and more accurate viable MAP counts being obtained. This is due to the fact that all viable MAP cells in the sample will contribute DNA for the final qPCR step in the assay, rather

TABLE 1 | Main findings of studies applying phage-based assays to detect viable MAP in naturally infected bovine milk, feces or blood.

Study	Type of phage assay	Sample type (no. of samples)	Comparator test(s)	Main findings
Foddai et al. (24)	PMS ^a -phage assay	Bulk tank milk (<i>n</i> = 44), feces (<i>n</i> = 39)	HPC ^b + culture or PMS-culture (milk), real-time qPCR (feces)	Bulk tank milk: 15/44 (34.1%) samples tested positive by PMS-phage assay, with numbers of viable MAP detected ranging from 1 to 110 PFU ^c /50 ml BTM. 5/44 (11.4%) samples were positive by culture after HPC decontamination or PMS. Feces: 20/39 (51.2%) samples tested positive by PMS-phage assay, with numbers of viable MAP detected ranging from 6 to 41,111 PFU/g. 35/39 (89.7%) feces samples had been positive by RT-qPCR when tested several months previously.
Swift et al. (14)	PMMS ^a -Phage-PCR	Bloods from milk-ELISA positive cattle (<i>n</i> = 9, Set A), cattle in JD-free herd (<i>n</i> = 5, Set B), and from cattle with strong, intermediate or negative milk-ELISA results (<i>n</i> = 10, Set C)	Serum-ELISA, Culture without decontamination	Set A: 9/9 (100%) bloods tested PMMS-phage-PCR positive, with MAP counts ranging from 3 to 35 PFU/ml blood, compared to 8/9 (88.9%) by serum-ELISA. Set B: 0/5 (0%) bloods tested PMMS-phage-PCR positive, same by serum-ELISA. Set C: 8/10 (80%) bloods tested PMMS-phage-PCR positive compared to 4/10 (40%) positive by serum-ELISA and 0/10 (0%) positive by culture.
Botsaris et al. (16)	Phage-PCR	Bulk tank milks (<i>n</i> = 225) in Cyprus	HPC + culture	218/225 (96.9%) milk samples yielded plaques, i.e., contained viable mycobacteria. Only 50/225 (22.2%) milk samples tested positive for presence of MAP DNA by plaque PCR. In contrast, just 2/225 (0.9%) milk samples yielded colonies confirmed to be MAP after HPC and culture.
Swift et al. (20)	PMMS-phage assay	Bloods from 4.5 year old cattle that had been orally inoculated with MAP at 3–4 months of age (<i>n</i> = 19)	Fecal culture, fecal qPCR and Serum-ELISA	7/19 (37%) blood PBMCs ^d tested positive by PMMS-Phage-PCR, with low numbers of MAP indicated (2–5 PFU). 2/19 (10.5%) and 1/19 (5.3%) tested positive by fecal culture and serum ELISA, respectively.
Foddai and Grant (27)	PMS-phage assay	Milk from individual cows in a JD affected dairy herd (<i>n</i> = 146), and bulk tank milk from Johne's affected dairy farms (<i>n</i> = 22).	PMS-IS900 qPCR and PMS-MGIT culture.	Limit of detection (LOD _{50%}) of the PMS-phage assay reported as 0.93 MAP cells/50 ml milk. Viable MAP detected in 31/146 (21.2%) milks from individual cows and from 13/22 (59.1%) bulk tank milks by the PMS-phage assay, with numbers of viable MAP detected ranging from 6 to 948 PFU/50 ml. Fewer MAP positive samples detected by PMS-qPCR (Individual: 9.1%, BTM 45.4%) and PMS-culture (Individual: 11.6%, BTM: 50.0%). "Moderate" agreement between PMS-phage assay and PMS-qPCR results for BTM (<i>p</i> = 0.0036), "poor to fair" agreement for individual milks (<i>p</i> = 0.1695).
O'Brien et al. (33)	PMS-phage assay	Milk from MAP test negative cattle (<i>n</i> = 105) and MAP test positive animals (<i>n</i> = 40)	Serum-ELISA, Fecal culture, PMS-culture	Diagnostic sensitivity (DSe) and specificity (DSp) of the PMS-phage assay were 0.325 and 1.000, respectively, compared to 0.250 and 0.962 for PMS-culture, and 0.525 and 0.962 for the PMS-phage assay and PMS-culture results combined.
Swift et al. (15)	Actiphage [®] Rapid assay	Bloods from experimentally MAP infected calves (<i>n</i> = 15) and non-infected control calves (<i>n</i> = 8)	Phage-PCR, IDEXX ELISA and tissue culture (at necropsy)	MAP infected calves: 13/15 (87%) blood PBMC samples Actiphage [®] Rapid assay positive and 6/15 (40%) Phage-PCR assay positive. No calves tested MAP positive by either serum-ELISA or tissue culture. Non-infected calves: 2/8 (25%) blood PBMC samples Actiphage [®] Rapid assay positive. No bloods positive by Phage-PCR or serum-ELISA, and no MAP cultured from tissues. Actiphage [®] Rapid assay had greater MAP detection sensitivity than original Phage-PCR assay. Limit of detection reported as 1–10 MAP cells/ml blood.
Foddai and Grant (29)	PhMS ^f -qPCR assay	Bulk tank milk (<i>n</i> = 100)	None	Limit of detection (LOD _{50%}) of the optimized PhMS-qPCR assay reported as 10 MAP cells/50 ml milk (95% CI: 1.20–82.83). 49/100 (49%) bulk tank milks tested PhMS-qPCR positive with number of viable MAP detected ranging from 3 to 126 MAP/50 ml milk.

(Continued)

TABLE 1 | Continued

Study	Type of phage assay	Sample type (no. of samples)	Comparator test(s)	Main findings
Foddai et al. (29)	PhMS-qPCR assay	Bulk tank milk ($n = 392$) and individual milks from cows on four MAP-infected farms ($n = 293$)	Milk-ELISA, PMS-culture	<p>Bulk tank milks: Viable MAP detected in 103/392 (26.5%) bulk tank milks by PhMS-qPCR, with MAP levels ranging from 1 to 8,432 MAP/50 ml; <2% of the 392 farms had MAP contamination levels >100 MAP cells/50 ml.</p> <p>Individual milks: 17–24% of animals in four of the above farms showing highest MAP contamination levels in their bulk tank milk tested PhMS-qPCR positive, with MAP levels between 6.7 and 42.1 MAP cells/50 ml.</p> <p>There was no significant correlation between parallel PhMS-qPCR and milk-ELISA results for either BTM or individual milks.</p> <p>When subjected to PMS-culture, 52/61 (85%) PhMS-qPCR positive milks yielded an IS900 qPCR positive Pozzato broth culture.</p>

^aPMS and PMMS, peptide-mediated magnetic separation. Swift et al. (14, 20) used beads coated with peptides as described by Foddai et al. (24).

^bHexadecylpyridinium chloride decontamination.

^cPFU, Plaque-forming units.

^dPBMC, peripheral blood mononuclear cells isolated from whole blood before testing.

^eLOD_{50%} is the microbial analyte concentration (and confidence limits) that corresponds to a 50 % probability of a positive result with the test method.

^fPhMS, phage-mediated magnetic separation (known as phagomagnetic separation).

than a random selection of 5–10 plaques that may or may not have arisen from lysed MAP cells picked from agar plates. In the author's opinion, these rapid phage-based assays should be less problematic for intending users, given that the test protocols have been streamlined to require fewer manipulations and transfers, are less reliant on accurate incubation times, and have qPCR as the endpoint detection step. Furthermore, many veterinary diagnostic laboratories will already be familiar with qPCR if they carry out fecal qPCR for Johne's or other animal disease diagnosis, for instance.

APPLICATION OF PHAGE-BASED TESTS FOR DIAGNOSIS OF MAP INFECTION IN CATTLE

To date, the University of Nottingham research group has principally focussed on applying their phage-based tests (PMMS-Phage-PCR and Actiphage Rapid[®] assay) to blood sample from cattle for detection of viable MAP and *M. bovis*. In contrast, the Queen's University Belfast research group has concentrated on applying their methods (PMS-phage assay and PhMS-qPCR) for detection of viable MAP in bulk tank milk and individual cows' milk primarily, but have also tested some bovine feces (24). In my experience, without magnetic separation to remove inhibitory components in feces the phage assay cannot be successfully applied to this specimen type. Table 1 summarizes the findings of published studies relating to detection of viable MAP in naturally contaminated cattle samples. Consistently, more viable MAP positive results are being obtained with the phage-based assays compared to culture, whether performed with prior chemical decontamination or PMS (20, 24, 27). The rapid, 1-day phage- and qPCR-based assays are proving to be more sensitive than either the Phage-PCR or PMS-phage assays, which are plaque assay-based tests (15, 29, 34). Phage assay results are often indicating the presence of viable MAP bacteraemia or MAP

shedding in milk and feces in animals that are serum- or milk-ELISA negative (14, 15, 20, 34). O'Brien et al. (33) determined the diagnostic specificity and sensitivity of the PMS-phage assay to be 1.00 and 0.325, respectively. PMS-culture specificity and sensitivity values when applied to the same samples were 0.962 and 0.250, respectively. Only a single herd was used as the "non-infected" cohort during this study and because four animals in that population were fecal culture positive (confirmed by IS900 PCR), the diagnostic specificity estimates may not be accurate.

CURRENT STATE-OF-PLAY AND WHAT NEXT

More validation data for the most recent rapid phage- and qPCR-based methods is urgently needed, in order to accumulate a convincing body of evidence demonstrating the tests' performance relative to culture results; although it must be remembered that depending on how culture is carried out it may not be a perfect comparator test. It will be important that follow-up longitudinal studies of animals that have tested phage assay positive (by whichever version of phage-based test applied and whichever sample type tested) but with discrepant serum- or milk-ELISA and fecal qPCR negative results are carried out. Ideally, further work to make the latest rapid phage-based tests higher throughput and more automated, with applicability for testing a broad range of veterinary specimen types, would also be undertaken. The development of more complex phage-based biosensor methods involving the D29 mycobacteriophage, or other more recently discovered mycobacteriophages that can or may be able to infect MAP (35–37), would not be considered a priority in relation to Johne's disease diagnosis. Veterinary diagnostic laboratories are unlikely to want to invest in expensive biosensor equipment that may require more skilled and knowledgeable operators.

AUTHOR CONTRIBUTIONS

The author confirms being the sole contributor of this work and has approved it for publication.

REFERENCES

- Stabel JR. Johne's disease: a hidden threat. *J Dairy Sci.* (1998) 81:283–8. doi: 10.3168/jds.S0022-0302(98)75577-8
- Geraghty T, Graham DA, Mullowney P, More SJ. A review of bovine Johne's disease control activities in 6 endemically infected countries. *Prev Vet Med.* (2014) 116:1–11. doi: 10.1016/j.prevetmed.2014.06.003
- Whittington R, Donat K, Weber MF, Kelton D, Nielsen SS, Eisenberg S, et al. Control of *paratuberculosis*: who, why and how. A review of 48 countries. *BMC Vet Res.* (2019) 15:198. doi: 10.1186/s12917-019-1943-4
- Kralik P, Nocker A, Pavlik I. *Mycobacterium avium* subsp. *paratuberculosis* viability determination using F57 quantitative PCR in combination with propidium monoazide treatment. *Int J Food Microbiol.* (2010) 141 (Suppl.):S80–6. doi: 10.1016/j.ijfoodmicro.2010.03.018
- Ricchi M, De Cicco C, Kralik P, Babak V, Boniotti MB, Savi R, et al. Evaluation of viable *Mycobacterium avium* subsp. *paratuberculosis* in milk using peptide-mediated separation and Propidium Monoazide qPCR. *FEMS Microbiol Lett.* (2014) 356:127–33. doi: 10.1111/1574-6968.12480
- Foddai ACG, Grant IR. Methods for detection of viable foodborne pathogens: current state-of-art and future prospects. *Appl Microbiol Biotechnol.* (2020) 104:4281–8. doi: 10.1007/s00253-020-10542-x
- Froman S, Will DW, Bogen E. Bacteriophage active against virulent *Mycobacterium tuberculosis*. I Isolation and activity. *Am J Publ Health Nations Health.* (1954) 44:1326–33. doi: 10.2105/AJPH.44.10.1326
- David HL, Clavel S, Clement F. Adsorption and growth of the bacteriophage-D29 in selected mycobacteria. *Annal Virol.* (1980) 131:167–84. doi: 10.1016/0769-2617(80)90031-3
- Rybníček J, Kramme S, Small PL. Host range of 14 mycobacteriophages in *Mycobacterium ulcerans* and seven other mycobacteria including *Mycobacterium tuberculosis* – application for identification and susceptibility testing. *J Med Microbiol.* (2006) 55:37–42. doi: 10.1099/jmm.0.46238-0
- Foley-Thomas EM, Whipple DL, Bermudez LE, Barletta RG. Phage infection, transfection and transformation of *Mycobacterium avium* complex and *Mycobacterium paratuberculosis*. *Microbiology.* (1995) 141:1173–81. doi: 10.1099/13500872-141-5-1173
- Kaiser G. *The Lytic Life Cycle of Bacteriophages.* (2021). Available online at: <https://chem.libretexts.org/@go/page/3244> (accessed March 3, 2021).
- McNerney R, Kambashi BS, Kinkese J, Tembwe R, Godfrey-Faussett P. Development of a bacteriophage phage replication assay for diagnosis of pulmonary tuberculosis. *J Clin Microbiol.* (2004) 42:2115–20. doi: 10.1128/JCM.42.5.2115-2120.2004
- Stanley EC, Mole RJ, Smith RJ, Glenn SM, Barer MR, McGowan M, et al. Development of a new, combined rapid method using phage and PCR for detection and identification of viable *Mycobacterium paratuberculosis* bacteria within 48 hours. *Appl Environ Microbiol.* (2007) 73:1851–7. doi: 10.1128/AEM.01722-06
- Swift BM, Denton EJ, Mahendran SA, Huxley JN, Rees CE. Development of a rapid phage-based method for the detection of viable *Mycobacterium avium* subsp. *paratuberculosis* in blood within 48 h. *J Microbiol Meth.* (2013) 94:175–9. doi: 10.1016/j.mimet.2013.06.015
- Swift BMC, Meade N, Sandoval Barron E, Bennett M, Perehenic T, Hughes V, et al. The development and use of Actiphage® to detect viable mycobacteria from bovine Tuberculosis and Johne's disease-infected animals. *Microb Biotechnol.* (2020) 13:738–46. doi: 10.1111/1751-7915.13518
- Botsaris G, Liapi M, Kakogianis C, Dodds CER, Rees CED. Detection of *Mycobacterium avium* subsp. *paratuberculosis* in bulk tank milk by combined phage-PCR assay: evidence that plaque number is a good predictor of MAP. *Int J Food Microbiol.* (2013) 164:76–80. doi: 10.1016/j.ijfoodmicro.2013.03.023
- Gerrard ZE, Swift BMC, Botsaris G, Davidson RS, Hutchings MR, Huxley JN, et al. Survival of *Mycobacterium avium* subspecies *paratuberculosis* in retail pasteurised milk. *Food Microbiol.* (2018) 74:57–63. doi: 10.1016/j.fm.2018.03.004
- Botsaris G, Slana I, Liapi M, Dodd C, Economides C, Rees C, et al. Rapid detection methods for viable *Mycobacterium avium* subspecies *paratuberculosis* in milk and cheese. *Int J Food Microbiol.* (2010) 141:S87–90. doi: 10.1016/j.ijfoodmicro.2010.03.016
- Botsaris G, Swift BMC, Liapi M, Christodoulou M, Hatzitofi N, Christodoulou V, et al. Detection of viable *Mycobacterium avium* subspecies *paratuberculosis* in powdered infant formula by phage-PCR and confirmed by culture. *Int J Food Microbiol.* (2016) 216:91–4. doi: 10.1016/j.ijfoodmicro.2015.09.011
- Swift BMC, Huxley JN, Plain KM, Begg DJ, de Silva K, Purdie AC, et al. Evaluation of the limitations and methods to improve rapid phage-based detection of viable *Mycobacterium avium* subsp. *paratuberculosis* in the blood of experimentally infected cattle. *BMC Vet Res.* (2016) 12:115. doi: 10.1186/s12917-016-0728-2
- Altic LC, Rowe MT, Grant IR. UV light inactivation of *Mycobacterium avium* subsp. *paratuberculosis* in milk assessed by FASTPlaqueTB™ phage assay and culture. *Appl Environ Microbiol.* (2007) 73:3728–33. doi: 10.1128/AEM.00057-07
- Donaghy J, Keyser M, Johnston J, Cilliers FP, Gouws PA, Rowe MT. Inactivation of *Mycobacterium avium* ssp. *paratuberculosis* in milk by UV treatment. *Lett Appl Microbiol.* (2009) 49:217–21. doi: 10.1111/j.1472-765X.2009.02644.x
- Foddai A, Elliott CT, Grant IR. Optimization of a phage amplification assay to permit accurate enumeration of viable *Mycobacterium avium* subsp. *paratuberculosis* cells. *Appl Environ Microbiol.* (2009) 75:3896–902. doi: 10.1128/AEM.00294-09
- Foddai A, Strain S, Whitlock RH, Elliott CT, Grant IR. Application of a peptide-mediated magnetic separation-phage assay for viable *Mycobacterium avium* subsp. *paratuberculosis* to bovine bulk tank milk and feces samples. *J Clin Microbiol.* (2011) 49:2017–9. doi: 10.1128/JCM.00429-11
- Foddai A, Elliott CT, Grant IR. Maximising capture efficiency and specificity of magnetic separation for *Mycobacterium avium* subsp. *paratuberculosis* cells. *Appl Environ Microbiol.* (2010) 76:7550–8. doi: 10.1128/AEM.01432-10
- Foddai ACG, Grant IR. An optimised milk testing protocol to ensure accurate enumeration of viable *Mycobacterium avium* subsp. *paratuberculosis* by the PMS-phage assay. *Int Dairy J.* (2015) 53:16–23. doi: 10.1016/j.idairyj.2015.07.004
- Foddai ACG, Grant IR. Sensitive and specific detection of viable *Mycobacterium avium* subsp. *paratuberculosis* in raw milk by the Peptide-mediated magnetic separation (PMS)-phage assay. *J Appl Microbiol.* (2017) 122:1357–67. doi: 10.1111/jam.13425
- Stewart LD, Foddai A, Elliott CT, Grant IR. Development of novel phage-mediated immunoassay for the rapid detection of viable *Mycobacterium avium* subsp. *paratuberculosis*. *J Appl Microbiol.* (2013) 115:808–17. doi: 10.1111/jam.12275
- Foddai ACG, Grant IR. A novel one-day phage-based test for rapid detection and enumeration of viable *Mycobacterium avium* subsp. *paratuberculosis* in cows' milk. *Appl Microbiol Biotechnol.* (2020) 104:9399–412. doi: 10.1007/s00253-020-10909-0
- Rees CD, Swift B. *Mycobacteria Detection Using Bacteriophages, PCT/GB2014/052970* (2014).
- Grant IR, Foddai ACG. *Detection of Mycobacterium Species, PCT/EP2020/076632* (2020).
- Butot S, Ricchi M, Sevilla IA, Michot L, Molina E, Tello M, et al. Estimation of the performance characteristics of analytical methods

SUPPLEMENTARY MATERIAL

The Supplementary Material for this article can be found online at: <https://www.frontiersin.org/articles/10.3389/fvets.2021.632498/full#supplementary-material>

- for *Mycobacterium avium* subsp. *paratuberculosis* detection in dairy products. *Front Microbiol.* (2019) 10:509. doi: 10.3389/fmicb.2019.00509
33. O'Brien LM, McAloon CG, Stewart LD, Strain SAJ, Grant IR. Diagnostic potential of the PMS-phage assay and PMS-culture to detect *Mycobacterium avium* subsp. *paratuberculosis* in naturally infected bovine milk samples. *Transbound Emerg Dis.* (2018) 65:719–26. doi: 10.1111/tbed.12794
 34. Foddai ACG, Watson G, McAloon C, Grant IR. Phagomagnetic separation-qPCR: a rapid, sensitive and specific surveillance tool for viable *Mycobacterium avium* subsp. *paratuberculosis* in bulk tank and individual cows' milk. *J Dairy Sci.* (2021). doi: 10.3168/jds.202-19626. [Epub ahead of print].
 35. Hatfull GF. Complete genome sequences of 138 mycobacteriophages. *J Virol.* (2012) 86:2382–4. doi: 10.1128/JVI.06870-11
 36. Endersen L, Coffey A, Neve H, McAuliffe O, Ross RP, O'Mahony JM. Isolation and characterisation of six novel mycobacteriophages and investigation of their antimicrobial potential in milk. *Int Dairy J.* (2013) 28:8–14. doi: 10.1016/j.idairyj.2012.07.010
 37. Basra S, Anany H, Brovko L, Kropinski AM, Griffiths MW. Isolation and characterization of a novel bacteriophage against *Mycobacterium avium* subspecies *paratuberculosis*. *Arch Virol.* (2014) 159:2659–74. doi: 10.1007/s00705-014-2122-3

Conflict of Interest: The author declares that the phagomagnetic (PhMS)-qPCR assay discussed was developed in her laboratory and is patent pending (Grant and Foddai, PCT/EP2020/076632).

Copyright © 2021 Grant. This is an open-access article distributed under the terms of the Creative Commons Attribution License (CC BY). The use, distribution or reproduction in other forums is permitted, provided the original author(s) and the copyright owner(s) are credited and that the original publication in this journal is cited, in accordance with accepted academic practice. No use, distribution or reproduction is permitted which does not comply with these terms.



Identification of Long Non-coding RNA Isolated From Naturally Infected Macrophages and Associated With Bovine Johne's Disease in Canadian Holstein Using a Combination of Neural Networks and Logistic Regression

OPEN ACCESS

Edited by:

Miguel Salgado,
Austral University of Chile, Chile

Reviewed by:

Marta Alonso-Hearn,
Animalien Osasuna, NEIKER-Instituto
Vasco de Investigación y Desarrollo
Agrario, Spain
Mohanned Naif Alhussien,
National Dairy Research Institute
(ICAR), India

*Correspondence:

Nathalie Bissonnette
nathalie.bissonnette@canada.ca

†ORCID:

Andrew Marete
orcid.org/0000-0003-2301-4168

Specialty section:

This article was submitted to
Veterinary Infectious Diseases,
a section of the journal
Frontiers in Veterinary Science

Received: 08 December 2020

Accepted: 15 February 2021

Published: 22 April 2021

Citation:

Marete A, Ariel O, Ibeagha-Awemu E
and Bissonnette N (2021)
Identification of Long Non-coding
RNA Isolated From Naturally Infected
Macrophages and Associated With
Bovine Johne's Disease in Canadian
Holstein Using a Combination of
Neural Networks and Logistic
Regression. *Front. Vet. Sci.* 8:639053.
doi: 10.3389/fvets.2021.639053

Andrew Marete^{1†}, Olivier Ariel^{1,2}, Eveline Ibeagha-Awemu¹ and Nathalie Bissonnette^{1*}

¹ Agriculture and Agri-Food Canada, Sherbrooke Research and Development Centre, Sherbrooke, QC, Canada, ² Faculty of Science, Sherbrooke University, Sherbrooke, QC, Canada

Mycobacterium avium ssp. *paratuberculosis* (MAP) causes chronic enteritis in most ruminants. The pathogen MAP causes Johne's disease (JD), a chronic, incurable, wasting disease. Weight loss, diarrhea, and a gradual drop in milk production characterize the disease's clinical phase, culminating in death. Several studies have characterized long non-coding RNA (lncRNA) in bovine tissues, and a previous study characterizes (lncRNA) in macrophages infected with MAP *in vitro*. In this study, we aim to characterize the lncRNA in macrophages from cows naturally infected with MAP. From 15 herds, feces and blood samples were collected for each cow older than 24 months, twice yearly over 3–5 years. Paired samples were analyzed by fecal PCR and blood ELISA. We used RNA-seq data to study lncRNA in macrophages from 33 JD(+) and 33 JD(–) dairy cows. We performed RNA-seq analysis using the “new Tuxedo” suite. We characterized lncRNA using logistic regression and multilayered neural networks and used DESeq2 for differential expression analysis and Panther and Reactome classification systems for gene ontology (GO) analysis. The study identified 13,301 lncRNA, 605 of which were novel lncRNA. We found seven genes close to differentially expressed lncRNA, including *CCDC174*, *ERI1*, *FZD1*, *TWSG1*, *ZBTB38*, *ZNF814*, and *ZSCAN4*. None of the genes associated with susceptibility to JD have been cited in the literature. lncRNA target genes were significantly enriched for biological process GO terms involved in immunity and nucleic acid regulation. These include the MyD88 pathway (*TLR5*), GO:0043312 (neutrophil degranulation), GO:0002446 (neutrophil-mediated immunity), and GO:0042119 (neutrophil activation). These results identified lncRNA with potential roles in host immunity and potential candidate genes and pathways through which lncRNA might function in response to MAP infection.

Keywords: bovine, genomics, long non-coding RNA, macrophages, paratuberculosis (*Mycobacterium avium* ssp. *paratuberculosis*), Johne's disease, MAP disease

INTRODUCTION

One of the most economically significant diseases in livestock is paratuberculosis (1). The etiological agent of paratuberculosis or Johne's disease (JD) is *Mycobacterium avium* ssp. *paratuberculosis* (MAP). Whitlock and Buergele described JD as chronic, wasting, incurable, and infectious ruminant enteritis (2). For dairy producers, MAP infection translates to significant financial losses related to reduced milk production, decreased pregnancy rates, increased replacement costs, and decreased slaughtered carcass weight (3, 4), not to mention diminished animal welfare. Around 24–66% of dairy herds in Canada are MAP infected (5). Horizontal transmission of infection via the fecal–oral route is the most important mode of spread of infection due to the high amounts of MAP excreted in the feces. After ingestion of contaminated water or food, MAP reaches the gastrointestinal tract; MAP shows an evident tropism for this site (1, 6). The first route of MAP entry is through the ileum and jejunum's organized lymphoid tissue, the Peyer's patch in the intestinal mucosa and submucosa (7). These early events of MAP infection occur in two functional stages: (1) invasion through the intestinal barrier via MAP discharge from epithelial M cells and (2) phagocytosis and survival in macrophages of the lamina propria (7–9). It is known that MAP uses tissue-resident macrophages as its primary reservoir for survival and multiplication (10–12). Interestingly, genetic variations in numerous candidate genes expressed in macrophages are associated with resistance/susceptibility to MAP infection, notably the *NOD2* (13, 14), *IL10* (15–18), *SLC11A1*, and Toll-like receptor genes (19, 20).

With a slow progression of the disease, the pathogenesis of JD makes diagnosis difficult, more so in the subclinical stage of infection before the clinical signs appear (21). The first clinical signs include gradual weight loss despite normal appetite or, sometimes, increased appetite. During this clinical period, there is a decrease in milk production, accompanied by a concomitant weight loss with a sometimes more fluid consistency of manure. Diarrhea may be intermittent at first, with periods of normal manure consistency leading to chronic diarrhea (2). During the prolonged incubation subclinical period of 4–7 years, scarce clinical signs are observed (22). Difficulty in JD diagnosis is further hindered by host genetics (23), herd management, MAP strain, and infectious dose (24).

MAP employs complex mechanisms to control macrophages, which turn into a duel that lasts for years with unpredictable disease progression. The T helper type 1 (Th1)-mediated response that usually effectively controls non-pathogenic intracellular mycobacterial infections fails for MAP infection (25). The pathogenesis of JD is still under investigation because macrophage-MAP cross talk in the subclinical stage of the disease is partially resolved. It is paramount to consider the study of alternative molecular avenues for identifying the product resulting from bacterial MAP infection that might become potential biomarkers of JD and evolve therapeutic tools.

Previous reports indicate that bacteria interfere with mammalian regulatory RNA expression that is not translated

to protein (such as long non-coding RNA–lncRNA) to modify immune signaling, autophagy, or apoptosis machinery (26, 27). lncRNAs are now emerging as important regulators of innate and adaptive immune responses (28–30). In humans, while they are widely investigated in aging, cancers, and epigenetics (31–33), there is growing evidence that lncRNAs interfere in the pathogenetic mechanisms of multifactorial disease like Crohn's disease and inflammatory bowel disease (34, 35).

In bovine, few studies have examined the occurrence of lncRNA in tissues, including muscle, skin, various tissues, and the mammary gland (36–40). Previous studies also report that lncRNA is involved with host cell response toward bacterial infections, including paratuberculosis (27, 41). lncRNA is unique from other RNA based on size (>199 nucleotides) and limited evidence of protein-coding potential (36, 37, 42–44). However, lncRNA's novel nature means there is no consensus on the best way to classify the protein-coding and non-coding potential of the lncRNA, so we use both logistic regression (45) and multilayered neural networks (46). The former implements human-designed features, such as open reading frame (ORF) length and integrity, GC content, and hexamer usage bias, whereas the latter identifies multilayered deep patterns solely on sequence information.

This study aims to use available deep learning and logistic regression approaches to study lncRNA associated with MAP in Canadian Holstein and provide novel insight into lncRNA's regulatory function in macrophages of dairy cattle during MAP infection. To this end, we investigated the presence of potentially novel lncRNA candidates and their role in MAP infection using RNA sequencing.

MATERIALS AND METHODS

Cow Selection and Johne's Disease Diagnosis

According to the Canadian Council on Animal Care guidelines for institutional animal use, we carried out all animal procedures and obtained ethical approval for the study from the Agriculture and Agri-Food Canada Animal Ethics Committee (protocol 362). To select cows for RNA-Seq, we analyzed fecal and blood samples from 15 commercial dairy herds positive for JD located in the province of Quebec, Canada, as described in the companion project (47).

Briefly, from each herd, we sampled cows twice yearly. The cows were older than 24 months to be enrolled in the study. They had calved twice or more at culling. We collected one fecal sample of a volume equivalent of 100 mL using a single-use veterinary glove. Consecutively, we also drew two blood samples per cow in dry tubes for serum collection (SST Serum Separation Tubes 8.5 mL; BD Biosciences, Ontario, Canada). Within 1 h of sampling, the tubes were centrifuged at $1,300 \times g$ at 20°C for 10 min and kept at 4°C during the transport to the laboratory. Sera were collected and then stored at –80°C until ELISA analysis. According to the manufacturer's instructions, we processed sera using the IDEXX MAP Ab test kit (IDEXX

Laboratories, USA). As described by Collins (48), we transformed optical density values into sample-to-positive (S/P) ratios and selected samples with an S/P ratio of at least 55% as positive. The presence of MAP in feces was tested by qPCR, and JD cows were confirmed infectious using the BD MGIT ParaTB culture medium and the BACTEC 960 detection 960 system described in Fock-Chow-Tho et al. (47). Cows that presented concordant serological and fecal culture or qPCR statuses, either positive or negative, were retained. A cow was designated JD (+) when a fecal culture and ELISA were positive at least two sampling periods. During macrophage analysis, the mean age of JD(−) cows was 6.4 ± 1.5 years, and 5.1 ± 1.8 years for the JD(+) cows. While JD(+) cows were promptly culled, the JD(−) cows were kept on-farm for >7 years to confirm their status definitively. In total, we selected 66 cows for RNA-Seq analysis, of which 33 were JD(+), and 33 were JD(−).

RNA Isolation, Library Preparation, and Sequencing

The monocyte-derived macrophages (MDM) were prepared in the absence of FBS and granulocyte-macrophage colony-stimulating factor (GM-CSF), or M-CSF, to avoid activation or bias in the differentiation toward M1 or M2 polarization, as described in Ariel et al. (49). Freshly isolated monocytes were confirmed exempt of MAP from both JD(+) and JD(−) cows, confirmed using qPCR and fluorescent microscopy. DNA was extracted from adherent monocytes, MDM, and PBMC using ZR Fecal DNA MiniPrep kit (Zymo Research Corp., Irvine, CA, USA), and qPCR was performed using the VETMAX Gold MAP Detection Kit (Life Technology Inc., Burlington, Ontario, Canada) as described previously (47). The absence of MAP in JD(+) and JD(−) MDM was also confirmed *in vitro* using fluorescence microscopy as described (49). To profile the lncRNA in resting macrophages (CTL, i.e., non-infected) and in response to MAP infection, the MDM were also infected with MAP. Our previous experimental design was used: 1 h, 4 h, 8 h, and 24 h post-infection with MAP at the multiplicity of infection of 10 (49).

In summary, we extracted total RNA from MDM from each experimental time point (CTL and MAP-infected at 1, 4, 8 h, and 24 hpi) in 66 cows [33 JD(−) and 33 JD(+)] using the RNeasy kit (Qiagen) total RNA extraction protocol. We quantified the RNA yield using a NanoDrop spectrophotometer (Thermo Fisher) and assessed RNA quality using the Bioanalyzer RNA 6000 kit (Agilent Technologies). We used the Ribo-Zero Gold kit to remove ribosomal RNA and Illumina TruSeq Stranded Total mRNA Sample Preparation kit (Illumina) to generate cDNA libraries. After quality control (size and absence of primer dimers) and qPCR library quantification [Kappa Library Quantification kit (Roche)], we performed paired-end sequencing using the Illumina HiSeq 2500 platform running HiSeq Control Software (v2.2.68). A subset of the sequencing data from the 66 cows is available from the Gene Expression Omnibus repository (accession number GSE98363). All processes followed manufacturer recommendations.

Transcriptome Assembly, Novel lncRNA Prediction, and Differential Expression (DE) Analysis

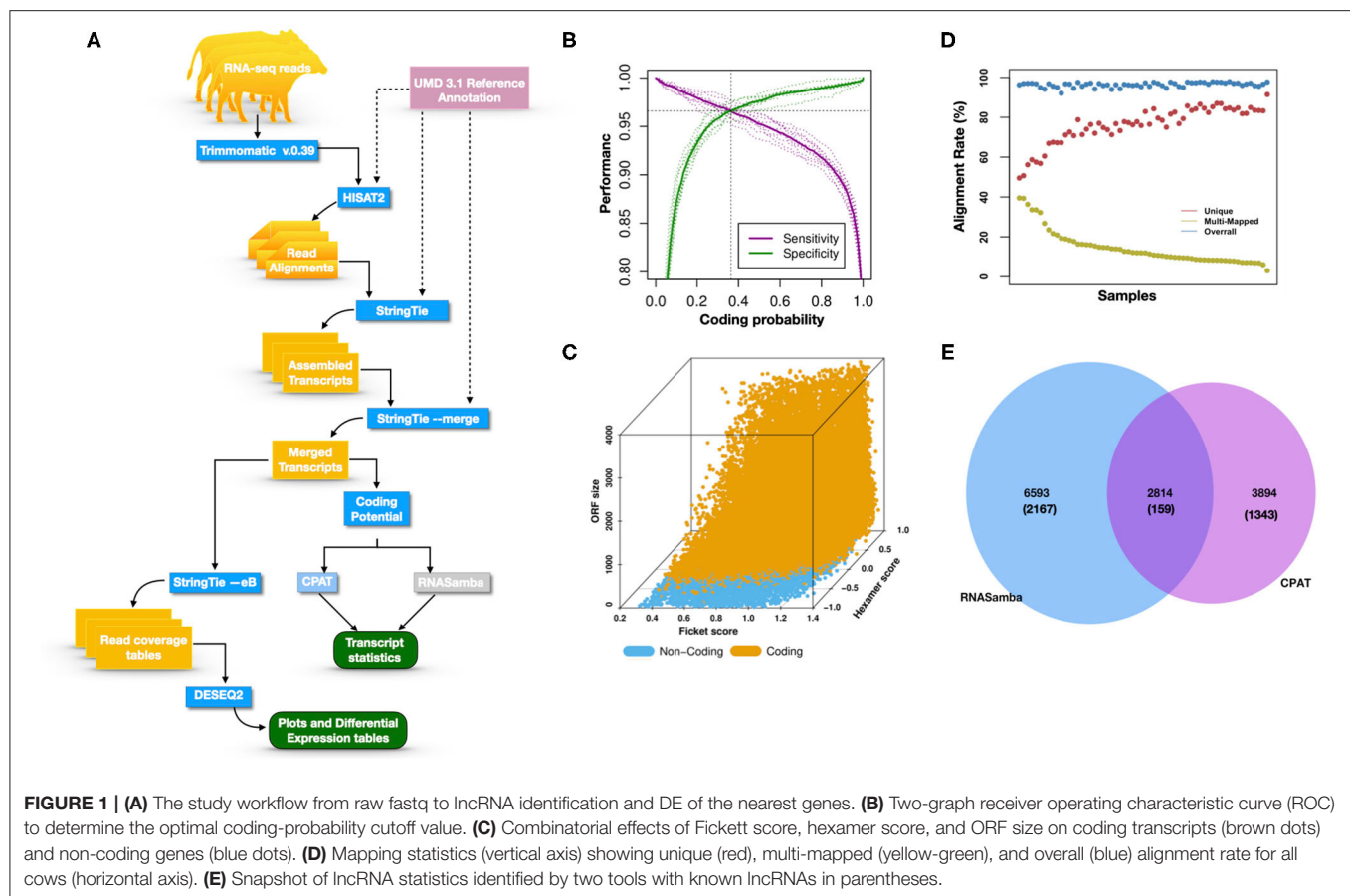
Figure 1A illustrates the steps of transcriptome assembly. Illumina adapter sequences were trimmed from each RNA-Seq read using Trimmomatic (V0.39), keeping reads longer than 36 bp and with a Phred score ≥ 30 . Reads were mapped to UMD 3.1.1 bovine genome assembly using HISAT2 (v2.2.0) and transcripts assembled using StringTie (v2.1.0). We merged assembled transcripts from all cows using the—merge option of StringTie, resulting in non-redundant assembled transcripts. Using Gffcompare (v0.10.1), transcripts were then compared with Ensembl bovine gene annotation (release 94) to identify transcripts overlapping with known protein-coding and non-coding regions. To identify lncRNA, we used the transcript classification codes of Gffcompare to select transcripts categorized as “u” and with a length of ≥ 200 nt.

Transcripts were analyzed using two approaches: (1) estimation of transcript coding probability and (2) differential expression (DE) analysis. Coding probability was estimated using two tools: RNAsamba (46) and CPAT (v2.0.0) (45). Both tools were tested using the *Bos taurus* dataset of known and unknown protein-coding sequences to train the models. RNAsamba computes RNA sequences' coding potential using a neural network classification model resulting in sequences classified as coding or non-coding based on an estimated coding score. The approach of CPAT uses a logistic regression model. Also, CPAT evaluates each base's unequal content frequency and asymmetrical distribution in the positions of codons in one sequence, i.e., the Fickett score and usage bias of adjacent amino acids in proteins, namely, the hexamer score. The models' respective outputs were evaluated using 20-fold cross-validation to determine the coding probability cutoff (**Figures 1B,C**). Using usearch (50), transcripts with a coding probability of ≤ 0.4 and ORF ≤ 300 bp were selected. Sequences were further filtered out if they blasted against the Swiss-Prot database ($e < 1 \times 10^{-05}$). The final dataset was compared to the NONCODEV5 database (51). Those annotated were qualified as known bovine lncRNA, and the remaining isoform transcripts (code = “j”) were classified as novel lncRNA.

We used DESeq2 (v1.26.0) for DE analysis using raw read counts of each sample from the final retained dataset. DESeq2 calculates each sample size factor to correct for library size and RNA composition bias (52). We considered lncRNA as truly expressed if normalized counts ≥ 5 in at least 10% of our libraries and an FDR < 0.5 . To explore the functions of significant DE lncRNA, we used bedtools to obtain the genes 100 kb of each lncRNA. We performed gene ontology (GO) term enrichment analysis using the Panther classification system (53) and Reactome pathways (54). Significance was expressed as *P*-value, with a lower *P*-value indicating higher significance.

RESULTS AND DISCUSSION

In most dairy cows, JD progression is slow, primarily due to the ability of MAP to lodge in intestinal tissue-resident phagocytic



cells and escape the immune system's surveillance. Myeloid cells, including monocytes, macrophages, and neutrophils, work in concert with lymphoid cells to initiate and amplify innate and adaptive immunity. Previous reports indicate that lncRNA plays a significant role in regulating the immune response toward several bacterial pathogens known to induce *Mycobacterium tuberculosis* infection in human macrophages (55). We hypothesized that lncRNA could be part of the mechanisms employed by MAP to control macrophages. The current study provides information (1) on potentially lncRNA-targeted genes affected by MAP infection to weaken the host and (2) on the biological pathways that might lead to susceptibility to MAP infection. In our study, RNA-Seq data from macrophages of 33 cows diagnosed JD positive (+), and 33 JD negative (-) cows were used, among which the study of differential gene expression of 12 cows was previously described (49).

Prediction of lncRNA From Expressed in Bovine Macrophages

To investigate the potential role of lncRNA in macrophages for JD susceptibility, we used RNA-Seq data of macrophages from JD(+) and JD(-) cows. Previous studies have demonstrated the importance of a strong correlation between read alignments and accurate transcript assembly and quantification since misaligned

reads usually decrease the number of reconstructed genes (56). In our previous study (49), we analyzed the differentially expressed (DE) genes in macrophages from JD(+) and JD(-) cows using a TopHat-Cufflink pipeline. In the current study, we used HISAT2 because this program, while aligning RNA-Seq reads to the genome, discovers transcript splice sites and provides an accurate representation of all transcript isoforms, creating a rigorous representation of lncRNA (56).

Identifying and inferring lncRNA's biological role is challenging, more so for dairy cattle, where the functional annotation of lncRNA is limiting (57). This study implemented a computational pipeline based on the "new Tuxedo" package (56). As illustrated in **Figure 1A**, we used HISAT2, StringTie, and Gffcompare to align transcripts to the reference genome, assemble the transcripts, and produce transcript statistics, thus allowing us to obtain results comparable to previous lncRNA studies in cattle (38, 40, 58). Furthermore, we obtained promising alignment statistics (>92% concordant alignment for all samples, **Figure 1D**) with HISAT2, which was more accurate compared to its preceding software (59, 60), and exhibited a faster search algorithm (61). After mapping a minimum of 13 million paired reads per cow to the UMD 3.1.1 bovine reference genome, on average, 71% were uniquely aligned, 14% were multi-mapped, and the average overall alignment rate was 92% (**Figure 1D**). Of the lncRNAs identified in this study, 45.05% had an average

length of 600 bp long with a range of 200–1,000 bp, most of which were mostly intergenic. This result concurred with previous reports that lncRNAs are mainly located between genes (i.e., intergenic) with a smaller overlap within genic regions (42, 44). Moreover, though previous studies indicate intergenic lncRNA may act in cis or trans to regulate gene activities (62, 63), the ever-continuing curation of the bovine functional lncRNA annotation posed a challenge to study how the identified lncRNA may act in trans to regulate distant genes.

With the low multi-mapped read rate and high overall alignment rate, we were confident that false-positive alignments would not disrupt StringTie's flow algorithm and skew the expression estimates of assembled transcripts. Parsed mapped files identified 47,683 potential transcripts, of which 13,301 were putative lncRNA (i.e., had a code = "u"). CPAT and RNAsamba predicted 3,894 and 6,593 as non-coding transcripts, respectively, with an intersection of 2,814 non-coding transcripts (Figure 1E). Most of the lncRNA were <1,000 base pairs, with the shortest lncRNA being on chromosomes 12, 26, 27, and X, with *ENSBTAG00000046640*, *LBX1*, *ER11*, and *AMELX* being the closest genes, respectively (Table 1). Chromosomes X and 18 report the highest number of lncRNAs identified in bovine macrophages, with 1,385 and 1,054 lncRNA, respectively (Figure 2).

Novel lncRNA in Bovine Macrophages

Among the 16,970 lncRNA predicted by the two tools, 3,669 were novel non-coding transcripts, and 385 were known lncRNA. Interestingly, most novel lncRNAs identified in bovine macrophages were mapped on chromosomes X and 18 (Figure 2 and Supplementary File 1). Chromosomes 26 and 28 had the least number of novel non-coding transcripts, with 148 and 161 lncRNAs, respectively (Supplementary File 1). CPAT predicted a smaller number of overall non-coding transcripts, but 35% of these were novel, whereas RNAsamba predicted a larger number of non-coding transcripts, of which 33% were novel lncRNA (Figure 1E).

Differential Expression (DE) of lncRNA in Macrophages From JD(+) and JD(−) Cows

The differential expression (DE) analysis method usually has the most substantial impact on results (64, 65). For this study, we used DESeq2 to study DE of lncRNA detected in macrophages from JD(+) and JD(−) cows. DESeq2 performs robustly in comparison to other existing DE tools (66). As presented in Table 1 and Figure 3, DE analysis using the two predictor tools identified the lncRNA having the greatest significance ($P < 0.05$) for all chromosomes. The two longest DE lncRNAs were on chromosomes 4 and 10, within a 0.5-Mb region ($P = 3.45 \times 10^{-03}$), at 49 Kb from the *FZD1* gene, and within a 0.1-Mb region ($P = 4.45 \times 10^{-04}$) close to the *FLRT2* gene, respectively (Table 2 and Figure 3). Interestingly, the Frizzled Class Receptor 1 gene (*FZD1*) was DE in our previous study, where fold change was estimated using FPKM: *FZD1* was 15.56 times more expressed in macrophages from JD(+) cows than JD(−) macrophages (49). The gene encodes a transmembrane domain protein acting as a receptor for Wnt signaling proteins, which are essential for

regulating pro-inflammatory cytokines in response to bacteria and mycobacterial infection (67).

Ten of the predicted lncRNAs were highly DE at $P < 0.05$ (Table 2). The most highly DE lncRNA was downregulated by ~3-fold change (FC) ($\text{Log}_2 -1.58 \pm 0.4$) in JD(+) compared to JD(−) macrophages. This lncRNA is located within a 0.4-Kb region on chromosome 24 and is close to the predicted twisted gastrulation protein homolog one gene (*TWSG1*) (Table 2). *TWSG1* was found expressed in bovine macrophages and, interestingly, was previously significantly downregulated by 0.70 Log_2FC in response to MAP infection at 4 h post-infection (4 hpi) (49). The second highest DE was an lncRNA of 0.3 Kb located on chromosome 20 with a Log_2FC of $-1.23 (\pm 0.4)$. The negative Log_2FC indicates that macrophages from JD(+) cows have 2.35 times fewer lncRNA transcripts than macrophages from JD(−) cows. This lncRNA is 13 Kb away from *Bos taurus* biorientation of chromosomes in cell division 1 gene (*BOD1*). Although *BOD1* is a provisional NCBI gene (accession no. NM_001076200), *BOD1* expression was detected in bovine macrophages (49) but was however not found DE between JD(−/+) groups. Two lncRNAs with the greatest Log_2FC are located in a 31-Kb region of chromosome 9 ($\text{FC} = 2.35$, $P = 6.65 \times 10^{-04}$, vicinity of *AKAP12*) and in a 108-Kb region of chromosome 10 ($\text{Log}_2\text{FC} = 2.81$, $P = 4.45 \times 10^{-04}$, vicinity of *FLRT2*). These lncRNAs' impact on *AKAP12* and *FLRT2* is unlikely because these computationally predicted genes were not found expressed in macrophages (49). However, these lncRNAs' role in JD should not be excluded considering their potential activity on trans-target genes. Overall, there were 255 DE genes within the neighborhood of the lncRNA transcripts (Supplementary Figure 1).

Functions of lncRNA on the Different Biological Systems in Macrophages

The 255 DE genes were used to explore the functions of significant DE lncRNAs. Part of the Reactome pathways and Panther classification system analysis are presented in Table 3 with some of the Gene Ontology (GO) terms. A detailed report is found in Supplementary File 1. The analysis revealed 14 significant enrichment in the Reactome pathways, among the 1,287 enriched pathways. The highest significant enriched Reactome pathway was the Nuclear Receptor transcription pathway (R-HSA-383280, $P = 1.69 \times 10^{-5}$). Interestingly, part of this pathway is the Nuclear Receptor Subfamily 3 Group C Member 1 gene (*NR3C1*). *NR3C1* was previously found expressed in bovine macrophages and being upregulated nearly 2-fold in response to MAP infection (Log_2FC 0.8; $P < 0.05$) (49). This gene encodes a glucocorticoid receptor and chiefly binds small diffusible signaling molecules in the cytoplasm. Upon ligand binding, it migrates to the nucleus to bind glucocorticoid response elements in the promoters of glucocorticoid-responsive genes (68). While its role in JD is not reported, upon glucocorticoid-receptor bindings, various physiological functions, notably those involved in metabolism, inflammatory processes, and stress, are affected (69). This *NR3C1* gene was also identified in the Panther classification system (Table 4 and Supplementary File 1). The *NR3C1*

TABLE 1 | Location of the highest DE lncRNAs in macrophages from JD(+) vs. JD(-) cows identified on *Bos taurus* autosomes 1–29 and chromosome X.

Chrom ^a	Start	End	Length (kb) ^b	Closest gene (kb) ^c	Gene ^d	Mean ^e	Fold change ^f	Wald statistic ^g	P-value ^h
1	128523379	128576527	53.15	—	<i>ZBTB38</i>	10198.41	0.25 (±0.08)	3.23	1.25e-03
2	59365700	59366021	0.32	10.25	<i>HNMT</i>	43.3	-0.23 (±0.15)	-1.48	1.30e-01
3	120249265	120249575	0.31	20.37	<i>ANKMY1</i>	56.44	-0.64 (±0.22)	-2.91	3.65e-03
4	7843837	8440753	596.92	49.92	<i>FZD1</i>	3159.91	0.53 (±0.18)	2.92	3.45e-03
5	28846068	28846987	0.92	0.12	<i>LETMD1</i>	111.3	-0.34 (±0.14)	-2.36	1.00e-02
6	52972592	52972837	0.24	964.81	<i>PCDH7</i>	8.3	1.12 (±0.54)	2.09	3.00e-02
7	21107248	21107521	0.27	7.63	<i>CREB3L3</i>	35.87	-0.59 (±0.21)	-2.78	5.51e-03
8	23054554	23054855	0.3	0.01	<i>ENSBTAG00000039963</i>	15.44	-1.41 (±0.79)	-1.79	7.00e-02
9	89536157	89567424	31.27	—	<i>bta-mir-2285e-2</i>	1033.91	1.23 (±0.36)	3.4	6.65e-04
10	98235095	98343170	108.08	—	<i>FLRT2</i>	218.23	1.49 (±0.42)	3.51	4.45e-04
11	43739783	43741807	2.02	24.14	<i>RF00026</i>	10148.11	0.18 (±0.1)	1.86	6.00e-02
12	52352608	52352826	0.22	0.28	<i>ENSBTAG00000046640</i>	18.24	-0.49 (±0.22)	-2.19	2.00e-02
13	46917583	46917875	0.29	82.89	<i>LARP4B</i>	14.21	-0.32 (±0.23)	-1.37	1.70e-01
14	57874677	57874911	0.23	89.6	<i>TMEM74</i>	5.22	1.09 (±0.41)	2.66	7.89e-03
15	22944062	22952348	8.29	23.66	<i>PTS</i>	5.9	0.67 (±0.29)	2.3	2.00e-02
16	44005434	44008857	3.42	0.77	<i>DFFA</i>	2764.31	-0.34 (±0.19)	-1.79	7.00e-02
17	6578427	6636825	58.4	—	<i>SH3D19</i>	129.96	0.64 (±0.27)	2.34	1.00e-02
18	65524855	65525608	0.75	1.97	<i>ENSBTAG00000013020</i>	314.44	0.36 (±0.11)	3.29	9.86e-04
19	43812878	43813292	0.41	0.64	<i>NBR1</i>	1843.89	0.29 (±0.15)	1.94	5.00e-02
20	5251758	5252057	0.3	13.05	<i>BOD1</i>	12.56	-1.23 (±0.37)	-3.35	8.22e-04
21	14494659	14522280	27.62	10.08	<i>ENSBTAG00000048002</i>	18545.49	0.21 (±0.12)	1.8	7.00e-02
22	58285995	58286273	0.28	0.45	<i>CCDC174</i>	9.15	1 (±0.3)	3.39	6.97e-04
23	9006094	9006521	0.43	1.1	<i>ANKS1A</i>	547.63	-0.2 (±0.1)	-1.93	5.00e-02
24	42014626	42014991	0.36	6.48	<i>TWSG1</i>	8.31	-1.58 (±0.04)	-4.19	2.81e-05
25	32467533	32467886	0.35	—	<i>RF00002</i>	25187.9	0.5 (±0.04)	1.23	2.10e-01
26	21892569	21892785	0.22	1.62	<i>LBX1</i>	8.22	-0.75 (±0.01)	-1.28	2.00e-01
27	24191077	24191301	0.22	1.82	<i>DPH1</i>	27.11	1.11 (±0.3)	3.77	1.63e-04
28	280436	280721	0.28	0.76	<i>CCSAP</i>	108.71	0.28 (±0.01)	1.42	1.50e-01
29	30263006	30263284	0.28	44.06	<i>KIRREL3</i>	1.65	-1.27 (±0.5)	-2.35	1.00e-02
X	137567452	137567677	0.22	10.99	<i>AMELX</i>	2.4	-1.88 (±0.6)	-2.87	4.07e-03

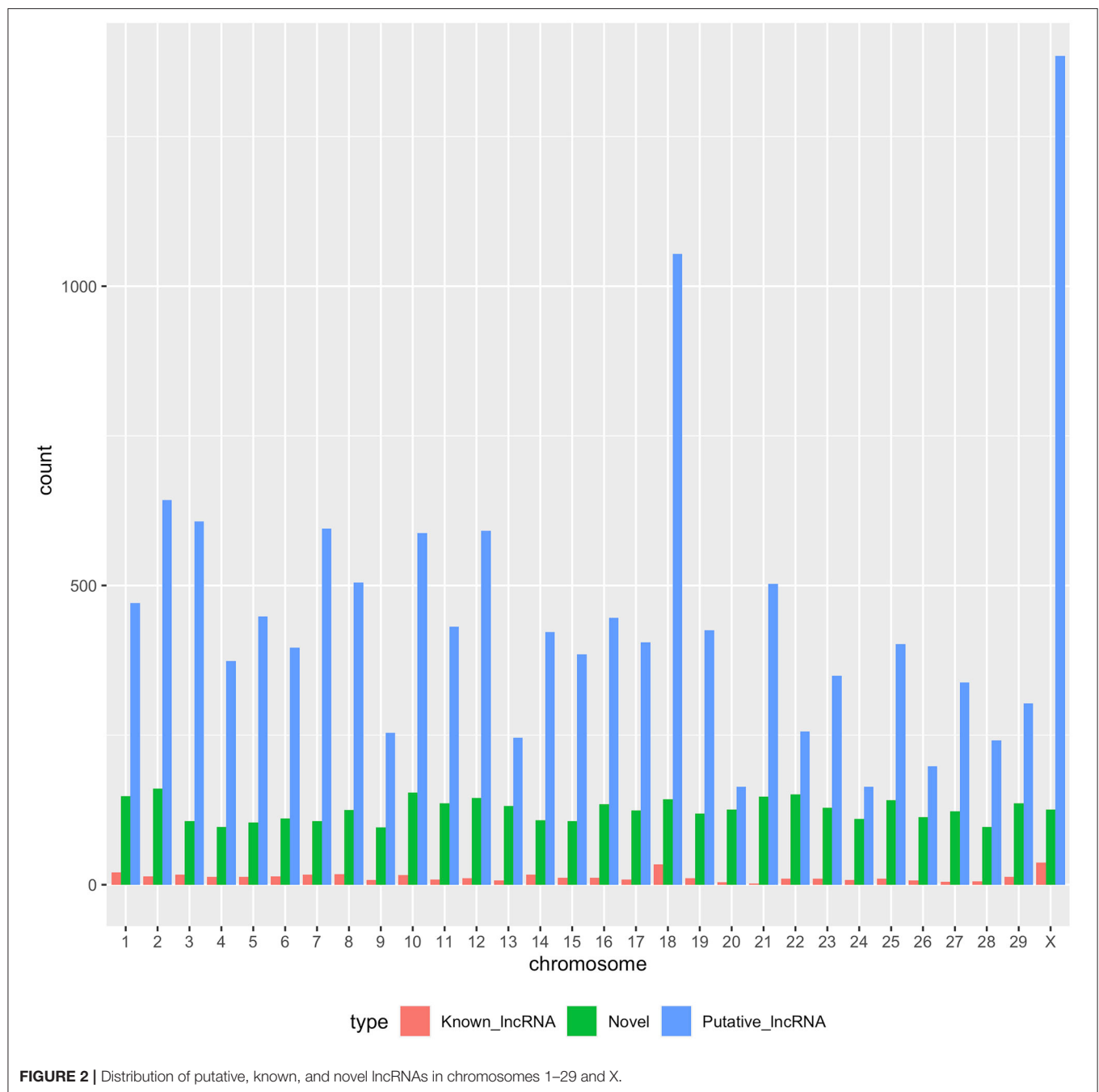
^aChrom: *Bos taurus* chromosome.^bLength (kb): length of the lncRNA transcript calculated as the difference between the start and end positions expressed as thousand base pairs.^cClosest gene (kb): the distance to the closest coding gene.^dGene: the gene closest to the significant transcript.^eMean: the average of normalized counts for all cows.^fFold change: for a particular gene, the log₂ fold change of -1 for cows scored as JD(+) vs. JD(-) cows means that *Mycobacterium avium* subspecies *paratuberculosis* (MAP) infection induces a DE level of 2⁻¹ in JD(+) macrophages compared to JD(-) macrophages.^gWald statistic: Results from a likelihood ratio test comparing the estimated standard error of a log₂ fold change to test if it is equal to zero between the cow status (negative, positive).^hP-value: False discovery rate adjusted P-value at 0.05.

molecular function falls in “glucocorticoid receptor activity” (GO:0004883; $P = 8.45 \times 10^{-03}$) of the biological activity “glucocorticoid mediated signaling pathway” (GO:0043402) with the highest fold (118.25) enrichment pathway (Table 3). As presented in Table 4, this nuclear receptor *NR3C1* gene was found in “RNA polymerase II cis-regulatory region sequence-specific DNA binding” (GO:0000978; $P = 1.16 \times 10^{-04}$), in “cis-regulatory region sequence-specific DNA binding” (GO:0000987; $P = 1.56 \times 10^{-04}$), and in “sequence-specific DNA binding” (GO:0043565; $P = 1.57 \times 10^{-04}$) pathways (70–72).

A second significant enriched pathway, which includes genes found expressed in bovine macrophages, is the RNA

Polymerase I Promoter Escape (Table 3). Interestingly, the *TWISTNB* gene, which encodes the RNA polymerase I subunit F, was upregulated to 2.42 FC ($P = 5 \times 10^{-04}$) in macrophages from JD(+) cows (49), suggesting increased recruitment of Pol I to rDNA promoters in macrophages from JD(+) cows.

The complete list of GO terms from categories of the Panther classification system, notably molecular function, cellular components, and biological processes, is presented in Supplementary File 1. The biological process category reported 3,144 pathways, of which 2,117 had 2-fold enrichment or better; molecular function reported 148 pathways with 132 having at least a 2-fold enrichment; and 153 pathways had a cellular



component with 26 pathways having a 2-fold enrichment or better (**Supplementary File 1**).

It is well-known for *M. tuberculosis* (73) and suggested for MAP (12) that preventing acidification or fusion of the phagosome to the lysosome is a surviving strategy. Interestingly, several lncRNAs were identified in cellular components associated with lytic vacuole membrane (GO:0098852), lysosomal membrane (GO:0005765), and endocytic vesicle membrane (GO:0030666). Two genes located in the lysosomal membrane were previously found

downregulated in macrophages in response to MAP infection, namely, the Solute Carrier Family 2 Member 8 gene (*SLC2A8*) and the Solute Carrier Family 48 Member 1 (*SLC48A1*) (data shown). It is of particular interest that *SLC48A1* encodes to a heme transporter in the context that MAP (70) as for other mycobacteria (71, 72) relies on the host for the acquisition of iron (Fe) which is critical for their growth. Other cellular components were the extracellular exosome (GO:0070062, $P = 3.18 \times 10^{-25}$) and vesicle (GO:1903561, $P = 5.63 \times 10^{-24}$) which were the most significant cellular components

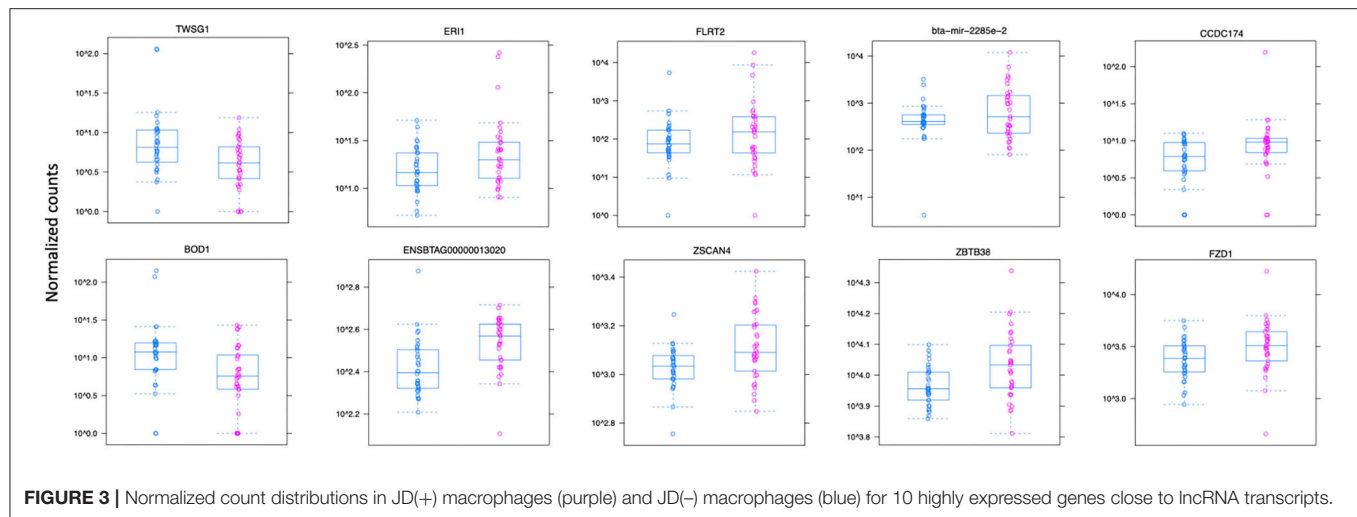


FIGURE 3 | Normalized count distributions in JD(+) macrophages (purple) and JD(-) macrophages (blue) for 10 highly expressed genes close to lncRNA transcripts.

with a similar high fold enrichment (~ 30). Interestingly, the histamine N-methyltransferase gene (*HNMT*) was significantly downregulated by 2.7-fold in macrophages infected by MAP at 4 hpi (49).

One of the longest significant lncRNAs, as mentioned above, is in the vicinity of the *FZD1*-encoded transmembrane protein, identified associated with the cellular component focal adhesion (GO:0005925). The molecule *FZD1* functions as protein binding (GO:0005515), a critical Wnt/ β -catenin negative feedback loop for repression of Toll-like receptor (TLR)-triggered inflammatory responses (74). This cell receptor in macrophages performs Wnt signaling to regulate pro-inflammatory cytokines in response to bacteria and mycobacterial infection (67). Interestingly, *FZD1* and its ligand Wnt3a are involved in reprogramming *Mycobacterium tuberculosis*-infected macrophages (75). This is particularly interesting for JD while supporting our hypothesis developed based on our previous study (49) and other studies (76) that JD(+) macrophages may be responsive because of tolerance, i.e., epigenetic reprogramming. *FZD1* was found more expressed in macrophages from JD(+) cows than JD(-) macrophages and might explain the phenotypes observed for JD(+) macrophages (49).



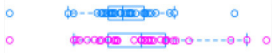


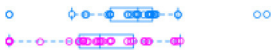
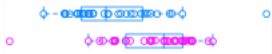



lncRNA's Putative Role of JD-Associated lncRNA in the Immune Response

Though not among the most significant GO terms, immunoreceptor activity (GO:0140375) had a 5.18-fold enrichment. This high fold enrichment is of interest because this function is responsible for receiving a signal and transmitting it in a cell to initiate an immune response during an invasion by a pathogen. The top 10 GO terms involved with biological processes were associated with neutrophils, for instance, neutrophil degranulation (GO:0043312, $P = 7.08 \times 10^{-12}$), which is involved in regulated exocytosis of secretory granules, neutrophil-mediated immunity (GO:0002446, $P = 3.2 \times 10^{-09}$), and neutrophil activation (GO:0042119, $P = 2.61 \times 10^{-08}$). For *Mtb* infection, secreted products from neutrophils regulate

the macrophage activity (77). Since neutrophils are part of the first line of innate immunity of healthy cows (78) and are the second type of cell migrating in lesions of experimentally MAP-infected calves (79), the involvement of these pathways to support neutrophils in their role for pathogen clearance is highly relevant. Interestingly, the “negative regulation of T cell-mediated cytotoxicity” (GO: GO:0001915, $P = 3.1 \times 10^{-04}$) was among the top enriched biological processes. Both genes associated with this pathway, notably *CEACAM1* and interleukin (IL) 7 receptor gene (*IL7R*), were expressed in bovine macrophages, and most interestingly is *IL7R* that was up to 7-fold increased in macrophages in response to MAP infection at 4–8 hpi (49). Aberrant plasma IL7 and soluble IL7 receptor levels indicate impaired T-cell response in human tuberculosis (80), and gene expression of *IL7R* had significant discriminatory power between tuberculosis-positive and -negative patients (81). The relevance of studying the lncRNA associated with *IL7R* in the pathogenesis of MAP also merits that *IL7R* is an immune biomarker validated for detecting clinical tuberculosis (82).

Gene ontology (GO) indicated that lncRNA influences, among others, the inflammation, the evidence of which is well-documented for macrophages (83–85). The myeloid differentiation primary response (MyD88) pathway was confirmed to be affected by MAP infection in our previous study (49). Interestingly, previous studies have shown that mice with knocked-out Myd88 are highly susceptible to infection by *M. tuberculosis* (86), implying that the MyD88-dependent toll-like receptor signaling pathway could be a mycobacterial target for pathogen evasion of host responses. As expected, lncRNA target genes were significantly enriched for biological process GO terms involved in this immune regulation (GO:0034146, GO:0002755). Previous studies report that lncRNA may bind to their target genes; hence, it is unsurprising that the nucleic acid regulation GO terms were enriched (87). GO terms (e.g., GO:0043312, GO:0002446, and GO:0042119) were characterized by pathways associated with neutrophils reported to provide the first line of cellular defense against bacterial colonization in cattle (88).

TABLE 2 | The top 10 most significant DE lncRNAs in macrophages ranked by the FDR corrected *P*-value.

Chromosome	Start	End	Dispersion ^a	Length (kb) ^b	Closest gene (kb) ^c	Gene ^d	Mean ^e	Log2 FC ^f	Wald statistic ^g	<i>P</i> -value ^h
24	42014626	42014991		0.36	6.48	<i>TWSG1</i>	8.31	-1.58 (± 0.4)	-4.19	2.81e-05
27	24191077	24191301		0.22	1.82	<i>DPH1</i>	27.11	1.11 (± 0.3)	3.77	1.63e-04
10	98235095	98343170		108.08	—	<i>FLRT2</i>	218.23	1.49 (± 0.4)	3.51	4.45e-04
9	89536157	89567424		31.27	—	<i>AKAP12</i>	1033.91	1.23 (± 0.4)	3.4	6.65e-04
22	58285995	58286273		0.28	0.45	<i>CCDC174</i>	9.15	1 (± 0.3)	3.39	6.97e-04
20	5251758	5252057		0.3	13.05	<i>BOD1</i>	12.56	-1.23 (± 0.4)	-3.35	8.22e-04
18	65524855	65525608		0.75	1.97	<i>ZNF814</i>	314.44	0.36 (± 0.1)	3.29	9.86e-04
18	65255175	65265109		9.93	13.44	<i>ZSCAN4</i>	1216.85	0.31 (± 0.1)	3.29	1.01e-03
1	128523379	128576527		53.15	—	<i>ZBTB38</i>	10198.41	0.25 (± 0.1)	3.23	1.25e-03
4	7843837	8440753		596.92	49.92	<i>FZD1</i>	3159.91	0.53 (± 0.2)	2.92	3.45e-03

^aDispersion: Visual representation of normalized count dispersion of lncRNA in a specific region of a selected chromosome in JD(+) macrophages (purple) and JD(-) macrophages (blue).

^bLength (kb): Length of the lncRNA transcript calculated as the difference between the start and end positions expressed as thousand base pairs.

^cClosest gene (kb): The distance from the significant lncRNA to the closest coding gene.

^dGene: The closest gene to the significant lncRNA transcript. Genes expressed in bovine macrophages are in bold characters.

^eMean: The average of normalized counts for all cows.

^fFold change: For a particular gene, the log₂ fold change of -1 for cows scored as Positive vs. cows scored as Negative means that infection of *Mycobacterium avium* subspecies *paratuberculosis* (MAP) for JD(+) cows induces a multiplicative change in macrophages, observed as the gene expression level of 2⁻¹ compared to the macrophages from JD(-) cows.

^gWald statistic: Result of a likelihood ratio test comparing the estimated standard error of a log₂ fold change to test if it is equal to zero between the cow status [JD(-), JD(+)].

^h*P*-value: False discovery rate adjusted *P*-value at 0.05.

TABLE 3 | Enriched Reactome pathways using 255 DE lncRNA.

Reactome pathway name	Genes			Reactions ratio ^c	Genes found ^d
	Found	Ratio ^a	P-value ^b		
Nuclear receptor transcription pathway	10/107	5.84e-03	1.69e-05	1.53e-04	<i>ATXN7</i> , <i>NR3C1</i>
Deletions in the AMER1 gene destabilize the destruction complex	1/1	6.79e-05	1.66e-02	7.63e-05	<i>AMER1</i>
RNA polymerase I promoter escape	4/64	4.35e-03	2.34e-02	1.53e-04	<i>CBX3</i> , <i>H2AFZ</i> , <i>POLR1B</i> , <i>TWISTNB</i>
Misspliced GSK3beta mutants stabilize beta-catenin	2/15	1.02e-03	2.66e-02	7.63e-05	<i>AMER1</i> , <i>PPP2R5A</i>
Phosphorylation site mutants of CTNNB1	2/16	1.09e-03	3.00e-02	3.05e-04	<i>AMER1</i> , <i>PPP2R5A</i>
Beta-catenin phosphorylation cascade	2/19	1.29e-03	4.09e-02	3.05e-04	<i>AMER1</i> , <i>PPP2R5A</i>
RUNX3 regulates YAP1-mediated transcription	2/20	6.11e-04	4.48e-02	2.29e-04	<i>TEAD4</i> , <i>TAZ</i>
Physiological factors	2/21	8.83e-04	4.89e-02	3.05e-04	<i>KAT2B</i> , <i>TAZ</i>
Defective ALG12 causes ALG12-CDG (CDG-1g)	1/3	2.04e-04	4.89e-02	7.63e-05	<i>ALG12</i>
MyD88 deficiency (<i>TLR5</i>)	1/3	2.04e-04	4.89e-02	7.63e-05	<i>TLR5</i>

^aRatio: the ratio of entities from this pathway to all Reactome entities.

^bP-value: the result of the statistical test for overrepresentation, for molecules of the type of the results selected which have been corrected for overrepresentation probability.

^cReactions ratio: the ratio of reactions from this pathway to all Reactome reactions.

^dGenes found: some of the genes associated with the Reactome pathway. Genes expressed in bovine macrophages are in bold characters.

We observed little overlap between predicted lncRNA candidates and the previously published cattle non-coding RNA. This little overlap may partially be because the lncRNA library is not fully curated in dairy cattle or that previously published non-coding RNA was identified in different tissues since lncRNAs show tissue- and cell-specific expressions. This study does have limitations; one is the incomplete bovine annotation where many unannotated genes exist, both protein- and non-protein-coding. In the current state, this would render the unknown transcripts in our data moot. Collaborative projects may eventually lead to creating a comprehensive map of functional elements in cattle's genome, allowing better identification of potential bovine lncRNA.

A good example is the Functional Annotation of Animal Genomes (FAANG) (89). Previous studies have identified lncRNA using *in vitro* infected macrophages (41). However, our study's novelty aimed to identify genome-wide lncRNAs using primary monocyte-derived macrophages for naturally MAP infected cows.

Our study's rigor also comes from the culture protocol of macrophages that do not bias macrophages' polarization. In Gupta et al. (41), macrophages were cultured in the presence of fetal bovine serum (FBS) and were differentiated in the presence of macrophage colony-stimulating factor (M-CSF). The effect of a culture medium on polarization when supporting monocytes' differentiation has been rigorously documented (90). It turns out that the presence of fetal bovine serum (FBS) and stimulating factors, such as GM-CSF or M-CSF allow a differentiation of the monocytes that activate and polarize them (90). The presence of FBS affects the functionality of monocyte-derived macrophages (91). FBS contains a considerable amount of immunoregulatory cytokines and bioactive molecules, notably the transforming growth factor- β (TGF- β) in notable concentrations (92) that yields a dominant immunosuppressive phenotype in the presence of M-CSF (93). This is all the more important since polarization impacts the

lncRNA profile in macrophages (30). An additional novelty of our study is that macrophages were differentiated in the absence of FBS and that no stimulating factors were used to avoid polarization bias. It might explain that we identified 3,669 novel lncRNAs in bovine macrophages compared to 397 novel lncRNAs in the previous study (41).

Dairy and beef studies continuously use underlying biological information of point mutations (e.g., SNP) and genomic features to discover which genomic variants are theoretically enriched (94). The bovine lncRNAs reported here could further extend the underlying biological information by including a new class for genomic variants exclusive in lncRNA regions to enrich bovine health traits.

Although human data studies show that single-exon lncRNAs are more likely to be conserved (95), we did not discriminate against lncRNAs from abundant lowly expressed single-exonic fragments. Furthermore, following stringent filtering criteria based on other genomic features like ORF length, protein-coding potential, and expression levels, we identified 16,970 lncRNAs, 3,669 of which were novel lncRNAs with 255 potential cis target genes.

CONCLUSION

In summary, we have provided the lncRNA expression profile of macrophages from JD cows, together with many potential co-regulated candidate protein-coding genes. We have identified 13,589 lncRNAs, 3,669 of which are novel. Among those lncRNAs significantly upregulated in JD(+) macrophages, three were linked (<1 kb) to genes expressed in bovine macrophages, notably *TWSG1*, *DPH1*, and *BOD1*. Bacteria interfere with mammalian regulatory RNA expression, including lncRNA, to modify molecular and cellular signaling. We identified lncRNAs as having the potential to play a significant role in regulating several cellular activities, including the immune response.

TABLE 4 | Gene ontology results using 255 DE lncRNAs.

GO Id ^a	Label ^b	Ratio ^c	P-value	Fold enrichment ^d	Genes ^e
CELLULAR COMPONENT					
GO:0070062	Extracellular exosome	31.75	3.18e-25	37.53	ACOT9, ADAD1, AHR , AKAP12,
GO:1903561	Extracellular vesicle	27.40	5.63e-24	32.39	ALCAM, ALG12, AMELX, AMER1,
GO:0043230	Extracellular organelle	25.97	1.59e-23	30.71	ATXN7, B4GALT4 , BCL2, BEX3,
GO:0043227	Membrane-bounded organelle	1.36	2.86e-16	1.61	BOD1 , CBX3, CCDC174, CCNO,
GO:0043226	Organelle	1.28	6.34e-16	1.51	CEACAM1 , CMTR2, CNOT11, COQ8B,
GO:0005622	Intracellular	1.21	5.43e-15	1.42	DENND4B, DFFA, DPH1 , EBF3,
GO:0031982	Vesicle	2.83	1.57e-13	3.34	FLRT2 , FOXJ2 , FTH1, GALNT6 , GLB1L3,
GO:0005737	Cytoplasm	1.32	2.27e-12	1.56	IRF2BPL, KAT2B, KIRREL3, KLHL9 ,
GO:0043229	Intracellular organelle	1.24	3.84e-12	1.46	NR3C1, NRIP1 , PLEKHM1 , POLR1B ,
					SAMD9 , SLC2A8 , SLC48A1,
					TWISTNB , ZSCAN4, CA8 , UPK1A
MOLECULAR FUNCTION					
GO:0005515	Protein binding	2.29	1.15e-44	2.70	CCNO, CCR6, CCSAR, CDA , CDH11,
GO:0005488	Binding	1.37	3.18e-24	1.62	DFFA, DOK5, DPH1 , EBF3, ENPP2,
GO:0046872	Metal ion binding	1.57	4.98e-06	1.85	ICE2, IFNAR1, IL12B, IL7R, IQSEC1 ,
GO:0043169	Cation binding	1.53	9.96e-06	1.81	MAP3K7CL, NBR1 , POLR1B , PPP2R5A ,
GO:0043167	Ion binding	1.34	1.10e-05	1.58	PRDM1, PRKAR2B, PTS , RHOU, RNF122,
GO:0000978	RNA polymerase II cis-regulatory region sequence-specific DNA binding	2.12	1.16e-04	2.5	RPE, RRAGB, SAE1 , SAMD14, SAMD9,
GO:0000987	cis-Regulatory region sequence-specific DNA binding	2.07	1.56e-04	2.44	SBSN, SCGB1A1, SESTD1, SH3D19,
GO:0043565	Sequence-specific DNA binding	1.81	1.57e-04	2.14	SLC48A1, SNX24, SNX32, SOD1, SPIN2,
GO:0003677	DNA binding	1.59	2.03e-04	1.88	SPNS3,
					STOM , TLR5, TMEM19 , TMEM74, TMEM9,
					TOP1, TRMT12, ELMSAN1, GALNT6 ,
					PCDH7,
					ZNF518A, SAE, ZNF350 , NBR1, TMEM74,
					TWGS1 , IQSEC1 , B4GALT4 ,
					CDA, PPP2R5A
BIOLOGICAL PROCESSES					
GO:0043312	Neutrophil degranulation	75.00	7.08e-12	141.90	ATP6AP2, CDA , CEACAM1, FTH1, MMP25,
GO:0019222	Regulation of metabolic process	1.53	1.25e-10	1.80	STOM, AHR, AKAP12, AMELX, AMER1,
GO:0002283	Neutrophil activation involved in immune response	60.00	4.38e-10	70.95	APPL1, ATXN7, BCL2, BEX3, BOD1 ,
GO:0050789	Regulation of biological process	1.22	8.09e-10	1.43	CBX3, CCNO, CNOT11, CREB3L3,
GO:0031323	Regulation of cellular metabolic process	1.55	9.18e-10	1.83	CREB3L4,
GO:0050794	Regulation of cellular process	1.22	2.46e-09	1.44	DFFA, DOK5, DPH1 , EBF3, ELMSAN1,
GO:0002446	Neutrophil-mediated immunity	42.86	3.20e-09	50.67	ENPP2, ERI1, FOXJ2, FZD1, GRSF1,
GO:0060255	Regulation of macromolecule metabolic process	1.51	3.81e-09	1.78	H2AFZ, HIVEP3, HMG20A , HOMEZ,
GO:0065007	Biological regulation	1.17	4.04e-09	1.38	IBTK , ICE2, IL12B, IL7R , IRF2BPL,
GO:0048518	Positive regulation of biological process	1.53	7.12e-09	1.81	KAT2B, LARP4B, LBX1, LOXL2, LPXN,
GO:0051171	Regulation of nitrogen compound metabolic process	1.53	1.04e-08	1.80	LSM2, MOSPD1, MYBL2 , NBR1, NR3C1,
GO:0042119	Neutrophil activation	30.00	2.61e-08	35.47	NRIP1, OXR1, PDE4B, PIK3R4, PKHD1,
GO:0080090	Regulation of primary metabolic process	1.49	3.38e-08	1.76	POLR1B , PPP2R5A, PRKAR2B, PUM3,
GO:0043299	Leukocyte degranulation	28.57	3.47e-08	33.78	RAD50, RAF1, RBBP6, RBM12B, RRAGB,
					SAE1, SCGB1A1, SH3D19, SNX32, SOD1,
					SPIN2, SPTLC2, TAZ, TEAD4, TIRAP , TLR5 ,
					PAG1 , SLC2A8, SNRK, ZFAND5, PRDM1

^aId: gene ontology (GO) symbol accepted by the broader scientific community and sorted by ascending p-value.

^bLabel: GO term accepted by the broader scientific community.

^cRatio: the proportion of genes submitted and those found to be associated with the GO term.

^dFold enrichment: statistical estimation of obtaining the GO term that is not attributed to random chance.

^eGenes: a snippet of genes associated with the GO domain, more detailed genes available in **Supplementary File 1**. Genes found expressed in bovine macrophages are in bold characters.

Although the mechanisms of MAP are currently unknown, we speculate that many of the identified lncRNAs are essential participants in the bovine innate immune response. At the same time, some could support MAP in macrophages in its duel to escape the surveillance of the immune system that lasts for years.

DATA AVAILABILITY STATEMENT

The datasets presented in this study can be found in online repositories. The names of the repository/repositories and accession number(s) can be found in the article/Supplementary Material.

ETHICS STATEMENT

The animal study was reviewed and approved by Agriculture and Agri-Food Canada Animal Ethics Committee. Written informed consent was obtained from the owners for the participation of their animals in this study.

AUTHOR CONTRIBUTIONS

NB: project administration, supervision, and funding acquisition. AM, OA, and NB: methodology. AM: data curation and formal analysis. AM and NB: writing. All authors provided the input in interpreting the results and have read and agreed to the published version of the manuscript.

FUNDING

This study was funded by Agri-Food and Agriculture Canada (Project AAFC J-000075 and AAFC J-000079). This research was supported by a contribution from the Dairy Research Cluster 3 (Dairy Farmers of Canada, Canadian Dairy Network and Agriculture, and Agri-Food Canada) under the Canadian

Agricultural Partnership AgriScience Program (Project AAFC J-002095).

ACKNOWLEDGMENTS

We appreciate the invaluable collaboration of the veterinarians and dairy producers in the Ontario and Quebec Provinces.

SUPPLEMENTARY MATERIAL

The Supplementary Material for this article can be found online at: <https://www.frontiersin.org/articles/10.3389/fvets.2021.639053/full#supplementary-material>

Supplementary File 1 | (A) Distribution of lncRNA per chromosome; **(B)** General Transfer Format (gtf) of identified lncRNA; **(C)** Reactome pathways; **(D)** General biological programs accomplished by the multiple molecular activities (Biological processes; GO terms); **(E)** Molecular-level activities performed by gene products (molecular functions; GO terms), and **(F)** The locations relative to cellular structures in which a gene product performs a function (Cellular component; GO terms).

Supplementary Figure 1 | Illustration of gene network including genes within 100 kb of highly expressed lncRNA.

REFERENCES

- Whittington R, Donat K, Weber ME, Kelton D, Nielsen SS, Eisenberg S, et al. Control of paratuberculosis: who, why and how. A review of 48 countries. *BMC Vet Res.* (2019) 15:198. doi: 10.1186/s12917-019-1943-4
- Whitlock RH, Buergele C. Preclinical and clinical manifestations of paratuberculosis (including pathology). *Vet Clin North Am Food Anim Pract.* (1996) 12:345–56. doi: 10.1016/S0749-0720(15)30410-2
- Smith RL, Strawderman RL, Schukken YH, Wells SJ, Pradhan AK, Espejo LA, et al. Effect of Johnes's disease status on reproduction and culling in dairy cattle. *J Dairy Sci.* (2010) 93:3513–24. doi: 10.3168/jds.2009-2742
- Garcia AB, Shalloo L. Invited review: the economic impact and control of paratuberculosis in cattle. *J Dairy Sci.* (2015) 98:5019–39. doi: 10.3168/jds.2014-9241
- Corbett CS, Naqvi SA, Bauman CA, De Buck J, Orsel K, Uehlinger F, et al. Prevalence of *Mycobacterium avium* ssp. *paratuberculosis* infections in Canadian dairy herds. *J Dairy Sci.* (2018) 101:11218–28. doi: 10.3168/jds.2018-14854
- Merkal RS, Larsen AB, Kopecky KE, Kluge JB, Monlux WS, Lehmann RP, et al. Experimental paratuberculosis in sheep after oral, intratracheal, or intravenous inoculation: serologic and intradermal tests. *Am J Vet Res.* (1968) 29:963–9.
- Momotani E, Whipple DL, Thiermann AB, Cheville NF. Role of M cells and macrophages in the entrance of *Mycobacterium paratuberculosis* into Domes of ileal Peyer's patches in calves. *Vet Pathol.* (1988) 25:131–7. doi: 10.1177/030098588802500205
- Arsenault RJ, Maattanen P, Daigle J, Potter A, Griebel P, Napper S. From mouth to macrophage: mechanisms of innate immune subversion by *Mycobacterium avium* subsp. *paratuberculosis*. *Vet Res.* (2014) 45:54. doi: 10.1186/1297-9716-45-54
- Koets AP, Eda S, Sreevatsan S. The within host dynamics of *Mycobacterium avium* ssp. *paratuberculosis* infection in cattle: where time and place matter. *Vet Res.* (2015) 46:61. doi: 10.1186/s13567-015-0185-0
- Bannantine JP, Stabel JR. Killing of *Mycobacterium avium* subspecies *paratuberculosis* within macrophages. *BMC Microbiol.* (2002) 2:2. doi: 10.1186/1471-2180-2-2
- Weiss DJ, Souza CD, Evanson OA, Sanders M, Rutherford M. Bovine monocyte TLR2 receptors differentially regulate the intracellular fate of *Mycobacterium avium* subsp. *paratuberculosis* and *Mycobacterium avium* subsp. *avium*. *J Leuk. Biol.* (2008) 83:48–55. doi: 10.1189/jlb.0707490
- Hussain T, Shah SZ, Zhao D, Sreevatsan S, Zhou X. The role of IL-10 in *Mycobacterium avium* subsp. *paratuberculosis* infection. *Cell Commun Signal.* (2016) 14:29. doi: 10.1186/s12964-016-0152-z
- Pinedo PJ, Buergele CD, Donovan GA, Melendez P, Morel L, Wu R, et al. Association between CARD15/NOD2 gene polymorphisms and paratuberculosis infection in cattle. *Vet Microbiol.* (2009) 134:346–52. doi: 10.1016/j.vetmic.2008.09.052
- Ruiz-Larranaga O, Garrido JM, Iriondo M, Manzano C, Molina E, Koets AP, et al. Genetic association between bovine NOD2 polymorphisms and infection by *Mycobacterium avium* subsp. *paratuberculosis* in Holstein-Friesian cattle. *Anim Genet.* (2010) 41:652–5. doi: 10.1111/j.1365-2052.2010.02055.x
- Pinedo PJ, Buergele CD, Donovan GA, Melendez P, Morel L, Wu R, et al. Candidate gene polymorphisms (BoIFNG, TLR4, SLC11A1) as risk factors for paratuberculosis infection in cattle. *Prev Vet Med.* (2009) 91:189–96. doi: 10.1016/j.prevetmed.2009.05.020
- Korou LM, Liandris E, Gazouli M, Ikononopoulos J. Investigation of the association of the SLC11A1 gene with resistance/sensitivity of goats (*Capra hircus*) to paratuberculosis. *Vet Microbiol.* (2010) 144:353–8. doi: 10.1016/j.vetmic.2010.01.009
- Ruiz-Larranaga O, Garrido JM, Manzano C, Iriondo M, Molina E, Gil A, et al. Identification of single nucleotide polymorphisms in the bovine solute carrier family 11 member 1 (SLC11A1) gene and their association with infection by *Mycobacterium avium* subspecies *paratuberculosis*. *J Dairy Sci.* (2010) 93:1713–21. doi: 10.3168/jds.2009-2438
- Verschoor CP, Pant SD, You Q, Schenkel FS, Kelton DF, Karrow NA. Polymorphisms in the gene encoding bovine interleukin-10 receptor alpha are associated with *Mycobacterium avium* ssp. *paratuberculosis* infection status. *BMC Genet.* (2010) 11:23. doi: 10.1186/1471-2156-11-23
- Cinar MU, Hizlisoy H, Akyüz B, Arslan K, Aksel EG, Gümüşsoy KS. Polymorphisms in toll-like receptor (TLR) 1, 4, 9 and SLC11A1 genes and their association with paratuberculosis susceptibility in Holstein and indigenous crossbred cattle in Turkey. *J Genet.* (2018) 97:1147–54. doi: 10.1007/s12041-018-1008-7
- Juste RA, Vazquez P, Ruiz-Larranaga O, Iriondo M, Manzano C, Agirre M, et al. Association between combinations of genetic polymorphisms and epidemiopathogenic forms of bovine paratuberculosis. *Heliyon.* (2018) 4:e00535. doi: 10.1016/j.heliyon.2018.e00535

21. Clarke CJ. The pathology and pathogenesis of paratuberculosis in ruminants and other species. *J Compar Pathol.* (1997) 116:217–61. doi: 10.1016/S0021-9975(97)80001-1
22. Sweeney RW. Pathogenesis of paratuberculosis. *Vet Clin North Am Food Anim Pract.* (2011) 27:537–46. doi: 10.1016/j.cvfa.2011.07.001
23. Kirkpatrick BW. *Genetics of Host Susceptibility to Paratuberculosis.* Cambridge, MA: CABI (2010).
24. Stevenson K. Genetic diversity of *Mycobacterium avium* subspecies *paratuberculosis* and the influence of strain type on infection and pathogenesis: a review. *Vet Res.* (2015) 46:64. doi: 10.1186/s13567-015-0203-2
25. Stabel JR. Host responses to *Mycobacterium avium* subsp. *paratuberculosis*: a complex arsenal. *Anim Health Res Rev.* (2006) 7:61–70. doi: 10.1017/S1466252307001168
26. Duval M, Cossart P, Lebreton A. Mammalian microRNAs and long noncoding RNAs in the host-bacterial pathogen crosstalk. *Semin Cell Dev Biol.* (2017) 65:11–9. doi: 10.1016/j.semcdb.2016.06.016
27. Zur Bruegge J, Einspanier R, Sharbati S. A long journey ahead: long non-coding RNAs in bacterial infections. *Front Cell Infect Microbiol.* (2017) 7:95. doi: 10.3389/fcimb.2017.00095
28. Fitzgerald KA, Caffrey DR. Long noncoding RNAs in innate and adaptive immunity. *Curr Opin Immunol.* (2014) 26:140–6. doi: 10.1016/j.coi.2013.12.001
29. Elling R, Chan J, Fitzgerald KA. Emerging role of long noncoding RNAs as regulators of innate immune cell development and inflammatory gene expression. *Eur J Immunol.* (2016) 46:504–12. doi: 10.1002/eji.201444558
30. Ahmad I, Valverde A, Ahmad F, Naqvi AR. Long noncoding RNA in myeloid and lymphoid cell differentiation, polarization and function. *Cells.* (2020) 9:269. doi: 10.3390/cells9020269
31. Kim J, Kim KM, Noh JH, Yoon JH, Abdelmohsen K, Gorospe M. Long noncoding RNAs in diseases of aging. *Biochim Biophys Acta.* (2016) 1859:209–21. doi: 10.1016/j.bbaggm.2015.06.013
32. Li L, Song X. The working modules of long noncoding RNAs in cancer cells. *Adv Exp Med Biol.* (2016) 927:49–67. doi: 10.1007/978-981-10-1498-7_2
33. Talebian S, Daghighi H, Yousefi B, Ozkul Y, Ilkhani K, Seif F, et al. The role of epigenetics and non-coding RNAs in autophagy: a new perspective for thorough understanding. *Mech Ageing Dev.* (2020) 190:111309. doi: 10.1016/j.mad.2020.111309
34. Zacharopoulou E, Gazouli M, Tzouvala M, Vezakis A, Karamanolis G. The contribution of long non-coding RNAs in inflammatory bowel diseases. *Dig Liver Dis.* (2017) 49:1067–72. doi: 10.1016/j.dld.2017.08.003
35. Ge Q, Dong Y, Lin G, Cao Y. Long noncoding RNA antisense noncoding RNA in the INK4 locus correlates with risk, severity, inflammation and infliximab efficacy in Crohn's disease. *Am J Med Sci.* (2019) 357:134–42. doi: 10.1016/j.amjms.2018.10.016
36. Weikard R, Hadlich F, Kuehn C. Identification of novel transcripts and noncoding RNAs in bovine skin by deep next generation sequencing. *BMC Genomics.* (2013) 14:789. doi: 10.1186/1471-2164-14-789
37. Billerey C, Boussaha M, Esquerre D, Rebours E, Djari A, Meersseman C, et al. Identification of large intergenic non-coding RNAs in bovine muscle using next-generation transcriptomic sequencing. *BMC Genomics.* (2014) 15:499. doi: 10.1186/1471-2164-15-499
38. Koufariotis LT, Chen YP, Chamberlain A, Vander Jagt C, Hayes BJ. A catalogue of novel bovine long noncoding RNA across 18 tissues. *PLoS ONE.* (2015) 10:e0141225. doi: 10.1371/journal.pone.0141225
39. Tong C, Chen Q, Zhao L, Ma J, Ibeagha-Awemu EM, Zhao X. Identification and characterization of long intergenic noncoding RNAs in bovine mammary glands. *BMC Genomics.* (2017) 18:468. doi: 10.1186/s12864-017-3858-4
40. Ibeagha-Awemu EM, Li R, Dudemaine PL, Do DN, Bissonnette N. Transcriptome analysis of long non-coding RNA in the bovine mammary gland following dietary supplementation with linseed oil and safflower oil. *Int J Mol Sci.* (2018) 19:3610. doi: 10.3390/ijms19113610
41. Gupta P, Peter S, Jung M, Lewin A, Hemmrich-Stanisak G, Franke A, et al. Analysis of long non-coding RNA and mRNA expression in bovine macrophages brings up novel aspects of *Mycobacterium avium* subspecies *paratuberculosis* infections. *Sci Rep.* (2019) 9:1571. doi: 10.1038/s41598-018-38141-x
42. Cabili MN, Trapnell C, Goff L, Koziol M, Tazon-Vega B, Regev A, et al. Integrative annotation of human large intergenic noncoding RNAs reveals global properties and specific subclasses. *Genes Dev.* (2011) 25:1915–27. doi: 10.1101/gad.17446611
43. Chen G, Yin K, Shi L, Fang Y, Qi Y, Li P, et al. Comparative analysis of human protein-coding and noncoding RNAs between brain and 10 mixed cell lines by RNA-Seq. *PLoS ONE.* (2011) 6:e28318. doi: 10.1371/journal.pone.0028318
44. Derrien T, Johnson R, Bussotti G, Tanzer A, Djebali S, Tilgner H, et al. The GENCODE v7 catalog of human long noncoding RNAs: analysis of their gene structure, evolution, and expression. *Genome Res.* (2012) 22:1775–89. doi: 10.1101/gr.132159.111
45. Wang L, Park HJ, Dasari S, Wang S, Kocher JP, Li W. CPAT: coding-potential assessment tool using an alignment-free logistic regression model. *Nucleic Acids Res.* (2013) 41:e74. doi: 10.1093/nar/gkt006
46. Camargo AP, Sourkov V, Pereira GAG, Carazzolle MF. RNAsamba: neural network-based assessment of the protein-coding potential of RNA sequences. *NAR Genom Bioinform.* (2020) 2:lqz024. doi: 10.1093/nargab/lqz024
47. Fock-Chow-Tho D, Topp E, Ibeagha-Awemu EA, Bissonnette N. Comparison of commercial DNA extraction kits and quantitative PCR systems for better sensitivity in detecting the causative agent of paratuberculosis in dairy cow fecal samples. *J Dairy Sci.* (2017) 100:572–81. doi: 10.3168/jds.2016-11384
48. Collins MT. Interpretation of a commercial bovine paratuberculosis enzyme-linked immunosorbent assay by using likelihood ratios. *Clin Diagn Lab Immunol.* (2002) 9:1367–71. doi: 10.1128/CDLI.9.6.1367-1371.2002
49. Ariel O, Gendron D, Dudemaine PL, Gevry N, Ibeagha-Awemu EM, Bissonnette N. Transcriptome profiling of bovine macrophages infected by *Mycobacterium avium* spp. *paratuberculosis* depicts foam cell and innate immune tolerance phenotypes. *Front Immunol.* (2019) 10:2874. doi: 10.3389/fimmu.2019.02874
50. Edgar RC. Search and clustering orders of magnitude faster than BLAST. *Bioinformatics.* (2010) 26:2460–1. doi: 10.1093/bioinformatics/btq461
51. Fang S, Zhang L, Guo J, Niu Y, Wu Y, Li H, et al. NONCODEV5: a comprehensive annotation database for long non-coding RNAs. *Nucleic Acids Res.* (2018) 46:D308–14. doi: 10.1093/nar/gkx1107
52. Love MI, Huber W, Anders S. Moderated estimation of fold change and dispersion for RNA-seq data with DESeq2. *Genome Biol.* (2014) 15:550. doi: 10.1186/s13059-014-0550-8
53. Mi H, Muruganujan A, Casagrande JT, Thomas PD. Large-scale gene function analysis with the PANTHER classification system. *Nat Protoc.* (2013) 8:1551–66. doi: 10.1038/nprot.2013.092
54. Jassal B, Matthews L, Viteri G, Gong C, Lorente P, Fabregat A, et al. The reactome pathway knowledgebase. *Nucleic Acids Res.* (2020) 48:D498–503. doi: 10.1093/nar/gkz1031
55. Yang X, Yang J, Wang J, Wen Q, Wang H, He J, et al. Microarray analysis of long noncoding RNA and mRNA expression profiles in human macrophages infected with *Mycobacterium tuberculosis*. *Sci Rep.* (2016) 6:38963. doi: 10.1038/srep38963
56. Pertea M, Kim D, Pertea GM, Leek JT, Salzberg SL. Transcript-level expression analysis of RNA-seq experiments with HISAT, StringTie and Ballgown. *Nat Protoc.* (2016) 11:1650–67. doi: 10.1038/nprot.2016.095
57. Weikard R, Demasius W, Kuehn C. Mining long noncoding RNA in livestock. *Anim Genet.* (2017) 48:3–18. doi: 10.1111/age.12493
58. Kern C, Wang Y, Chitwood J, Korf I, Delany M, Cheng H, et al. Genome-wide identification of tissue-specific long non-coding RNA in three farm animal species. *BMC Genomics.* (2018) 19:684. doi: 10.1186/s12864-018-5037-7
59. Kim D, Pertea G, Trapnell C, Pimentel H, Kelley R, Salzberg SL. TopHat2: accurate alignment of transcriptomes in the presence of insertions, deletions and gene fusions. *Genome Biol.* (2013) 14:R36. doi: 10.1186/gb-2013-14-4-r36
60. Kim D, Langmead B, Salzberg SL. HISAT: a fast spliced aligner with low memory requirements. *Nat Methods.* (2015) 12:357–60. doi: 10.1038/nmeth.3317
61. Baruzzo G, Hayer KE, Kim EJ, Di Camillo B, Fitzgerald GA, Grant GR. Simulation-based comprehensive benchmarking of RNA-seq aligners. *Nat Methods.* (2017) 14:135–9. doi: 10.1038/nmeth.4106
62. Ponjavic J, Oliver PL, Lunter G, Ponting CP. Genomic and transcriptional co-localization of protein-coding and long non-coding RNA pairs in the developing brain. *PLoS Genet.* (2009) 5:e1000617. doi: 10.1371/journal.pgen.1000617

63. Kotake Y, Nakagawa T, Kitagawa K, Suzuki S, Liu N, Kitagawa M, et al. Long non-coding RNA ANRIL is required for the PRC2 recruitment to and silencing of p15(INK4B) tumor suppressor gene. *Oncogene*. (2011) 30:1956–62. doi: 10.1038/ncr.2010.568
64. Teng M, Love MI, Davis CA, Djebali S, Dobin A, Graveley BR, et al. A benchmark for RNA-seq quantification pipelines. *Genome Biol*. (2016) 17:74. doi: 10.1186/s13059-016-1060-7
65. Williams CR, Baccarella A, Parrish JZ, Kim CC. Empirical assessment of analysis workflows for differential expression analysis of human samples using RNA-Seq. *BMC Bioinformatics*. (2017) 18:38. doi: 10.1186/s12859-016-1457-z
66. Merino GA, Conesa A, Fernandez EA. A benchmarking of workflows for detecting differential splicing and differential expression at isoform level in human RNA-seq studies. *Brief Bioinform*. (2019) 20:471–81. doi: 10.1093/bib/bbx122
67. Schaale K, Neumann J, Schneider D, Ehlers S, Reiling N. Wnt signaling in macrophages: augmenting and inhibiting mycobacteria-induced inflammatory responses. *Eur J Cell Biol*. (2011) 90:553–9. doi: 10.1016/j.ejcb.2010.11.004
68. Bray PJ, Cotton RG. Variations of the human glucocorticoid receptor gene (NR3C1): pathological and *in vitro* mutations and polymorphisms. *Hum Mutat*. (2003) 21:557–68. doi: 10.1002/humu.10213
69. Vitellius G, Trabado S, Bouligand J, Delemer B, Lombes M. Pathophysiology of glucocorticoid signaling. *Ann Endocrinol*. (2018) 79:98–106. doi: 10.1016/j.ando.2018.03.001
70. Behr MA, Collins DM. *Paratuberculosis: Organism, Disease, Control*. Cambridge, MA: CABI (2010).
71. Olakanmi O, Kesavalu B, Abdalla MY, Britigan BE. Iron acquisition by *Mycobacterium tuberculosis* residing within myeloid dendritic cells. *Microb Pathog*. (2013) 65:21–8. doi: 10.1016/j.micpath.2013.09.002
72. Chao A, Sieminski PJ, Owens CP, Goulding CW. Iron acquisition in *Mycobacterium tuberculosis*. *Chem Rev*. (2019) 119:1193–220. doi: 10.1021/acs.chemrev.8b00285
73. Harriff MJ, Purdy GE, Lewinsohn DM. Escape from the phagosome: the explanation for MHC-i processing of mycobacterial antigens? *Front Immunol*. (2012) 3:40. doi: 10.3389/fimmu.2012.00040
74. Li Y, Shi J, Yang J, Ma Y, Cheng L, Zeng J, et al. A Wnt/beta-catenin negative feedback loop represses TLR-triggered inflammatory responses in alveolar epithelial cells. *Mol Immunol*. (2014) 59:128–35. doi: 10.1016/j.molimm.2014.02.002
75. Neumann J, Schaale K, Farhat K, Endermann T, Ulmer AJ, Ehlers S, et al. Frizzled1 is a marker of inflammatory macrophages, and its ligand Wnt3a is involved in reprogramming *Mycobacterium tuberculosis*-infected macrophages. *FASEB J*. (2010) 24:4599–612. doi: 10.1096/fj.10-160994
76. Khare S, Lawhon SD, Drake KL, Nunes JE, Figueiredo JF, Rossetti CA, et al. Systems biology analysis of gene expression during *in vivo* *Mycobacterium avium paratuberculosis* enteric colonization reveals role for immune tolerance. *PLoS ONE*. (2012) 7:e42127. doi: 10.1371/journal.pone.0042127
77. Scordo JM, Arcos J, Kelley HV, Diangelo L, Sasindran SJ, Youngmin E, et al. *Mycobacterium tuberculosis* cell wall fragments released upon bacterial contact with the human lung mucosa alter the neutrophil response to infection. *Front Immunol*. (2017) 8:307. doi: 10.3389/fimmu.2017.00307
78. Alhussien MN, Dang AK. Potential roles of neutrophils in maintaining the health and productivity of dairy cows during various physiological and physiopathological conditions: a review. *Immunol Res*. (2019) 67:21–38. doi: 10.1007/s12026-019-9064-5
79. Khare S, Nunes JS, Figueiredo JF, Lawhon SD, Rossetti CA, Gull T, et al. Early phase morphological lesions and transcriptional responses of bovine ileum infected with *Mycobacterium avium* subsp. *paratuberculosis*. *Vet Pathol*. (2009) 46:717–28. doi: 10.1354/vp.08-Vp-0187-G-FL
80. Lundtoft C, Afum-Adjei Awuah A, Rimpler J, Harling K, Nausch N, Kohns M, et al. Aberrant plasma IL-7 and soluble IL-7 receptor levels indicate impaired T-cell response to IL-7 in human tuberculosis. *PLoS Pathog*. (2017) 13:e1006425. doi: 10.1371/journal.ppat.1006425
81. Mihret A, Loxton AG, Bekele Y, Kaufmann SH, Kidd M, Haks MC, et al. Combination of gene expression patterns in whole blood discriminate between tuberculosis infection states. *BMC Infect Dis*. (2014) 14:257. doi: 10.1186/1471-2334-14-257
82. Jenum S, Dhanasekaran S, Lodha R, Mukherjee A, Kumar Saini D, Singh S, et al. Approaching a diagnostic point-of-care test for pediatric tuberculosis through evaluation of immune biomarkers across the clinical disease spectrum. *Sci Rep*. (2016) 6:18520. doi: 10.1038/srep18520
83. Carpenter S, Aiello D, Atianand MK, Ricci EP, Gandhi P, Hall LL, et al. A long noncoding RNA mediates both activation and repression of immune response genes. *Science*. (2013) 341:789–92. doi: 10.1126/science.1240925
84. Hu G, Gong AY, Wang Y, Ma S, Chen X, Chen J, et al. LincRNA-Cox2 promotes late inflammatory gene transcription in macrophages through modulating SWI/SNF-mediated chromatin remodeling. *J Immunol*. (2016) 196:2799–808. doi: 10.4049/jimmunol.1502146
85. Covarrubias S, Robinson EK, Shapleigh B, Vollmers A, Katzman S, Hanley N, et al. CRISPR/Cas-based screening of long non-coding RNAs (lncRNAs) in macrophages with an NF-kappaB reporter. *J Biol Chem*. (2017) 292:20911–20. doi: 10.1074/jbc.M117.799155
86. Arsenault RJ, Li Y, Maattanen P, Scruten E, Doig K, Potter A, et al. Altered Toll-like receptor 9 signaling in *Mycobacterium avium* subsp. *paratuberculosis*-infected bovine monocytes reveals potential therapeutic targets. *Infect Immun*. (2013) 81:226–37. doi: 10.1128/IAI.00785-12
87. Flintoft L. Non-coding RNA: structure and function for lncRNAs. *Nat Rev Genet*. (2013) 14:598. doi: 10.1038/nrg3561
88. Hammon DS, Evjen IM, Dhiman TR, Goff JP, Walters JL. Neutrophil function and energy status in Holstein cows with uterine health disorders. *Vet Immunol Immunopathol*. (2006) 113:21–9. doi: 10.1016/j.vetimm.2006.03.022
89. Andersson L, Archibald AL, Bottema CD, Brauning R, Burgess SC, Burt DW, et al. Coordinated international action to accelerate genome-to-phenome with FAANG, the functional annotation of animal genomes project. *Genome Biol*. (2015) 16:57. doi: 10.1186/s13059-015-0622-4
90. Emam M, Tabatabaei S, Sargolzaei M, Sharif S, Schenkel F, Mallard B. The effect of host genetics on *in vitro* performance of bovine monocyte-derived macrophages. *J Dairy Sci*. (2019) 102:9107–16. doi: 10.3168/jds.2018-15960
91. Rey-Giraud F, Hafner M, Ries CH. *In vitro* generation of monocyte-derived macrophages under serum-free conditions improves their tumor promoting functions. *PLoS ONE*. (2012) 7:e42656. doi: 10.1371/journal.pone.0042656
92. Oida T, Weiner HL. Depletion of TGF-beta from fetal bovine serum. *J Immunol Methods*. (2010) 362:195–8. doi: 10.1016/j.jim.2010.09.008
93. Mia S, Warnecke A, Zhang XM, Malmstrom V, Harris RA. An optimized protocol for human M2 macrophages using M-CSF and IL-4/IL-10/TGF-beta yields a dominant immunosuppressive phenotype. *Scand J Immunol*. (2014) 79:305–14. doi: 10.1111/sji.12162
94. Koufariotis L, Chen YP, Bolormaa S, Hayes BJ. Regulatory and coding genome regions are enriched for trait associated variants in dairy and beef cattle. *BMC Genomics*. (2014) 15:436. doi: 10.1186/1471-2164-15-436
95. Washietl S, Kellis M, Garber M. Evolutionary dynamics and tissue specificity of human long noncoding RNAs in six mammals. *Genome Res*. (2014) 24:616–28. doi: 10.1101/gr.165035.113

Conflict of Interest: The authors declare that the research was conducted in the absence of any commercial or financial relationships that could be construed as a potential conflict of interest.

Copyright © 2021 Marete, Ariel, Ibeagha-Awemu and Bissonnette. This is an open-access article distributed under the terms of the Creative Commons Attribution License (CC BY). The use, distribution or reproduction in other forums is permitted, provided the original author(s) and the copyright owner(s) are credited and that the original publication in this journal is cited, in accordance with accepted academic practice. No use, distribution or reproduction is permitted which does not comply with these terms.



Engineering Synthetic Lipopeptide Antigen for Specific Detection of *Mycobacterium avium* subsp. *paratuberculosis* Infection

Sylvie Bay^{1,2*}, Douglas Begg³, Christelle Ganneau^{1,2}, Maxime Branger⁴, Thierry Cochard⁴, John P. Bannantine⁵, Heike Köhler⁶, Jean-Louis Moyaen⁷, Richard J. Whittington³ and Franck Biet^{4*}

OPEN ACCESS

Edited by:

Miguel Salgado,
Austral University of Chile, Chile

Reviewed by:

Ad Koets,
Wageningen Bioveterinary Research
(WBVR), Netherlands
Marta Alonso-Hearn,
NEIKER-Instituto Vasco de
Investigación y Desarrollo
Agrario, Spain
Philip John Griebel,
University of Saskatchewan, Canada

*Correspondence:

Sylvie Bay
sylvie.bay@pasteur.fr
Franck Biet
franck.biet@inrae.fr

Specialty section:

This article was submitted to
Veterinary Infectious Diseases,
a section of the journal
Frontiers in Veterinary Science

Received: 04 December 2020

Accepted: 24 March 2021

Published: 23 April 2021

Citation:

Bay S, Begg D, Ganneau C,
Branger M, Cochard T, Bannantine JP,
Köhler H, Moyaen J-L, Whittington RJ
and Biet F (2021) Engineering
Synthetic Lipopeptide Antigen for
Specific Detection of *Mycobacterium*
avium subsp. *paratuberculosis*
Infection. *Front. Vet. Sci.* 8:637841.
doi: 10.3389/fvets.2021.637841

¹ Institut Pasteur, Unité de Chimie des Biomolécules, Département de Biologie Structurale et Chimie, Paris, France, ² CNRS UMR 3523, Paris, France, ³ School of Veterinary Science, University of Sydney, Camden, NSW, Australia, ⁴ INRAE, Université de Tours, ISP, Nouzilly, France, ⁵ USDA-Agricultural Research Service (USDA-ARS), National Animal Disease Center, Ames, IA, United States, ⁶ Friedrich-Loeffler-Institut, Federal Research Institute for Animal Health, Jena, Germany, ⁷ Laboratoire Départementale d'Analyse et de Recherche de Dordogne, Coulounieix Chamiers, France

Unlike other MAC members, *Mycobacterium avium* subsp. *paratuberculosis* (MAP) does not produce glycopeptidolipids (GPL) on the surface of the cell wall but a lipopeptide called L5P (also termed Lipopeptide-I or Para-LP-01) characterized in C-type (bovine) strains. This lipopeptide antigen contains a pentapeptide core, D-Phenylalanine-N-methyl-L-Valine-L-Isoleucine-L-Phenylalanine-L-Alanine, in which the N-terminal D-Phenylalanine is amido-linked with a fatty acid (C18–C20). The molecular and genetic characterization of this antigen demonstrated that L5P is unique to MAP. Knowledge of the structure of L5P enabled synthetic production of this lipopeptide in large quantities for immunological evaluation. Various studies described the immune response directed against L5P and confirmed its capability for detection of MAP infection. However, the hydrophobic nature of lipopeptide antigens make their handling and use in organic solvents unsuitable for industrial processes. The objectives of this study were to produce, by chemical synthesis, a water-soluble variant of L5P and to evaluate these compounds for the serological diagnosis of MAP using well-defined serum banks. The native L5P antigen and its hydrosoluble analog were synthesized on solid phase. The pure compounds were evaluated on collections of extensively characterized sera from infected and non-infected cattle. ROC analysis showed that L5P and also its water-soluble derivative are suitable for the development of a serological test for Johne's disease at a population level. However, these compounds used alone in ELISA have lower sensitivity (Se 82% for L5P and Se 62% for the water-soluble variant of L5P) compared to the Se 98% of a commercial test. Advantageously, these pure synthetic MAP specific antigens can be easily produced in non-limiting quantities at low cost and in standardized batches for robust studies. The fact that L5P has not been validated in the context of ovine paratuberculosis highlights the need to better characterize the antigens expressed

from the different genetic lineages of MAP to discover new diagnostic antigens. In the context of infections due to other mycobacteria such as *M. bovis* or the more closely related species *M. avium* subsp. *hominissuis*, the L5P did not cross react and therefore may be a valuable antigen to solve ambiguous results in other tests.

Keywords: *Mycobacterium avium* subsp. *paratuberculosis*, Johne's disease, lipopeptide, diagnosis, antibody response, chemical synthesis

INTRODUCTION

Mycobacteria are well-known for their cell envelope containing abundant mycolic acids and specific lipid components (1, 2). These molecules play a crucial role to maintain the integrity of the cell wall and are considered to be involved in bacterial virulence through influence on the host immune response (3). The outer membrane contains diverse surface lipids that are species-dependent. This likely reflects differences in the cell biochemical organization and probably impacts significantly the way *Mycobacterium* species interact with the host. *Mycobacterium avium* complex (MAC) is a group of non-tuberculous mycobacteria that cause tuberculosis-like diseases in humans and in animals and that produces glycopeptidolipids (GPLs) (4, 5). GPLs form the basis for a commercial test that can be useful for rapid diagnosis of MAC pulmonary disease (MAC-PD) and for differentiating MAC-PD from pulmonary tuberculosis (PTB) in humans (6). Although belonging to the MAC, the subspecies *paratuberculosis* (MAP), causing paratuberculosis or Johne's Disease in ruminants (7), is distinguished by the absence of production of GPL (8). Subspecies *paratuberculosis* produces lipopeptides (LPs) whose biosynthetic pathway is likely to be homologous to that of GPL, based on the structural relatedness between GPL and LP. The main difference between GPL and LP is the absence of sugars, explained by absence of an hydroxyl group in the peptidyl moiety of LP, and the absence of a double bond in the fatty acid moiety. Within subsp. *paratuberculosis* the first LP described contains a pentapeptide core, D-Phenylalanine-N-methyl-L-Valine-L-Isoleucine-L-Phenylalanine-L-Alanine, in which the N-ter D-Phenylalanine is amido-linked with a fatty acid (C18–C20) (Figure 1). This LP is termed L5P for lipopentapeptide (8), and is also known as Lipopeptide-I or Para-LP-01 (9, 10). It is an abundant molecule in *Mycobacterium avium* subsp. *paratuberculosis* (MAP) and found in the outermost layers of the cell envelope (8, 11). Previously we deciphered the genetic organization, including the nonribosomal peptide synthase genes *mps1*, that participate in the biosynthesis of the peptidic moiety of the L5P (8). Thanks to the exact knowledge of the composition of this MAP-specific LP antigen, it was possible to produce synthetic high quality L5P in large quantity for immunological studies. Indeed, various studies by us and others described the immune response directed against this native or synthetic L5P and confirmed its potential for the detection of MAP infection (8, 10, 12–16). However, the hydrophobic nature of this LP antigen necessitates its handling and use in organic solvent, which is not suitable for industrial processes.

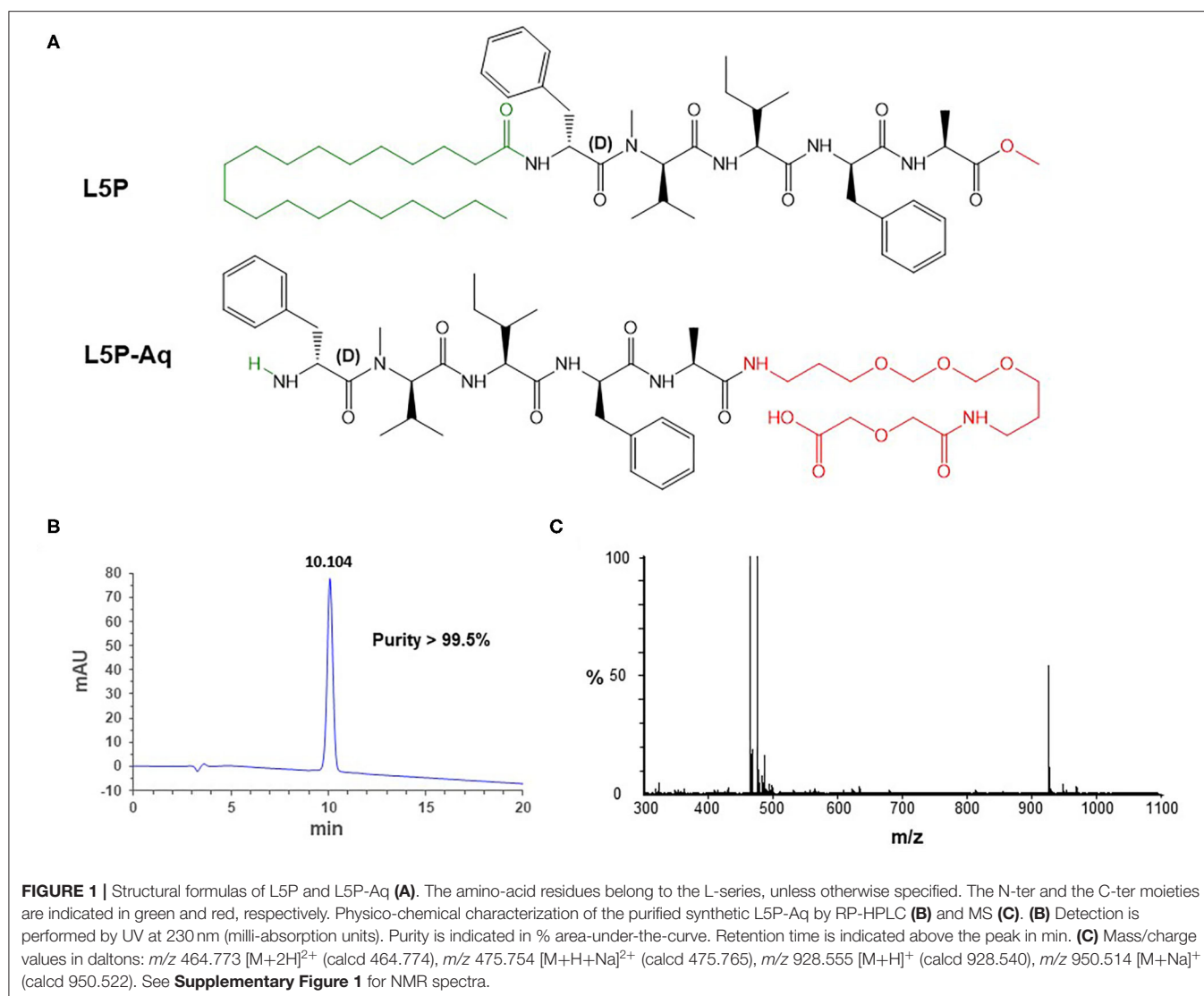
Despite the establishment of control programs in most developed countries, with substantial financial efforts, the prevalence rate of paratuberculosis remains at a very high level, around 50% for European herds (17, 18) and around 80% in the USA. The disease controls implemented may be different depending on the country: control, surveillance, certification, border quarantine, and on-farm biosecurity (19). For routine screening, the majority of analyses are performed by ELISA serological tests. The bovine antibody response to MAP changes over the course of disease progression. Serial bleeds collected from experimentally infected calves over a 1-year period was performed to temporally examine the humoral immune response using a MAP protein array (20). Antibody reactivity declined between day 194 and day 321 for a group of 11 proteins while reactivity to other proteins increased over the experimental timepoints. As disease enters the clinical stage, the antibody response is more consist and predominant, which enables reliable detection by ELISA (20). Currently available serological diagnostic tests are based on the use of whole cell antigens that may cross-react with closely related mycobacteria and require culture of this slow growing pathogen to produce the antigen. Specificity of commercial tests require a pre-absorption step with antigens of *M. phlei* to remove cross-reactivity. The preparation of antigen from the culture of mycobacteria is a critical element that can be a bottleneck for these tests. Conversely, pure synthetic antigens make it possible to secure and standardize the production of specific MAP antigen at low cost, thus improving existing tests. In this study we produced, by chemical synthesis, a hydrosoluble variant of L5P termed L5P-Aqueous (L5P-Aq) and evaluated these compounds for the serological diagnosis of MAP from well-defined serum banks. We also included sera from animals infected with *M. avium* subsp. *hominissuis*, a species close to MAP, and *M. bovis* because of the interest in antigens that do not cross-react with this species.

MATERIALS AND METHODS

Chemical Synthesis of the Lipopentapeptide Antigen and Hydrosoluble Analog

The antigens were synthesized manually on a solid phase using Fmoc chemistry. The lipopentapeptide L5P was obtained using a 4-hydroxymethylbenzoyl resin (HMBA-AM resin, Novabiochem) as previously described (8).

The L5P-Aq antigen was prepared by attaching *N*-(Fmoc-13-amino-4,7,10-trioxatridecyl)-diglycolic acid (Novabiochem) to a Wang resin (Novabiochem) using



1-(mesitylene-2-sulfonyl)-3-nitro-1,2,4-triazole and *N*-methylimidazole (21). The capping, coupling and deprotection steps were performed as previously described (8). The product was cleaved from the resin with aqueous trifluoroacetic acid (TFA)/triisopropylsilane/ H_2O 95/2.5/2.5 v/v/v for 2 h at room temperature. After filtration of the resin, the filtrate was concentrated, and diluted with CH_2Cl_2/H_2O 50/50. The organic phase was extracted twice with H_2O . The aqueous phases were pooled and lyophilized. The crude L5P-Aq was purified by reverse-phase (RP) flash chromatography using a gradient of H_2O +0.1%TFA/ CH_3CN +0.1%TFA from 70/30 to 50/50 and 126 mg of the peptide derivative were obtained (yield 88%). The purified compound was analyzed by RP high performance liquid chromatography (HPLC) using an Agilent 1200 pump system with a UV detector at 220 nm. A Kromasil C18 column (5 μm , 100 \AA , 4.6 mm \times 250 mm) (Agilent, France) was used, and a gradient of acetonitrile (A)/water + 0.1%TFA (B) was applied over a period of 20 min, from 33 to 50% A (1 mL/min, retention

time 10.1 min). L5P-Aq was also characterized by electrospray ionization mass spectrometry (MS) (positive mode, Q-ToF Micro Waters), quantitative amino acid analysis (AAA) (after hydrolysis with 6N HCl at 110°C for 48 h and using a Beckman 6300 analyzer), and nuclear magnetic resonance (NMR) (Bruker 400 MHz instrument). The NMR spectra and the corresponding structural formula are shown in **Supplementary Figure 1**.

MS: $C_{47}H_{73}N_7O_{12}$ m/z 928.538 $[M+H]^+$ (calcd 928.540), 950.510 $[M+Na]^+$ (calcd 950.522).

AAA: Ala 1 (1), Phe 1.79 (1), Ile 0.90 (1), and an extra peak typical of *N*-Methyl-Val.

1H NMR (MeOD): δ 0.68 (d, 3H, $CH_3\gamma$ Val, $J = 6.56$ Hz), 0.79 (d, 3H, $CH_3\gamma$ Val, $J = 6.64$ Hz), 0.81 (d, 3H, $CH_3\gamma$ Ile, $J = 6.89$ Hz), 0.85 (t, 3H, $CH_3\delta$ Ile, $J = 7.38$ Hz), 1.01–1.09 (m, 1H, $1CH_2\gamma$ Ile), 1.30 (d, 3H, $CH_3\beta$ Ala, $J = 7.12$ Hz), 1.45–1.51 (m, 1H, $1CH_2\gamma$ Ile), 1.70–1.81 (m, 5H, $CH\beta$ Ile, CH_2 D, and K), 2.08–2.14 (m, 1H, $CH_2\beta$ Val), 2.92 (dd, 1H, $1CH_2\beta$ Phe), 3.01 (dd, 1H, $1CH_2\beta$ Phe), 3.05 (s, 3H, NCH₃), 3.13 (dd, 1H, $1CH_2\beta$ Phe), 3.20

(dd, 1H, 1CH₂β Phe), 3.23 (t, 2H, CH₂ C or L, $J = 6.86$ Hz), 3.33 (t, 2H, CH₂ C or L, $J = 6.84$ Hz), 3.48–3.54 (m, 4H, CH₂ E and J), 3.56–3.64 (m, 8H, CH₂ F, G, H, and I), 4.04 (s, 2H, CH₂ B), 4.06–4.10 (m, 1H, CHα Ile), 4.18 (s, 2H, CH₂ A), 4.23–4.28 (q, 1H, CHα Ala), 4.47 (d, 1H, CHα Val, $J = 10.96$ Hz), 4.61 (dt, 1H, CHα Phe), 4.68 (dt, 1H, CHα Phe), 7.16–7.19 (m, 2H, NH PEG), 7.21–7.38 (m, 10H, 2Ph), 7.97 (d, NH Ile), 8.13 (d, NH Phe). ¹³C NMR (MeOD): δ 11.34 (CH₃δ Ile), 15.75 (CH₃γ Ile), 18.34 (CH₃β Ala), 19.87, 20.00 (2CH₃γ Val), 26.10 (CH₂γ Ile), 28.50 (CHβ Val), 30.35, 30.38 (CH₂ D and K), 32.05 (NCH₃), 37.69, 37.90 (CH₂ C and L), 38.14, 38.61 (2CH₂α Phe), 50.56 (CHα Ala), 53.35, 55.93 (2CHα Phe), 59.50 (CHα Ile), 64.94 (CHα Val), 69.22 (CH₂ A), 69.82, 70.11 (CH₂ E and J), 71.28, 71.31, 71.52, 71.58 (CH₂ B, F, G, H, and I), 127.87, 129.08, 129.56, 130.27, 130.35, 130.59, 135.26, 138.28 (Ph), 171.06, 171.92, 172.20, 172.85, 173.25, 173.63, 174.43 (CO).

Animal Sera

A bank of serum samples of bovine origin, constituted by CERVACODA, was provided by Dr. M. Govaerts. The status of the sera was characterized by several diagnostic tests: fecal culture, Pourquier ELISA, and ID-Vet ELISA. The negative sera came from farms known to be free from paratuberculosis, this status was awarded after 3 consecutive years of whole-herd negative serology. Sera were defined as being true positive ($n = 60$) when they were positive in all three tests or as true negative ($n = 50$) when they were negative in all three tests. The same serum bank was used for the discovery of new antigenic candidates in previous reports (22, 23). The sera were stored at -20°C and verified in IDEXX test (IDEXX Paratuberculosis Screening Ab, Montpellier, France) (Supplementary Tables 1, 2 and Supplementary Figure 2). In addition, a panel of sera were collected from cattle from a herd that was free of paratuberculosis but included in an official eradication campaign for bovine tuberculosis. Eleven sera were collected from cattle from which *M. bovis* had been isolated and confirmed by IS6110 PCR and spoligotyping (24).

In the context of ovine paratuberculosis, 54 serum samples were carefully selected (25, 26). Fifteen negative sera were from unexposed sheep and 39 positive sera were from sheep experimentally infected with Telford 9.2 MAP strain (25). The positive sera, verified by commercial test (Supplementary Table 1 and Supplementary Figure 3) were classified in five groups according to the histopathological stage of the infection (27), (1) exposed but uninfected, (2) infected with low grade lesions, (3) paucibacillary 3a, (4) multibacillary 3b, and (5) macroscopical lesions 3c.

Serum samples collected from unexposed goats ($n = 25$) or goats experimentally infected either with MAP ($n = 27$) strain JII-1961 (28, 29) or with *Mycobacterium avium* subsp. *hominissuis* (MAH) field isolate ($n = 26$) (30, 31) were provided by Dr. Heike Koehler. Infection with MAP or MAH was confirmed by cultural isolation of the respective strains from tissues after necropsy and/or by histopathology (lesions) and immunohistochemistry (presence of mycobacteria) of tissue sections. Positive sera were from animals with severe lesions that

tested positive in commercial diagnostic ELISA IDEXX (IDEXX Paratuberculosis Screening Ab, Montpellier, France).

ELISA Procedure

ELISA using IDEXX commercial test (IDEXX Paratuberculosis Screening Ab, Montpellier, France) were performed according to manufacturer's instructions. ELISA experiments using synthetic antigens were performed as described previously (8). Briefly, L5P antigens were diluted at 25 μg/mL in ethanol. Water-soluble L5P-Aq variant was diluted at 80 μg/mL in PBS (10 mM PBS, pH 7.4). Maxisorp microtiter plates (Nunc, Roskilde, Denmark) were coated with 50 μL of antigen preparation. Microtiter plates coated with L5P were air-dried for 18 h at 37°C to allow the solvent to evaporate. Microtiter plates coated with L5P-Aq were incubated for 18 h at 4°C . Following each incubation step, the plates were washed three times with PBS supplemented with 0.1% (v/v) Tween 20 (PBST) (Sigma). After washing, the wells were blocked with 50 μL of Blocking Buffer (PBSTG: PBS+0.05% Tween 20, 0.5% Gelatin) (Gibco) at room temperature for 2 h. Fifty microliters of serum (diluted at 1:100 in PBSTG) were then added to each well and incubated for 1 h 30 min at 37°C . Microtiter plates were washed five times with PBST and 50 μL of solution of Recombinant Protein G Peroxidase Conjugated (Thermo Scientific) diluted at 0.5 μg/mL in PBST, were added to each well and incubated for 1 h at room temperature. After washing five times with PBST the reaction was visualized using 3,3',5,5'-tetramethylbenzidine (Sigma) and 0.5% v/v H₂O₂. The reaction was stopped with 1N sulfuric acid after 2 min of incubation in the dark and ODs were read at 450 nm on a Multiskan RC reader (Labsystems, Helsinki, Finland).

Data Analysis

The ELISA results of positive sera compared to negative sera control, for each antigen were subjected to receiver-operator characteristic (ROC) curve analysis. This method estimates the sensitivity and specificity of the ELISA, calculate likelihood ratios and provides an overall measure of test accuracy as area under the ROC curve (AUC) to evaluate the performance of the tests (32, 33). The optimal cut-off value is provided by ROC analysis as being associated with the maximal likelihood ratio.

Statistical differences between groups of goats unexposed or goats experimentally infected either with MAP or MAH or between groups of cattle naturally infected by *M. bovis* or Map was evaluated by Wilcoxon's matched pairs test. Differences were considered significant at $p < 0.05$. All statistical analyses were performed using statistical software (GRAPHPAD PRISM version 6.07 for Windows, GraphPad software, San Diego, CA, <http://www.graphpad.com>).

RESULTS

Chemical Synthesis of Pure L5P and Hydrosoluble Analog L5P-Aq

The L5P is very hydrophobic and does behave very differently as compared to conventional protein antigens which are hydrophilic. It is soluble in DMSO, CHCl₃, CH₂Cl₂, MeOH, and EtOH, but insoluble in water or aqueous buffers. Glass containers

have to be used, and contact with polypropylene surfaces must be minimized. Material handling like dilution and transfer steps also needs to be minimized. These properties of L5P would cause difficulties if a diagnostic test was based on the L5P antigen. To circumvent these difficulties, we have designed a hydrosoluble derivative of L5P, L5P-Aq. The N-ter non-immunogenic lipidic moiety of L5P was suppressed and the C-ter methyl ester was replaced by polyethylene glycol chain ending with a carboxyl group (Figure 1A).

The resulting L5P-Aq was obtained by solid-phase peptide synthesis using 9-fluorenylmethoxycarbonyl chemistry. After cleavage from the resin, by contrast with its hydrophobic counterpart, the crude product was actually extracted in aqueous phase. Purification by reverse-phase chromatography then afforded 126 mg of L5P-Aq with a 88 % overall yield. To ensure both its purity and its identity, the L5P-Aq was analyzed by RP-HPLC (Figure 1B, >99.5%), MS (Figure 1C), quantitative AAA, and NMR (Supplementary Figures 1A,B).

Antigenic Evaluation of L5P and L5P-Aq on a Bank of Bovine Sera

In previous studies, the antibody response against L5P was investigated with a limited panel of sera and it has not been subjected to comprehensive, large scale evaluation. Synthetic L5P and the hydrosoluble derivative L5P-Aq were therefore both assessed using a bank of well-defined sera including 60 sera from MAP-naturally infected cattle and 50 sera from healthy cattle (details in the method section). In receiver operating characteristic analysis (ROC analysis) of L5P, the area under the curve and its standard error were 0.97 (95% confidence interval, 0.9418 to 0.9942) and 0.01336, respectively (Figure 2 and Supplementary Table 1). The L5P-Aq was evaluated in ethanol and in PBS and the area under the curve and its standard error were 0.937 (95 % confidence interval, 0.8909 to 0.9831) and 0.02354, and 0.9427 (95% confidence interval, 0.9021 to 0.9832) and 0.02068, respectively (Figure 2 and Supplementary Table 1). The sensitivity of L5P and L5P-Aq in comparison to commercial test were 81.67, 61.67, and 98%, respectively. The specificity of L5P and L5P-Aq were 98% identical to the commercial test. When tested in same conditions, the acidic derivative of the L5P lipid moiety (eicosanoic acid) was not antigenic, showing that the serum response was not directed against the L5P lipid (Supplementary Figure 4) according to previous report. These results confirm that both L5P and L5P-Aq have potential to discriminate MAP infected and uninfected cattle at a population level.

L5P Antigenic Response in the Context of Ovine Paratuberculosis

Although ovine paratuberculosis is comparable to the disease in cattle, it is well-documented that MAP strains isolated from sheep have host-dependent features. To investigate the immune response in MAP infected sheep, we used the L5P described as the native antigen in strains of MAP of subtype II isolated from cattle. The results presented in Figure 3 show that synthetic L5P is not able to significantly discriminate MAP positive sheep from

uninfected sheep. As discussed in detail below, this result is likely due to the minor lipopeptide differences present in the cell walls of sheep vs. cattle strains of MAP.

Diagnostic Value of L5P in Goats Infected With MAP or MAH

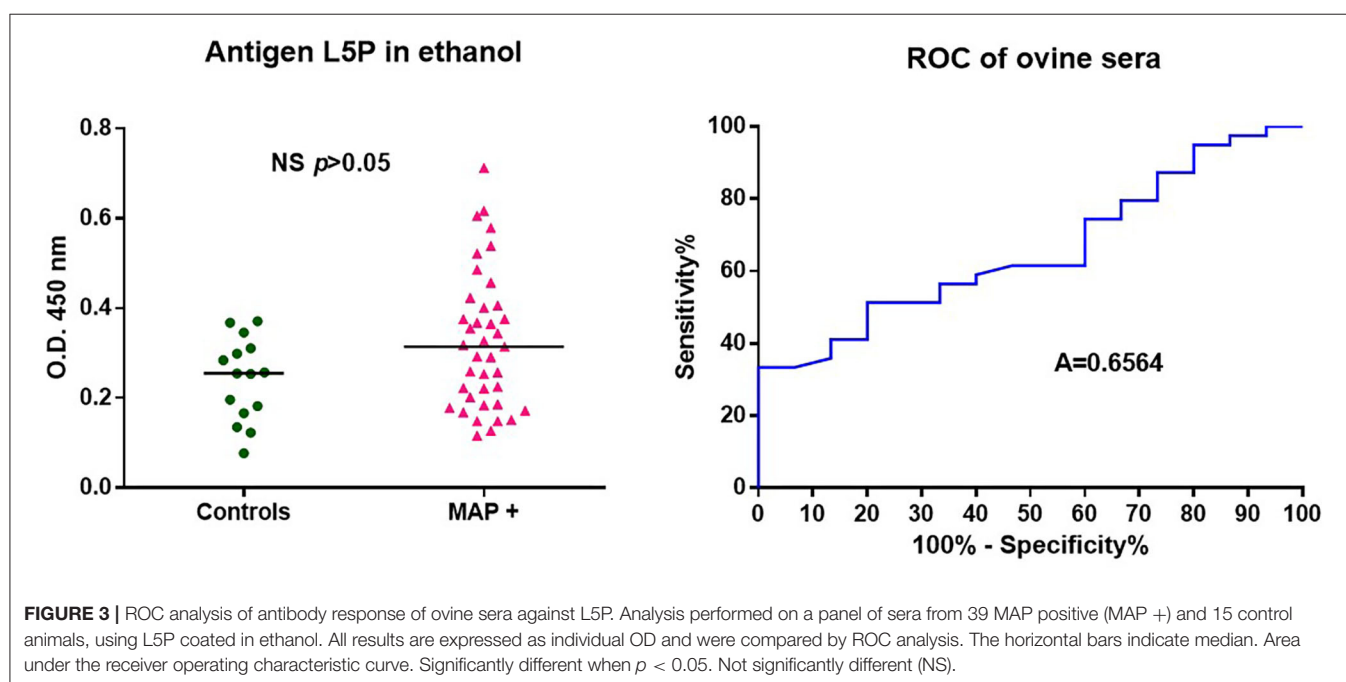
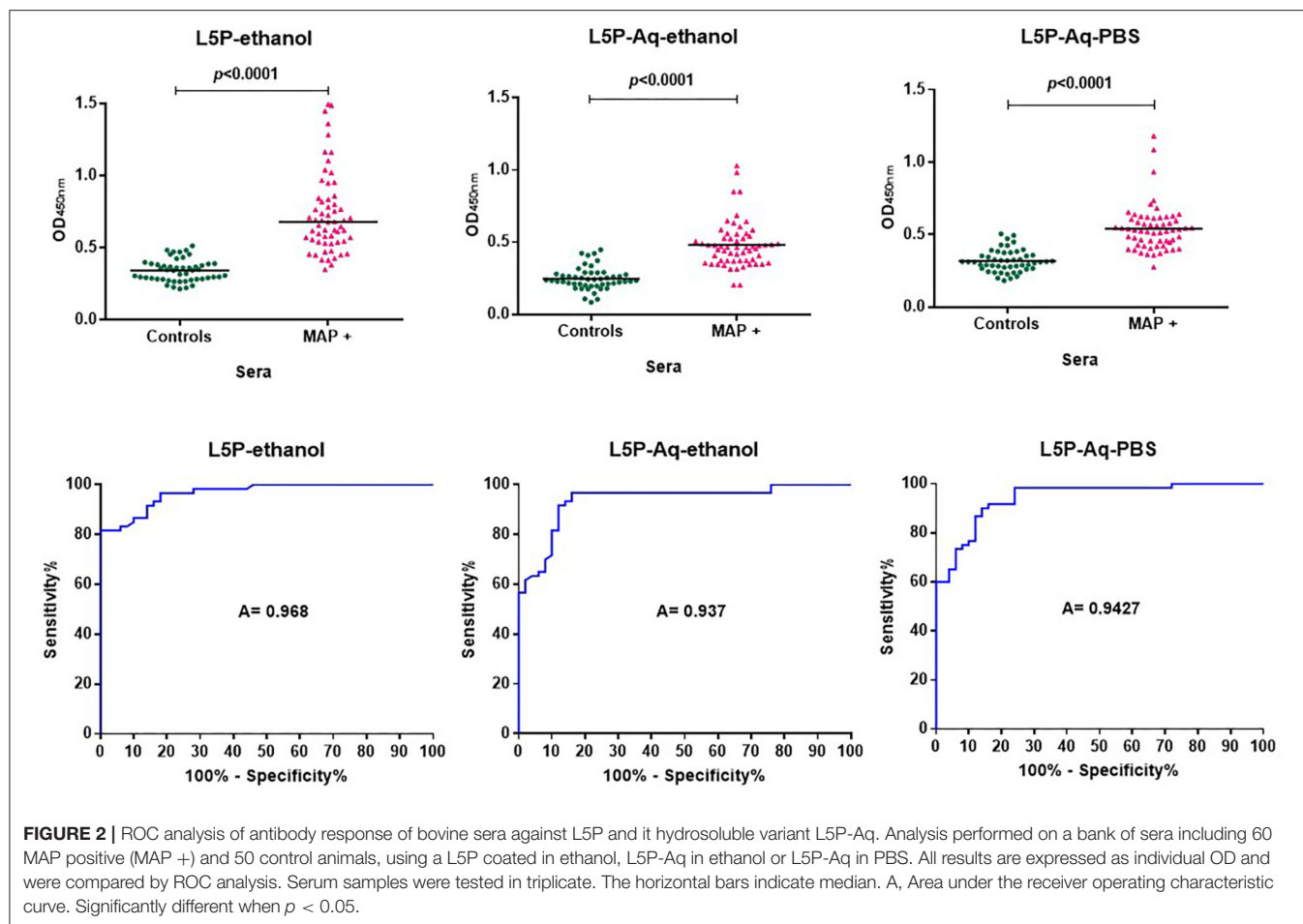
In their environment animals are naturally exposed to different mycobacteria. In the context of farm animals, it is recognized that this exposure can hamper diagnostic tests. To gain specificity, commercial serologic screening tests for MAP use a serum adsorption step with antigens prepared from an environmental bacterium *Mycobacterium phlei*. Knowing that L5P is specific to MAP we investigated its use without any pre-adsorption step against serum from animals experimentally infected with MAP, or MAH mycobacteria very close to MAP. As expected, the commercial IDEXX test makes it possible to distinctly detect animals infected with MAP from animals infected with MAH and from non-infected animals. Compared to the commercial test, L5P used alone without a pre-adsorption step with *Mycobacterium phlei* extracts, lacked sensitivity with MAP positive sera but didn't react with sera of animals infected with MAH (Figure 4).

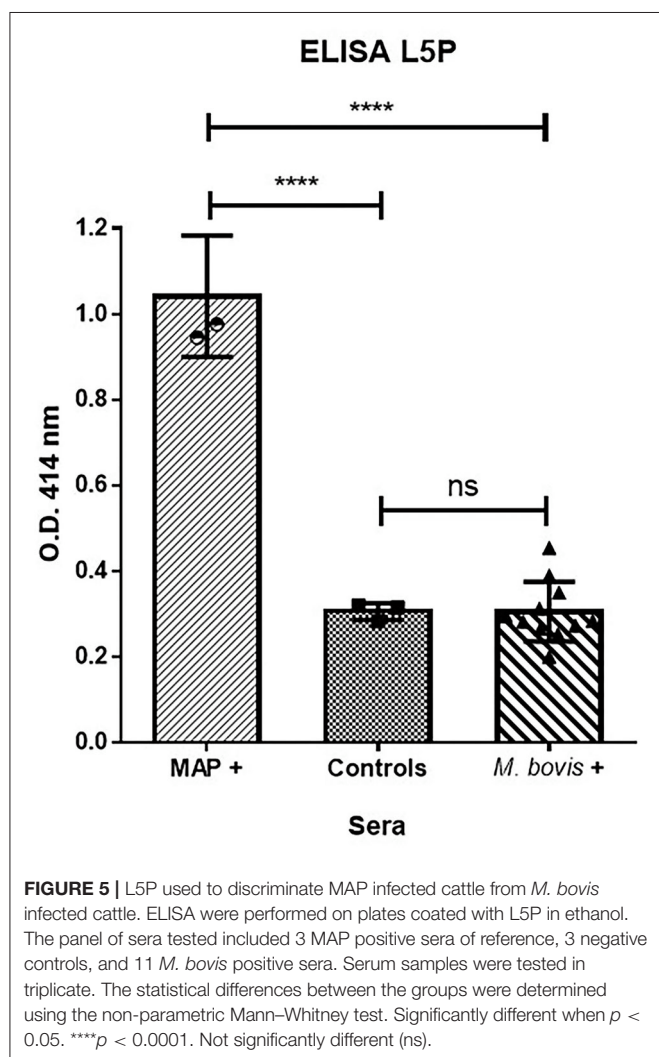
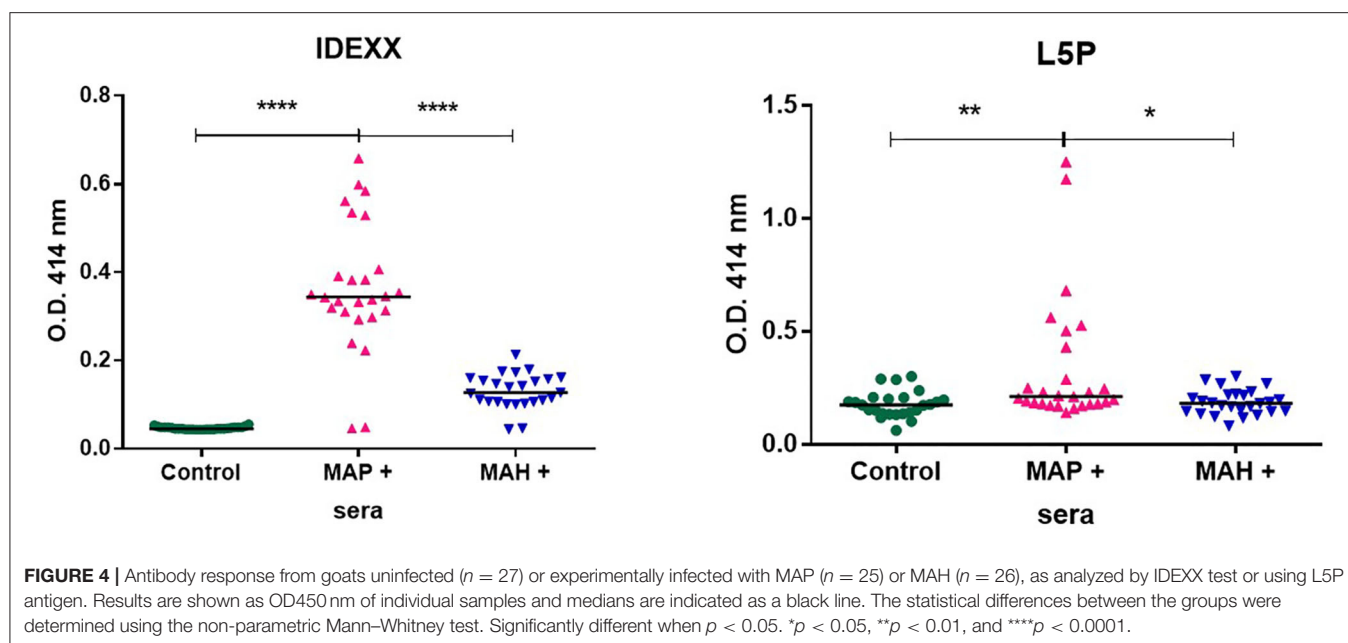
L5P as a Biomarker Able to Discriminate MAP From/Between *M. bovis* Infection

Bovine tuberculosis (bTB) is a major zoonotic disease of cattle that is endemic in much of the world. The antemortem diagnostic methods currently approved for use in cattle have limitations. The intradermal tuberculin test has suboptimal sensitivity and inconsistent performance (34, 35). Nontuberculous mycobacteria (NTM) and MAP, in particular, have been repeatedly shown to interfere with the detection of *M. bovis* (36). There have been a number of projects with aims to improve the diagnosis of bTB and JD by generating specific tools that do not compromise sensitivity or specificity due to co-infections or testing regimes. We therefore evaluated the L5P antigen against field sera from cattle naturally infected with *M. bovis*. The results in Figure 5 show that ELISA based on synthetic L5P did not react to field sera from *M. bovis* positive cattle in comparison to sera from MAP positive cattle.

DISCUSSION

The high lipid contents of mycobacterial cells has been recognized for a long time and much effort has been devoted to the identification of the various types of lipids present, many of which are glycolipids, unique to mycobacteria (37). *M. avium* isolates are characterized by their production of highly antigenic glycopeptidolipids or GPLs, which are suitable for specific serodiagnosis (6, 38). Surprisingly, subspecies *paratuberculosis* isolates produce lipopeptides instead of GPLs; these are characterized by the absence of sugars and the absence of both hydroxylation and double bonds in the fatty acid moiety (8). Attempts to develop serological assays based on the native L5P structure are problematic due to the apolar nature of the molecule and its lack of solubility in the aqueous buffers





typically used in ELISA. To overcome this issue, we engineered a hydrophilic variant of the native lipopeptide, named L5P-Aq, and we validated its antigenicity using a bank of MAP positive bovine sera. Used alone without a pre-adsorption step, the L5P ELISA test developed in this study can discriminate MAP infected goats from MAH infected goats. Interestingly, the sera from MAP infected sheep did not react with L5P, suggesting that lineage of strains of MAP specific for the sheep enrolled in this study may have another lipopeptide which has not yet been reported. This report also shows that L5P may have utility as a reagent to assist in the diagnosis of bTB.

Attempts to overcome the apolar nature of antigens in serological assays have been performed on bacterial glycolipids (39). For example, the Tween detergent has been used to optimize the antigen coating. On the other hand, the use of Tween was shown to be problematic as the detergent interacts with the lipid portion of the molecule causing its detachment from the plastic (39). From our results, 100% ethanol or methanol solutions enabled the efficient coating of antigen onto microtiter plate wells. Both our past and current studies show that the critical L5P epitopes are located on the peptide portion (8). Therefore, modifications to improve solubility were focused on (i) suppressing the hydrophobic lipid and (ii) extending the peptide with a hydrophilic chain. The resulting modification of L5P will yield numerous advantages. The hydrosolubility of the resulting L5P-Aq is an important benefit for its use in an ELISA test, especially for high throughput formats. Furthermore, safety issues associated with the use of organic solvents, including alcohols, are avoided. Finally, handling of antigenic material is much easier and reliable allowing repeatable procedures.

In most countries, the majority of routine screening for MAP (control, surveillance, certification, control at introduction) (99%) is carried out by serological ELISA tests (18, 40). The other methods such as PCR, bacteriological culture, direct examination (Ziehl-Neelsen staining) are used for clinical case

confirmation. The final purpose of this project was to know if synthetic lipopeptide antigen derivatives are able to specifically discriminate sera from MAP-infected and uninfected cattle in a serological assay. Until now L5P (hydrophobic) was evaluated in just a few animals. We have thus assembled here a large panel of thoroughly characterized sera, to test the recognition of these synthetic antigens. ROC analysis of results obtained with the L5P and its hydrosoluble variant, L5P-Aq, demonstrated a cut-off value corresponding to a relative sensitivity of 82 and 62% and a specificity of 98 and 98%, respectively (**Supplementary Table 1** and **Supplementary Figure 2**). These results show that synthetic L5P antigen, used alone, is able to discriminate MAP-infected animals and controls at a population level although the lower sensitivity compared with the commercial test remains an issue to improve. Likewise, the lack of sensitivity of L5P observed with sera from experimentally infected goats suggests that there is a “technical barrier” to be overcome to improve this parameter. Indeed to achieve the best assay performances, more research is needed to improve not only on the ELISA procedure (antigen presentation, buffer composition, coating process, secondary reagent...), but also on the target antigen(s). It is accepted that one universal antigen probably does not exist and that an efficient diagnostic test for paratuberculosis will require a cocktail of antigens. In this context, if used within an optimal combination, such synthetic individual MAP antigens have potential to assist in the improvement of the antigens used commercially. In addition, the use of synthetic antigen rather than crude protein extracts or culture-derived antigens has the advantage of avoiding the culture of slow growing pathogenic mycobacteria, such as MAP. The L5P-Aq synthesis can be easily performed by organic chemistry that offers the possibility of having large quantities of pure material. Numerous other advantages also come from the synthetic production of antigen, including the ability to standardize the batches and also to modify the antigens and/or their formulation, for example to graft fluorescent markers to monitor their handling. In the future, it would be interesting to have access to a bovine serum panel built to cover all the stages of JD infection and to be able to investigate the early stages of infection with these synthetic antigens. Preliminary data on the use of L5P for the early diagnosis of MAP infection by detection of interferon should be consolidated (15).

A very interesting issue of this study came from the “negative” result obtained with the sera from MAP infected sheep. Our current knowledge on the composition of lipids of the external layer of the wall of the subspecies *paratuberculosis* allows us to understand this result. According to genomic analysis, the S-type strains, which are more adapted in sheep, have evolved in two distinct subtype S-I and S-III (41). In a recent report we described that the SIII-type strain S397, produced a unique lipid, a tripeptide Phe-N-Methyl-Val-Ala with a N-ter lipid moiety, termed lipotriptide (L3P) instead of the L5P detected in cattle strains (11). In addition, at the present time no L5P nor L3P has been detected in the lipids extracted from the S-I strain Telford that was used in the experimental sheep infections (data not shown). These observations may explain why L5P was not significantly recognized by the sera of infected sheep. While most MAP strains isolated from bovine are of C-type, infections with S type do occur, a situation which cannot be detected by this

antigen if it is used alone. These results highlight the great need to characterize the antigens of MAP broadly across many strains, regardless of their protein or lipidic nature, and to consider the genetic diversity of this subspecies. Not only are lipids different among MAP strain types, but they can change based on the environment. For example, the L5P lipid was shown to be absent in MAP exposed to milk, but present in MAP cultured in Middlebrook media (42). Therefore, additional experiments should be conducted to determine the extent to which L5P is produced across many different environments, including feces and milk. However, from a bovine diagnostics standpoint, it is clear that MAP replicating inside cows do produce L5P as we and others have shown a bovine antibody response to L5P.

In conclusion, using an engineered synthetic antigen, we have identified a potent hydrosoluble mimic of the native L5P and established ELISA conditions for the specific diagnosis of bovine paratuberculosis. Ongoing research into the characterization of the non-protein antigens produced naturally by the different genetic lineages of MAP should identify new antigens that could contribute to achieve a diagnostic test with optimal sensitivity and specificity. In addition, it would be important to identify the L5P homolog in SI-type strains. New developments, including chemical tailoring and formulation of these synthetic antigens need to be investigated to gain sensitivity observed in this report. Other investigations should evaluate animal responses according to the disease progression and excretory status of the animal. These synthetic antigens could also be useful for the improvement of existing commercial tests especially regarding the strong demand from diagnostic laboratories for no batch-to-batch variation and elimination of the pre-absorption step.

DATA AVAILABILITY STATEMENT

The original contributions presented in the study are included in the article/**Supplementary Material**, further inquiries can be directed to the corresponding author/s.

AUTHOR CONTRIBUTIONS

SB, RW, HK, JB, and FB conceived and designed the study. All authors made substantial contributions to the analysis and writing of the manuscript.

FUNDING

This study was funded by EMIDA-EraNet Mycobacdiagnosis (Convention: 2011-EMID-005-02).

SUPPLEMENTARY MATERIAL

The Supplementary Material for this article can be found online at: <https://www.frontiersin.org/articles/10.3389/fvets.2021.637841/full#supplementary-material>

Supplementary Figure 1 | ^1H (A) and ^{13}C (B) NMR spectra of L5P-Aq. The corresponding structural formula is depicted in panel (C).

Supplementary Figure 2 | ROC analysis of antibody response of a bank of bovine sera in the IDEXX test. ROC analysis was performed on a bank of sera including 60 MAP positive and 50 control animals, using the commercial test IDEXX. All results are expressed as individual OD and were compared by ROC analysis. Serum samples were tested in triplicate. Significantly different when $p < 0.05$. **** $p < 0.0001$. The horizontal bars indicate median. Not significantly different (ns).

Supplementary Figure 3 | ROC analysis of antibody response of the ovine serum panel in the IDEXX test. ROC analysis performed on a bank of sera including 39 MAP positive and 15 control animals, using the commercial test

IDEXX. All results are expressed as individual S/P (OD sample-OD negative control/ meanOD positive control—Mean negative control) and were compared by ROC analysis. Serum samples were tested in triplicate. Area under the receiver operating characteristic curve (A).

Supplementary Figure 4 | ROC analysis of antibody response of bovine sera against lipid part of L5P. ROC analysis was performed on a bank of sera including 60 MAP positive and 50 control animals, using the lipid part of L5P coated in ethanol. All results are expressed as individual OD and were compared by ROC analysis. Serum samples were tested in triplicate. The horizontal bars indicate median. Not significantly different (ns).

Supplementary Table 1 | Statistical detail of ROC analysis.

Supplementary Table 2 | Detail of bank of sera.

REFERENCES

- Daffe M, Crick DC, Jackson M. Genetics of capsular polysaccharides and cell envelope (Glyco)lipids. *Microbiol Spectr.* (2014) 2:1–2. doi: 10.1128/microbiolspec.MGM2-0021-2013
- Marrakchi H, Laneelle MA, Daffe M. Mycolic acids: structures, biosynthesis, and beyond. *Chem Biol.* (2014) 21:67–85. doi: 10.1016/j.chembiol.2013.11.011
- Nakata N, Fujiwara N, Naka T, Yano I, Kobayashi K, Maeda S. Identification and characterization of two novel methyltransferase genes that determine the serotype 12-specific structure of glycopeptidolipids of *Mycobacterium intracellulare*. *J Bacteriol.* (2008) 190:1064–71. doi: 10.1128/JB.01370-07
- Pourshafie M, Ayub Q, Barrow WW. Comparative effects of *Mycobacterium avium* glycopeptidolipid and lipopeptide fragment on the function and ultrastructure of mononuclear cells. *Clin Exp Immunol.* (1993) 93:72–9. doi: 10.1111/j.1365-2249.1993.tb06499.x
- Ortalo-Magne A, Lemassu A, Laneelle MA, Bardou F, Silve G, Gounon P, et al. Identification of the surface-exposed lipids on the cell envelopes of *Mycobacterium tuberculosis* and other mycobacterial species. *J Bacteriol.* (1996) 178:456–61. doi: 10.1128/JB.178.2.456-461.1996
- Kitada S, Yoshimura K, Miki K, Miki M, Hashimoto H, Matsui H, et al. Validation of a commercial serodiagnostic kit for diagnosing pulmonary *Mycobacterium avium* complex disease. *Int J Tuberc Lung Dis.* (2015) 19:97–103. doi: 10.5588/ijtld.14.0564
- Rathanaiah G, Zinniel DK, Bannantine JP, Stabel JR, Grohn YT, Collins MT, et al. Pathogenesis, molecular genetics, and genomics of *Mycobacterium avium* subsp. *paratuberculosis*, the Etiologic Agent of Johne's Disease. *Front Vet Sci.* (2017) 4:187. doi: 10.3389/fvets.2017.00187
- Biet F, Bay S, Thibault VC, Euphrasie D, Grayon M, Ganneau C, et al. Lipopeptide induces a strong host humoral response and distinguishes *Mycobacterium avium* subsp. *paratuberculosis* from *M. avium* subsp. *avium*. *Vaccine.* (2008) 26:257–68. doi: 10.1016/j.vaccine.2007.10.059
- Riviere M, Puzo G, Wright EL, Barrow WW. A unique phenylalanine-containing lipopeptide isolated from a rough-colony variant of *Mycobacterium avium*. *Eur J Biochem.* (1996) 241:682–90. doi: 10.1111/j.1432-1033.1996.00682.x
- Eckstein TM, Chandrasekaran S, Mahapatra S, McNeil MR, Chatterjee D, Rithner CD, et al. A major cell wall lipopeptide of *Mycobacterium avium* subspecies *paratuberculosis*. *J Biol Chem.* (2006) 281:5209–15. doi: 10.1074/jbc.M512465200
- Bannantine JP, Etienne G, Laval F, Stabel JR, Lemassu A, Daffe M, et al. Cell wall peptidolipids of *Mycobacterium avium*: from genetic prediction to exact structure of a nonribosomal peptide. *Mol Microbiol.* (2017) 105:525–39. doi: 10.1111/mmi.13717
- Costanzo G, Pinedo FA, Mon ML, Viale M, Gil A, Illia MC, et al. Accuracy assessment and screening of a dairy herd with *paratuberculosis* by three different ELISAs. *Vet Microbiol.* (2012) 56:183–8. doi: 10.1016/j.vetmic.2011.10.029
- Thirunavukkarasu S, Plain KM, Eckstein TM, de Silva K, Whittington RJ. Cellular and humoral immunogenicity of *Mycobacterium avium* subsp. *paratuberculosis* specific lipopeptide antigens. *Res Vet Sci.* (2013) 95:123–9. doi: 10.1016/j.rvsc.2013.03.002
- Verdier J, Deroche L, Allez M, Loy C, Biet F, Bodier CC, et al. Specific IgG response against *Mycobacterium avium* *paratuberculosis* in children and adults with Crohn's disease. *PLoS One.* (2013) 8:e62780. doi: 10.1371/journal.pone.0062780
- Holbert S, Branger M, Souriau A, Lamoureux B, Ganneau C, Richard G, et al. Interferon gamma response to *Mycobacterium avium* subsp. *paratuberculosis* specific lipopeptide antigen L5P in cattle. *Res Vet Sci.* (2015) 102:118–21. doi: 10.1016/j.rvsc.2015.07.017
- Niegowska M, Rapini N, Biet F, Piccinini S, Bay S, Lidano R, et al. Seroreactivity against specific L5P antigen from *Mycobacterium avium* subsp. *paratuberculosis* in children at risk for T1D. *PLoS One.* (2016) 11: e0157962. doi: 10.1371/journal.pone.0157962
- Barkema HW, Hesselink JW, McKenna SLB, Benedictus G, Groenendaal H. Global prevalence and economics of infection with *Mycobacterium avium* subsp. *paratuberculosis* in ruminants. In: Behr MA, Collins DM, editors. *Paratuberculosis: Organism, Disease, Control*. Oxfordshire: Wallingford (2010). p. 10–21.
- Barkema HW, Orsel K, Nielsen SS, Koets AP, Rutten V, Bannantine JP, et al. Knowledge gaps that hamper prevention and control of *Mycobacterium avium* subspecies *paratuberculosis* infection. *Transbound Emerg Dis.* (2018) 65(Suppl 1):125–48. doi: 10.1111/tbed.12723
- Whittington R, Donat K, Weber MF, Kelton D, Nielsen SS, Eisenberg S, et al. Control of *paratuberculosis*: who, why and how. A review of 48 countries. *BMC Vet Res.* (2019) 15:198. doi: 10.1186/s12917-019-1943-4
- Bannantine JP, Bayles DO, Waters WR, Palmer MV, Stabel JR, Paustian ML. Early antibody response against *Mycobacterium avium* subspecies *paratuberculosis* antigens in subclinical cattle. *Proteome Sci.* (2008) 6:5. doi: 10.1186/1477-5956-6-5
- Blankemeyer-Menge B, Nimtz M, Frank R. An efficient method for anchoring fmoc-amino acids to hydroxyl-functionalised solid supports. *Tetrahedron Lett.* (1990) 31:1701–4. doi: 10.1016/S0040-4039(00)88858-9
- Leroy B, Roupie V, Noel-Georis I, Rosseels V, Walravens K, Govaerts M, et al. Antigen discovery: a postgenomic approach to *paratuberculosis* diagnosis. *Proteomics.* (2007) 7:1164–76. doi: 10.1002/pmic.200600988
- Leroy B, Viart S, Trincherio N, Roupie V, Govaerts M, Letesson JJ, et al. Use of *Mycobacterium avium* subsp. *paratuberculosis* specific coding sequences for serodiagnosis of bovine *paratuberculosis*. *Vet Microbiol.* (2009) 135:313–9. doi: 10.1016/j.vetmic.2008.09.065
- Courcoul A, Moya JL, Brugere L, Faye S, Henault S, Gares H, et al. Estimation of sensitivity and specificity of bacteriology, histopathology and PCR for the confirmatory diagnosis of bovine tuberculosis using latent class analysis. *PLoS One.* (2014) 9:e90334. doi: 10.1371/journal.pone.0090334
- Begg DJ, de Silva K, Di Fiore L, Taylor DL, Bower K, Zhong L, et al. Experimental infection model for Johne's disease using a lyophilised, pure culture, seedstock of *Mycobacterium avium* subspecies *paratuberculosis*. *Vet Microbiol.* (2010) 141:301–11. doi: 10.1016/j.vetmic.2009.09.007
- Dukkipati VSR, Ridler AL, Thompson KG, Buddle BM, Hedgspeth BA, Price-Carter M, et al. Experimental infection of New Zealand Merino sheep with a suspension of *Mycobacterium avium* subspecies *paratuberculosis* (Map)

- strain Telford: kinetics of the immune response, histopathology and Map culture. *Vet Microbiol.* (2016) 195:136–43. doi: 10.1016/j.vetmic.2016.09.018
27. Perez V, Garcia Marin JF, Badiola JJ. Description and classification of different types of lesion associated with natural paratuberculosis infection in sheep. *J Comp Pathol.* (1996) 114:107–22. doi: 10.1016/S0021-9975(96)80001-6
 28. Kruger C, Kohler H, Liebler-Tenorio EM. Cellular composition of granulomatous lesions in gut-associated lymphoid tissues of goats during the first year after experimental infection with *Mycobacterium avium* subsp. *Paratuberculosis*. *Vet Immunol Immunopathol.* (2015) 163:33–45. doi: 10.1016/j.vetimm.2014.11.002
 29. Mobius P, Nordsiek G, Holzer M, Jarek M, Marz M, Kohler H. Complete genome sequence of JII-1961, a bovine *Mycobacterium avium* subsp. *paratuberculosis* field isolate from Germany. *Genome Announc.* (2017) 5:e00870–17. doi: 10.1128/genomeA.00870-17
 30. Kohler H, Soschinka A, Meyer M, Kather A, Reinhold P, Liebler-Tenorio E. Characterization of a caprine model for the subclinical initial phase of *Mycobacterium avium* subsp. *paratuberculosis* infection. *BMC Vet Res.* (2015) 11:74. doi: 10.1186/s12917-015-0381-1
 31. Schinkothe J, Mobius P, Kohler H, Liebler-Tenorio EM. Experimental infection of goats with *Mycobacterium avium* subsp. *hominissuis*: a Model for Comparative Tuberculosis Research. *J Comp Pathol.* (2016) 155:218–30. doi: 10.1016/j.jcpa.2016.06.008
 32. Bewick V, Cheek L, Ball J. Statistics review 13: receiver operating characteristic curves. *Crit Care.* (2004) 8:508–12. doi: 10.1186/cc3000
 33. Gardner IA, Greiner M. Receiver-operating characteristic curves and likelihood ratios: improvements over traditional methods for the evaluation and application of veterinary clinical pathology tests. *Vet Clin Pathol.* (2006) 35:8–17. doi: 10.1111/j.1939-165X.2006.tb00082.x
 34. Schiller I, Oesch B, Vordermeier HM, Palmer MV, Harris BN, Orloski KA, et al. Bovine tuberculosis: a review of current and emerging diagnostic techniques in view of their relevance for disease control and eradication. *Transbound Emerg Dis.* (2010) 57:205–20. doi: 10.1111/j.1865-1682.2010.01148.x
 35. Lyashchenko KP, Grandison A, Keskinen K, Sikar-Gang A, Lambotte P, Esfandiari J, et al. Identification of novel antigens recognized by serum antibodies in bovine tuberculosis. *Clin Vaccine Immunol.* (2017) 24:e00259–17. doi: 10.1128/CVI.00259-17
 36. Biet F, Boschirolu ML. Non-tuberculous mycobacterial infections of veterinary relevance. *Res Vet Sci.* (2014) 97(Suppl):S69–77. doi: 10.1016/j.rvsc.2014.08.007
 37. Brennan PJ, Nikaido H. The envelope of mycobacteria. *Annu Rev Biochem.* (1995) 64:29–63. doi: 10.1146/annurev.bi.64.070195.000333
 38. Jeong BH, Kim SY, Jeon K, Lee SY, Shin SJ, Koh WJ. Serodiagnosis of *Mycobacterium avium* complex and *Mycobacterium abscessus* complex pulmonary disease by use of IgA antibodies to glycopeptidolipid core antigen. *J Clin Microbiol.* (2013) 51:2747–9. doi: 10.1128/JCM.00702-13
 39. Spencer JS, Brennan PJ. The role of *Mycobacterium leprae* phenolic glycolipid I (PGL-I) in serodiagnosis and in the pathogenesis of leprosy. *Lepr Rev.* (2011) 82:344–57. doi: 10.47276/lr.82.4.344
 40. Mikkelsen H, Aagaard C, Nielsen SS, Jungersen G. Review of *Mycobacterium avium* subsp. *paratuberculosis* antigen candidates with diagnostic potential. *Vet Microbiol.* (2011) 152:1–20. doi: 10.1016/j.vetmic.2011.03.006
 41. Biet F, Sevilla IA, Cochard T, Lefrancois LH, Garrido JM, Heron I, et al. Inter- and intra-subtype genotypic differences that differentiate *Mycobacterium avium* subspecies *paratuberculosis* strains. *BMC Microbiol.* (2012) 12:264. doi: 10.1186/1471-2180-12-264
 42. Alonso-Hearn M, Eckstein TM, Sommer S, Bermudez LE. A *Mycobacterium avium* subsp. *paratuberculosis* LuxR regulates cell envelope and virulence. *Innate Immun.* (2010) 16:235–47. doi: 10.1177/1753425909339811

Conflict of Interest: The authors declare that the research was conducted in the absence of any commercial or financial relationships that could be construed as a potential conflict of interest.

Copyright © 2021 Bay, Begg, Ganneau, Branger, Cochard, Bannantine, Köhler, Moyen, Whittington and Biet. This is an open-access article distributed under the terms of the Creative Commons Attribution License (CC BY). The use, distribution or reproduction in other forums is permitted, provided the original author(s) and the copyright owner(s) are credited and that the original publication in this journal is cited, in accordance with accepted academic practice. No use, distribution or reproduction is permitted which does not comply with these terms.



Functional Variants Surrounding Endothelin 2 Are Associated With *Mycobacterium avium* Subspecies *paratuberculosis* Infection

Jennifer N. Kiser¹, Zeping Wang¹, Ricardo Zanella¹, Erik Scraggs¹, Mahesh Neupane¹, Bonnie Cantrell¹, Curtis P. Van Tassell², Stephen N. White^{3,4,5}, Jeremy F. Taylor⁶ and Holly L. Neibergs^{1*}

¹ Department of Animal Sciences, Washington State University, Pullman, WA, United States, ² Animal Genomics and Improvement Laboratory, United States Department of Agriculture, Agricultural Research Service, Beltsville, MD, United States, ³ Animal Disease Research, United States Department of Agriculture, Agricultural Research Service, Pullman, WA, United States, ⁴ Department of Veterinary Microbiology and Pathology, Washington State University, Pullman, WA, United States, ⁵ Center for Reproductive Biology, Washington State University, Pullman, WA, United States, ⁶ Division of Animal Sciences, University of Missouri, Columbia, MO, United States

OPEN ACCESS

Edited by:

Miguel Salgado,
Austral University of Chile, Chile

Reviewed by:

Kieran G. Meade,
University College Dublin, Ireland
Amanda Jane Gibson,
Aberystwyth University,
United Kingdom

*Correspondence:

Holly L. Neibergs
neibergs@wsu.edu

Specialty section:

This article was submitted to
Veterinary Infectious Diseases,
a section of the journal
Frontiers in Veterinary Science

Received: 02 November 2020

Accepted: 04 March 2021

Published: 05 May 2021

Citation:

Kiser JN, Wang Z, Zanella R, Scraggs E, Neupane M, Cantrell B, Van Tassell CP, White SN, Taylor JF and Neibergs HL (2021) Functional Variants Surrounding Endothelin 2 Are Associated With *Mycobacterium avium* Subspecies *paratuberculosis* Infection. *Front. Vet. Sci.* 8:625323. doi: 10.3389/fvets.2021.625323

Bovine paratuberculosis, caused by *Mycobacterium avium* subspecies *paratuberculosis* (MAP), continues to impact the dairy industry through increased morbidity, mortality, and lost production. Although genome-wide association analyses (GWAAAs) have identified loci associated with susceptibility to MAP, limited progress has been made in identifying mutations that cause disease susceptibility. A 235-kb region on *Bos taurus* chromosome 3 (BTA3), containing a 70-kb haplotype block surrounding endothelin 2 (*EDN2*), has previously been associated with the risk of MAP infection. *EDN2* is highly expressed in the gut and is involved in intracellular calcium signaling and a wide array of biological processes. The objective of this study was to identify putative causal mutations for disease susceptibility in the region surrounding *EDN2* in Holstein and Jersey cattle. Using sequence data from 10 Holstein and 10 Jersey cattle, common variants within the 70-kb region containing *EDN2* were identified. A custom SNP genotyping array fine-mapped the region using 221 Holstein and 51 Jersey cattle and identified 17 putative causal variants ($P < 0.01$) located in the 5' region of *EDN2* and a SNP in the 3' UTR ($P = 0.00009$) associated with MAP infection. MicroRNA interference assays, mRNA stability assays, and electrophoretic mobility shift assays were performed to determine if allelic changes at each SNP resulted in differences in *EDN2* stability or expression. Two SNPs [*rs109651404* (G/A) and *rs110287192* (G/T)] located within the promoter region of *EDN2* displayed differential binding affinity for transcription factors in binding sequences harboring the alternate SNP alleles. The luciferase reporter assay revealed that the transcriptional activity of the *EDN2* promoter was increased ($P < 0.05$) with the A allele for *rs109651404* and the G allele for *rs110287192*. These results suggest that the variants *rs109651404* and *rs110287192* are mutations that alter transcription and thus may alter susceptibility to MAP infection in Holstein and Jersey cattle.

Keywords: paratuberculosis, dairy cattle, *EDN2*, functional variant, functional assays

INTRODUCTION

Paratuberculosis, also referred to as Johne's disease, is an infectious and incurable disease that afflicts many wild and domestic ruminant species, including cattle, sheep, goats, and deer. Caused by *Mycobacterium avium* ssp. *paratuberculosis* (MAP), most cattle with bovine paratuberculosis initially present with decreased production and progress to severe diarrhea, emaciation, and eventually death. With no effective vaccines available for the disease and limited treatment options for livestock, many countries rely on voluntary or mandatory management and prevention programs to help producers limit the spread of infection both within and between herds (1). The financial burden incurred by producers due to bovine paratuberculosis is substantial. In the U.S. dairy industry alone, MAP infections result in an estimated \$1.5 billion annual loss stemming from decreases in production (2).

While the economic impact of bovine paratuberculosis is substantial, the situation is made worse by a lack of sensitive diagnostic tests and limited treatment options. There are multiple diagnostic tests available to test for MAP infection including polymerase chain reaction (PCR) analyses of tissues or feces; enzyme-linked immunosorbent assays (ELISAs) for serum, milk, or fecal samples; and culturing of tissue or feces, all of which have similar specificity for MAP (3, 4). However, the sensitivity of these diagnostic methods varies. For example, McKenna et al. (5) reported that when 160 cattle identified as MAP positive by tissue culture were tested for MAP infection by fecal ELISAs, the ELISAs only identified 6.9% ($n = 11$) to 16.9% ($n = 27$) of the cattle as being MAP positive. Among the various diagnostic methods available for MAP testing, tissue culturing is considered the gold standard (6, 7). However, tissue culturing is a time-consuming method and studies have shown that quantitative PCR of tissue samples is equally effective in identifying MAP-positive animals and considerably faster (8), making the use of the two diagnostic methods comparable. The differences among some testing methods have likely contributed to the lack of success in curbing the spread of the disease.

The identification of genetic markers from studies with high-quality phenotypes can be implemented to the population at large to help to reduce the prevalence of the disease. Previous studies have identified loci associated with disease susceptibility that could be used to help producers select less susceptible cattle. These include candidate gene studies (9–14) and genome-wide association studies (11, 15–24). To date, there have been few loci that have been associated with MAP in more than one study, which may be due to differences in MAP diagnostic testing sensitivity, genotyping densities, and disease phenotype definition (22). However, some concordance among associations has been found on *Bos taurus* chromosome 1 (BTA1) (15, 19), BTA12 (16, 19), and BTA3 (15, 25). The overlapping regions between studies on BTA1 and BTA12 do not harbor any positional candidate genes within 50 kb of the associated loci, but the region on BTA3 harbored a 70 kb haplotype block that is located near endothelin 2 (*EDN2*) and HIVEP zinc finger 3 (*HIVEP3*).

In a study by Zanella et al. (18), the original 235-kb candidate region on BTA3 was further refined to 10.6 kb (104,738,280 to 104,748,953 bp on ARS-UCD 1.2) near *EDN2*. The objective of the current study was to validate and refine the 10.6-kb region and to further identify putative causal mutations within this 10.6-kb region associated with susceptibility to MAP tissue infection in both Holstein and Jersey cattle. To determine if loci located in the 10.6-kb region were associated with differences between MAP-positive and MAP-negative cattle, microRNA interference assays, mRNA stability assays, electrophoretic mobility shift assays (EMSAs), and an association analysis were utilized.

MATERIALS AND METHODS

Study Populations

Sample collection and MAP diagnostic methods for the Holstein population used in this study have been described in detail in previous MAP studies (15, 18, 22, 25, 26). Briefly, 245 Holstein cows from four herds in the Eastern United States had tissue and fecal samples collected at slaughter. To determine if the animals were MAP tissue infected, MAP was cultured from tissues taken from the ileum, ileo-cecal valve, and two adjacent ileo-cecal lymph nodes using the method described by Whitlock et al. (3). Samples with colony-forming units (cfus) of MAP > 0 were classified as MAP infected. After testing, 94 cattle were classified as cases, and 138 cattle were classified as controls. An additional 13 cattle were not tissue cultured and were removed from further analyses. The mean ages of cases (60.7 months) and controls (58.5 months) did not differ ($P = 0.44$).

As with the Holstein population, sample collection and diagnostic testing methods of the Jersey population have also been previously described (22). The Jersey population consisted of 48 cows from an Oregon dairy and 9 Jersey steers from a dairy in Pennsylvania. Briefly, fecal and tissue samples from ileum and ileo-cecal lymph nodes were harvested at slaughter, and determination of the infection status of the animals was conducted using the AgPath-IDtm real-time qPCR assay using 300 mg of tissue sample (ileo-cecal lymph node and ileum) for the Northern Oregon animals. Quantitative PCR results were also confirmed in a subset of samples with qPCR results from the Washington State University Veterinary Diagnostic Laboratory. All qPCR diagnostic testing was performed in triplicate. Animals with MAP DNA copies/ μ l > 1 in at least one of the tissues were considered MAP infected. After testing, 16 cattle were classified as cases and 41 were classified as controls. The mean age of cases (46.2 months) did not differ from the mean age of controls (52.6 months) ($P = 0.48$).

Genotyping and Quality Assurance

To develop a custom fine-mapping array, single-nucleotide polymorphisms (SNPs) within the previously defined region on BTA3 (104,677,793 to 104,748,725 bp on ARS-UCD 1.2) were identified using the whole genome sequences of 10 Holstein and 10 Jersey cattle previously sequenced for a different study (MAP status unknown) (Animal Genomics and Improvement Laboratory, United States Department of Agriculture). The non-coding region between *HIVEP3* and *EDN2* was observed to

be highly conserved when compared to six species (human, macaque, horse, elephant, dog, and dolphin) with blocks of conservation that exceeded the conservation of the coding regions of *HIVEP3* and *EDN2*. Non-coding regions commonly contain regulatory elements such as enhancers and promoters that may be evolutionarily conserved across species (27). Conserved sequences across species commonly indicate regions constrained against mutation due to the functional consequences of such a variant. Given the lack of annotation of the bovine genome assembly, sequence comparison across species allows for the identification of DNA sequences previously identified as regulatory elements in other, better annotated species like humans and identify conserved sequences that typically have functional roles. This region between *EDN2* and *HIVEP3* contains a multitude of transcription factor binding sites and over 100 putative functional modifications that modify the binding of transcription factors based on *in silico* analysis of the observed DNA variants. From the whole genome sequence data, 528 SNPs with a median spacing of 132 bp were identified in the candidate region. From these 528 SNPs, 96 were incorporated in a custom 96-SNP assay (Illumina, San Diego, CA). These 96 SNPs were selected based on a lack of repetitive regions surrounding the SNP, their nucleotide location based on the UMD 3.0 assembly, high minor allele frequency (MAF) among the 20 sequenced animals, whether the SNP had previously been validated (or, if not validated, SNPs predicted to be segregating in both breeds were preferred), conservation of SNP flanking sequences in the six species listed previously, and the predicted presence of transcription or other regulatory motifs using the Transfac public database for gene regulation (<http://gene-regulation.com/pub/databases.html>) and with Illumina design scores >70 (28).

DNA was extracted from tissue from each animal using the Puregene DNA extraction kit following the manufacturer's instructions (Gentra, Minneapolis, MN). DNA was quantified using a NanoDrop1000 spectrophotometer (ThermoScientific, Wilmington, DE) and then genotyped at Igenix (Seattle, WA) using the custom array. Genotypes were called using Illumina's BeadStudio (v3.2.23) software, and samples were removed from the analysis when more than 10% of genotypes failed. After quality control, 210 Holstein cattle (90 cases and 120 controls) and 56 Jersey cattle (15 cases and 41 controls) remained for analysis. SNPs were removed if the MAF was <1% ($n = 39$ in Holstein; $n = 9$ in Jersey), if SNP call rates were <90% ($n = 7$ in Holstein; $n = 30$ in Jersey), or if the SNPs failed the Hardy-Weinberg equilibrium test ($P < 0.001$; $n = 6$ in Holstein; $n = 4$ in Jersey). After filtering, 44 SNPs remained for analysis in Holsteins and 53 in Jerseys.

To test for population stratification between the cases and controls prior to the association analysis, multi-dimensional scaling (MDS) plots were constructed using PLINK (version 1.07) in the R statistical environment for the Holstein and Jersey cattle populations (29). No population stratification was detected among the Holstein or Jersey cattle populations.

Association Analysis

An allelic chi-square test was performed using PLINK v1.07 between SNPs to identify loci associated with MAP infection (29).

Two separate analyses were conducted; the first compared cases and controls within the Holstein populations and the second compared cases and controls within the Jersey population. A significance threshold for the association analysis of $P < 0.05$ was used after 10^6 permutations comparing each observed test statistic against the maximum of all permuted statistics over all SNPs for each single replicate. The linkage disequilibrium levels between SNPs were computed using the D' function in Haploview 4.2 (30).

Functional Analyses

Cell Culture, Transfection, and Dual Luciferase Reporter Assay

Human embryonic kidney (HEK293) cells were cultured in Dulbecco's modified eagle medium (DMEM) supplemented with 10% fetal bovine serum (FBS), 100 units/ml penicillin, and 100 μ g/ml streptomycin. Cells were maintained at 37°C in a humidified atmosphere of 95% air and 5% CO₂. HEK293 cells were seeded at 10^5 cells per well in a 24-well plate the day before transfection and co-transfected with 0.8 μ g of the luciferase reporter construct and 0.1 μ g of pRL-TK (*Renilla* luciferase) plasmid. Thirty hours after transfection, firefly and *Renilla* luciferase activities were measured consecutively using a dual Luciferase assay kit (Promega, Madison, WI). *Renilla* luciferase values were normalized to firefly and the ratio of *Renilla*/firefly values was reported. Each experiment was carried out more than three times in triplicate (repeatability = 0.93).

Electrophoretic Mobility Shift Assays

Eighteen significant SNPs from the association analysis were further investigated using EMSAs. Nuclear extracts were prepared from cattle ileo-cecal lymph nodes using NE-PER Nuclear and Cytoplasmic Extraction Reagents (Pierce, Rockford, IL) according to the manufacturer's instructions. The EMSAs were performed using the LightShift Chemiluminescent EMSA kit (Pierce, Rockford, IL) according to the manufacturer's instructions. Double-stranded oligonucleotide probes consisting of 31 bp of sequence complementary to each allele were synthesized (Supplementary Table 1). Probes were pre-incubated with poly (dI-dC), a competitor for nonspecific DNA binding proteins, for 2 h at room temperature and then incubated with 20 μ g of nuclear extract for 20 min at room temperature. The products were then separated by electrophoresis on a 6% non-denaturing polyacrylamide gel with 0.5 \times tris-borate-EDTA buffer (pH 8.3). The protein-oligonucleotide complexes were visualized by auto-radiography. For competition studies, unlabeled oligonucleotide probes of 5- to 125-fold excess concentration were pre-incubated with the nuclear extract before the biotin-labeled probes were added. All EMSAs were repeated at least three times to assess the reproducibility of the observed band shifts ($r = 1.0$).

3' MicroRNA Analysis of EDN2 mRNA Stability

The MAP infection-associated SNP272 (*rs109490418*) is located within the 3' UTR of *EDN2*, 189 bp from the transcription stop site. Putative target sites for microRNA in the 3-UTR around SNP272 were screened using Targetscan (www.targetscan.org)

to investigate their potential involvement in mRNA stability. microRNAs were investigated for their role in mRNA stability as SNPs within microRNAs or their binding sites in the 3' UTR have been demonstrated to influence regulation of gene expression (31). This occurs through the binding of microRNA to the 3' UTR of mRNA in conjunction with other RNA binding proteins that are responsible for the localization, translation, or degradation of mRNA with the cell (32, 33). Two microRNAs (bta-miR-2339 and bta-miR-1197) were predicted within the 600-bp 3' UTR of *EDN2* and were investigated using EMSA.

Within the 3' UTR, bta-miR-2339 was located between 409 and 415 bp while bta-miR-1197 was located 413 to 419 bp from the *EDN2* transcription start site. To determine if the alleles at this site influenced mRNA stability, genomic DNA from two cattle that were homozygous for SNP272 for either the A or G allele were used as the PCR template for the analysis. Sequences for the amplified fragments of 31 bp are in **Supplementary Table 2**. The 3' PCR amplified DNA was cloned into the XhoI and NotI multiple cloning sites distal to the *Renilla* luciferase coding region of the psiCHECK-2 vector (Promega, Madison, WI). microRNA precursors (bta-miR-1197 and bta-miR-2339) and a negative control were purchased from Ambion (Austin, TX). HEK293 cells were co-transfected with 50 nmol/L microRNA and 200 ng of psiCHECK-2 constructs, using Lipofectamine 2000 (Invitrogen, Carlsbad, CA). The assay for firefly and *Renilla* luciferase activities were as described above in the "Cell culture, transfection, and dual luciferase reporter assay" subsection. The two alternative allele SNP272 sequences were confirmed by sequencing both cloned strands. Results were assessed using a two-tailed *t* test with a significance threshold of $P < 0.05$.

5' Region Analysis of *EDN2*

Since SNPs located in the 5' region of a gene or in a promoter region could alter gene expression through the modification of transcription binding factors, enhancers, or suppressors, any SNP that was confirmed to exhibit differential allelic binding through EMSA was further investigated to determine the alleles' impact on *EDN2* expression ($n = 2$). As SNP208 (*rs110287192*) and SNP105 (*rs109651404*) were confirmed to have different allele binding affinities by EMSAs, both were further examined to determine if there were allele-specific *EDN2* expression differences. SNP208 is found 671 bases 5' of the transcription start site for *EDN2* located at 104,700,352 (ARS-UCD 1.2). This SNP was part of a 718-bp construct of the *EDN2* promoter (104,699,956–104,700,673 bp) flanked by XhoI and HindIII restriction endonuclease sites and inserted into a pGL3-basic vector (**Supplementary Figure 1A**; Promega, Madison, WI). Constructs were created containing each of the two SNP208 alleles.

SNP105 is located 11 kb 5' to the transcription start site of *EDN2*. Considering the substantial physical distance between SNP105 (G/A) and *EDN2*, luciferase assays were not performed on this SNP alone. Instead, it was co-transfected into pGL3-basic vectors that contained SNP208 (G/T) to determine if allele-specific interactions between the SNP105 and SNP208 influenced *EDN2* expression (**Supplementary Figure 1B**).

A 31-bp (104,689,846–104,689,876 bp) PCR fragment containing either of the SNP105 alleles was amplified from individuals with DNA that were homozygous for the allele. The amplified products for each allele were separately cloned into the plasmids that contained SNP208 and a portion of the *EDN2* promoter. The sequences of the cloned PCR fragments were verified by sequencing both the sense and antisense strands of the cloned fragments. Relative luciferase activities were compared between the four plasmid constructs containing the four different allelic combinations: (1) SNP105-G and SNP208-G, (2) SNP105-G and SNP208-T, (3) SNP105-A and SNP208-G, and (4) SNP105-A and SNP208-T. Luciferase results were analyzed using a two-tailed *t* test, and interactions with $P < 0.05$ were considered significant.

RESULTS

Association Analyses

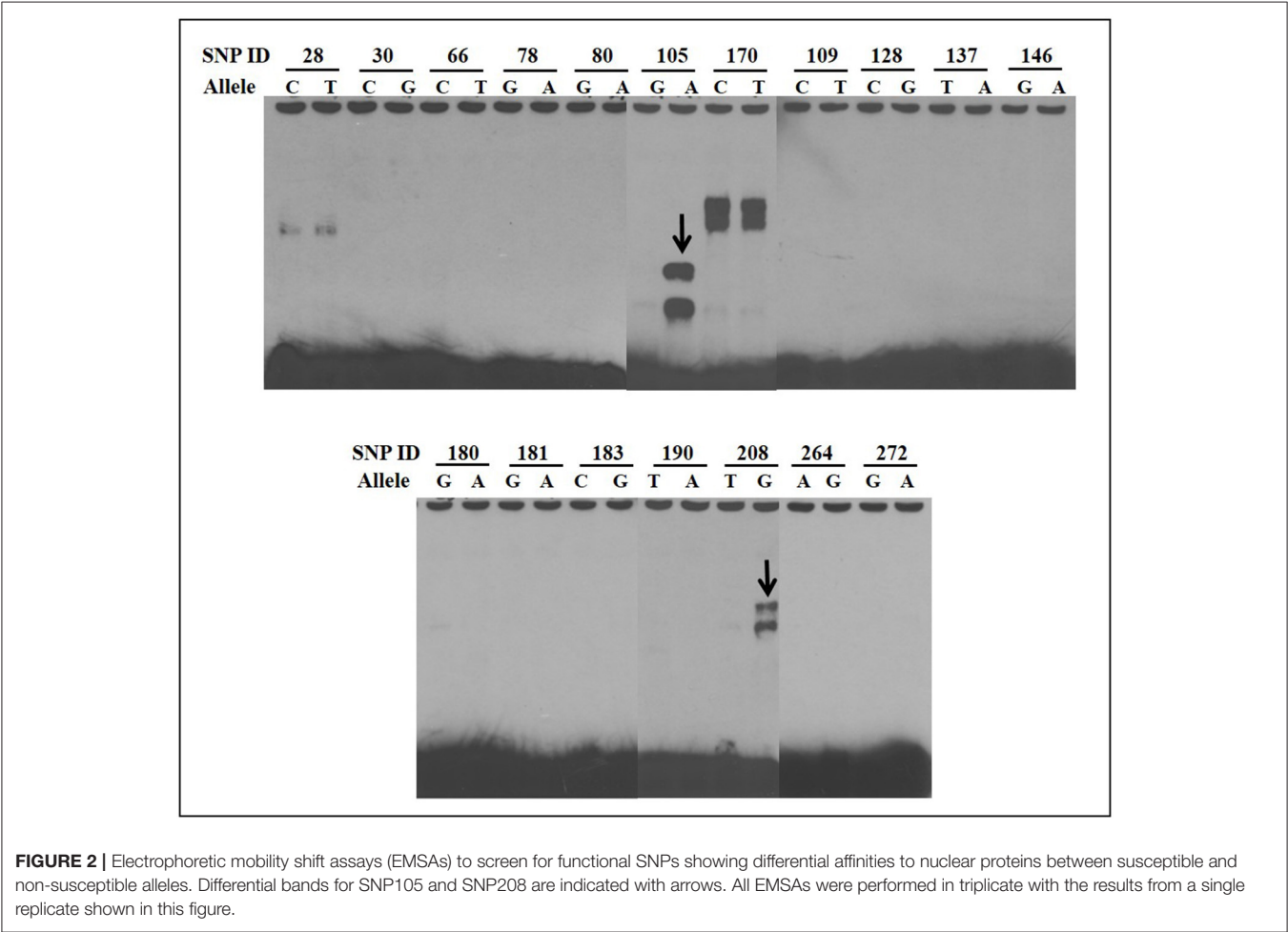
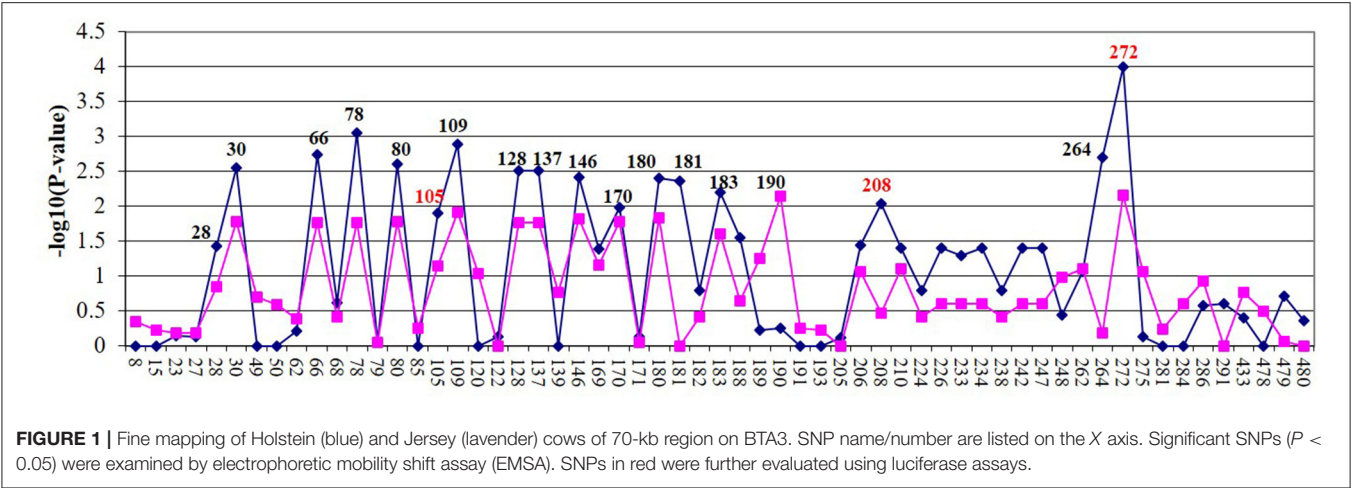
Allelic association tests were conducted to determine if there was an association between MAP tissue infection and the selected SNPs. The allelic chi-square test identified 24 SNPs ($P < 0.05$) associated in the Holstein population and 13 SNPs in the Jersey population (**Figure 1**). The most significant SNP in both populations was SNP272 (Holstein: $P < 9.9 \times 10^{-5}$; Jersey: $P < 6.8 \times 10^{-3}$). The 18 SNPs most strongly associated with MAP tissue infection across both breeds were selected for further functional analyses. Apart from a single SNP (SNP190, no rs#), all significant SNPs were in strong linkage disequilibrium with each other ($r^2 > 0.9$). Additional investigation determined that SNP272 was located within the 3' UTR of *EDN2* while the remaining SNPs were located 5' of *EDN2*.

Electrophoretic Mobility Shift Assays

EMSAs were used to determine if allelic variants at the 18 most significant SNPs from the association analysis had a functional role in binding ileo-cecal lymph node nuclear proteins, since binding proteins have a known role in controlling the production of mRNA within a cell (34). Only 2 of the 18 SNPs (SNP105 or *rs109651404* and SNP208 or *rs110287192*) exhibited differential nuclear protein binding affinities between alleles (**Figure 2**). Additional competition EMSAs were conducted for these two SNPs (**Figure 3**), confirming the differential binding affinity of alleles.

3' MicroRNA Analysis of mRNA Stability

SNPs within microRNAs or their binding sites in the 3' UTR have been demonstrated to influence regulation of gene expression (31). No significant change of luciferase activities was observed ($P > 0.05$) (**Figure 4**) when A vs. G alleles were compared for SNP272 luciferase constructs. Similarly, no significant changes in reporter activities were identified ($P > 0.05$; **Figure 5**) for the allele-specific effects of SNP272 when the binding of microRNA (bta-miR-2339 or bta-miR-1197) to the 3' UTR was compared. These results indicate that the microRNAs are not influenced by SNP272 variation and that this variant is not influencing mRNA stability through alterations of the microRNA binding sites.



5' Region Analysis

When SNP208 and SNP105 were investigated, the G allele of SNP208 had twice the luciferase activity as the T allele of SNP208 when paired with the *EDN2* promoter (**Figure 6A**; $P = 0.01$). The increased luciferase activity of the G allele at SNP208 when

paired with the *EDN2* promoter was further supported by the results from the luciferase assay on the co-transfected plasmids containing alleles for SNP208 and SNP105. When the G allele for SNP208 and the A allele for SNP105 were paired with the *EDN2* promoter, there was a significant increase in luciferase activity

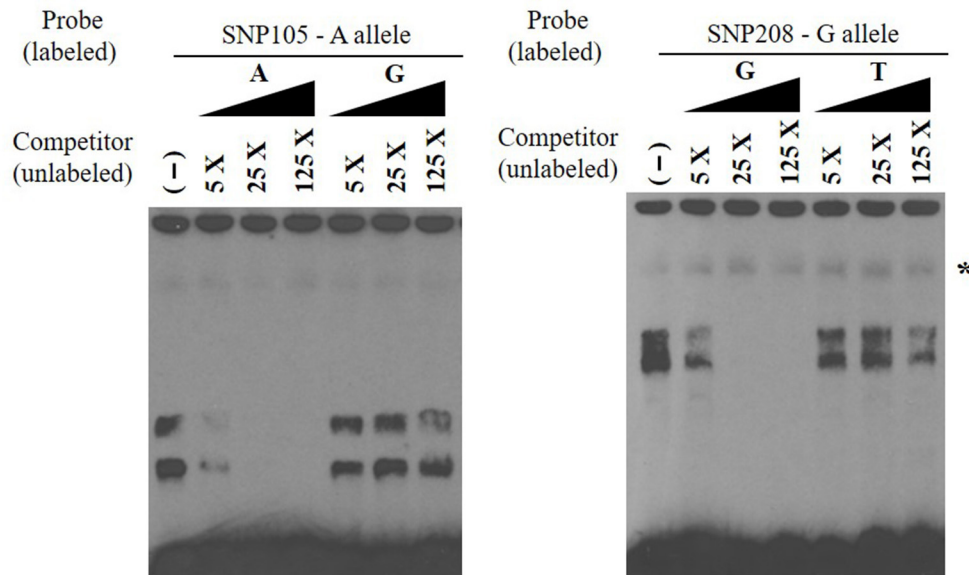


FIGURE 3 | Electrophoretic mobility shift competition assay for SNP105 (left) and SNP208 (right). DNA-protein complexes were competed away in a concentration-dependent manner by unlabeled oligonucleotide with A allele for SNP105 and with allele G for SNP208 (non-specific binding was indicated with star). All EMSAs were performed in triplicate with the results from a single replicate shown in this figure.

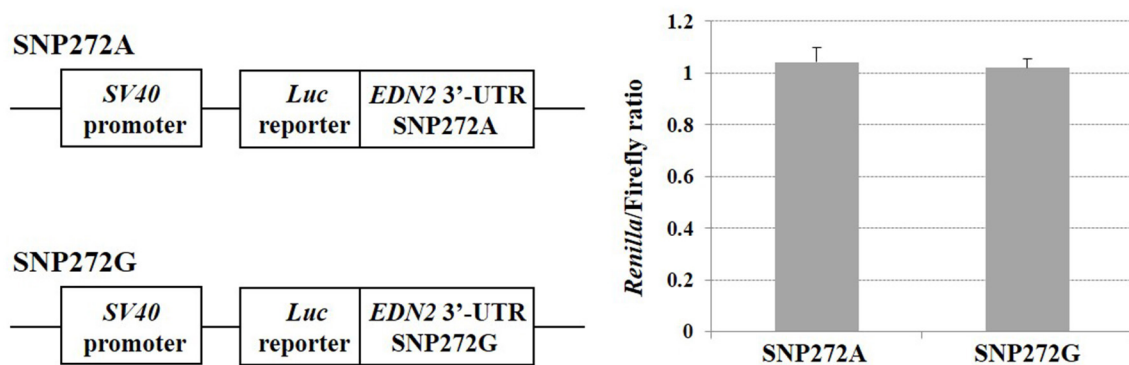


FIGURE 4 | SNP272 effect on mRNA stability. HEK293 cells were transfected with *EDN2*-3'-UTR luciferase constructs (SNP272 A/G). Luciferase activities (in triplicates) were measured 24 h post-transfection. *Renilla* luciferase activities were normalized against firefly luciferase activities, and mean normalized *Renilla* luciferase activities (\pm SD) from three independent experiments were determined. There was no difference ($P > 0.05$) in luciferase activities between the A and G alleles at SNP272.

($P = 0.02$) compared to all other allelic combinations with the *EDN2* promoter (Figure 6B).

DISCUSSION

Numerous studies have attempted to identify the genetic variation involved in susceptibility to *MAP* infection. Various approaches have been applied to identify genes and chromosomal regions associated with *MAP* infection, including genome-wide association, candidate gene, and linkage analyses. An initial genome-wide association study (15) and subsequent fine-mapping study (18) revealed a region of 10.6 kb on BTA3

associated with *MAP* infection. The current study expanded on these two studies by identifying 18 SNPs associated with *MAP* tissue infection through re-sequencing and fine-mapping in both Holstein and Jersey breeds when the region between *EDN2* and *HIVEP3* was evaluated. Of the 18 SNPs tested in the EMSA analyses, three (SNP272, SNP208, and SNP105) showed evidence of binding nuclear proteins. This study provides the basis for further investigations to identify the proteins that bind these regions and the mechanism used to regulate *EDN2*. This investigation is needed for a full understating of the role of these SNPs in regulating *EDN2* and *Map* infection.

An *in silico* analysis of the 18 SNPs associated with *MAP* infection did not provide evidence that the SNPs were

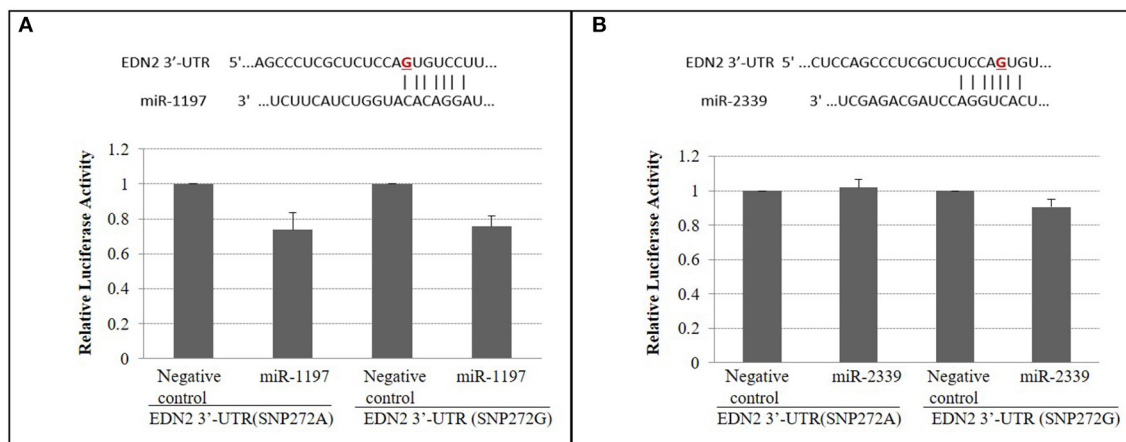


FIGURE 5 | (A) SNP272 is not responsible for bta-miR-1197's targeting of *EDN2* 3'-UTR ($P > 0.05$). miR-1197 and its predicted seed binding site in the 3'-UTR of *EDN2* (top). SNP272 is highlighted in red. **(B)** bta-miR-2339 does not target 3'-UTR of *EDN2* ($P > 0.05$). miR-2339 and its predicted seed binding site in the 3'-UTR of *EDN2* (top). HEK293 cells were co-transfected with *EDN2*-3'-UTR luciferase constructs (SNP272 A/G) and microRNA precursors (miR-1197 or miR-2339). microRNA negative control oligonucleotides were used as negative controls. Luciferase activities (in triplicates) were measured 24 h after transfection. *Renilla* luciferase activities were normalized against firefly luciferase activities, and mean normalized *Renilla* luciferase activities (\pm SD) from three independent experiments were determined and expressed relative to control values.

within transcription factor binding sites using the PROMO transcription regulatory element search tool (35, 36). However, given the level of sequence conservation across species in this region and the limited availability of annotated regulatory regions in cattle, further investigation was warranted. The regulatory function of SNP208 and SNP105 was confirmed through the use of luciferase assays, while the variant alleles at SNP272 did not regulate *EDN2*. The favorable allele of SNP208 and SNP105 increased luciferase activity alone and when coupled together, indicating that these two SNPs may synergistically regulate *EDN2* expression. Previous studies have also used luciferase assays to determine if SNPs located within microRNA binding sites were associated with certain disease traits in the 3' UTR of genes. For example, Zou et al. (33) performed luciferase assays on 10 SNP located within microRNA binding sites in the 3' UTR of genes associated with oxidative damage and age-related cataracts. They found that an allele in the 3' UTR of the XPC gene differed in luciferase reporter gene expression and was linked to an increased risk of nuclear type of age-related cataracts. Similar to the results of Zou et al. (33), this study also identified that SNPs within microRNA binding sites in the 3' UTR may be associated with disease traits.

The role of *EDN2* in *MAP* infection may be through its interaction with macrophages in providing intestinal immunity or in its role in the contraction and permeability of the intestine. During initial infection, *MAP* enters the host most commonly through the fecal-oral route where it is then transported across the intestinal epithelial barrier and into the host macrophages. Once *MAP* infects the host macrophages, it is able to avoid the host's phagosome-lysosome response (37). While the mechanism that *MAP* employs to avoid the phagosome-lysosome response is unknown, other mycobacteria are capable of avoiding the phagosome-lysosome interaction within macrophages

through the secretion of phosphatase, an acid that can arrest phagosomal maturation (38). Several studies have indicated that *EDN2* produces a chemoattractant for macrophages, such that an increased expression of *EDN2* attracts macrophages to a given area (39). While *EDN2* is commonly associated with female reproduction and ovulation (40–42), it is also present in the gastrointestinal tract of multiple species where it is highly expressed (Human Protein Atlas available from [https://www.proteinatlas.org/ENSG00000127129-EDN2/tissue/small\\$+intestine](https://www.proteinatlas.org/ENSG00000127129-EDN2/tissue/small$+intestine)) (43, 44). A study in mice by Takizawa et al. (43) found that localization of *EDN2* was predominantly observed in the epithelial cells of the basal membrane and that *EDN2* could be secreted into the lamina propria and the dome region of Peyer's patch, suggesting a role in modulating mucosal defense. Previous work has indicated that Peyer's patches in the small intestines of calves and kid goat play a key role in mediating *MAP* uptake across the intestinal barrier (45, 46).

In addition to its potential role in intestinal mucosal defense in mice, *Edn2* also has a function in intestinal architecture. Bianchi et al. (47) found that in mouse intestinal villi, *EDN2* exhibited a gradient localization, with increased presence near the base or crypt of the villi. The researchers postulated that the increased localization of *EDN2* near the crypts of intestinal villi was correlated with smooth muscle contraction (mobility) of the villi, contributing to the overall structure of the intestinal villi. It was also suggested that the gradient expression of *EDN2* might be associated with villi permeability through changes in the fibroblast network (47).

Given the roles that *EDN2* has in macrophage signaling, intestinal mucosa, intestinal structure, and how important these functions are during *MAP* infection, the hypothesis that potential

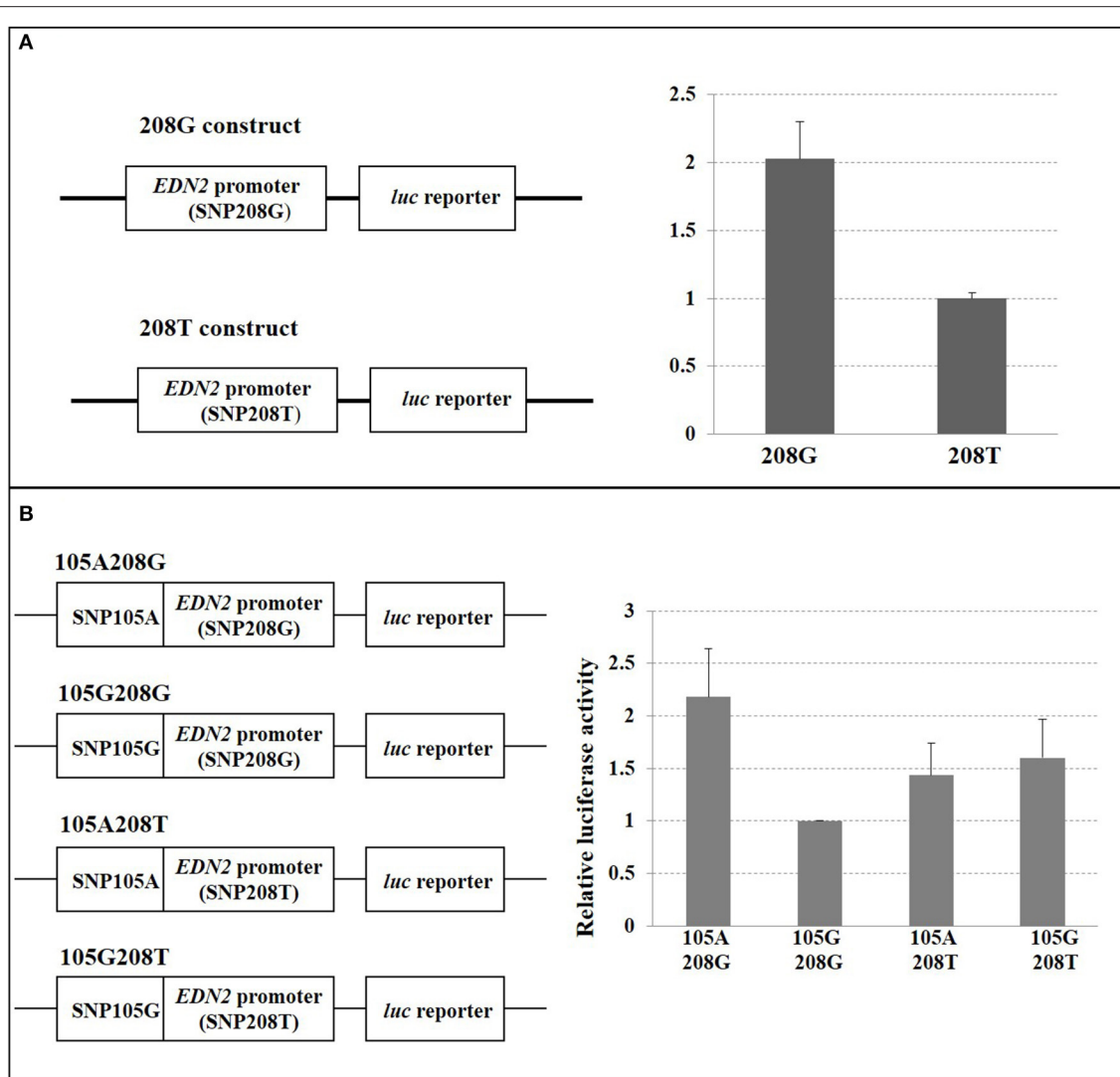


FIGURE 6 | (A) SNP208 Luciferase reporter assay. HEK293 cells were transfected with *EDN2* promoter-pGL3 reporter constructs containing either G or T at the location of SNP208. The relative luciferase activities were calculated and expressed as mean \pm SD. The relative luciferase activity of the genotype G at SNP208 was significantly higher ($P = 0.01$) compared with that of the genotype T. **(B)** SNP105 and SNP208 interaction. HEK293 cells were transfected with *EDN2* promoter-pGL3 reporter constructs containing different combination of SNP105(A/G) and SNP208(G/T). The relative luciferase activities were calculated and normalized to construct 105G/208G. The mean of relative luciferase activity (\pm SD) from three independent experiments was shown. The relative luciferase activity of the G genotype at SNP208 and the A genotype at SNP105 was significantly higher ($P = 0.02$) than genotype combinations.

causal mutations associated with *MAP* tissue infection lie near or within the gene is supported. The identification of SNP208 to be associated with *MAP* infection across breeds in different parts of the world provides further evidence that this region surrounding *EDN2* is associated with the disease. Çınar et al. (48) also investigated SNP272, SNP208, and SNP105 for their roles in *MAP* infection and identified SNP208 to be associated with *MAP* infection in East Anatolian Red crossbred cattle, Anatolian Black crossbred cattle, and Holstein cattle. Çınar et al. (48) found that *MAP* infection differed between animals with different genotypes at SNP208 ($P < 0.05$) where cattle with the TG or GG genotypes were more often controls and cattle

with TT genotypes were cases, suggesting that animals with the G may be less susceptible to *MAP* infection. Çınar et al. (48) did not identify any differences in *MAP* infection for SNP105 or SNP272.

The use of a SNP identified across breeds to be associated with *MAP* infection for genomic selection would be advantageous as it would be predictive for disease susceptibility in multiple breeds. The use of a causal variant for disease is even more desirable as the accuracy of prediction would not decay over time. Although SNP208 has not yet been proven to be a causal variant for *MAP* infection, these results are supportive of its role in *MAP* infection and suggest that it

may be of value for genomic selection to reduce disease. The selection of cattle less susceptible to *MAP* infection could reduce the prevalence of bovine paratuberculosis and lower the cattle suffering and the economic costs associated with it.

DATA AVAILABILITY STATEMENT

The data presented in the study are deposited in the CattleQTLdb repository, and can be found at: <https://www.animalgenome.org/QTLdb/supp/?t=TaEg1A5OgI>.

ETHICS STATEMENT

The animal study was reviewed and approved by Washington State University Institutional Animal Care and Use Committee (Study# 4073). Written informed consent for participation was not obtained from the owners because for the Jersey population, verbal consent was obtained from dairy owners prior to sample collection which occurred post mortem. For the Holstein population, these samples were collected from the Regional Dairy Quality Management Alliance (RDQMA) study herds for other analyses.

REFERENCES

- Geraghty T, Graham DA, Mullenwey P, More SJ. A review of bovine Johne's disease control activities in 6 endemic countries. *Prev Vet Med.* (2014) 116:1–11. doi: 10.1016/j.prevetmed.2014.06.003
- Harris NB, Barletta RG. *Mycobacterium avium* subsp. *paratuberculosis* in veterinary medicine. *Clin Microbiol Rev.* (2001) 14:489–512. doi: 10.1128/CMR.14.3.489-512.2001
- Whitlock RH, Wells SJ, Sweeney RW, Van Tiem J. ELISA and fecal culture for paratuberculosis (Johne's disease): Sensitivity and specificity of each method. *Vet Microbiol.* (2000) 77:387–98. doi: 10.1016/S0378-1135(00)00324-2
- White R, Marotti KR, Hines MEH, Whittington L, Goins K, et al. Evaluation of new enzyme-linked immunosorbent assay (ELISA) for Johne's disease in goat serum. *SOJ Vet Sci.* (2016) 2:1–6. doi: 10.15226/2381-2907/2/1/00112
- McKenna SLB, Keefe GP, Barkema HW, Sockett DC. Evaluation of three ELISA for *Mycobacterium avium* subsp. *paratuberculosis* using tissue and fecal culture as comparison standards. *Vet Microbiol.* (2005) 110:105–11. doi: 10.1016/j.vetmic.2005.07.010
- Martinson SA, Hanna PE, Ikeda BO, Lewis JP, Miller LM, et al. Comparison of bacterial culture, histopathology, and immunohistochemistry for the diagnosis of Johne's disease in culled dairy cows. *J Vet Diagn Invest.* (2008) 20:51–7. doi: 10.1177/104063870802000109
- Whittington R. Cultivation of *Mycobacterium avium* ssp. *paratuberculosis*. In: Behr MA, Collins DM, editors. *Paratuberculosis: Organism, Disease, Control*. Wallingford: CABI (2010). p. 244–266.
- Acharya KR, Dhand NK, Whittington RJ, Plain KM. Culture-independent identification of *Mycobacterium avium* subspecies *paratuberculosis* in ovine tissues: comparison with bacterial culture and histopathological lesions. *Front Vet Sci.* (2017) 4:232. doi: 10.3389/fvets.2017.00232
- Pinedo PJ, Buerge CD, Donovan GA, Melendez P, More L, et al. Association between CARD15/NOD2 gene polymorphisms and paratuberculosis infection in cattle. *Vet Microbiol.* (2009) 134:346–52. doi: 10.1016/j.vetmic.2008.09.052
- Mucha R, Bhide MR, Chakurkar EB, Novak M, Mikula IS. Toll-like receptors TLR1, TLR2 and TLR4 gene mutations and natural resistance to *Mycobacterium avium* subsp. *paratuberculosis* infection in cattle. *Vet Immunol Immunopathol.* (2009) 128:381–8. doi: 10.1016/j.vetimm.2008.12.007

AUTHOR CONTRIBUTIONS

HN, JT, and SW designed the study. HN, RZ, and ES collected the samples. SW and CT provided sequencing and transcription factor data. ZW, RZ, ES, MN, JK, and BC performed the experiments. JK wrote and edited the manuscript. HN reviewed and edited the manuscript. All authors read and approved the final manuscript.

FUNDING

This project was funded through an anonymous donation.

ACKNOWLEDGMENTS

The authors would like to thank the dairies that provided access to the cattle used in this study.

SUPPLEMENTARY MATERIAL

The Supplementary Material for this article can be found online at: <https://www.frontiersin.org/articles/10.3389/fvets.2021.625323/full#supplementary-material>

- Pant SD, Schenkel FS, Verschoor CP, You Q, Kelton DF, et al. A principal component regression based genome wide analysis approach reveals the presence of a novel QTL on BTA7 for MAP resistance in holstein cattle. *Genomics.* (2010) 95:176–82. doi: 10.1016/j.ygeno.2010.01.001
- Pant SD, Verschoor CP, Schenkel FS, You Q, Kelton DF, et al. Bovine *PGLYRP1* polymorphisms and their association with resistance to *Mycobacterium avium* ssp. *paratuberculosis*. *Anim Genet.* (2011) 42:354–60. doi: 10.1111/j.1365-2052.2010.02153.x
- Verschoor CP, Pant SD, You Q, Schenkel FS, Kelton DF, et al. Polymorphisms in the gene encoding bovine interleukin-10 receptor alpha are associated with *Mycobacterium avium* ssp. *paratuberculosis* infection status. *BMC Genetics.* (2010) 11:23. doi: 10.1186/1471-2156-11-23
- Singh SV, Dhama K, Chaubey KK, Kumar N, Singh PK, et al. Impact of host genetics on susceptibility and resistance to *Mycobacterium avium* subspecies *paratuberculosis* infection in domestic ruminants. *Pak J Biol Sci.* (2013) 16:251–66. doi: 10.3923/pjbs.2013.251.266
- Settles M, Zanella R, McKay SD, Schnabel RD, Taylor JF, et al. A whole-genome association analysis identifies loci associated with *Mycobacterium avium* ssp. *paratuberculosis* infection status in US Holstein cattle. *Anim Genet.* (2009) 40:655–62. doi: 10.1111/j.1365-2052.2009.01896.x
- Minozzi G, Buggiotti L, Stella A, Strozzi F, Luini M, et al. Genetic loci involved in antibody response to *Mycobacterium avium* ssp. *paratuberculosis* in cattle. *PLoS ONE.* (2010) 5:e11117. doi: 10.1371/journal.pone.0011117
- Kirkpatrick BW, Shi X, Shook GE, Collins MT. Whole-Genome association analysis of susceptibility to paratuberculosis in Holstein cattle. *Anim Genet.* (2011) 42:149–60. doi: 10.1111/j.1365-2052.2010.02097.x
- Zanella R, Settles ML, McKay SD, Schnabel R, Taylor J, et al. Identification of loci associated with tolerance to Johne's disease in Holstein cattle. *Anim Genet.* (2011) 42:28–38. doi: 10.1111/j.1365-2052.2010.02076.x
- Minozzi G, Williams JL, Stella A, Strozzi F, Luini M, et al. Meta-analysis of two genome-wide association studies of bovine paratuberculosis. *PLoS ONE.* (2012) 7:e32578. doi: 10.1371/journal.pone.0032578
- van Hulzen KJ, Schopen GC, van Arendonk JA, Nielsen M, Koets AP, et al. Genome-wide association study to identify chromosomal regions associated with antibody response to *Mycobacterium avium* subspecies *paratuberculosis* in milk of Dutch Holstein-Friesians. *J Dairy Sci.* (2012) 95:2740–8. doi: 10.3168/jds.2011-5005

21. Alpay F, Zare Y, Kamalludin MH, Huang X, Shi X, et al. Genome-wide association study of susceptibility to infection by *Mycobacterium avium* subspecies *paratuberculosis* in Holstein cattle. *PLoS ONE*. (2014) 9:e111704. doi: 10.1371/journal.pone.0111704
22. Kiser JN, White SN, Johnson KA, Hoff JL, Taylor JF, et al. Identification of loci associated with susceptibility to *Mycobacterium avium* subspecies *paratuberculosis* (Map) tissue infection in cattle. *J Anim Sci*. (2017) 95:1080–91. doi: 10.2527/jas.2016.1152
23. Gao Y, Jiang J, Yang S, Cao J, Han B, et al. Genome-wide association study of *Mycobacterium avium* subspecies *paratuberculosis* infection in Chinese Holstein. *BMC Genomics*. (2018) 19:972. doi: 10.1186/s12864-018-5385-3
24. Mallikarjunappa S, Sargolzaei M, Brito LF, Meade KG, Karrow NA, et al. *Short communication*: Uncovering quantitative trait loci associated with resistance to *Mycobacterium avium* ssp. *paratuberculosis* infection in Holstein cattle using a high-density single nucleotide polymorphism panel. *J Dairy Sci*. (2018) 101:7280–6. doi: 10.3168/jds.2018-14388
25. Neibergs HL, Settles ML, Whitlock RH, Taylor JF. GSEA-SNP identifies genes associated with John's disease in cattle. *Mamm Genome*. (2010) 21:419–25. doi: 10.1007/s00335-010-9278-2
26. Kiser JN, Neupane M, White SN, Neibergs HL. Identification of genes associated with susceptibility to *Mycobacterium avium* ssp. *paratuberculosis* (map) tissue infection in Holstein cattle using gene set enrichment analysis-SNP. *Mamm Genome*. (2018) 29:539–49. doi: 10.1007/s00335-017-9725-4
27. Huh I, Mendizabal I, Park T, Yi SV. Functional conservation of sequence determinants at rapidly evolving regulatory regions across mammals. *PLoS Comput Biol*. (2018) 14:e1006451. doi: 10.1371/journal.pcbi.1006451
28. Liu Y, Qin X, Song XZ, iang H, Shen Y, Durbin KJ, et al. Bos taurus genome assembly. *BMC Genomics*. (2009) 10:180. doi: 10.1186/1471-2164-10-180
29. Purcell S, Neale B, Todd-Brown K, Thomas L, Ferreira MA, et al. PLINK: A tool set for whole-genome association and population-based linkage analyses. *Am J Hum Genet*. (2007) 81:559–75. doi: 10.1086/519795
30. Barrett JC, Fry B, Maller J, Daly MJ. Haploview: analysis and visualization of LD and haplotype maps. *Bioinformatics*. (2005) 21:263–5. doi: 10.1093/bioinformatics/bth457
31. Haas U, Sczakiel G, Laufer SD. MicroRNA-mediated regulation of gene expression is affected by disease-associated SNPs within the 3'-UTR via altered RNA structure. *RNA Biol*. (2012) 9:924–37. doi: 10.4161/rna.20497
32. Ambros V. The functions of animal microRNAs. *Nature*. (2004) 431:350–5. doi: 10.1038/nature02871
33. Zou X, Kang L, Yang M, Wu J, Guan H. MicroRNA binding mediated functional sequence variant in 3'-UTR of DNA repair gene XPC in age-related cataract. *Sci Rep*. (2018) 8:15198. doi: 10.1038/s41598-018-33071-0
34. Gilbertson S, Federspiel JD, Hartenian E, Cristea IM, Glaunsinger B. Changes in mRNA abundance drive shuttling of RNA binding proteins, linking cytoplasmic RNA degradation to transcription. *eLife*. (2018) 7:e37663. doi: 10.7554/eLife.37663
35. Messeguer X, Escudero R, Farré D, Nuñez O, Martiez J, et al. PROMO: Detection of known transcription regulatory elements using species-tailored searches. *Bioinformatics*. (2002) 18:333–4. doi: 10.1093/bioinformatics/18.2.333
36. Farré D, Roset R, Huerta M, Adsua JE, Roselló L, et al. Identification of patterns in biological sequences at the ALGEN server: PROMO and MALGEN. *Nucleic Acids Res*. (2003) 31:3651–3. doi: 10.1093/nar/gkg605
37. Woo SR, Heintz JA, Albrecht R, Barletta RG, Czuprynski CJ. Life and death in bovine monocytes: the fate of *Mycobacterium avium* subsp. *paratuberculosis*. *Microb Pathog*. (2007) 43:106–13. doi: 10.1016/j.micpath.2007.04.004
38. Vergne I, Chua J, Deretic V. *Mycobacterium tuberculosis* phagosome maturation arrest: selective targeting of PI3P-dependent membrane trafficking. *Traffic*. (2003) 4:600–6. doi: 10.1034/j.1600-0854.2003.00120.x
39. Grimshaw MJ, Wilson JL, Balkwill FR. Endothelin-2 is a macrophage chemoattractant: implications for macrophage distribution in tumors. *Eur J Immunol*. (2002) 32:2393–400. doi: 10.1002/1521-4141(200209)32:9<2393::AID-IMMU2393>3.0.CO;2-4
40. Klipper E, Levit A, Mastich Y, Berisha B, Schams D, et al. Induction of endothelin-2 expression by luteinizing hormone and hypoxia: possible role in bovine corpus luteum formation. *Endocrinology*. (2010) 151:1914–22. doi: 10.1210/en.2009-0767
41. Choi DH, Kim EK, Kim KH, Lee KA, Kang DW, et al. Expression pattern of endothelin system components and localization of smooth muscle cells in the human pre-ovulatory follicle. *Hum Reprod*. (2011) 25:1171–80. doi: 10.1093/humrep/der066
42. Cacioppo JA, Lin PCP, Hannon PR, McDougall DR, Gal A, et al. Granulosa cell endothelin-2 expression is fundamental for ovulatory follicle rupture. *Sci Rep*. (2017) 7:817. doi: 10.1038/s41598-017-00943-w
43. Takizawa S, Uchida T, Adur J, Kozakai T, Kotake-Nara E, et al. Differential expression of endothelin-2 along the mouse intestinal tract. *J Mol Endocrinol*. (2005) 35:201–9. doi: 10.1677/jme.1.01787
44. Uhlén M, Fagerberg L, Hallström BM, Lindskog C, Oksvold P, et al. Tissue-based map of the human proteome. *Science*. (2015) 347:1260419. doi: 10.1126/science.1260419
45. Sigur-Dardóttir OG, Press CM, Evensen O. Uptake of *Mycobacterium avium* subsp. *Paratuberculosis* through distal small intestinal mucosa in goats: an ultrastructural study. *Vet Pathol*. (2001) 38:184–9. doi: 10.1354/vp.38-2-184
46. Facciolo A, Gonzalez-Cano P, Napper S, Griebel PJ, Mutharia LM. Marked differences in mucosal immune responses induced in ileal versus jejunal Peyer's patches to *Mycobacterium avium* subsp. *Paratuberculosis* secreted proteins following targeted enteric infection in young calves. *PLoS ONE*. (2016) 11:e0158747. doi: 10.1371/journal.pone.0158747
47. Bianchi M, Adur J, Takizawa S, Saida K, Casco VH. Endothelin system in intestinal villi: A possible role of endothelin-2/vasoactive intestinal contractor in the maintenance of intestinal architecture. *Biochem Biophys Res Commun*. (2012) 417:1113–8. doi: 10.1016/j.bbrc.2011.12.053
48. Çınar MU, Akyüz B, Arslan K, White SN, Neibergs HL, Gümüşsoy KS. The EDN2 rs110287192 gene polymorphism is associated with paratuberculosis susceptibility in multibreed cattle population. *PLoS ONE*. (2020) 15:e0238631. doi: 10.1371/journal.pone.0238631

Conflict of Interest: The authors declare that the research was conducted in the absence of any commercial or financial relationships that could be construed as a potential conflict of interest.

Copyright © 2021 Kiser, Wang, Zanella, Scraggs, Neupane, Cantrell, Van Tassell, White, Taylor and Neibergs. This is an open-access article distributed under the terms of the Creative Commons Attribution License (CC BY). The use, distribution or reproduction in other forums is permitted, provided the original author(s) and the copyright owner(s) are credited and that the original publication in this journal is cited, in accordance with accepted academic practice. No use, distribution or reproduction is permitted which does not comply with these terms.



Early Detection of *Mycobacterium avium* subsp. *paratuberculosis* Infected Cattle: Use of Experimental Johnins and Innovative Interferon-Gamma Test Interpretative Criteria

OPEN ACCESS

Edited by:

Kumi de Silva,
The University of Sydney, Australia

Reviewed by:

Eduard Otto Roos,
Pirbright Institute, United Kingdom
Santhamani Ramasamy,
Public Health Research Institute
(PHRI), United States

*Correspondence:

Linda Petrucci
l.petrucci@izsum.it

[†]These authors have contributed
equally to this work and share first
authorship

Specialty section:

This article was submitted to
Veterinary Infectious Diseases,
a section of the journal
Frontiers in Veterinary Science

Received: 07 December 2020

Accepted: 30 March 2021

Published: 14 May 2021

Citation:

Corneli S, Di Paolo A, Vitale N,
Torricelli M, Petrucci L, Sebastiani C,
Ciullo M, Curcio L, Biagetti M, Papa P,
Costarelli S, Cagiola M, Dondo A and
Mazzone P (2021) Early Detection of
Mycobacterium avium subsp.
paratuberculosis Infected Cattle: Use
of Experimental Johnins and
Innovative Interferon-Gamma Test
Interpretative Criteria.
Front. Vet. Sci. 8:638890.
doi: 10.3389/fvets.2021.638890

Sara Corneli^{1†}, Antonella Di Paolo^{1†}, Nicoletta Vitale², Martina Torricelli¹, Linda Petrucci^{1*}, Carla Sebastiani¹, Marcella Ciullo¹, Ludovica Curcio¹, Massimo Biagetti¹, Paola Papa¹, Silva Costarelli¹, Monica Cagiola¹, Alessandro Dondo² and Piera Mazzone¹

¹ Istituto Zooprofilattico Sperimentale dell'Umbria e delle Marche "Togo Rosati", Perugia, Italy, ² Istituto Zooprofilattico Sperimentale del Piemonte Liguria e Valle d'Aosta, Torino, Italy

Paratuberculosis (PTB), also known as Johne's disease, is a chronic proliferative enteritis of ruminants caused by *Mycobacterium avium* subsp. *paratuberculosis* (MAP). To date, PTB diagnosis, based on serology, fecal culture, and real-time polymerase chain reaction, has identified animals in advanced stages of infection. To detect MAP infection in animals earlier, the interferon-gamma (IFN- γ) test may be applied. This assay detects cytokines produced by T-lymphocytes of infected subjects after stimulation with purified protein derivatives (PPDs), extracted from *Mycobacterium bovis* (MB) and from *M. avium* (MA). The study involved three bovine herds: one PTB-infected herd, one PTB-free herd, and one with an outbreak of bovine tuberculosis. The IFN- γ test was performed on 235 animals, using bovine PPD (PPDB), avian PPD (PPDA), and three experimental PPD Johnins (PPDJs) extracted from a synthetic liquid medium culture of MAP (PPDJ A, B, and C), to assess early MAP detection and avoid false reactions to MB. Furthermore, IFN- γ results were evaluated using 12 interpretative criteria (ICs), based on the differences and ratio between PPD optical density (OD) and IFN- γ basal OD values after lymphocytic stimulation. IC accuracy was expressed as area under the receiver operating characteristic curve. Through a longitudinal study, PPDJs proved to be specific and sensitive in the detection of MAP-infected animals. Among the evaluated ICs, six showed the best performance in terms of accuracy ($p < 0.0001$), highlighting PTB subclinical infections. In particular, the two best criteria reached sensitivity values of 100% [confidence interval (CI) 95%, 94.1–100%] with a specificity of 91.8% (CI 95%, 81.9–97.3%) and sensitivity levels of 80.6% (CI 95%, 69.1–89.2%) with a specificity of 100% (CI 95%, 94.1–100%). Thus, the IFN- γ assay proved to be a useful diagnostic tool to identify early subclinical MAP-infected animals, in order to manage infected cattle or those exposed to MAP and to monitor younger calves within a herd. Furthermore, the IFN- γ test can be considered an additional test to avoid the introduction of MAP-infected

animals, especially in herds where disease has already been eradicated and preservation of the health status is required to maintain the PTB certification level.

Keywords: *Mycobacterium avium* subsp. *paratuberculosis*, Johne's disease, bovine paratuberculosis, IFN- γ test, purified protein derivatives, Johnin PPD, interpretative criteria, cattle

INTRODUCTION

Mycobacterium avium subsp. *paratuberculosis* (MAP) is a slow-growing mycobacterium (1) and the causal agent of Johne's disease (JD) or paratuberculosis (PTB), a chronic inflammatory bowel disease seen in farmed ruminants and wildlife species worldwide (2, 3). Infected animals may shed MAP through their feces, and the live bacteria can survive in pastures (4) for a long time, representing a risk to other animals and even humans (5, 6). In fact, MAP may also act as a zoonotic agent in some human diseases (7–10). In particular, for more than a century, it has been associated with Crohn's disease, a chronic inflammatory bowel disease characterized by transmural inflammation and granuloma formation. Recently, other diseases have been associated with MAP, such as sarcoidosis, Blau syndrome, type 1 diabetes, Hashimoto's thyroiditis, and multiple sclerosis (9, 11–16). Regarding the transmission sources, MAP may contaminate food for human consumption, such as dairy and meat products, infant formula (17–19), and water (6, 20); and MAP seems to resist pasteurization treatment of milk at 72°C for 15 s [high-temperature, short-time (HTST) pasteurization] (21–23).

JD causes major economic losses to the global dairy industry due to reduced milk production (24), weight loss, infertility, premature culling, and increased cow replacement costs (25, 26). The prevalence of MAP-infected farms in countries with advanced animal husbandry is growing rapidly and varies worldwide between 7 and 55% (27–29). Control programs to manage PTB in cattle and sheep herds have been adopted and in some cases re-adopted over the past couple of decades, in different countries, such as Australia, the USA, the Netherlands, Japan, and Denmark (28–32). The effectiveness of several recent control programs is yet to be demonstrated, since no countries have yet been able to eradicate the infection and there is no international agreement on PTB eradication plans (29, 30, 33).

A major problem in PTB control is the identification of animals in the early stages of MAP infection. The animals become most frequently infected at a young age, rarely *in utero*, but more often as newborns (34–36). The fecal–oral route is the main route of transmission, including the ingestion of contaminated feed, fodder, milk, and colostrum (35, 37, 38).

The initial host defense against MAP infection is mediated by the lymphocyte T-helper 1 (Th1) response, characterized by the production of IFN- γ and other pro-inflammatory cytokines (39–41). Nevertheless, MAP can use its evasion mechanisms and can survive by interfering with the host immune response (42). In particular, MAP is captured and processed by macrophages, in which mycobacteria can replicate and avoid phagolysosome maturation (43, 44). This step is followed by the activation of the cell-mediated immune response, which attempts to contain

MAP infection (45). Humoral immune response, mediated by lymphocyte Th2, also appears in mycobacterial infection but generally only appears late when the disease is already established (46). This is an oversimplification of what happens in animals during MAP infection, since it has been demonstrated that an overlap between Th1 and Th2 responses could exist (47, 48). In the animals that “lose the battle against infection,” two or more years can pass before the appearance of the first clinical symptoms, and the evolution of the infection is not obvious in all subjects (49). Clinical disease is characterized by intermittent diarrhea, progressive weight loss, inappetence, and death (36, 45). The progression of the infection depends on both the containment action of innate and cell-mediated immunity (CMI) and is related to host genetics (50) and environmental factors. Therefore, PTB can be defined as a conditioned disease (43, 49, 51). The diagnosis of PTB, based on enzyme-linked immunosorbent assay (ELISA) for antibody detection, MAP fecal culture, and real-time quantitative polymerase chain reaction (qPCR) to detect MAP DNA, is particularly difficult (52). In fact, during the initial and subclinical stages, in MAP-infected animals, specific antibodies are absent or present at low levels, while MAP can be excreted intermittently at low concentrations (49, 53–55). When the infection advances, circulating antibodies gradually increase and are easily detectable by ELISA; however, they have no protective effect (46, 56, 57). Generally, animals that are positive for PTB ELISA are in advanced stages of infection; therefore, diagnostic tests based on measuring CMI, such as IFN gamma-release assays (IGRAs), could be more suitable for revealing subclinical stages of infection (48, 49, 57–62). IGRAs, which are used for the diagnosis of mycobacterial infections, consist of the quantification of IFN- γ released after mycobacterial antigen stimulation of peripheral blood lymphocytes. The test is performed using commercial ELISA kits to detect the amount of cytokines produced and secreted by T-cells of infected animals in culture supernatants (63, 64). The IFN- γ assay, developed in Australia in the late 1980s, is an *in vitro* blood test used as an ancillary test in combination with the skin test for the diagnosis of bovine tuberculosis (bTB) due to *Mycobacterium bovis* (MB) (63–67). Recently, it has also been used for the early diagnosis of PTB (60). As reported in the literature, the specificity (Sp) of the method varies from 67 to 94%, while the sensitivity (Se) varies from 13 to 85%, depending on the type and quantity of purified protein derivatives (PPDs) and, particularly, on the interpretative criteria (ICs) adopted for the tests (57, 58, 60). The antigens normally used during the stimulation phase of lymphocytes in the IFN- γ test are the traditional bovine and avian tuberculin PPDs extracted from MB AN5 (PPDB) and *M. avium* D4ER (PPDA), respectively. Johnin (PPDJ), similar to the other tuberculins, is a crude PPD obtained from a MAP culture in a synthetic liquid medium, inactivated by heat treatment, precipitated with

trichloroacetic acid, and re-suspended in phenol and glycerin (57, 68).

In the present study, we used three different experimental PPDJs, which are produced in Italy at Istituto Zooprofilattico Sperimentale dell'Umbria e delle Marche "Togo Rosati" (IZSUM) and described by Corneli et al. (69).

The commercial diagnostic ELISA tests available today that are used for bTB have not been validated by the manufacturer for the diagnosis of PTB (57, 58). The interpretation of the values of secreted IFN- γ , expressed as absorbance values in optical density (OD) and relative cutoff points, is crucial for defining the outcome of the IFN- γ test and thus to clarify the state of mycobacterial infection in the animal (58, 70–74). However, there is a substantial difference between the use of the IFN- γ test for bTB diagnosis and the use of the IFN- γ test for PTB diagnosis. In the first case, the aim of the test is to detect the infected animal earlier than the skin test can (63) to facilitate prompt slaughter of the positive animals, according to the "test and cull" strategy. By contrast, in the case of PTB, the IFN- γ test still aims to identify the infected animal, but a different destination can be assigned to this animal depending on the prevalence of the disease in the herd. In a herd where the prevalence is low or PTB is not present, with an advanced health certification for PTB, the animal has to be removed from the herd. Conversely, in a herd with a high prevalence of PTB, animals with a positive reaction to the IFN- γ test for MAP infection diagnosis might be at risk of MAP shedding, and therefore, animals need to be checked more often than others. As reported by several authors (49, 75), these cattle could also include the animals able to contain the evolution of the MAP infection, without ever developing the subclinical and clinical forms of PTB, and therefore, they represent a genetic resource to be preserved and enhanced.

The aim of this longitudinal study was to evaluate the performance of three new experimental PPDJs and their potential application, in association with Italian PPDA and PPDB, in the IFN- γ test for the early detection of animals infected with MAP.

MATERIALS AND METHODS

Production of Purified Protein Derivative Johnin

For the production of the new Italian Johnin, 20 Italian MAP strains were genotyped by amplification of mini- and microsatellite loci at the Italian National Reference Center for PTB (76). Two field strains, identified as strain A (used for PPDJA) and strain B (used for PPDJB), were selected based on their geographical distribution, growth characteristics, and protein yield. The MAP American Type Culture Collection (ATCC) strain 19698 represented strain C and was used for a third batch of Johnin (PPDJC) only as a production control and for methodical optimization. The three MAP strains were cultured for 4 months at 37°C in Watson–Reid modified broth, and then the bottles were autoclaved at 100°C for 3 h. The cells were removed, and the proteins were extracted by precipitation with trichloroacetic acid. The precipitate was then washed and dissolved in phosphate phenolate buffer and glycerine, with a

final protein concentration of 1 mg/ml, as required for PPDB by the European regulation Annex B, Directive 64/432/EEC (77), and European regulation (EC) No. 1226/2002 (78).

Field Trial

Animal Population Characteristics and Ethics Statement

All samples were assessed as per the periodic tests required by the Italian National Health Programs (78–80) and during farmers' voluntary health controls for PTB, provided by the Italian National Guidelines (81).

A total of 235 cattle from farms in central Italy were enrolled in the study and divided into three groups, as follows:

- The first group consisted of 87 dairy cattle from three bTB Officially Free (OF) herds, where clinical cases of PTB had been reported.
- The second group consisted of 61 beef cattle from a bTB OF herd without PTB cases, and the herd had tested negative for serological tests in the last 4 years.
- The third group included 87 beef cattle from a bTB-positive herd with an ongoing outbreak when the study was performed.

Paratuberculosis Status Assessment

Each animal from the bTB OF herds with previous PTB cases or without PTB was assessed in parallel to traditional PTB tests, as follows:

- PTB ELISA test on serum ("ID Screen® paratuberculosis Indirect"—IDVet Innovative Diagnostics, Montpellier, France) in accordance with the manufacturer's instructions;
- MAP isolation on selective solid media following the OIE terrestrial manual (82);
- IS900 qPCR for MAP DNA detection from feces (83, 84) in fast mode (85).

As part of the longitudinal study, cattle were monitored for 4 years to check the evolution of their health status in relation to PTB, and animals were considered positive for PTB if at least one of the three tests (ELISA and/or qPCR and/or MAP culture) yielded a positive result.

Interferon- γ Assay and Interpretative Criteria

Whole Blood *in vitro* Stimulation and Interferon- γ Detection

Jugular blood samples were collected and delivered to the laboratory within 12 h at room temperature. The heparinized blood samples of each animal were dispensed in aliquots of 1 ml and stimulated, respectively, with phosphate-buffered saline (PBS 0.01 M, pH 7.2), used as a nil control antigen, which represented the IFN- γ basal value in the single animal (PBS); 10 μ g of Italian PPDB and 10 μ g of Italian PPDA; 20 and 10 μ g of the three experimental PPDJs (strains A, B, and C, respectively), with two different dilutions 1:5 and 1:10; Pokeweed Mitogen (PWM; Thermo Fisher Scientific™, Waltham, MA, USA) included at a final concentration of 1 μ g/ml, as a positive control of lymphocyte viability. IFN- γ secretion was evaluated

using the Bovigam IFN- γ kit (Thermo Fisher Scientific™) in the plasma collected after 24 h of incubation at $37 \pm 1^\circ\text{C}$ in 5% CO_2 . The obtained values were expressed in units of OD measured at 450 nm (OD 450 nm).

Interferon- γ Interpretative Criteria

For the PTB IFN- γ performance evaluation, a comparison among PPDB, PPDA, and PPDJ was carried out, applying differences or ratios among the PPD OD values obtained. For each criterion, different cutoffs were applied to interpret the results. In particular, 12 possible ICs were adopted in the first and second groups to assess the presence or absence of MAP (MAP reactive or MAP negative) and to evaluate the stage of MAP infection. In the third group, to verify the test performance and reliability in the presence of another mycobacterial infection, three of the best criteria, chosen among those evaluated, were adopted. The ICs, shown in **Table 1**, were applied to all PPDJs (A, B, and C) at two dilutions (1:5 and 1:10) in association with Italian bovine and avian PPDs. Briefly, from the first to fifth criteria, we considered the difference between the PPDs OD values obtained after lymphocyte stimulation and the OD basal value with three different cutoff values (if PPDA or PPDJ – PBS > 0.05; 0.1; 0.2 = MAP infection) and twice the OD basal value at two different cutoff values (if PPDA or PPDJ – 2 * PBS > 0; 0.04 = MAP infection). From the sixth to ninth criteria, we considered the ratio between the PPD OD values obtained (PPDB or PPDA/PPDJ \leq 0.09 = MAP infection; PPDJ/PPDB or PPDA > 1 = MAP infection). For the 10th criterion, we compared the ratio between PPDs (PPDB/PPDA > PPDB/PPDJ = MAP infection); and finally, for the 11th and 12th criteria, we considered the difference between PPDA and PPDJs and two different cutoff values (PPDJ – PPDA > 0.05; 0.1 = MAP infection).

For every criterion, a maximum threshold of the basal value (PBS \leq 0.150 OD) was introduced to verify the eligibility of the sample. As reported in the literature (73, 86), this additional quality control is already used in the diagnosis of bTB to exclude animals with high basal values due to pre-existing pathologies or to avoid contaminated blood samples. This quality control (PBS \leq 0.150 OD) was validated by the Istituto Zooprofilattico Sperimentale del Piemonte, Liguria e Valle d'Aosta Laboratory, with the sixth criterion applied to eradicate bTB in Piedmont from 2004 to 2016, to obtain European official tuberculosis-free status (87), and it is still being used (88–90).

The sixth criterion is currently also adopted in the IZSUM for the official diagnosis of bTB.

Statistical Analysis

The performance of the PPDJs in the 12 IFN- γ test ICs was evaluated on the OD values obtained from a total of 235 cattle, including 87 cattle from PTB affected herds, 61 cattle from a bTB OF herd, without PTB cases in the last 4 years, and another group of 87 cattle from a bTB-positive herd.

To establish the diagnostic accuracy and to compare the diagnostic efficiency of PPDJs, a receiver operating characteristic (ROC) curve analysis was performed. For each criterion, the Se, Sp, accuracy, area under the ROC curve (AUC), and Youden

index were calculated. Differences in accuracy, Se, and Sp among the criteria were assessed using a binomial exact test.

The association statistics, the AUC with its standard error, and a confidence interval (CI) for each model were calculated. Differences between the AUC for PPDJA, PPDJB, and PPDA were performed by ROCCONTRAST statements using the non-parametric approach of DeLong (91).

For the purpose of the study, Se was defined as the proportion of samples with positive results from the expected true-positive animals, while Sp was defined as the proportion of samples with negative results to the expected true-negative animals.

The Se of PPDJ (A, B, and C) in the detection of MAP-infected subjects was calculated considering positive animals with a positive outcome in ELISA and/or qPCR and/or fecal culture. The Sp of PPDJ (A, B, and C) was calculated considering negative animals with a negative outcome in ELISA, qPCR, and fecal culture from the herd PTB-free for at least 4 years.

The PPDJ OD distribution was analyzed using histograms, and comparisons between dilutions and strains are shown in box plot graphs.

Two types of analysis of variance were performed using Proc generalized linear models and SAS software v. 9.2 to evaluate the “dilution factor” (1:5 and 1:10) and “strain factor” (A, B, and C) of the PPDJs, in particular if the PPDJ OD concentration values were different among the three strains and between the two dilutions.

RESULTS

Paratuberculosis Status Assessment

Animals belonging to the three groups underwent traditional PTB tests: ELISA PTB, qPCR, and MAP isolation from feces (57). Each subject was considered positive for PTB if at least one of the three tests was positive.

In the first group, among the 87 cattle coming from bTB OF herds with previous PTB cases, 71 were positive for at least one of the traditional tests and 16 were negative to all the PTB tests. In particular, considering only the serological test, 68 subjects were positive, three were doubtful, and 16 were negative. Eighteen cattle were positive for real-time PCR from feces, and 28 were positive for MAP fecal culture. In the next 4 years, among the 16 subjects negative for the three PTB traditional tests at the first examination, five became positive during the follow-up (**Supplementary Table 1**). Specifically, one subject became positive for the culture test 3 months later, one was positive for ELISA and MAP isolation 10 months later, and two cattle became positive for ELISA (**Supplementary Figure 1**).

In the second group, among 61 cattle belonging to an OF bTB herd and without cases of PTB in the last 4 years, 100% of the animals were negative using conventional diagnostic tests.

The third group consisted of 87 cattle from a herd in which bTB positivity to the skin test was registered and then confirmed by the isolation of MB. In the first sampling of the study, the bTB outbreak was still present and PPDA reactivity was found in the comparative skin test. For this reason, the IFN- γ test and ELISA PTB test were performed in support of the official bTB diagnosis to avoid false-positive

TABLE 1 | Interpretative criteria of the IFN- γ test and cutoff values applied in the study for the diagnosis of *Mycobacterium avium* subsp. *paratuberculosis* (MAP) infected cattle.

Interpretative criteria		
1	Difference between PPD _{Av} and PBS value > 0.05 Difference between PPD _{Ja} or Jb and PBS value > 0.05	If PPD _{Av} – PBS > 0.05 = MAP If PPD _J – PBS > 0.05 = MAP
2	Difference between PPD _{Av} and PBS value > 0.1 Difference between PPD _{Ja} or Jb and PBS value > 0.1	If PPD _{Av} – PBS > 0.1 = MAP If PPD _J – PBS > 0.1 = MAP
3	If the difference between the PPD _{Av} value and PPD _{Ja} or Jb and PBS value is >0.2, the animal is considered MAP reactive	PPD _{Av} – PBS > 0.2 = MAP
4	If the reaction to Italian PPD _{Av} or PPD _{Ja} or Jb is two-fold the PBS value, the animal is considered MAP reactive	PPD _J – PBS > 0.2 = MAP PPD _{Av} – (2 * PBS) > 0 = MAP
5	Difference between PPD _{Av} and twice the PBS value > 0.04 Difference between PPD _{Ja} or Jb and twice the PBS value > 0.04	PPD _J – (2 * PBS) > 0 = MAP If PPD _{Av} – (2 * PBS) > 0.04 = MAP If PPD _J – (2 * PBS) > 0.04 = MAP
6	First level: Second level: In case of intermediate values, the result is inconclusive or not discriminant (ND).	If PPDBov and PPD _J > 2 * PBS then apply PPDBov/PPD _J If PPDBov/PPD _J ≤ 0.9 = MAP and if PPDBov/PPD _J ≥ 1.1 = MB If PPDBov/PPD _{Av} ≤ 0.9 = MAP and if PPDBov/PPD _{Av} ≥ 1.1 = MB
7	First level: Second level: In case of intermediate values, the result is inconclusive or non-discriminant (ND).	If PPD _{Av} and PPD _J > 2 * PBS then apply PPDBov/PPD _J If PPD _{Av} /PPD _J ≤ 0.9 = MAP and if PPD _{Av} /PPD _J ≥ 1.1 = MA
8	PPD _{Ja} or Jb and PPDBov ratio	If PPD _J /PPDBov > 1 = MAP
9	PPD _{Ja} or Jb and PPD _{Av} ratio	If PPD _J /PPD _{Av} > 1 = MAP
10	Comparison of the ratios between PPDBov and PPD _{Av} and between PPDBov and PPD _{Ja} or Jb ratio	If PPDBov/PPD _{Av} > PPDBov/PPD _J = MAP
11	Difference between PPD _{Ja} or Jb and PPD _{Av} > 0.1	If PPD _J – PPD _{Av} > 0.1 = MAP
12	Difference between PPD _{Ja} or Jb and PPD _{Av} > 0.05	If PPD _J – PPD _{Av} > 0.05 = MAP

PPD, purified protein derivative; PPDBov, bovine PPD; PPD_{Av}, avian PPD; PPD_J, Johnin PPD; PPD_{Ja}, Johnin PPD from strain A; PPD_{Jb}, Johnin PPD from strain B; PBS, phosphate-buffered saline. The asterisk symbol (*) is used to indicate the mathematical operation of multiplication.

bTB outcomes in eventually PTB-positive animals. The herd was monitored for another 2 years until the bTB-free status was regained and all animals were negative in the two ELISA tests performed annually.

Evaluation of Purified Protein Derivatives Johnin Performance and IFN- γ Innovative Interpretative Criteria in the First and Second Groups

To evaluate the Se and Sp of the PPDJs using the different ICs, 128 animals were enrolled and followed up for 4 years. Among them, 67 from the first group were positive for at least one test for PTB, and 61 from the second group were always negative on the traditional tests for PTB. **Table 2** shows the accuracy of the IFN- γ test according to the 12 ICs using PPD_{Ja} and PPD_{Jb}. Sp and Se values obtained with PPD_{Jc} are not shown

because ATCC 19698 was used only for production control and method optimization.

Out of 71 animals that tested positive for traditional PTB tests, four were considered outliers (PBS > 0.150 OD) and were therefore excluded from the performance evaluation.

The amount of IFN- γ produced by the PTB-positive subjects, in response to stimulation with the various PPDs, expressed in OD values, is represented graphically in **Figure 1**.

Regarding the assessment of PPD_J efficiency, analysis of variance showed no statistically significant differences between the mean OD 450 nm of the PPDJs and the dilution factor (F -test = 1.61; p = 0.2060) (**Figure 2A**) or for the strain factor (F -test = 0.37; p = 0.6907) (**Figure 2B**).

As shown in **Table 2**, among the 12 applied ICs, the PPDJs achieved the best performance within the first six ICs, with values of accuracy ranging from 90.6% (CI 95%: 85.5–95.7%)

TABLE 2 | Specificity and sensitivity values obtained with 12 interpretative criteria of the IFN- γ test and cutoff values applied in the study for the diagnosis of *Mycobacterium avium* subsp. *paratuberculosis* (MAP) infected cattle.

Interpretative criteria	SP (CI 95%)	SE (CI 95%)	Accuracy (A CI 95%)	AUC*	Y
1					
A-PBS > 0.05 = MAP	88.5% (80.3–96.7%)	85.1% (76.3–93.8%)	86.8% (80.7–92.7%)	0.868	73.6%
Ja-PBS > 0.05 = MAP	93.4% (84.1–98.2%)	88.1% (77.8–94.7%)	90.6% (85.5–95.7%)	0.908	81.5%
Jb-PBS > 0.05 = MAP	91.8% (81.9–97.3%)	100.0% (94.1–100.0%)	89.8% (84.5–95.1%)	0.899	79.9%
2					
A-PBS > 0.1 = MAP	95.1% (89.5–100%)	76.1% (65.6–86.6%)	85.2% (78.9–91.4%)	0.856	71.2%
Ja-PBS > 0.1 = MAP	100.0% (94.1–100.0%)	77.6% (65.8–86.9%)	88.3% (82.6–93.9%)	0.888	77.6%
Jb-PBS > 0.1 = MAP	100.0% (94.1–100.0%)	80.6% (69.1–89.2%)	89.8% (84.5–95.1%)	0.903	80.6%
3					
A-PBS > 0.2 = MAP	100.0% (94.1–100.0%)	58.2% (45.5–70.0%)	78.1% (70.8–85.3%)	0.791	58.2%
Ja-PBS > 0.2 = MAP	100.0% (94.1–100.0%)	67.2% (54.6–78.2%)	82.8% (76.1–89.4%)	0.836	67.2%
Jb-PBS > 0.2 = MAP	100.0% (94.1–100.0%)	62.7% (50.1–74.2%)	80.4% (73.5–87.4%)	0.813	62.7%
4					
A-(2 * PBS) > 0 = MAP	90.2% (79.8–96.3%)	79.0% (67.4–88.1%)	84.3% (77.9–90.7%)	0.846	69.2%
Ja-(2 * PBS) > 0 = MAP	98.4% (91.2–99.9%)	79.1% (67.4–88.1%)	88.2% (82.6–93.9%)	0.887	77.5%
Jb-(2 * PBS) > 0 = MAP	93.4% (84.1–98.2%)	82.1% (70.8–90.4%)	87.5% (81.6–93.3%)	0.878	75.5%
5					
A-(2 * PBS) > 0.04 = MAP	95.1% (86.3–99.0%)	73.1% (60.9–83.2%)	83.6% (77.1–90.1%)	0.841	68.2%
Ja-(2 * PBS) > 0.04 = MAP	100.0% (94.1–100.0%)	71.6% (59.3–82.0%)	85.1% (78.9–91.3%)	0.858	71.6%
Jb-(2 * PBS) > 0.04 = MAP	100.0% (94.1–100.0%)	70.2% (57.7–80.7%)	83.5% (77.0–90.0%)	0.85	70.2%
6					
If PPD _{Bov} and/or PPD _{Av} and/or PPD _J > 2 * PBS, then apply PPD _{Bov} /PPD _{Av} and/or PPD _{Bov} /PPD _J					
B/A \leq 0.9 = MAP	90.2% (79.8–96.3%)	81.3% (69.5–89.9%)	83.6% (77.1–90.1%)	0.857	71.4%
B/Ja \leq 0.9 = MAP	100.0% (93.5–100.0%)	78.7% (66.3–88.1%)	82.8% (76.1–89.4%)	0.893	77.0%
B/Jb \leq 0.90 = MAP	94.9% (85.8–98.9%)	81.5% (70.0–90.1%)	85.1% (78.9–91.3%)	0.882	69.3%
7					
If PPD _{Av} and PPD _J > 2 * PBS, then apply PPD _{Av} /PPD _J					
A/Ja \leq 0.90 = MAP	100.0% (93.5–100.0%)	68.4% (51.3–82.5%)	63.2% (54.8–71.7%)	0.842	68.4%
A/Jb \leq 0.90 = MAP	98.2% (90.3–99.9%)	73.7% (56.9–86.6%)	64.0% (55.6–72.4%)	0.859	73.2%
8					
Ja/B > 1 = MAP	75.0% (62.7–85.5%)	88.0% (77.8–94.7%)	82.0% (75.2–88.7%)	0.817	63.0%
Jb/B > 1 = MAP	69.0% (55.7–80.1%)	94.0% (85.4–98.4%)	82.0% (75.2–88.7%)	0.814	63.0%
9					
Ja/A > 1 = MAP	90.2% (79.8–96.3%)	55.2% (42.6–67.4%)	71.8% (63.9–79.7%)	0.727	45.4%
Jb/A > 1 = MAP	85.3% (73.8–93.0%)	53.7% (41.1–66.0%)	68.7% (60.6–76.8%)	0.695	39.0%
10					
B/A > B/Ja = MAP	90.2% (79.8–96.3%)	55.0% (42.6–67.4%)	71.8% (63.9–79.7%)	0.727	45.0%
B/A > B/Jb = MAP	85.0% (73.8–93.0%)	54.0% (41.1–66.0%)	68.7% (60.6–76.8%)	0.695	39.0%
11					
Ja-A > 0.1 = MAP	100.0% (94.1–100.0%)	25.4% (15.5–37.5%)	60.9% (52.3–69.5%)	0.627	25.4%
Jb-A > 0.1 = MAP	100.0% (94.1–100.0%)	28.9% (16.8–39.1%)	61.7% (53.1–70.2%)	0.634	28.9%
12					
Ja-A > 0.05 = MAP	100.0% (94.1–100.0%)	35.0% (24.5–48.5%)	66.4% (58.1–74.6%)	0.679	35.0%
Jb-A > 0.05 = MAP	98.4% (91.2–99.9%)	37.3% (25.8–50.0%)	66.4% (58.1–74.6%)	0.678	35.7%

PPD, purified protein derivative; PPD_{Bov} or B, bovine PPD; PPD_{Av} or A, avian PPD; PPD_J, Johnin PPD; Ja, Johnin PPD from strain A; Jb, Johnin PPD from strain B; PBS, phosphate-buffered saline; SP CI 95%, specificity and confidence interval 95%; SE CI 95%, sensitivity and confidence interval 95%; A CI 95%, accuracy and confidence interval 95%; AUC, area under the ROC curve; ROC, receiver operating characteristic; Y, Youden's index. The asterisk symbol (*) is used to indicate the mathematical operation of multiplication.

to 80.4% (CI 95%: 73.5–87.4%). The accuracy of the first six criteria was higher than that of the last six criteria, and the difference was statistically significant (binomial exact test, $p < 0.0001$). The first criterion achieved a higher accuracy for criteria 3, 4, 5, and 6; and the difference was statistically significant for each criterion (binomial exact test, $p < 0.05$). No statistically significant differences were observed between the accuracy of the

first and second ICs; however, there were differences between the Se and Sp values. In particular, as shown in **Table 2**, PPDJB with the first criterion achieved better Se values (binomial exact test, $p = 0.02$; Se 100.0% CI: 94.1–100.0%), while PPDJB with the second criterion achieved the best Sp values (binomial exact test, $p < 0.0001$; Sp 100.0% CI: 94.1–100.0%), but the accuracy was the same (89.8% CI: 84.5–95.1%).

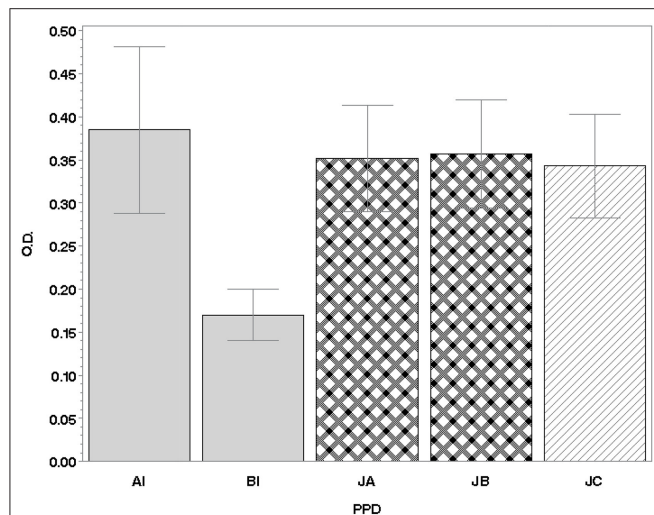


FIGURE 1 | IFN- γ production in lymphocytes of 71 PTB-positive animals. Values are expressed as the mean of the differences between the OD_{450nm} of PPDs and the OD_{450nm} of PBS (\pm SD). IFN, interferon; PTB, paratuberculosis; PBS, phosphate-buffered saline; PPD, purified protein derivative; SD, standard deviation; OD, optical density; AI, Italian avian PPD; BI, Italian bovine PPD; JA, JB, JC, Johnins produced by the three strains of MAP: A and B (field strains) and C [strain American Type Culture Collection (ATCC) 19698].

Regarding the comparison of the diagnostic accuracy of PPDJs vs. PPDA, within the same criterion, statistically significant differences were observed in the second criterion (binomial exact test, $p = 0.0397$). In addition, in the second criterion, the Sp of PPDJs was higher than that of PPDA, and the difference was statistically significant (binomial exact test, $p = 0.0381$).

Results of ROC analysis obtained with PPDA, PPDJA, and PPDJB according to the first three criteria are shown in **Figure 3** and in **Supplementary Tables 2, 3**. Regarding the comparison between AUC of PPDJs and AUC of PPDA, the differences were statistically significant; in particular, the AUCs of PPDJA and of PPDJB were higher than those of PPDA, with a $p < 0.001$ and $p < 0.05$, respectively. No difference was observed between AUC of PPDJA and PPDJB, since DeLong's test for two correlated ROC curves was statistically not significant ($p > 0.05$).

As shown in **Table 2**, the IC that showed the best performance in terms of Se and Sp was derived from a comparison between the OD value obtained after PPD stimulation and the OD value of basal IFN- γ of each animal (PBS) (from the first to fifth criteria). All the ICs based on the simple difference or ratio between OD values relative to PPDs (from the eight to 12th criterion), not considering the baseline value of IFN- γ (OD value of PBS), elicited the worst results. The comparison between the criteria that provided difference and ratio showed that the criteria based on PPDs OD ratio, such as the sixth and seventh criteria, yielded numerous inconclusive outcomes (ND) for values in the cutoff range, despite good results in terms of Se and Sp. Furthermore, all the ICs that provided a difference or ratio between the PPDJs and the PPDA showed inefficacy, especially in terms of Se, with values ranging from 25.4% (CI 95%: 15.5–37.5%) to 55.2% (CI 95%: 42.6–67.4%).

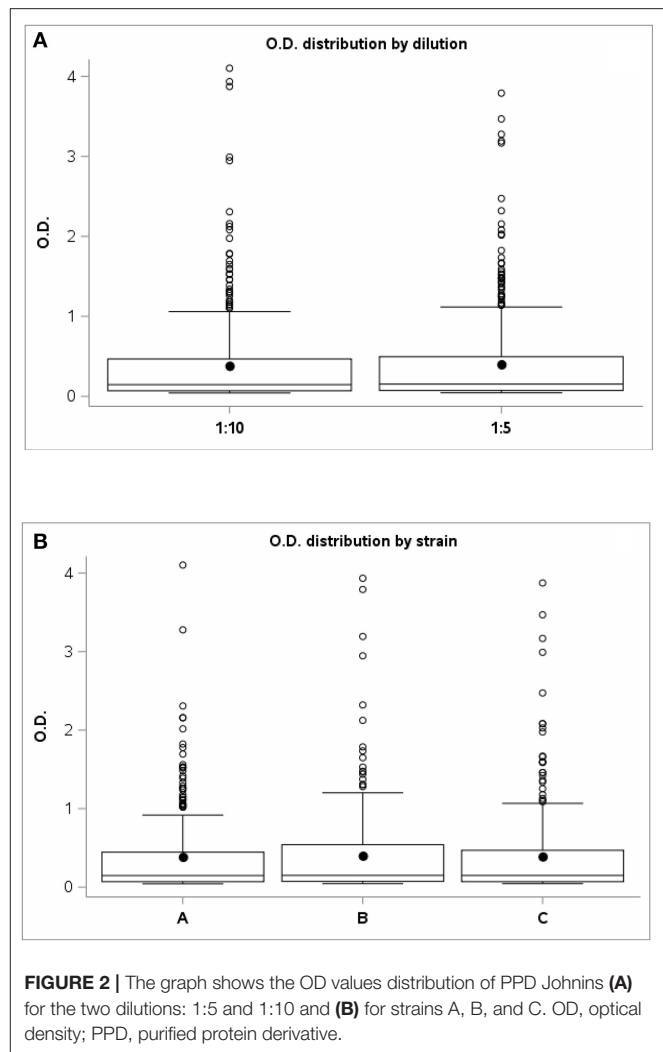


FIGURE 2 | The graph shows the OD values distribution of PPD Johnins **(A)** for the two dilutions: 1:5 and 1:10 and **(B)** for strains A, B, and C. OD, optical density; PPD, purified protein derivative.

Evaluation of Purified Protein Derivatives Johnin Performance and IFN- γ Innovative Interpretative Criteria in the Third Group

In the third group, based on the data obtained from the application of the 12 criteria in the first and second groups on positive and negative PTB animals, respectively, the criteria with the best performance were used. In particular, in a herd with an ongoing bTB outbreak, the criteria that reported Sp values of 100% (second, third, and fifth ICs) were adopted with the aim of verifying the Sp of PPDJs.

Out of 87 animals that were negative to ELISA PTB tests, seven subjects were considered outliers (PBS > 0.150 OD) and therefore excluded from the performance evaluation. As shown in **Table 3**, for the second criterion (if PPDJ – PBS > 0.1 = MAP), the PPDJA at 1:10 dilution reached 95.0% Sp (CI 95%: 87.69–98.62%) and the PPDJB at 1:10 dilution provided 87.50% Sp (CI 95%: 78.21–93.84%). In the third criterion (if PPDJ – PBS > 0.2 = MAP), PPDJA at 1:10 dilution provided 100.0% Sp (CI 95%: 95.49–100.0%) and 95.0% Sp for PPDJB (CI 95%: 87.69–98.62%).

Finally, in the fifth criterion (if $PPDJ - 2 \times PBS > 0.04 = MAP$), the PPDJA at 1:10 dilution reached 96.25% Sp (CI 95%: 89.43–99.22%) and PPDJB reached 91.25% Sp (CI 95%: 82.80–96.41%). With the third criterion, PPDJA reached Sp values higher than those of the other two ICs (binomial exact test, $p < 0.0001$) and PPDA (binomial exact test, $p = 0.0006$).

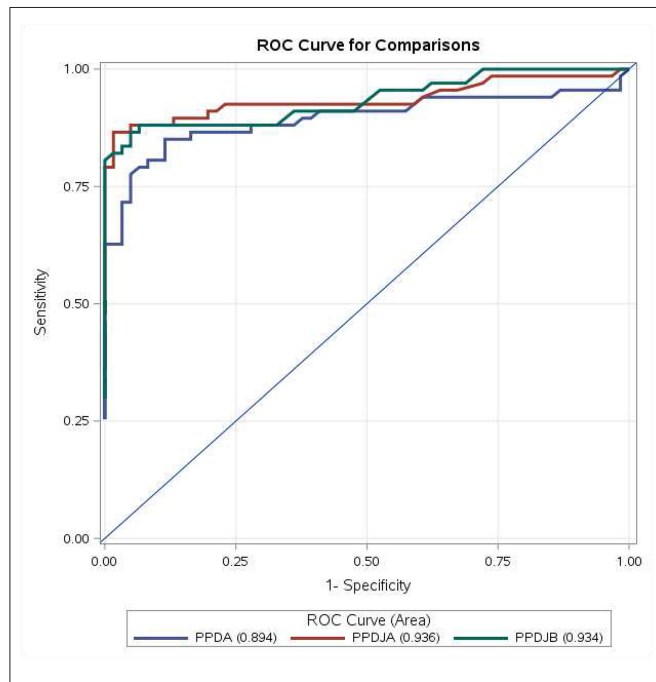


FIGURE 3 | ROC curve for comparisons of PPDA-PBS, PPDJA-PBS, and PPDJB-PBS according to the first three interpretative criteria of the IFN- γ test applied in the study for the diagnosis of *Mycobacterium avium* subsp. *paratuberculosis* (MAP)-infected cattle. PPDJA and PPDJB showed higher AUC than PPDA, and the difference is statistically significant ($p < 0.05$). ROC, receiver operating characteristic; IFN, interferon; PPD, purified protein derivative; PPDA, avian PPD; PPDJA, PPD Johnin strain A; PPDJB, PPD Johnin strain B; AUC, area under the ROC curve.

DISCUSSION

The IFN- γ test, in association with the tuberculin skin test, is used in many European countries for bTB diagnosis (63, 64). Both methods show the CMI response of the infected animals following stimulation with mycobacterial antigens, PPDB and PPDA (58, 63, 82). The immunologic evaluation to identify animals infected with MB is often limited by cross-reactions observed in animals exposed to other species of mycobacteria, particularly those belonging to the *Mycobacterium avium* complex (MAC), mainly MAP (86, 92).

In a single intradermal comparative cervical tuberculin (SICCT) test and in the IFN- γ release assay, a reaction to PPDA can identify animals affected by PTB (58, 82, 93–95). For this reason, in cattle, the IFN- γ test has also been used recently for the early diagnosis of PTB, although the Sp of the method varies from 67 to 94%, depending on the type and amount of PPDs used, and particularly on the IC of the test (57, 60).

With the aim of producing new batches of PPDJ obtained from the field strains of MAPs common in our territory and to develop a more sensitive and specific IFN- γ test for the early diagnosis of MAP infection, three experimental PPDJs were produced at IZSUM, and different IFN- γ ICs were evaluated.

From the first contact with mycobacteria, the immune response is characterized by a complex series of events aimed at controlling the infection before it can compromise homeostasis in the organism (45). In this context, the secretion of pro-inflammatory cytokines, such as IFN- γ , is involved in the containment of infection caused by mycobacteria (48) and can be detected only by the IFN- γ test. However, the humoral immune response, detectable by ELISA, appears only in the late stage when the disease is clinically manifested (60). The animals become infected at a young age, but the clinical PTB form does not occur until 2–3 years, probably because of the control role of innate and CMI, genetic susceptibility of the animal, and environmental factors (45, 47, 48, 50, 75). Therefore, it is strategically advantageous to decide in which categories include animals with a positive reaction to the IFN- γ test and tested

TABLE 3 | Specificity values obtained in the 3rd group of animals, adopting the 2nd, 3rd, and 5th interpretative criteria of the IFN- γ test.

Interpretative criteria	N	TN	FP	%FP	SP	CI 95% SP	
2							
A-PBS > 0.1 = MAP	80	73	7	8.75%	91.25%	82.80%	96.41%
Ja-PBS > 0.1 = MAP	80	76	4	5.00%	95.00%	87.69%	98.62%
Jb-PBS > 0.1 = MAP	80	70	10	12.50%	87.50%	78.21%	93.84%
3							
A-PBS > 0.2 = MAP	80	79	1	1.25%	98.75%	93.23%	99.97%
Ja-PBS > 0.2 = MAP	80	80	0	0.00%	100.00%	95.49%	100.00%
Jb-PBS > 0.2 = MAP	80	76	4	5.00%	95.00%	87.69%	98.62%
5							
A-(2 * PBS) > 0.04 = MAP	80	74	6	7.50%	92.50%	84.39%	97.20%
Ja-(2 * PBS) > 0.04 = MAP	80	77	3	3.75%	96.25%	89.43%	99.22%
Jb-(2 * PBS) > 0.04 = MAP	80	73	7	8.75%	91.25%	82.80%	96.41%

Specificity for IFN- γ test criteria estimated on a sample of 80 animals from a *Mycobacterium avium* subsp. *paratuberculosis* (MAP) free herd with an ongoing bovine tuberculosis outbreak. N, number of assessed animals; TN, true negative; FP, false positive; SP CI 95%, specificity and confidence interval 95%; A, avian PPD; Ja, Johnin PPD from strain A; Jb, Johnin PPD from strain B; PBS, phosphate-buffered saline.

negative to traditional tests for MAP infection diagnosis (49, 75). The production of IFN- γ by lymphocytes, after stimulation with PPDs, indicates an “immunological memory” and therefore a previous contact with a mycobacterium, and in the case of the PTB, the presence of a MAP infection. Thus, as an oversimplification, an IFN- γ -positive reactor is a MAP-infected animal that is probably in the stage of infection in which the animal, through CMI, keeps the pathogen under control and avoids its spread, as reported by recent studies (44). At this stage of infection, the animal, even if infected, does not yet eliminate MAP with feces and does not present any antibodies. To date, it is not predictable how long the animal will remain in this stage of infection. Certainly, in a herd with a high PTB prevalence, an IFN- γ -positive reactor could be a possible future MAP shedder and will therefore need to be checked more often than other cattle. However, if this IFN- γ -positive reactor will never test positive in conventional tests, it could be a subject able to contain the MAP infection, which will never develop the disease. It will be an important challenge for future studies to understand whether these animals with these characteristics will be identified as resistant or resilient PTB cattle (49, 75).

As stated earlier, the “infected” animals that do not yet shed MAP and do not yet show clinical signs are the most difficult category to identify with ELISA, fecal culture, and qPCR, due to low antibody production and low or absent MAP shedding. In addition, the “subclinical infected” animals may contaminate the environment, but their detection by serological test and the direct MAP identification has lower probability of success, representing a significant challenge for the control and management of PTB (57). “Affected” animals often present a clinical form and shed large quantities of MAP, representing the main source of infection, and are frequently positive in serological tests and can be easily detected by MAP isolation and biomolecular approaches.

In the present study, through a 4-year follow-up, it was possible to define the different stages of MAP infection in cattle of the first group from three PTB-affected herds, using new Italian Johnins in the IFN- γ assay. The obtained data represent the first assessment of the performance of experimental Italian PPDJs in the IFN- γ test and the first evidence of their ability to detect MAP-infected animals by adopting different ICs.

The critical aspect of this study was the comparison between two different diagnostic approaches, one based on the IFN- γ test and the other based on traditional tests (ELISA, fecal culture, and qPCR). The first approach is able to detect animals in the preliminary stages of MAP infection, while the second is useful when affected subjects are in the advanced stages of the disease or already have the clinical form of PTB. Therefore, the Se and Sp of the IFN- γ assay are related to the tests adopted to define the “positive animal.” These parameters are calculated on the basis of tests applied at the different stages of infection, in animal producing antibodies against MAP and/or in animal shedding MAP, while the IFN- γ test reveals infected animals that generally do not yet produce antibodies and do not yet shed MAP in their feces. This may have a negative effect on the performance of the IFN- γ test.

Simultaneously to the performance evaluation of the new PPDJs, different criteria for the PTB IFN- γ test interpretation were developed and compared, particularly IC based on the difference between OD values and IC based on the OD ratio (**Table 1**). Moreover, different cutoff values have been applied to each criterion, some of which are often used for the diagnosis of bTB in cattle and buffalo (72, 92, 96).

The PPDJs achieved the best performance within the first six ICs, among the 12 applied ICs (**Table 2**), with values of accuracy ranging from 90.6% (CI 95%: 85.5–95.7%) to 80.4% (CI 95%: 73.5–87.4%). In particular, the accuracy achieved by the PPDJs adopting the first six criteria resulted in a higher accuracy than that using the last six criteria, and the difference was statistically significant (binomial exact test, $p < 0.0001$). In addition, both PPDJs with the first criterion achieved a higher accuracy related to values reached adopting IC from the third to sixth, and the difference was statistically significant for each criterion (binomial exact test, $p < 0.05$).

From the perspective of the field use of PPDJs, we wanted to identify the IC that would maximize their performance, both in terms of Se, as in the case of the first criterion (PPDJB Se 100.0%, CI: 94.1–100.0%), and in terms of Sp, as in the case of the second IC (PPDJs Sp 100.0%, CI: 94.1–100.0%). In fact, even though no statistically significant differences were observed between the first and second ICs, in terms of accuracy, PPDJB with the first criterion achieved better Se values (binomial exact test, $p = 0.02$), while PPDJB with the second criterion achieved the best Sp values (binomial exact test, $p < 0.0001$), despite the accuracy being equal. As stated before, the Sp and Se are greatly affected by the tests used to detect the positive animal. On the basis of the six best ICs, in the first group, among 16 subjects with negative outcomes in the three PTB conventional tests, six were IFN- γ positive. The follow-up allowed monitoring of PTB progression, and five animals became PTB positive to traditional tests. In particular, two animals that reacted to both PPDA and PPDJs had PTB-positive bacterial culture 3 months later and also to the ELISA 10 months later. Among the three bovines reactive only to PPDJs, two animals became ELISA-positive 6 months later and a one bovine 18 months later. In the first step, these animals were considered “false positive” by statistical analysis, but the IFN- γ test with the six best ICs detected and unveiled MAP-infected cattle earlier than did the other traditional tests (**Supplementary Table 1** and **Supplementary Figure 1**).

In terms of the mean IFN- γ production following stimulation with PPDJs and PPDA, there were no statistically significant differences (**Figure 1**) except in the second criterion, where the Sp of PPDJs was higher than the Sp of PPDA, and the difference was statistically significant (binomial exact test $p = 0.0381$). However, the analysis of the ROC curves of the PPDJA, PPDJB, and PPDA, according to the first three criteria (**Figure 3** and **Supplementary Tables 2, 3**), shows that there were no statistical difference between AUC of PPDJA and of PPDJB, since DeLong's test for two correlated ROC curves was statistically not significant ($p > 0.05$). Instead, it is important to highlight that AUC of PPDA was different from PPDJA and PPDJB and that the difference was statistically significant ($p < 0.05$).

This result can be explained since MAP is part of the MAC; therefore, the remarkable similarities between PPD extracted from MAP and PPD extracted from MA do not permit the use of one against the other. However, in the criteria where both PPDJs and PPDA were used (**Table 2**), the first ones reached better values in terms of accuracy and proved to be more specific, particularly when used with the second criterion. Moreover, the comparison between the two PPDJs did not reveal statistically significant differences, even if the PPDJB seemed to be more sensitive and the PPDJA seemed more specific (**Table 2**, first and second ICs). These aspects, related to the performance of PPDJs and the robustness of IC validation, could be improved by enrolling more animals in future investigations. In addition, a further evolution of our study could be the use of recombinant antigens, peptides, or proteins from MAP, to increase the Sp of the IFN- γ test (97). These antigens have already been widely used in the IFN- γ test for the diagnosis of bTB in bovines (98, 99) and buffalo (92), and the most widely used antigens are ESAT6/CFP10, or other antigen cocktails, with the aim of increasing the Sp of the IFN- γ test. In the literature, the results obtained with recombinant proteins of MAP have not been completely satisfactory (100). Nevertheless, we are evaluating possible candidates for future inclusion in the lymphocyte stimulation phase of the IFN- γ test, such as the more promising MAP2698C (62) and MAP0586C (101) proteins. However, it should be noted that our experimental PPDJs achieved Sp values of 100%, without compromising Se values and therefore maintaining high accuracy values, when the second, third, and fifth ICs were adopted (**Table 2**) and when used with the third criterion in a bTB outbreak (**Table 3**). However, recombinant antigens tend to favor Sp but penalize Se because of their high discriminating power.

Although valid criteria were highlighted in this study, in particular the first and the second, in our opinion, the main aspect is the adoption of different criteria in relation to the PTB status in each farm. In particular, it is advisable to use those criteria with a major Se, such as the first criterion, in herds with a high prevalence of PTB; on the contrary, apply more specific IC, such as the second criterion, in herds with low PTB prevalence, similar to the protocol described by Keck et al. (73) used in France during the bTB eradication plans for cattle from 2003 to 2014.

In this regard, it was of great interest to include in the experiment a particularly problematic herd, the third enrolled group, which consisted of animals from a herd with a bTB outbreak at the time of the survey. In addition, animals have always been brought to pasture in the summer months; hence, they are subject to infections due to atypical mycobacteria, particularly those belonging to the MAC. Therefore, in these animals, non-specific reactions in the PTB IFN- γ test related to possible cross-reactions to MB and MAC were predictable. In these cases, it was useful to assess the Sp of PPDJs to avoid false-positive outcomes for MAP in animals that have always been negative on ELISA tests for PTB. In particular, in this third group, with the aim of verifying the Sp of PPDJs, the second, third, and fifth ICs were adopted because they reached Sp values of 100% (CI 95%: 94.1–100.0%) in the other groups. PPDJA achieved Sp values of 100% (CI 95%: 95.49–100%) when adopted in the

third criterion, and the difference with other ICs was statistically significant (binomial exact test, $p < 0.0001$). Always regarding the third criterion, PPDJA has shown higher Sp than PPDA, and the difference was statistically significant (Binomial exact test, $p = 0.0006$). Other authors (100) included a group of animals from a bTB outbreak in their assessment of the efficiency of the IFN- γ test for PTB diagnosis and did not find the same performance achieved in the present study. The authors concluded that the IC that they used led to several inconclusive results, and the use of a PPDJ would have resulted in a more precise classification of the animals within the bTB outbreak. Therefore, the use of the PPDJs investigated in the present study and the IC with the best performance could be recommended in herds where bTB and PTB co-infection is suspected, a scenario that could be an additional challenge for us.

In conclusion, the use of PPDJs and the interpretation of the IFN- γ test with the first or second criterion achieved high performance in the identification of MAP-infected cattle. Therefore, it can be assumed that the IFN- γ test could be a useful tool for identifying early subclinical MAP-infected animals, managing cattle infected or exposed to MAP, and monitoring younger calves within a herd.

CONCLUSIONS

The IFN- γ test should be used for the early diagnosis of MAP infection, and it can be efficiently used to detect pre-maturely MAP-infected subjects within a herd. Considering that infected cattle may never shed MAP or show clinical signs of PTB, this would allow veterinarians and farmers to decide together about the future of infected animals. The future of the animal, that is, to keep or to cull, must be considered carefully based on PTB prevalence on a farm. In particular, in herds with high PTB prevalence, culling IFN- γ positive reactors could mean eliminating animals that are “controlling” the infection, and paradoxically these animals may be “resistant” to the disease, and as such, should be kept in the herd.

On the contrary, in herds with low PTB prevalence or that are PTB-free, an animal that reacts positively to the IFN- γ test is definitely an animal that has been exposed to MAP or has contracted the infection; therefore, it has to be removed in order to maintain the low PTB or PTB-free status in the herd. Furthermore, the IFN- γ test can be considered as an additional test for animals that may be admitted to the herd, to avoid the introduction of MAP-infected subjects, especially in herds that have already eradicated the disease. Hence, the IFN- γ test will provide an additional diagnostic tool that farmers could adopt voluntarily to reach and preserve health status certification regarding PTB.

DATA AVAILABILITY STATEMENT

The raw data supporting the conclusions of this article will be made available by the authors, without undue reservation.

AUTHOR CONTRIBUTIONS

PM: conceptualization. SC, ADi, CS, LC, PP, SCo, NV, ADo, and PM: methodology. NV: software. SC, ADi, and PM: validation. NV, LP, CS, MCi, LC, and PM: formal analysis. SC, ADi, CS, MCi, LC, MB, PP, SCo, and PM: investigation. SC, ADi, MB, ADo, and PM: resources. SC, ADi, NV, and PM: data curation. SC, ADi, MT, LP, and PM: writing original draft preparation. SC, ADi, MT, LP, MCa, and PM: writing review and editing. SC, NV, ADi, LP, and PM: visualization. SC, ADi, NV, MT, LP, MCa, ADo, and PM: supervision. All authors contributed to the article and approved the submitted version.

FUNDING

The present study was supported by the Italian Ministry of Health, RC IZSUM 011/2008, RC IZSUM 04/2011 research projects. LP was funded by a grant from RC IZSUM 06/2019 research project, financed by the Italian Ministry of Health.

REFERENCES

- Lambrecht RS, Carriere JF, Collins MT. A model for analyzing growth kinetics of a slowly growing *Mycobacterium* sp. *Appl Environ Microbiol.* (1988) 54:910–6. doi: 10.1128/AEM.54.4.910-916.1988
- Chiodini RJ, Van Kruiningen HJ, Merkal RS. Ruminant paratuberculosis (John's disease): the current status and future prospects. *Cornell Vet.* (1984) 74:218–62.
- Harris NB, Barletta RG. *Mycobacterium avium* subsp. paratuberculosis in veterinary medicine. *Clin Microbiol Rev.* (2001) 14:489–512. doi: 10.1128/CMR.14.3.489-512.2001
- Fecteau ME, Whitlock RH, Buerge CD, Sweeney RW. Exposure of young dairy cattle to *Mycobacterium avium* subsp. paratuberculosis (MAP) through intermediate grazing of contaminated pastures in a herd positive for John's disease. *Can Vet J.* (2010) 51:198–200.
- Garvey M. *Mycobacterium avium* subspecies paratuberculosis: a possible causative agent in human morbidity and risk to public health safety. *Open Vet J.* (2018) 8:172–81. doi: 10.4314/ovj.v8i2.10
- Mazzoni P, Corneli S, Di Paolo A, Maresca C, Felici A, Biagetti M, et al. Survival of *Mycobacterium avium* subsp. paratuberculosis in the intermediate and final digestion products of biogas plants. *J Appl Microbiol.* (2018) 125:36–44. doi: 10.1111/jam.13762
- Hermion-Taylor J. *Mycobacterium avium* subspecies paratuberculosis, Crohn's disease and the Doomsday scenario. *Gut Pathog.* (2009) 1:15. doi: 10.1186/1757-4749-1-15
- Wynne JW, Bull TJ, Seemann T, Bulach DM, Wagner J, Kirkwood CD, et al. Exploring the zoonotic potential of *Mycobacterium avium* subspecies paratuberculosis through comparative genomics. *PLoS ONE.* (2011) 6:e22171. doi: 10.1371/journal.pone.0022171
- Sechi LA, Dow CT. *Mycobacterium avium* ss. paratuberculosis Zoonosis—the hundred year war—beyond Crohn's disease. *Front Immunol.* (2015) 6:96. doi: 10.3389/fimmu.2015.00096
- Eslami M, Shafiei M, Ghasemian A, Valizadeh S, Al-Marzoqi AH, Shokouhi Mostafavi SK, et al. *Mycobacterium avium* paratuberculosis and *Mycobacterium avium* complex and related subspecies as causative agents of zoonotic and occupational diseases. *J Cell Physiol.* (2019) 234:12415–21. doi: 10.1002/jcp.28076
- Scanu AM, Bull TJ, Cannas S, Sanderson JD, Sechi LA, Dettori G, et al. *Mycobacterium avium* subspecies paratuberculosis infection in cases of irritable bowel syndrome and comparison with Crohn's disease and John's disease: common neural and immune

ACKNOWLEDGMENTS

The authors would like to thank the Italian National Reference Center for Paratuberculosis, in particular Dr. Norma Arrigoni and Dr. Matteo Ricchi, for the genotyping of MAP field strains; the veterinary services of the Marche region; and Dr. Marco Ermini, Dr. Luigi Bonifazi, Dr. Martina Sebastianelli, and Dr. Piermario Mangili of IZSUM for their support in the field trials. Finally, a special thanks to Mrs. Angela Caporali for her excellent technical support. We would like to thank the reviewers for the useful observations and comments that enabled us to improve the manuscript quality, contributing to its better understanding.

SUPPLEMENTARY MATERIAL

The Supplementary Material for this article can be found online at: <https://www.frontiersin.org/articles/10.3389/fvets.2021.638890/full#supplementary-material>

pathogenicities. *J Clin Microbiol.* (2007) 45:3883–90. doi: 10.1128/JCM.01371-07

- Sisto M, Cucci L, D'Amore M, Dow TC, Mitolo V, Lisi S. Proposing a relationship between *Mycobacterium avium* subspecies paratuberculosis infection and Hashimoto's thyroiditis. *Scand J Infect Dis.* (2010) 42:787–90. doi: 10.3109/00365541003762306
- Dow CT. *M. paratuberculosis* heat shock protein 65 and human diseases: bridging infection and autoimmunity. *Autoimmune Dis.* (2012) 2012:150824. doi: 10.1155/2012/150824
- Frau J, Cossu D, Coghe G, Lorefice L, Fenu G, Melis M, et al. *Mycobacterium avium* subsp. paratuberculosis and multiple sclerosis in Sardinian patients: epidemiology and clinical features. *Mult Scler.* (2013) 19:1437–42. doi: 10.1177/1352458513477926
- Waddell LA, Rajić A, Stärk KD, McEWEN SA. The zoonotic potential of *Mycobacterium avium* ssp. paratuberculosis: a systematic review and meta-analyses of the evidence. *Epidemiol Infect.* (2015) 143:3135–57. doi: 10.1017/S095026881500076X
- Recht J, Schuenemann VJ, Sánchez-Villagra MR. Host diversity and origin of zoonoses: the ancient and the new. *Animals (Basel).* (2020) 10:1672. doi: 10.3390/ani10091672
- Grant IR, Ball HJ, Rowe MT. Incidence of *Mycobacterium paratuberculosis* in bulk raw and commercially pasteurized cows' milk from approved dairy processing establishments in the United Kingdom. *Appl Environ Microbiol.* (2002) 68:2428–35. doi: 10.1128/AEM.68.5.2428-2435.2002
- Hruska K, Bartos M, Kralik P, Pavlik I. *Mycobacterium avium* subsp. paratuberculosis in powdered infant milk: paratuberculosis in cattle—the public health problem to be solved. *Vet Med Praha.* (2005) 50:327–35. doi: 10.17221/5631-VETMED
- Eltholth MM, Marsh VR, Van Winden S, Guitian FJ. Contamination of food products with *Mycobacterium avium* paratuberculosis: a systematic review. *J Appl Microbiol.* (2009) 107:1061–71. doi: 10.1111/j.1365-2672.2009.04286.x
- Waddell L, Rajić A, Stärk K, McEwen SA. *Mycobacterium avium* ssp. paratuberculosis detection in animals, food, water and other sources or vehicles of human exposure: a scoping review of the existing evidence. *Prev Vet Med.* (2016) 132:32–48. doi: 10.1016/j.prevetmed.2016.08.003
- Grant IR, Williams AG, Rowe MT, Muir DD. Efficacy of various pasteurization time-temperature conditions in combination with homogenization on inactivation of *Mycobacterium avium* subsp. paratuberculosis in milk. *Appl Environ Microbiol.* (2005) 71:2853–61. doi: 10.1128/AEM.71.6.2853-2861.2005
- Gerrard ZE, Swift BMC, Botsaris G, Davidson RS, Hutchings MR, Huxley JN, et al. Survival of *Mycobacterium avium* subspecies

- paratuberculosis in retail pasteurised milk. *Food Microbiol.* (2018) 74:57–63. doi: 10.1016/j.fm.2018.03.004
23. Fechner K, Dreyman N, Schimkowiak S, Czerny CP, Teitzel J. Efficacy of dairy on-farm high-temperature, short-time pasteurization of milk on the viability of *Mycobacterium avium* ssp. paratuberculosis. *J Dairy Sci.* (2019) 102:11280–90. doi: 10.3168/jds.2019-16590
 24. Bates A, O'Brien R, Liggett S, Griffin F. The effect of sub-clinical infection with *Mycobacterium avium* subsp. paratuberculosis on milk production in a New Zealand dairy herd. *BMC Vet Res.* (2018) 14:93. doi: 10.1186/s12917-018-1421-4
 25. Garcia AB, Shalloo L. Invited review: the economic impact and control of paratuberculosis in cattle. *J Dairy Sci.* (2015) 98:5019–39. doi: 10.3168/jds.2014-9241
 26. Barratt AS, Arnoult MH, Ahmadi BV, Rich KM, Gunn GJ, Stott AW. A framework for estimating society's economic welfare following the introduction of an animal disease: the case of John's disease. *PLoS ONE.* (2018) 13:e0198436. doi: 10.1371/journal.pone.0198436
 27. Bulletin of the International Dairy Federation, No. 362/2001, *Mycobacterium paratuberculosis*, (2001). Available online at: <https://fil-idf.org/publications/bulletin/mycobacterium-paratuberculosis/>
 28. Nielsen SS, Toft N. A review of prevalences of paratuberculosis in farmed animals in Europe. *Prev Vet Med.* (2009) 88:1–14. doi: 10.1016/j.prevetmed.2008.07.003
 29. Whittington R, Donat K, Weber MF, Kelton D, Nielsen SS, Eisenberg S, et al. Control of paratuberculosis: who, why and how. A review of 48 countries. *BMC Vet Res.* (2019) 15:198. doi: 10.1186/s12917-019-1943-4
 30. Benedictus G, Verhoeff J, Schukken YH, Hesselink JW. Dutch paratuberculosis programme history, principles and development. *Vet Microbiol.* (2000) 77:399–413. doi: 10.1016/S0378-1135(00)00325-4
 31. Nielsen SS, Toft N. Assessment of management-related risk factors for paratuberculosis in Danish dairy herds using Bayesian mixture models. *Prev Vet Med.* (2007) 81:306–17. doi: 10.1016/j.prevetmed.2007.05.001
 32. Benedictus A, Mitchell RM, Linde-Widmann M, Sweeney R, Fyock T, Schukken YH, et al. Transmission parameters of *Mycobacterium avium* subspecies paratuberculosis infections in a dairy herd going through a control program. *Prev Vet Med.* (2008) 83:215–27. doi: 10.1016/j.prevetmed.2007.07.008
 33. Webb Ware JK, Larsen JW, Kluser P. Financial effect of bovine John's disease in beef cattle herds in Australia. *Aust Vet J.* (2012) 90:116–21. doi: 10.1111/j.1751-0813.2012.00896.x
 34. Sweeney RW. Pathogenesis of paratuberculosis. *Vet Clin North Am Food Anim Pract.* (2011) 27:537–46. doi: 10.1016/j.cvfa.2011.07.001
 35. Rathnaiah G, Zinniel DK, Bannantine JP, Stabel JR, Gröhn YT, Collins MT, et al. Pathogenesis, molecular genetics, and genomics of *Mycobacterium avium* subsp. paratuberculosis, the etiologic agent of John's disease. *Front Vet Sci.* (2017) 4:187. doi: 10.3389/fvets.2017.00187
 36. Fecteau ME. Paratuberculosis in cattle. *Vet Clin North Am Food Anim Pract.* (2018) 34:209–22. doi: 10.1016/j.cvfa.2017.10.011
 37. Sweeney RW. Transmission of paratuberculosis. *Vet Clin North Am Food Anim Pract.* (1996) 12:305–12. doi: 10.1016/S0749-0720(15)30408-4
 38. Lombard JE. Epidemiology and economics of paratuberculosis. *Vet Clin North Am Food Anim Pract.* (2011) 27:525–35. doi: 10.1016/j.cvfa.2011.07.012
 39. Coussens PM. Model for immune responses to *Mycobacterium avium* subspecies paratuberculosis in cattle. *Infect Immun.* (2004) 72:3089–96. doi: 10.1128/IAI.72.6.3089-3096.2004
 40. Baquero MM, Plattner BL. Bovine WC1(+) $\gamma\delta$ T lymphocytes modify monocyte-derived macrophage responses during early *Mycobacterium avium* subspecies paratuberculosis infection. *Vet Immunol Immunopathol.* (2016) 170:65–72. doi: 10.1016/j.vetimm.2015.12.002
 41. Baquero MM, Plattner BL. Bovine peripheral blood WC1+ and WC1neg $\gamma\delta$ T lymphocytes modulate monocyte-derived macrophage effector functions during *in vitro* *Mycobacterium avium* subspecies paratuberculosis infection. *Cell Immunol.* (2017) 315:34–44. doi: 10.1016/j.cellimm.2017.01.009
 42. Arsenault RJ, Maattanen P, Daigle J, Potter A, Griebel P, Napper S. From mouth to macrophage: mechanisms of innate immune subversion by *Mycobacterium avium* subsp. paratuberculosis. *Vet Res.* (2014) 45:54. doi: 10.1186/1297-9716-45-54
 43. Koets AP, Eda S, Sreevatsan S. The within host dynamics of *Mycobacterium avium* ssp. paratuberculosis infection in cattle: where time and place matter. *Vet Res.* (2015) 46:61. doi: 10.1186/s13567-015-0185-0
 44. Park HE, Park HT, Jung YH, Yoo HS. Gene expression profiles of immune-regulatory genes in whole blood of cattle with a subclinical infection of *Mycobacterium avium* subsp. paratuberculosis. *PLoS ONE.* (2018) 13:e0196502. doi: 10.1371/journal.pone.0196502
 45. Stabel JR, Kimura K, Robbe-Austerman S. Augmentation of secreted and intracellular gamma interferon following Johnin purified protein derivative sensitization of cows naturally infected with *Mycobacterium avium* subsp. paratuberculosis. *J Vet Diagn Invest.* (2007) 19:43–51. doi: 10.1177/104063870701900107
 46. Ganusov VV, Klinkenberg D, Bakker D, Koets AP. Evaluating contribution of the cellular and humoral immune responses to the control of shedding of *Mycobacterium avium* ssp. paratuberculosis in cattle. *Vet Res.* (2015) 46:62. doi: 10.1186/s13567-015-0204-1
 47. Begg DJ, de Silva K, Carter N, Plain KM, Purdie A, Whittington RJ. Does a Th1 over Th2 dominance really exist in the early stages of *Mycobacterium avium* subspecies paratuberculosis infections? *Immunobiology.* (2011) 216:840–6. doi: 10.1016/j.imbio.2010.12.004
 48. Stabel JR, Bannantine JP. Divergent antigen-specific cellular immune responses during asymptomatic subclinical and clinical states of disease in cows naturally infected with *Mycobacterium avium* subsp. paratuberculosis. *Infect Immun.* (2019) 88:e00650–19. doi: 10.1128/IAI.00650-19
 49. Jungersen G, Mikkelsen H, Grell SN. Use of the Johnin PPD interferon-gamma assay in control of bovine paratuberculosis. *Vet Immunol Immunopathol.* (2012) 148:48–54. doi: 10.1016/j.vetimm.2011.05.010
 50. Purdie AC, Plain KM, Begg DJ, de Silva K, Whittington RJ. Candidate gene and genome-wide association studies of *Mycobacterium avium* subsp. paratuberculosis infection in cattle and sheep: a review. *Comp Immunol Microbiol Infect Dis.* (2011) 34:197–208. doi: 10.1016/j.cimid.2010.12.003
 51. Koets AP, Gröhn YT. Within- and between-host mathematical modeling of *Mycobacterium avium* subspecies paratuberculosis (MAP) infections as a tool to study the dynamics of host-pathogen interactions in bovine paratuberculosis. *Vet Res.* (2015) 46:60. doi: 10.1186/s13567-015-0205-0
 52. van den Esker MH, Koets AP. Application of transcriptomics to enhance early diagnostics of mycobacterial infections, with an emphasis on *Mycobacterium avium* ssp. paratuberculosis. *Vet Sci.* (2019) 6:59. doi: 10.3390/vetsci6030059
 53. Sweeney RW, Whitlock RH, Rosenberger AE. *Mycobacterium paratuberculosis* cultured from milk and supramammary lymph nodes of infected asymptomatic cows. *J Clin Microbiol.* (1992) 30:166–71. doi: 10.1128/JCM.30.1.166-171.1992
 54. Chiodini RJ. Immunology: resistance to paratuberculosis. *Vet Clin North Am Food Anim Pract.* (1996) 12:313–43. doi: 10.1016/S0749-0720(15)30409-6
 55. Arango-Sabogal JC, Paré J, Labrecque O, Côté G, Roy JP, Buczinski S, et al. Incidence of fecal excretion of *Mycobacterium avium* subsp. paratuberculosis in dairy cows before and after the enrolment in the Québec voluntary program. *Prev Vet Med.* (2017) 148:94–105. doi: 10.1016/j.prevetmed.2017.10.006
 56. Jungersen G, Huda A, Hansen JJ, Lind P. Interpretation of the gamma interferon test for diagnosis of subclinical paratuberculosis in cattle. *Clin Diagn Lab Immunol.* (2002) 9:453–60. doi: 10.1128/CDLI.9.2.453-460.2002
 57. World Organisation for Animal Health OIE. *Manual of Diagnostic Tests and Vaccines for Terrestrial Animals; Paratuberculosis (John's disease) - Chapter 8.13.1 (NB. Version adopted in 2004)*. Paris: OIE (2009). Available online: https://www.oie.int/index.php?id=169&L=0&ndhtml=chapitre_paratuberculosis.htm (accessed December 2020).
 58. Kalis CH, Collins MT, Hesselink JW, Barkema HW. Specificity of two tests for the early diagnosis of bovine paratuberculosis based on cell-mediated immunity: the Johnin skin test and the gamma interferon assay. *Vet Microbiol.* (2003) 97:73–86. doi: 10.1016/j.vetmic.2003.07.003
 59. Huda A, Jungersen G, Lind P. Longitudinal study of interferon-gamma, serum antibody and milk antibody responses in cattle infected with

- Mycobacterium avium* subsp. paratuberculosis. *Vet Microbiol.* (2004) 104:43–53. doi: 10.1016/j.vetmic.2004.08.011
60. Nielsen SS, Toft N. Ante mortem diagnosis of paratuberculosis: a review of accuracies of ELISA, interferon-gamma assay and faecal culture techniques. *Vet Microbiol.* (2008) 129:217–35. doi: 10.1016/j.vetmic.2007.12.011
 61. Plain KM, Begg DJ, de Silva K, Purdie AC, Whittington RJ. Enhancement of the interferon gamma assay to detect paratuberculosis using interleukin-7 and interleukin-12 potentiation. *Vet Immunol Immunopathol.* (2012) 149:28–37. doi: 10.1016/j.vetimm.2012.05.023
 62. Gurung RB, Begg DJ, Purdie AC, de Silva K, Bannantine JP, Whittington RJ. Lymphoproliferative and gamma interferon responses to stress-regulated *Mycobacterium avium* subsp. paratuberculosis recombinant proteins. *Clin Vaccine Immunol.* (2014) 21:831–7. doi: 10.1128/CVI.00775-13
 63. de la Rua-Domenech R, Goodchild AT, Vordermeier HM, Hewinson RG, Christiansen KH, Clifton-Hadley RS. Ante mortem diagnosis of tuberculosis in cattle: a review of the tuberculin tests, gamma-interferon assay and other ancillary diagnostic techniques. *Res Vet Sci.* (2006) 81:190–210. doi: 10.1016/j.rvsc.2005.11.005
 64. Bezos J, Casal C, Romero B, Schroeder B, Hardegger R, Raeber AJ, et al. Current ante-mortem techniques for diagnosis of bovine tuberculosis. *Res Vet Sci.* (2014) 97:S44–52. doi: 10.1016/j.rvsc.2014.04.002
 65. Wood PR, Corner LA, Plackett P. Development of a simple, rapid *in vitro* cellular assay for bovine tuberculosis based on the production of gamma interferon. *Res Vet Sci.* (1990) 49:46–9. doi: 10.1016/S0034-5288(18)31044-0
 66. Wood PR, Corner LA, Rothel JS, Baldock C, Jones SL, Cousins DB, et al. Field comparison of the interferon-gamma assay and the intradermal tuberculin test for the diagnosis of bovine tuberculosis. *Aust Vet J.* (1991) 68:286–90. doi: 10.1111/j.1751-0813.1991.tb03254.x
 67. Wood PR, Jones SL. BOVIGAM: an *in vitro* cellular diagnostic test for bovine tuberculosis. *Tuberculosis.* (2001) 81:147–55. doi: 10.1054/tube.2000.0272
 68. Tameni S, Amadori M, Scaccaglia P, Quondam-Giandomenico R, Tagliabue S, Achetti IL, et al. Quality controls and *in vitro* diagnostic efficiency of bovine PPD tuberculin. *Biologicals.* (1998) 26:225–35. doi: 10.1006/biol.1998.0147
 69. Corneli S, Corte L, Roscini L, Di Paolo A, Colabella C, Petrucci L, et al. Spectroscopic characterization of bovine, avian and Johnin purified protein derivative (PPD) with high-throughput Fourier transform infrared-based method. *Pathogens.* (2019) 8:136. doi: 10.3390/pathogens8030136
 70. Wood PR, Rothel JS. *In vitro* immunodiagnostic assays for bovine tuberculosis. *Vet Microbiol.* (1994) 40:125–35. doi: 10.1016/0378-1135(94)90051-5
 71. Faye S, Moya JL, Gares H, Benet JJ, Garin-Bastuji B, Boschirolu ML. Determination of decisional cut-off values for the optimal diagnosis of bovine tuberculosis with a modified IFN gamma assay (Bovigam®) in a low prevalence area in France. *Vet Microbiol.* (2011) 151:60–7. doi: 10.1016/j.vetmic.2011.02.026
 72. EFSA (European Food Safety Authority). EFSA panel on animal health and welfare (AHAW); scientific opinion on the use of a gamma interferon test for the diagnosis of bovine tuberculosis. *EFSA J.* (2012) 10:2975. doi: 10.2903/j.efsa.2012.2975
 73. Keck N, Boschirolu ML, Smye F, Vogler V, Moya JL, Desvieux S. Successful application of the gamma-interferon assay in a bovine tuberculosis eradication program: the french bullfighting herd experience. *Front Vet Sci.* (2018) 5:27. doi: 10.3389/fvets.2018.00027
 74. Nuñez-García J, Downs SH, Parry JE, Abernethy DA, Broughan JM, Cameron AR, et al. Meta-analyses of the sensitivity and specificity of ante-mortem and post-mortem diagnostic tests for bovine tuberculosis in the UK and Ireland. *Prev Vet Med.* (2018) 153:94–107. doi: 10.1016/j.prevetmed.2017.02.017
 75. Wright K, Plain K, Purdie A, Saunders BM, de Silva K. Biomarkers for detecting resilience against mycobacterial disease in animals. *Infect Immun.* (2019) 88:e00401–19. doi: 10.1128/IAI.00401-19
 76. Ricchi M, Barbieri G, Taddei R, Belletti GL, Carra E, Cammi G, et al. Effectiveness of combination of Mini-and Microsatellite loci to sub-type *Mycobacterium avium* subsp. paratuberculosis Italian type C isolates. *BMC Vet Res.* (2011) 7:54. doi: 10.1186/1746-6148-7-54
 77. European Community. Consolidated (English) version of Council Directive 64/432/EEC of 26 June 1964 on animal health problems affecting intra-Community trade in bovine animals and swine. *Off J Eur Commu.* (1964) Annex B 121:1977–2012.
 78. European Community. *Commission Regulation (EC)1226/2002 of 8 July 2002 Amending Annex B to Council Directive 64/332/EEC.* Available online at: <https://eur-lex.europa.eu/legal-content/EN/TXT/HTML/?uri=CELEX:32002R1226&from=EN> (accessed August 10, 2020).
 79. Italian Ministry of Health Decree No 196 of 22May 1999. *Implementation of Q21 Directive 97/12/EC Amending and Updating Directive 64/432/EEC on Animal Q26 Health Problems Affecting Intra-Community Trade in Bovine Animals and Swine.* *Gazzetta Ufficiale Della Repubblica Italiana-Serie Generale* 146 (1999). Available online at: <https://www.gazzettaufficiale.it/eli/id/1999/06/24/099G0224/sg> (accessed August 10, 2020).
 80. Italian Ministry of Health. *Decree No 592 of 15 December 1995. Regulation Q21 on the National Plan for the Eradication of Tuberculosis in Cattle and Buffalo Q26 Herds-and Subsequent Amendments.* *Gazzetta Ufficiale Della Repubblica Italiana Serie Generale* 125. Available online at: <https://www.gazzettaufficiale.it> (accessed December 2020).
 81. Agreement. *Agreement Between the Government, the Regions and the Autonomous Provinces of Trento and Bolzano on Guidelines for the adoption of control and certification plans for bovine paratuberculosis.* (Rep. Acts n. 146/CSR). (13a09123) *GU General Seriesn.* 271 of 19-11-2013 - Ordinary Suppl. n.79). (2013). Available online at: <https://www.gazzettaufficiale.it/eli/gu/2013/11/19/271/so/79/sg/pdf> (accessed December 2020).
 82. Mazzone P, Agnetti F, Biagetti M, Cagiola M, Mangili PM, Nardini R, et al. Infezione da *Mycobacterium avium* subsp. Paratuberculosis e gamma-interferon test. *Argomenti.* (2010) 1:44–7. Available online at: https://sivemp.it/post_rivista/argomenti-nr-1-2010-anno-xiii/
 83. Donaghy JA, Rowe MT, Rademaker JL, Hammer P, Herman L, De Jonghe V, et al. An inter-laboratory ring trial for the detection and isolation of *Mycobacterium avium* subsp. paratuberculosis from raw milk artificially contaminated with naturally infected faeces. *Food Microbiol.* (2008) 25:128–35. doi: 10.1016/j.fm.2007.06.007
 84. Ricchi M, Manini F, Cammi G, Donaghy J, Arrigoni N. Comparison of four different PCR methods for the detection of *Mycobacterium avium* subsp. paratuberculosis in milk. In: *Proceedings of 10 International Colloquium on Paratuberculosis - ICP.* Minneapolis Minnesota (2009). p. 56–9.
 85. Sebastiani C, Curcio L, Ciullo M, Mazzone P, Pezzotti G, Biagetti M. Development of IS900 and F57 fast real-time PCR assays for the detection of *Mycobacterium paratuberculosis*. In: *Proceedings of XII International Colloquium on Paratuberculosis - ICP.* Parma (2014). p. 84.
 86. Roupie V, Alonso-Velasco E, Van Der Heyden S, Holbert S, Duytschaevera L, Berthon P, et al. Evaluation of mycobacteria-specific gamma interferon and antibody responses before and after a single intradermal skin test in cattle naturally exposed to *M. avium* subsp. paratuberculosis and experimentally infected with *M. bovis*. *Vet Immunol Immunopathol.* (2018) 196:35–47. doi: 10.1016/j.vetimm.2017.12.007
 87. European Commission. *Commission Decision of 5 February 2016 Amending Decision 2003/467/EC and Declaring Piedmont Officially free of Bovine Tuberculosis (2016/168/EC).* Available online at: <https://eur-lex.europa.eu/legal-content/EN/TXT/?uri=celex%3A32016D0168> (accessed August 10, 2020).
 88. Dondo A, Goria M, Moda G, Cesano L, Garanzini A, Giammartino M, et al. La prova del g-interferone per la diagnosi della tubercolosi bovina: determinazione della sensibilità e della specificità in prove di campo. *Med Vet Prevent.* (1996) 13:14–8.
 89. Chiavacci L, Dondo A, Goria M, Moda G, Ruocco L, Vignetta P, et al. Tuberculosis eradication in Italy. In: Thoen CO, editor. *Zoonotic Tuberculosis: Mycobacterium bovis and Other Pathogenic Mycobacteria.* Hoboken, NJ: Wiley and Sons (2014). p. 357–69.
 90. Moda G. Non-technical constraints to eradication: the Italian experience. *Vet Microbiol.* (2006) 112:253–8. doi: 10.1016/j.vetmic.2005.11.021
 91. DeLong ER, DeLong DM, Clarke-Pearson DL. Comparing the areas under two or more correlated receiver operating characteristic curves: a nonparametric approach. *Biometrics.* (1988) 44:837–45. doi: 10.2307/2531595

92. Martucciello A, Vitale N, Mazzone P, Dondo A, Archetti I, Chiavacci L, et al. Field evaluation of the interferon gamma assay for diagnosis of tuberculosis in water buffalo (*Bubalus bubalis*) comparing four interpretative criteria. *Front Vet Sci.* (2020) 7:563792. doi: 10.3389/fvets.2020.563792
93. Dunn JR, Kaneene JB, Grooms DL, Bolin SR, Bolin CA, Bruning-Fann CS. Effects of positive results for *Mycobacterium avium* subsp. Paratuberculosis as determined by microbial culture of feces or antibody ELISA on results of caudal fold tuberculin test and interferon-g assay for tuberculosis in cattle. *J Am Vet Med Assoc.* (2005) 226:429–35. doi: 10.2460/javma.2005.226.429
94. Aranaz A, De Juan L, Bezos J, Alvarez J, Romero B, Lozano F, et al. Assessment of diagnostic tools for eradication of bovine tuberculosis in cattle co-infected with *Mycobacterium bovis* and *M. avium* subsp. paratuberculosis. *Vet Res.* (2006) 37:593–606. doi: 10.1051/vetres:2006021
95. Álvarez J, de Juan L, Bezos J, Romero B, Sáez JL, Marqués S, et al. Effect of paratuberculosis on the diagnosis of bovine tuberculosis in a cattle herd with a mixed infection using interferongamma detection assay. *Vet Microbiol.* (2009) 135:389–93. doi: 10.1016/j.vetmic.2008.09.060
96. Antognoli MC, Remmenga MD, Bengtson SD, Clark HJ, Orloski KA, Gustafson LL, et al. Analysis of the diagnostic accuracy of the gamma interferon assay for detection of bovine tuberculosis in U.S. herds. *Prev Vet Med.* (2011) 101:35–41. doi: 10.1016/j.prevetmed.2011.05.012
97. Hughes V, McNair J, Strain S, Barry C, McLuckie J, Nath M, et al. Gamma interferon responses to proteome-determined specific recombinant proteins in cattle experimentally- and naturally-infected with paratuberculosis. *Res Vet Sci.* (2017) 114:244–53. doi: 10.1016/j.rvsc.2017.04.018
98. Aagaard C, Govaerts M, Meikle V, Vallecillo AJ, Gutierrez-Pabello JA, Suarez-Güemes F, et al. Optimizing antigen cocktails for detection of *Mycobacterium bovis* in herds with different prevalences of bovine tuberculosis: ESAT6-CFP10 mixture shows optimal sensitivity and specificity. *J Clin Microbiol.* (2006) 44:4326–35. doi: 10.1128/JCM.01184-06
99. Casal C, Bezos J, Díez-Guerrier A, Álvarez J, Romero B, de Juan L, et al. Evaluation of two cocktails containing ESAT-6, CFP-10 and Rv-3615c in the intradermal test and the interferon- γ assay for diagnosis of bovine tuberculosis. *Prev Vet Med.* (2012) 105:149–54. doi: 10.1016/j.prevetmed.2012.02.007
100. Dernivoix K, Roupie V, Welby S, Roelandt S, Viart S, Letesson, et al. Field performance of six *Mycobacterium avium* subsp. Paratuberculosis antigens in a 20h interferon gamma release assay in Belgium. *Vet Immunol Immunopathol.* (2017) 189:17–27. doi: 10.1016/j.vetimm.2017.05.008
101. Roupie V, Holbert S, Viart S, Tholoniati C, Leroy B, Cappoen D, et al. Immunological analysis of 35 recombinant antigens of *M. avium* subsp. paratuberculosis in mice and cattle. In: *Proceedings of XIII International Colloquium on Paratuberculosis - ICP.* Nantes (2016). p. 159

Conflict of Interest: The authors declare that the research was conducted in the absence of any commercial or financial relationships that could be construed as a potential conflict of interest.

Copyright © 2021 Corneli, Di Paolo, Vitale, Torricelli, Petrucci, Sebastiani, Ciullo, Curcio, Biagetti, Papa, Costarelli, Cagiola, Dondo and Mazzone. This is an open-access article distributed under the terms of the Creative Commons Attribution License (CC BY). The use, distribution or reproduction in other forums is permitted, provided the original author(s) and the copyright owner(s) are credited and that the original publication in this journal is cited, in accordance with accepted academic practice. No use, distribution or reproduction is permitted which does not comply with these terms.



Development of a Method to Detect *Mycobacterium paratuberculosis* in the Blood of Farmed Deer Using Actiphage[®] Rapid

Anton Kubala^{1,2}, Tania M. Perehinec¹, Catherine Evans¹, Andrea Pirovano², Benjamin M. C. Swift³ and Catherine E. D. Rees^{1,2*}

¹ School of Biosciences, University of Nottingham, Loughborough, United Kingdom, ² PBD Biotech Ltd., Link House, Elm Farm Park, Thurston, United Kingdom, ³ Pathobiology and Population Sciences, The Royal Veterinary College, Hatfield, United Kingdom

OPEN ACCESS

Edited by:

Kumi de Silva,
The University of Sydney, Australia

Reviewed by:

Eduard Otto Roos,
Pirbright Institute, United Kingdom
Heike Uta Köhler,
Friedrich-Loeffler-Institute, Germany

*Correspondence:

Catherine E. D. Rees
cath.rees@nottingham.ac.uk

Specialty section:

This article was submitted to
Veterinary Infectious Diseases,
a section of the journal
Frontiers in Veterinary Science

Received: 08 February 2021

Accepted: 21 June 2021

Published: 29 July 2021

Citation:

Kubala A, Perehinec TM, Evans C, Pirovano A, Swift BMC and Rees CED (2021) Development of a Method to Detect *Mycobacterium paratuberculosis* in the Blood of Farmed Deer Using Actiphage[®] Rapid. *Front. Vet. Sci.* 8:665697. doi: 10.3389/fvets.2021.665697

Mycobacterium avium subsp. *paratuberculosis* (MAP) is the causative agent of Johne's disease, which is an economically and clinically relevant pathogen for commercial deer production. The purpose of this study was to develop a method that could be used to rapidly detect MAP infection in deer using the Actiphage Rapid blood test. This test has previously been used to detect MAP in cattle blood following the purification of buffy coat using Ficoll gradients, however this method is quite laborious and costly. The purpose of this study was to develop a simpler method of blood preparation that was also compatible with deer blood and the Actiphage test. Initially differential lysis of RBCs using Ammonium Chloride-Potassium (ACK) blood lysis buffer was compared with the Ficoll gradient centrifugation method using cattle blood samples for compatibility with the Actiphage reagents, and it was found that the simpler ACK method did not have an impact on the Actiphage test reagents, producing an equivalent sensitivity for detection of low levels of MAP. When the two methods were compared using clinical blood samples from farmed deer, the ACK lysis method resulted in a cleaner sample. When a blinded test of 132 animals from 4 different production groups was carried out, the majority of the positive test results were found to be from animals in just one group, with a small number identified in a second group. The test results were found to be reproducible when a small set of positive animals were tested again 1 month after their initial testing. Finally a set of negative animals which had been previously screened using an ELISA test, all animals gave a negative Actiphage result. This study shows that this improved sample preparation method and Actiphage blood testing can be used to test blood samples from deer, and the full diagnostic potential of the method can now be evaluated.

Keywords: *Mycobacterium paratuberculosis*, Actiphage, deer, bacteriophage, qPCR

INTRODUCTION

Mycobacterium avium subsp. *paratuberculosis* (MAP) is a slow growing acid-fast bacterium that is the causative agent of Johne's disease in a range of farmed ruminants including cattle, sheep, goats and deer (1). Johne's disease is a chronic inflammation (granulomatous enteritis of the intestine primarily affecting the jejunum and ileum) resulting in inhibition of nutrient absorption and

leading to chronic wasting of the animal resulting in reduced meat yields, reduced fertility and premature death of the animals (2). Although good estimates of the economic impact of Johne's disease for commercial deer farming are not available, it is known that the disease does pose a significant cost to other farmed species susceptible to Johne's disease (3, 4).

In farmed, captive and free-living deer, diarrhoea, loss of weight and body condition are clinical signs of disease (5). Two clinical syndromes have been described in red deer: sporadic disease with low morbidity and high mortality in adult populations, and severe outbreaks in young deer (8–15 months old) resulting in both high morbidity and high mortality (2). In infected animals, MAP is increasingly shed in faeces as the disease progresses [see (6)]. Contaminated faeces then acts as a source of transmission within herds by the faecal-oral route (7). MAP can also be transmitted through ingestion of colostrum from infected dams or *in utero* via the placenta and this is reported to be very high in both symptomatic and asymptomatic red deer (8, 9). Therefore, for control of the disease in farmed deer, it is important to have accurate tests that can detect infection at an early stage of infection (4, 10).

Culture-based diagnostic approaches that can be used for other pathogenic organisms are not appropriate for mycobacterial pathogens due to their very slow *in vitro* growth rates. Culture-based tests require from 4 weeks (automated liquid culture) to 20 weeks [culture on solid media; (11)]. The main diagnostic tool currently employed for the rapid detection of Johne's disease is an antibody ELISA which detects the presence of MAP-specific antibodies in either blood or milk produced by the animal in response to infection. In cattle populations, the MAP ELISA is often used as a front line test due to its availability and fast sample throughput, but its shortcomings include low sensitivity and accuracy especially during early stages of the infection (4, 6, 10). As intracellular pathogens, MAP is known to infect and replicate inside macrophages and have the ability to evade immune surveillance and signalling pathways, allowing them to persist in the intracellular environment for long periods of time before shedding becomes evident. In cattle animal's immune response to MAP is not consistent over time and antibody production is slow to develop [see (6)]. However, it has been shown that IgG ELISA tests that have been optimised for cattle samples do not retain their performance characteristics when used to test blood samples from other species (12, 13). In contrast to cattle, farmed deer do seem to raise a detectable antibody response (14), and surveys have been performed to evaluate the performance of different ELISA tests (13) but there are still limited numbers of commercial validated tests available for deer. The IgG1 ELISA for detection of paratuberculosis in deer (Paralisa™) has been developed in New Zealand and has been shown to be of value for screening deer herds to identify high shedding animals (15), although this was also not found to have a good predictive value in earlier stages of infection. Therefore, new tests that can directly detect the bacterium in the early stages of infection could be used to help implement control or eradication programmes.

Phage-based assays, such as the Actiphage® assay (PBD Biotech Ltd., UK), have been shown to be able to detect MAP

in the blood of cattle (16, 17). The assay uses mycobacteriophage D29 as a lysing agent to efficiently release genomic DNA from low numbers of mycobacterial cells which can be detected by signature specific PCR assays (16, 17). In addition to using phage-based assays to detect MAP in blood as a sign of infection, we have previously shown that the appearance of detectable levels of mycobacteria in the circulating blood is a good marker of disease for infections caused by both *Mycobacterium bovis* and *Myobacterium tuberculosis* (16–20). In all species of animal, mononucleocytes are the main targets of infection of mycobacterial pathogens in blood (21–23). When developing the phage-based assay, it was found that one of the critical steps was the removal of red blood cells (RBCs) from the sample as these can inhibit phage infection (16). Traditionally density gradient separation, such as the Ficoll buoyancy gradient method, has been widely used for the separation of monocytes and other white blood cells (24). However, this method is time consuming, requiring several centrifugation steps, and is sensitive to variation in both sample age and temperature. Recently, we have shown that differential sedimentation methods developed for the isolation of human white blood cells are compatible with the Actiphage assay (18). In addition we have shown that recovery of infected white blood cells from milk by centrifugation is also a suitable method to prepare samples prior to the phage assay (25).

In this study we wanted to investigate whether a differential lysis approach to remove the RBCs from a blood sample using Ammonium Chloride-Potassium (ACK) lysis buffer was compatible with the Actiphage assay. The Ammonium Chloride-Potassium (ACK) lysis method lyses erythrocytes as a result of osmotic stress caused by the uptake of ammonium chloride before cell debris is removed by washing in a buffer that is osmotically balanced for the white blood cells and has been shown to be effective for obtaining purified white blood cells from whole blood samples (26, 27). The performance of ACK lysis buffer method for the removal of RBCs was first compared to the traditional Ficoll method using cattle blood. The ACK method was then evaluated to see if it could be used to detect MAP in the blood of naturally infected, farmed deer.

MATERIALS AND METHODS

Bacterial Strains and Media

MAP (strain K10; ATCC BAA-968) was used as the positive control for Actiphage assays. MAP was propagated in Middlebrook 7H9 broth (Difco, UK) supplemented with oleic albumin dextrose catalase (OADC) at a ratio of 1:10 and Mycobactin-J (2 µg ml⁻¹; Synbiotic Corporation, France), grown with aeration at 37°C (28). The Actiphage (PBD Biotech Ltd., UK) phage reagent and Media Plus were prepared according to the manufacturer's instructions. Briefly Media Plus is prepared by supplementing the base media supplied in the kit with a sterile supplement at a 1 in 10 dilution rate. Media Plus is then used to reconstitute the freeze dried Actiphage reagent.

Blood Samples

All clinical blood samples were handled under BS level 2 containment. For method optimisation experiments superfluous material from commercial bovine blood samples sent to PBD Biotech Ltd. for Actiphage testing was used. The clinical cervid blood samples originated from farmed deer in the East Midlands area of the UK. The deer were kept on outdoor pastures and in four different production groups. Blood was collected for diagnostic purposes by veterinarians in Heparin Vacutainer tubes (Beckton Dickinson, UK) and stored and transported at ambient temperatures (15–20°C) to ensure that the mycobacteria remained in an active growth phase required for productive D29 infection (28). The blood separation procedures were carried out within 12 h of collection. Samples for MAP blood ELISA assays were sent to Axiom Veterinary Laboratories (Devon, UK).

Animal Groups for Testing

All the experiments in this study was performed using superfluous blood samples sent to PBD Biotech Ltd. for commercial testing and therefore were samples of convenience rather than taken from particular cohorts of animals of known infection status. Initial comparison of the Ficoll and ACK methods was carried out using superfluous blood from 43 cattle of unknown infection status, but with a known low herd prevalence of MAP infection.

All the deer samples were from females that were part of the commercial breeding stock on the farm which had experienced low levels of sporadic MAP infection in the past. Set 1 included 29 animals of a range of ages that were being screened before being sale. Blood samples from these animals were used to determine if the ACK method was compatible with deer blood, and to confirm that this method did not affect the performance of the Actiphage reagents. Set 2 included most of the mature breeding animals on the farm (ages 5–10 years) and were from different breeding groups and animals within these groups had shown signs on John's disease on previous occasions. These animals were used to determine whether the ACK/Actiphage method could detect MAP in the deer. Set 3 included only young animals that were being screened prior to the rut to identify which animals would be retained on the farm. This set was also used to determine whether MAP could be detected in the blood of these animals. A small number of animals from this group that gave a positive Actiphage results were included in a set of animals (set 4) that were screened using Actiphage 1 month later and allowed the reproducibility of the test results to be examined. Animals in set 5 were selected by the farm to be screened before sale using both MAP ELISA tests and Actiphage and included only animals that had previously been given a negative test result using Actiphage.

Blood Preparation Methods

For separation of peripheral blood mononucleocytes (PBMCs) using Ficoll gradients (Ficoll paque Plus; GE Healthcare), a 10 ml Leucosep™ gradient tube (Greiner, Austria) was filled with 3 ml Ficoll density medium. 2.5 ml of Phosphate Buffered Saline (PBS) was gently mixed with a 2 ml sample of whole heparinised blood sample. The sample was then layered onto the top of the leucosep filter membrane. The sample was centrifuged (300

× g, 20 min, 19°C, swing out rotor with no deceleration). The buffy coat layer located above the filter membrane, was collected and mixed with 6 ml PBS before centrifuging (200 × g, 10 min, 19°C, swing out rotor with deceleration set at maximum. The pellet containing the blood mononucleocytes was resuspended in 1 ml of Actiphage Media Plus to induce lysis of the white blood cells and release the intracellular mycobacteria into the media. The samples were then either processed immediately (samples inoculated with laboratory cultured MAP) or incubated at room temperature for up to 12 h (clinical samples) prior to performing the Actiphage assay.

For purification of blood leukocytes (both mononucleocytes and granulocytes) using ACK buffer, a modification of the method described by Brown et al. (27) was used. Briefly, a sample (2 ml) of whole blood was added to 40 ml of ACK buffer (an aqueous solution of 150 mM Ammonium chloride, 10 mM Potassium bicarbonate, 0.1 mM EDTA, filter sterilised using 0.45 µm pore size). On addition of ACK the blood samples became more opaque, but this disappeared after gently agitating the sample for 5 min. The lysis process was determined to be complete when the sample became a dark red, transparent solution. The blood leukocytes were recovered by centrifugation (300 × g, 5 min at 20°C) and the supernatant discarded. The pellet was then washed twice to remove traces of erythrocyte debris using 5 ml of PBS with the intact white blood cells being recovered after each wash by centrifugation (300 × g, 5 min at 20°C). Finally the pellet was resuspended in 1 ml of Actiphage Media Plus and was stored at room temperature for upto 2 days before testing as described above.

Actiphage Assay and qPCR

The Actiphage assay was carried out according to manufacturer's instruction. Briefly, after lysis of the white blood cells, any mycobacteria released into the Actiphage Media Plus were collected by centrifugation (13,000 × g, 3 min). The pellet was resuspended in 110 µl of rehydrated Actiphage reagent and then transferred into an Actiphage Rapid tube before incubating at 37°C for 3.5 h to allow phage absorption, infection and complete lysis of the mycobacterial cells. After the phage lysis step, the Actiphage Rapid tubes were centrifuged (13,000 × g, 3 min) and the lysate containing the released mycobacterial DNA was recovered from the collection tube. For the assay positive controls (Actiphage Media Plus inoculated with ~10² MAP K10 cells) and negative controls (Media Plus and Actiphage reagent) were prepared according to the manufacturer's instructions.

DNA recovered from the Actiphage assay was concentrated using a Zymo™ clean and concentrator kit (Zymo, USA) and eluted in a total volume of 14 µl using 55°C water pre-warmed to 55°C. Detection of MAP DNA was carried out using the BactoReal kit for the detection of MAP (Ingenetix, Austria) which targets the IS900 element. qPCR reactions were performed according to the manufacturer's instructions using 5 µl of purified DNA per reaction. The positive control DNA sample provided with this kit contains ~10,000 target copies per reaction and the PCR Mastermix includes an Internal Positive control (IPC) labelled with VIC-TAMRA for detection of PCR inhibition. A test sample was determined positive if its C_q-value

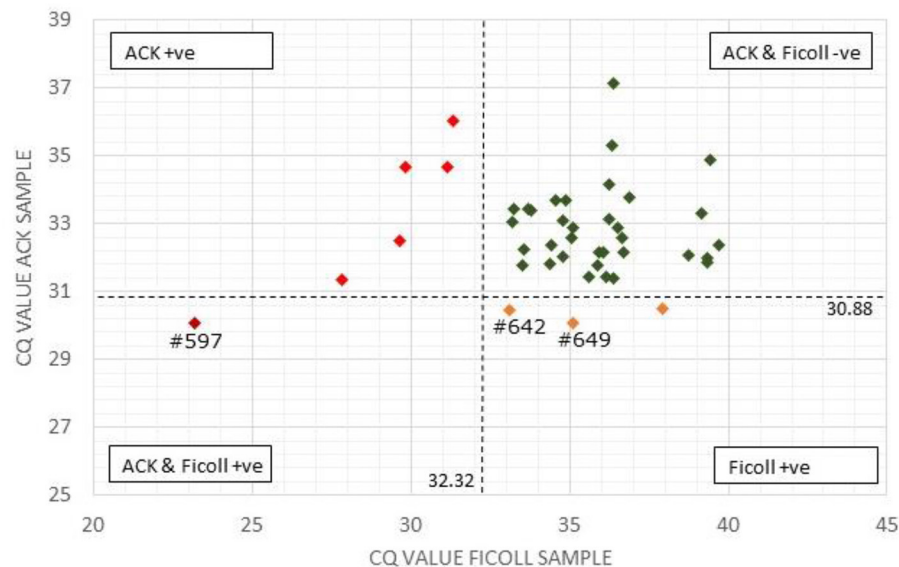


FIGURE 1 | Comparison of Actiphage pPCR test results using Ficoll and ACK methods to purify white blood cells. The Cq-values for the paired blood samples are compared using a scatter plot. Vertical and horizontal dashed lines are set at the cut off values for the Ficoll and ACK samples, respectively. Samples falling within each quadrant are colour coded and cut off values are given next to each line. The position of individual samples (#) referred to in the text are indicated.

was 2 cycles lower than that of the Actiphage negative control sample ($\Delta Cq \geq 2$). A sample producing a Cq-value between 1.5 and 2 units lower than the negative control was scored as weak positive ($\Delta Cq = 1.5-2$).

Statistical Analysis

Excel 2010 statistical add on package was used carry out a correlated *T*-Test when values for paired samples was compared. Significance was determined at $p < 0.05$. PCR efficiency was determined by plotting Ct-value against \log_{10} (cell number) using Excel 2013, and determining the slope of the curve from the trend line and R^2 -values for each set of data points (R^2 over 90% = acceptable). PCR efficiency was then calculated using the equation $\text{Efficiency (\%)} = [10^{(-1/\text{slope})} - 1] \times 100$; acceptable range = 90–110%.

RESULTS

Determining Compatibility of ACK Method With the Actiphage Assay

The Actiphage test is currently being performed by PBD Biotech Ltd. as a commercial blood test for detecting MAP in bovine blood samples and the kit instructions describe the isolation of white blood cells using a Ficoll density gradient method. To determine whether the ACK lysis method could be used as an alternative method to purify white blood cells prior to performing the Actiphage assay, superfluous blood from bovine samples set to PBD Biotech Ltd. were used. On the day of commercial testing, white blood cells were also prepared from blood of 43 cattle of unknown infection status using the ACK lysis method described by Brown et al. (27). Visible inspection showed that

the ACK lysis method also produced purified white blood cells with low visible erythrocyte contamination which is key indicator for samples to be successfully tested using the Actiphage kit so that the results could be compared with the results reported for the commercial tests using the Ficoll method. Purified DNA was tested for the presence of MAP using a commercial qPCR kit (Bactoreal, Ingenetix) which includes an internal positive control (IPC) in the qPCR Mastermix to detect PCR inhibition. The signal from the IPC indicated that no PCR inhibition was detected when the DNA the samples prepared using either Ficoll or ACK were tested indicating that changing the extraction method did not result in a lower quality DNA sample (data not shown).

The IS900 target DNA positive control sample provided in the kit that contained $\sim 10,000$ copies of the MAP-specific target sequence gave a Cq-value of 20.54 (expected range 19–22). For the Actiphage assay, a positive control containing $\sim 10^2$ freshly grown MAP K10 cells is used, and in this experiment produced a Cq-value of 21.13. Based on the Cq-value of the positive control the expected range for the MAP positive control would be 21–22 as the K10 strain contains 17 copies of the IS900 element (i.e., 10^2 cells contain 1,700 copies of the IS900 target sequence). For the Actiphage test, a negative control sample is also prepared using the media supplied in the kit and the Actiphage reagent alone but still contain high levels of phage DNA and residual DNA from the *Mycobacterium smegmatis* strain used to propagate the Actiphage reagent which may result in PCR bridging events. In this case the negative control samples give Cq-values in the range of 30–32 and therefore these values are used to establish a base line for identifying positive test results (see Figure 1).

TABLE 1 | Comparison of qPCR result for deer blood samples prepared using Ficoll and ACK methods.

Sample	Blood preparation method				Ratio ACK:Ficoll Cq ^c
	ACK Cq	ΔCq ^b	Ficoll Cq	ΔCq ^b	
Act. +ve ^a	20.83	n/a	22.24	n/a	0.94
Act. -ve ^a	30.29	n/a	32.36	n/a	0.94
1	33.45	-3.2	40.72	-8.4	0.82
2	36.09	-5.8	35.49	-3.1	1.02
3	33.32	-3.0	32.51	-0.1	1.02
5	33.94	-3.7	33.00	-0.6	1.03
6	32.38	-2.1	32.33	0.0	1.00
7	34.40	-4.1	38.02	-5.7	0.90
8	33.57	-3.3	34.80	-2.4	0.96
9	28.38	1.9	33.76	-1.4	0.84
10	32.40	-2.1	34.00	-1.6	0.95
11	33.03	-2.7	34.35	-2.0	0.96
12	33.61	-3.3	33.86	-1.5	0.99
13	32.86	-2.6	31.86	0.5	1.03
14	33.63	-3.3	33.80	-1.4	0.99
15	32.79	-2.5	30.48	1.9	1.08
16	31.85	-1.6	33.44	-1.1	0.95
17	33.10	-2.8	35.57	-3.2	0.93
19	31.94	-1.7	33.84	-1.5	0.94
20	31.32	-1.0	31.96	0.4	0.98
21	43.93	-13.6	31.40	1.0	1.40
22	36.38	-6.1	35.09	-2.7	1.04
23	31.95	-1.7	36.73	-4.4	0.87
24	31.40	-1.1	35.03	-2.7	0.90
25	33.29	-3.0	34.40	-2.0	0.97
26	33.10	-2.8	33.20	-0.8	1.00
27	32.20	-1.9	30.82	1.5	1.04
29	31.95	-1.7	30.62	1.7	1.04

^aActiphage positive control = Media Plus inoculated with $\sim 10^2$ MAP K10 cells; Actiphage negative control = Media Plus and Actiphage reagents alone.

^bΔCq, difference in Cq sample compared to the Actiphage negative control; n/a, not applicable; Positive test result = ΔCq = ≥ 2 ; A weak positive test result = ΔCq 1.5-2 (weak positive results shaded in grey).

^cRatio of Cq-values = Cq[ACK]/Cq[Ficoll] for each paired sample. Average value = 0.99. The one sample where this ratio was significantly larger highlighted in bold.

A comparison of the qPCR analysis of the 43 bovine samples prepared using the two different methods is shown in **Figure 1**. Using the standard Ficoll isolation method, MAP DNA was detected in 4 of the clinical bovine blood samples, two with a clear positive result (ΔCq = ≥ 2 ; #597, #649) and two gave a weak positive result (ΔCq = 1.5–2) indicating that very low levels of Map (~ 5 cells) had been detected. In comparison, using the ACK lysis method, 6 positive results and no weak positive results were obtained. Comparing the pattern of results, the sample with the highest ΔCq-value using the ACK group matched one of the two positive results for the Ficoll samples (**Figure 1**; #597). Animal #642 gave a weak positive result with the Ficoll method and had a ΔCq of 1.2 for the ACK method, indicating that it was just below the threshold for a weak positive score. The two other positive results from the Ficoll set gave negative test results using ACK. When low levels of MAP are being detected in samples, some stochastic variation in number of cells per sample is to be expected [see (25)].

For PCR efficiency determination, 10-fold dilutions of a MAP positive control culture with a starting titre of 1.2×10^4 cfu ml⁻¹ were used to inoculate white blood cells extracted using the two different methods with cell numbers from ~ 10 – 10^4 cells. For the Ficoll method the PCR efficiency value was 89.6% ($R^2 = 0.996$), with an intercept Ct-value of 30.85, whereas for the ACK method the PCR efficiency value as 98.2% ($R^2 = 0.994$), with an intercept Ct-value of 31.24 indicating that sensitivity achieved using the two sample preparation methods was very similar (**Supplementary Figure 1**). Overall from these results it was concluded that the ACK method was compatible with the Actiphage reagents as there was no evidence of inhibition and positive test results were achieved.

Comparison of Blood Processing Methods for Clinical Cervid Blood Samples

Ficoll can be used to isolate white blood cells from many species of animal, including cervids, and ACK has been shown

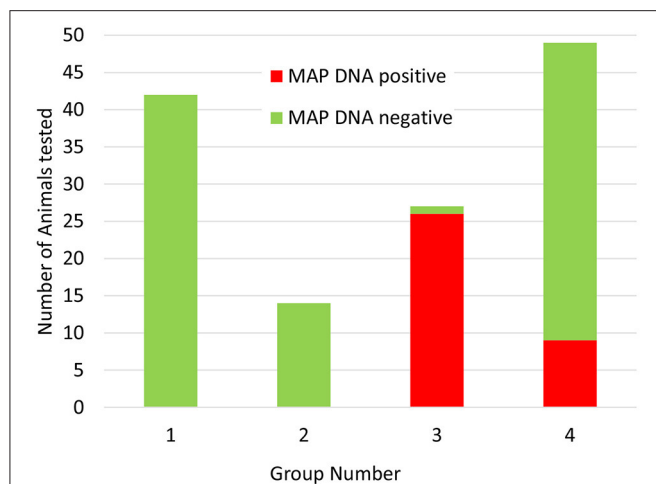


FIGURE 2 | Distribution of Actiphage MAP test results in commercial deer herd production groups. Blood samples were taken from 132 female deer prior to the rutting season. The samples were supplied to the lab blinded to production group. After the test results were available, the samples were unblinded and sorted by production group. Green bars indicate negative MAP test results; red bars indicate positive MAP test results.

to be able to remove contaminating erythrocytes from cervid buffy coat preparations (29). However, deer blood is known to exhibit unusual properties due to sickling which can be associated with increased fragility of erythrocytes (30). Therefore, to determine whether the ACK lysis method was an appropriate method for bulk isolation of white blood cells from whole blood, surplus material from 29 deer blood samples (set 1) provided for commercial Actiphage testing were obtained. White blood cells were recovered from 2 ml samples using either the recommended Ficoll method or the ACK lysis method. Although buffy coat was recovered from deer blood samples using Ficoll, the position of the buffy coat layer was inconsistent, and often formed a layer underneath the porous frit of the Leucosep tubes making extraction more difficult. In contrast a pellet of purified blood leukocytes was formed using the ACK method that on visible inspection was cream in colour indicating very little contamination with erythrocytes.

After the Actiphage assay had been performed, no PCR inhibition was detected by the IPC for either set of DNA samples, again confirming that the ACK method was compatible with the Actiphage assay reagents. Similarly the Actiphage assay positive control ($\sim 10^2$ MAP cells) and negative control (Actiphage reagents) samples gave Cq-values in the expected range (Table 1) but for this set of animals no clear positive test results were obtained, although tests were scored as weak positive for 4 animals (Table 1). The Cq-values for the paired samples was compared (Table 1) and were not found to be statistically different ($p = 0.16$), with an average ACK:Ficoll Cq of 0.99 with only 1 sample (#21) significantly deviating from this value. These results indicated that using the ACK method of white blood cell preparation did not affect the assay performance.

Detecting MAP in Deer Blood

Having established that the ACK method could be used to purify leukocytes from whole deer blood, the method was used to screen blood samples from a set of 132 female red deer immediately prior to the autumn rutting season (set 2). Again, positive and negative control samples gave the expected results and no qPCR inhibition was detected. In this set of animals MAP was detected in the blood samples of 35 animals (27%). Approximately 2/3 of the positive samples (21/31) produced strong positive results ($\Delta Cq > 5$), and the remaining 10 samples were scored as weak positive ($\Delta Cq 1.5-2$). Interestingly, when the animals were assigned to their production groups, it was found that all but nine of the animals that gave a positive test results belonged to one production group, and the rest were all found to belong to a second production group (see Figure 2 and Supplementary Table 1).

The following year, a set of 298 yearling animals from the same farm were tested using the ACK blood preparation method but as the farm only chose to test young animals on this occasion, this group did not include any of the animals tested the previous year (set 3). In this set of animals, 16% gave a positive test result (Supplementary Table 2). The following month a small set of 11 animals from this group that gave a positive test result were included in the blood samples set for screening (set 4; Table 2). At the second time of sampling all these animals again gave a positive test result, although 3 only gave a weak positive results ($\Delta Cq 1.5-2$).

A set of 38 animals were also chosen by the farm for commercial testing prior to sale that had given a negative test result the previous year and provided an opportunity to investigate the reproducibility of negative test results (set 5). On this occasion, blood samples were taken for both commercial MAP blood ELISA and Actiphage testing using the ACK method. In this case all blood samples from these animals produced a negative Actiphage test result and the ELISA test results were also all negative (data not shown).

DISCUSSION

We have previously shown that phage-based assays can be used to detect MAP in blood mononucleocytes of infected cattle (16) and more recently have described a new, more rapid and sensitive phage-based test that can be used to detect infection at any age [Actiphage; (17)]. In these previous studies Ficoll gradients were used to recover blood mononucleocytes, however this method has its disadvantages in that it is laborious and requires costly reagents. In this study we have demonstrated that the ACK differentiation lysis method, developed for the rapid recovery of stem cells, is compatible with the Actiphage assay. Unlike INF- γ assays, the physiological state of the white blood cells is not important for phage-based detection assays. Rather it is the physiological state of the MAP cells that is critical, and the leukocytes are lysed during the first steps of the assay to release any

TABLE 2 | Comparison of Actiphage-test results after 1 month.

Sample	Test date: 27/08/20			Test date: 22/09/20		
	Test result ^b	Cq-value	Δ Cq ^c	Test result ^b	Cq-value	Δ Cq ^c
Act. +ve ^a	+ve	25.72	n/a	+ve	18.68	n/a
Act. -ve ^a	-ve	30.43	n/a	-ve	32.44	n/a
1	+ve	21.44	9.0	+ve	29.75	2.7
2	+ve	22.34	8.1	+ve (w)	30.97	1.5
3	+ve	22.97	7.5	+ve	29.78	2.7
4	+ve	23.15	7.3	+ve (w)	30.59	1.9
5	+ve	24.98	5.5	+ve	29.25	3.2
6	+ve	26.02	4.4	+ve (w)	30.49	1.9
7	+ve	26.22	4.2	+ve	29.34	3.1
8	+ve	27.43	3.0	+ve	29.95	2.5
9	+ve	27.96	2.5	+ve	29.61	2.8
10	+ve	28.05	2.4	+ve	30.21	2.2
11	+ve	28.09	2.3	+ve	30.22	2.2

All animals tested were female, and were born in the same year (2019).

^aActiphage positive control = Media Plus inoculated with $\sim 10^2$ MAP K10 cells; Actiphage negative control = Media Plus and Actiphage reagents alone.

^bTest result; Positive = Δ Cq = ≥ 2 ; Positive weak (w) = Δ Cq 1.5-2.

^c Δ Cq; difference in Cq sample compared to the Actiphage negative control; n/a, not applicable.

intracellular MAP into a growth medium to keep them in a metabolically active state required for phage infection (28). Indeed the additional osmotic stress that the leukocytes experience during the ACK procedure may make them more susceptible to lysis which would also facilitate phage-based detection.

When preparing samples from deer blood, it was noted that there was less detectable erythrocyte contamination when using the ACK method. Contamination of the Ficoll purified buffy coats may have been due to the fact that the buffy coat layer was formed very close to the surface of the erythrocyte layer, some of which may have been picked up while pipetting off the delicate buffy coat layer or may be due to the higher fragility of the erythrocytes causing premature lysis (30). Hence for cervid blood samples, the ACK method had another advantage over standard Ficoll gradients.

In this study, the ACK method was used to screen animals from a commercial herd of farmed deer. The farm had had sporadic problems with JD after some animals had been purchased, but no cases of clinical disease had been detected recently. Initially a set of female animals were tested, with blood samples provided simply in the order the animals entered the testing pen. In this set of results there was an unusual pattern, with a cluster of positive results occurring in samples collected at the end of the process. This pattern of results was explained when the test results were compared with information provided about the production groups, when it became evident that there was one main group (group 3) which had the highest level of MAP infection and a lower level of infection detected in group 4, whereas groups 1 and 2 did not give any positive test results. Since these groups are geographically separated on the farm, this information is now being integrated into the farm management plan to ensure that infected animals are not moved

to the uninfected groups, and animals known to be infected are being prioritised for culling when numbers need to be reduced.

When the farm testing program allowed, it was also possible to carry out some small scale test reproducibility evaluation work, and it was found that when repeat tests were performed within 1 month that the results gained were consistent. The variation in the levels of DNA detected in the same animal (Table 2) is to be expected as there will be stochastic variation in the number of MAP cells detected when only very low number of infected macrophage are present in the blood and only small (2 ml) blood samples are being tested [see (25)]. Our previous studies of MAP in bovine blood have detected only 5–50 MAP cells per sample using phage-based assays (16, 31) and therefore only a very small percentage of the PBMCs in a sample ($\sim 10^6$) are likely to be infected. If larger samples could be tested, this would reduce the stochastic variation, but currently the viscosity of the sample which contains large amounts of bovine DNA derived from the lysed macrophages prevents larger volumes of blood processed using the Actiphage kit. Similarly when a set of animals that had previously given a negative Actiphage test result were tested again using both ELISA and Actiphage, both tests gave negative results. Since a commercial qPCR kit was used to detect the MAP DNA, and the specificity of the detection event comes from the qPCR step, this provides confidence that these are true positive results. However, it was also clear that this non-optimised qPCR assay resulted in high background noise levels. The Bactoreal kit is optimised for the detection of MAP DNA in faecal samples and PCR bridging can lead to positive Cq-values when the sample DNA contains high concentrations of off targets and primer concentrations have not been optimised (32–34). If the PCR reagents are optimised, this may allow lower levels of cells to be detected with confidence. Further studies are required to fully validate the Actiphage method for detecting MAP infections in deer, including comparison with

other standard diagnostic test methods, but these results provide first evidence that Actiphage is specific and in combination with the ACK lysis method can be used to detect MAP infection in farmed deer.

The inherent specificity of bacteriophage D29 towards its Mycobacterial host cells, coupled with the high specificity and sensitivity of PCR-based detection methods has led to the development of the new, more sensitive Actiphage assay. The replacement of Ficoll gradients further simplifies the method and the chemicals required for the production of ACK lysis buffer (Ammonium chloride, Potassium bicarbonate and EDTA) are widely available and inexpensive. This proof of principle study demonstrates that Actiphage is a new tool that can directly detect the presence of MAP in cervid blood samples and clearly has potential for the control of Johne's disease.

DATA AVAILABILITY STATEMENT

The original contributions presented in the study are included in the article/**Supplementary Material**, further inquiries can be directed to the corresponding author.

ETHICS STATEMENT

Ethical review and approval was not required for the animal study because Superfluous blood samples from commercial testing

program provided. Written informed consent was obtained from the owners for the participation of their animals in this study.

AUTHOR CONTRIBUTIONS

AK developed and evaluated the ACK method for use with deer blood, and contributed to writing the manuscript. AP and CE generated results for commercial samples using the Ficoll method. TP and BS contributed to the design, supervision of experiments, writing, and reviewing the manuscript. CR contributed to design of experiments, data analysis, and writing the manuscript. All authors contributed to the article and approved the submitted version.

FUNDING

BS was funded by a Research England—Connecting Capabilities Fund—BloomsburySET Research Fellowship. AK and CE are UoN students sponsored by PBD Biotech Ltd.

SUPPLEMENTARY MATERIAL

The Supplementary Material for this article can be found online at: <https://www.frontiersin.org/articles/10.3389/fvets.2021.665697/full#supplementary-material>

REFERENCES

- Bauerfeind R, Benazzi S, Weiss R, Schliesser T, Willems H, Baljer G. Molecular characterization of *Mycobacterium paratuberculosis* isolates from sheep, goats, and cattle by hybridization with a DNA probe to insertion element IS900. *J Clin Microbiol.* (1996) 34:1617–21. doi: 10.1128/jcm.34.7.1617-1621.1996
- Mackintosh C, de Lisle G, Collins D, Griffin J. Mycobacterial diseases of deer. *N Z Vet J.* (2004) 52:163–74. doi: 10.1080/00480169.2004.36424
- de Lisle G, Yates G, Montgomery R. The emergence of *Mycobacterium paratuberculosis* in farmed deer in New Zealand—a review of 619 cases. *N Z Vet J.* (2003) 51:58–62. doi: 10.1080/00480169.2003.36341
- Whittington R, Donat K, Weber MF, Kelton DF, Nielsen SS, Eisenberg SWF, et al. Control of paratuberculosis: who, why and how. A review of 48 countries. *BMC Vet Res.* (2019) 15:198. doi: 10.1186/s12917-019-1943-4
- Palmer MV, Kanipe C, Cox R, Robbe-Austerman S, Thacker TC. Characteristics of subclinical *Mycobacterium avium* subsp. paratuberculosis infection in a captive white-tailed deer herd. *J Vet Diagn Invest.* (2019) 31:844–51. doi: 10.1177/1040638719873028
- Magombedze G, Shiri T, Eda S, Stabel JR. Inferring biomarkers for *Mycobacterium avium* subsp. paratuberculosis infection and disease progression in cattle using experimental data. *Sci Rep.* (2017) 7:44765. doi: 10.1038/srep44765
- Raizman EA, Wells SJ, Godden SM, Bey RF, Oakes MJ, Bentley DC, et al. The distribution of *Mycobacterium avium* subsp. paratuberculosis in the environment surrounding Minnesota dairy farms. *J Dairy Sci.* (2004) 87:2959–66. doi: 10.3168/jds.S0022-0302(04)73427-X
- van Kooten H, Mackintosh C, Koets A. Intra-uterine transmission of paratuberculosis (Johne's disease) in farmed red deer. *N Z Vet J.* (2006) 54:16–20. doi: 10.1080/00480169.2006.36598
- Thompson BR, Clark RG, Mackintosh CG. Intra-uterine transmission of *Mycobacterium avium* subsp. paratuberculosis in subclinically affected red deer (*Cervus elaphus*). *N Z Vet J.* (2007) 55:308–13. doi: 10.1080/00480169.2007.36786
- Schiller I, Oesch B, Vordermeier HM, Palmer MV, Harris BN, Orloski KA, et al. Bovine tuberculosis: a review of current and emerging diagnostic techniques in view of their relevance for disease control and eradication. *Transbound Emerg Dis.* (2010) 57:205–20. doi: 10.1111/j.1865-1682.2010.01148.x
- Whittington RJ, Marsh I, Turner MJ, McAllister S, Choy E, Eamens GJ, et al. Rapid detection of *Mycobacterium paratuberculosis* in clinical samples from ruminants and in spiked environmental samples by modified BACTEC 12B radiometric culture and direct confirmation by IS900 PCR. *J Clin Microbiol.* (1998) 36:701–7. doi: 10.1128/JCM.36.3.701-707.1998
- Reyes-García R, Pérez-de-la-Lastra JM, Vicente J, Ruiz-Fons F, Garrido JM, Gortázar C. Large-scale ELISA testing of Spanish red deer for paratuberculosis. *Vet Immunol Immunopathol.* (2008) 124:75–81. doi: 10.1016/j.vetimm.2008.01.032
- Prieto JM, Balseiro A, Casais R, Abendaño N, Fitzgerald LE, Garrido JM, et al. Sensitive and specific enzyme-linked immunosorbent assay for detecting serum antibodies against *Mycobacterium avium* subsp. paratuberculosis in fallow deer. *Clin Vaccine Immunol.* (2014) 21:1077–85. doi: 10.1128/01.00159-14
- Griffin JF, Spittle E, Rodgers CR, Liggett S, Cooper M, Bakker D, et al. Immunoglobulin G1 enzyme-linked immunosorbent assay for diagnosis of Johne's Disease in red deer (*Cervus elaphus*). *Clin Diagn Lab Immunol.* (2005) 12:1401–9. doi: 10.1128/CDLI.12.12.1401-1409.2005
- O'Brien R, Hughes A, Liggett S, Griffin F. Composite testing for ante-mortem diagnosis of Johne's disease in farmed New Zealand deer: correlations between bacteriological culture, histopathology, serological reactivity and faecal shedding as determined by quantitative PCR. *BMC Vet Res.* (2013) 9:72. doi: 10.1186/1746-6148-9-72
- Swift BM, Denton EJ, Mahendran SA, Huxley JN, Rees CE. Development of a rapid phage-based method for the detection of viable *Mycobacterium*

- avium* subsp. paratuberculosis in blood within 48 h. *J Microbiol Meth.* (2013) 94:175–9. doi: 10.1016/j.mimet.2013.06.015
17. Swift BMC, Meade N, Sandoval Barron E, Bennett M, Perehinec T, Hughes V, et al. The development and use of Actiphage® to detect viable mycobacteria from bovine tuberculosis and John's disease-infected animals. *Microb Biotechnol.* (2020) 13:738–46. doi: 10.1111/1751-7915.13518
 18. Verma R, Swift BMC, Handley-Hartill W, Lee JK, Woltmann G, Rees CED, et al. A novel, high-sensitivity, bacteriophage-based assay identifies low-level *Mycobacterium tuberculosis* bacteremia in immunocompetent patients with active and incipient Tuberculosis. *Clin Infect Dis.* (2020) 70:933–6. doi: 10.1093/cid/ciz548
 19. Molenaar FM, Burr PD, Swift BMC, Rees CED, Masters N. Conservation challenges: the limitations of antemortem tuberculosis testing in captive Asiatic Lions (*Panthera Leo persica*). *J Zoo Wildl Med.* (2020) 51:426–32. doi: 10.1638/2019-0084
 20. Swift BM, Convery TW, Rees CE. Evidence of *Mycobacterium tuberculosis* complex bacteraemia in intradermal skin test positive cattle detected using phage-RPA. *Virulence.* (2016) 7:779–88. doi: 10.1080/21505594.2016.1191729
 21. Silver R, Li Q, Ellner J. Expression of virulence of *Mycobacterium tuberculosis* within human monocytes: virulence correlates with intracellular growth and induction of tumor necrosis factor alpha but not with evasion of lymphocyte-dependent monocyte effector functions. *Infect Immun.* (1998) 66:1190–9. doi: 10.1128/IAI.66.3.1190-1199.1998
 22. Rathnaiah G, Zinniel DK, Bannantine JP, Stabel JR, Gröhn YT, Collins MT, et al. Pathogenesis, molecular genetics, and genomics of *Mycobacterium avium* subsp. paratuberculosis, the etiologic agent of John's Disease. *Front Vet Sci.* (2017) 4:187. doi: 10.3389/fvets.2017.00187
 23. Bower KL, Begg DJ, Whittington RJ. Culture of *Mycobacterium avium* subsp. paratuberculosis (MAP) from blood and extra-intestinal tissues in experimentally infected sheep. *Vet Microbiol.* (2011) 147:127–32. doi: 10.1016/j.vetmic.2010.06.016
 24. Menck K, Behme D, Pantke M, Reiling N, Binder C, Pukrop T, et al. Isolation of human monocytes by double gradient centrifugation and their differentiation to macrophages in teflon-coated cell culture bags. *J Vis Exp.* (2014) 9:e51554. doi: 10.3791/51554
 25. Gerrard ZE, Swift BMC, Botsaris G, Davidson RS, Hutchings MR, Huxley JN, et al. Survival of *Mycobacterium avium* subsp. paratuberculosis in retail pasteurised milk. *Food Microbiol.* (2018) 74:57–63. doi: 10.1016/j.fm.2018.03.004
 26. Chernyshev AV, Tarasov PA, Semianov KA, Nekrasov VM, Hoekstra AG, Maltsev VP. Erythrocyte lysis in isotonic solution of ammonium chloride: theoretical modeling and experimental verification. *J Theor Biol.* (2008) 251:93–107. doi: 10.1016/j.jtbi.2007.10.016
 27. Brown WE, Hu JC, Athanasiou KA. Ammonium-chloride-potassium lysing buffer treatment of fully differentiated cells increases cell purity and resulting neotissue functional properties. *Tissue Eng Part C Methods.* (2016) 22:895–903. doi: 10.1089/ten.tec.2016.0184
 28. Swift BM, Gerrard ZE, Huxley JN, Rees CE. Factors affecting phage D29 infection: a tool to investigate different growth states of mycobacteria. *PLoS ONE.* (2014) 9:e106690. doi: 10.1371/journal.pone.0106690
 29. Dugovich B, Crane L, Alcantar B, Beechler B, Dolan B, Jolles A. Multiple innate antibacterial immune defense elements are correlated in diverse ungulate species. *PLoS ONE.* (2019) 14:e0225579. doi: 10.1371/journal.pone.0225579
 30. Esin A, Bergendahl LT, Savolainen V, March JA, Warnecke T. The genetic basis and evolution of red blood cell sickling in deer. *Nat Ecol Evol.* (2018) 2:367–76. doi: 10.1038/s41559-017-0420-3
 31. Swift BM, Huxley JN, Plain KM, Begg DJ, de Silva K, Purdie AC, et al. Evaluation of the limitations and methods to improve rapid phage-based detection of viable *Mycobacterium avium* subsp. paratuberculosis in the blood of experimentally infected cattle. *BMC Vet Res.* (2016) 12:115. doi: 10.1186/s12917-016-0728-2
 32. Liu S, Thaler DS, Libchaber A. Signal and noise in bridging PCR. *BMC Biotechnol.* (2002) 2:13. doi: 10.1186/1472-6750-2-13
 33. Ruiz-Villalba A, van Pelt-Verkuil E, Gunst QD, Ruijter JM, van den Hoff MJ. Amplification of nonspecific products in quantitative polymerase chain reactions (qPCR). *Biomol Detect Quantif.* (2017) 14:7–18. doi: 10.1016/j.bdq.2017.10.001
 34. Park M, Won J, Choi BY, Lee CJ. Optimization of primer sets and detection protocols for SARS-CoV-2 of coronavirus disease 2019 (COVID-19) using PCR and real-time PCR. *Exp Mol Med.* (2020) 52:963–77. doi: 10.1038/s12276-020-0452-7

Conflict of Interest: CR and BS are founder members and shareholders of PBD Biotech Ltd., and AP is an employee of the company. AP and CE are UoN students sponsored by the company, but they can declare that the research was conducted in the absence of any commercial or financial relationships that could be construed as a potential conflict of interest. TP is an employee of UoN and has no commercial or financial relationship with the company.

The remaining author declares that the research was conducted in the absence of any commercial or financial relationships that could be construed as a potential conflict of interest.

Publisher's Note: All claims expressed in this article are solely those of the authors and do not necessarily represent those of their affiliated organizations, or those of the publisher, the editors and the reviewers. Any product that may be evaluated in this article, or claim that may be made by its manufacturer, is not guaranteed or endorsed by the publisher.

Copyright © 2021 Kubala, Perehinec, Evans, Pirovano, Swift and Rees. This is an open-access article distributed under the terms of the Creative Commons Attribution License (CC BY). The use, distribution or reproduction in other forums is permitted, provided the original author(s) and the copyright owner(s) are credited and that the original publication in this journal is cited, in accordance with accepted academic practice. No use, distribution or reproduction is permitted which does not comply with these terms.

Advantages of publishing in Frontiers



OPEN ACCESS

Articles are free to read
for greatest visibility
and readership



FAST PUBLICATION

Around 90 days
from submission
to decision



HIGH QUALITY PEER-REVIEW

Rigorous, collaborative,
and constructive
peer-review



TRANSPARENT PEER-REVIEW

Editors and reviewers
acknowledged by name
on published articles

Frontiers

Avenue du Tribunal-Fédéral 34
1005 Lausanne | Switzerland

Visit us: www.frontiersin.org

Contact us: frontiersin.org/about/contact



REPRODUCIBILITY OF RESEARCH

Support open data
and methods to enhance
research reproducibility



DIGITAL PUBLISHING

Articles designed
for optimal readership
across devices



FOLLOW US

@frontiersin



IMPACT METRICS

Advanced article metrics
track visibility across
digital media



EXTENSIVE PROMOTION

Marketing
and promotion
of impactful research



LOOP RESEARCH NETWORK

Our network
increases your
article's readership